

SIMULTANEOUS DETERMINATION OF VAPOUR- AND LIQUID-SIDE VOLUMETRIC MASS TRANSFER COEFFICIENTS IN DISTILLATION COLUMN

V. LINEK*, T. MOUCHA, E. PROKOPOVÁ and J. F. REJL

Prague Institute of Chemical Technology, Department of Chemical Engineering, Prague, Czech Republic

The method for the determination of $k_L a$ and $k_V a$ in distillation column consists in a fitting of the concentration profile along the column obtained by the integration of a differential model to the experimental one. Preliminary test of the method is presented using concentration profile measured in the binary distillation of the ethanol-water system at total reflux on metal Pall Ring 25 mm. The distillation is modelled as a simultaneous heat and mass transfer process and the mathematical model includes mass and energy balances and the heat and mass transfer equations. By using the Maxwell-Stefan flux expressions the convective transport contributions have been considered in the transfer equations. Vapour and liquid phases are supposed to be at their saturated temperatures along the column. Concentration and temperature dependent physical parameters and the liquid phase thermodynamic non-idealities have been taken into account. The distillation mass transfer coefficients in the liquid and vapour phases obtained by the fitting procedure are compared with those calculated from absorption data using Onda's, Billet's and Linek's correlations. The distillation heat transfer coefficients calculated from the model assuming saturated temperatures in both phases are compared with those calculated from the Chilton-Colburn and penetration model analogy.

Keywords: mass transfer coefficient; HETP; distillation; packed column.

INTRODUCTION

Absorption and distillation have the same physical background—interfacial mass transfer between gas and liquid phase, which is characterized by a volumetric mass transfer coefficient on the vapour/gas- ($k_V a$) and the liquid- ($k_L a$) side. In spite of this fact, a design of distillation columns from absorption mass transfer data is not successful because large errors in estimation of the height equivalent to theoretical plate for distillation (HETP) exist (up to 100%, see Linek *et al.*, 1995). It indicates that the correlations based on the absorption mass transfer coefficients do not fit the influence of physical properties accurately in the range needed for temperature extrapolation from absorption (around 20°C) to distillation conditions.

Measurements of the fundamental mass transfer data in distillation columns, i.e., vapour- and liquid-mass transfer coefficients, are rare. In distillation, it is not possible to measure individual mass transfer coefficients under conditions where the overall resistance to the process is

mainly due to one of the phases and to study behaviour of the individual coefficients separately as it is possible in absorption. The transfer of heat simultaneously with the transfer of mass have to be considered in experimental analysis of the process of distillation as it is important in determining the individual phase transfer coefficients. It is normally assumed that the rate of heat transfer is such as to keep the vapour and liquid phases just at their dew and boiling points respectively, as they pass through the column. This was supported by experiments carried out by Kayihan *et al.* (1977) in a wetted wall column using the methanol-water system. Confirmation of the liquid phase saturation was made through a comparison of the experimentally measured liquid temperature with the calculated bubble point temperature. From the observed fact that the liquid phase was saturated the authors deduced that all of the resistance to mass transfer was in the vapour phase. The experimental vapour phase mass transfer coefficients were in good agreement with published correlations based on absorption and evaporation data. It was concluded that interphase diffusion is responsible for mass transfer in distillation and that there is no additional evaporation within the liquid phase caused by heat transferred from the vapour phase as proposed by some previous investigators (Liang and Smith, 1962). Honorat and Sandall (1978)

*Correspondence to: Dr V. Linek, Prague Institute of Chemical Technology, Department of Chemical Engineering, CZ-166 28 Prague 6, Czech Republic.
E-mail: linekv@vscht.cz

confirmed the same in a distillation column packed with 1/4 in Raschig rings using the toluene–trichloroethylene system, i.e., the zero resistance to mass transfer in the liquid phase and the agreement between vapour mass transfer coefficients obtained from the distillation experiments and those predicted from correlations of gas absorption data.

An assumption that all of the resistance to mass transfer is in the vapour phase has been used in many applications of simultaneous heat and mass transfer model for multi-component distillation. For example, Dribika and Sandall (1979) used the model for evaluation of the vapour phase mass transfer coefficient in a wetted wall column in the benzene–toluene–ethylbenzene ternary system. Pelkonen *et al.* (1997) assumed a total resistance to mass transfer in the vapour phase in a case study with nonideal multi-component distillation mixtures (methanol–isopropyl alcohol–water, acetone–methanol–isopropyl alcohol–water) performed to investigate which parameters affect the profile of the rectification line. To eliminate the heat transfer coefficients, Dribika and Sandall (1979) used the Chilton–Colburn analogy in contrast to Pelkonen *et al.* (1997), who neglected the contribution of the sensible heat flux.

Arwikar and Sandall (1980) re-examined the previous mass transfer data (Kayihan *et al.*, 1977; Honorat and Sandall, 1978) from which the negligible liquid phase mass transfer resistance in distillation was deduced. They determined the absorption liquid phase mass transfer coefficients on the same column and revealed that the liquid phase mass transfer resistance is small but not negligible constituting approximately 12–18% of the total mass transfer resistance. The authors (Kayihan *et al.*, 1977; Honorat and Sandall, 1978) neglected the resistance to the mass transfer in the liquid phase, so their k_{va} data cannot be considered reliable.

In the paper a method, which enables to determine k_{La} and k_{va} in distillation column, is presented. The method consists in fitting the concentration profile obtained by integration of the differential model of a distillation column to the experimental one. The aim of this paper is to point out the practicability of the simultaneous determination of both partial mass transfer coefficients in a distillation column.

THEORETICAL

The model is based on the application of mass and energy balances and heat and mass transfer equations to a differential control volume $S dz$ of the column, i.e., combined heat and mass transfer processes are taken into account. The following assumptions have been made: (1) the piston flow in both phases; (2) the processes are in steady state; (3) the pressure in the column is constant; (4) the rate of heat transfer is such as to keep the vapour and liquid phases just at their dew and boiling points respectively and heat losses to the environment are neglected; (5) equilibrium at the interface is considered (no interfacial resistance); (6) the heat and mass transfer areas are equal; (7) the liquid leaving the condenser is saturated; (8) the total reflux is considered.

The Differential Model of a Distillation Column

Global mass, component and enthalpy balances over the differential volume of packing with length dz for the

distillation of binary mixture lead to

$$\frac{dL}{dz} - \frac{dV}{dz} = 0 \Rightarrow L - V = \text{const.} \quad (1)$$

$$L \frac{dx_A}{dz} + x_A \frac{dL}{dz} - V \frac{dy_A}{dz} - y_A \frac{dV}{dz} = 0 \quad (2)$$

$$L \frac{dh_L}{dz} + h_L \frac{dL}{dz} - V \frac{dh_V}{dz} - h_V \frac{dV}{dz} = 0 \quad (3)$$

The following simplifications hold at the total reflux under adiabatic conditions: $L = V$ and $x_A = y_A$ and

$$L \left(\frac{dh_L}{dz} - \frac{dh_V}{dz} \right) + \frac{dL}{dz} (h_L - h_V) = 0 \quad (4)$$

Liquid phase mass balances of components A and B (the molar fluxes $N_{A,B}$ are defined to be positive from the vapour to the liquid) are

$$L \frac{dx_A}{dz} + x_A \frac{dL}{dz} - N_A = L \frac{dx_B}{dz} + x_B \frac{dL}{dz} - N_B = 0 \quad (5)$$

$N_{A,B}$ are given by following rate and equilibrium relations and by the mass continuity requirement at the interface (an equal mass transport in the liquid and vapour phases)

$$\begin{aligned} N_A &= k_{va} \cdot c_v \cdot r \cdot \ln \left[\frac{y_{Aw} - r}{x_A - r} \right] \cdot S \\ &= k_{La} \cdot c_L \cdot r \cdot \ln \left[\frac{x_A - r}{x_{Aw} - r} \right] \cdot S \end{aligned} \quad (6)$$

$$\frac{N_B}{N_A} = \left(\frac{1}{r} \right) - 1 \quad (7)$$

$$y_{Aw} = K \cdot x_{Aw} \quad (8)$$

The molar flux N_A between the vapour and liquid phases results from the combined contribution of molecular diffusion and a bulk transport of material through the interface. A detailed derivation of the equation is given elsewhere (Bird *et al.*, 1960).

Energy balances of liquid and vapour phases (heat transfer is defined to be positive from the vapour to the liquid phase)

$$L \frac{dh_L}{dz} + h_L \frac{dL}{dz} - Q_{TL} - (N_A h_{LA} + N_B h_{LB}) = 0 \quad (9)$$

$$L \frac{dh_V}{dz} + h_V \frac{dL}{dz} - Q_{TV} - (N_A h_{VA} + N_B h_{VB}) = 0 \quad (10)$$

The sensible heats transferred from the interface to the bulk liquid Q_{TL} and from the bulk vapour to the interface Q_{TV} are given by following relation (Bird *et al.*, 1960)

$$Q_{TL} = \alpha_L a \frac{C_{pL}}{1 - \exp(-C_{pL})} (t_w - t_L) S \quad (11)$$

$$Q_{TV} = \alpha_V a \frac{C_{pV}}{1 - \exp(-C_{pV})} (t_V - t_w) S \quad (12)$$

$$C_{pi} = \frac{N_A c_{piA} + N_B c_{piB}}{\alpha_i a} \quad (i = L, V) \quad (13)$$

From equation (4) through (13), by some rearrangements, the following set of differential equations can be obtained, an integration of which gives the concentration profile in a column and the heat transfer coefficients in both phases which are necessary to keep the phases at the saturated temperatures

$$\frac{dL}{dz} = (N_A + N_B) \quad (14)$$

$$\frac{dx_A}{dz} = \frac{N_A - x_A(N_A + N_B)}{L} \quad (15)$$

$$\frac{dh_L}{dz} = \frac{dx_A}{dz} \cdot \left(\frac{dh_L}{dx_A} + \frac{dh_L}{dt_L} \cdot \frac{dt_L}{dx_A} \right) \quad (16)$$

$$\frac{dh_V}{dz} = \frac{dx_A}{dz} \cdot \left(\frac{dh_V}{dx_A} + \frac{dh_V}{dt_V} \cdot \frac{dt_V}{dx_A} \right) \quad (17)$$

$$\frac{dL}{dz} \cdot (h_V - h_L) + L \cdot \left(\frac{dh_V}{dz} - \frac{dh_L}{dz} \right) = 0 \quad (18)$$

$$Q_{TL} = \frac{dh_L}{dz} \cdot L - N_A(h_{LA} - h_L) - N_B(h_{LB} - h_L) \quad (19)$$

$$Q_{TV} = \frac{dh_V}{dz} \cdot L - N_A(h_{VA} - h_V) - N_B(h_{VB} - h_V) \quad (20)$$

$$\alpha_{LA} = Q_{TL} \cdot \frac{1 - \exp(-C_{pL})}{C_{pL} \cdot (t_w - t_L) \cdot S} \quad (21)$$

$$\alpha_{VA} = Q_{TV} \cdot \frac{1 - \exp(-C_{pV})}{C_{pV} \cdot (t_V - t_w) \cdot S} \quad (22)$$

with N_A and N_B given by equations (6)–(8). When the following auxiliary relations are added to the model equations

$$h_L(x_A, t_L) = [c_{pLA}x_A + c_{pLB}(1 - x_A)]t_L + \Delta h_{\text{mix}} \quad (23)$$

$$h_V(x_A, t_V) = [c_{pVA}t_{\text{bpA}} + \Delta h_{\text{vapA}}]x_A + [c_{pVB}t_{\text{bpB}} + \Delta h_{\text{vapB}}](1 - x_A) + c_{pVA}x_A(t_V - t_{\text{bpA}}) + c_{pVB}(1 - x_A)(t_V - t_{\text{bpB}}) \quad (24)$$

we obtain a system with 10 equations [equations (6)–(8), (14)–(18), (23) and (24)], 10 variables (L , x_A , x_{Aw} , N_A , N_B , t_w , t_L , t_V , h_L , h_V) and two coefficients (k_{La} , k_{Va}).

In the calculation following thermodynamic properties: c_{pLA} , c_{pLB} , Δh_{mix} , c_{pVA} , c_{pVB} , Δh_{vapA} , Δh_{vapB} , c_V and c_L were considered to be functions of the concentration and the temperature and hence change along the column. The corresponding functions are: the molar heat of mixing Δh_{mix} was calculated by Christensen *et al.* (1984), the molar densities of the liquid mixtures by Barner–Quinlan's rule using data from Vargaftik (1975), the vapour phase was ideal, the vapour–liquid equilibrium was calculated by Wilson equation using binary coefficients given by Gmehling *et al.* (1981) and diffusion coefficients were calculated according to Zarzycki and Chacuk (1993). The dependences of the volumetric mass transfer coefficients on phase flows and on physical properties of phases

which change along the column were considered in two forms: in the form of correlations suggested by Billet *et al.* (1993)

$$k_{La} = C_L \left(\frac{\rho_L g}{\eta_L} \right)^{1/6} \left(\frac{D_L}{l_\tau} \right)^{1/2} a_t^{2/3} u_L^{1/3} \left(\frac{a}{a_t} \right)$$

$$k_{Va} = C_V \frac{1}{(\varepsilon - U)^{1/2}} \frac{a_t^{3/2}}{l_\tau^{1/2}} D_V \left(\frac{u_V \rho_V}{a_t \eta_V} \right)^{3/4}$$

$$\times \left(\frac{\eta_V}{D_V \rho_V} \right)^{1/3} \left(\frac{a}{a_t} \right)$$

$$\frac{a}{a_t} = 1.5(a_t l_\tau)^{-0.5} \left(\frac{u_L l_\tau \rho_L}{\eta_L} \right)^{-0.2} \left(\frac{u_L^2 \rho_L l_\tau}{\sigma_L} \right)^{0.75} \left(\frac{u_L^2}{g l_\tau} \right)^{-0.45}$$

$$U = \left(12 \frac{1}{g} \frac{\eta_L}{\rho_L} u_L a_t^2 \right)^{1/3}; \quad l_\tau = 4 \frac{\varepsilon}{a_t} \quad (25)$$

and in a simple form of

$$k_{La} = b_L u_L^{2/3} D_L^{1/2}$$

$$k_{Va} = b_V u_V^{0.7} D_V^{2/3} \quad (26)$$

Optimization of the shape or optionally of the values of some exponents in correlations (25) and (26) is not possible until more extensive data collection will be treated.

The concentration profile obtained by integration of the differential equations is fitted to the experimental one, optimizing the empirical parameters C_L and C_V in case of correlation (25) and b_L and b_V in case of correlation (26).

COMPUTING METHOD

Integration of the Differential Model of a Distillation Column and Parameters Estimation Method

The set of the differential equations has been solved using a finite difference numerical method. The column has been divided in a finite number of elements with an incremental length of Δz . An iterative calculation was started at the top of the column. The following input parameters are used: cross-section of the column S , packing height Z , pressure in the column p , the total reflux conditions (molar flow L_0 , concentration x_{A0} and corresponding saturated temperatures t_{L0} and t_{V1}). The calculation procedure of flow and concentration profiles in the column and the optimizing procedure used for evaluation of the parameters b_V and b_L is summarized as follows:

- (1) Guess the parameters b_V and b_L (or C_L and C_V) and evaluate all thermodynamic properties, coefficients k_{La} and k_{Va} from (25) or (26) and derivatives dh_L/dx_A , dh_L/dt_L , dt_L/dx_A , dh_V/dx_A , dh_V/dt_V , dt_V/dx_A (a numerical differentiation was used).
- (2) Guess the interface temperature t_w at the top section of the column.
- (3) Calculate x_{Aw} and y_{Aw} with the assumed temperature t_w and column pressure from (8).
- (4) Calculate r from (6).
- (5) Calculate the fluxes N_A and N_B from (6) and (7).

- (6) Calculate dL/dz and dx_A/dz from (14) and (15).
- (7) Using the dx_A/dz calculate dh_L/dz and dh_V/dz from (16) and (17).
- (8) Calculate dL/dz from (18). If the value agrees with that calculated from (14) go to step (9), otherwise guess a new value of t_w and return to the step (3).
- (9) Using equations (14) and (15), calculate the new flow L_1 and concentration x_{A1} of the liquid at the next section ($z + \Delta z$).
- (10) If $(z + \Delta z) = Z$ go to step (11), if $(z + \Delta z) < Z$ guess a value of t_w for next section ($z + \Delta z$) and go to step (3).
- (11) The calculated concentration profile compare with the experimental one. If a matching criterion is fulfilled stop the calculation, otherwise guess new values of the parameters b_L and b_V and go to step (2).

As the matching criterion was used the following objective function representing the minimum of the sum of squared relative molar fractions differences between the calculated and measured values along the column

$$\min f = \sum_{\substack{\text{point} \\ \text{series}j}} \left(\left(\frac{(x_{A,i})_{\text{exp}} - (x_{A,i})_{\text{cal}}}{(x_{A,i})_{\text{exp}}} \right)^2 \right)_j$$

$$(i = 1, \dots, 7, j = 1, \dots, 8) \quad (27)$$

The simplex method was used for determination of the model parameters b_L and b_V or C_L and C_V by minimizing the objective function. The computational program was written in FORTRAN 90.

HETP and Liquid Side Mass Transfer Resistance

The height equivalent to the theoretical plate (HETP) is calculated according to the relation

$$\text{HETP} = u_L \left(\frac{1}{k_L a} + \frac{m_A}{k_V a} \right) \frac{\ln(m_A(u_L/u_V))}{m_A(u_L/u_V) - 1} \quad (28)$$

The ratio of the liquid phase mass transfer resistance to the overall resistance R_L was calculated from

$$R_L = \frac{1/k_L a}{1/k_L a + m_A/k_V a} \quad (29)$$

where the slope of equilibrium m_A is expressed as (Seader and Henley, 1998)

$$m_A = \frac{c_{LA}^* - c_{LA,w}}{c_{VA} - c_{VA,w}} = \left(\frac{c_L}{c_V} \right) \left(\frac{x_A^* - x_{A,w}}{y_A - Kx_{A,w}} \right)$$

$$\text{TOT.REFLUX} \left(\frac{c_L}{c_A} \right) \left(\frac{x_A^* - x_{A,w}}{x_A - Kx_{A,w}} \right) \quad (30)$$

The alterations of the slope of equilibrium, which take place independently along the distillation column, enable to determine the individual coefficients $k_L a$ and $k_V a$ separately. The distillation system ethanol–water is convenient in this respect because its slope changes considerably.

Heat Transfer Coefficients

As the bulks of the liquid and the vapour phase differ in temperature, a convective heat transfer occurs in the system, an intensity of which depends on the values of volumetric heat transfer coefficients in the liquid and the vapour phase, i.e., $\alpha_L a$ and $\alpha_V a$. Because of the above-mentioned assumption of the temperature saturation of the phases it is possible to calculate the values of $\alpha_L a$ and $\alpha_V a$ for each cross-section of the column from relations (21) and (22), i.e., from enthalpy balance.

On the other hand, it is possible to treat the process of convective heat transfer in a distillation column as analogic to the process of diffusional mass transfer, and thus to calculate the values of the heat transfer coefficients from the knowledge of the mass transfer coefficients. Using the Chilton–Colburn analogy for the vapour phase and assuming a penetration-theory type mechanism for the liquid phase we obtain following relations:

$$\frac{\alpha_V a}{k_V a} = 1000 \cdot \left(\frac{Sc_V}{Pr_V} \right)^{2/3} \left(\frac{\rho_V c_{pV}}{M_V} \right)$$

$$= 1000 \cdot \left(\frac{\lambda_V}{D_V} \right)^{2/3} \left(\frac{\rho_V c_{pV}}{M_V} \right)^{1/3} \quad (31)$$

$$\frac{\alpha_L a}{k_L a} = 1000 \cdot \left(\frac{Sc_L}{Pr_L} \right)^{1/2} \left(\frac{\rho_L c_{pL}}{M_L} \right)$$

$$= 1000 \cdot \left(\frac{\lambda_L}{D_L} \right)^{1/2} \left(\frac{\rho_L c_{pL}}{M_L} \right)^{1/2} \quad (32)$$

According to Krishnamurthy and Taylor (1985): ‘The analogies used above to predict the heat transfer coefficients cannot be taken very reliable. Alternative methods for the estimation of the heat transfer coefficients are hard to come by. The only solution to this stalemate is to use analogies with caution and evaluate the significance of errors in the estimation of α_V and α_L on the final results.’

By comparison of the values obtained from the balance equations (21) and (22) and from the analogies (31) and (32) the quality of the prediction of the analogies can be judged.

EXPERIMENTAL

The experiments were carried out in a stainless steel packed column of 0.15 m i.d. The column was equipped with six openings for placing thermistors and sampling devices for withdrawal of liquid samples along the column. 25 mm metal Pall rings were used as a packing. The height of the packing was 2.04 m and the packing density was $n_t = 46\,418 \text{ pcs m}^3$ ($a_t = 193 \text{ m}^{-1}$, $\varepsilon = 0.959$). The packing support (stainless steel grid) was designed to provide 95% free space to avoid premature flooding. A countercurrent condenser was situated above the packing. Flow rate of the liquid, which returned from the condenser, was measured by Omega FTB-900 flow meter and the liquid was led to the distributor situated as close as possible to the top of the packing. A uniform liquid distribution was achieved with a specially designed distributor. Electrically heated reboiler equipped with electric power regulator (up to 60 kW) was used to maintain a constant boiling rate.

The column, reboiler and condenser were insulated with 4 cm thick Orsil insulation and wrapped with duct tape. The

effectiveness of the insulation was determined by some heat loss experiments, which showed that the total heat loss was less than 3% of the heat delivered to the reboiler.

The experiments were run at total reflux and steady state conditions. About 45 litres of ethanol–water mixture were poured into the reboiler and electric power input to the reboiler was adjusted to 25 kW. The column was operated for some time to achieve steady state, which took one hour usually. After this period the liquid samples (5 ml) were withdrawn by glass syringes from all the sampling devices simultaneously. Series of eight experiments were performed at the same power input to the reboiler but at different concentrations of ethanol in the liquid in the reboiler. After finishing the run densities of the samples were measured using a digital densimeter (A.Paar, DMA 4500) with an accuracy of 0.05 kg m^{-3} , so the accuracy for the measurements of concentration values was better 0.002 in molar fraction.

RESULTS AND DISCUSSION

Concentration Profile and Parameters Evaluated

In order to assure, that the pairs of parameters obtained by the fitting represent the global minimum, different values of the parameters were used as an initial guess for the fitting procedure. The parameters for different initial guesses do not differ by more than 0.3%. The following pairs of the ‘best fit’ parameters were obtained: $\{C_L = 1.77; C_V = 0.454\}$ in case of correlation (25); $\{b_L = 9890; b_V = 8110\}$ in case of correlation (26). The comparison of the resulting theoretical concentrations with the experimental ones is shown in Figures 1 and 2. Individual SERIEs cover different concentration range (the concentration in reboiler was changed), i.e., also the initial conditions for the integration of individual SERIEs vary. Using the ‘best fit’ parameters, we integrated the model for both correlations (25) and (26) in concentration range that covered all the experimental concentration data. These theoretical profiles are plotted in Figures 1 and 2. The individual experimental SERIEs in the figures

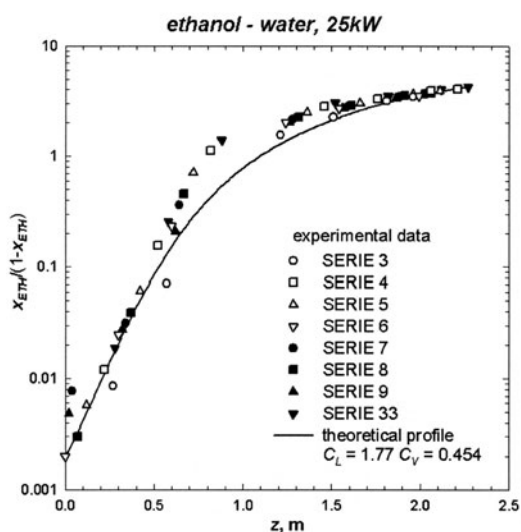


Figure 1. Comparison of the experimental ethanol concentrations with that calculated from the model using correlation (25) with $C_L = 1.77$ and $C_V = 0.454$ for volumetric mass-transfer coefficients calculation.

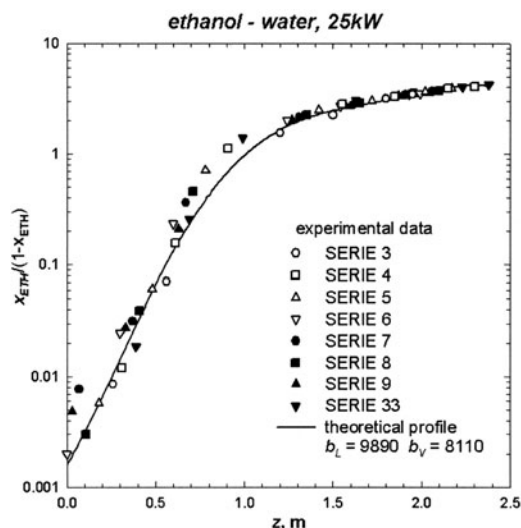


Figure 2. Comparison of the experimental ethanol concentrations with that calculated from the model using correlation (26) with $b_L = 9890$ and $b_V = 8110$ for volumetric mass-transfer coefficients calculation.

are shifted in z -coordinate so as the ‘initial condition’ for each SERIE ‘sits’ on the different theoretical profile. The same SERIE in both figures thus has the same concentrations, i.e., the same x -values, but is shifted in the z -coordinate differently. It is evident that the theoretical profile calculated using correlation (25) does not correspond well to the pattern of the experimental profile, especially within the range 20–60 mol% of ethanol, the correlation (25) is too complex for the description of the set of data restricted to only one reboiler duty and one distillation system. An average relative deviation of the theoretical profile is 18.3%. Simplification of the mass transfer correlation to the form of correlation (26) results in a lowering of the average relative deviation of the theoretical profile to 14.8%. The match with the experimental data is better for the correlation (26) and thus the correlation (25) is not further considered.

Vapour- and Liquid-Side Mass Transfer Coefficients

The dependence of the volumetric mass transfer coefficients on liquid and vapour side calculated from the correlation (26) using the ‘best fit’ parameters (b_L, b_V) on concentration of ethanol in liquid phase is in Figures 3 and 4 compared with the values calculated according to correlations based on absorption experiments, i.e., correlation by Onda *et al.* (1968), Billet *et al.* (1993) (i.e., correlation (25) using constants $C_L = 1.44$ and $C_V = 0.336$ given in the original paper Billet *et al.* (1993) for metal Pall-ring 25) and Linek *et al.* (1995) recalculation procedure.¹

It is seen in Figure 3, that the $k_L a$ values evaluated from the relation (26) agree the best with the values calculated

¹ The recalculation procedure of the absorption data to the distillation conditions is based only on the difference in diffusivities D and in numbers of pieces of packing per unit volume n according to the relation $k_{va} \sim D_G^{2/3} \cdot n$ and $k_L a \sim D_L^{1/2} \cdot n$. Following absorption systems were chosen as suitable ones: absorption of SO_2 into NaOH solution to determine k_{va} and absorption of O_2 into water to determine $k_L a$.

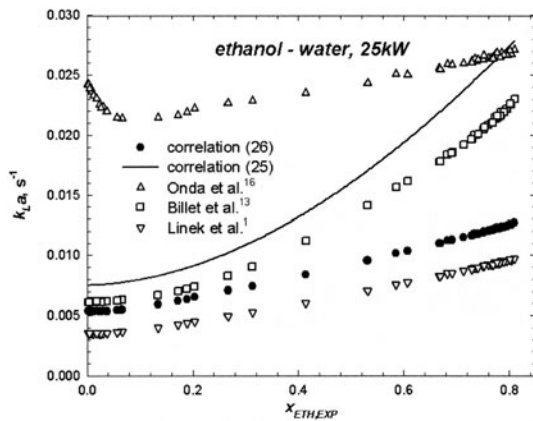


Figure 3. Comparison of the k_{La} calculated from correlation (26) ($b_L = 9890$) with the coefficients calculated from correlations given in literature, i.e., Onda *et al.* (1968), Billet and Schultes (1993) ($C_L = 1.44$), Linek *et al.* (1995) along the column. Line represents Billet and Schultes (1993) correlation (25) with $C_L = 1.77$ (value obtained in this work).

from the absorption correlation by Linek *et al.* (1995). The values predicted by the correlation are by cca $0.0025 s^{-1}$ lower (representing 25–30 relative percent) over the whole concentration range. In case of the vapour phase, which is illustrated in Figure 4, the absorption correlations by Onda *et al.* (1968) and by Billet *et al.* (1993) predict an increase of the k_{Va} with an increase of x_{ETH} . The relation (26) and Linek *et al.*'s (1995) absorption correlation result in almost constant value of k_{Va} and the maximum difference between them reaches 20%. Relatively worse agreement of the correlations by Onda and by Billet (reaching multiples of the values) is probably due to the large temperature extrapolation from absorption (around $20^\circ C$) to distillation conditions.

HETP, Liquid-Side Mass Transfer Resistance

In Figure 5 is shown the development of $HETP$ values calculated from the relation (28), into which the values of the mass transfer coefficients obtained from the correlation (26) and from the absorption correlations were inserted,

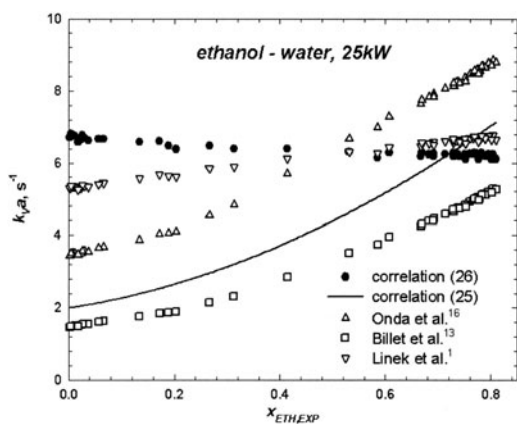


Figure 4. Comparison of the k_{Va} calculated from correlation (26) ($b_V = 8110$) with the coefficients calculated from correlations given in literature, i.e., Onda *et al.* (1968), Billet and Schultes (1993) ($C_V = 0.336$), Linek *et al.* (1995) along the column. Line represents Billet and Schultes (1993) correlation (25) with $C_V = 0.454$ (value obtained in this work).

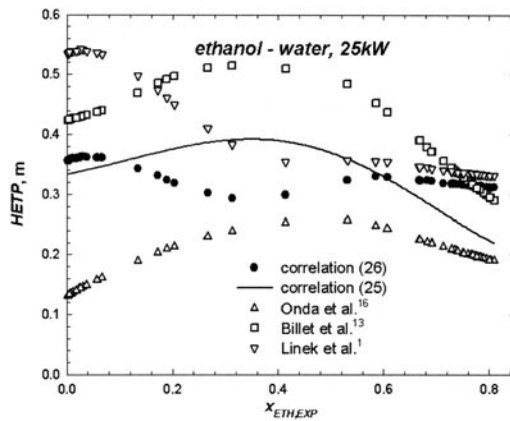


Figure 5. Development of the $HETP$ calculated from (28) using mass-transfer coefficients predicted by correlation (26) ($b_L = 9890$, $b_V = 8110$) and by the correlations given in literature, i.e., Onda *et al.* (1968), Billet and Schultes (1993) ($C_L = 1.44$, $C_V = 0.336$), Linek *et al.* (1995) along the column. Line represents Billet and Schultes (1993) correlation (25) with $C_L = 1.77$, $C_V = 0.454$ (values obtained in this work).

with the conditions (represented by the concentration of ethanol) in the column. The 'local $HETP$ values' obtained by such way differ the most in the bottom of the column, where Onda *et al.*'s (1968) correlation gives $HETP$ value approximately 0.15 m, while Linek *et al.*'s (1995) correlation gives for the same conditions $HETP$ value 0.54 m. If the top of the column the values of $HETP$ predicted by individual correlations come closer to each other, they fall into the range 0.19–0.33 m. The values predicted by the correlation (26) are fitted the best by the Linek *et al.*'s (1995) correlation at ethanol concentrations higher than $x_{ETH} = 0.4$.

The relative resistances to mass transfer ascribed to the liquid phase by individual correlations of mass transfer coefficients are compared in Figure 6. The pattern of the dependence of the relative liquid side resistance on the concentration of ethanol in the liquid phase is for all the correlations similar—the highest resistance is ascribed to the lowest concentration, towards the top of the

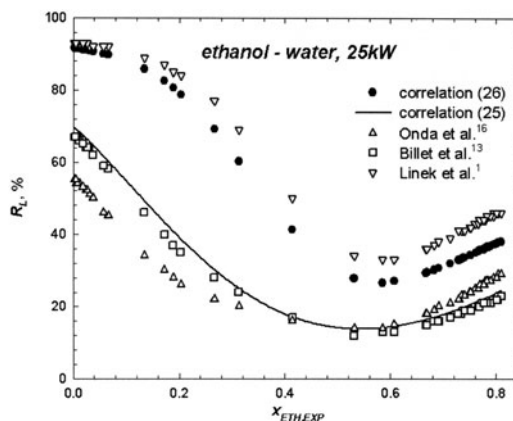


Figure 6. Development of the relative liquid side resistance calculated from (29) using mass-transfer coefficients predicted by correlation (26) ($b_L = 9890$, $b_V = 8110$) and by the correlations given in literature, i.e., Onda *et al.* (1968), Billet and Schultes (1993) ($C_L = 1.44$, $C_V = 0.336$), Linek *et al.* (1995) along the column. Line represents Billet and Schultes (1993) correlation (25) with $C_L = 1.77$, $C_V = 0.454$ (values obtained in this work).

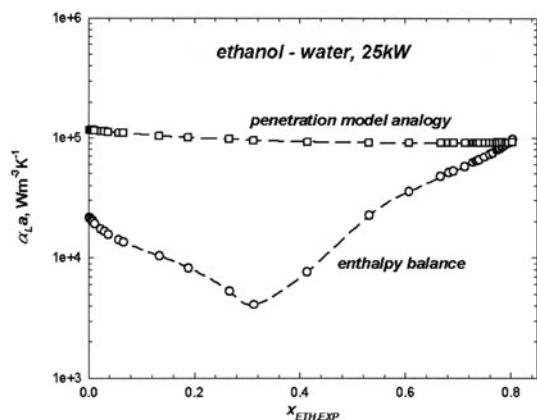


Figure 7. Comparison of the values of the $\alpha_L a$ calculated from the enthalpy balance with the values predicted by the penetration model analogy for the volumetric mass transfer coefficients calculated by correlations (26).

column the resistance sharply decreases, reaches its minimum for the concentration of approximately 50 mol% of ethanol and then slightly increases, but does not reach its bottom value. On the other hand, the magnitude of the resistance predicted by individual correlations considerably differs—while Onda *et al.*'s (1968) correlation ascribes to liquid phase 14–55%, Linek *et al.*'s (1995) correlation ascribes to the liquid phase 33–93% of the overall resistance.

Heat Transfer Coefficients

The values of $\alpha_L a$ calculated from the enthalpy balance (21) and from the analogy (31) are compared in Figure 7. The analogy was applied on $k_L a$ values calculated from the correlation (26) using the 'best fit' parameters. It is evident, that while the analogy results in almost constant $\alpha_L a$ values, the enthalpy balance predicts strong dependence of $\alpha_L a$ on conditions in the column represented by the concentration of ethanol. The balance coefficients agree with the analogy coefficients only for the highest concentrations of ethanol (in the top of the column), the largest deviation occurs at the concentration 31 mol% of ethanol, where the balance coefficients reach their minima, which differ by order from the analogy values.

In Figure 8 are shown the values of $\alpha_V a$ calculated from the enthalpy balance (22) and from the analogy (32) applied on the correlation (26). In contrast to the situation in the liquid phase, the best agreement between the enthalpy balance and analogy in vapour phase occurs in the bottom of the column (for the lowest concentration of ethanol), while the coefficients in the top of the column (for the highest concentrations) show the largest deviation, which is, however, much smaller than in case of the liquid phase.

CONCLUSIONS

The practicability of the simultaneous determination of both partial mass transfer coefficients in a distillation column based on fitting the concentration profile obtained by integration of the differential model of a distillation

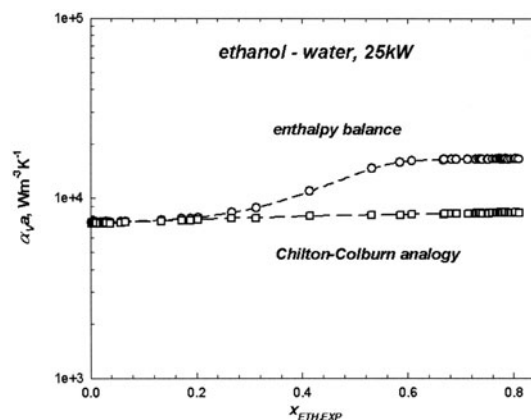


Figure 8. Comparison of the values of the $\alpha_V a$ calculated from the enthalpy balance with the values predicted by the Chilton–Colburn analogy for the volumetric mass transfer coefficients calculated by correlations (26).

column to the experimental one was demonstrated on a limited collection of experimental data (one reboiler duty and one distillation system) but the method is applicable generally (what follows from our recent results).

The theoretical concentration profile calculated using Billet's correlation (25) does not fit well the experimental profile, especially within the range 20–60 mol% of ethanol. Simplification of the mass transfer correlation (25) to the form of correlation (26) results in a lowering of the average relative deviation of the theoretical profile from 18.3% to 14.8%. As the relation (26) describes only the dependence on diffusion coefficients and superficial velocities of individual phases, resulting values and trends of $k_L a$ and $k_V a$ approximate the most to the coefficients calculated according to the simple recalculation rule by Linek *et al.* (1995), in which the dependence of the coefficients on diffusion coefficients and flow rates of the phases is respected. Therefore the *HETP* values are for these two correlations the closest to each other as well.

The values of volumetric heat transfer coefficients calculated from the analogies are direct functions of the values of volumetric mass transfer coefficient. As the mass transfer coefficients calculated according to the relation (26) show only slight dependence on the ethanol concentration along the column, also the heat transfer coefficients calculated from the analogies are almost concentration-independent. The analogy is hence unable to describe the strong concentration dependence predicted by the enthalpy balance for the liquid phase. The values of the heat transfer coefficients predicted by the Chilton–Colburn analogy for the vapour phase correspond well to the enthalpy-balance values. Heat transfer coefficients in the liquid phase calculated according to the penetration model analogy are considerably higher compared to the enthalpy balance data with exception of the region of high ethanol-concentration (approximately $x_{ETH} > 0.7$).

NOMENCLATURE

a	effective heat/mass transfer area, m^{-1}
a_t	geometrical area of packing, m^{-1}
$b_{L,V}$	empirical constants
$C_{L,V}$	empirical constants

C_p	dimensionless molar heat, defined by equation (13)
c	molar concentration in the bulk, kmol m^{-3}
c_p	molar heat, $\text{kJ kmol}^{-1} \text{K}^{-1}$
D	diffusion coefficient, $\text{m}^2 \text{s}^{-1}$
g	gravitational constant, m s^{-2}
h	molar enthalpy, kJ kmol^{-1}
Δh_{mix}	heat of mixing, kJ kmol^{-1}
Δh_{vap}	molar heat of vaporization, kJ kmol^{-1}
K	equilibrium ratio
$k_L a$	liquid-side volumetric mass transfer coefficient, s^{-1}
$k_V a$	vapour-side volumetric mass transfer coefficient, s^{-1}
L	liquid phase molar flow, kmol s^{-1}
M	molecular weight, kg kmol^{-1}
m_A	slope of equilibrium defined by equation (30)
N	molar flux transferred per unit height of packing, $\text{kmol m}^{-1} \text{s}^{-1}$
n_t	number of pieces of packing per unit volume, m^{-3}
Pr	Prandtl number
Q_T	sensible heat transferred per unit height of packing, kW m^{-1}
R_L	relative liquid phase mass transfer resistance
r	ethanol to total molar flux transferred ratio
S	column cross-section, m^2
Sc	Schmidt number
t	temperature, $^{\circ}\text{C}$
u	superficial velocity, m s^{-1}
V	gas phase molar flow, kmol s^{-1}
x	liquid phase molar fraction of ethanol
y	gas phase molar fraction of ethanol
Z	packing height, m
z	column height coordinate, m

Greek symbols

α	heat transfer coefficient, $\text{W m}^{-2} \text{K}^{-1}$
$\alpha_L a$	liquid-side volumetric heat transfer coefficient, $\text{W m}^{-3} \text{K}^{-1}$
$\alpha_V a$	vapour-side volumetric heat transfer coefficient, $\text{W m}^{-3} \text{K}^{-1}$
λ	heat conductivity, $\text{kW m}^{-1} \text{K}^{-1}$
η	dynamic viscosity, Pa s^{-1}
ρ	density, kg m^{-3}
σ	surface tension, kg s^{-2}
ε	porosity

Subscripts

V	vapour phase
L	liquid phase
w	interface
A	ethanol
B	water
ETH	ethanol
exp	experimental
calc	calculated

Superscripts

*	equilibrium value
---	-------------------

REFERENCES

- Arwika, K.J. and Sandall, O.C., 1980, Liquid phase mass transfer resistance in a small scale packed distillation column, *Chem Eng Sci*, 35: Q2337–2343.
- Billet, R. and Schultes, M., 1993, Predicting mass transfer in packed columns, *Chem Eng Technol*, 16: 1–9.
- Bird, R.B., Stewart, W.E. and Lightfoot, E.N., 1960, *Transport Phenomena* (John Wiley and Sons, New York, USA).
- Christensen, C., Gmehling, J., Rasmussen, P. and Weidlich, U., 1984, *Chemistry Data Series*, Vol. III, Part 1 (Dechema, Frankfurt, Germany).
- Dribika, M.M. and Sandall, O.C., 1979, Simultaneous heat and mass transfer for multicomponent distillation in a wetted-wall column, *Chem Eng Sci*, 34: 733–739.
- Gmehling, J., Onken, N. and Arlt, W., 1981, *Chemistry Data Series* (Dechema, Frankfurt, Germany).
- Honorat, A. and Sandall, O.C., 1978, Simultaneous heat and mass transfer in a packed binary distillation column, *Chem Eng Sci*, 33: 635–640.
- Kayihan, F., Sandall, O.C. and Mellichamp, D.A., 1977, Simultaneous heat and mass transfer in binary distillation II experimental, *Chem Eng Sci*, 32: 747–754.
- Krishnamurthy, R. and Taylor, R., 1985, Simulation of packed distillation and absorption columns, *Ind Eng Chem Process Des Dev*, 24: 513–524.
- Liang, Y. and Smith, W., 1962, The effect of heat transfer between the phases on the performance of countercurrent distillation columns, *Chem Eng Sci*, 17: 11–21.
- Linek, V., Sinkule, J. and Brekke, K., 1995, A critical evaluation of the use of absorption mass transfer data for the design of packed distillation columns, *Trans IChemE, Part A, Chem Eng Res Des*, 73: 398–405.
- Onda, K., Takeuchi, H. and Okumoto, Y., 1968, Mass transfer coefficients between gas and liquid phases in packed columns, *J Chem Eng Japan*, 1: 56–61.
- Pelkonen, S., Kaesemann, R. and Górak, A., 1997, Distillation lines for multicomponent separation in packed columns: Theory and comparison with experiments, *Ind Eng Chem Res*, 36: 5392–5398.
- Seader, J.D. and Henley, E.J., 1998, *Separation Process Principles* (John Wiley & Sons, New York, USA).
- Vargaftik, N.B., 1975, *Tables on the Thermophysical Properties of Liquids and Gases* (John Wiley, New York, USA).
- Zarzycki, R. and Chacuk, A., 1993, *Absorption* (Pergamon Press Ltd, Oxford, UK).

ACKNOWLEDGEMENTS

This work was supported by the Grant Agency of Czech Republic through the project no. 104/00/0574 and by Czech Ministry of Education through the scientific project no. 223400007.

The manuscript was received 31 July 2003 and accepted for publication after revision 4 May 2005.

Vapour- and liquid-side volumetric mass transfer coefficients measured in distillation column. Comparison with data calculated from absorption correlations

J.F. Rejl, V. Linek*, T. Moucha, E. Prokopová, L. Valenz, F. Hovorka

Prague Institute of Chemical Technology, Department of Chemical Engineering, CZ-166 28 Prague 6, Czech Republic

Received 13 December 2005; received in revised form 22 May 2006; accepted 1 June 2006

Available online 12 June 2006

Abstract

Volumetric mass transfer coefficients in liquid and vapour phases in distillation column were measured by the method consisting of a fitting of the concentration profile of liquid phase along the column obtained by the integration of a differential model to the experimental one. The mathematical model of distillation process includes mass and energy balances and the heat and mass transfer equations. The film model flux expressions with the convective transport contributions have been considered in the transfer equations. Vapour and liquid phases are supposed to be at their saturated temperatures along the column. Effect of changes of phase flows and physical properties of phases on the mass transfer coefficients along the column and non-ideal thermodynamic behaviour of the liquid phase have been taken into account. The concentration profiles of liquid phase are measured in the binary distillation of the ethanol–water and methanol–ethanol systems at total reflux on metal Pall Rings and Intalox saddles 25 mm in the column with diameter of 150 mm. The distillation mass transfer coefficients obtained by the fitting procedure are compared with those calculated from absorption data using Onda's, Billet's and Linek's correlations. The distillation heat transfer coefficients calculated from the model assuming saturated temperatures in both phases are compared with those calculated from the Chilton–Colburn and penetration model analogy between mass and heat transfer. The results have confirmed an agreement neither between distillation and from absorption correlations calculated mass transfer coefficients nor between analogy and from enthalpy balance calculated heat transfer coefficients. Also the concentration profiles obtained by the integration of the differential model of the distillation column using the coefficients from absorption correlation have differed from the experimental profiles considerably.

© 2006 Elsevier Ltd. All rights reserved.

Keywords: Mass transfer; *HETP*; Distillation; Packed column; Absorption

1. Introduction

Distillation columns are the most widely used large-scale separation equipments in chemical, food and pharmaceutical industry. Energy demands of the distillation are extremely high and its recovery for further purposes is difficult, therefore the capital and operational costs of the distillation process are high. Even though alternative separation techniques are still developed, they cannot replace the distillation process completely, what makes its future use indubitable. An attention hence should be paid to the distillation as a small improvement in its

design or performance has a large financial impact. Despite the earnest effort of many chemical engineers and a huge number of original works submitted up to present time, the design of distillation columns has long been relying on experience and is essentially empirical in nature.

The idea of the height equivalent to a theoretical plate is most commonly used to the column design. An integral character of *HETP* makes it impossible to find the universal rule for *HETP* data transfer among different systems and conditions. Another approach employs the fact, that absorption and distillation have the same physical background—interfacial mass transfer between gas and liquid phase which is characterised by mass transfer coefficients in liquid $k_L a$ and gas $k_V a$ phase. An effort to calculate the *HETP* using absorption mass transfer coefficients recalculated to the conditions in distillation column has

* Corresponding author: Tel.: +420 2 2044 3298; fax: +420 2 3333 7335.
E-mail address: linekv@vscht.cz (V. Linek).

mostly led to large deviations from the experimental data (often higher than 50%). The discrepancy can be ascribed partially to large extrapolation in temperature used in the data transfer from absorption to distillation. However, the measurements of mass transfer coefficients directly in distillation columns are rare (Kayihan et al., 1977; Honorat and Sandall, 1978; Dribika and Sandall, 1979). In distillation namely, it is not possible to measure individual mass transfer coefficients by using a proper distillation system in which the overall resistance to the interfacial mass transfer is mainly due to one of the phases and to study behaviour of the individual coefficients separately as it is possible in absorption. An assumption that all of the resistance to mass transfer is in the vapour phase has been used in the mentioned papers in which the mass transfer coefficients in distillation columns were measured. Arwika and Sandall (1980) have shown, however, that this assumption is mistaken and thereby they in firm the principal conclusion of the previous works, namely that the mass transfer coefficients calculated from absorption correlations (to be specific the correlation by Onda et al., 1968) fit well the coefficients in distillation columns.

Recently, Linek et al. (2005) presented a method of simultaneous determination of volumetric mass transfer coefficients in both phases in distillation column. The method consists of a fitting of the concentration profile along the column obtained by the integration of a differential model to the experimental one. The importance of the calculation methods based on the integration of differential equations describing a distillation column has increased. The methods, designed as “rate-based” or “non-equilibrium”, require thorough understanding of the processes occurring inside a distillation column as they utilize a numerical solution of energy and mass balances with transport equations describing components, phases and energy flows within the column, covering all the process determining phenomena (Mori et al., 1996, 1999, 2002, 2006; Taylor and Krishna, 1993; Wesselingh, 1997). The lack of available and reliable values of the coefficients, which characterise rates of the phenomena included in the rate-based models, has braked the development of more accurate and reliable models for the design of distillation columns. The use of the mass transfer coefficients determined under the conditions of distillation columns would significantly improve the reliability of the simulation models.

Practicability of the method proposed by Linek et al. (2005) was preliminary verified on the limited data set (Pall-ring 25, ethanol–water (E–W), reboiler duty 25 kW). The E–W distillation system was used for sharp changes of the equilibrium coefficient with concentration (i.e., along the column), which makes it possible to separate the individual phase contributions to interfacial mass transfer resistance and thus to evaluate mass transfer coefficients in both phases simultaneously.

The aim of this work is to apply this method on wider set of data, i.e., on another type of packing (Intalox-25) and distillation system (methanol–ethanol (M–E)). The distillation system M–E shows small changes of the equilibrium coefficient with concentration in comparison with the originally used E–W system. The distillation mass transfer parameters measured by this

method are compared with those calculated from absorption correlations.

2. Theoretical

2.1. Differential model of distillation column

Linek et al. (2005) presented the model with some errors. This is why we present it here again. The model is based on the application of mass and energy balances and heat and mass transfer equations to a differential control volume Sdz of the column (see Fig. 1). The balances and transfer equations have been developed under following assumptions: (i) distillation of binary mixture under total reflux; (ii) process is adiabatic and steady state; (iii) the overall pressure is constant through out the column; (iv) the plug flow in both phases; (v) interfacial mass and heat transport are described using a film model in which the convective flow is taken into account; (vi) the rate of heat transfer is such as to keep the vapour and liquid phases just at their dew and boiling points respectively; (vii) interfacial area for the mass and heat transfer is identical.

Global mass, component and enthalpy balances simplify under the total reflux and adiabatic conditions to

$$L - V = 0, \quad (1)$$

$$x_A - y_A = 0, \quad (2)$$

$$L \left(\frac{dh_L}{dz} - \frac{dh_V}{dz} \right) + \frac{dL}{dz} (h_L - h_V) = 0. \quad (3)$$

Liquid phase mass balances of components A and B (the molar fluxes $N_{A,B}$ are defined to be positive from the vapour to the liquid) are

$$L \frac{dx_A}{dz} + x_A \frac{dL}{dz} - N_A = 0,$$

$$L \frac{dx_B}{dz} + x_B \frac{dL}{dz} - N_B = 0. \quad (4)$$

$N_{A,B}$ are given by following rate and equilibrium relations and by the mass continuity requirement at the interface (an equal

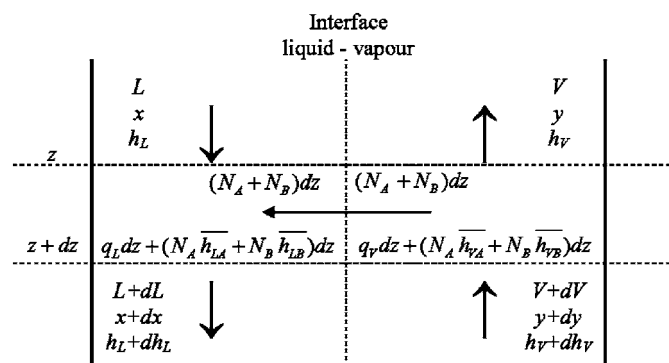


Fig. 1. Differential control volume of distillation column.

mass transport in the liquid and vapour phases)

$$N_A = k_V a \cdot c_V \cdot r \cdot \ln \left[\frac{y_{Aw} - r}{x_A - r} \right] \cdot S$$

$$= k_L a \cdot c_L \cdot r \cdot \ln \left[\frac{x_A - r}{x_{Aw} - r} \right] \cdot S, \quad (5)$$

$$r = \frac{N_A}{N_A + N_B}, \quad (6)$$

$$y_{Aw} = K \cdot x_{Aw}. \quad (7)$$

The molar flux N_A between the vapour and liquid phases results from the combined contribution of molecular diffusion and a bulk transport of material through the interface. A detailed derivation of the equation is given elsewhere (Bird et al., 1960).

Energy balances of liquid and vapour phases (heat transfer is defined to be positive from the vapour to the liquid phase)

$$L \frac{dh_L}{dz} + h_L \frac{dL}{dz} - q_L - Q_L = 0, \quad (8)$$

$$L \frac{dh_V}{dz} + h_V \frac{dL}{dz} - q_V - Q_V = 0. \quad (9)$$

The sensible heats transferred from the interface to the bulk liquid q_L and from the bulk vapour to the interface q_V are given by following relations (Bird et al., 1960)

$$q_L = \alpha_L a \frac{-C_{pL}}{1 - \exp(C_{pL})} (t_w - t_L) S,$$

$$q_V = \alpha_V a \frac{C_{pV}}{1 - \exp(-C_{pV})} (t_V - t_w) S, \quad (10)$$

$$C_{pi} = \frac{N_A c_{piA} + N_B c_{piB}}{\alpha_i a S}, \quad (i = L, V) \quad (11)$$

and the enthalpy transferred by the convective mass flux into the liquid Q_L and from the vapour Q_V are given by following relations:

$$Q_L = N_A \overline{h_{LA}} + N_B \overline{h_{LB}},$$

$$Q_V = N_A \overline{h_{VA}} + N_B \overline{h_{VB}} \quad (12)$$

\overline{h} are the components partial molar enthalpies at the conditions of the interface.

From Eqs. (3)–(12), by some rearrangements, the following set of differential equations can be obtained, an integration of which gives the concentration profile in a column and the heat transfer coefficients in both phases that are necessary to keep the phases at the saturated temperatures

$$\frac{dL}{dz} = (N_A + N_B), \quad (13)$$

$$\frac{dx_A}{dz} = [N_A - x_A(N_A + N_B)]/L, \quad (14)$$

$$\frac{dh_L}{dz} = \frac{dx_A}{dz} \cdot \left(\frac{dh_L}{dx_A} + \frac{dh_L}{dt_L} \cdot \frac{dt_L}{dx_A} \right), \quad (15)$$

$$\frac{dh_V}{dz} = \frac{dx_A}{dz} \cdot \left(\frac{dh_V}{dx_A} + \frac{dh_V}{dt_V} \cdot \frac{dt_V}{dx_A} \right), \quad (16)$$

$$\frac{dL}{dz} \cdot (h_V - h_L) + L \cdot \left(\frac{dh_V}{dz} - \frac{dh_L}{dz} \right) = 0, \quad (17)$$

$$q_L = \frac{dh_L}{dz} \cdot L - N_A (\overline{h_{LA}} - h_L) - N_B (\overline{h_{LB}} - h_L), \quad (18)$$

$$q_V = \frac{dh_V}{dz} \cdot L - N_A (\overline{h_{VA}} - h_V) - N_B (\overline{h_{VB}} - h_V), \quad (19)$$

$$\alpha_L a = q_L \cdot \frac{\exp(C_{pL}) - 1}{C_{pL} \cdot (t_w - t_L) \cdot S}, \quad (20)$$

$$\alpha_V a = q_V \cdot \frac{1 - \exp(-C_{pV})}{C_{pV} \cdot (t_V - t_w) \cdot S}, \quad (21)$$

with N_A and N_B given by Eqs. (5)–(7). When the following auxiliary relations are added to the model equations, a system with 10 equations (Eqs. (5)–(7), (13)–(17), (22) and (23)), 10 variables ($L, x_A, x_{Aw}, N_A, N_B, t_w, t_L, t_V, h_L, h_V$) and 2 coefficients ($k_L a, k_V a$) is obtained.

$$h_L(x_A, t_L) = [c_{pLA} x_A + c_{pLB} (1 - x_A)] t_L + \Delta h_{\text{mix}}, \quad (22)$$

$$h_V(x_A, t_V) = [c_{pLA} t_{bPA} + \Delta h_{\text{vapA}}] x_A + [c_{pLB} t_{bPB} + \Delta h_{\text{vapB}}] \times (1 - x_A) + c_{pVA} x_A (t_V - t_{bPA}) + c_{pVB} (1 - x_A) (t_V - t_{bPB}). \quad (23)$$

The set of the differential equations has been solved using a finite difference numerical method. The computing procedure has been described in detail elsewhere (Linek et al., 2005).

In the calculation following thermodynamic properties: $c_{pLA}, c_{pLB}, \Delta h_{\text{mix}}, c_{pVA}, c_{pVB}, \Delta h_{\text{vapA}}, \Delta h_{\text{vapB}}, c_V$ and c_L were considered to be functions of the concentration and the temperature and hence they change along the column. The corresponding functions were taken from the literature: Δh_{mix} by Christensen et al. (1984), the molar densities of the liquid mixtures by Barner–Quinlan's rule using data from Vargaftik (1975) and Stephan and Hildwein (1987), the vapour phase was considered as ideal, the vapour–liquid equilibria have been taken from Gmehling et al. (1988) and diffusion coefficients from Zarzycki and Chacuk (1993).

The dependences of the volumetric mass transfer coefficients on phase flows and on physical properties of phases which change along the column were considered in two forms: in the form of correlations suggested by Billet et al. (1999)

$$k_L a = C_L \left(\frac{\rho_L g}{\eta_L} \right)^{1/6} \left(\frac{D_L}{l_\tau} \right)^{1/2} a_t^{2/3} u_L^{1/3} \left(\frac{a}{a_t} \right),$$

$$k_V a = C_V \frac{1}{(\varepsilon - U)^{1/2}} \frac{a_t^{3/2}}{l_\tau^{1/2}} D_V \left(\frac{u_V \rho_V}{a_t \eta_V} \right)^{3/4} \left(\frac{\eta_V}{D_V \rho_V} \right)^{1/3} \left(\frac{a}{a_t} \right),$$

$$\frac{a}{a_t} = 1.5 (a_t l_\tau)^{-0.5} \left(\frac{u_L l_\tau \rho_L}{\eta_L} \right)^{-0.2} \left(\frac{u_L^2 \rho_L l_\tau}{\sigma} \right)^{0.75} \left(\frac{u_L^2}{g l_\tau} \right)^{-0.45},$$

$$U = \left(12 \frac{1}{g} \frac{\eta_L}{\rho_L} u_L a_t^2 \right)^{1/3}, \quad l_\tau = 4 \frac{\varepsilon}{a_t} \quad (24)$$

and by Onda et al. (1968)

$$k_L = b_L \left(\frac{u_L \rho_L}{a \eta_L} \right)^{2/3} \left(\frac{\eta_L}{\rho_L D_L} \right)^{-1/2} (a_t d_p)^{2/5} \left(\frac{\rho_L}{\eta_L g} \right)^{-1/3},$$

$$k_V = b_V \left(\frac{u_V \rho_V}{a_t \eta_V} \right)^{0.7} \left(\frac{\eta_V}{\rho_V D_V} \right)^{1/3} (a_t d_p)^{-2} (a_t D_V),$$

$$\frac{a}{a_t} = 1 - \exp \left\{ -1.45 \left(\frac{\sigma_C}{\sigma_L} \right)^{0.75} \left(\frac{u_L \rho_L}{a_t \eta_L} \right)^{0.1} \times \left(\frac{u_L^2 a_t}{g} \right)^{-1/20} \left(\frac{u_L^2 \rho_L}{a_t \sigma_L} \right)^{1/5} \right\}. \quad (25)$$

The concentration profile obtained by integration of the differential equations is fitted to the experimental one, optimising the empirical parameters C_L and C_V in case of correlation (24) and b_L and b_V in case of correlation (25).

As the matching criterion was used the following objective function representing the minimum of the sum of squared molar fractions differences between the calculated and measured values along the column

$$\min f = \sum_{\substack{\text{point } i \\ \text{series } j \\ q_{\text{reb}}^k}} [(x_{A,i,j,k})_{\text{exp}} - (x_{A,i,j,k})_{\text{cal}}]^2,$$

$$(i = 1, \dots, 7, j = 1, \dots, 8, k = 1, \dots, 3 \text{ or } 4). \quad (26)$$

All data from all experiments (i.e., data measured at seven positions along the column, in each of eight series and at all three or four reboiler duties used) were taken into account. Series loaded with gross error were excluded from the evaluation. There were two such series in the data presented. The simplex method was used for determination of the model parameters [C_L , C_V] or [b_L , b_V] by minimizing the objective function.

2.2. HETP and liquid side mass transfer resistance

The height equivalent to the theoretical plate is calculated according to the relation

$$HETP = u_L \left(\frac{1}{k_{LA}} + \frac{m_A}{k_{VA}} \right) \frac{\ln(m_{AU_L}/u_V)}{m_{AU_L}/u_V - 1}. \quad (27)$$

The ratio of the liquid phase mass transfer resistance to the overall resistance R_L was calculated from

$$R_L = \frac{1/k_{LA}}{1/k_{LA} + m_A/k_{VA}}, \quad (28)$$

where the slope of equilibrium m_A is expressed by Seader and Henley (1998) as

$$m_A = \frac{c_{LA}^* - c_{LA,w}}{c_{VA} - c_{VA,w}} = \left(\frac{c_L}{c_V} \right) \left(\frac{x_A^* - x_{A,w}}{y_A - K x_{A,w}} \right)_{\text{TOT.REFLUX}} \left(\frac{c_L}{c_A} \right) \times \left(\frac{x_A^* - x_{A,w}}{x_A - K x_{A,w}} \right). \quad (29)$$

Substituting local values of concentration and mass transfer coefficient into the relations the local HETP and R_L values were calculated.

2.3. Heat transfer coefficients

Because of the above-mentioned assumption of the saturation temperature of the phases it is possible to calculate the values of volumetric heat transfer coefficients in liquid $\alpha_L a$ and vapour $\alpha_V a$ phase from relations (20) and (21) (i.e., from enthalpy balance) which are necessary to keep the vapour and liquid phases just at their dew and boiling points, respectively, as they pass through the column.

The values $\alpha_L a$ and $\alpha_V a$ calculated from the enthalpy balance are compared with values deduced from an analogy of heat and mass transfer. Using the Chilton–Colburn analogy for the vapour phase and assuming a penetration-theory type mechanism for the liquid phase we obtain following relations for the heat transfer coefficients:

$$\alpha_V a / k_V a = (Sc_V / Pr_V)^{2/3} (\rho_V c_{pV} / M_V) = (\lambda_V / D_V)^{(2/3)} (\rho_V c_{pV} / M_V)^{1/3}, \quad (30)$$

$$\alpha_L a / k_L a = (Sc_L / Pr_L)^{1/2} (\rho_L c_{pL} / M_L) = (\lambda_L / D_L)^{(1/2)} (\rho_L c_{pL} / M_L)^{1/2}. \quad (31)$$

From the comparison the quality of the prediction of the analogies can be judged.

3. Experimental

A stainless steel column of inner diameter of 0.15 m was packed to the height of 2.04 m. The column was equipped with six openings for placing thermistors and sampling devices for withdrawal of liquid samples along the column see Fig. 2. Platinum thermometer (Pt 100, accuracy $\pm 0.05^\circ\text{C}$) has been installed in the collecting channel of the sampling device, Fig. 3. Total spiral condenser has been mounted at the top of the column. The column was operated under total reflux, which has been maintained by PI regulation of liquid level in the reflux head (see Fig. 2). Reflux flow was distributed on the packing using shower distributor (Fig. 4, 1472 holes/m²). Reflux flow was measured by radial turbine flowmeter (Omega FTB9510, accuracy $\pm 0.001 \text{ l min}^{-1}$). Two distillation systems were used: M–E and E–W. 25 mm metal all rings at the packing density $n_t = 46418 \text{ pcs/m}^3$ ($a_t = 193 \text{ m}^{-1}$, $\varepsilon = 0.959$) were used in distillation of M–E system and 25 mm metal Intalox saddles at the packing density $n_t = 46418 \text{ pcs/m}^3$ ($a_t = 193 \text{ m}^{-1}$, $\varepsilon = 0.959$) were used in distillation of E–W system. Electrically heated reboiler equipped with electric power regulator (up to 60 kW) was used to maintain a constant boiling rate. The column was covered with Orsil insulation. The heat loss, measured by independent experiments, was less than 3% of the reboiler duty.

About 45 l of distillation mixture were poured into the reboiler and electric power input to the reboiler was adjusted to desired level. Four ($q_{\text{reb}} = 15, 25, 35$ and 45 kW) and three ($q_{\text{reb}} = 10, 20$ and 30 kW) of the power input levels were used

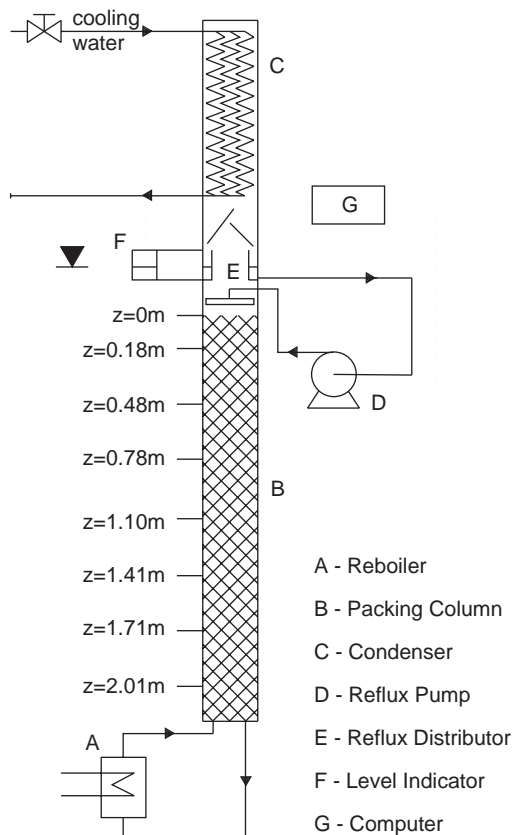


Fig. 2. Schematic drawing of packed bed column operating at total reflux.

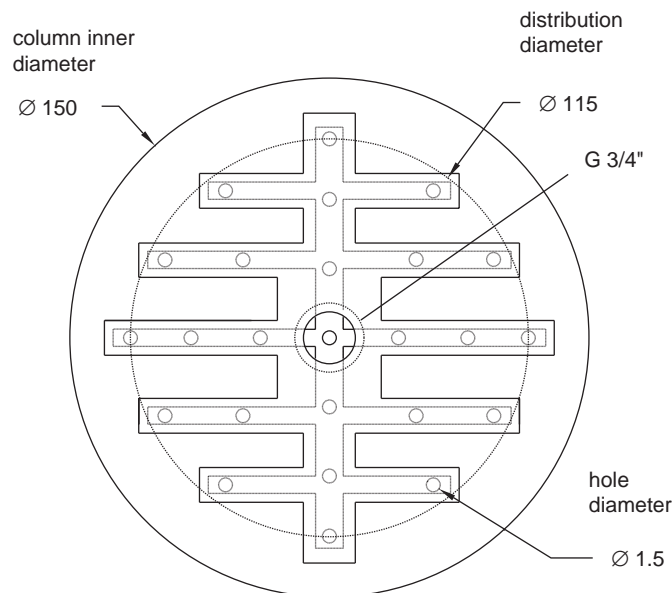


Fig. 4. Schematic drawing of liquid distributor. (Dimensions given in mm.)

The column was operated for some time to achieve steady state, what took 1 h usually. After this period the liquid samples (5 ml) were withdrawn by glass syringes from all the sampling devices simultaneously. Series of eight experiments were performed at the same power input to the reboiler but at different concentrations of the liquid in the reboiler covering whole concentration range. After finishing the run densities of the samples were measured using a digital densimeter (A.Paar, DMA 4500) with an accuracy of 0.05 kg/m^3 , so the accuracy for the measurements of concentration values was better 0.002 in molar fraction.

4. Results and discussion

4.1. Temperature of phases

Liquid phase overheating evaluated from the measured temperatures and boiling points of the withdrawn liquid samples are plotted as a function of position in the column for both distillation systems in Fig. 5. The results indicate an overcooled reflux by $1\text{--}2^\circ\text{C}$, slightly overheated liquid phase by approx. 0.5°C along practically whole the column. A notably overheated liquid (by up to 4°C) was observed at the bottom of the column for E–W system at the lowest reboiler duty of 15 kW. It is there, where the largest temperature difference between phases and the extremely low liquid loading ($B = 1.51 \text{ m/h}$, see Table 1) exist in the column.

Negligible effect of pressure drop in the column on saturation temperatures was verified as follows: Pure water has been distilled under two reboiler duties 15 and 45 kW at atmospheric pressure of 99.33 kPa. Temperatures of vapour phase were monitored (see Table 2). Temperature difference between top and bottom of the column are lower than 0.3°C , which is substantially less than the maximum revealed overheating.

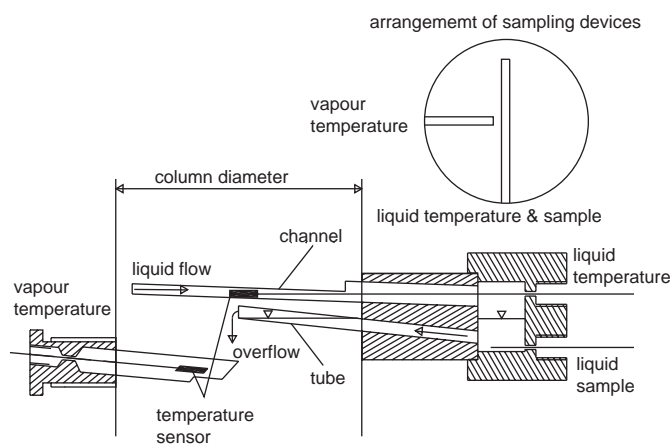


Fig. 3. Sampling and measuring device assembly.

in distillation E–W and M–E systems, respectively. The power into the reboiler was measured by three-phase wattmeter (Orbit Merret 405, accuracy $\pm 240 \text{ W}$). Illustrative vapour and liquid flow rates in the column calculated out of the reboiler¹ duties (heat losses neglected) are given in Table 1.

¹ The values in the table have been calculated as follows: for given composition saturation enthalpies of liquid h_L and vapour h_V phases have been calculated. Molar flow of phases L, V have been calculated from the condition $L = V = q_{\text{reb}} / (h_V - h_L)$.

Table 1
Vapour and liquid flow rates in the distillation column at limiting reboiler duties

q_{reb} (kW)	x_A	L, V (mol/s)	$u_L \times 10^3$ (m/s)	B (m/h)	u_V (m/s)	F (Pa ^{1/2})
Methanol–ethanol 100 kPa						
10	0.95	0.279	0.7	2.49	0.444	0.48
10	0.05	0.253	0.9	3.17	0.418	0.52
20	0.95	0.558	1.4	4.98	0.888	0.96
20	0.05	0.507	1.8	6.35	0.836	1.04
30	0.95	0.837	2.1	7.46	1.333	1.44
30	0.05	0.760	2.6	9.52	1.254	1.57
Ethanol–water 100 kPa						
15	0.8	0.384	1.15	4.13	0.634	0.75
15	0.05	0.360	0.42	1.51	0.630	0.50
25	0.8	0.640	1.91	6.79	1.06	1.24
25	0.05	0.601	0.70	2.52	1.05	0.83
35	0.8	0.896	2.68	9.65	1.48	1.74
35	0.05	0.841	0.98	3.53	1.47	1.17
45	0.8	1.152	3.45	12.4	1.90	2.24
45	0.05	1.081	1.26	4.54	1.89	1.50

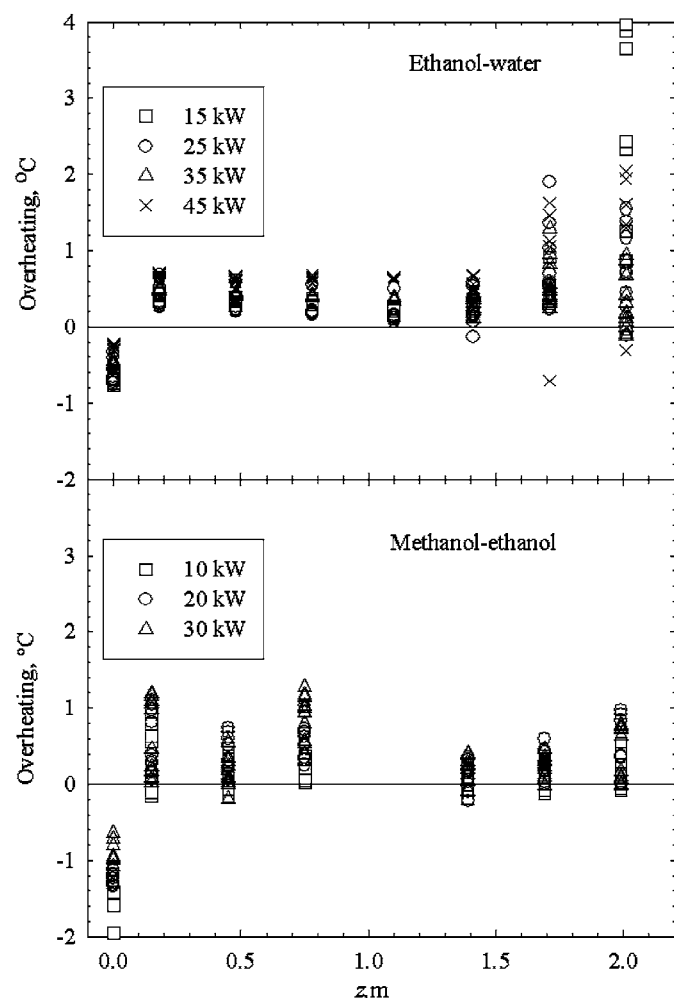


Fig. 5. Liquid phase overheating in methanol–ethanol and ethanol–water distillation systems. (Top of the column: $z = 0$ m.)

Table 2

Demonstrations of negligible effect of pressure drop in the distillation column

z (m)	t_V (15 kW) (°C)	t_V (45 kW) (°C)
0.18	99.43	99.48
0.48	99.38	99.44
0.78	99.55	99.59
1.1	99.68	99.72
1.41	99.56	99.64
1.71	99.64	99.71

Table 3

Concentrations, temperatures and overheating of vapour phase measured in ethanol–water system at reboiler duty of 15 kW

z (m)	y_A	t_V (°C)	$t_{V\text{dew}}$ (°C)	Overheating (°C)
1.41	0.6436	79.63	79.67	−0.04
1.71	0.4969	83.67	83.95	−0.28
2.01	0.1564	95.36	95.37	−0.01

At the end of experiments—more or less tentatively—samples of vapour phase were withdrawn in three points along the column and measured their concentration. The samples were withdrawn to the syringe with needle inserted in thermometrical basin in lieu of vapour thermometers. Temperature of vapour phase was measured just before withdrawal of the vapour sample. The results, given in Table 3 together with dew points of the vapour, clearly show that the vapour phase is at its dew point in the column.

4.2. Concentration profile and parameters evaluated

The pairs of parameters obtained by minimizing the objective function (26) represent the global minimum. This was confirmed so that the parameters for different initial guesses do not differ by more than 0.3%. The pairs of the “best fit”

Table 4
The “best fit” parameters evaluated from distillation concentration profiles and from absorption experiments

System	Packing	C_L	C_V	s_x	$b_L \times 10^3$	b_V	s_x
Methanol–ethanol	Pall r. 25	0.335	0.447	0.0220	2.59	4.92	0.0209
Absorption	Pall r. 25	1.44 ^a	0.336 ^a	–	5.10 ^b	5.23 ^b	–
Ethanol–water	Intalox 25	0.681	0.681	0.0449	4.98	5.81	0.0315
Absorption	Intalox 25	1.36 ^c	0.779 ^c	–	5.10 ^b	5.23 ^b	–

^aBillet and Schultes (1999).

^bOnda et al. (1968).

^cMoucha et al. (2005).

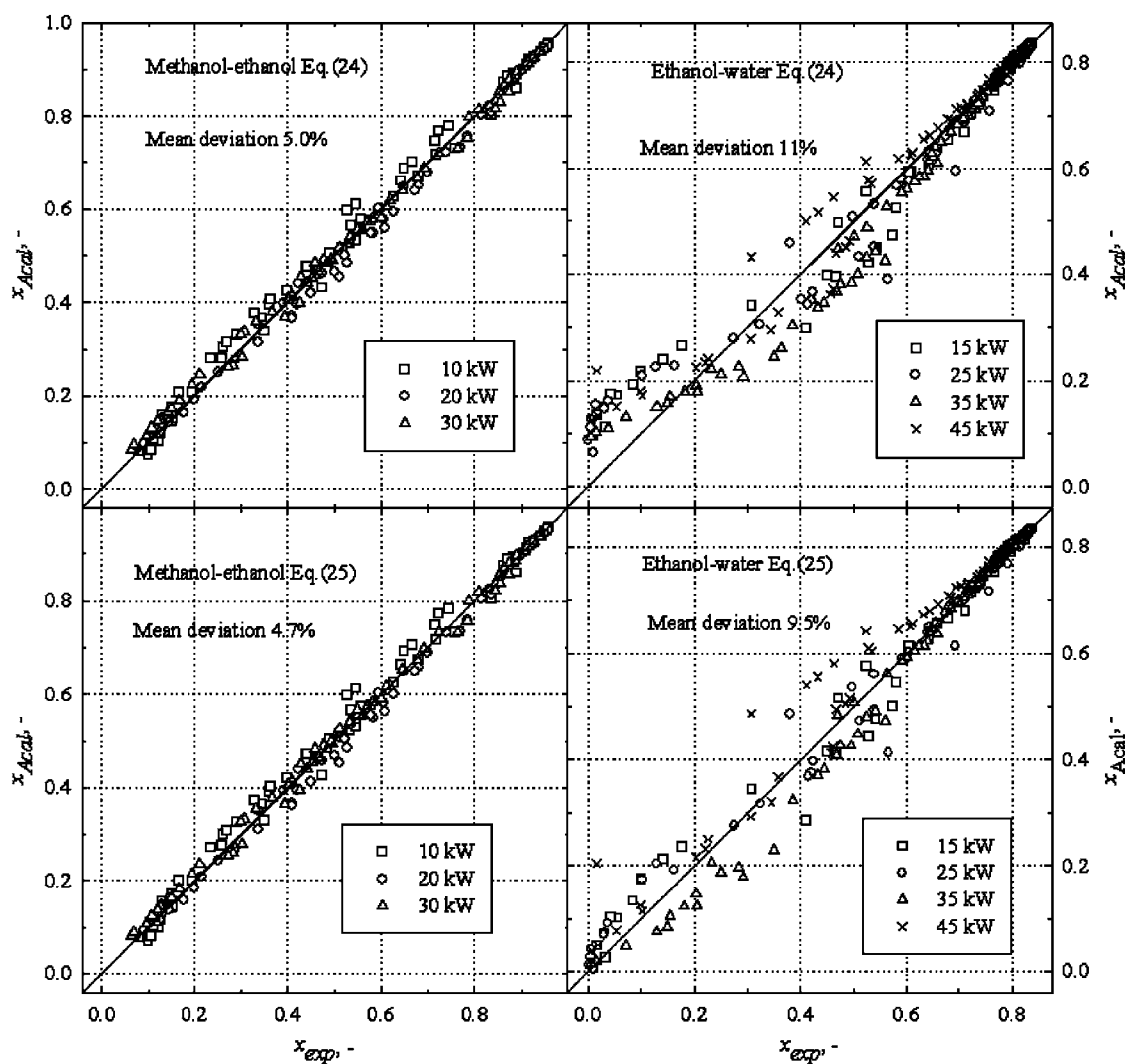


Fig. 6. Comparison of concentrations measured experimentally $x_{A,exp}$ with those $x_{A,fit}$ calculated from correlations (24) and (25) using the fitted parameters $[C_L, C_V]$ and $[b_L, b_V]$.

parameters $[C_L, C_V]$ and $[b_L, b_V]$ are given in Table 4. Concentrations measured experimentally $x_{A,exp}$ are compared with those $x_{A,fit}$ calculated from the fitted parameters $[C_L, C_V]$ and $[b_L, b_V]$ in Fig. 6. Mean absolute deviations s_x of the experimental and the calculated concentrations evaluated from

$$s_x = \sqrt{f/n} \quad (32)$$

(n is a number of experimental points) are given in Table 4 also. The s_x -values show that correlation (25) fits concentration profiles more precisely than the correlation (24) and the figure shows that the correlation (24) does not suit for E–W distillation system at low ethanol concentrations.

Thus, just those parameters obtained by fitting the profiles using correlation (25) are further used only. Optimisation of

Table 5
Sensitivity of the objective function f on parameters b_L and b_V

Distillation system	A_L	A_V	A_V/A_L
Methanol–ethanol	2.88	8.84	3.07
Ethanol–water	0.828	108.8	131.0

the shape or optionally of the values of some exponents in the correlation (25) is not possible until more extensive distillation data collection will be treated.

Sensitivity of the objective function f to parameters b_L and b_V were compared through values of normalized partial derivative of the objective function (26) with respect to the parameters round the global minima. The derivatives have been evaluated numerically

$$A_L = \frac{b_{L,OPT}}{f_{OPT}} \left(\frac{\partial f}{\partial b_L} \right)_{b_V} \cong \frac{b_{L,OPT}}{f(b_{L,OPT}; b_{V,OPT})} \left(\frac{\Delta f}{\Delta b_L} \right)_{b_V}$$

$$A_V = \frac{b_{V,OPT}}{f_{OPT}} \left(\frac{\partial f}{\partial b_V} \right)_{b_L} \cong \frac{b_{V,OPT}}{f(b_{L,OPT}; b_{V,OPT})} \left(\frac{\Delta f}{\Delta b_V} \right)_{b_L} \quad (33)$$

Results given in Table 5 show much higher sensitivity of the objective function to parameter b_V and thus the higher reliability of mass transfer coefficients measured in vapour phase for both distillation systems compared to liquid coefficients.

4.3. Vapour- and liquid-side volumetric mass transfer coefficients

Dependences of the volumetric mass transfer coefficients calculated from correlation (25) using the “best fit” parameters $[b_L, b_V]$ on volatile component concentration in liquid phase along distillation column are given in Figs. 7 and 8. To reduce scatter of experimental points in the figures calculated for different reboiler duties the mass transfer coefficients are divided by u_L and u_G values powered to exponents suggested by correlation (25), i.e., $k_L a / u_L^{0.761}$ and $k_V a / (u_L^{0.284} u_V^{0.7})$.

Mass transfer coefficients calculated from absorption correlations presented in literature and obtained by Linek et al. (1995) recalculation procedure² are also given in Figs. 7 and 8. For the sake of lucidity the literature data are plotted for boundary values of reboiler duty only. Onda et al. (1968) have set values of $b_{L,abs} = 5.1 \times 10^{-3}$ and $b_{V,abs} = 5.23$ for packings of nominal size higher than 15 mm. For metal Pall rings 25 mm Billet et al. (1999) have indicated values of $C_{L,abs} = 1.44$ and $C_{V,abs} = 0.336$ and for metal Intalox saddles 25 mm Moucha et al. (2005) have determined values of $C_{L,abs} = 1.36$ and $C_{V,abs} = 0.779$. All the absorption parameters $[b_{L,abs}, b_{V,abs}]$ and $[C_{L,abs}, C_{V,abs}]$ are

² The recalculation procedure of the absorption data to the distillation conditions is based only on the difference in diffusivities D and in numbers of pieces of packing per unit volume n according to the relation $k_V a \sim D_V^{2/3} \cdot n$ and $k_L a \sim D_L^{1/2} \cdot n$. Following absorption systems were chosen as suitable ones: absorption of SO_2 into NaOH solution to determine $k_V a$ and absorption of O_2 into water to determine $k_L a$. Linek et al. (1995) and Moucha et al. (2005) have presented correlations of the parameters for Pall rings and Intalox saddles, respectively.

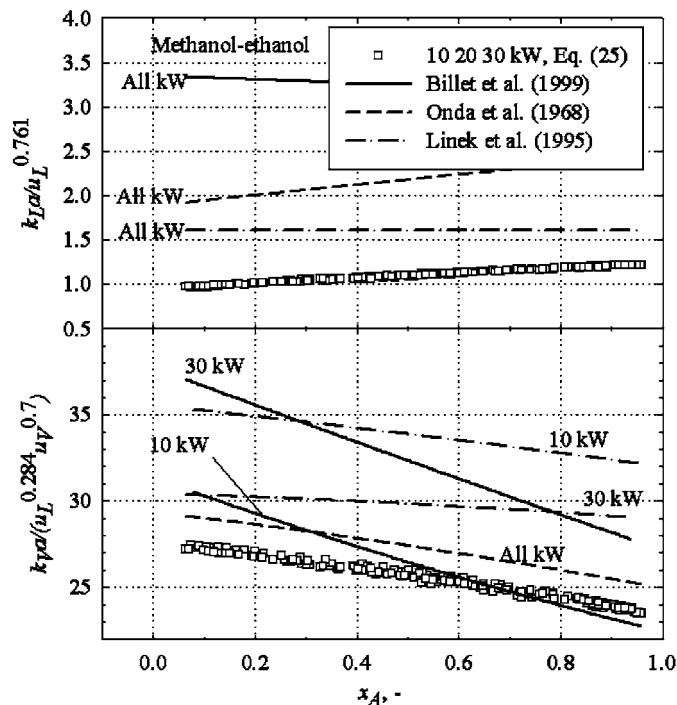


Fig. 7. Volumetric mass transfer coefficients calculated from correlation (25) using the “best fit” parameters $[b_L, b_V]$ for M–E system (symbols). Comparison with the coefficients calculated from absorption correlations given in literature (lines).

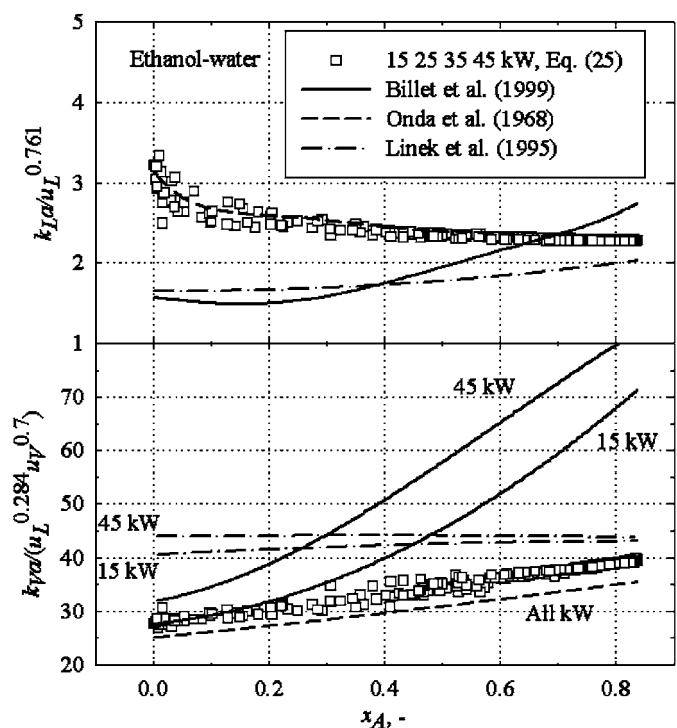


Fig. 8. Volumetric mass transfer coefficients calculated from correlation (25) using the “best fit” parameters $[b_L, b_V]$ for E–W system (symbols). Comparison with the coefficients calculated from absorption correlations given in literature (lines).

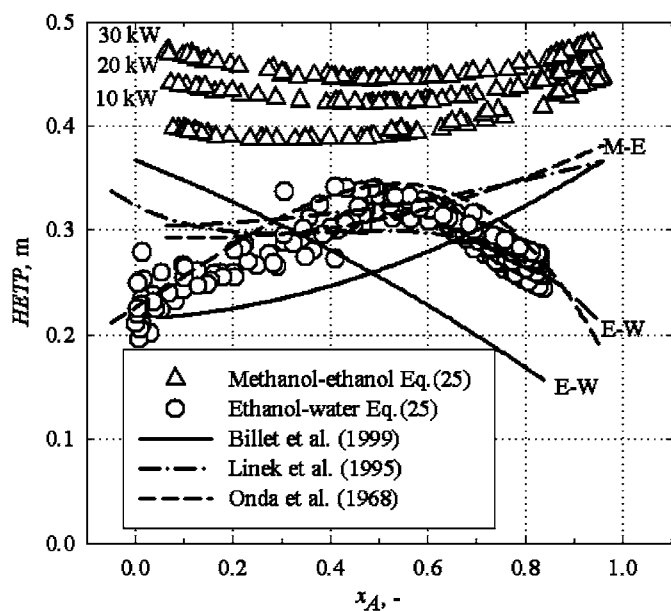


Fig. 9. Local values of $HETP$ calculated from (27) with the mass transfer coefficients obtained from correlation (25) (symbols) and from absorption correlations given in literature (lines) for E–W and M–E distillation systems.

summarised in Table 4. Onda et al. (1968) absorption correlation matches the best with the distillation mass transfer coefficients: differences between the coefficients for vapour phase in both distillation systems and between the coefficients for liquid phase in E–W system did not exceed 10%. However, Onda's absorption correlation predicts by 100% higher $k_L a$ -values in M–E distillation system, Linek's procedure overestimates these coefficients up to by 50% and Billet's absorption correlation up to by 300%. Billet's correlations as well as Linek's procedure overestimate mass transfer coefficients for vapour phase in M–E system up to by 50%. In E–W distillation system, they predict $k_L a$ -values lower up to by 50% and overestimate $k_V a$ -values up to by 100%.

Conclusion from the comparison is that any of the absorption correlations does not describe distillation mass transfer coefficients sufficiently accurately under all distillation conditions used in this work.

4.4. $HETP$, liquid-side mass transfer resistance, equimolar counter-diffusion

Local values of $HETP$ calculated from Eq. (27) with the mass transfer coefficients obtained from the correlation (25) using the “best fit” parameters $[b_L, b_V]$ are shown in Fig. 9. The values depend slightly on reboiler duty and concentration, i.e., on the position in the column but the data lie within the interval 0.39–0.47 m and 0.20–0.33 m with the mean value of 0.43 and 0.28 m for M–E and E–W distillation system, respectively. Very similar $HETP$ data are predicted by Onda's absorption correlation for the system E–W. In the other situations the absorption correlations fail: for the system M–E the absorption correlations predict markedly lower values by 30–50% and for

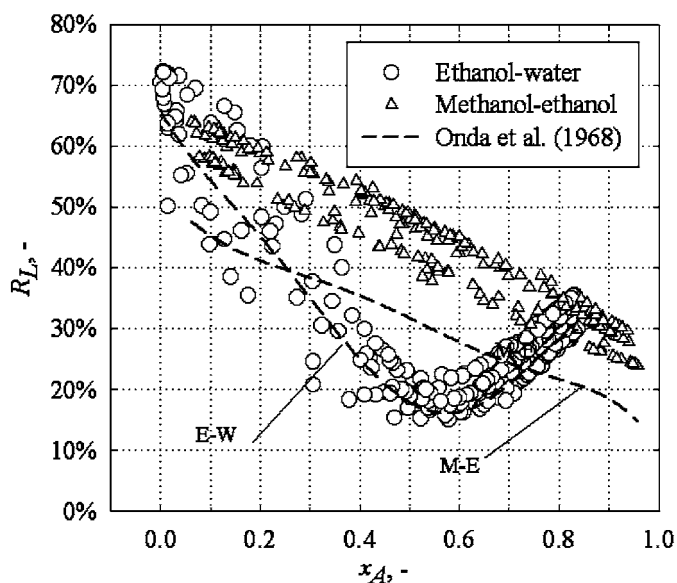


Fig. 10. Relative liquid side mass transfer resistances calculated from (28) with the mass transfer coefficients obtained from correlation (25) for M–E and E–W distillation systems. Comparison with the values predicted by absorption correlation by Onda et al. (1968).

the E–W system Linek's correlation fits the data at high ethanol concentration only.

Relative liquid side mass transfer resistance calculated from Eq. (28) with the mass transfer coefficients obtained from the correlation (25) using the “best fit” parameters $[b_L, b_V]$ are shown in Fig. 10. The highest liquid side resistance occur at the lowest concentration of the more volatile component in both distillation systems, i.e., at the bottom of column where the resistance reaches 70%. Towards the top of the column the relative resistance sharply decreases, reaching its minimum 15% and 25% at concentration x_A of approx. 0.5 and 0.95 in E–W and M–E distillation system, respectively. Absorption correlation by Onda et al. (1968) predicts the R_L -values for E–W system well but it predicts lower values for M–E system by 15%.

Convective flow of A-component $x_A(N_A + N_B)$ induced by total flow of the mixture through an interface $N_A + N_B$ relative to the flow N_A is presented as a function of the concentration of A-component in Fig. 11. The convective flow reaches up to 10% of the flow of A-component at the top of column and flows from liquid into vapour along the whole column in M–E system. In the system E–W, the convective flow reaches up to 5% in concentration range $x_A > 0.1$. At $x_A = 0.1$ the equimolar counter-diffusion occurs as $N_A + N_B = 0$ and in concentration range $x_A < 0.1$, the direction of the convective flow is opposite, i.e., from vapour into liquid.

4.5. Heat transfer and heat transfer coefficients

The heat transfer fluxes and heat transfer coefficients in both phases which are necessary to keep the phases at their saturation temperatures can be calculated from equations of the model.

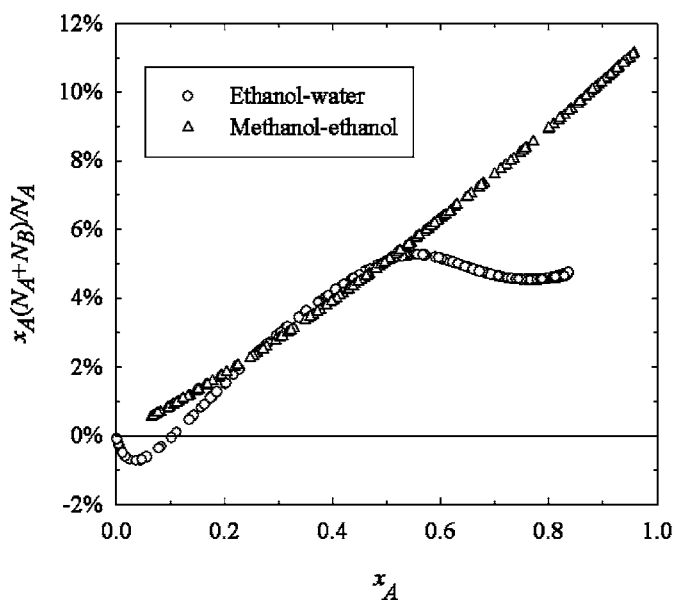


Fig. 11. Convective flow of A-component $x_A(N_A + N_B)$ relative to the flow N_A as a function of concentration of the component A.

The sensible heats transferred from the interface to the bulk liquid q_L and from the bulk vapour to the interface q_V and the enthalpy transferred by the convective mass flux into the liquid Q_L and from the vapour Q_V evaluated from Eqs. (12), (18) and (19) with correlation (25) are presented in Fig. 9. To reduce scatter of experimental points in the figure calculated for different reboiler duties the coefficients are divided by the due reboiler duty. The data fulfil the energy continuity at the interface, i.e.

$$q_L + Q_L = q_V + Q_V. \quad (34)$$

Two transfer mechanisms, conduction q and convection Q , take significant role in the heat transfer in both phases. In M–E distillation system, the energy ($q + Q$) flows from vapour to liquid phase along whole the column. In liquid phase, the same amount of the heat is transferred by each of the two mechanisms while in vapour phase smaller part of heat (20–40%) is transferred by conduction. In E–W system, only the heat transferred by conduction flows from vapour to liquid along whole the column. The heat transferred by convection flows from liquid to vapour and only in vapour phase at low ethanol concentrations at the column bottom, it flows in opposite direction, i.e., from vapour into liquid. That is the region, where also total flux of mixture occurs in this direction (see Fig. 12).

Volumetric heat transfer coefficients in liquid and vapour phases calculated from the enthalpy balance, i.e., Eqs. (20) and (21), and from the analogy between heat and mass transfer, i.e., Eqs. (30) and (31), for M–E and E–W distillation systems are plotted in Figs. 13 and 14. Again, to reduce scatter of the data in the figures calculated for different reboiler duties the coefficients are divided by superficial velocity of phases with the same exponents as were used with the mass transfer coefficients, i.e., $\alpha_L a / u_L^{0.761}$ and $\alpha_V a / (u_L^{0.284} u_V^{0.7})$. The analogy was applied on the mass transfer coefficients calculated from the

correlation (25) using the “best fit” parameters $[b_L, b_V]$. The heat transfer coefficients calculated from the Chilton–Colburn analogy for the vapour phase agree with the data calculated from the enthalpy balance better than the coefficients calculated from analogy of the penetration-theory mechanism used for the liquid phase. $\alpha_V a$ -values calculated from the analogy for both distillation systems are at maximum by 50% lower than the data evaluated from the enthalpy balance whereas $\alpha_L a$ -values calculated from the analogy are considerably higher (up to by two orders) than the data evaluated from the enthalpy balance. The $\alpha_V a$ -values were evaluated using the assumption of saturated liquid phase, however, which has not been fully confirmed. Therefore the resulting values and unsatisfactory agreement with data resulting from analogies have to be taken with caution.

4.6. Simulated concentration profiles

Concentration profiles obtained by integration of the differential model of the distillation column using the mass transfer coefficients calculated either from correlations (24) and (25) (the best fit parameters $[b_L, b_V]$ and $[C_L, C_V]$ used) or from the absorption correlation are plotted for distillation systems M–E and E–W in Figs. 15 and 16, respectively, together with experimental concentration data series measured at the same reboiler duty but at different concentrations of the liquid in the reboiler covering whole concentration range. The individual experimental series in the figures are shifted in z -coordinate so as the “initial condition” for each series “sits” on the different theoretical profile. The profiles calculated using the absorption mass transfer coefficients do not correspond well to the experimental profile, especially for M–E distillation system. For the system E–W, the absorption mass transfer coefficients obtained by Linek’s recalculating procedure smooth the experimental profiles quite well but Onda’s and especially Billet’s absorption coefficients lead to profiles very different from the experimental ones.

Utilization of absorption mass transfer coefficients in “rate based” distillation models is risky as it might lead to incorrect concentration profiles.

5. Conclusions

Method for the simultaneous determination of both partial mass transfer coefficients in a distillation column was successfully used in the distillation system M–E which is characterized by small change of the equilibrium coefficient along the column in comparison with the originally used E–W system. The concentration profiles were better-fitted using correlation (25) than the one of (24) to describe the effect of the changes of phase velocities and physical properties of phases on the coefficients along the column.

The distillation mass transfer coefficients agree with Onda et al. (1968) absorption correlation better than with the other absorption correlations. Differences between the distillation and Onda’s coefficients for vapour phases in both distillation

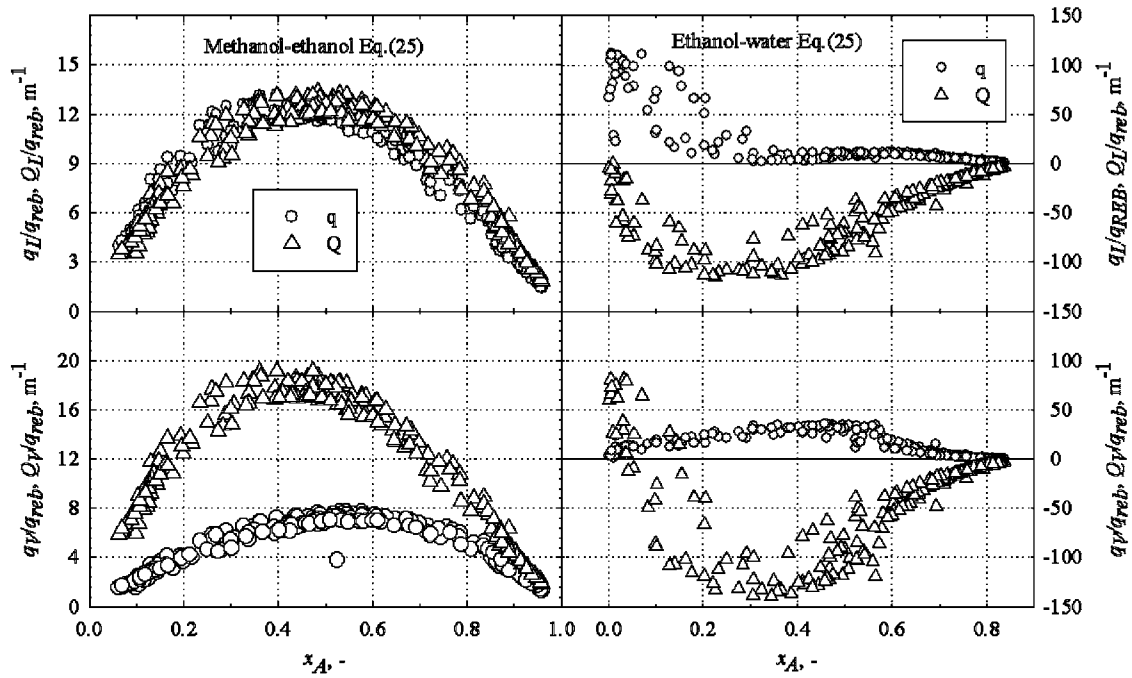


Fig. 12. Sensible heats flux q and enthalpy transfer by the convective mass flux Q on liquid and vapour side of interface.

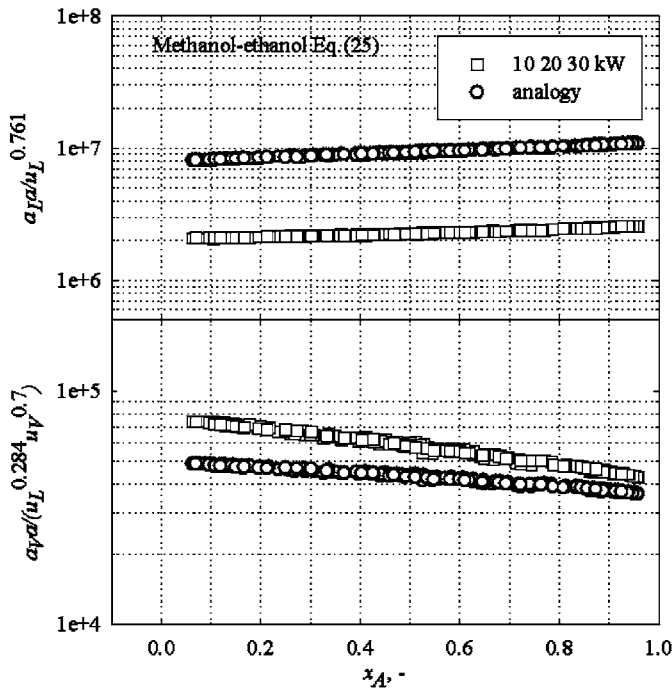


Fig. 13. Volumetric heat transfer coefficients in liquid and vapour phases calculated from the enthalpy balance and from the analogy for M–E distillation system.

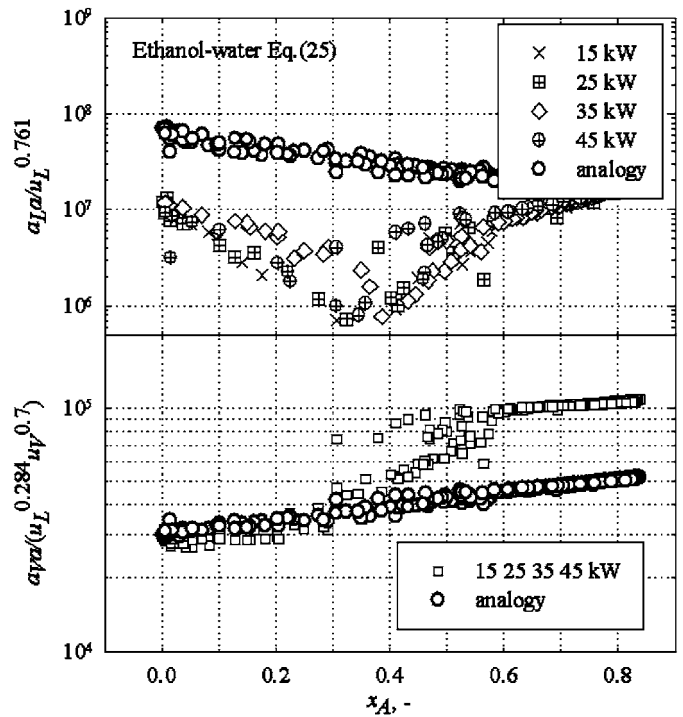


Fig. 14. Volumetric heat transfer coefficients in liquid and vapour phases calculated from the enthalpy balance and from the analogy for E–W distillation system.

systems and for liquid phase in E–W distillation system did not exceed 10%. However, Onda’s absorption correlation predicts by 100% higher $k_L a$ -values in M–E distillation system, Linek’s procedure overestimates the coefficients up to by 50% and Billet’s absorption correlation up to by 300%. Conclusion from the comparison is that none of the absorption correlations

describe distillation mass transfer coefficients sufficiently accurately under all distillation conditions used in this work.

Local values of $HETP$ calculated from the mass transfer coefficients obtained by the fitting of distillation profiles lie within the interval 0.39–0.47 m and 0.20–0.33 m with the mean value

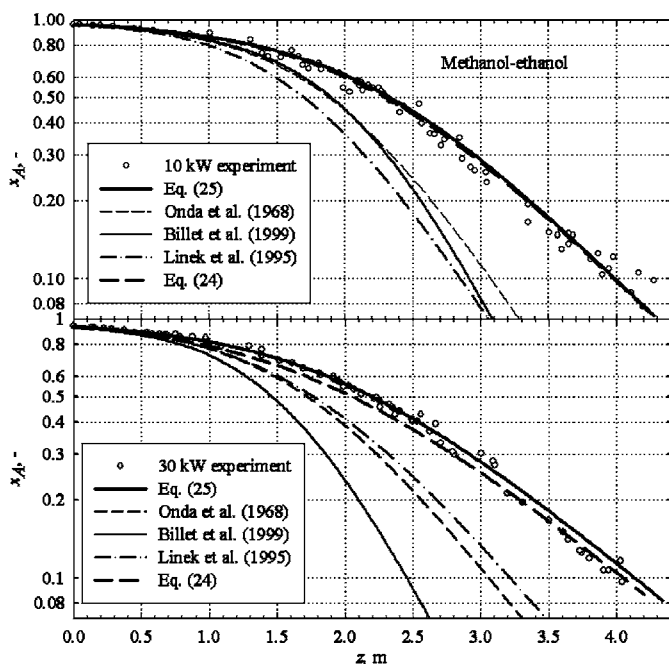


Fig. 15. Concentration profiles obtained by integration of the differential model of the distillation column using k_{La} - and k_{Va} -values either from Eqs. (24) and (25) or from the absorption correlations for M–E distillation system at reboiler duties of 10 and 30 kW.

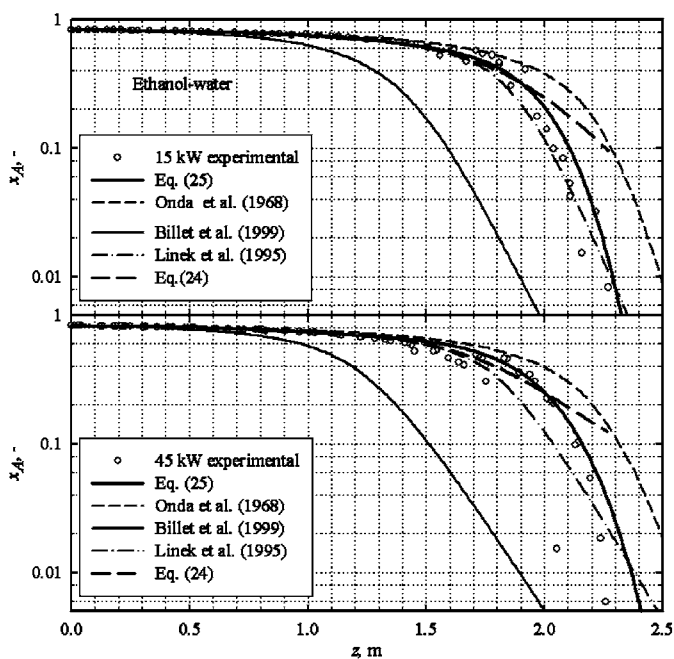


Fig. 16. Concentration profiles obtained by integration of the differential model of the distillation column using k_{La} - and k_{Va} -values either from Eqs. (24) and (25) or from the absorption correlations for E–W distillation system at reboiler duties of 15 and 45 kW.

of 0.43 and 0.28 m for M–E and E–W distillation system, respectively.

Relative liquid side mass transfer resistance calculated from the fitted mass transfer coefficients depends strongly upon

concentration. The highest resistance occur at the lowest concentration in both distillation systems, i.e., at the bottom of column where it reaches 70%. Towards the top of the column the relative resistance sharply decreases, reaching its minimum of about 20% in both distillation systems.

The convective flow of A-component induced by the total flow of mixture through an interface reaches up to 10% and 5% of the flow of A-component in M–E and E–W system, respectively. The equimolar counter-diffusion occurs at $x_A=0.1$ in E–W system only.

Two transfer mechanisms, conduction and convection, take significant role in the heat transfer in both phases. The values of the heat transfer coefficients predicted by the Chilton–Colburn analogy between heat and mass transfer used for the vapour phase are at maximum one and half order higher than the enthalpy-balance values. The coefficients in the liquid phase calculated from the analogy based on the penetration-theory mechanism are up to two-orders higher compared to the enthalpy balance data.

Utilization of absorption mass transfer coefficients in simulating distillation model leads to very incorrect concentration profiles.

Notation

a	effective heat/mass transfer area, m^{-1}
a_t	geometrical area of packing, m^{-1}
$A_{L,V}$	normalized partial derivative of objective function, defined by Eq. (33)
$b_{L,V}$	empirical constants
B	liquid load, $m^3 m^{-2} h^{-1}$
c	molar concentration in the bulk, $kmol m^{-3}$
c_p	molar heat, $kJ kmol^{-1} K^{-1}$
$C_{L,V}$	empirical constants
C_p	dimensionless molar heat, defined by Eq. (11)
D	diffusion coefficient, $m^2 s^{-1}$
f	matching criterion, defined by Eq. (26)
F	$=u_V \sqrt{\rho_V}$, gas capacity factor, $Pa^{1/2}$
g	gravitational constant, $m s^{-2}$
h	molar enthalpy, $kJ kmol^{-1}$
Δh_{mix}	heat of mixing, $kJ kmol^{-1}$
Δh_{vap}	molar heat of vapourization, $kJ kmol^{-1}$
k_{La}	liquid-side volumetric mass transfer coefficient, s^{-1}
k_{Va}	vapour-side volumetric mass transfer coefficient, s^{-1}
K	equilibrium ratio, dimensionless
L	liquid phase molar flow, $kmol s^{-1}$
m_A	slope of equilibrium defined by Eq. (29), dimensionless
M	molecular weight, $kg kmol^{-1}$
n_t	number of pieces of packing per unit volume, m^{-3}
N	molar flux transferred per unit height of packing, $kmol m^{-1} s^{-1}$
Pr	Prandtl number, dimensionless

q	sensible heat transfer per unit height of packing, kW m^{-1}
q_{reb}	reboiler power input, kW
Q	convective enthalpy transfer per unit height of packing, kW m^{-1}
r	flux of component A to total molar flux transferred defined by Eq. (6), dimensionless
R_L	relative liquid phase mass transfer resistance defined by Eq. (28), dimensionless
s_x	mean deviation defined by Eq. (32), dimensionless
S	column cross-section, m^2
Sc	Schmidt number, dimensionless
t	temperature, $^{\circ}\text{C}$
u	superficial velocity, m s^{-1}
V	gas phase molar flow, kmol s^{-1}
x	liquid phase molar fraction of volatile component, dimensionless
y	gas phase molar fraction of volatile component, dimensionless
z	packing height coordinate taken from top ($z=0$), m
Z	packing height, m

Greek letters

α	heat transfer coefficient, $\text{kW m}^{-2} \text{K}^{-1}$
ε	porosity, dimensionless
η	dynamic viscosity, Pa s
λ	heat conductivity, $\text{kW m}^{-1} \text{K}^{-1}$
ρ	density, kg m^{-3}
σ	surface tension, kg s^{-2}
σ_c	critical surface tension of a packing material, kg s^{-2}

Subscripts

A	volatile component
B	less volatile component
cal	calculated from fitted parameters [C_L, C_V] or [b_L, b_V]
exp	experimental
i	number of measuring place
j	number of series (repetition)
k	number of reboiler duty
L	liquid phase
V	vapor phase
w	interface

Superscript

*	equilibrium value
---	-------------------

Acknowledgements

The support from the Ministry of Education (MSM 6046137306) is gratefully acknowledged.

References

- Arwika, K.J., Sandall, O.C., 1980. Liquid phase mass-transfer resistance in a small scale packed distillation column. *Chemical Engineering Science* 35, 2337–2343.
- Billet, R., Schultes, M., 1999. Prediction of mass transfer in columns with dumped and arranged packings updated summary of the calculation method of Billet and Schultes. *Chemical Engineering Research Design* 77 (Part A), 979–986.
- Bird, R.B., Stewart, W.E., Lightfoot, E.N., 1960. *Transport Phenomena*. Wiley, New York.
- Christensen, C., Gmehling, J., Rasmussen, P., Weidlich, U., 1984. *Chemistry Data Series*, vol. III, Part 1, Dechema, Frankfurt am Main.
- Dribika, M.M., Sandall, O.C., 1979. Simultaneous heat and mass transfer for multicomponent distillation in a wetted wall column. *Chemical Engineering Science* 34, 733–739.
- Gmehling, J., Onken, N., Rarey-Nies, J.R., 1988. *Vapour-liquid Equilibria Data Collection*, vol. 1. Part 2e, Supplement 3, *Chemistry Data Series*, Dechema, Frankfurt am Main.
- Honorat, A., Sandall, O.C., 1978. Simultaneous heat and mass transfer in a packed distillation column. *Chemical Engineering Science* 33, 635–640.
- Kayihan, F., Sandall, O.C., Mellichamp, D.A., 1977. Simultaneous heat and mass transfer in binary distillation—II (experimental). *Chemical Engineering Science* 32, 747–754.
- Linek, V., Sinkule, J., Brekke, K., 1995. A critical evaluation of the use of absorption mass transfer data for the design of packed distillation columns. *Chemical Engineering Research and Design* 73, 398–405.
- Linek, V., Moucha, T., Prokopová, E., Rejl, J.F., 2005. Simultaneous determination of vapour- and liquid-side volumetric mass transfer coefficients in distillation column. *Chemical Engineering Research and Design* 83, 979–986.
- Mori, H., Oda, A., Aragaki, T., Kunimoto, Y., 1996. Packed column distillation simulation with a rate-based method. *Journal Chemical Engineering Japan* 29, 307–314.
- Mori, H., Ito, Ch., Oda, A., Aragaki, T., 1999. Total reflux simulation of packed column distillation. *Journal Chemical Engineering Japan* 32, 69–75.
- Mori, H., Ito, C., Taguchi, K., Aragaki, T., 2002. Simplified heat and mass transfer model for distillation column simulation. *Journal Chemical Engineering Japan* 35, 100–106.
- Mori, H., Ibukia, R., Taguchia, K., Futamura, K., Olujic, Ž., 2006. Three-component distillation using structured packings: performance evaluation and model validation. *Chemical Engineering Science* 61, 1760–1766.
- Moucha, T., Linek, V., Prokopová, E., 2005. Effect of packing geometrical details: influence of free tips on volumetric mass transfer coefficients of Intalox saddles. *Chemical Engineering Research and Design* 83, 88–92.
- Onda, K., Takeuchi, H., Okumoto, Y., 1968. Mass transfer coefficients between gas and liquid phases in packed columns. *Journal of Chemical Engineering Japan* 1, 56–61.
- Seader, J.D., Henley, E.I., 1998. *Separation Process Principles*. Wiley, New York.
- Stephan, K., Hildwein, H., 1987. *Recommended Data of Selected Compounds and Binary Mixtures*. Dechema, Frankfurt am Main.
- Taylor, R., Krishna, R., 1993. *Multicomponent Mass Transfer*. Wiley, New York.
- Vargaftik, N.B., 1975. *Tables on the Thermophysical Properties of Liquids and Gases*. Wiley, New York.
- Wesselingh, J.A., 1997. Non-equilibrium modeling of distillation. *Chemical Engineering Research Design* 75, 529–538.
- Zarzycki, R., Chacuk, A., 1993. *Absorption*. Pergamon Press Ltd.

Effect of Gas- and Liquid-Phase Axial Mixing on the Rate of Mass Transfer in a Pilot-Scale Distillation Column Packed with Mellapak 250Y

L. Valenz,* F. J. Rejl, and V. Linek*

Department of Chemical Engineering, Prague Institute of Chemical Technology, CZ-166 28 Prague 6, Czech Republic

ABSTRACT: Using the “profile method”, the vapor- and liquid-side volumetric mass-transfer coefficients (k_{Va} , k_{La}) were evaluated by comparing the vapor and liquid concentration profiles with those calculated from a rate-based distillation model taking into account axial mixing in both phases. The method was applied for the atmospheric distillation of three different mixtures of primary alcohols: methanol–ethanol, ethanol–propanol, and methanol–propanol on structured packing Mellapak 250Y. The column was operated at total reflux; liquid and vapor samples were withdrawn at seven sampling points distributed regularly along the column. Bodenstein numbers Bo were determined by means of the “cold” air–water dynamic experiments performed under hydraulic conditions, by which the concentration profiles were measured in the distillation column. The mass-transfer coefficients were compared with those obtained in our previous work (Rejl et al. *Ind. Eng. Chem., Res.* **2010**, *49*, 4383) using the plug flow model for their evaluation. The axial dispersion model reproduces the experimental profiles with a 2-fold decreased relative difference between the experimental and the calculated concentrations in comparison with the plug flow model. The individual transport coefficients are higher (by up to 2 times) and are less dependent on the phase flow rate in comparison with the plug flow model. The correspondence with the mass-transfer correlations designed for the packed columns (Rocha et al. *Ind. Eng. Chem. Res.* **1996**, *35*, 1660; Billet and Schultes *Trans IChemE* **1999**, *77*, 498; Olujić et al. *Chem. Eng. Process.* **1999**, *38*, 683) is not improved by using the dispersion model: the differences reach multiples of the measured values. The parameters k_{La} , k_{Va} , Bo_L , and Bo_V were studied for their relative influences on the separation efficiency of the column. The relative contribution of k_{Va} is predominant (60%), whereas the axial mixing of vapor Bo_V has practically no effect. The contribution of k_{La} constitutes about 25%, and the one of the axial mixing of the liquid Bo_L increases from about 15 to 40% with a decrease in the liquid flow rate at the expense of the contribution of k_{Va} .

1. INTRODUCTION

Absorption and distillation in packed columns are analogical processes of interfacial mass and heat transfer, and the creation of a unique database for their design remains a challenging problem for chemical engineers. Chemical engineering as a branch of science is targeted toward the description and design of various processes carried out in various equipments using the combination of hydrodynamic, heat- and mass-transfer models deduced from the first principles. To improve reliability and accuracy of the predictive models used for design of separation columns, we should better understand all underlying phenomena which would lead to obtaining parameters of the models with a clear physical meaning, which underlies their applicability to other conditions and their transferability to similar processes. This work is devoted to axial mixing, as neglecting its effect may substantially reduce the applicability and the transferability of the column mass-transfer parameters.

Axial mixing is an undesirable phenomenon, occurring during a phase flow through the column-type mass-transfer exchangers (e.g., absorption or distillation columns), as it lowers the driving force of the interfacial mass transfer. As a result, it is necessary to use a higher number of transfer units, i.e. a deeper bed of packing, to maintain the same output concentration for the axial dispersion flow of the phases in the column, compared with the plug flow model. At extreme ratios of liquid-to-gas flow, which are common in column-type mass-transfer exchangers, axial mixing

and mass-transfer resistance are usually significant during the phase with a lower interstitial velocity and its effects can be ignored in the high-velocity phase. The significance of axial mixing in these situations is illustrated in Figure 1. In this figure, the relative increase in the packing depth, $H_{\text{true}}/H_{\text{plug}}$, eliminating the effect of the axial dispersion in one phase that is characterized by the Bo number, is plotted as a function of the number of the plug flow transfer units, N_{plug} . Equation 1 is taken from ref 1:

$$\exp(-N_{\text{plug}}) = \frac{4b \exp(Bo/2)}{(1+b)^2 \exp(bBo/2) - (1-b)^2 \exp(-bBo/2)} \quad (1a)$$

$$b = \sqrt{1 + 4 \frac{N_{\text{true}}}{Bo}}; \quad Bo = \frac{u_i H_{\text{true}}}{D_e} \quad (1b)$$

In their study,² Furzer and Ho explained the increase of the HETP values measured in the columns of different heights (0.15, 0.3, 0.6, and 1.2 m) in terms of the differential backmixing

Received: August 3, 2010

Accepted: December 8, 2010

Revised: November 23, 2010

Published: January 24, 2011

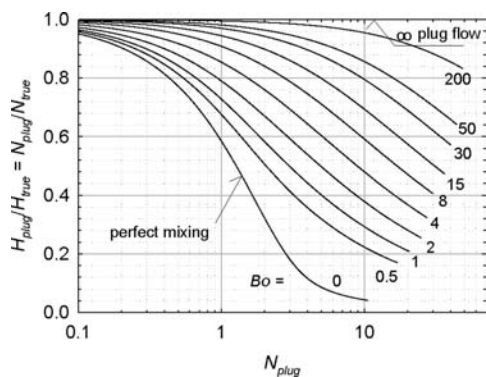


Figure 1. Relative increase of the column packing height, $H_{\text{true}}/H_{\text{plug}}$ eliminating an effect of the axial dispersion in one phase characterized by the Bo number.

rate-based distillation model. The Peclet numbers of the liquid phase used in this model were eight times higher in comparison to those obtained by dynamic measurements in a “cold” air–water simulation system. Furzer and Ho have stated in their other study³ that improved correlations could be obtained if the $HETP_{\text{true}}$ are correlated instead of $HETP_{\text{plug}}$ calculated from the end compositions assuming plug flow in both phases.

Steiner et al.⁴ compared the liquid and the vapor concentration profiles measured in a packed distillation column (height, 1.9 m; diameter, 0.1 m; Raschig rings, 33 mm; 10 sampling points) with the profiles evaluated from a stagewise backflow model. This model reproduced the experimental profiles well using rather low backmixing coefficients in the liquid phase (the equivalent eddy diffusivity $D_{e,L}$ of the order of $10^{-3} \text{ m}^2/\text{s}$ with the plug flow in the vapor phase) while the plug flow model of both phases failed, especially close to the ends of the column. As Furzer and Ho³ anticipated, their⁴ mass-transfer coefficients based on the backflow model correlated with the vapor flow rate with a substantially lower level of scatter than the ones based on the plug flow model.

With the aim of establishing general correlations for the design of packed absorption, desorption, and distillation columns, Kolev and Semkov^{5–7} have studied whether the model parameters derived from cold absorption experiments are also valid for distillation. They analyzed⁷ the effects of all possible types of side phenomena (e.g., axial mixing, radial mixing, thermal rectification, and interfacial turbulence induced by the surface tension gradient—the Marangoni effect) associated with the main mass-transfer process and concluded that only the effects of axial mixing and the Marangoni effect need to be taken into account when the cold data are transferred onto the distillation. They have demonstrated⁵ that the plug flow model is inadequate because the calculated height of the packing was not more than half the actual height. The Marangoni effect⁶ on column efficiency depends on the performance concentrations and the packing geometry reaching 29% for the random packing of Raschig rings and 49% for the arranged sheets packing of HOLPACK. They concluded⁷ that the diffusion model with dimensionless correlations of the mass-transfer coefficients corrected for the axial mixing effect and for the correlation between axial mixing and the Marangoni parameters, all derived from cold experiments employing the same packing, represents a promising unified approach for gas or vapor–liquid column design.

In all previous studies,^{2–7} the mass-transfer coefficients used in the distillation models were calculated from dimensionless

correlations derived from cold absorption experiments, and the phase flow rates were considered to be constant along the distillation column. In our most recent study,⁸ the profile method was presented which enables the determination of vapor- and liquid-side volumetric mass-transfer coefficients directly in the distillation by comparing the concentration profiles measured in both phases in a distillation column with the simulated profiles. The coefficients predicted by the three most frequently used correlations for the packed distillation columns design, namely, those of Rocha et al.⁹ (RBF), Billet and Schultes¹⁰ (BS), and Olujić et al.^{11,12} (DELFT), were compared with the coefficients measured directly in the distillation column by the profile method. The coefficients measured⁸ using the profile method on Mellapak 250Y structured packing differ substantially (by up to 6 times) from those calculated using the original correlations.

During work,⁸ the plug flow model for both phases was used in the simulated model and the phase flow changes along the column were evaluated using the enthalpy balance equation. This work aims to recalculate the $k_{L,A}$ and $k_{V,A}$ data measured by the profile method by the application of the differential axial dispersion model instead of the plug flow model described in our last paper.⁸ Liquid- and vapor-phase axial dispersion coefficients measured by cold experiments¹³ have been utilized. The values of $k_{L,A}$ and $k_{V,A}$ and their dependence on the rate of phases are compared with those predicted by the RBF, BS, and DELFT models.

2. DISTILLATION COLUMN MODEL

A complete set of corresponding model equations based on the use of the plug flow model for both phases can be found in Rejl et al.⁸ and the algorithm for solving them in Linek et al.¹⁴ Here, we provide only those equations that differ from those of the previous plug flow model and the principal features of the present model. Plug flow with axial dispersion in both phases is utilized, interfacial mass transport is described by a film model in which the convective flow is taken into account, and it is assumed that the vapor and liquid phases in the column are at their dew point and boiling point, respectively. The corresponding altered relations, representing the component balances over the differential volume of packing of the length dz for the distillation of the two-component mixture at total reflux (for which $L = V$ applies), are as follows:

$$(L - c_{L,S_{i,L}} \frac{dD_{e,L}}{dz}) \frac{dx_A}{dz} + x_A \frac{dL}{dz} - c_{L,S_{i,L}} D_{e,L} \frac{d^2 x_A}{dz^2} = N_A \quad (2a)$$

$$(L - c_{V,S_{i,V}} \frac{dD_{e,V}}{dz}) \frac{dx_A}{dz} + x_A \frac{dL}{dz} - c_{V,S_{i,V}} D_{e,V} \frac{d^2 x_A}{dz^2} = N_A \quad (2b)$$

$$S_{i,L} D_{e,L} = \frac{L}{u_{i,L}} D_{e,L} = L \frac{H}{Bo_L};$$

$$S_{i,V} D_{e,V} = \frac{L}{u_{i,V}} D_{e,V} = L \frac{H}{Bo_V} \quad (2c)$$

The molar fluxes transferred per unit height of packing N_A and N_B were calculated with convective flow taken into account from the equation

$$N_A = k_{V,A} c_{V,r} \ln \frac{y_{A,w} - r}{y_{A,r} - r} S = k_{L,A} c_{L,r} \ln \frac{x_{A,r} - r}{x_{A,w} - r} S \quad (3a)$$

$$r = \frac{N_A}{N_A + N_B}; \quad y_{A,w} = K_A x_{A,w} \quad (3b)$$

Table 1. Vapor and Liquid Flow Rates in the Distillation Column at Limiting Reboiler Duties, for Methanol–Propanol, and Axial Dispersion $Bo_{L,V}$ Numbers (from Equations 4 and 5) Used in the Calculation

$z, \text{ m}$	$P = 10 \text{ kW}$					$P = 20 \text{ Kw}$					$P = 40 \text{ kW}$			
	$B, \text{ m/h}$	u_V	10 m/s	Bo_L	Bo_V	$B, \text{ m/h}$	u_V	10 m/s	Bo_L	Bo_V	$B, \text{ m/h}$	$u_V, \text{ m/s}$	Bo_L	Bo_V
0.00	2.08	3.73	7.32	271	5.014	7.87	11.7	226.9	10.2	1.78	15.9	155		
0.15	2.09	3.72	7.36	271	5.241	7.80	12.18	226.4	10.4	1.77	16.1	155		
0.45	2.15	3.71	7.52	270	5.835	7.63	13.43	225.4	10.8	1.76	16.7	154		
0.75	2.28	3.69	7.90	270	6.442	7.55	14.64	223.8	11.7	1.73	17.9	153		
1.08	2.56	3.61	8.79	269	6.884	7.55	15.40	221.8	13.2	1.69	20.0	151		
1.39	2.91	3.54	9.87	268	7.076	7.56	15.70	220.6	14.6	1.67	21.8	149		
1.69	3.17	3.52	10.6	266	7.150	7.57	15.81	220.1	15.4	1.68	22.7	146		
1.99	3.30	3.53	10.9	265	7.178	7.58	15.85	219.9	15.8	1.68	23.1	144		

The complete model also includes the physicochemical properties and the equilibrium relations of the alcoholic distillation systems utilized in this work, which are given in ref 8. The dispersion coefficients $D_{e,L,V}$ and their dependences on the flow rates and the physicochemical properties were taken from the following Bo -numbers correlations deduced¹³ by means of the cold air–water dynamic experiments performed under hydraulic conditions by which the concentration profiles were measured in the distillation column for Mellapak 250Y structured packing (Bo numbers are related to the packing height of 1 m):

$$Bo_L = 1.022Fi^{0.478} \frac{3}{\sin^2 \alpha} \frac{1.159}{(da_p)^{6.337}} \quad (4)$$

$$Bo_V = 2.807 \cdot 10^6 Re_V^{-0.00895} 10^{-0.00394Re_L} (da_p)^{-7.792} \quad (5)$$

are valid in the following ranges of phase flow rates: $0 < B < 40 \text{ m/h}$; $0 < u_V < 2 \text{ m/s}$. The correlations reproduce the experimental data of Bo_L and Bo_V to better than within ± 15 and $\pm 22\%$ divergence between the measured and the predicted values, respectively, for most of the data.

The dependence of the volumetric mass-transfer coefficients $k_L a$ and $k_V a$ on phase flows and physicochemical properties which change along the length of the column has been left in the form utilized in the RBF, the BS, or the DELFT original models. Their variability, required for the purpose of optimization, has been retained by the application of the corrective multiplication parameters b_L and b_V .

$$\begin{aligned} k_L a &= b_L (k_L a)_{\text{model, orig}} \\ k_V a &= b_V (k_V a)_{\text{model, orig}} \end{aligned} \quad (6)$$

where index model = RBF, BS, or DELFT. The explicit expressions of the original models are given in ref 8. The optimization procedure used for obtaining b_L and b_V parameters is based on minimizing the standard deviation of the experimental and the calculated molar fractions.

$$s = \sqrt{\frac{\sum_{i=1}^n (x_{A,i, \text{calc}} - x_{A,i, \text{expt}})^2 + \sum_{i=1}^n (y_{A,i, \text{calc}} - y_{A,i, \text{expt}})^2}{2n}} \quad (7)$$

Table 2. b_L and b_V Parameters Calculated with Fixed and Optimized Initial Conditions (System Methanol–Propanol, Model RBF)

$P, \text{ kW}$	fixed initial conditions			optimized initial conditions			
	b_L	b_V	s	b_L	b_V	s	shift x_A^a
10	0.668	3.47	0.0248	0.899	2.81	0.0127	0.0026
20	0.682	1.88	0.0241	1.004	1.46	0.0168	0.0055
30	0.917	1.42	0.0221	1.328	1.16	0.0165	0.0087
40	1.054	1.26	0.0272	1.701	1.04	0.0140	0.0057

^a Absolute value of the difference between the optimized $x_A(z=0)$ and the fixed (measured) $x_{A,0,\text{expt}}$.

3. EXPERIMENTAL SECTION

3.1. Distillation Column. The atmospheric distillation column used has been described in detail in ref 8. The column with an inner diameter of 0.15 m was packed with 10 pieces of Mellapak 250Y, to the height of 2.1 m. The characteristics of the packing are $a_p = 250 \text{ m}^{-1}$, $d = 0.01606 \text{ m}$, and $F_{SE} = 0.35$. The column was operated under total reflux which was applied to the packing by a shower distributor with 25 openings (1472 holes/m^2). The column was equipped with seven openings for the placing of thermistors and sampling devices for the withdrawal of liquid and vapor samples along the column. Three distillation systems were used: methanol–ethanol (M–E), ethanol–propanol (E–P), and methanol–propanol (M–P). The experiments were performed at four levels of electric power input to the reboiler, namely, 10, 20, 30, and 40 kW.

3.2. Source Experimental Data. The experiments were repeated four times for each reboiler duty with different concentrations of the distillation mixture in order to encompass the entire concentration range of the measured concentration profiles in the column. A complete list of the source experimental data including the set of seven liquid, $x_{A,i}$, and vapor concentrations, $y_{A,i}$, along the packing, the liquid concentration in the reflux tube $x_{A,0,\text{expt}}$, the vapor concentration leaving the reboiler $y_{A,8}$, the volumetric flow rate of the liquid reflux, the barometric pressure, and the average temperature of each phase at the time of withdrawal $t_{L,i}$ and $t_{V,i}$ are provided in the paper⁸ together with the illustrative vapor and liquid flow rates and their physical properties in the distillation column for the reboiler duties used. For illustration, the vapor and liquid flow rates in the distillation column for limiting reboiler duties, for the M–P distillation

Table 3. Effect of Experimental Errors of the Bo Number of Vapor ($\Delta_{\text{rel}}Bo_V = 0.22$) and Liquid Phase ($\Delta_{\text{rel}}Bo_L = 0.15$) on the Parameters b_L and b_V Evaluated from Equation 8

no.	model	conditions				$\Delta_{\text{rel}}b_V/\Delta_{\text{rel}}Bo_V$	$\Delta_{\text{rel}}b_V/\Delta_{\text{rel}}Bo_L$	$\Delta_{\text{rel}}b_L/\Delta_{\text{rel}}Bo_V$	$\Delta_{\text{rel}}b_L/\Delta_{\text{rel}}Bo_L$	$\pm b_V, \%$	$\pm b_L, \%$
		$P, \text{ kW}$	system	Bo_V	Bo_L						
1	BS	10	M-E	270	8.31	0.025	0.74	0.013	0.45	12	7
2		40		150	17.9	0.024	0.12	0.025	0.43	2	7
3		10	M-P	269	9.05	0.048	0.45	0.071	0.56	8	10
4		40		150	18.7	0.029	0.14	0.002	0.23	3	3

Table 4. Best Fit Parameters b_L and b_V Obtained by the Profile Method

model	$b_{L,\text{orig}}^a$	$b_{V,\text{orig}}^a$	$P, \text{ kW}$	methanol-ethanol			ethanol-propanol			methanol-propanol		
				b_L	b_V	$s \cdot 10^2$	b_L	b_V	$s \cdot 10^2$	b_L	b_V	$s \cdot 10^2$
Axial Dispersion Model												
RBF	1	1	10	0.983	3.22	1.00	0.690	2.88	0.98	0.899	2.81	1.27
			20	0.914	1.81	0.78	0.830	1.54	1.46	1.004	1.46	1.68
			30	1.196	1.45	0.81	1.107	1.28	1.14	1.328	1.16	1.65
			40	1.479	1.30	0.55	1.397	1.17	0.79	1.701	1.04	1.40
Plug Flow Model (Data from Reference 8)												
RBF	1	1	10	0.474	2.00	1.8	0.418	2.14	2.5	0.449	2.05	3.4
			20	0.564	1.50	1.4	0.580	1.38	2.2	0.628	1.29	3.0
			30	0.763	1.27	1.4	0.794	1.18	2.0	0.861	1.06	3.0
			40	0.971	1.16	1.2	1.025	1.09	1.5	1.098	0.97	2.7
Axial Dispersion Model												
BS ^b	1.334	0.385	10	1.910	0.880	0.97	1.232	0.851	1.00	1.585	0.784	1.28
			20	1.597	0.528	0.78	1.336	0.477	1.46	1.676	0.430	1.70
			30	1.991	0.433	0.81	1.670	0.406	1.14	2.110	0.348	1.64
			40	2.335	0.398	0.55	1.969	0.377	0.77	2.534	0.319	1.38
Axial Dispersion Model												
DELFT	1	1	10	0.427	2.53	1.01	0.264	2.66	0.99	0.374	2.35	1.26
			20	0.449	1.94	0.79	0.364	1.93	1.47	0.497	1.66	1.66
			30	0.676	1.83	0.81	0.529	1.87	1.15	0.767	1.54	1.60
			40	0.906	1.84	0.55	0.692	1.90	0.80	1.044	1.55	1.37

^a Values of the multiplication parameters used in the original models. ^b Billet and Schultes¹⁰ did not present the constant for Mellapak 250Y. For comparison, the constants are presented for similar packing Ralu-Pak YC-250.

system, are given in Table 1, together with the axial dispersion Bo_L and Bo_V numbers (calculated from eqs 4 and 5) used in the calculation.

3.3. Data Evaluation Method. The effect of the fixed or optimized initial condition on the best-fit parameters b_L and b_V was tested in a manner similar to what was carried out⁸ for the plug flow model. The parameters evaluated on the basis of the fixed initial conditions $x_A(z=0) = y_A(z=0) = x_{A,0,\text{expt}}$ were compared with the values evaluated using the initial conditions $x_A(z=0) = y_A(z=0)$ optimized simultaneously with the parameters b_L and b_V . From the results summarized in Table 2 it is apparent that the parameters evaluated with the fixed and with the optimized initial conditions differ by between 15 and 39%, but the optimized initial concentrations $x_A(z=0)$ differ from the measured values $x_{A,0,\text{expt}}$ on average by less than 0.005(!). It is evident that the sensitivity of the parameters to the initial condition is high and that the accuracy of the experimental

$x_{A,0,\text{expt}}$ values is not sufficient. Because the optimized values $x_A(z=0)$ differ from the experimental values by less than the standard margin for experimental error and the calculated profiles better fit the experimental profiles (see s -values in Table 2), we have assumed that the optimization of the initial conditions together with the parameters b_L and b_V is the correct method, and therefore this method has been used subsequently in the same manner as it was used in the evaluation with the plug flow model.

4. RESULTS

4.1. Sensitivity of the Parameters b_L and b_V on the Experimental Scatter of Bo Numbers. The parameters b_L and b_V were studied for their sensitivity to the scatter of Bo numbers used in the evaluation. The following expressions 8 representing the ratio of relative errors of the parameter p , b_L , or

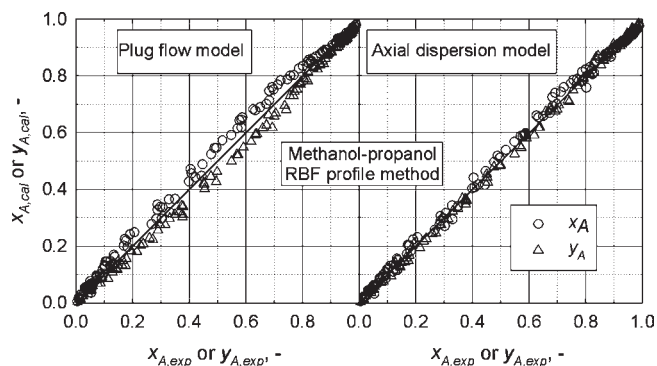


Figure 2. Comparison of experimental concentration profiles with those calculated from the RBF model with the correcting parameters b_L and b_V evaluated by the profile method using the plug flow or the axial dispersion model. Methanol–propanol distillation system.

b_V , and of the Bo numbers, were evaluated by numerical derivation for some representative experiments.

$$\frac{\Delta_{\text{rel}} b_i}{\Delta_{\text{rel}} Bo_i} = \frac{\partial b_i}{\partial Bo_i} \frac{Bo_i}{b_i}; \quad (8)$$

$$\pm b_i = \pm \sum_{i=L,V} \frac{\Delta_{\text{rel}} b_i}{\Delta_{\text{rel}} Bo_i} \Delta_{\text{rel}} Bo_i$$

where index $i = L$ or V . In Table 3, the ratios calculated for some experiments performed at low and high flow rates (low and high reboiler duties), using the BS model, are given, together with the relative errors of b_L and b_V induced by the probable experimental errors of Bo_L and Bo_V by correlations (4) and (5); namely, $\Delta_{\text{rel}} Bo_L = 0.15$ and $\Delta_{\text{rel}} Bo_V = 0.22$, respectively. The resulting scatter of both parameters is acceptably low, by approximately 10%. Similar results were obtained using the RBF and DELFT models.

4.2. Temperature of Phases. The main findings presented in our previous work⁸ were the following: (i) the liquid phase is overheated for all three distillation systems, with the highest level being for the M–P system, reaching 3 °C; (ii) the vapor is unevenly saturated, with the highest deviation of –1 °C for the M–P system; (iii) there is no correlation between the overheating of the phases and the reboiler duty; (iv) the overheating correlates with the concentration phase more closely than with its position in the column; (v) subcooling of the vapor phase and overheating of the liquid phase reach their maximum approximately at the equimolar concentration of the mixture, at which the temperature difference of the phases and their mass-transfer intensity reach their maximum.

4.3. Concentration Profiles Evaluated by the Profile Method. The best-fit parameters b_L and b_V are shown in Table 4 together with the standard deviations s of the experimental and the calculated concentrations. The s -values show that all of the models with the correcting parameters obtained by the profile method match the concentration profiles with practically the same precision: the best data of the M–E system and the worst data of the M–P system. The data for the M–P system are used to illustrate the data behavior obtained using the profile method in this work because the deviations using this system are the largest and therefore our conclusions are on the safe side. The axial dispersion model reproduces the experimental profiles better than does the plug flow model. The average relative

difference between the experimental and the calculated concentrations decreased from 17 to 10% for the M–P distillation system as illustrated in Figure 2. Similar decreases were observed for M–E (from 8 to 4%) and E–P (from 11 to 6%) distillation systems.

4.4. Parameters b_L and b_V and $k_L a$ and $k_V a$ Evaluated According to the Profile Method. The volumetric mass-transfer coefficients calculated from the models RBF, BS, and DELFT for all distillation systems, using the correcting parameters b_L and b_V based on the axial dispersion model, are plotted in Figure 3 as a function of the superficial vapor- and liquid-phase velocity. Also plotted in the figure are the coefficients calculated from the plug flow model and those calculated from the original models. The volumetric mass-transfer coefficients obtained by the profile method with the plug flow model and with the axial dispersion model differ considerably from those calculated from the original RBF, BS, and DELFT models. The application of the dispersion model increases both the liquid and the vapor mass-transfer coefficients in comparison with the plug flow model but it does not substantially diminish the differences between the coefficients determined by the profile method and those calculated from the original models. The mutual compatibility of the coefficients evaluated by the profile method with these three different RBF, BS, and DELFT models, using the axial dispersion model, is slightly worse than when the plug flow model is used (compare the distance apart of the blue lines and the red ones in Figure 3).

The parameters b_L and b_V depend on the reboiler duty P (see Table 4) or, in other words, on the phase flow rates. The b_L -values increase and the b_V -values decrease with P as much as 2-fold in the range of the reboiler duties utilized. This indicates that the models do not fit the dependence of volumetric mass-transfer coefficients on phase velocities well. This is discussed further.

4.5. Dependence of $k_L a$ and $k_V a$ on Physicochemical Properties and Phase Flow Rates. As was described in our previous paper,⁸ the dependence of volumetric mass-transfer coefficients on phase flow rates predicted by the original models^{9–11} under total reflux and below the loading point may be expressed as follows:

$$(k_L a)_{\text{model, orig}} = b_{L, \text{orig}} A_{L, \text{model}} (\text{phys. properties}) u_L^\alpha$$

$$(k_V a)_{\text{model, orig}} = b_{V, \text{orig}} A_{V, \text{model}} (\text{phys. properties}) u_V^\beta \quad (9)$$

where index model = RBF, BS, or DELFT. $A_{L,V,\text{model}}$ are functions only of the physicochemical properties of the system, which are given by the original RBF, BS, or DELFT model. The multiplication parameters $b_{L,V,\text{orig}}$ and the exponents α and β evaluated from the individual models are given in Tables 4 and 5, respectively. It has been shown⁸ that the exponents α and β do not, within the range of the conditions of our experiments, depend in practical terms on the rate, the concentration, or the distillation system utilized and that the physicochemical properties of the alcohol systems utilized in this work do not vary much. As a result, changes to them have a much lesser effect on the volumetric mass-transfer coefficients compared with the effect of the rate of the phases. This is why the dependence of the volumetric mass-transfer coefficients on the rate of the phases predicted by the models RBF, BS, and DELFT was tested, because the rates only varied in a wider range, by a factor of

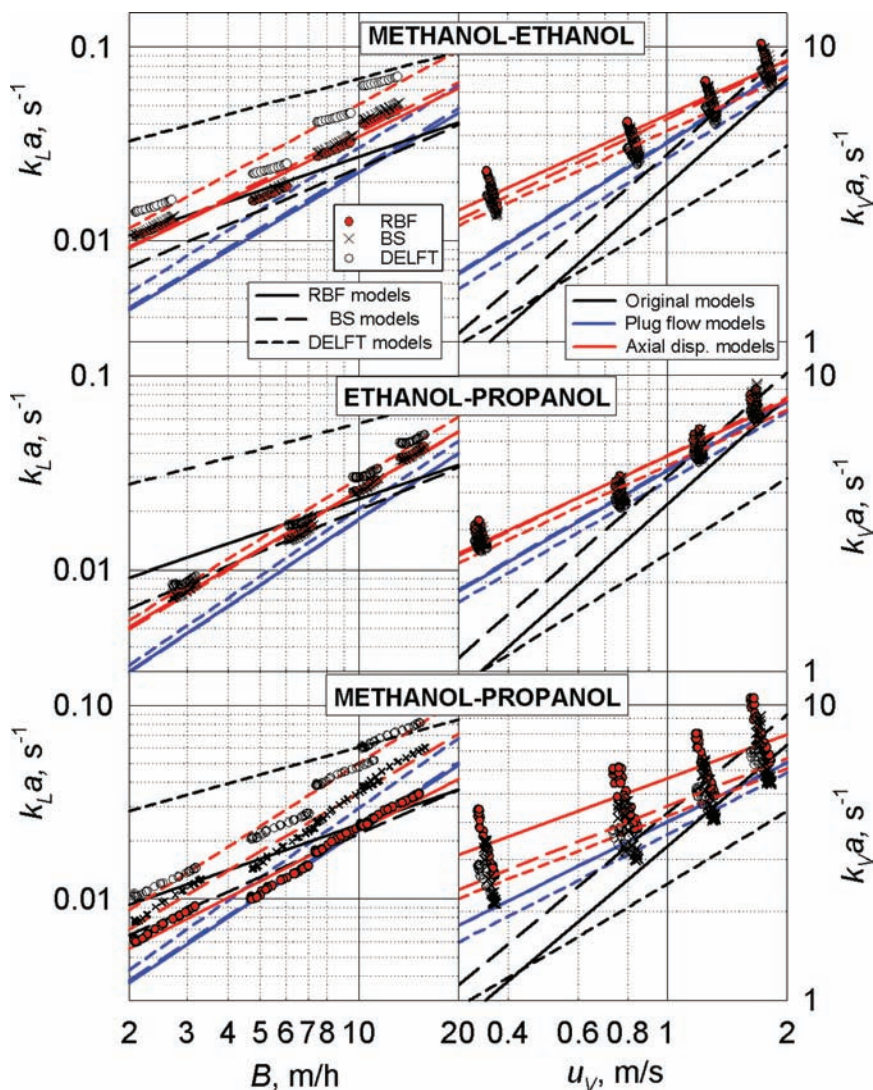


Figure 3. Volumetric mass-transfer coefficients calculated from RBF, BS, and DELFT models using the best-fit parameters b_L and b_V and from the original model correlations as a function of the superficial vapor- and liquid-phase velocity.

Table 5. Values of Exponents in Relations 9 (for Systems Methanol–Ethanol, Ethanol–Propanol, and Methanol–Propanol Using Models RBF, BS, and DELFT)

	methanol–ethanol			ethanol–propanol			methanol–propanol		
	RBF	BS	DELFT	RBF	BS	DELFT	RBF	BS	DELFT
α	0.582	0.733	0.445	0.576	0.733	0.445	0.580	0.733	0.450
λ	0.294	0.138	0.581	0.491	0.320	0.675	0.466	0.318	0.782
$\alpha + \lambda$	0.876	0.871	1.03	1.07	1.05	1.12	1.05	1.05	1.23
β	1.19	1.16	0.823	1.20	1.16	0.872	1.20	1.16	0.844
v	−0.619	−0.543	−0.224	−0.629	−0.572	−0.243	−0.691	−0.634	−0.295
$\beta + v$	0.571	0.617	0.599	0.571	0.588	0.629	0.509	0.526	0.549

approximately four times, by changing the input into the reboiler (10, 20, 30, and 40 kW).

4.6. $k_L a$ and $k_V a$ Dependence on the Rate of Phases Improved by the Profile Method. In our experiments performed under total reflux, the flow rate of liquid and vapor in the column rises proportionately to the power input to the reboiler. If the $k_L a$ - and $k_V a$ -dependence on the rates

predicted by the RBF, BS, and DELFT models is described properly, the correcting parameters b_L and b_V , obtained by optimization, should not be dependent on the reboiler duty. However, the value of the parameter b_L increases and of the parameter b_V decreases for all of the models in accordance with the power used. In analogy to eq 9 for the transport coefficients, the power dependence of the experimentally

Table 6. Best Fit Parameters $b_{L,PM}$ and $b_{V,PM}$ Obtained by the Profile Method

	$P, \text{ kW}$	methanol–ethanol			ethanol–propanol			methanol–propanol		
		$b_{L,PM}$	$b_{V,PM}$	$s \cdot 10^2$	$b_{L,PM}$	$b_{V,PM}$	$s \cdot 10^2$	$b_{L,PM}$	$b_{V,PM}$	$s \cdot 10^2$
RBF	10	7.625	1.721	1.0	20.84	1.520	1.0	22.57	1.426	1.3
	20	5.538	1.690	0.8	16.80	1.373	1.5	17.32	1.322	1.7
	30	6.346	1.785	0.8	18.08	1.506	1.1	18.52	1.424	1.7
	40	7.155	1.957	0.5	19.52	1.686	0.8	20.52	1.590	1.4
BS	10	4.915	0.5270	1.0	11.36	0.483	1.0	14.80	0.430	1.3
	20	3.619	0.4968	0.8	9.43	0.426	1.5	11.56	0.391	1.7
	30	4.208	0.5176	0.8	10.22	0.465	1.1	12.48	0.418	1.7
	40	4.715	0.5638	0.5	10.89	0.519	0.8	13.53	0.468	1.4
DELFT	10	26.23	2.011	1.0	29.27	2.127	1.0	87.26	1.806	1.2
	20	16.96	1.942	0.8	23.20	1.903	1.5	62.31	1.637	1.7
	30	19.62	2.021	0.8	24.95	2.046	1.1	66.80	1.725	1.6
	40	21.78	2.177	0.6	26.31	2.238	0.8	71.28	1.894	1.4

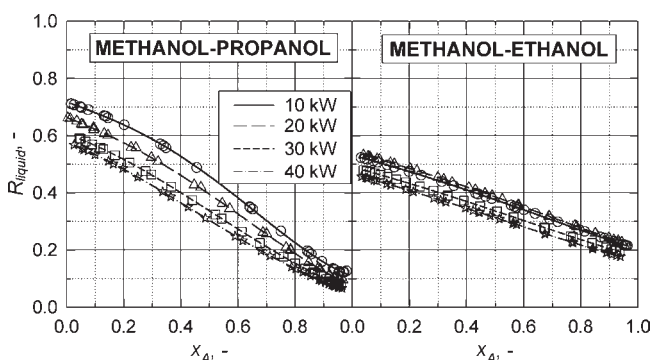


Figure 4. Relative liquid-side mass-transfer resistances calculated using $k_{L,a}$ and $k_{V,a}$ obtained by the profile method, using the RBF model with corrected dependence on the velocity of the phases, i.e., from eq 11 with $b_{L,PM}$, $b_{V,PM}$ taken from Table 6.

determined parameters b_L and b_V on the reboiler duty P was utilized.

$$\begin{aligned}
 b_L &\propto P^\lambda \propto u_L^\lambda \\
 b_V &\propto P^\nu \propto u_V^\nu
 \end{aligned}
 \tag{10}$$

The exponents λ and ν obtained by regression are shown in Table 5. The correcting values of the exponents presented in the table show that the RBF, BS, and DELFT models considerably underestimate the $k_{L,a}$ -dependence on the rate (positive exponents λ of about 0.4) and considerably overestimate the $k_{V,a}$ -dependence (negative exponents ν of about -0.5).

The best-fit parameters $b_{L,PM}$, $b_{V,PM}$ were obtained by the profile method, with the corrected dependence of the volumetric mass-transfer coefficients on the velocity of the phases, using the following relations in the place of the relation in eq 6 in the optimization procedure

$$\begin{aligned}
 k_{L,a} &= b_{L,PM} u_L^\lambda (k_{L,a})_{\text{model,orig}} \\
 k_{V,a} &= b_{V,PM} u_V^\nu (k_{V,a})_{\text{model,orig}}
 \end{aligned}
 \tag{11}$$

where index model = RBF, BS, or DELFT. The $b_{L,PM}$, $b_{V,PM}$, and the standard deviations s are given in Table 6. Practically the

identical s -values as in Table 3 demonstrate that the concentration profiles have the same accuracy as previously, but that the $b_{L,PM}$ and $b_{V,PM}$ values are now practically independent of the phase flow rates, and therefore the dependence of the coefficients on the rate is substantively better defined.

4.7. Relative Liquid-Side Mass-Transfer Resistance and HETP. Variations of the relative liquid-side mass-transfer resistance along the column, calculated from eq 12 using the RBF model with corrected dependence on the velocity of the phases, is shown in Figure 4. The resistance decreases from the base to the top of the column in all of the distillation systems used. The greatest change in the resistance occurs in the M–P system at the lowest reboiler duty of 10 kW (from 70 to 10%), and the least change occurs in the system M–E at the highest reboiler duty of 40 kW (from 45 to 15%). The changes are very similar to those revealed by the plug flow model.⁸

In any case, the variation of the relative resistance along the column, which underlies the applicability of the profile method for the separate evaluation of $k_{L,a}$ and $k_{V,a}$ from the concentration profile, is sufficient for its successful application.

$$R_{\text{liquid}} = \frac{m_A k_{V,a}}{k_{L,a} + m_A k_{V,a}}
 \tag{12a}$$

$$m_A = \frac{c_V x_A - K x_{Aw}}{c_L x_A - x_{Aw}} = \frac{c_V x_A - K x_{Aw}}{c_L x_A / K - x_{Aw}}
 \tag{12b}$$

where m_A is the local slope of the equilibrium curve.

4.8. $k_{L,a}$ and $k_{V,a}$ Original RBF, BS, and DELFT Models Corrected for the Dependence on the Phase Flow Rates by the Profile Method. The corrected values of the overall exponents ($\alpha + \lambda$) and ($\gamma + \nu$) are presented in Table 5. The encouraging fact is that the exponents differ very little for different models and distillation systems from each other. Their mean values $\bar{\alpha} + \bar{\lambda}$ and $\bar{\gamma} + \bar{\nu}$ are listed in Table 7 together with the mean scatters of individual values from the mean value. The scatters are small and lower than 9%. According to the profile method with axial dispersion model, $k_{L,a}$ depends on phase flow in accordance with the relation $k_{L,a} \propto u_L^{1.04}$, which is larger than what the original RBF, BS, and DELFT models predict (approximately $k_{L,a} \propto u_L^{0.58}$) but lower than what the plug flow model $k_{L,a} \propto u_L^{1.18}$ predicts and $k_{V,a}$ is dependent in accordance

Table 7. Mean Values of the Corrected Overall Exponents and the Best Fit Parameters

model	all systems RBF	all systems BS	all systems DELFT	all models and systems
$\alpha + \lambda$	0.999 ± 0.08	0.990 ± 0.08	1.13 ± 0.07	1.04 ± 0.07
$\beta + \nu$	0.550 ± 0.03	0.577 ± 0.03	0.592 ± 0.03	0.573 ± 0.03
$b_{L,PM}$	15.07 ± 5.6	9.31 ± 3.3	39.66 ± 21	
$b_{V,PM}$	1.58 ± 0.15	0.475 ± 0.04	1.96 ± 0.14	
$\bar{\lambda}$	0.417	0.259	0.679	
$\bar{\nu}$	-0.646	-0.583	-0.254	

with the relation $k_V a \propto u_V^{0.573}$, which is considerably less than what the original models predict (approximately $k_V a \propto u_V^{1.2}$) and lower than what the plug flow model predicts $k_V a \propto u_V^{0.771}$.

The best-fit parameters $b_{L,PM}$ and $b_{V,PM}$, presented in Table 6, differ for different models and distillation systems from each other to a larger extent than the difference between corresponding exponents ($\alpha + \lambda$) and ($\gamma + \nu$). Their mean values $\bar{b}_{L,PM}$ and $\bar{b}_{V,PM}$ are listed in Table 7 together with the scatters of the individual values. The scatters are large and reach up to 53%, whereas for the plug flow model they reached⁸ 35% at maximum. The large differences between b_{PM} parameters we ascribe to an improper description of an effect of the physical properties of the phases on the mass-transfer coefficients involved in the original RBF, BS, or DELFT model. The description cannot be improved until the data of the distillation systems with broader variance in their physicochemical properties has been obtained.

Making use of these mean values of the mean parameters and the exponents, the final forms of the mass-transfer correlations referred to in the literature, adjusted according to the profile method, are as follows.

The corrected RBF⁹ model,

$$(k_L a)_{PM,RBF} = 15.07(u_L)^{0.417}(k_L a)_{RBF,orig} \quad (13a)$$

$$(k_V a)_{PM,RBF} = 1.58(u_V)^{-0.646}(k_V a)_{RBF,orig} \quad (13b)$$

fits the experimental concentration profiles of all distillation systems utilized with the mean difference of 19.5% between the experimental concentrations and those concentrations calculated from the correlation (13), while the original RBF correlation was with 180%.

The corrected BS¹⁰ model,

$$(k_L a)_{PM,BS} = 9.31(u_L)^{0.259}(k_L a)_{BS,orig} \quad (14a)$$

$$(k_V a)_{PM,BS} = 0.475(u_V)^{-0.583}(k_V a)_{BS,orig} \quad (14b)$$

fits the profiles with the mean difference of 19.6%, while the original BS correlation was with 104%.

The corrected DELFT¹¹ model,

$$(k_L a)_{PM,DELFT} = 39.66(u_L)^{0.679}(k_L a)_{DELFT,orig} \quad (15a)$$

$$(k_V a)_{PM,DELFT} = 1.96(u_V)^{-0.592}(k_V a)_{DELFT,orig} \quad (15b)$$

fits the profiles with the mean difference of 18.8%, while the original DELFT correlation was with 125%. As elaborated in detail elsewhere,⁸ the present database is too narrow to allow us to come with a more appropriate nondimensional form of the correlations.

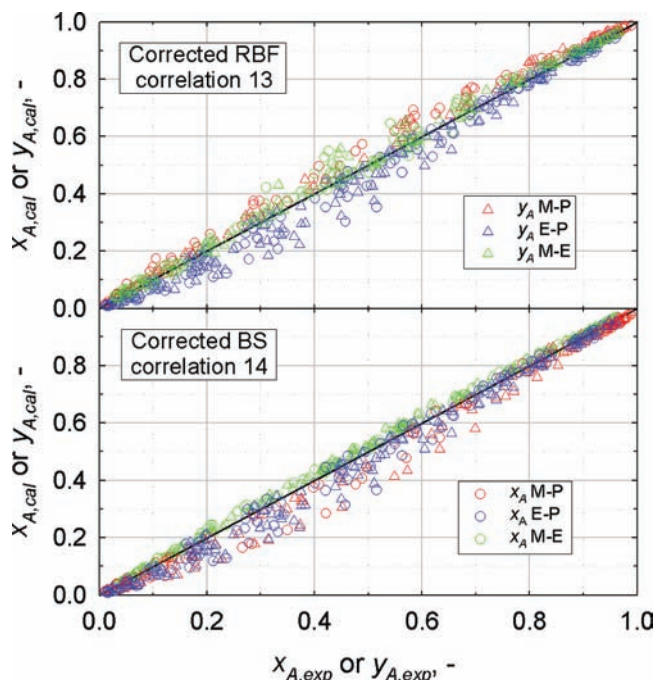


Figure 5. Comparison of the experimental concentrations with those calculated from the corrected RBF and BS models, i.e., from eqs 13 and 14, respectively.

In Figure 5, the experimental concentration profiles are compared with those calculated from the corrected RBF and BS models, i.e., from eqs 13 and 14, respectively, for all distillation systems used. Similar comparisons are shown for the original RBF and BS models in Figure 6. The most accurate are the fitted data of the M-E system and the least accurate those of the E-P system. The mean relative differences between the experimental concentrations and those concentrations calculated from eq 13 for the M-P, M-E, and E-P systems are 17.2, 14.7, and 26.6%, respectively, and from eq 14 for the same systems are 19.7, 14.7, and 24.3%. In any case, correlation 13 is much more precise than the original RBF and BS models with the mean deviations 37.5, 78, 87 and 198, 57.3, 57.7, respectively, for these same systems. A similar improved accuracy is shown in the DELFT model.

4.9. Relative Effects of $k_L a$, $k_V a$, Bo_L , and Bo_V on the Column Separation Efficiency. The parameters $k_L a$, $k_V a$, Bo_L , and Bo_V were studied for their relative effects on the designed column height H using the following relationship.

Relative effect R_{pi} of parameters pi ($i = 1$ to 4)

$$R_{pi}[\%] = 100 \cdot pi \frac{\Delta H}{\Delta pi} \bigg/ \sum_{j=1}^4 pj \frac{\Delta H}{\Delta pj};$$

$$pi = k_L a, k_V a, Bo_L, \text{ or } Bo_V \quad (16)$$

The ratios in the equation were evaluated by numerical derivation using the relative changes of the parameters $\Delta pi/pi = 0.1$. This expression represents the change of the column height H due to a 10% change of the parameter pi in relation to the sum of the changes induced by changes to all the parameters pi ($k_L a$, $k_V a$, Bo_L , and Bo_V). The results in Table 8 show that the effects of the parameters are not dependent on the separation efficiency of the

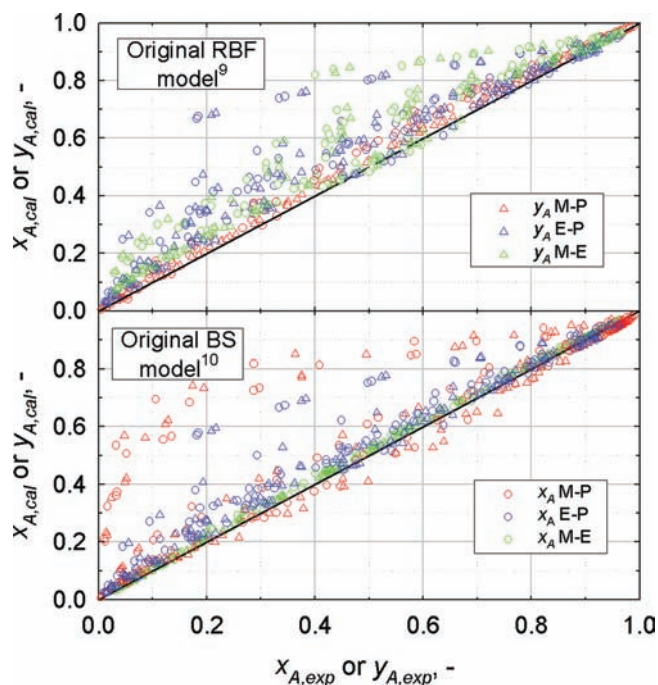


Figure 6. Comparison of the experimental concentrations with those calculated from the original RBF and BS models.

Table 8. Relative Effects of the Parameters $k_L a$, $k_V a$, Bo_L , and Bo_V on the Column Height H Using the RBF or BS Model with the Best Fit Parameters b_L and b_V Obtained by the Profile Method

model	P , kW	system	top–bottom H , m	mole fraction	relative effect of the given parameter, %			
					$k_L a$	$k_V a$	Bo_L	Bo_V
Mellapak 250Y								
RBF	40	M–E	2.06	0.84–0.16	24	58	16	2
			5.91	0.99–0.01	23	60	15	2
			9.02	0.999–0.001	22	60	16	2
10			2.34	0.983–0.10	22	39	38	1
Mellapak 250Y								
BS	40	M–P	1.97	0.95–0.05	19	69	10	2
			3.35	0.99–0.01	18	70	10	2
			2.77	0.9–0.10	21	61	16	2
10		M–P	2.60	0.99–0.01	25	44	29	2
			2.39	0.9–0.1	20	42	37	1
Intalox Saddles 25 ^a								
RBF	40	M–E	2.08	0.825–0.175	8	41	45	6
			8.84	0.998–0.002	6	39	50	5

^aData taken from our paper which is in preparation.

column and, not surprisingly, are very similar for all the models used though they differ with respect to structured or random packing.

For a column packed with Mellapak 250Y structured packing, the effect of $k_V a$ is predominant (60%), whereas axial mixing in vapor Bo_V has practically no effect (2%). The effect of $k_L a$

constitutes about 25%, and the effect of axial mixing of the liquid-phase Bo_L increases from about 15 to 40% with a decreasing liquid flow rate, at the expense of the effect of $k_V a$. For a column packed with Intalox saddles 25 random packing, the effects of mass transfer in vapor and of the liquid-phase axial mixing are predominant and are of the same size of 40%. The effects of $k_L a$ and of the axial mixing of the liquid-phase Bo_L are also of the same size of approximately 10%.

5. CONCLUSIONS

(1) In the profile method, the dependence of the coefficients $k_L a$ and $k_V a$ on phase flows and physicochemical properties has been considered in the form assumed in the RBF, BS, or DELFT original models. The application of the dispersion model increases both the liquid and the vapor mass-transfer coefficients in comparison with the plug flow model, but it does not diminish substantially the differences between the coefficients determined by the profile method and those calculated from the original models which remains in multiples.

(2) An effect of the convective flow of components induced by the total flow of the mixture through an interface was negligible. It reaches 6% at the most on the coefficients $k_L a$ and $k_V a$ in comparison with their values, evaluated assuming equimolar counterdiffusion.

(3) The axial dispersion model reproduces the experimental concentration profiles better than does the plug flow model. The difference between the experimental and the calculated concentrations is two times lower.

(4) The parameters Bo_L , Bo_V , $k_L a$, and $k_V a$ were studied for their relative effects on the designed column height made of the structured packing Mellapak 250Y. The effect of the axial mixing of the liquid Bo_L increases, at the expense of the effect of $k_V a$, from about 15 to 40% with a decrease in the liquid flow rate. The axial mixing of vapor Bo_V has practically no effect. The effect of $k_V a$ is predominant (60%), and that of $k_L a$ constitutes about 25%; i.e., the liquid-side mass-transfer resistance is not negligible (as it is usually assumed). It tends to decrease from the base to the top of the column in all the distillation systems used; the decrease is greatest in the M–P system at the lowest flow rate (from 70 to 10%), and the least change occurs in the system M–E at the highest flow rate (from 45 to 15%).

(5) The profile method with the axial dispersion flow model predicts $k_L a$ and $k_V a$ are less dependent on phase flow velocity ($k_L a \propto u_L^{1.04}$ and $k_V a \propto u_V^{0.573}$) in comparison with the dependences predicted with the plug flow model ($k_L a \propto u_L^{1.18}$ and $k_V a \propto u_V^{0.0771}$). An encouraging fact is that the exponents differ very little for different models and distillation systems.

(6) The best-fit parameters $b_{L,PM}$ and $b_{V,PM}$ evaluated by the profile method using this corrected dependence of the coefficients on the velocity of phases does not depend on reboiler duty, but they differ for the models (RBF, BS, or DELFT) and distillation systems from each other to a larger extent than the corresponding exponents ($\alpha + \lambda$) and ($\gamma + \nu$) differ. The differences between b_{PM} parameters we ascribe to an improper description of an effect of the physicochemical properties of the phases on the mass-transfer coefficients involved in the original RBF, BS, or DELFT model. The description cannot be improved until the data of the distillation systems with broader variance in their physicochemical properties have been obtained.

AUTHOR INFORMATION

Corresponding Author

* E-mail: linekv@vscht.cz (V.L.); valenzl@vscht.cz (L.V.).

ACKNOWLEDGMENT

Financial support from the Ministry of Education (Grant MSM 6046137306) is gratefully acknowledged. Sulzer Ltd. is acknowledged for providing the packing free of charge

NOMENCLATURE

a = effective specific mass-transfer area, 1/m
 a_p = specific geometrical area of the packing, 1/m
 B = superficial liquid velocity, m/h
 $Bo_j = u_{i,j}H/D_{e,j}$ ($j = L, V$), Bodenstein number
 b = parameter of axial dispersion model defined by eq 1
 $b_{L,PM}$ = empirical correction factors obtained by using eq 11 in the profile method, $(m/s)^{-\lambda}$
 $b_{L,V}$ = empirical correction factors obtained by using eq 6 in the profile method
 $b_{L,V,orig}$ = multiplication factors used in original models RBF, BS, and DELFT
 $b_{V,PM}$ = empirical correction factors obtained by using eq 11 in the profile method, $(m/s)^{-v}$
 c = molar concentration, mol/m³
 D_e = axial dispersion coefficient, m²/s
 d = packing characteristic dimension, m
 H = packing height, m
 HETP = height equivalent to a theoretical plate, m
 $Fi = \eta_L u_L / d^2 \rho_L g$
 $F_V = u_V \sqrt{\rho_V}$ gas capacity factor, Pa^{1/2}
 g = gravity acceleration, m/s²
 K_A = equilibrium coefficient in eq $y_A = K_A x_A$
 k_L = liquid-side mass-transfer coefficient, m/s
 k_V = vapor-side mass-transfer coefficient, m/s
 $k_{L,a}$ = liquid-side volumetric mass-transfer coefficient, 1/s
 $k_{V,a}$ = vapor-side volumetric mass-transfer coefficient, 1/s
 L = liquid-phase molar flow, kmol/s
 m_A = local slope of equilibrium curve $m_A = dc_{AV}^*/dc_{AL}^*$ defined by eq 12
 N = number of transfer units
 N_{AB} = molar flux transferred per unit height of packing, kmol/(m s)
 P = reboiler duty, kW
 pi = various process parameters ($k_{L,a}$, $k_{V,a}$, Bo_L , Bo_V)
 r = quantity defined by eq 3
 $Re_V = u_V d \rho_V / \eta_V$
 R_{liquid} = relative liquid-phase mass-transfer resistance calculated from eq 12
 R_{pi} = relative effect of parameter pi defined by eq 16, %
 S = column cross-section, m²
 $S_{i,L/V}$ = i-phase ($i = V, L$) flow cross-section, m²
 s = objective function defined by eq 7
 u_i = interstitial velocity ($i = V, L$), m/s
 u_j = superficial velocity ($j = V, L$), m/s
 V = vapor-phase molar flow, kmol/s
 x_A = mole fraction of more volatile component in liquid phase
 y_A = mole fraction of more volatile component in vapor phase
 z = packing height coordinate taken from top of the packing ($z = 0$), m

Subscripts

L = liquid phase

orig = original RBF, BS, or DELFT model

PM = profile method

p1 to p4 = $k_{L,a}$, $k_{V,a}$, Ba , Bo_V

true = corrected for the axial mixing effect

V = vapor/gas phase

w = vapor–liquid interface

Superscripts

α, β = exponents in relations 9

λ, v = exponents in relations 10

* = equilibrium value

Greek Symbols

α = corrugation angle, deg

η = viscosity, Pa s

ρ = density, kg/m³

REFERENCES

- Miyachi, T.; Vermeulen, T. Longitudinal dispersion in two-phase continuous-flow operations. *Ind. Eng. Chem. Fundam.* **1963**, *2*, 113.
- Furzer, I. A.; Ho, G. E. Differential backmixing in distillation columns. *Chem. Eng. Sci.* **1970**, *25*, 1297.
- Furzer, I. A.; Ho, G. E. Distillation in packed columns: The relationship between HTU and packed height. *AIChE J.* **1967**, *13*, 614.
- Steiner, L.; Barendrecht, H. P.; Hartland, S. Concentration profiles in a packed distillation column. *Chem. Eng. Sci.* **1978**, *33*, 255.
- Kolev, N.; Semkov, K. Über den Einfluss der Axialvermischung bei Rektifikationskolonnen mit ungeordneten Fullkoperschüttungen (On the influence of axial mixing in distillation columns with random packing). *Chem. Eng. Process.* **1985**, *19*, 175.
- Semkov, K.; Kolev, N. On the evaluation of the interfacial turbulence (the Marangoni effect) in gas (vapour)–liquid mass transfer. Part I. A method for estimating the interfacial turbulence effect. *Chem. Eng. Process.* **1991**, *29*, 77.
- Semkov, K.; Kolev, N. On the evaluation of the interfacial turbulence (the Marangoni effect) in gas (vapour)–liquid mass transfer. Part II. Modeling of packed columns accounting for axial mixing and Marangoni effects. *Chem. Eng. Process.* **1991**, *29*, 83.
- Rejl, F. J.; Valenz, L.; Linek, V. “Profile method” for the measurement of $k_{L,a}$ and $k_{V,a}$ in distillation columns. Validation of rate-based distillation models using concentration profiles measured along the column. *Ind. Eng. Chem. Res.* **2010**, *49*, 4383.
- Rocha, J. A.; Bravo, J. L.; Fair, J. R. Distillation columns containing structured packings: A comprehensive model for their performance. 2. Mass-transfer model. *Ind. Eng. Chem. Res.* **1996**, *35*, 1660.
- Billet, R.; Schultes, M. Prediction of mass transfer columns with dumped and arranged packings. Updated summary of the calculation method of Billet and Schultes. *TranslChemE* **1999**, *77*, 498.
- Olujic, Ž.; Kamerbeek, A. B.; de Graauw, J. A. Corrugation geometry based model for efficiency of structured distillation packing. *Chem. Eng. Process.* **1999**, *38*, 683.
- Fair, J. R.; Seibert, A. F.; Behrens, M.; Saraber, P. P.; Olujic, Z. Structured packing performance—Experimental evaluation of two predictive models. *Ind. Eng. Chem. Res.* **2000**, *39*, 1788.
- Valenz, L.; Rejl, F. J.; Linek, V. Gas and liquid axial mixing in the column packed with Mellapak 250Y, Pall rings 25, and Intalox saddles 25 under flow conditions prevailing in distillation columns. *Ind. Eng. Chem. Res.* **2010**, *49*, 10016.
- Linek, V.; Moucha, T.; Prokopova, E.; Rejl, J. F. Simultaneous determination of vapour- and liquid-side volumetric mass transfer coefficients in distillation column. *Chem. Eng. Res. Des.* **2005**, *83* (A8), 979.

Contents lists available at [ScienceDirect](http://www.sciencedirect.com)

Chemical Engineering Research and Design

journal homepage: www.elsevier.com/locate/cherd

Hydraulic and mass-transfer characteristics of Raschig Super-Pak 250Y

F.J. Rejl*, L. Valenz, J. Haidl, M. Kordač, T. Moucha

University of Chemistry and Technology Prague Technická 5, 166 28 Praha 6, Czech Republic

ARTICLE INFO

Article history:

Received 17 October 2014

Received in revised form 16 March 2015

Accepted 14 April 2015

Available online 20 April 2015

Keywords:

Absorption

Mass transfer

Structured packing

Raschig

Super-Pak

ABSTRACT

Our paper presents hydraulic, hydrodynamic and mass-transfer characteristics of the Raschig Super-Pak 250Y high-capacity structured packing measured under absorption conditions. The measurements were performed in the absorption column of inner diameter of 0.29 m using proven aqueous test systems. Measured data reveal excellent gas-phase mass-transfer performance and improved hydraulic behavior which is in agreement with the data provided by the vendor. There was found significant degree of the liquid-phase axial mixing on the packing. All six packing constants of the model proposed by [Billet and Schultes \(1999\)](#) were evaluated. The HETP values for distillation of C_6/C_7 and methanol/*n*-propanol mixtures were predicted using the BS-model with the evaluated constants and plug flow assumption. Predicted HETPs were found to be in a poor agreement with those measured under distillation conditions. However, we do not address this disagreement to fundamental impropriety of the test systems or the inability of the BS model to transfer the data from absorption conditions to distillation ones. We demonstrate that rather accurate values of HETP can be obtained when the influence of the liquid phase axial mixing is involved into the HETP prediction. The need for incorporation of the more sophisticated hydrodynamic models into simulation software becomes evident.

© 2015 Published by Elsevier B.V. on behalf of The Institution of Chemical Engineers.

1. Introduction

The structured packings exhibit low pressure drop and excellent capacity per efficiency unit and therefore are widely used in the chemical industry. After the packings made of wire gauze (Sulzer BX, CY) for the manufacture less demanding variants made of metal sheets have been introduced. Sulzer's Mellapak 250Y is a classical example of the structured packing of this generation and is considered a standard.

In the late 1990s a new structured packings generation evolved which provided substantially better capacity with only marginally decreased separation efficiency. This so called high-capacity packings have channels bended to the vertical direction near the packing element edges and thus reduce sudden changes of the gas velocity at the element interface, where the flooding of the bed is normally initiated. Sulzer's

Mellapak 252Y or Koch-Glitsch's Flexipac HC are typical examples of this class of packing.

Another approach to the high-capacity packing design has been adopted by Raschig Company with its Raschig Super-Pak packing (RSP 250Y). The packing is fundamentally different to the well known corrugated perforated or non-perforated, textured sheet metal structured packings. It consists of a systematic sequence of smooth sinusoidal waves above and below the plain of the metal sheet ([Chambers and Schultes, 2007](#)). As both the sides of the channel are formed by the single sheet of the metal which alternately forms its upper and lower side, the channels are 50% open and thus the intense radial mixing of the phases can be anticipated.

The design of the packed columns can be based on two basic distinctive approaches. (1) stage-wise approach utilizing the concept of the height of the packing equivalent to the

* Corresponding author. Tel.: +420 220 44 3299.

E-mail address: frantisek.rejl@vscht.cz (F.J. Rejl).<http://dx.doi.org/10.1016/j.cherd.2015.04.014>

0263-8762/© 2015 Published by Elsevier B.V. on behalf of The Institution of Chemical Engineers.

Nomenclature

a	effective interfacial area (m^2/m^3)
a_g	geometrical area of the packing (m^2/m^3)
B	superficial liquid velocity (m/h)
Bo_L	Bodenstein number of the liquid phase; $Bo_L = \frac{u_L H}{h_L E_L}$
$C_L, C_V, C_{P,0}, C_S, C_{F1}, C_H$	packing characteristic constants in Billet and Schultes model
d	diameter (m)
d_{eq}	packing characteristic diameter; $d_{eq} = 4\epsilon/a_g$ (m)
D	diffusion coefficient (m^2/s)
E	axial dispersion coefficient (m^2/s)
Fi_L	film number of the liquid phase; $Fi_L = \frac{u_L S \mu_L}{d_{eq}^2 \rho_L g}$
H	height of the packing (m)
$HETP$	height of the packing equivalent to the theoretical plate (m)
h_L	liquid hold-up (m^3/m^3)
$k_L a$	volumetric mass-transfer coefficient in the liquid phase (s^{-1})
k_G	mass-transfer coefficient in the gas phase (m/s)
$k_G a$	volumetric mass-transfer coefficient in the gas phase (s^{-1})
$N_{eq, stages}$	number of equilibrium stages
$\Delta p/H$	specific pressure drop (Pa/m)
u	phase velocity (m/s)
Indexes	
g	geometrical
G	gas phase
L	liquid phase
S	superficial
exp	experimental
$calc$	calculated
Greek symbols	
ϵ	packing void fraction (m^3/m^3)
ρ	density (kg/m^3)
μ	dynamic viscosity (Pa s)
θ	inclination of the channels from horizontal plane ($^\circ$)

theoretical plate, $HETP$. (2) Rate-based approach utilizing the mass-transfer coefficients and the effective interfacial area as a mass-transfer characteristic determining the packing mass-transfer performance.

Whatever design approach is chosen, the utilization of the specific packing desires knowledge of its hydraulic and mass-transfer characteristics. Uncertainty in this respect may necessitate undesirable overdesign. For the stage-wise concept the $HETP$ data needs to be measured for each new packing and system involved as the $HETP$ is not transferable to other conditions.

For the rate-based approach, which more closely relates packing separation efficiency with the individual physical phenomena on the packing, there exist elaborate models enabling estimation of the mass-transfer coefficients and the effective interfacial area for given physical properties, hydrodynamic conditions and packing geometry. The models are verified against experimentally obtained mass-transfer characteristics measured with the specific systems, preferably with those for which the mass-transfer rate is controlled

dominantly by single parameter (e.g. effective interfacial area only). Discussion of the suitable systems is performed e.g. in Hoffmann et al. (2007) and Onken and Arlt (1989).

The models may or may not involve packing specific constants which reflect the influence of the packing type geometry on the mass transfer. Classical example of such model incorporated also into the simulation software (e.g. Aspen Plus) is Billet–Schultes model (Billet and Schultes, 1999). This model involves six packing parameters which have to be evaluated out of the experimental data. These parameters are not published for the newer packings as there are no updates of the model published in the open literature. The aim of this paper is to provide hydraulic, hydrodynamic and mass-transfer characteristics of the metal RSP 250Y packing measured under absorption conditions with standard systems. In order to enable recalculation of the data to other conditions the Billet–Schultes model constants have been evaluated. Recalculation of the absorption data to the distillation conditions and their utilization for the distillation design is also discussed.

2. Literature survey and theory

The absorption mass transfer characteristics of RSP 250Y were measured previously by Wang et al. (2012) and Wang et al. (2014) in ID 0.42 m counter-current absorption column equipped with 108 drip points per square meter liquid distributor.

Their experimental methods are briefly described here:

For the effective area, a , determination they used CO_2 chemisorption into the lye. The experiments have been carried out with the $100 \text{ mol}/\text{m}^3$ initial concentration of the sodium hydroxide solution and the gas has been analyzed by IR analyzer. The physical quantities describing the reaction – mass-transfer phenomena have been acquired by independent experiments.

For the $k_L a$ measurements the stripping of toluene from the water into the air stream was used. The $k_L a$ data determined on the toluene/water system was recalculated to the oxygen/water system used in this work using

$$k_L a_{\text{O}_2} = k_L a_{\text{toluene}} \left(\frac{D_{\text{O}_2, \text{water}}}{D_{\text{toluene, water}}} \right)^{0.5} \quad (1)$$

The power of 0.5 used in Eq. (1) is taken from the penetration theory. Diffusivity of toluene, $D_{\text{toluene, water}} = 7.74 \times 10^{-10} \text{ m}^2/\text{s}$, and oxygen, $D_{\text{O}_2, \text{water}} = 1.83 \times 10^{-9} \text{ m}^2/\text{s}$, in water at 20°C were calculated using the method of Wilke and Chang taken from Reid et al. (1987).

The volumetric mass-transfer coefficient in the gas phase, $k_G a$, was measured using sulphur dioxide chemisorption into the lye. It is a standard system with negligible mass-transfer resistance in the liquid phase due to the instantaneous reaction of the sulphur dioxide at the interface (Rejl et al., 2009). Two analyzers calibrated to 0–100 ppm and 0–100 ppb SO_2 have been used for the inlet and outlet concentration determination.

The results of the experiments with the deep (3.05 m) bed provided in the Wang et al. (2012) paper were later found to be unreliable¹ by the their authors due to the significant effect of any water condensation in the outlet sample line, which was not fully eliminated even by the heating of the

¹ Correspondence with the authors.

sample line. Modified experimental procedure with reduced bed height and corresponding increase in the outlet SO₂ concentration (500–5000 ppb), which was less prone to the effect of the issue, revealed relative increase of the k_{Ga} results. The improved data has been published in the Wang et al. (2014).

The distillation performance of RSP 250Y has been tested by standard measurements of HETP at F.R.I. (column of ID 1.22 m) with C₆/C₇ and o-/p-xylene systems and at SRP (column of ID 0.42 m) with C₆/C₇ systems. The hydraulic characteristics were measured at SRP facility using air/water system. The liquid loads 0–73.44 m³/(m² h) and gas loads from 0 to 4 m/s were utilized. Both results were published by Chambers and Schultes (2007) and can be found also on the websites of the packing vendor (www.raschig.com/Rings-Downloads).

The recalculation of the data from the conditions given by the measuring system to the operational ones can be performed using some of the hydraulic/mass-transfer models. The models which do not utilize any packing specific constant could be used for comparison of the predicted and measured results, but adjustment of the mass-transfer model according to the experimental data is naturally more convenient for the models with intentionally introduced constants.

Out of the possible models we have chosen the BS model (Billet and Schultes, 1993, 1999). The BS model is incorporated in the Aspen Plus simulation software which enables the user to set the model constants to the arbitrary values. The model has been derived for random and structured packings and involves six packing specific constants (C_L , C_V , $C_{P,0}$, C_S , C_{FL} , C_h) which are related to the liquid phase mass-transfer, gas phase mass-transfer, dry and irrigated pressure drop, loading and flooding point specification and liquid hold-up calculation. The model assumes plug flow of both phases.

3. Experimental

The absorption and hydraulic measurements were performed in the counter-current atmospheric absorption column of 0.29 m inner diameter packed with four elements of the RSP 250Y (six for the dynamic experiments). The column is equipped with four openings in which sampling devices for the withdrawal of liquid and gas samples can be placed. Each element of the packing was horizontally drilled by electrical discharge machinery to enable installation of a sampling device for the withdrawal of the gas or liquid samples. The samples were withdrawn from sampling devices placed in the packing elements ($H=0.21, 0.42, 0.63$ m) or from those placed right above and below the packed bed ($H=0.94, 1.40$ m). Uniform liquid distribution over the cross-section of the column was carried out by the pipe-type liquid distributor with drip-point density of 630 drip points/m² together with 2 elements of Raschig Initial Distribution System. The gas phase was saturated with the water vapor, enriched with the tracer gas (SO₂ for the k_{Ga} and CO₂ for the a measurements) and fed to the absorption column through the large drum equipped with the lattice at the outlet which provided necessary pressure drop for stabilization of the gas flow. The inlet temperatures of both phases were maintained at 20 °C. Flow rate of the liquid phase (distilled water for the Δp , h_L , Bo_L and $k_{L,a}$ measurements or 1 kmol/m³ solution of NaOH for the k_{Ga} and a measurements) was measured with turbine flow meter; flow rate of air was determined on the basis of the pressure drop at the orifice plate. The tracer gas (k_{Ga} , a measurements) or nitrogen ($k_{L,a}$) flow rate was controlled by means of Bronkhorst low- Δp flow

meter. For more details of the column setup see Valenz et al. (2011) and Rejl et al. (2014).

Systems and methods used for the mass transfer and hydraulic measurements together with the methods of analysis and range of flow rates are given in Table 1. For detailed descriptions of the methods see the references listed in the table.

The distillation experiments with the methanol-*n*-propanol (M/P) and cyclohexane-*n*-heptane (C₆/C₇) test mixtures were performed in a stainless steel atmospheric distillation column with an inner diameter of 0.15 m (for more details see Rejl et al., 2010). The column was packed with nine pieces of the Raschig Super-Pak 250Y, to the height of 2.12 m. An electrically heated reboiler, equipped with an electric power regulator (up to 60 kW), was used to maintain a constant rate of boiling. The total condenser was mounted at the top of the column. Reflux flow was distributed on the packing using a pipe-type distributor with 25 openings (1472 drip points/m²); the reflux flow rate was determined using the turbine flow meter. Vapor from the reboiler was introduced into the column by a chimney type distributor with four chimneys regularly distributed over the column base cross section. The column was operated under the total reflux conditions. The samples of the liquid reflux and of the vapor entering and leaving the packed bed were withdrawn for the HETP determination. The samples taken during each run were analyzed immediately using the Atago RX5000 refractometer.

HETP values from the distillation data were calculated from the concentration of the vapor samples taken at the top and bottom of the packed bed. The stage-to-stage approach to the HETP calculation was used; the fraction of the last, incomplete equilibrium stage was calculated using the linear interpolation of the concentration between two closest complete stages. The HETP was calculated according to Eq. (2)

$$HETP_{\text{exp}} = \frac{H_{\text{exp}}}{N_{\text{eq.stages}}} \quad (2)$$

Prediction of the distillation HETP from the absorption data was based on the simulation of the vapor and liquid concentration profiles along the column using the differential model of a distillation (Rejl et al., 2010). The mass transfer coefficients were calculated using the BS model with the parameters (C_L , C_V , $C_{P,0}$, C_S , C_{FL}) evaluated from the absorption experiments (Table 3). The concentration profiles were calculated assuming: (1) the plug flow model in both phases, (2) the axial mixing in the liquid phase and the plug flow model in the vapor phase. The axial mixing in the liquid phase was described using the plug flow model with axial dispersion with the Bodenstein numbers calculated from Eq. (8). To enable a direct comparison of the calculated and experimental HETP values the experimental head and bottom concentrations and reflux flow rates were used as an input into the simulation.

The $HETP_{\text{calc}}$ values were calculated according to Eq. (3) with the value of H_{calc} obtained from the simulation.

$$HETP_{\text{calc}} = \frac{H_{\text{calc}}}{N_{\text{eq.stages}}} \quad (3)$$

² The data measured on the metal structured packing RSP 250Y are compared with the literature data available for metal random packing Pall Ring 25 and metal structured packing Mellapak 250Y.

Table 1 – Overview of systems and methods used for the mass transfer and hydraulic measurements.

Measurement	Method	Analysis	Flow rates	References
$k_L a$	Stripping of oxygen into the nitrogen stream; $H = 0.63$ m $H_{BED} = 0.94$ m	Oxygen dissolved in the water, Pre-Sens oxygen probes (0–21 kPa O_2)	$B = 5$ –100 m/h $u_G = 0.1$ m/s	Valenz et al. (2011)
$k_G a^*$	Absorption of SO_2 from the air into the NaOH solution; $H = 0.21, 0.42, 0.94$ m $H_{BED} = 0.94$ m	SO_2 in the air stream, SICK 710 IR spectrometer (15–3000 ppm SO_2) + Horiba AP5A-370 UV fluorescence analyzer (50–1000 ppb SO_2)	$B = 5$ –100 m/h $u_G = 0.5$ –3.0 m/s	Rejl et al. (2014)
a	Absorption of CO_2 from the air into the NaOH solution; $H = 0.63$ m $H_{BED} = 0.94$ m	CO_2 in the air stream, SICK 710 IR spectrometer (15–8000 ppm CO_2)	$B = 5$ –100 m/h $u_G = 0.5$ –3.0 m/s	Valenz et al. (2011)
Bo_L h_L	Dynamic method based on monitoring of the response on the step change of the tracer concentration (NaCl solution) in the inlet water; $H_{BED} = 1.40$ m	Conductivity	$B = 5$ –20 m/h $u_G = 0$ m/s	Valenz et al. (2010)
Δp	The pressure drop of air-water system; $H_{BED} = 0.94$ m	Digital manometer (0–1000 Pa)	$B = 24$ –75 m/h $u_G = 1.0$ –3.2 m/s	

* Most of the $k_G a$ data were measured on 0.21–0.42 m of the packing using SICK 710 analyzer for the determination of SO_2 concentration in the air at both, upper and lower, positions of the packed bed. Some experiments have been later repeated on 0.94 m of the packing (4 elements) using the Horiba AP5A-370 analyzer for determination of SO_2 in the air at the top of the packed bed. The $k_G a$ values measured on the higher bed agreed with those measured on the lower bed within 5%.

4. Results²

4.1. Effective interfacial area, a

In agreement with the general behavior of the packings the effective interfacial area of the RSP 250Y increases with the liquid velocity and is less dependent of the gas velocity (see Fig. 1, Eq. (4)). The effective area of the RSP 250Y is larger than its geometrical area for the liquid loads above $B \sim 10$ m/h which is in contrast with what was found for Mellapak 250Y and other structured packings. That implies that – at least for the higher liquid loads – some additional effective area is present over

that formed by the films flowing down the metal sheets. Formation of droplets can be the possible explanation. Depending on the liquid load, the effective interfacial area of the RSP 250Y is 20–50% higher than that of Mellapak 250Y.

$$a = 215 \cdot B^{0.0774} \cdot u_G^{-0.031} \quad (4)$$

The effective interfacial area data of the RSP 250Y are found 10% higher than the ones obtained by Wang et al. (2012) with the same system.

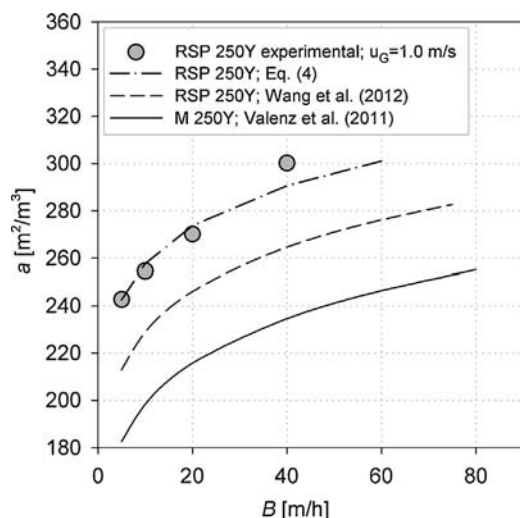


Fig. 1 – Comparison of experimental and from Eq. (4) calculated effective interfacial area, a . Comparison with the data published by Wang et al. (2012) and with data of Mellapak 250Y packing published by Valenz et al. (2011). All data presented for $u_G = 1.0$ m/s.

4.2. Volumetric mass-transfer coefficient in the liquid phase, $k_L a$

Resulting dependence of $k_L a$ on the liquid superficial velocity B follows approximately power law relation with the power of 0.662.

$$k_L a = 2.74 \times 10^{-3} \cdot B^{0.662} \quad (5)$$

The power law behavior corresponds well to that of the Mellapak 250Y and suggests common liquid phase mass-transfer mechanism for both packings. The absolute $k_L a$ values of the packings are quite similar up to the $B \sim 40$ m/h, at higher liquid loads the $k_L a$ of RSP 250Y are 10–15% larger (see Fig. 2). The $k_L a$ data has been correlated using BS model (Billet and Schultes, 1999) with the relative mean deviation of 16% and resulting C_L value is 1.446 (see Table 3).

The $k_L a$ data for RSP 250Y provided by Wang et al. (2012) recalculated to the nitrogen/oxygen/water systems according to Eq. (1) are $\sim 40\%$ lower.

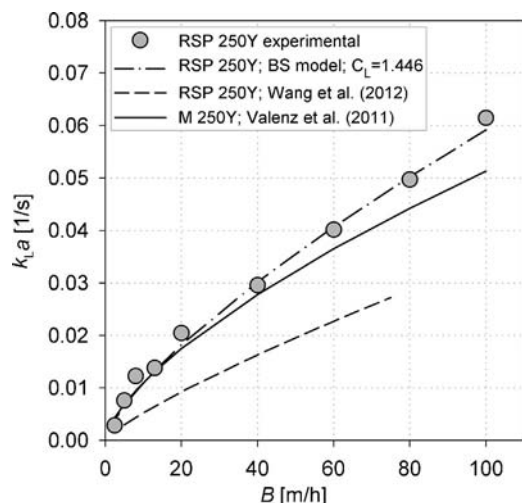


Fig. 2 – Comparison of experimental and from BS model (with parameters from Table 3) calculated volumetric mass-transfer coefficient in the liquid phase, $k_L a$. Comparison with the data published by Wang et al. (2012) and with data of Mellapak 250Y packing published by Valenz et al. (2011).

4.3. Volumetric mass-transfer coefficient in the gas phase, $k_G a$

The volumetric mass-transfer coefficient in the gas phase, $k_G a$, has been measured using chemisorption of the sulphur dioxide into the lye under various gas and liquid loads (see Fig. 3). Resulting $k_G a$ depend significantly on the gas-phase velocity and just slightly on the liquid one (Eq. (6)). The dependence of the $k_G = k_G a / a$ on the phase velocities evaluated from Eqs. (4) and (6) exhibits only negligible dependence on the liquid phase velocity (Eq. (7)).

$$k_G a = 8.394 \cdot B^{0.0632} \cdot u_G^{0.575} \quad (6)$$

$$k_G a = 39.86 \times 10^{-3} \cdot B^{-0.0258} \cdot u_G^{0.609} \quad (7)$$

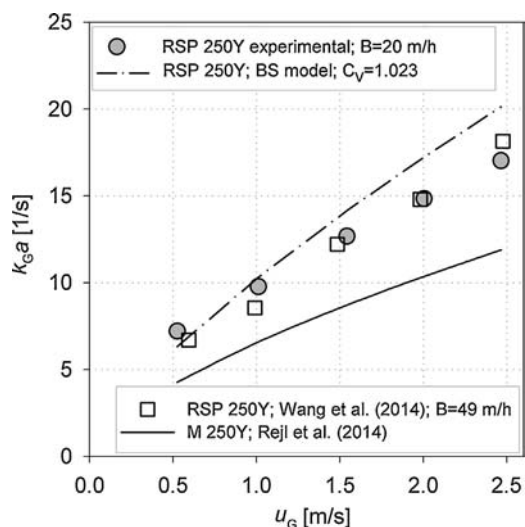


Fig. 3 – Comparison of experimental and from BS model (with parameters from Table 3) calculated volumetric mass-transfer coefficient in the gas phase, $k_G a$. Comparison with the data published by Wang et al. (2012) and with data of Mellapak 250Y packing published by Valenz et al. (2011). All data presented for $B = 20$ m/h.

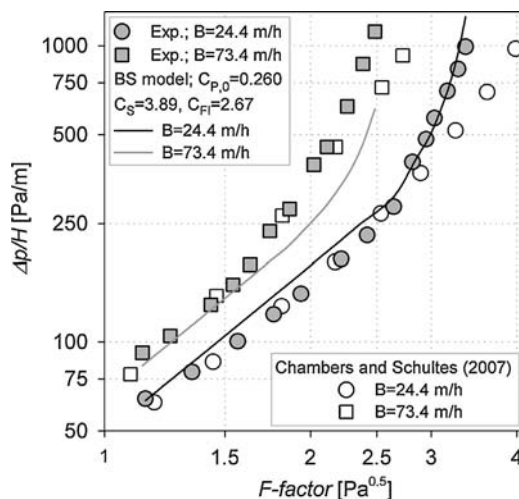


Fig. 4 – Comparison of experimental and from BS model (with parameters from Table 3) calculated specific pressure drop of the packing, $\Delta p/H$. Comparison with the data published by Chambers and Schultes (2007). Data presented for $B = 24.4$ m/h and $B = 73.4$ m/h.

The power of 0.609 in the dependence of the k_G on the gas velocity u_G agrees well with the results obtained on Mellapak 250Y (power of 0.642, see Rejl et al., 2014). It differs significantly, however, from the results obtained on the wetted-wall columns³ (power in range from 0.8 to 1.0) and from the dependences incorporated in many structured packing mass-transfer models (power in range from 0.7 to 1.0).

Resulting $k_G a$ are 40–80% higher than those of the Mellapak 250Y which is caused by both, higher effective interfacial area as well as higher mass-transfer coefficient k_G under similar phase flows. The $k_G a$ data of Wang (Wang et al., 2014) agree with the $k_G a$ data presented in this paper with an average error of 11%. Our data has been also correlated using BS model with relative mean deviation of 26% and resulting C_V value 1.023 (see Table 3). Relatively poor fit of the data by the BS model is caused by significantly larger effect of the liquid flow on the $k_G a$ values predicted by the BS model ($k_G a \sim B^{0.41}$) than was found experimentally. With the C_V of 1.023 the BS model predicts the $k_G a$ fairly well (relative mean deviation of 15%) for the liquid velocities in the range $B = 10$ – 20 m/h.

4.4. Specific pressure drop, $\Delta p/H$

The specific pressure drop of the packing has been measured under various gas and liquid loads (see Fig. 4) with the air-water system. The observed power law dependence of the specific pressure drop on the gas velocity with the power of 1.85–1.90 suggests gas flow regime close to the turbulent one. The obtained data correspond well with the ones published for RSP 250Y by Chambers and Schultes (2007) up to the loading point achieved at our column. The capacity is about 20% lower in comparison with these data possibly as a result of different experimental arrangement differing in the column inner diameter and packed bed height. The capacity of the packing is higher in comparison with M250Y packing

³ The flow of the gas phase through the structured packing is usually modeled as a flow through the short inclined channel (models of Olujic' et al., 1999; Rocha et al., 1996) with the correlations for the k_G adopted from the wetted wall column experiments.

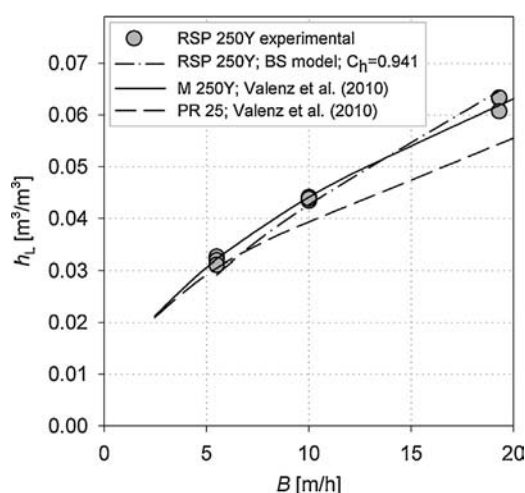


Fig. 5 – Comparison of experimental and from BS model (with parameters from Table 3) calculated total liquid hold-up, h_L . Comparison with the data of Mellapak 250Y structured packing and of Pall ring 25 random packing published by Valenz et al. (2010).

measured in the same column. The specific pressure drop values have been correlated using BS model with relative mean deviation of 16% and resulting hydraulic parameters, C_S , C_{F1} , C_{P0} , are summarized in Table 3.

4.5. Liquid hold-up, h_L

The comparison of total liquid hold-up, h_L , of the structured packings Raschig Super-Pak 250Y and Mellapak 250Y and random packing Pall ring 25 is shown in Fig. 5. The liquid hold-up increases with the power 0.63 of the liquid velocity and reaches 6% for $B=20$ m/h. Qualitatively as well as quantitatively the behavior matches that of Mellapak 250Y and is also very similar to that found for Pall ring 25, although the geometry of these packings differ significantly. As the effective interfacial area of the RSP 250Y is at least 20% higher than that of Mellapak 250Y, the equal hold-up is apparently formed by thinner films. C_h parameter of the value 0.941 has been evaluated out of the data (see also Table 3).

4.6. Axial mixing of the liquid phase (expressed as Bo_L parameter of the axial dispersion model)

Bodenstein numbers, Bo_L , of the structured packings Raschig Super-Pak 250Y and Mellapak 250Y and of the random packing Pall ring 25 (related to packing height $L=1$ m) are plotted in Fig. 6. For all the packings, the axial dispersion decreases (Bodenstein number increases) with increasing liquid velocity.

Values of the Bodenstein number reach the value of approx. 15 for liquid velocity $B=20$ m/h. In the entire flow range the values are about half of that found for Mellapak 250Y, implicating more significant axial dispersion of the liquid on the RSP 250Y packing. Axial dispersion is an undesirable phenomenon as it degrades efficiency of the separation equipment through reduction of the mass-transfer driving force, and in the limit, a column behaves like a single equilibrium stage (Henley et al., 2011).

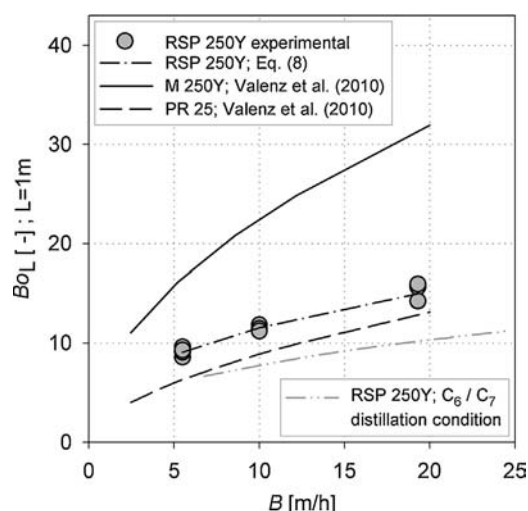


Fig. 6 – Comparison of experimental and from Eq. (8) calculated axial mixing in the liquid phase, Bo_L . Comparison with the data of Mellapak 250Y structured packing and of Pall ring 25 random packing published by Valenz et al. (2010).

The dimensionless correlation for the Bodenstein number in the form suggested by Macías-Salinas and Fair (1999) has been successfully used for correlation of the data resulting in

$$Bo_L = 0.0582 \cdot Fi_L^{0.398} \left(\frac{3}{\sin^2 \theta} \right)^{1.159} (d_{eq} a_g)^{6.337} \quad (8)$$

4.7. Distillation (HETP) data

For both distillation systems (methanol-*n*-propanol, cyclohexane-*n*-heptane) the dependence of the HETP on the F-factor exhibit expected behavior being almost constant in the preloading region and decreases when loading begins. For the C_6/C_7 system the mean value of the HETP in the preloading regime is 0.40 m, for M/P system it is 0.38 m.

Separation efficiency of the packing depends on the composition of the distilled mixture for the C_6/C_7 system, the HETP for the cyclohexane rich mixture are significantly higher than those for the mixture with low content of cyclohexane (Valenz et al., 2013). To eliminate this influence to the HETP only the values obtained at approx. 50 mol.% of cyclohexane in the middle of the packed bed are compared with the literature data.

The distillation data are compared with those measured at SRP of University of Texas and F.R.I at 1.62–1.65 bar for C_6/C_7 system. The absolute values of HETP are in very good agreement (especially with the F.R.I data) in the preloading region. In the loading region and just before flooding the SRP and F.R.I. HETP data tend to increase sharply which was not observed in our column (see Fig. 7). The different behavior in the loading and near flooding region could be perhaps explained by different column diameters.

The HETPs have also been calculated on the basis of the distillation column rate-based simulation using BS model with the constants taken from Table 3. As these constants were evaluated from the absorption experiments, comparison of the experimental HETP and those revealed by the simulation examines the mutual transferability of the data between absorption and distillation.

The HETPs calculated out of the simulations are barely half of the experimental ones when the plug-flow hydrodynamic model is used. On the other hand, when axial dispersion in the

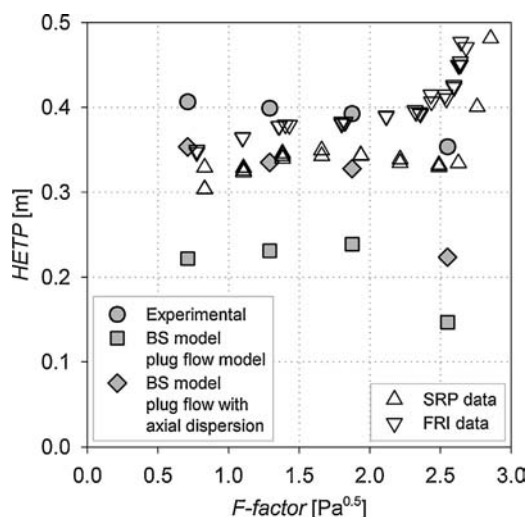


Fig. 7 – Comparison of experimental and from BS model (with parameters from Table 3) calculated distillation separation efficiency for C_6/C_7 system, HETP. Comparison with the experimental data measured by SRP and F.R.I.

liquid phase is taken into account, the out of simulation calculated HETPs match the experimental ones with only about 16% and 9% error (for C_6/C_7 (see Fig. 7) and M/P (see Fig. 8) system, respectively). The acquisition of the absorption mass-transfer data and their recalculation from absorption to the distillation conditions seems to be therefore successful in this particular case, but incorporation of the more sophisticated hydrodynamic model is clearly inevitable.

The C_V constant of the BS-model has been obtained with the SO_2 -NaOH system, for which the efficiency and the resulting volumetric mass-transfer coefficients are not diminished by the axial mixing of the liquid phase (due to the zero concentration of the solute at the interface). The C_L constant has been evaluated in the experimental setup exhibiting rather low number of the liquid phase mass-transfer units (1.4–3.5) and is therefore affected only slightly. The test systems therefore provide true values of the volumetric mass-transfer coefficients uncoupled with the hydrodynamic effects and

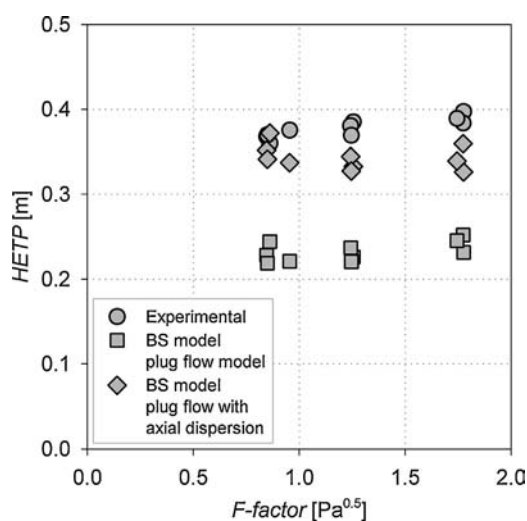


Fig. 8 – Comparison of experimental and from BS model (with parameters from Table 3) calculated distillation separation efficiency for M/P system, HETP, in the preloading regime.

Table 2 – Geometrical characteristics of the Raschig Super-Pak 250Y.

a_g (m^2/m^3)	ε (m^3/m^3)	d_{eq} (m)	θ ($^\circ$)
250	0.98	0.0157	45

these unaffected values also result from the BS-model with C_L , C_V constants listed in Table 2.

The use of these constants together with the plug flow model can be therefore recommended only for the simulation of the processes with low changes of the liquid phase concentration along the column, which are immune against axial dispersion effects. When the liquid phase axial dispersion is taken into account in the process simulation e.g. with the Bo_L values given by Eq. (8), the usage of the C_L , C_V constants given in Table 2 shall be appropriate universally.

5. Conclusions

Mass-transfer, hydraulic and hydrodynamic characteristics of the Raschig Super-Pak structured high-capacity packing has been measured using standard aqueous test systems in the ID 0.29 m absorption column. The data have been compared with those obtained for the standard first generation $250\text{ m}^2/\text{m}^3$ structured packing with 45° angle of corrugation (Mellapak 250Y). The results has been also used for optimization of the constants of the BS model, which are not presented in the literature and thus prevented the use of this model for the RSP 250Y packing e.g. in the simulation software.

Out of the measured characteristics of the packing we would like to stress its interfacial area which is found to be larger than its geometrical area for the liquid loads above $B \sim 10\text{ m/h}$ – what is in contrast with what was found on the Mellapak 250Y packing and resembles more the behavior of the random packings. It suggests that there exists some phenomenon forming additional mass-transfer area, possibly generation of the droplets. Depending on the liquid load the effective interfacial area of the RSP 250Y is 20–50% higher than that of Mellapak 250Y. The finding is also supported by the results of Wang.

But perhaps the most impressive quality of the packing is its gas-phase mass-transfer efficiency. The volumetric mass-transfer coefficient in the gas phase, $k_G a$, of the RSP 250Y is 40–80% higher than that of the Mellapak 250Y under the same conditions. The gas-phase efficiency of the RSP 250Y packing is exceptional and should be beneficial for the processes controlled solely by the gas-phase mass-transfer (e.g. fast chemisorptions). For other processes the usage of the presented C_V constant together with the plug flow model is not recommended.

From the mass-transfer modeling point of view the $k_G \sim u_G^{0.609}$ dependence suggests different mass-transfer mechanism in the gas-phase for the RSP 250Y packing from that which occurs in the wetted wall column and generally for the flows in the straight channels. As this is found also for Mellapak packings, rather different geometry, modeling of the structured packing as a set of the straight, independent tubular channels seems more convincingly to be inappropriate.

The specific pressure drop and the capacity of the RSP 250Y packing correspond to the packing “high capacity” character. Liquid hold-up of the packing is comparable with that found for the standard packing and for the random packing (Mellapak 250Y, Pall Ring 25). Interestingly, the axial mixing of the

Table 3 – Hydraulic and mass transfer parameters of Billet–Schultes model (Billet and Schultes, 1999).

Parameter	C_S	C_{Fl}	C_{p0}	C_h	C_L	C_V
Value	3.89	2.67	0.260	0.941	1.446	1.023
Mean relative deviation		16.4%		6.0%	15.8%	25.7%

liquid phase on the RSP 250Y is found to be approximately two times higher than that on the Mellapak 250Y.

The HETP data of the RSP 250Y packing for C_6/C_7 system obtained at three independent facilities correspond mutually in the preloading region. The distillation efficiency of the packing is similar to that found for the standard structured packing, which means, that the separation efficiency is not compromised by the high capacity gain of the packing. It seems probable that even better distillation efficiency is not found only because of the axial mixing of the liquid phase on the packing.

The HETP prediction for distillation of C_6/C_7 and M/P mixtures with the evaluated constants and plug flow assumption led to poor results. However, we do not address this disagreement to fundamental impropriety of the test systems or the inability of the BS model to transfer the data from absorption conditions to distillation ones. We demonstrate that reasonably accurate values of HETP can be obtained for the RSP 250Y packing when the influence of the liquid phase axial mixing is involved into the HETP prediction.

We would rather encourage the further development of the process simulation software with respect to the description of the phase hydrodynamics. It was shown that incorporation of the more sophisticated hydrodynamic models into the simulation software can lead to easier transferability of the data among the processes.

Acknowledgements

Authors are grateful to Raschig GmbH for providing of the packings, to the Czech Science Foundation for supporting the project through grant 13-01251S and for the financial support from Specific University Research (MSMT No 20/2015).

References

- Billet, R., Schultes, M., 1993. Predicting mass transfer in packed columns. *Chem. Eng. Technol.* 16, 1–9.
- Billet, R., Schultes, M., 1999. Prediction of mass transfer columns with dumped and arranged packings. Updates summary of the calculation method of Billet and Schultes. *Trans IChemE* 77 (Part A), 498–504.
- Chambers, S., Schultes, M., 2007. Reaching new performance levels with surface enhanced Raschig Super-Pak structured packings. In: 2007 Spring AIChE Meeting, Houston, Texas, April 22–26.
- Henley, E., Seader, J., Roper, D., 2011. *Separation Process Principles*. Wiley.
- Hoffmann, A., Maćkowiak, J.F., Górak, A., Haas, M., Loning, J.-M., Runowski, T., Hallenberger, K., 2007. Standardization of mass transfer measurements. A basis for the description of absorption processes. *Trans IChemE* 85 (Part A1), 40–49.
- Macías-Salinas, R., Fair, J.R., 1999. Axial mixing in modern packings, gas and liquid phases: I. Single-phase flow. *AIChE J.* 45 (2), 222–239.
- Olujic', Ž., Kamerbeek, A.B., de Graauw, J., 1999. A corrugation geometry based model for efficiency of structured distillation packing. *Chem. Eng. Proc.* 38, 683–695.
- Onken, U., Arlt, W., 1989. Recommended Test Mixtures for Distillation Columns, 2nd ed. Institution of Chemical Engineers.
- Reid, R.C., Prausnitz, J.M., Poling, B.P., 1987. *The Properties of Gases & Liquids*, 4th ed. McGraw-Hill Book Company, New York.
- Rejl, J.F., Linek, V., Moucha, T., Valenz, L., 2009. Methods standardization in the measurement of mass-transfer characteristics in packed absorption columns. *Chem. Eng. Res. Des.* 87, 695–704.
- Rejl, F.J., Valenz, L., Haidl, J., Kordač, M., Moucha, T., 2015. On the modeling of gas-phase mass-transfer in metal sheet structured packings. *Chem. Eng. Res. Des.* 93, 194–202.
- Rejl, F.J., Valenz, L., Linek, V., 2010. Profile method for the measurement of k_{La} and K_{Va} in distillation columns. Validation of rate-based distillation models using concentration profiles measured along the column. *Ind. Eng. Chem. Res.* 49, 4383–4398.
- Rocha, J.A., Bravo, J.L., Fair, J.R., 1996. Distillation columns containing structured packings: a comprehensive model for their performance. 2. Mass transfer model. *Ind. Eng. Chem. Res.* 35, 1660–1667.
- Valenz, L., Haidl, J., Linek, V., 2013. The effect of column diameter and packing height on the pressure. *Ind. Eng. Chem. Res.* 52, 5967–5974.
- Valenz, L., Rejl, F.J., Linek, V., 2010. Gas and liquid axial mixing in the column packed with Mellapak 250Y, Pall Rings 25, and Intalox Saddles 25 under flow conditions prevailing in distillation columns. *Ind. Eng. Chem. Res.* 49, 10016–10025.
- Valenz, L., Rejl, F.J., Šíma, J., Linek, V., 2011. Absorption mass-transfer characteristics of Mellapak packings series. *Ind. Eng. Chem. Res.* 50, 12134–12142.
- Wang, C., Perry, M., Seibert, A.F., Rochelle, G.T., 2014. Packing characterization for post combustion CO_2 capture: mass transfer model development. *Energy Procedia* 63, 1727–1744.
- Wang, C., Perry, M., Rochelle, G.T., Seibert, A.F., 2012. Packing characterization: mass transfer properties. *Energy Procedia* 23, 23–32.



Absorption in wetted-wall column with phase properties close to distillation conditions



J. Haidl^a, F.J. Rejl^{a,*}, L. Valenz^a, M. Kordač^a, T. Moucha^a, L. Labík^a, M. Schultes^b

^a University of Chemistry and Technology Prague, Technická 5, 166 28 Praha 6, Czech Republic

^b Raschig GmbH, Germany

HIGHLIGHTS

- Wetted wall column as a device with known interfacial area for absorption and distillation.
- Absorption experiments with distillation-like systems and flow rates.
- The mass-transfer coefficients dependent on the approx. square root of diffusivities for both phases.
- Quality of the diffusion coefficient data essential for k_L recalculation.

ARTICLE INFO

Article history:

Received 17 June 2015

Received in revised form

17 December 2015

Accepted 20 December 2015

Available online 6 January 2016

Keywords:

Absorption

Distillation

Mass transfer

Wetted-wall column

ABSTRACT

Our present research re-opens the problem of recalculation of the mass-transfer data between absorption and distillation by performing both processes in devices of the same geometry and using absorption and distillation systems whose physical properties are as similar as possible. The wetted wall column has been chosen as an experimental device which assures identical and known effective interfacial area for both processes. In this paper we present results of the absorption experiments while the follow up article will focus on the distillation ones and their mutual comparison. The liquid side mass-transfer coefficients were measured using desorption of oxygen from primary alcohols to the stream of nitrogen in the range of the liquid phase Reynolds numbers from 30 to 560. The experiments were carried out at ambient and at elevated temperatures providing the range of liquid phase Schmidt numbers from 66 to 1300. The gas phase mass-transfer coefficient was measured using absorption of sulfur dioxide from various carrier gasses—air, helium and sulfur hexafluoride—into the sodium hydroxide aqueous solution for Reynolds numbers from 300 to 11,800. Due to the significantly different properties of the carrier gases the range of the gas phase Schmidt number from 0.45 to 2.75 was achieved. The range of Reynolds numbers and Schmidt numbers covered by the absorption experiments overlaps the range of the distillation experiments, thus no extrapolation will be needed for the recalculation of the mass-transfer coefficients from absorption to distillation conditions. The results of the absorption experiments have been correlated in the dimensionless form $Sh_L = 0.33Re_L^{0.12}Sc_L^{0.47}$ and $Sh_G = 0.012Re_{LG}^{0.90}Sc_G^{0.61}$ with RSD of 6% and 4% respectively.

© 2016 Published by Elsevier Ltd.

1. Introduction

Distillation as well as absorption performed in packed column can be treated as similar process of simultaneous flow of liquid and gas phase on the packing accompanied with interfacial transfer processes (and optionally a chemical reaction). In principle both processes can be described by a unified general model describing identical set of individual phenomena with parameters

defined by identical functions of process conditions. More specifically – there should be possible to express mass transfer coefficients for individual by the same correlation for both processes. This assumption is utilized but has been never fully experimentally approved.

The general unified model valid simultaneously for absorption and for distillation is rarely used in its complete form for modeling of the processes as it is difficult to obtain all the necessary parameters. Individual phenomena do not have the same importance in these processes therefore the general model is simplified to fit the needs of each specific operation.

* Corresponding author. Tel.: +420 220 44 3299.

E-mail address: frantisek.rejl@vscht.cz (F.J. Rejl).

The parameters are obtained through experiments with the conditions set in a way that the process is sensitive to the specific parameter; we will denote them as “standard experiments”. Unfortunately the process conditions vary dramatically for standard absorption and distillation experiments. If the evaluated parameters are to be recalculated from one process to another, we need to know their dependence on the relatively broad range of conditions. The values of the parameters evaluated from absorption and distillation experiments may also diverge due to different effects of usual simplifications of the general model.

Not surprisingly, the results of recalculation of the parameters from absorption to distillation conditions are rarely accurate and the design of the packed distillation column on the basis of absorption experiments remains one of the Holy Grails of chemical engineering. The problem is therefore often revisited.

Our recalculation attempt is based on bringing the conditions of the standard absorption and distillation experiments as close together as possible. In an ideal case, the phase hydrodynamics and their physical properties would be the same. In order to minimize the number of phenomena which affect the process and to decrease unknown process parameters we decided to utilize the experimental apparatus for which the wet surface area is known, the wetted wall column.

Although the character of the liquid flow in the wetted wall column may not be uniform (rippling occurs in the whole range of the utilized liquid flows), we can say that the effective interfacial area in the column corresponds with the geometrical area much more accurately than in the packed column. Its utilization leaves us with the mass-transfer coefficients k_L , k_G as the only mass-transfer parameters of the processes.

Approaching the distillation conditions with standard absorption measurements and their recalculation to the distillation ones have been performed by interpolation in Reynolds and Schmidt numbers. Rationalization of the relation between mass-transfer, hydrodynamics and physical properties of the phases has been performed in the form of dimensionless criteria, namely Sherwood, Reynolds and Schmidt numbers. The absorption experiments were performed using such type of liquids and gases, and at such temperatures and flows, that the distillation mass-transfer coefficients k_L^{DIST} , k_G^{DIST} could be evaluated by interpolation in Reynolds and Schmidt numbers.

This paper presents the results of absorption experiments performed in the wetted wall column constructed in such a way that would make it usable both for absorption and distillation experiments. It provides values of liquid side mass-transfer coefficient k_L obtained by desorption of O₂ from cold and hot primary alcohols into the stream of nitrogen, and of gas side mass-transfer coefficient k_G obtained by chemisorption of SO₂ from He, N₂ and SF₆ into aqueous sodium hydroxide. It presents recalculation of this data to the conditions of atmospheric distillation of methanol-n-propanol mixture, which is intended for future distillation experiments.

2. Literature survey and theory

A wetted wall column is a device which was often used for the study of the mass transfer phenomena in packed absorption and distillation columns. Therefore, numerous papers dealing with the mass-transfer characteristics of this device under both absorption and distillation conditions can be found.

2.1. The mass transfer characteristics of the free falling liquid film

Mass transfer within liquid film has usually been studied by absorption/desorption of slightly soluble gas (O₂, CO₂, H₂, He) into

water (Emmert and Pigford, 1954; Kamei and Oishi, 1955; Kulov and Malysov, 1967; Krashennnikov and Durasova, 1958; Yih and Chen, 1982; Nielsen et al., 1998) or into organic solvents (alcohols, benzene, ethylene glycol solution) (Hikita et al., 1959; Won and Mills, 1982). The experimental data are usually published in a dimensionless form as the dependence of Sh_L on Re_L and Sc_L .

The characteristic dimensions used in Sh_L and Re_L in their standard form are the film thickness, δ , and the mean film velocity u_L . However, when used in the problems involving flowing films, substitution for these not easily measurable quantities is usually performed on the basis of the Nusselt's theory (Nusselt, 1916) replacing them with more convenient ones: diameter of the column, d , and mass flow related to the wetted perimeter, Γ . Resulting expression for Re_L is further multiplied by factor of 4 for the formal agreement with the definition of Re_G . Sh_L is divided by $\sqrt[3]{4}Re_L$. Throughout this article the following definition of the Reynolds and Sherwood number is therefore used:

$$Re_L = \frac{4\Gamma}{\mu_L} \quad (2.1)$$

$$Sh_L = \frac{k_L}{D_{12,L}} \sqrt{\frac{\mu^2}{\rho_L^2 g}} \quad (2.2)$$

Based on hydrodynamic studies, five regimes of the film flow can be distinguished (Brauer, 1958; Ishigai et al., 1972; Portalski, 1973). At very low values of Reynolds numbers ($Re_L < 20$) liquid flows in a smooth laminar layer with a semi-parabolic velocity distribution and with a film thickness described by the Nusselt's equations (Nusselt, 1916). Under these conditions the mass transfer in the film is caused only by the diffusion of the solute in the solvent, and the expressions for mass-transfer rate can be derived from Fick's law and material balance (Pigford, 1941). With the increasing value of Reynolds number, irregular waves appear on the film surface causing disturbances in the flow pattern and significant enhancement of the mass-transfer performance. For $Re_L = 20 - Re_{L,c}$ (pseudo-laminar regime) the film Sherwood number, Sh_L , increases with Re_L powered to $1/3 - 2/3$. As Re_L reaches the critical value $Re_{L,c}$ the flow regime changes to pseudo-turbulent¹ and Sh_L becomes almost independent of Re_L ; the power of Re_L varies between 0 and 0.2. The film flow becomes fully turbulent at $Re_L \approx 1200$ and the sharp increase of Sh_L with Re_L can be observed. In this regime the power of 0.6–1 at Reynolds number is observed. The critical Reynolds number at which the pseudo-laminar regime changes to the pseudo-turbulent depends generally on the system properties. According to Brauer (1958) $Re_{L,c}$ is a function of the liquid Kapitza number only

$$Re_{L,c} = 0.072Ka^{\frac{1}{3}} \quad (2.3)$$

while Hikita et al. (1959) proposed Eq. (2.4).

$$Re_{L,c} = 93.3Sc_L^{-0.24}Ga_L^{0.08} \left(\frac{\sigma}{0.072}\right)^{0.3} \quad (2.4)$$

While the dependence of Sh_L on Re_L changes with the flow regimes, the dependence $Sh_L \propto Sc_L^{0.5}$ is reported by most authors for all regimes. The results of Hikita et al. (1959) and Won and Mills (1982) show that the power of 0.5, which is in agreement with the penetration theory (Higbie, 1935) and VTDM (Henstock and Hanratty, 1979), holds also for non-aqueous systems where the change of Schmidt number is caused by the change of the solvent and not only of the solute.

¹ According to Ishigai et al. (1972) and Portalski (1973) two regimes – transitional and pseudo-turbulent – exist between the pseudo-laminar and fully turbulent regimes. However no such regime change can be observed on the mass-transfer characteristics.

Table 1
Overview of correlations for liquid phase Sherwood number.

Author	Correlation		System
Kamei and Oishi (1955)	$Sh_L = 4.6 \cdot 10^{-3} Re_L^{0.46} Sc_L^{0.58}$ ^a $Sh_L = 4.3 \cdot 10^{-2} Re_L^{0.18} Sc_L^{0.48}$ ^a $Sh_L = 1.2 \cdot 10^{-3} Re_L^{0.63} Sc_L^{0.52}$ ^a	$Re = 50\text{--}300$ $Re = 300\text{--}1400$ $Re > 1400$	CO ₂ /water at various temperatures
Hikita et al. (1959)	$Sh_L = 1.1 \cdot 10^{-2} \sigma_{rel}^{-0.15} Re_L^{0.5} Sc_L^{0.62} Ga_L^{-0.04}$ $Sh_L = 0.11 Sc_L^{0.5}$ $Re_{L,c} = 93.3 Sc_L^{-0.24} Ga_L^{0.08} \sigma_{rel}^{0.3}$ $\sigma_{rel} = \sigma/0.072$	$Re_L < Re_{L,c}$ $Re_L > Re_{L,c}$	CO ₂ /benzene, <i>n</i> -butanol, methanol and its aqueous solutions CO ₂ , Cl ₂ , SO ₂ , O ₂ , He and H ₂ S/water
Kulov and Malyusov (1972)	$Sh_L = 3.5 \cdot 10^{-3} Re_L^{2/3} Sc_L^{0.5}$ $Sh_L = 0.11 Sc_L^{0.5}$ $Sh_L = 11 \cdot 10^{-5} Re_L Sc_L^{0.5}$	$Re_L = 40\text{--}180$ $Re_L = 180\text{--}1000$ $Re_L > 1000$	CO ₂ /water
Won and Mills (1982)	$Sh_L = 8.7 \cdot 10^{-2} Re_L^{0.20} Sc_L^{0.36}$ ^a $Sh_L = 6.97 \cdot 10^{-9} Re_L^n Sc_L^{1-\alpha} Ka^{0.5}$ $n = 3.49 Ka^{-0.068}$ $\alpha = 0.137 Ka^{0.055}$	$Re = 500\text{--}2000$ $Re > 2000$	CO ₂ /methanol, water, <i>n</i> -propanol H ₂ , O ₂ , CO ₂ /ethanol
Yih and Chen (1982)	$Sh_L = 1.1 \cdot 10^{-2} Re_L^{0.40} Sc_L^{0.5}$ $Sh_L = 3.0 \cdot 10^{-2} Re_L^{0.21} Sc_L^{0.5}$ $Sh_L = 9.8 \cdot 10^{-4} Re_L^{0.68} Sc_L^{0.5}$	$Re_L = 49\text{--}200$ $Re_L = 200\text{--}1600$ $Re_L = 1600\text{--}10,500$	CO ₂ , O ₂ , H ₂ , He/water
Nielsen et al. (1998)	$Sh_L = 0.016 Re_L^{0.43} Re_G^{0.66} Sc_L^{0.5} \left(\frac{\mu^2}{\rho^2 g d^3} \right)^{1/3}$	$Re_L = 4000\text{--}12,000$ $Re_G = 7500\text{--}18,300$	O ₂ /water

^a The equation is not given in the paper and was obtained by correlation of original data.

Hikita et al. (1959) and Won and Mills (1982) also evaluated the influence of the liquid surface tension on Sh_L . Hikita et al. (1959) report the dependence $Sh_L \propto \sigma^{-0.15}$ for the pseudo-laminar regime and no distinguishable dependence for the pseudo-turbulent regime. For the turbulent film, Won and Mills (1982) observed a significant influence of the liquid Kapitza number on Sherwood number and proposed a rather complicated correlation for the prediction of Sh_L for both aqueous and organic systems (see Table 1).

2.2. The gas-phase mass-transfer characteristics

For the gas (fluid in general) flowing through the column there are two limiting regimes of the flow which can usually be distinguished according to gas Reynolds number, Re_G . At low values of Re_G the flow is assumed laminar with parabolic velocity profile. As Reynolds number increases, the flow pattern becomes more irregular and for $Re_G > 10,000$ the flow is usually assumed to be fully turbulent with a flat velocity profile. The transition between laminar and turbulent regime starts at $Re_G \approx 2000$ (Figs. 1 and 2).

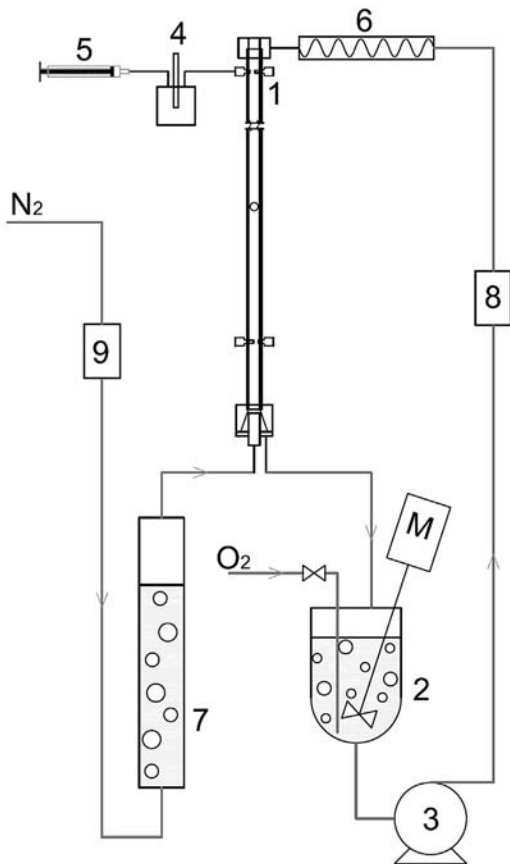
The gas phase mass-transfer characteristics of the wetted wall column in transitional and turbulent regime were usually experimentally studied by evaporation of pure liquids and their mixtures into the air stream (Gilliland and Sherwood, 1934; McCarter and Stutzman, 1959; Kafesjian et al., 1961; Strumillo and Porter, 1965; Crause and Nieuwoudt, 1999), by absorption (Nielsen et al., 1998) and by distillation (Johnstone and Pigford, 1942; Jackson and Ceaglske, 1950). The experimental data are usually correlated in a dimensionless form. A list of correlations is given in Table 2. Gilliland and Sherwood performed extensive measurements of the rate of vaporization of nine liquids into the air in the range of $Re_G = 2000\text{--}40,000$. They found that Sh_G increases with Re_G powered to 0.83 and with Sc_G powered to 0.44. Their data were taken by Chilton and Colburn (1934) and correlated together with the

pressure drop and heat transfer data in terms of j -factors resulting in the dependence $Sh_G \propto Sc_G^{1/3}$ which is in agreement with the boundary layer mass transfer model. The dependence $Sh_G \propto Sc_G^{0.5}$ was found by Crause and Nieuwoudt (1999) who used evaporation of seven solvents in a short column. While the power of the gas phase Reynolds number found by various authors varies significantly—from 0.68 to 1.05, the predictions of Sh_G , according to individual authors, provide similar results (see Fig. 8).

3. Experimental

Two glass columns of ID 25 mm (geometrical area $a_G = 4/d = 160 \text{ m}^2/\text{m}^3$) and lengths of 1.4 m and 2.1 m were used. The columns are equipped with 5 (7) pairs of holes which enable placing the liquid and gas sampling devices along the column. Each pair consists of two holes positioned on the opposite sides of the column and it is rotated by 90 degrees with respect to the previous one. The distance between the sampling points is 30 cm; the first sampling point is approx. 5 (15) cm below the upper edge of the column. The liquid and gas sampling devices are PVDF plugs with the openings which enable placing the oxygen probes and the withdrawal of the liquid and gas samples from the column (see Fig. 4).

The liquid is fed to the inner wall of the column by means of 8 needles which are inserted into the liquid distributor body. The needles of inner diameter of 0.8 mm and of length of 25 mm are aligned tangentially with respect to the column perimeter and inclined by 30 degrees with respect to the column axis (see Fig. 3). With this installment the liquid flow entering the column has tangential component of the velocity which ensures fusion of individual rivulets into the uniform liquid film along the whole perimeter at the top of the column. It was visually observed that the rotation of the liquid along the column perimeter is suppressed via the viscous forces before the liquid reaches the first



1 - glass column, 2 - stirred vessel, 3 - gear pump, 4 - measuring cell, 5 - syringe pump, 6 - glass heat exchanger, 7 - bubbled column, 8 - liquid flow meter, 9 - gas flow meter

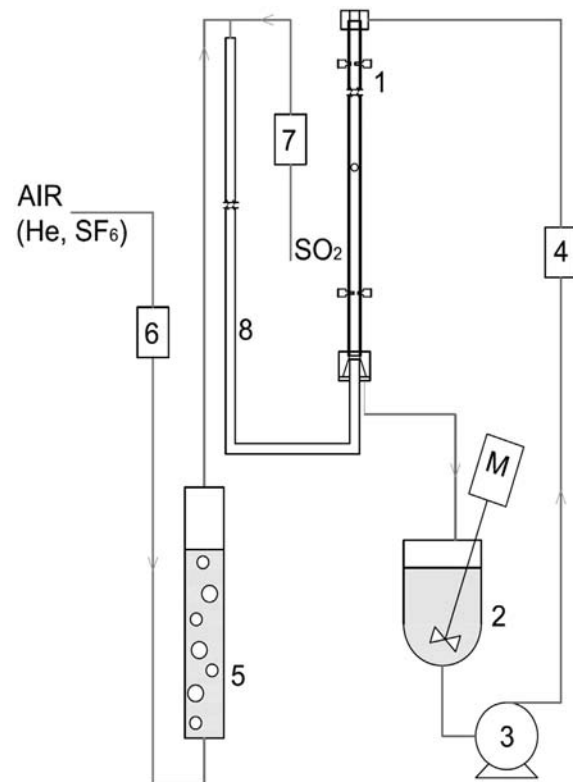
Fig. 1. The experimental setup for k_L measurements – desorption of oxygen from liquid into the nitrogen stream.

sampling point. The liquid distributor is capable of providing a stable wavy film for the flow rates higher than 110 ml/min for pure water and 80 ml/min for NaOH solution and organic solvents.

At the bottom of the column, the liquid collector/gas distributor was placed. During the measurements the column was equipped with both liquid and gas sampling devices providing the same setup as will be used for distillation experiments.

Before each set of measurements the column was dismantled, purged with chromic acid and distilled water. The vertical position of the column was checked with a plumb bob with the maximal allowed declination of 0.5 mm/m. For the measurements performed at elevated temperatures the column was insulated with a heating jacket. Liquid was fed to the column by means of a micro-gear pump. The flow rate of the liquid was controlled using the Bronkhorst mini-CoriFlow flow-meter (up to 36 kg/h). The gas phase entering the column (N_2 for the k_L measurements; air, He, SF_6 for hydraulics and k_G measurements) was saturated with vapors of the absorption liquid at the desired temperature in the bubble column. The flow rate of the gas phase was controlled with two Bronkhorst flow-meters (4–46 l/min and 20–200 l/min of air).

The conditions utilized for the measurements were chosen with respect to the conditions expected in the distillation column: $Q_L=80\text{--}320$ ml/min, $Re_L=100\text{--}400$, $Sc_L \approx 130$, $u_G=1.5\text{--}6$ m/s, $Re_G=5000\text{--}20,000$, $Sc_G=0.5\text{--}1$.



1 - glass column, 2 - stirred vessel, 3 - gear pump, 4 - liquid flow meter, 5 - bubbled column, 6 - gas flow meter, 7 - tracer gas flow meter, 8 - mixing tube

Fig. 2. The experimental setup for k_G and a_{eff} measurements – absorption of SO_2 and CO_2 from carrier gas into the NaOH solution.

3.1. k_L measurement

The k_L was measured by the desorption of O_2 from the liquid into the stream of nitrogen in the 1.4 m long column. The absorption liquid (water, methanol, ethanol, *n*-propanol, *n*-heptane and equimolar mixture of methanol and *n*-propanol) was saturated with pure oxygen at the desired temperature in the large (approx. 10 l), tempered and well stirred vessel and fed to the column. An additional glass exchanger was installed in the very front of the liquid distributor to ensure that the liquid entering the column had the desired temperature. Flow rates from 60 up to 600 ml/min and temperatures from 20 to 75 °C were used (the complete list of conditions is given in Table 3). The liquid samples were withdrawn from the column (the top and bottom samples were taken from the sampling points located on the same side of the column, $h=0.6$ m) to the tempered cell containing the optical oxygen probe. The flow rate of the liquid withdrawn from the column was maintained by means of the syringe pump at 1.5 ml/min. The oxygen probe was calibrated to measure the partial pressure of the O_2 from 1 to 100 kPa. The list of conditions used during the measurements is given in Table 3. The local k_L for each pair of sampling points was calculated from the partial pressure of oxygen from Eq. (3.1). The k_L for each series of conditions was taken as the average of the local values measured along the column.

$$k_L = \frac{Q_L}{\pi \cdot d \cdot h} \ln \left(\frac{p_{O_2, \text{top}}}{p_{O_2, \text{bottom}}} \right) \quad (3.1)$$

Table 2
Overview of correlations for gas phase Sherwood number.

Gilliland and Sherwood (1934)	$Sh_G = 0.023 Re_G^{0.83} Sc_G^{0.44}$	$Re_G > 2000$ $Sc_G = 0.6-2.26$	Evaporation of nine solvents into the air
Chilton and Colburn (1934)	$Sh_G = 0.029 Re_G^{0.78} Sc_G^{1/3}$	$Re_G > 30,000$	Distillation of five binary systems
Johnstone and Pigford (1942)	$Sh_G = 0.0328 Re_G^{0.77} Sc_G^{1/3} \left(\frac{u_G}{u_G + 1.5u_L} \right)^{0.23}$	$Re_G = 4000-30,000$	
McCarter and Stutzman (1959)	$Sh_G = 0.024 Re_G^{0.8} Sc_G^{0.4} \left(\frac{u_G + 1.5u_L}{u_G} \right)^{0.8}$	$Re_G = 3000-40,000$	Evaporation of seven solvents into the air
Kafesjian et al. (1961)	$Sh_G = 0.0065 Re_G^{0.83} Re_L^{0.15} \left(\frac{p}{p_{air}} \right)$	$Re_G = 2000-20,000$ $Re_L = 25-1200$	Evaporation of water into the air
Strumillo and Porter (1965)	$Sh_G = 0.0093 Re_G^{0.68} Re_L^{0.34} \left(\frac{p}{p_{air}} \right)$	$Re_G = 3000-10,000$ $Re_L = 100-800$	Evaporation of carbon tetrachloride into the air
Nielsen et al. (1998)	$Sh_G = 0.00031 Re_G^{1.05} Re_L^{0.207} Sc_G^{0.5}$	$Re_G = 7500-18,300$ $Re_L = 4000-12,000$	Absorption of SO ₂ from air into the sodium hydroxide sol
Crause and Nieuwoudt (1999)	$Sh_G = 0.00283 Re_G Sc_G^{0.5} Re_L^{0.08}$	$Re_G = 2000-10,000$	Evaporation of seven liquids into the air (short tube)

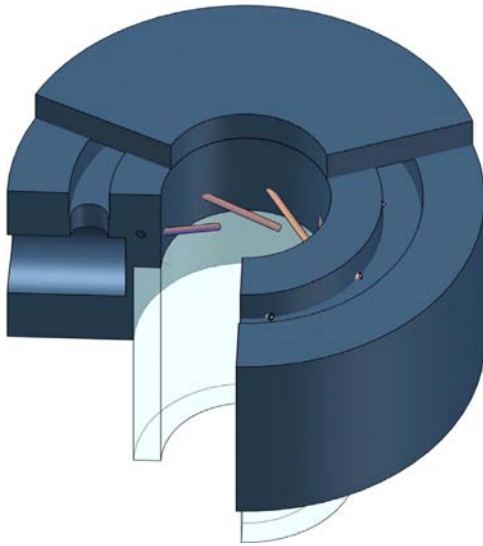


Fig. 3. The liquid distributor.

3.2. k_G measurement

The k_G measurements were performed in 2.1 m long column using the SO₂/NaOH system known for its negligible mass-transfer resistance in the liquid phase (Rejl et al., 2009). For those measurements a 0.6 m long glass tube of 25 mm inner diameter was installed below the gas distributor providing the calming section for the gas flow which should be sufficient for the velocity profile development. Three carrier gases (air, He, SF₆) saturated with the vapors of water at 20 °C were utilized providing a wide range of the gas phase physical properties ($Sc_G = 0.45-2.75$). SO₂ was injected into the carrier gas in a 2.5 m long mixing tube before entering the column. The gas samples collected from the column (sample points distance, $h = 1.8$ m) were dried by magnesium perchlorate and analyzed by IR spectrometer Sick S710 calibrated for the range of 30–3000 ppm of SO₂. Eq. (3.2) was used for the k_G calculation (Table 4).

$$k_G = \frac{u_G \cdot d}{4 \cdot h} \ln \left(\frac{c_{SO_2, bottom}}{c_{SO_2, top}} \right) \quad (3.2)$$

3.3. a_{eff} measurement

The effective interfacial area, a_{eff} , was measured using the air/CO₂/NaOH system according to the recommendation of Rejl et al. (2009). The same column setup as for the k_G measurement was used, the gas samples were dried by calcium dichloride and analyzed by the IR spectrometer calibrated for the range of 800–

Table 3
Overview of conditions used in the k_L measurements.

Methanol	Ethanol	<i>n</i> -Propanol
20 °C: $Sc_L = 136$; $Re_L = 250-430$	20 °C: $Sc_L = 417$; $Re_L = 40-310$	20 °C: $Sc_L = 1166$; $Re_L = 30-170$
40 °C: $Sc_L = 82$; $Re_L = 130-400$	40 °C: $Sc_L = 200$; $Re_L = 120-460$	40 °C: $Sc_L = 490$; $Re_L = 40-330$
50 °C: $Sc_L = 66$; $Re_L = 560$	60 °C: $Sc_L = 109$; $Re_L = 260-520$	60 °C: $Sc_L = 235$; $Re_L = 160-320$
		75 °C: $Sc_L = 147$; $Re_L = 280-410$
Water	<i>n</i> -Heptane	Methanol–propanol mixture ^a
20 °C: $Sc_L = 514$ $Re_L = 100-400$	20 °C: $Sc_L = 87$; $Re_L = 360-540$	20 °C: $Sc_L = 344$; $Re_L = 170-330$
		40 °C: $Sc_L = 186$; $Re_L = 335$

^a 50 mol% of methanol.

8000 ppm of CO₂. The concentration of the NaOH (1 kmol/m³) was determined by titration with HCl solution. For conditions where the mass-transfer resistance is concentrated only in the liquid film the effective interfacial area can be calculated by Eq. (3.3). The parameter of $K_a = 0.00243$ m/s related to 1 kmol/m³ NaOH solution was determined independently by still level experiments.

$$a_{eff,0} = \frac{u_G}{h \cdot K_a} \ln \left(\frac{c_{CO_2, bottom}}{c_{CO_2, top}} \right) \quad (3.3)$$

The influence of the gas-phase mass-transfer resistance was taken into the account and the value of $a_{eff,0}$ was therefore re-evaluated according to Eq. (3.4).

$$a_{eff} = \left(\frac{1}{a_{eff,0}} - \frac{K_a}{k_g a} \right)^{-1} \quad (3.4)$$

The $k_g a$ values of CO₂/air system in Eq. (3.4) were calculated using Eq. (4.6).

4. Results

4.1. Liquid phase diffusivity data

The value of Sherwood numbers calculated from the experimental k_L data as well as the front factor and the power at the Schmidt number in Eq. (4.1) depend on the diffusivity data which are generally known and reliable only for some, mostly aqueous systems. As there are only a few data on diffusivities of gases in cold alcohols (which, in addition, often differ by more than 20%)

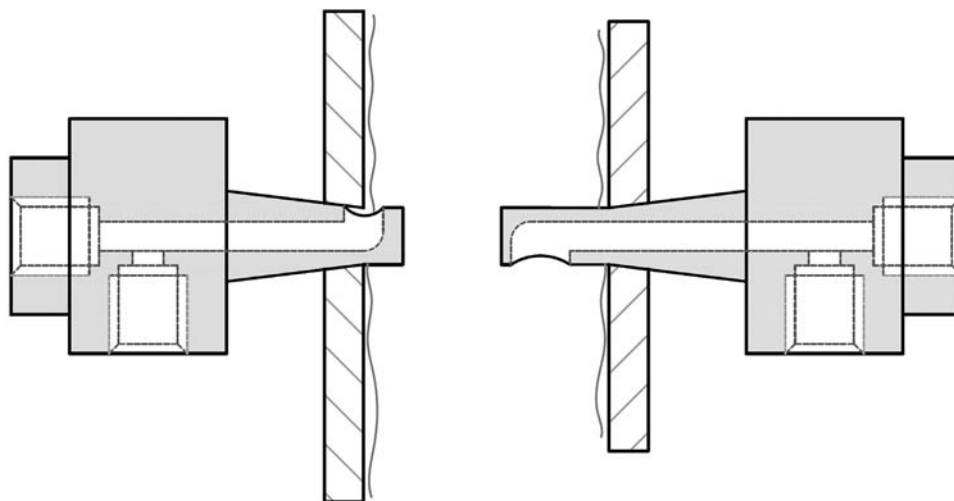


Fig. 4. The drawing of the liquid (left) and the gas (right) sampling devices.

Table 4
Overview of conditions used in the k_G and a_{eff} measurements.

k_G			a_{eff}
SO ₂ /air	SO ₂ /He	SO ₂ /SF ₆	CO ₂ /air
$Sc_G=1.22$	$Sc_G=2.75$	$Sc_G=0.45$	$Q_L=170\text{--}345$ ml/min
$Q_L=80\text{--}370$ ml/min	$Q_L=170$ ml/min	$Q_L=170$ ml/min	$u_G=0.9\text{--}1.9$ m/s
$Re_G=500\text{--}11,200$	$Re_G=300\text{--}2100$	$Re_G=3900\text{--}11,800$	

Table 5
Methods for liquid diffusivity calculation.

Wilke and Chang (1955) (W-C)	Tyn and Calus (1975) (T-C)
$D_{12} = \frac{7.4 \cdot 10^{-15} (\phi_2 M_2)^{0.5} T}{\mu_2 V_1^{0.6}}$	
$D_{12} = \frac{8.93 \cdot 10^{-15} T \left(\frac{V_{b,1}}{V_{b,2}}\right)^{1/6} \left(\frac{P_2}{P_1}\right)^{0.6}}{\mu_2}$	
<p>For non-polar solutes diffusing into monohydroxy alcohols the values of P_2 and V_2 should be multiplied by factor of $8000 \cdot \mu_2$</p>	
<p>MeOH: $V_b=43$ cm³/mol; $P=89$; $\phi=1.9$; $M=32$ g/mol EtOH: $V_b=59$ cm³/mol; $P=133$; $\phi=1.5$; $M=46$ g/mol PrOH: $V_b=82$ cm³/mol; $P=165$; $\phi=1.2$; $M=60$ g/mol O₂: $V_b=25.6$ cm³/mol; $P=40$ CO₂: $V_b=34$ cm³/mol; $P=49$</p>	

and none on gases in hot alcohols, we had to use some estimation methods for their calculation. Methods of Wilke and Chang (1955) – further referred to as W-C, and Tyn and Calus (1975) – further T-C, with their parameters listed in Table 5 were examined. The predictions of both methods are compared to the literature data of diffusivities of CO₂ and O₂ in primary alcohols in Table 6. Both methods provide predictions in poor agreement with experimental data – the average relative deviation of predicted and literature data is 50% for both methods. The method of T-C was chosen as more suitable for this paper as it seems to provide more reliable data for the methanol–propanol system and it is also recommended by Reid et al. (1987).

Table 6
Liquid diffusivities for several systems.

System	t (°C)	D_{12}^0 (10 ⁹ m ² /s)		
		Ref.	W-C	T-C
O ₂ /MeOH	20	1.88 ^a	4.13	5.34
	20	1.64 ^a	2.13	3.61
	25	5.24 ^b	2.39	3.94
	29.6	2.64 ^c	2.66	4.28
O ₂ /PrOH	20	1.48 ^a	1.19	2.35
	25	8.37 ^d	3.78	5.29
CO ₂ /MeOH	25	8.21 ^e		
	25	3.86 ^d	2.02	3.66
	25	3.42 ^f		
	25	4.50 ^g		
	25	2.73 ^d	1.15	2.43
	30	0.80 ^h	1.15	0.97
PrOH/MeOH		1.97 ^h	2.42	2.17

- ^a Sada et al. (1975).
- ^b Won and Mills (1982).
- ^c Krieger et al. (1967).
- ^d Won et al. (1981).
- ^e Hikita et al. (1959).
- ^f Davies et al. (1967).
- ^g Simons and Ponter (1975).
- ^h Shuck and Toor (1963).

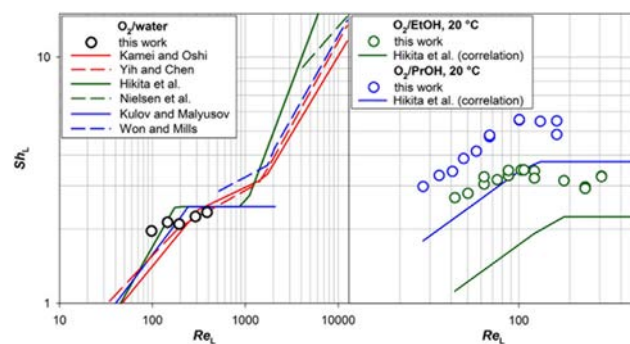


Fig. 5. Sh_L data measured on O₂/water, ethanol and *n*-propanol at 20 °C in dependence on liquid Reynolds number. Comparison with literature data.

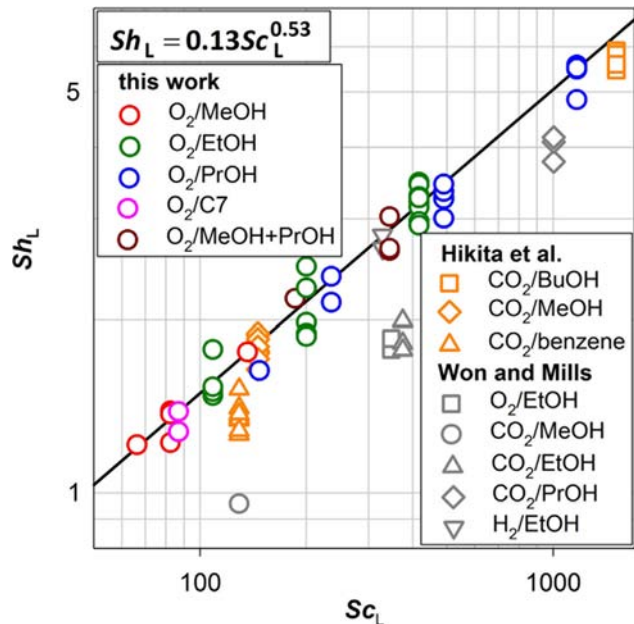


Fig. 6. The experimental Sh_L data correlated as a function of Sc_L only. Comparison with literature data for non-aqueous systems.

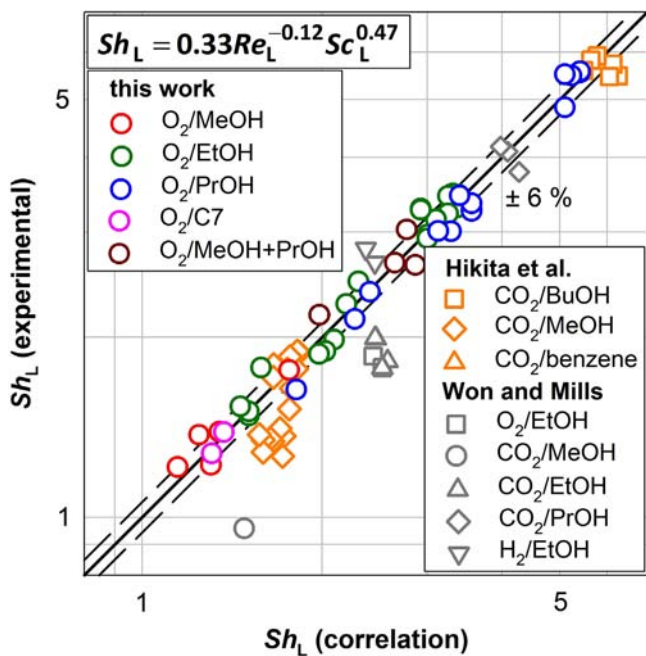


Fig. 7. The experimental Sh_L data correlated as a function of Re_L and Sc_L . Comparison with literature data for non-aqueous systems.

4.1.1. Effective interfacial area

Effective interfacial area in the device has been found 158–161 m^2/m^3 for several gas and liquid velocities, which is in excellent agreement with the area of the column inner surface divided by its volume (160 m^2/m^3). This result is in agreement with the findings of Portalski and Clegg (1971) stating that the interfacial area provided in the wetted wall column is almost independent of hydrodynamic conditions.

4.1.2. Mass transfer in the liquid phase

Liquid phase Sherwood numbers, Sh_L , in dependence on liquid phase Reynolds number, Re_L , measured with O_2 –water system are presented in Fig. 5. The data measured with this system were

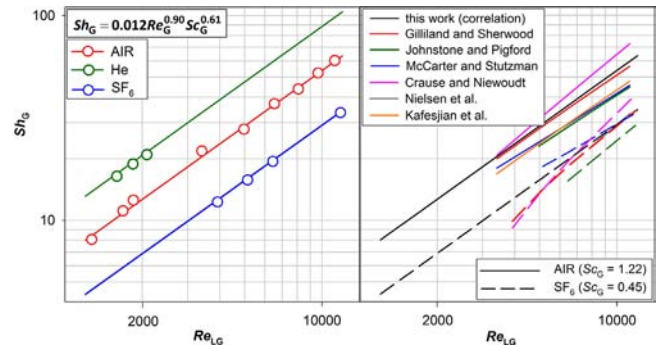


Fig. 8. The experimental Sh_G data correlated as a function of Re_{LG} and Sc_G . Comparison of correlation (4.6) with literature data for air and SF_6 as a carrier gas.

possible to be acquired in a relatively narrow range of flow rates and served for the test of the experimental set-up. The results fall in the area observed by other authors.

Liquid phase Sherwood numbers, Sh_L , of ethanol and n-propanol at 20 °C were found to increase with Reynolds number up to the critical Reynolds number, Re_{LC} (pseudo-laminar regime). Above the Re_{LC} the pseudo-turbulent flow occurs and Sh_L dependence on the Re_L sharply ceases (see Fig. 5). This behavior qualitatively agrees with observations of other authors (Table 1); critical Reynolds number observed in this work $Re_{LC}=85$ (ethanol) or $Re_{LC}=100$ (n-propanol) are higher than those calculated according to Brauer (1958) $Re_{LC}=51$ (ethanol) or $Re_{LC}=23$ (n-propanol). For other conditions (temperatures higher than 20 °C and for water, methanol, n-heptanes) the pseudo-laminar regime was not achieved due to the experimental set-up limitations.

The data acquired for all organic solvents at all temperatures have been correlated by

$$Sh_L = 0.33 Re_L^{-0.12(\pm 0.02)} Sc_L^{0.47(\pm 0.02)} \quad (4.1)$$

for $Re_L > Re_{LC}$ with RSD of 6%. The diffusivity of oxygen in the solvents has been estimated by Tyn–Calus method.

The data have been compared with those of Hikita et al. (1959) and Won and Mills (1982) which were measured with non-aqueous systems. Although the correlation of Hikita et al. (1959) seriously underestimates our experimental Sh_L values (see Fig. 5), Hikita's raw k_L data for non-aqueous systems fit well with our correlation when diffusivities calculated by T–C method are used for Sh_L and Sc_L calculation (see Figs. 6 and 7).

Our data (O_2 /EtOH) are approx. 30% higher than those by Won Mills.

Absolute values of Sh_L as well as power of the Sc_L in the resulting correlation depend on the method of diffusivity calculation (Tyn–Calus or Wilke–Chang method). However, the success of the correlation is the same regardless of the selected method. Interestingly, the incorporation of experimental diffusivities provided by Hikita and Won and Mills leads to a significant deviation of the data from correlation (4.1).

The shape of the correlation determines

$$k_L \sim D_{12,L}^{0.53} \mu_L^{-0.077} \rho_L^{0.197} m_L^{-0.12} d^{0.12} g \quad (4.2)$$

The dependence of the mass transfer coefficient on the diffusivity is close to the prediction of the penetration theory and the VDT model. The mass-transfer data in terms of Sh_L obtained for different solvents, flows and temperatures fit well with the correlation and mutually overlap, supporting the rationality of their description in the terms of chosen dimensionless numbers Re_L and Sc_L .

The success of the correlation suggests that, in the range of Reynolds and Schmidt numbers used, it will be valid for similar organic solvents. The agreement with Hikita's data measured with carbon dioxide suggests its applicability also for different solutes.

4.1.3. Mass transfer in the gas phase

The mass transfer in the gas phase of the wetted-wall column has been studied by chemisorption of SO₂ from the air, He, and SF₆ into the aqueous solution of sodium hydroxide. The character of the dependence

$$Sh_G = f(Re_{LG}) \quad (4.3)$$

has been investigated for the SO₂/air/aq. NaOH system in the range of Reynolds numbers 500–11,000. The only significant change in this dependence suggesting a change of the hydrodynamic regime has been found at around $Re_{LG,c} = 1200$.

$$Sh_G = f(Re_{LG}^\alpha) \quad (4.4)$$

For $Re_{LG} < Re_{LG,c}$ the power of Reynolds criteria, α , was approximately 1.41 and for $Re_{LG} > Re_{LG,c}$ the power was 0.9. The mass transfer data measured for the $Re_{LG} < Re_{LG,c}$ have been excluded from the evaluation for all gases.

Liquid phase velocity influence has been studied with the SO₂/air/NaOH system by changing the liquid phase velocity for several fixed gas flows. The optimal value of the β coefficient in the following relation

$$Re_{LG} = \frac{(u_L + \beta u_L) d \rho_G}{\eta_G} \quad (4.5)$$

has been determined as a value for which the scatter of dependence 4.4 achieved a minimum. The optimal value was found to be $\beta = 1.15$, however, for all calculations the rounded value of $\beta = 1$ has been adopted. The data acquired for all gases has been correlated by common correlation

$$Sh_G = 0.012 Re_{LG}^{0.90(\pm 0.01)} Sc_G^{0.61(\pm 0.02)} \quad (4.6)$$

for $Re_{GL} > 1200$ and Sc_G in the range 0.45–2.75 with RSD of 4%. Expression of the mass-transfer coefficient dependence on the dimensional quantities yields

$$k_G \sim D_{12,G}^{0.39} \mu_G^{-0.29} \rho_L^{0.29} (u_G + u_L)^{0.9} d^{-0.1} \quad (4.7)$$

In the range of validity the correlation (4.6) agrees well with the results of Gilliland and Sherwood (1934) and within 20% also with those obtained by Crause and Nieuwoudt (1999), Johnstone and Pigford (1942), McCarter and Stutzman (1959) and Kafesjian et al. (1961). On the other hand our Sh_G data are significantly higher than those found by Strumillo and Porter (1965) and Nielsen et al. (1998). The disagreement with Nielsen's data despite the same measurement system is annoying, although Nielsen's data have been acquired under much higher liquid velocities.

The power of Reynolds criteria 0.9 falls in between 0.68 and 1.05 found by the other investigators. The correlation provides 0.61 power of the Schmidt number, which is higher than that predicted by Gilliland and Sherwood (1934), McCarter and Stutzman (1959) and it is also higher than 1/3 predicted by Chilton–Colburn analogy. The value is close, however, to the value of 0.566 found by Crause and Nieuwoudt (1999).

5. Conclusions

This article brings mass-transfer data of the organic liquid phase and of the several carrier gasses in a wetted wall column for absorption/desorption conditions. Such data have been rarely provided in literature.

It was shown that the obtained correlations of the mass-transfer data in terms of the dimensionless Sh , Re and Sc numbers

$$Sh_L = 0.33 Re_L^{-0.12} Sc_L^{0.47}$$

$$Sh_G = 0.012 Re_{LG}^{0.90} Sc_G^{0.61}$$

fit the mass-transfer data for any of the studied system and therefore seem to be universal.

The comparison and correlation of the data measured with different systems was found to be difficult due to the mutual disagreement of the experimentally found diffusivities of individual systems and also due to the disagreement among the predictions of various diffusivity models. These discrepancies contribute to the disagreement of the treated mass-transfer data. Apparently, the best solution was found in the systematic use of Tyn and Calus (liquid phase)/Wilke-Lee (gas phase) model for the diffusivity calculation and recalculation of the literature data according to the chosen models. The predictive ability of the correlations is also limited to the use of these models for diffusivity.

The aim of the work has been to obtain absorption data under conditions approaching those found for atmospheric distillation of methanol-n-propanol system in the same column. Comparison of the data will be used in the broader scope of study of the transfer of the data between absorption and distillation. The revealed correlations predict relative mass-transfer resistance in the liquid phase in the range of 5–45% which will be sufficient for its more precise determination.

Nomenclature

a_{eff}	effective interfacial area of the column, $\text{m}^2 \cdot \text{m}^{-3}$
a_G	geometrical area of the column, $a_G = 4/d$, $\text{m}^2 \cdot \text{m}^{-3}$
c	molar concentration, $\text{mol} \cdot \text{m}^{-3}$
D	diffusivity, $\text{m}^2 \cdot \text{s}^{-1}$
d	column diameter, m
g	gravity acceleration, $9.82 \text{ m} \cdot \text{s}^{-2}$
h	height of the column, distance between sampling points, m
K_a	reactive-diffusion parameter in Eq. (3.3), $K_a = 0.00243 \text{ m/s}$
k_G	gas phase mass-transfer coefficient, m/s
k_L	liquid phase mass-transfer coefficient, m/s
l	column length, m
M	molar mass, $\text{g} \cdot \text{mol}^{-1}$
m	slope of the equilibrium line, $m = \frac{dc_G}{dc_L}$
\dot{m}	mass flow, $\text{kg} \cdot \text{s}^{-1}$
P	parachor, $P = \frac{1000 \cdot M \cdot \sigma^{1/4}}{\rho_L}$, $\text{N}^{1/4} \text{ m}^{11/4} \text{ mol}^{-1}$
p	pressure, Pa
Q	volumetric flow rate, $\text{m}^3 \cdot \text{s}^{-1}$
R_L	relative resistance of the liquid phase to the mass transfer
$Re_{L,c}$	critical Reynolds number of the liquid phase
u_G	gas velocity, m/s
u_L	liquid film velocity according to the Nusselt's theory, $u_L = \left(\frac{Re_L^2 \mu_L g}{48 \rho_L} \right)^{1/3}$, m/s
u_{LG}	gas velocity relative to the liquid surface, $u_{LG} = u_L + u_G$, m/s
V_1	molar volume of solute at boiling point, $\text{cm}^3 \cdot \text{mol}^{-1}$

Greek symbols

Γ	liquid mass flow rate per wetted perimeter, $\Gamma = \frac{\dot{m}_L}{\pi \cdot d}$, $\text{kg} \cdot \text{m}^{-1} \cdot \text{s}^{-1}$
δ	film thickness according to the Nusselt's theory, $\delta = \left(\frac{3 \mu_L^2 Re_L}{4 \rho_L^2 g} \right)^{1/3}$, m
μ	viscosity, $\text{Pa} \cdot \text{s}$
θ	association parameter
ρ	density, $\text{kg} \cdot \text{m}^{-3}$
σ	surface tension, $\text{N} \cdot \text{m}^{-1}$

Subscripts

bottom	bottom position
G	gas phase
L	liquid phase
top	top position
1	solute (diffusivity calculation)
2	solvent (diffusivity calculation)

Superscripts

0	in infinite dilution
DIST	distillation

Dimensionless numbers

$$Ga_L = \frac{g \rho_L^2 l^3}{\mu_L} \quad \text{liquid phase Galilei number}$$

$$Ka = \frac{\rho_L \sigma^3}{\mu_L^2 g} \quad \text{liquid Kapitza number}$$

$$Re_G = \frac{d \cdot u_G \cdot \rho_G}{\mu_G} \quad \text{gas phase Reynolds number relative to the column wall}$$

$$Re_L = \frac{4 \cdot \Gamma}{\mu_L} = \frac{4 \cdot \dot{m}_L}{\pi \cdot d \cdot \mu_L} \quad \text{liquid phase Reynolds number}$$

$$Re_{LG} = \frac{d \cdot u_G \cdot \rho_G}{\mu_G} \quad \text{gas phase Reynolds number relative to the liquid surface}$$

$$Sc = \frac{\mu}{\rho \cdot D_{12}} \quad \text{Schmidt number}$$

$$Sh_G = \frac{k_G d}{D_{12,G}} \quad \text{gas phase Sherwood number}$$

$$Sh_L = \frac{k_L}{D_{12,L}} \left(\frac{\mu_L^2}{\rho_L^2 \cdot g} \right)^{1/3} \quad \text{liquid phase Sherwood number}$$

Acknowledgement

Authors are grateful to Raschig GmbH for financial support of the project and to the Czech Science Foundation for supporting the project through Grant 13-01251S and to the financial support from Specific University Research (MSMT no. 20/2015).

Appendix A. Supplementary material

Supplementary data associated with this article can be found in the online version at <http://dx.doi.org/10.1016/j.ces.2015.12.027>.

References

- Brauer, H., 1958. Stoffaustausch beim Rieselfilm. *Chem. Ing. Tech.* 30 (2), 75–84.
- Crause, J.C., Nieuwoudt, I., 1999. Mass transfer in a short wetted-wall column. 1. Pure components. *Ind. Eng. Chem. Res.* 38, 4928–4932.
- Chilton, T.H., Colburn, A.P., 1934. Mass transfer (absorption) coefficients—prediction from data on heat transfer and fluid friction. *Ind. Eng. Chem.* 26 (11), 1183–1187.
- Davies, G.A., Ponter, A.B., Craine, K., 1967. Diffusion of carbon dioxide in organic liquids. *Can. J. Chem. Eng.* 45 (6), 372–376.
- Emmert, R.E., Pigford, R.L., 1954. Interfacial resistance. A study of gas absorption in falling liquid films. *Chem. Eng. Prog.* 50, 87–93.
- Gilliland, E.R., Sherwood, T.K., 1934. Diffusion of vapors into air streams. *Ind. Eng. Chem.* 26 (5), 516–523.
- Hikita, H., Nakanishi, K., Kataoka, T., 1959. Liquid-phase mass transfer in wetted-wall columns. *Kagaku Kogaku* 23, 459–466.
- Henstock, W.H., Hanratty, T.J., 1979. Gas absorption by a liquid layer flowing on the wall of a pipe. *AIChE J.* 25 (1), 122–131.
- Higbie, R., 1935. The rate of absorption of a pure gas into a still liquid during short periods of exposure. *Trans. Am. Inst. Chem. Eng.* 35, 365–389.
- Ishigai, S., Nakanishi, S., Koizumi, T., Oyabu, Z., 1972. Hydrodynamics and heat transfer of vertical falling liquid films—Part 1, classification of flow regimes. *Bull. JSME* 15 (83), 594–602.
- Jackson, M.L., Ceaglske, N.H., 1950. Distillation, vaporization, and gas absorption in a wetted-wall column. *Ind. Eng. Chem.* 42 (6), 1188–1198.
- Johnstone, H.F., Pigford, R.L., 1942. Distillation in a wetted-wall column. *Trans. Am. Inst. Chem. Eng.* 38, 25–51.
- Kafesjian, R., Plank, C.A., Gerhard, E.R., 1961. Liquid flow and gas phase mass transfer in wetted-wall towers. *AIChE J.* 7 (3), 463–466.
- Kamei, S., Oishi, J., 1955. Mass and heat transfer in a falling liquid film of wetted wall tower. *Mem. Fac. Eng. Kyoto Univ.* 17, 277–289.
- Krashennnikov, S.A., Durasova, S.A., 1958. Absorption of carbon dioxide by water. *Khimiya Khimicheskaya Tekhnol.* 5, 136–141.
- Krieger, I.M., Mulholland, G.W., Dickey, C.S., 1967. Diffusion coefficients for gases in liquids from the rates of solution of small gas bubbles. *J. Phys. Chem.* 71 (4), 1123–1129.
- Kulov, N.N., Malyshev, V.A., 1967. Mass transfer in wetted-wall column with a stirred liquid film. *Teor. Osn. Khimicheskoi Tekhnol.* 1 (2), 213–223.
- McCarter, R.J., Stutzman, L.F., 1959. Transfer resistance and fluid mechanics. *AIChE J.* 5 (4), 502–505.
- Nielsen, C.H.E., Kiil, S., Thomsen, H.W., Dam-Johansen, K., 1998. Mass transfer in wetted-wall columns: correlations at high Reynolds numbers. *Chem. Eng. Sci.* 53 (3), 495–503.
- Nusselt, W., 1916. Die Oberflächenkondensation des Wasserdampfes. *VDI Z.* 60, 541–546.
- Pigford, R.L., 1941. Counter-diffusion in a wetted wall column (Dissertation thesis). University of Illinois.
- Portalski, S., 1973. Phase velocities on liquid films flowing on a smooth vertical plate. *AIChE J.* 19 (6), 1244–1246.
- Portalski, S., Clegg, A.J., 1971. Interfacial area increase in rippled film flow on wetted wall columns. *Chem. Eng. Sci.* 26 (6), 773–784.
- Reid, R.C., Prausnitz, J.M., Poling, B.E., 1987. The properties of gases and liquids, 4th ed. MacGraw Hill, New York.
- Rejl, J.F., Linek, V., Moucha, T., Valenz, L., 2009. Methods standardization in the measurement of mass-transfer characteristics in packed absorption columns. *Chem. Eng. Res. Des.* 87 (5), 695–704.
- Sada, E., Kito, S., Oda, T., Ito, Y., 1975. Diffusivities of gases in binary mixtures of alcohols and water. *Chem. Eng. J.* 10, 155–159.
- Shuck, F.O., Toor, H.L., 1963. Diffusion in the three-component liquid system methyl alcohol-n-propyl alcohol-isobutyl alcohol. *J. Phys. Chem.* 67, 540–545.
- Simons, J., Ponter, A.B., 1975. Diffusivity of carbon dioxide in ethanol-water mixtures. *J. Chem. Eng. Jpn.* 8 (5), 347–350.
- Strumillo, C., Porter, K.E., 1965. The evaporation of carbon tetrachloride in a wetted-wall column. *AIChE J.* 11 (6), 1139–1142.
- Tyn, M.T., Calus, W.F., 1975. Diffusion coefficients in dilute binary liquid mixtures. *J. Chem. Eng. Data* 20 (1), 106–109.
- Wilke, C.R., Chang, P., 1955. Correlation of diffusion coefficients in dilute solutions. *Am. Inst. Chem. Eng. J.* 1, 264–270.
- Won, Y.S., Mills, A.F., 1982. Correlation of the effects of viscosity and surface tension on gas absorption rates into freely falling turbulent liquid films. *Int. J. Heat Mass Transf.* 25 (2), 223–229.
- Won, Y.S., Chung, D.K., Mills, A.F., 1981. Density, viscosity, surface tension, and carbon dioxide solubility and diffusivity of methanol, ethanol, aqueous propanol, and aqueous ethylene glycol at 25 °C. *J. Chem. Eng. Data* 26 (2), 140–141.
- Yih, S.M., Chen, K.Y., 1982. Gas absorption into wavy and turbulent falling liquid films in a wetted-wall column. *Chem. Commun.* 17 (1–6), 123–136.



Analogy of absorption and distillation processes. Wetted-wall column study



F.J. Rejl^{a,*}, J. Haidl^a, L. Valenz^a, T. Moucha^a, M. Schultes^b

^a University of Chemistry and Technology Prague, Technická 5, 166 28 Praha 6, Czech Republic

^b Raschig GmbH, Germany

HIGHLIGHTS

- Wetted wall column for absorption as well as distillation experiments.
- Profile method for evaluation of distillation mass-transfer coefficients.
- Different dependence of absorption/ distillation k_G on the gas velocity.
- Quality of the diffusivity data/correlations essential for rate-based design.

ARTICLE INFO

Article history:

Received 15 January 2016

Received in revised form

8 July 2016

Accepted 14 July 2016

Available online 16 July 2016

Keywords:

Absorption

Distillation

Mass transfer

Wetted-wall column

ABSTRACT

This article is the second one from a pair focusing on the mass transfer fundamentals and the analogy between the processes of absorption and distillation. The wetted wall column, a device with known interfacial area, was built for this purpose enabling evaluation of the mass-transfer coefficients instead of the volumetric mass-transfer coefficients usually provided by experiments in the packed columns. The analogy of the processes has been assessed by comparison of the mass-transfer characteristics (*HETP*, individual mass-transfer coefficients k_L and k_G) evaluated on the basis of the absorption experiments with those found under the distillation conditions. In the prior paper the results of the absorption experiments performed under distillation-like conditions have been published in the form of dimensionless correlations $Sh_L = 0.33 Re_L^{-0.12} Sc_L^{0.47}$ and $Sh_G = 0.012 Re_{LG}^{0.90} Sc_G^{0.61}$.

In this paper we present results of the distillation experiments in the form of the *HETP* data and mass-transfer coefficients evaluated by the profile method. The experimental data are compared with those predicted on the basis of the absorption experiments results. The experimental *HETP* data acquired on the methanol-*n*-propanol and ethanol-*n*-propanol systems agree within 10–20% with the data predicted. The distillation mass-transfer coefficients evaluated by the profile method were correlated in the dimensionless form $Sh_L = 0.25 Re_L^{-0.12} Sc_L^{0.47}$ and $Sh_G = 2.3 \cdot 10^{-3} Re_{LG}^{1.07} Sc_G^{0.61}$. The distillation k_L values have been found to be 24% lower and the k_G values 13% lower than the ones predicted according to absorption correlations. The gas-phase mass-transfer coefficient, k_G , exhibits higher dependence on the vapor velocity than it was found in standard absorption measurements. Similar difference was found also for packed columns in previous works. Apparently, there is at least one unaccounted phenomenon which affects differently the mass-transfer performance of absorption and distillation packed columns. Poor results of the present diffusion models have been noticed in this work preventing deeper study of these differences. Improvement of these models is found to be inevitable for the further research in this area as well as for the reliable rate-based modeling of the industrial absorption and distillation columns.

© 2016 Elsevier Ltd. All rights reserved.

1. Introduction

Distillation and absorption in the packed column can be treated as the analogical processes of the mass transfer between the gas/vapor and the liquid flowing on the packing. The assumed analogy implies that the phenomena occurring in both the processes can

Abbreviations: EtOH, ethanol; MeOH, methanol; PrOH, *n*-propanol

* Corresponding author.

E-mail address: frantisek.rejl@vscht.cz (F.J. Rejl).

Nomenclature

a	effective interfacial area of the column, (m^2/m^3)
a_G	geometrical area of the column, $a_G=4/d$, (m^2/m^3)
b_L, b_G	parameters optimized by the profile method, (dimensionless)
B	liquid superficial velocity, (m/h)
c	total molar concentration, (mol/m^3)
d	column diameter, (m)
D	diffusivity, (m^2/s)
F_G	gas-load factor, $F_G = u_G \cdot \sqrt{\rho_G}$, ($\text{Pa}^{0.5}$)
g	gravity acceleration, $g = 9.82 \text{ m/s}^2$
h	height of the column, distance between sampling points, (m)
$HETP$	height of the packing equivalent to one theoretical plate, (m)
k_G	gas phase mass-transfer coefficient, (m/s)
k_L	liquid phase mass-transfer coefficient, (m/s)
$k_G a$	volumetric gas phase mass-transfer coefficient, (1/s)
$k_L a$	volumetric liquid phase mass-transfer coefficient, (1/s)
m_1	slope of the equilibrium line, $m_1 = \frac{dy_1}{dx_1}$, (dimensionless)
\dot{m}	mass flow rate, (kg/s)
n_G	gas/vapor phase molar flow-rate, (mol/s)
S	column cross-section, (m^2)
u_L	liquid film velocity according to the Nusselt's theory, $u_L = \left(\frac{Re_L^2 \mu_L g}{48 \rho_L} \right)^{1/3}$, (m/s)
u_{LG}	gas velocity relative to the liquid surface, $u_{LG} = u_L + u_G$, (m/s)
x_1	Liquid molar fraction of component 1, (dimensionless)
y_1	gas/vapor molar fraction of component 1, (dimensionless)
z	coordinate, (m)

Greek symbols

α_{12}	relative volatility of mixture, (dimensionless)
μ	viscosity, (Pa s)
ρ	density, (kg/m^3)
σ_i	standard deviation of quantity i
σ_{ri}	relative standard deviation of quantity i

Subscripts

bottom	bottom position
exp	experimental
G	gas/vapor phase
L	liquid phase
top	top position
1	solute (diffusivity calculation)
2	solvent (diffusivity calculation)
pred	predicted
R, reflux	reflux

Dimensionless numbers

$Re_L = \frac{4 \cdot \dot{m}_L}{\pi \cdot d \cdot \mu_L}$	liquid phase (film) Reynolds number
$Re_{LG} = \frac{d \cdot u_{LG} \cdot \rho_G}{\mu_G}$	gas phase Reynolds number relative to the liquid surface
$Sc = \frac{\mu}{\rho \cdot D_{12}}$	Schmidt number
$Sh_G = \frac{k_G d}{D_{12,G}}$	gas phase Sherwood number
$Sh_L = \frac{k_L}{D_{12,L}} \left(\frac{\mu_L^2}{\rho_L^2 \cdot g} \right)^{1/3}$	liquid phase (film) Sherwood number

be described with the same set of models dealing with the hydrodynamic of the phases, phase equilibria and the mass-transfer phenomena. In principle, it should be possible to use the packing mass-transfer characteristic ($k_L a$, $k_G a$ and a) measured by standardized experiments under the absorption conditions to predict the packing mass-transfer efficiency under the distillation ones. Despite all the effort already given to this topic the successful recalculation of the mass-transfer parameters from absorption to distillation conditions has never been mastered. Such situation lies the question whether the failures are caused only by the seriously different process conditions (absorption experiments are usually based on cold air/water system while the distillation is performed with hot organic systems) or whether there is a principal difference between those processes, i.e. the processes are not analogical. We re-open this question in this paper, as the rate-based modeling of the absorption and distillation columns relies on the validity of the analogy.

There are too many variables and uncertainties in testing the recalculation from absorption to distillation conditions if the ordinary distillation on the packing is considered. Our attempt to bring some new insight in the situation is based on the following ideas:

- 1) Utilizing direct method of determination of the mass-transfer coefficients under the distillation conditions – the profile method – which enables their direct comparison with results of absorption experiments.
- 2) Bringing the conditions of the absorption and distillation experiments as close together as possible. In an ideal case the phase hydrodynamics and their physical properties should be the same.

- 3) Minimizing the number of phenomena and quantities which affect the mass-transfer process by utilizing the experimental apparatus with known interfacial area – the wetted wall column – and by its utilization for both the absorption as well as the distillation experiments.

This paper is second of a pair. In the prior paper (Haidl et al., 2016a), the results of absorption experiments have been published in the form of the dimensionless correlations for the gas and liquid phase Sherwood numbers:

$$Sh_L = 0.33 Re_L^{-0.12} Sc_L^{0.47} \quad (1)$$

$$Sh_G = 0.012 Re_{LG}^{0.90} Sc_G^{0.61} \quad (2)$$

The absorption experiments were performed under several conditions using different liquids, gases, their temperatures and flow-rates covering the range of distillation Reynolds and Schmidt numbers so we expect that they can be used for the reliable calculation of the Sh_L and Sh_G (and $HETP$) values also for the distillation conditions. If so, the results would support rationality of the

- 1) Contemporary way of the rate based modeling of both processes
- 2) Description of the mass-transfer coefficients dependence on the process conditions.

The disagreement of the calculated and measured mass-transfer data should alarm us, that

- 1) The number of process affecting phenomena is incomplete
- 2) or/and models of the individual phenomena are insufficient
- 3) or/and the description of the mass-transfer coefficients dependence on the process conditions is poor.

In this paper we bring the separation efficiency of the wetted wall column under distillation conditions in form of the *HETP* and also as the correlations for gas and liquid Sherwood numbers evaluated by the profile method and their comparison with the values predicted using (Eqs. (1) and 2).

2. Literature

2.1. Distillation in wetted wall column

Although the wetted wall column was intensively used for the mass-transfer research in the last century, only a few of papers are dealing with its mass-transfer characteristics under distillation conditions. Several attempts to evaluate the contribution of the liquid-side resistance to the overall mass-transfer resistance, i.e. the relative resistance of the liquid phase, $R_{L,rel}$, have been made.

Johnstone and Pigford (1942) measured the height of transfer unit (*HTU*) for distillation of five binary mixtures under the total and partial reflux conditions ($Re_G=4000$ – 25000 ; $Sc_G=0.54$ – 0.72). The dependence of *HTU* on vapor loads and on L/V ratio was studied. According to their findings the relative liquid-side mass-transfer resistance of selected distillation systems is small (authors evaluated the effect of the liquid-side resistance to be less than 10% of overall mass-transfer resistance. The correlation $Sh_G \propto Re_G^{0.77} Sc_G^{1/3}$ is presented in the paper. The range of vapor Schmidt numbers did not allow evaluating its effect on the Sherwood number so the power of $1/3$ is taken from Chilton and Colburn (1934) correlation.

Surowiec and Furnas (1942) measured the overall gas-phase mass-transfer coefficients, K_G , by the distillation of ethanol-water system at various reflux ratios. They found the liquid phase mass-transfer resistance to be responsible for 30–50% of the overall mass-transfer resistance if the correlation of Gilliland and Sherwood (1934) is used for the calculation of k_G .

Jackson and Ceaglske (1950) performed the distillation experiments with 2-propanol-water system and total reflux conditions. They found the overall gas-phase mass-transfer coefficient in a good agreement with the value of k_G calculated according to the correlation of Chilton and Colburn (1934). Therefore, they concluded that distillation is a gas-side controlled operation.

Kayihan et al. (1975) developed a theoretical model for the simultaneous heat and mass transfer in distillation. The mass and heat transfer analogy assumption is involved into the model and numerous justified simplifications are applied. According to this model the liquid-side mass-transfer resistance in distillation can be evaluated from the molar fraction and temperature profiles measured in the liquid phase. The model was applied to evaluate such profiles measured by distillation of the methanol-water mixture under total reflux conditions (Kayihan et al., 1976). According to the model prediction made for this system, if there is any liquid-side mass-transfer resistance present in distillation, the liquid should be over-heated. As the liquid temperature measured agreed with its bubble-point, it was concluded that no mass-transfer resistance is present in the liquid during the distillation.

2.2. Mass-transfer coefficient determination under distillation conditions in the packed columns and comparison of their dependence on the phase flows with absorption results

Direct comparison of the absorption and distillation mass-transfer coefficients and their dependence on the phase flows is

Table 1

Dependencies of $k_L a \propto B^\alpha$ and $k_G a \propto u_G^\beta$ for Mellapak 250Y evaluated out of the distillation and absorption experiments and predicted by individual mass-transfer models.

	α	β
Rejl et al. (2010) – distillation	1.18	0.771
Valenz et al. (2011a) – absorption $k_L a$	0.734	0.651
Rejl et al. (2015) – absorption $k_G a$		
Rocha et al. (1996)	0.58	1.2
Billet and Schultes (1999)	0.733	1.16
Olujic et al. (1999)	0.45	0.844
Hanley and Chen (2012)	0.992	0.992

only possible, when some method of their determination is developed under distillation conditions. It is possible by introduction of serious simplifications (e.g. by presumption of the mass-transfer resistance in the gas phase only). As far as we know, the only other option is the analysis of the molar fraction profile along the column by the “profile method”.

The profile method has been applied to the molar fraction profiles measured along the ID 150 mm distillation column filled with Mellapak 250Y packing. The data measured on methanol-ethanol, methanol-*n*-propanol and ethanol-*n*-propanol systems and various reboiler duties were processed and the dependencies of $k_L a \propto B^\alpha$ and $k_G a \propto u_G^\beta$ were evaluated (Rejl et al., 2010; Valenz et al., 2011b). The dependencies of $k_L a$ and $k_G a$ on the phase flow-rates evaluated out of distillation and absorption (Valenz et al., 2011a, 2011b; Rejl et al., 2015) experiments and dependencies predicted by individual mass-transfer models are shown in Table 1. The table reveals significant differences in the individual models predictions and also in the behavior of the mass-transfer coefficients under absorption and distillation conditions.

2.3. Conclusions following from the literature survey

It cannot be clearly decided whether the distillation is solely gas-side controlled operation, as the conclusions made by individual authors are often contradictory. Clear conclusion about the possibility of the re-calculation of the mass-transfer coefficients between absorption and distillation conditions also cannot be made. Disagreement of the data presented in Table 1 indicates insufficient level understanding of the mass-transfer phenomena in packed columns. The differences in the phase-flow dependencies evaluated out of the absorption and distillation results together with findings of Valenz et al. (2011b) might indicate some fundamental unaccounted difference between absorption and distillation performed in packed columns.

3. Experimental

3.1. Wetted wall column

A glass column of ID 25 mm (geometrical area $a_G=4/d=160 \text{ m}^2/\text{m}^3$) and length of 2.1 m was used. The column was equipped with seven pairs of holes to enable placing liquid and gas sampling devices along the column. Each pair consisted of two conical shaped holes positioned on the opposite sides of the column and was rotated by 90 degrees with respect to the previous one. The vertical distance between the sampling points was 30 cm. The first sampling point was placed 15 cm below the upper column edge. Such positioning provided sufficient domain for the film flow development.

Liquid was fed to the column by means of 8 needles which are inserted in to the liquid distributor body. The needles of the inner

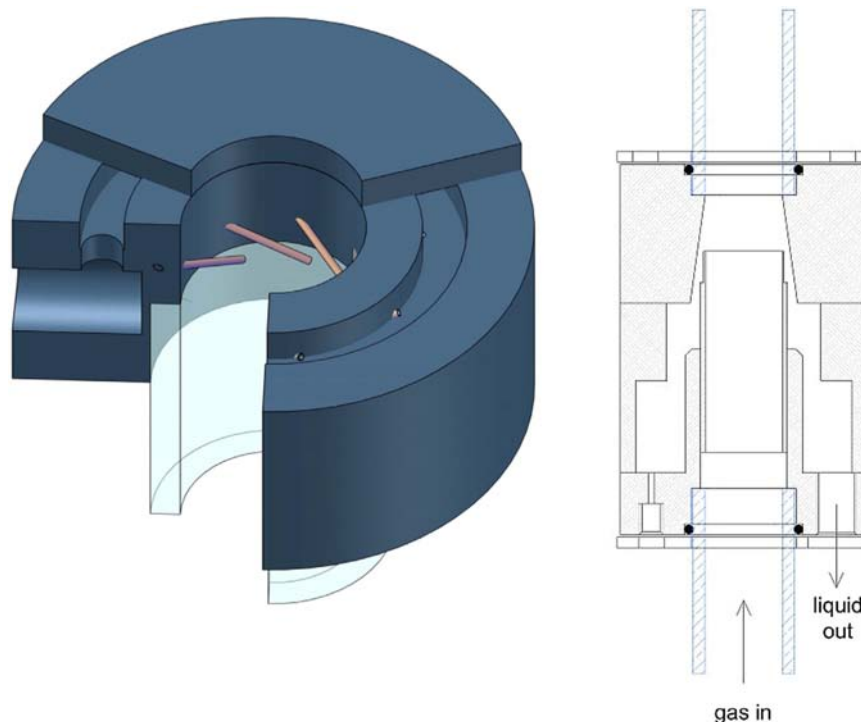


Fig. 1. The liquid (left) and the vapor (right) distributors.

diameter of 0.8 mm and the length of 25 mm were aligned tangentially with respect to the column perimeter and inclined by 30 degrees with respect to the column axis (see Fig. 1 – left).

With this installment the liquid flow entering the column has tangential component of the velocity which ensures connection of individual rivulets and a formation of the uniform liquid film at the top of the column. It was visually observed that the rotation of the liquid along the column perimeter is suppressed via the viscous forces before the liquid reaches the first sampling point. On the bottom of the column, there was placed a liquid collector/vapor distributor separating the liquid outlet from the vapor inlet.

Vapors of test mixtures were generated in an electrically heated reboiler with the maximal power output of 6 kW; the reboiler duty was controlled with a wattmeter and set according to the desired reflux flow rate. A bed of random packing was installed in the upper part of the reboiler to separate the drops of liquid from the vapor stream. The vapor was fed to the gas distributor through a 0.5 m long calming section and after passing through the column it was condensed in a glass total condenser. The condensate was collected in a small tank (of volume approx. 50 ml), cooled to approx. 20 °C (to prevent the liquid flow meter overheating) and fed through pre-heater to the liquid distributor as a reflux. The reflux flow rate, i.e. the gear pump revolutions, was controlled by the level of liquid in the condensate tank and measured by means of the Bronkhorst[®] mini-CoriFlow flow-meter. The reflux entering the column was sub-cooled by 2–3 °C with respect to its normal boiling point;¹ its temperature was measured with a Pt100 probe placed right before the distributor. The temperature of vapors leaving the column was measured using Pt100 probe placed above the liquid distributor. The column was insulated with two layers of Kaiflex EPDM thermal insulation. The experimental setup is illustrated in Fig. 2.

The liquid and vapor sampling devices were PVDF plugs with the openings permitting withdrawal of the liquid and gas samples

from the column (see Fig. 3). The secure placing of the sampling points was ensured by a conical shape of the devices which fits perfectly into the conical holes in the column wall. Two experimental setups were utilized:

- A) for reflux flow rates up to 2 g/s the column was fully equipped with seven pairs of vapor and liquid sampling devices to allow taking vapor and liquid samples along the column
- B) for reflux flow rates 2.5 and 3.0 g/s the vapor sampling devices were modified as shown in the Fig. 3b.

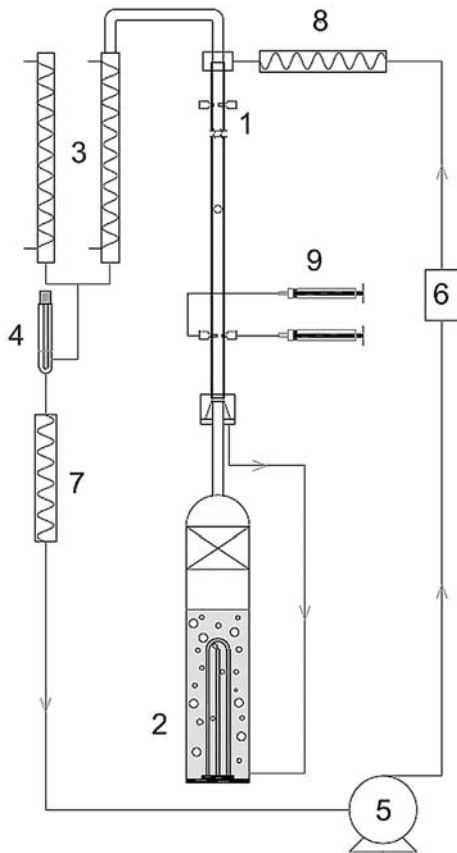
The experimental setup A does not allow performing the distillation experiments at the reflux flow rate higher than 2.2 g/s. At higher liquid- and vapor loads the flooding occurs at the sampling point positions. The modified vapor sampling devices used in setup B covers less of the column cross-section and permits to reach higher liquid- and vapor loads.

Eq. (2) taken from Haidl et al. (2016a, 2016b) is based on the results of k_G measurements performed on the column setup A. Its validity for column setup B was validated by the performing of the k_G measurements using the SO₂/air system. It was found that the column setup B provides Sh_G values 25% lower when compared to the results obtained under identical conditions on column setup A, therefore Eq. (2a) was used for the predictions of Sh_G in column setup B in this work.

$$Sh_G = 0.0096 Re_{LG}^{0.90} Sc_G^{0.61} \quad (2a)$$

The distillation experiments with methanol-*n*-propanol (MeOH-PrOH) and ethanol-*n*-propanol (EtOH-PrOH) systems were performed under the atmospheric pressure and total reflux conditions. The column was operated in the steady state which was determined by the constant reflux flow rate and composition and by the constant temperature of the vapor leaving the column; reflux samples were analyzed every 30 minutes and considered to be the same if the change in the composition was smaller than 0.003 mol fraction. Once the steady state was reached the sampling procedure was initiated.

¹ We were not able to heat up the reflux right up to the boiling without its occasional partial evaporation. To prevent such behavior the reflux was fed intentionally slightly subcooled.



1 - glass column, 2 - electric reboiler with demister, 3 - total condenser, 4 - liquid level meter, 5 - gear pump, 6 - liquid flow meter, 7 - reflux cooler, 8 - reflux pre-heater, 9 - syringe pump

Fig. 2. The experimental setup.

Two ml of the liquid and vapor (as condensate) samples from the same sampling point position were taken simultaneously to glass syringes. The sample flow rate of 1 ml/min was controlled by a syringe pump. Before the samples were taken, both syringes were purged twice by a withdrawal and re-insertion of the sample. The composition of the samples was analyzed using the Atago RX refractometer. The reproducibility of the concentration measurement was determined by repeated sampling – seven liquid and vapor samples were taken at the same sampling point. The composition of liquid varies within 0.9 mol% and the composition of vapor within 0.4 mol% from the average value.

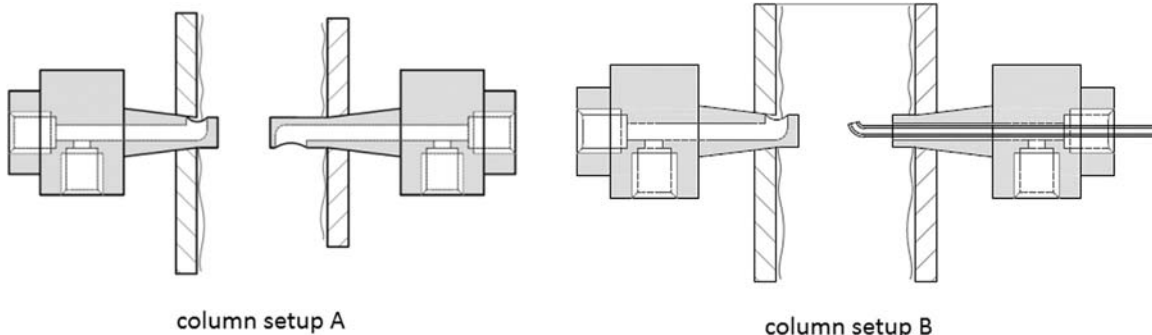


Fig. 3. The liquid (left side) and gas (right side) sampling devices.

The molar fraction profiles were measured for several reflux flow rates/vapor loads, the minimal reflux flow rate was limited by the stability of the liquid film, the maximal flow rate by the capacity of the column. As the wetted wall column exhibit relatively low separation efficiency ($HETP=1-2.5$ m), three batches of MeOH-PrOH mixture and four batches of EtOH-PrOH mixtures differing in concentration had to be used to obtain the profiles in the whole concentration range. The molar fraction profiles were evaluated by the profile method and in form of $HETP$.

3.2. Evaluation of the mass-transfer coefficients by the profile method

In this work the profile method (Linek et al., 2005; Rejl et al., 2010) was used to evaluate the mass-transfer coefficients from the vapor molar fraction profiles measured along the wetted wall column in distillation experiments. The rate-based model of the column with the following assumptions was used to calculate the theoretical molar fraction profiles:

- (i) distillation of binary mixture under total reflux conditions:
- (ii) the plug flow of the vapor and liquid phase
- (iii) process is adiabatic and steady state
- (iv) constant pressure along the column
- (v) thermodynamic equilibrium is established on the liquid-vapor interphase
- (vi) the effective interfacial area for the mass transfer is identical with the geometrical area of the column
- (vii) the liquid and vapor phase are at their boiling point and dew point, respectively; the reflux is fed on its boiling point
- (viii) the mass transfer between the vapor and liquid phase is carried through the vapor-liquid interface only
- (ix) the mass transfer across the interface consists of diffusional one (characterized by mass-transfer coefficients) and convective one due to the different enthalpies of vaporization of individual components.

The local k_L and k_G values were calculated from dimensionless correlations (3) and (4) with $Sh_{L,abs}$ and $Sh_{G,abs}$ calculated on basis of the absorption experiments results (Eqs. (1), (2) and (2a)).

$$Sh_L = b_L \cdot Sh_{L,abs} \quad (3)$$

$$Sh_G = b_G \cdot Sh_{G,abs} \quad (4)$$

Each hypothetical profile was calculated using the experimental reflux flow rate and composition as initials conditions. As the profile depends strongly on the reflux composition, a correction in the form of Eq. (5) has been introduced with an optimized parameter ϕ_i for each experimental profile.

$$x_{1,z=0} = x_{1,reflux} + \phi_i \cdot 0.05 \quad -1 \leq \phi_i \leq 1 \quad (5)$$

The parameters b_L , b_G , $\theta_1 - \theta_N$ were used as optimization parameters. Altogether $N+2$ parameters were optimized for each set of N experimental profiles. The sum of squares of differences between calculated and experimental molar fraction of methanol in vapor on each sampling point has been used as an optimization function.

3.3. HETP

The experimental $HETP$ values were calculated by the Fenske's equation (Eq. (6)). The vapor molar fractions of light component, y_1 , measured on the first and the last sampling point ($h=1.8$ m) were used as the $y_{1,top}$ and $y_{1,bottom}$, respectively. The value of the relative volatility, α_{12} , was calculated as a geometrical mean of relative volatilities calculated for conditions at the top and at the bottom of the column.

$$HETP_{exp} = \frac{h \cdot \ln(\bar{\alpha}_{12})}{\ln\left(\frac{y_{1,top}}{1-y_{1,top}} \cdot \frac{y_{1,bottom}}{1-y_{1,bottom}}\right)} \quad (6)$$

To enable the direct comparison of the experimental $HETP$ with the values predicted based on the absorption results, the $HETP_{pred}$ have been calculated from molar fraction profiles obtained as the solution of the rate-based model of the distillation column described above. Following conditions have been used for the calculation of each profile:

$$z = 0: \quad x_1 = y_1 = y_{1,top}$$

$$z = h_{pred} \quad x_1 = y_1 = y_{1,bottom}$$

The relations (1), (2) and (2a) have been used for the Sh_L and Sh_G calculations. For each experimental condition the value of $HETP_{pred}$ was calculated according to Eq. (6) using h_{pred} as the column height h .

4. Results

The liquid and vapor molar fraction profiles along the column were measured by atmospheric distillation of methanol-*n*-propanol and ethanol-*n*-propanol systems under total reflux conditions. Altogether 24 M fraction profiles on methanol-*n*-propanol (MeOH-PrOH) system and 13 profiles on ethanol-*n*-propanol (EtOH-PrOH) system were measured in range of reflux flow rate from 1 to 3 g/s.

For each experimental profile the overall $HETP_{exp}$ value has been calculated according to Eq. (6). The molar fraction of methanol and ethanol, respectively, in vapor taken on the first and the last sampling point has been used as $y_{1,top}$ and $y_{1,bottom}$, respectively. For each experimental profile the $HETP_{pred}$ has been also calculated on the basis of absorption results. The methods of Wilke–Chang and Tyn and Calus were used for calculation of diffusion coefficients in vapor and liquid phase, respectively. The $HETP_{exp}$ and $HETP_{pred}$ values for both distillation systems in dependence on the gas-load factor, F_G , are depicted in Fig. 4. The tabular data are attached to this paper as a supplementary material.

Fig. 4 demonstrates that the experimental $HETP$ values depend strongly on the concentration range they are measured in and that the $HETP$ values are slightly increasing with the gas load factor. Both the dependencies qualitatively agree with the dependencies predicted on the basis of absorption results. The experimental $HETP$ values measured on methanol-*n*-propanol system are approx. 10% higher than predicted values. The data measured on ethanol-*n*-propanol system agree within 8% with the values predicted on the basis of absorption experiments results.

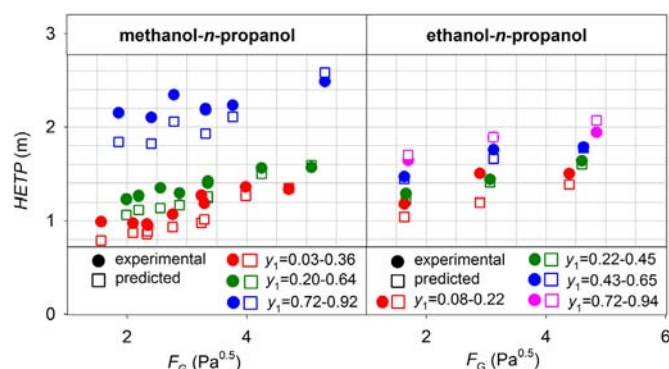


Fig. 4. The experimental $HETP$ values compared to the corresponding $HETP_{pred}$ values.

The uncertainty of the $HETP_{exp}$ values is a result of the uncertainty of the measured molar fraction of methanol and ethanol, respectively. For both the systems the relative error of $HETP_{exp}$ has been found to be in the range from 2% to 6%. The uncertainty of the $HETP_{abs}$ and $HETP_{local}$ values is a result of the uncertainties of the mass-transfer coefficients, k_L and k_G , calculated according to (Eqs. (1), (2) and 2a). Their uncertainties can be estimated on the basis of the uncertainties of individual quantities used for their calculations.

The relative uncertainties of most of the individual quantities required for calculation of Sh_L and Sh_G are either known (usually as the standard deviation of the correlation used for their calculation) or can be estimated from the accuracy of their measurement. The only quantities without easily obtainable uncertainty data are the diffusivities. The uncertainty of liquid diffusivity data is estimated from the results of a comparison of the values predicted by the individual models – Tyn and Calus (1975) and Wilke and Chang (1955) for liquid diffusivity data at infinite dilution and Wilke and Lee (1955) and Fuller et al. (1966) for gas/vapor diffusivity data – with experimental values found in the literature. In Table 2 are given the experimental and estimated diffusivity data for systems similar to those used in this work.

It can be seen that both the gas diffusivity models provide the values of $D_{12,G}$ for alcohol/air systems which are in excellent agreement with the experimental values. For the vapor mixtures, however, the methods provide values which differ mutually up to 30%. Based on this discrepancy, the uncertainty of 20% is estimated for $D_{12,G}$ under the distillation conditions. For the only liquid diffusivity data available for mixture of alcohols the difference of

Table 2

Literature vapor diffusivity data for alcohol/air systems compared with predicted data.

Gas phase diffusivity	$D_{12,G}$ (10^5 m ² /s)		
	Ref.	Fuller et al.	Wilke and Lee
MeOH/air, 0 °C	1.33 ^a	1.38	1.31
EtOH/air, 0 °C	1.02 ^a	1.06	1.05
PrOH/air, 0 °C	0.85 ^a	0.88	0.9
MeOH/PrOH, 50 mol%, 86.0 °C	–	1.18	0.91
EtOH/PrOH, 50 mol%, 88.7 °C	–	0.92	0.75
Liquid phase diffusivity	$D_{12,L}$ (10^9 m ² /s)		
		Wilke and Chang	Tyn and Calus
MeOH in PrOH, 30 °C	0.80 ^b	0.97	1.15
PrOH in MeOH, 30 °C	1.97 ^b	2.17	2.42

^a Washburn (2003).

^b Shuck and Toor (1963).

Table 3
Estimation of relative uncertainties of physical properties of distillation systems.

Y	$\sigma_r(Y) = \frac{\sigma(Y)}{Y}$	Y	$\sigma_r(Y) = \frac{\sigma(Y)}{Y}$
\dot{m}	0.005	u_{GL}	0.05
ρ_L	0.02	ρ_G	0.02
μ_L	0.05	μ_G	0.05
$D_{12,L}$	0.30	$D_{12,G}$	0.20

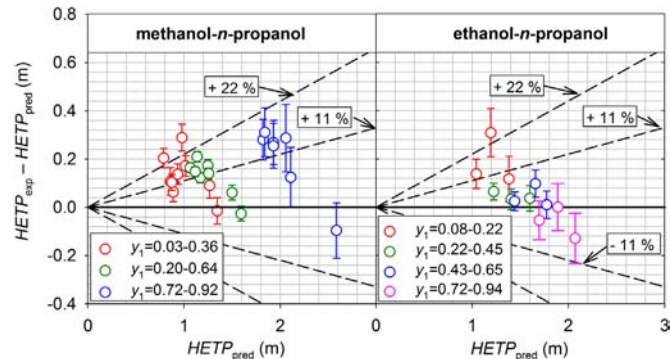


Fig. 5. Differences of experimental and predicted $HETP$ values of distillation systems.

20–40% was found. The uncertainty of only 30% for $D_{12,L}$ is estimated for distillation conditions.

The uncertainties of k_L and k_G values calculated from (Eqs. (1), (2) and 2a) were estimated using the error propagation law. The uncertainties of the individual quantities are given in Table 3. It can be concluded that the relative uncertainties of k_L and k_G are predominantly affected by the uncertainties of the diffusion coefficients and are $\sigma_r(k_L) \approx 15\%$, $\sigma_r(k_G) \approx 10\%$. The relative uncertainty of $HETP_{pred}$, $\sigma_r(HETP_{pred}) \approx 11\%$ was estimated.

For the methanol-*n*-propanol system the $HETP_{exp}$ values are systematically higher than $HETP_{pred}$. However, almost all the values lie within the extended confidence band of $HETP_{exp}$ – see Fig. 5. For the ethanol-*n*-propanol system all the $HETP_{exp}$ values except the two outlined lie in the confidence interval of $HETP_{pred}$. Hence, with respect to the uncertainties of the predicted and experimental $HETP$ values, a good agreement of both the values can be concluded.

The agreement of the results demonstrates that the overall mass-transfer efficiency of the wetted wall column under distillation conditions, i.e. $HETP$, can be successfully calculated using the rate-based model and with the mass-transfer coefficients determined on the basis of the dimensionless correlations derived from absorption experiments.

However the accuracy of the calculated $HETP$ data is seriously affected by the quality of physical property data, namely the gas and liquid diffusivity data. In this work the uncertainty of $HETP_{pred}$ of 11% was estimated on the basis of the statistical analysis of individual uncertainties. The absorption-distillation data transfer and process modeling can be considered successful only if this uncertainty of the result is accepted. Minor effect of some additional non-accounted phenomena might be obscured by this uncertainty.

4.1. Mass-transfer coefficients under distillation conditions evaluated by profile method

The molar fraction profiles measured on the MeOH-PrOH² system have been evaluated using the profile method as described

² The profile method showed low sensitivity for EtOH-PrOH system due to its significantly lower relative volatility in comparison with MeOH-PrOH system.

in the Section 3. Eqs. (3) and (4) have been used for the calculation of k_L and k_G , respectively. The parameters of b_L and b_G have been optimized for each reflux flow-rate. The values of b_L and b_G parameters evaluated by the profile method are listed in Table 4.

The b_L and b_G values with their standard deviations for the methanol-*n*-propanol system are shown in Fig. 6 in dependence on Re_L and Re_{LG} , respectively. The standard deviations of the parameters have been calculated by the Monte Carlo method as described in Hu et al. (2015).

For the methanol-*n*-propanol system the optimized k_L values have been found to be 24% lower than the values calculated using Eq. (1); the obtained values of k_G are 13% lower than the ones predicted using (Eqs. (2) and 2a), respectively.³ The lower values of k_L and k_G evaluated by the profile method are in agreement with the higher values of $HETP_{exp}$ discussed earlier.

Due to the high standard deviations of individual b_L values no dependency of b_L on Re_L can be deduced. On the other hand, the b_G values conclusively increase with Re_{LG} values. The b_G values have been correlated by Eq. (7) (respecting the weights of the individual values). The non-zero power of 0.17 at Re_{LG} in Eq. (7) implies that the correlations 1 and 2 do not fit the dependence of distillation Sh_G on Re_{LG} well. This observation is in agreement with the previous findings on ID 150 mm distillation column packed with Mellapak 250 Y – see the Literature section.

$$b_G = 0.19 Re_{LG}^{0.17} \quad (7)$$

On the basis of the profile method results the correlations (8), (9) (column setup A) and (9a) (column setup B) are built for the prediction of the distillation Sh_L and Sh_G values.

$$Sh_L = 0.25 Re_L^{-0.12} Sc_L^{0.47} \quad (8)$$

$$Sh_G = 2.3 \cdot 10^{-3} Re_{LG}^{1.07} Sc_G^{0.61} \quad (9)$$

$$Sh'_G = 1.7 \cdot 10^{-3} Re_{LG}^{0.7} Sc_G^{0.61} \quad (9a)$$

While the lower values of the distillation Sh_L and Sh_G values are possibly explainable by the poor quality of the diffusivity models, simultaneous occurrence of different dependences of absorption and distillation Sh_G on Re_{LG} suggests that there exists some additional difference between the absorption and distillation process not governed by the rate-based model described in the Experimental section. Two phenomena which could possibly provide explanations of the different absorption and distillation correlations of Sh_L and Sh_G have been identified (i) axial mixing of the phases; (ii) simultaneous occurrence of the mass and heat transfer in the column. Both the phenomena will be analyzed and briefly discussed in the following paragraphs.

Axial mixing is an undesirable phenomenon as it degrades efficiency of the separation equipment through a reduction of the mass-transfer driving force, and in the limit, a column behaves like a single equilibrium stage (Henley et al., 2011). In the distillation under the total reflux conditions and the plug-flow of both the phases the molar fraction profiles of the component in the liquid and vapor phase coincides and the mass-transfer driving force is maximal. The axial mixing of phases, if present, would demonstrate itself as the systematic spacing between a liquid and vapor molar fraction profiles – molar fraction of the light component in the liquid phase would be lower than that in the vapor reducing the driving force as the compositions would get closer to the equilibrium (Haidl et al., 2016b). Despite the presence of the intrusive, asymmetric sample points no such systematic spacing has been observed on the experimental molar fraction profiles

³ These findings are based on the average values of b_L and b_G parameters.

Table 4

Results of the profile method with k_L and k_G values calculated according to Eqs. (4) and (5). The standard deviations of the b_L and b_G values of MeOH-PrOH systems evaluated by the Monte-Carlo method (Hu et al., 2015).

Approx. reflux flow rate (g/s)	b_L (dimensionless)	b_G (dimensionless)	No. of exp. points (dimensionless)	No. of points excluded (dimensionless)	$\sigma(y_1)$ (dimensionless)
1.0	0.65 ± 0.28	0.88 ± 0.05	21	0	0.0052
1.3	1.30 ± 0.21	0.85 ± 0.01	21	4	0.0019
1.5	0.87 ± 0.15	0.87 ± 0.03	21	3	0.0027
1.7	0.69 ± 0.09	0.91 ± 0.03	28	5	0.0031
2.0	0.66 ± 0.09	0.94 ± 0.03	35	4	0.0043
2.5	0.99 ± 0.60	0.95 ± 0.11	14	0	0.0068
3.0	0.96 ± 0.26	0.98 ± 0.06	21	1	0.0051
Weighted average values	0.76^a ± 0.17	0.87^a ± 0.03			0.004

^a The reciprocal squares of standard deviations are used as the weights of the individual b_L and b_G values.

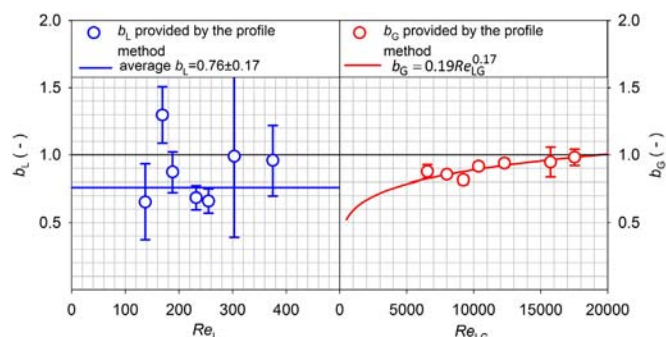


Fig. 6. The b_L and b_G values of MeOH-PrOH system with their standard deviations.

supporting the idea of the plug flow of the phases in the column and no or only negligible influence of the axial mixing on the mass-transfer characteristics of the wetted wall column.

According to the assumption (vii) stated in the Experimental section the liquid and the vapor phases in the column are at its boiling and dew point, respectively. This assumption implies the temperature difference between the phases and the occurrence of the heat transfer in the column. A simultaneous heat and mass transfer model (SHMT model) has been derived in order to enable the inspection of the heat transfer effect on the mass-transfer characteristics of the column.⁴ The model predicts subcooling of the liquid bulk of about 3 °C with respect to its boiling point (see Fig. 7), however, the b_L and b_G values evaluated by the profile method utilizing this model do not differ significantly from those listed in Table 4; for the conditions used in this paper the maximal difference in the component flux of 2% has been found. Therefore it was concluded that the heat transfer phenomena has also no or negligible influence on the mass-transfer characteristics of the wetted wall column.

5. Conclusions

This article brings a mass-transfer data ($HETP$ and k_L , k_G) obtained under distillation conditions in the wetted-wall column

⁴ Three mechanisms of the heat and mass transfer are assumed in the model: (i) the interfacial heat and mass flux controlled via the mass and heat transfer coefficients, respectively; (ii) the flux via bubbles potentially generated in the overheated liquid bulk; (iii) the flux via mist potentially generated in the subcooled vapor bulk. The overheating of the vapor and subcooling of the liquid are allowed. Heat transfer coefficients for the vapor phase are estimated according to the Dittus and Boelter (1930) and the liquid film heat transfer coefficient is estimated according to the Chun and Seban (1971). The model is solved for the corresponding boundary values and provides the concentration and temperature profiles along the column. The model is described in detail in the dissertation of Haidl (2016c).

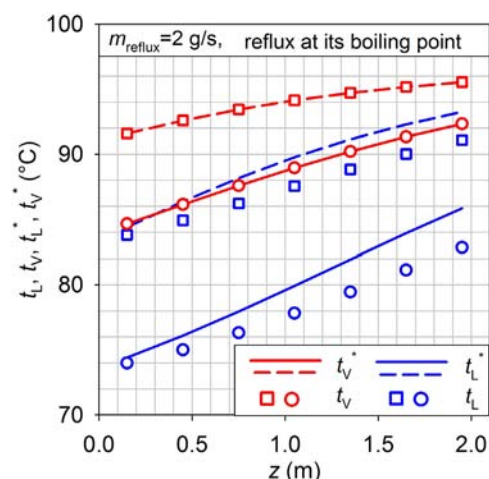


Fig. 7. The temperature profiles provided by the SHMT model. Squares and dashed-lines depict data for light component lean mixture, while circles and full-lines depict the data for light component rich mixture. Asterisk marks the saturated temperature of the phase bulk.

distilling methanol–n-propanol mixture under atmospheric pressure and the total reflux. The same type of the column was earlier used for the measurements of the mass-transfer coefficients under absorption conditions with the Reynolds and Schmidt numbers of the phases set to cover their whole range achieved during distillation experiments. The results of the absorption experiments have been correlated in the form of $Sh=f(Re, Sc)$ dependences.

The distillation $HETP$ values measured in the wetted wall column were found in average 10% higher than those calculated out of the Sh_L and Sh_G correlations based on the results of the experiments under absorption conditions. However, the precision of predicted $HETP$ depends strongly on the accuracy of the quantities used for the calculation of the utilized dimensionless criteria. Very poor reliability of widely used diffusivity models – especially those used for the calculation of the liquid diffusivity – has been noticed in this work and therefore the relative uncertainty of the predicted $HETP$ values is approximately 10–20%. In the frame of this uncertainty it must be only concluded, that the absorption and distillation data mutually agree. This finding, standing alone, supports rationality of several assumptions and approaches: 1) the rate based modeling of the processes 2) the possibility of the absorption mass-transfer coefficients transfer to distillation conditions through dimensionless correlations and 3) usual simplifications in description of the processes omitting phase flow non-ideality and thermal effects.

When the profile method has been applied to the distillation experimental data, the values of both mass-transfer coefficients

have been found lower than those predicted from the absorption results. This finding is in agreement with the *HETP* results. More importantly the higher dependence of the distillation Sh_G values on Re_{LG} has been revealed, confirming the results obtained earlier on the structured packings. While the lower values of distillation Sh_L and Sh_G (approximately 25% and 13% lower) can be explained as the result of the uncertainty of the diffusivity data, no such simple explanation can be found for the different phase flow dependence of Sh_G . As the observed difference was found not only for structured packings, but now also for the wetted wall column, it can't be accounted to the different formation of the interfacial area. Apparently, there is at least one unaccounted phenomenon which affects differently the mass-transfer performance of the absorption and distillation packed columns. Axial mixing of the phases and the heat-transfer influence were studied as such potential phenomena with both of them found to have marginal effects on the results of this work.

Any further study of the differences observed in this work is most probably not possible until more reliable diffusivity data are available, as the uncertainty of the results already precludes clear decisions. The uncertainty of the results has also implications for the application of the packed absorption/distillation rate-based modeling. While the rate-based modeling is physically more sound way of modeling of the packed columns, precision of the results depends on that of the input parameters. Out of the physical quantities necessary for their calculation we consider the diffusivities to be the most important aim for further studies due to their strong influence on the calculated mass-transfer coefficient values and in the same time due to their contemporary low precision.

Acknowledgment

Authors are grateful to Raschig GmbH for financial support of the project and to the Czech Science Foundation for supporting the project through Grant 13-01251S.

References

- Billet, R., Schultes, M., 1999. Prediction of mass transfer columns with dumped and arranged packings. Updates summary of the calculation method of Billet and Schultes. *Trans. IChemE* 77 (Part A), 498–504.
- Chilton, T.H., Colburn, A.P., 1934. Mass transfer (Absorption) coefficients – prediction from data on heat transfer and fluid friction. *Industrial and Engineering Chemistry* 26 (11), 1183–1187.
- Chun, K.R., Seban, R.A., 1971. Heat transfer to evaporating liquid films. *J. Heat Transf.* 93 (4), 391–396.
- Dittus, F.W., Boelter, L.M.K., 1930. Heat Transfer in Automobile Radiator of the Tubular Type, 2nd ed. University of California at Berkley Publications in Engineering.
- Fuller, E.N., Schettler, P.D., Giddings, J.C., 1966. A new method for prediction of Binary gas-phase diffusion coefficients. *Ind. Eng. Chem.* 58 (5), 18–27.
- Gilliland, E.R., Sherwood, T.K., 1934. Diffusion of Vapors into Air Streams. *Industrial and engineering chemistry* 26 (5), 516–523.
- Haidl, J., Rejl, F.J., Valenz, L., Kordač, M., Moucha, T., Labík, L., Schultes, M., 2016a. Absorption in wetted-wall column with phase properties close to distillation conditions. *Chem. Eng. Sci.* 144, 126–134.
- Haidl, J., Rejl, F.J., Valenz, L., Moucha, T., Schultes, M., 2016b. Analogy of mass transfer in absorption and distillation columns: wetted wall column study distillation. AIChE Spring Meeting, Houston, Texas.
- Haidl, J., 2016c. Wetted-wall column study of absorption and distillation process analogy. Dissertation defendend at UCT Prague.
- Hanley, B., Chen, Ch., 2012. New mass-transfer correlations for packed towers. *AIChEJ* 58 (1), 132–152.
- Henley, E.J., Seader, J.D., Roper, D.K., 2011. *Separation Process Principles*, 3rd ed. John Wiley & Sons, Asia.
- Hu, W., Xie, J., Chau, H.W., Si, B.C., 2015. Evaluation of parameter uncertainties in nonlinear regression using Microsoft Excel Spreadsheet. *Environm. Syst. Res.* 4, 4.
- Jackson, M.L., Ceaglske, N.H., 1950. Distillation, vaporization, and gas absorption in a wetted-wall column. *Ind. Eng. Chem.* 42 (6), 1188–1198.
- Johnstone, H.F., Pigford, R.L., 1942. Distillation in a wetted-wall column. *Trans. Am. Inst. Chem. Eng.* 38 (38), 25–51.
- Kayihan, F., Sandall, O.C., Mellichamp, A., 1975. Simultaneous Heat and Mass Transfer in Binary Distillation – 1. *Theor. Chem. Eng. Sci.* 30 (11-C), 1333–1339.
- Kayihan, F., Sandall, O.C., Mellichamp, A., 1976. Simultaneous heat and mass transfer in binary distillation – 2. *Exp. Chem. Eng. Sci.* 32, 747–754.
- Linek, V., Moucha, T., Prokopova, E., Rejl, J.F., 2005. Simultaneous determination of vapour- and liquid-side volumetric mass transfer coefficients in distillation column. *Chem. Eng. Res. Des.* 83 (A8), 979–986.
- Olujić, Z., Kamerbeek, A.B., de Graauw, J., 1999. A corrugation geometry based model for efficiency of structured distillation packing. *Chem. Eng. Process.* 38 (38), 683–695.
- Rejl, F.J., Valenz, L., Haidl, J., Kordač, M., Moucha, T., 2015. On the modeling of gas-phase mass-transfer in metal sheet structured packings. *Chem. Eng. Res. Des.* 93, 194–202.
- Rejl, F.J., Valenz, L., Linek, V., 2010. Profile method for the measurement of kLa and kVa in distillation columns. validation of rate-based distillation models using concentration profiles measured along the column. *Ind. Eng. Chem. Res.* 49 (9), 4383–4398.
- Rocha, J.A., Bravo, J.L., Fair, J.R., 1996. Distillation columns containing structured packings: a comprehensive model for their performance. 2. Mass-Transfer Model. *Ind. Eng. Chem. Res.* 35 (35), 1660–1667.
- Shuck, F.O., Toor, H.L., 1963. Diffusion in the three-component liquid system methyl alcohol-n-propyl alcohol-isobutyl alcohol. *J. Phys. Chem.* 67 (67), 540–545.
- Surowiec, A.J., Furnas, C.C., 1942. Distillation in a wetted-wall tower. *Trans. Am. Inst. Chem. Eng.* 38, 53–89.
- Tyn, M.T., Calus, W.F., 1975. Diffusion coefficients in dilute binary liquid mixtures. *J. Chem. Eng. Data* 20 (1), 106–109.
- Valenz, L., Rejl, F.J., Šíma, J., Linek, V., 2011a. Absorption mass-transfer characteristics of Mellapak packings series. *Ind. Eng. Chem. Res.* 50 (21), 12134–12142.
- Valenz, L., Rejl, F.J., Linek, V., 2011b. Effect of gas- and liquid-phase axial mixing on the rate of mass transfer in a pilot-scale distillation column packed with Mellapak 250Y. *Ind. Eng. Chem. Res.* 50 (50), 2262–2271.
- Washburn, E.W., 2003. *International Critical Tables of Numerical Data, Physics, Chemistry and Technology. Interdiffusion of Gases and Vapors*, Knovel, pp. 1926–1930.
- Wilke, C.R., Chang, P., 1955. Correlation of diffusion coefficients in dilute solutions. *Am. Inst. Chem. Eng. J.* 1 (1), 264–270.
- Wilke, C., Lee, C., 1955. Estimation of diffusion coefficients for gases and vapors. *Ind. Eng. Chem.* 47 (47), 1253–1257.

HYDRAULIC AND MASS TRANSFER CHARACTERISTICS OF PACKINGS FOR ABSORPTION AND DISTILLATION COLUMNS. RAUSCHERT-METALL-SATTEL-RINGS

V. LINEK, T. MOUCHA AND F. J. REJL

Department of Chemical Engineering, Prague Institute of Chemical Technology, Prague, Czech Republic.

Hydraulic and mass transfer data including pressure drop, liquid holdup, gas- and liquid-side volumetric mass transfer coefficients and interfacial area are measured for Rauschert-Metall-Sattel-Rings (RMSR) 25, 40 and 50. The volumetric gas- and liquid-side mass transfer coefficients are measured using the absorption systems SO₂/air-1 M NaOH and O₂/air-water, respectively. The interfacial area is measured by the CO₂/air-1 M NaOH absorption system. The data are described by 2- or 3-parameter empirical correlations and, with significantly larger scatter, also by well-known models taken from the literature. The results are compared with those for classical 25 and 50 mm metal Pall rings and with the results given by the Norton company for geometrically similar Intalox metal tower packing—packings for which a similar range of applications can be expected. Height equivalent to a theoretical plate (HETP) calculated from the mass transfer characteristics of the RMSR packings are compared with the experimentally measured HETP for the atmospheric distillation of isooctane-toluene, methanol-ethanol and ethanol-water.

Keywords: absorption; mass-transfer; packed-column; volumetric-mass-transfer-coefficient; HETP; pressure-drop.

INTRODUCTION

Hydraulic and transport characteristics of column packings are used for absorption and distillation column design as well as for comparison of the efficiency of individual packing types. Models of mass transfer in packed columns do not properly take account of the dependency of the characteristics on the shape and size of the packing. Therefore experimental characterization is necessary for each new packing type. Experimental data are the most reliable and accurate basis for packed column design. Further development of efficiency models for columns must await the accumulation of an improved data bank but it is likely that for random packings there will always be an empirical, experience-related ingredient in any predictive models, simply because of the randomness in the bed elements¹.

Absorption experiments, unlike distillation, are suitable for this task as they can directly address each characteristic by selecting a suitable absorption system. The series of articles by Linek *et al.*²⁻⁴ gives a complete set of transport characteristics for some selected packings (Combi-Pack 250 and NFOV 350^{2,4} which correspond with Mellapak 250 and 350; Razel rings which correspond with Pall rings³). The characteristics include pressure-drop, liquid hold-up, effective interfacial area and gas-side and liquid-side volumetric mass transfer coefficients.

This work gives a complete set of characteristics for RMSR 25, 40 and 50 mm packings. The procedure of

HETP calculation from the mass transfer characteristics is shown. The reliability of the calculation is tested by comparing the HETP values from the absorption data with experimental HETP values for various atmospheric distillation systems.

EXPERIMENTAL

Packing

The characteristics of the packings used in this study are given in Table 1. The shape of Rauschert-Metall-Sattel-Rings corresponds with the Intalox packing of Norton.

Apparatus

Absorption experiments were performed in the apparatus described earlier⁵. The absorption column was constructed of a perspex tube of 0.29 m inner diameter packed to the height of 1.2 m. Although the column diameter is only six times the diameter of RMSR 50-4, it was used because experimental results obtained in our laboratory earlier showed a negligible wall effect (with a column of i.d. 0.39 m the same values $k_L a$ and $k_G a$ were obtained for a packing of nominal size 50 mm as in a column of i.d. 0.29 m). Two liquid distributors were used: for lower liquid flow rates ($B < 20 \text{ m}^3 \text{ m}^{-2} \text{ h}^{-1}$) a disk liquid distributor with 2500 openings of 3 mm diam. per square meter and at

Table 1. Characteristics of the packings in experimental columns.

Packing	n [pcs m ⁻³]		a_r [m ² m ⁻³]			F_{pd}	
	Our data	Norton ⁹	Our data	Norton	Rauschert	Our	Ref ⁸
RMSR 25-3; Intalox 25	123 834 118 175*	168 425	200 191*	272**	223	39.2	43
RMSR 40-3; Intalox 40	50 465	50 140	142	143**	175	24.6	26
RMSR 50-4; Intalox 50	13 914	14 685	86	91**	115	16.4	17
Pall ring metal 25 mm	48 215		200				
Pall ring metal 50 mm	5 495		99				

* In distillation column. The other one in absorption column.

** Calculated from our experimental a_r values using the number of pieces per m³ given by Norton⁹.

higher liquid flow rates an eleven-armed liquid distributor with 630 openings per square meter. The temperature of both inlet streams was maintained at $20 \pm 0.3^\circ\text{C}$. Gas and liquid could be sampled at three different levels along the packed bed. The gas sample was sucked from 3 gas samplers distributed regularly over the column cross-section. The liquid samples were taken from a free-flow channel placed across the column diameter. The height of a measuring section of the packing, i.e., the distance between the sampling points, was 1.04 m for measurements of a and $k_L a$ and 0.5 m for measurement of $k_G a$. A polarographic oxygen probe was used to measure the oxygen concentration in the liquid samples. The CO₂ and SO₂ concentrations in the gas samples were measured by IR analyzers (UNOR 4N, Maihak). The absorption experiments were performed at liquid velocities from 1 to 120 m h⁻¹ and at gas velocities corresponding to F values in the range from 0.023 to 2.49 Pa^{1/2}.

Measurement of Liquid Hold-Up

Liquid hold-up was calculated from a mean residence time (RT) of the liquid flowing through the packed column. The RT was determined by tracer experiments. The NaCl solution (100 g NaCl l⁻¹) was injected into the liquid distributor at the column top and the conductivity probe response was recorded in the liquid withdrawn from the column bottom by a peristaltic pump. The liquid phase mean residence time was calculated from the conductivity probe response curve $s(t)$ using the equation:

$$\tau_L = \frac{\int_0^{t_s} t \cdot s(t) dt}{\int_0^{t_s} s(t) dt} \quad (1)$$

The RT in the packing was calculated as the difference between the RT measured at the two different packing heights. The RT measured with a packing height of 0.3 m was subtracted from that measured for the 1.2 m packing height. The difference represents the liquid residence time for the packing height of 0.9 m. In this way the effect of both liquid distributor and the sampling channel with the conductivity probe on the liquid residence time were eliminated. The volume fraction of liquid held in the packing, ε_L was calculated from:

$$\varepsilon_L = \frac{[(\tau_L)_{1.2} - (\tau_L)_{0.3}]B}{0.9 \cdot 3600} \quad (2)$$

The water circulating in the column was replenished when the conductivity probe signal reached the limit of the linearity range.

Measurement of Interfacial Area

Chemisorption of diluted CO₂ (1 vol% in air) into aqueous NaOH solution of initial concentration 1 kmol m⁻³ was used. The method employs the fact that the resistance to mass transfer is limited to the liquid film in this absorption system and, further, the mass transfer coefficient is independent of the hydrodynamics of both phases. The method was described in detail elsewhere^{5,6}. The specific interfacial area a was evaluated from the relation⁶

$$a = \frac{K_G a}{2.24 \cdot 10^{-3} \sqrt{c_{\text{OH}}}} \quad (3)$$

where the value of $2.24 \cdot 10^{-3} \text{ m s}^{-1}$ is the mass transfer coefficient of CO₂ into 1 M NaOH solution at 20°C and c_{OH} is the concentration of OH⁻ ions in the NaOH solution circulated through the column. The latter was determined by titration. The overall volumetric mass transfer coefficient of carbon dioxide, $K_G a$, was determined experimentally employing the relationship⁵:

$$K_G a = \frac{v_G}{H} \ln \frac{x_{G1}}{x_{G2}} \quad (4)$$

where x_{G1} and x_{G2} CO₂ concentrations in the lower and upper cross sections, respectively and the height of the measuring section of the packing H was equal to 1.04 m.

Measurement of $k_L a$

The volumetric liquid side mass transfer coefficient, $k_L a$, was measured using the system O₂/air-water in which the main resistance to the mass transfer is on the liquid side. Oxygen from air saturated water was desorbed into a stream of nitrogen at low gas velocity $F = 0.023 \text{ Pa}^{1/2}$. The method was described in detail elsewhere^{5,6}. The $k_L a$ value was calculated from the oxygen probe readings r_1 and r_2 in liquid samples taken from the upper and the lower sampling point of the measuring section, respectively, from the equation:

$$k_L a = \frac{v_L}{H} \ln \frac{r_1}{r_2} \quad (5)$$

The height of the measuring section was $H = 1.04 \text{ m}$.

Measurement of $k_G a$

The volumetric mass transfer coefficient in gas, $k_G a$, was determined by absorption of diluted SO_2 (0.02 vol% in air) into an aqueous solution of NaOH with initial concentration 1 kmol m^{-3} . The main resistance in this system is in the gas phase as all transferred SO_2 reacts in an instantaneous reaction at the interface. This was verified earlier⁶. The solution was circulated and replenished when the NaOH concentration decreased below 0.1 kmol m^{-3} . The $k_G a$ value was calculated from the relationship:

$$k_G a = \frac{v_G}{H} \ln \frac{x_{G1}}{x_{G2}} \quad (6)$$

where x_{G1} and x_{G2} are the SO_2 gas concentrations at the lower and the upper sampling points, respectively. The height of the measuring section was $H = 0.5 \text{ m}$. A higher layer of packing than 0.5 m lead to SO_2 output concentration below 5% of the input, which produced an unacceptable error in $k_G a$. The experiments were performed at four gas velocities ($F = 0.255, 0.575, 1.21$ and $2.49 \text{ Pa}^{1/2}$) for liquid flow rate B from 1 to $100 \text{ m}^3 \text{ m}^{-2} \text{ h}^{-1}$.

Measurement of HETP

The distillation experiments were performed on RMSR 25-3 using the systems methanol-ethanol and ethanol-water at atmospheric pressure. The column, of diameter 0.1 m and height of packing 1.67 m, operated under total reflux. Measured quantities included compositions of reflux and the liquid leaving the packing and flow rate of reflux. The HETP value was evaluated as the ratio of the height of packing to the number of theoretical plates. The vapour-liquid equilibria were taken from the literature⁷, together with HETP values for the system isooctane-toluene¹⁵.

The model used for calculation of HETP from absorption mass transfer data was described in detail elsewhere⁶. The formula relating HETP to the mass transfer kinetic parameters based on plug flow of both phases in the column was used:

$$\text{HETP} = \frac{v_L}{K_L a} \frac{\ln \left(m \frac{v_L}{v_G} \right)}{m \frac{v_L}{v_G} - 1} \quad (7)$$

where

$$m = \frac{dx_i}{dy_i} \frac{\rho_L}{\rho_G} \frac{M_G}{M_L}; \quad K_L a = \left(\frac{1}{k_L a} + \frac{m}{k_G a} \right)^{-1} \quad (8)$$

The local slope of the equilibrium curve m and the overall volumetric mass transfer coefficient $k_G a$ are substituted into Equation (7) at the temperature and pressure of the theoretical plate. The absorption mass transfer characteristics of the packing ($(k_G a)_A$ and $(k_L a)_A$), measured at the same flow rates as they are in the distillation column, were transformed to conditions at a given distillation theoretical plate (temperature, pressure, physical properties of both phases

and number n of pieces of packing per m^3), $(k_G a)_D$ and $(k_L a)_D$ using following relations:

$$\frac{(k_G a)_D}{(k_G a)_A} = \left(\frac{D_{GD}}{D_{GA}} \right)^{2/3} \frac{n_D}{n_A} \quad (9)$$

$$\frac{(k_L a)_D}{(k_L a)_A} = \left(\frac{D_{LD}}{D_{LA}} \right)^{2/3} \frac{n_D}{n_A} \quad (10)$$

The ratio of diffusivities of components transferred in absorption D_A (oxygen or sulphur dioxide) and distillation D_D (methanol, ethanol, water, isooctane and toluene) were estimated from semiempirical correlations by Fuller *et al.*¹⁴. This simple transformation based only on difference in diffusivities for the absorption and distillation systems has provided (see the model 3⁶) the best results compared with transformations based on more general correlations given in the literature¹¹⁻¹³, indicating that the influence of other physical properties and geometry of the packing are not well established in the general correlations when large extrapolation (in temperature) is needed. The HETP value depends on the position in the column. In the figure the mean values are given which were calculated as an arithmetic mean of the values calculated for the liquid compositions on individual stages along the column from the top to the bottom of the packing. For the system isooctane-toluene the mean values of HETP were calculated in the interval 0.2 to 0.7 of mole fraction of isooctane as the experimental values of the concentrations at the bottom and the top of column are not given¹⁵.

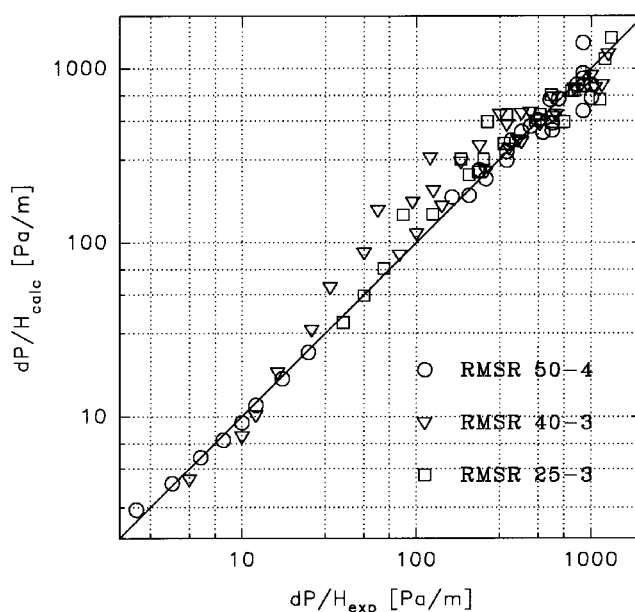


Figure 1. Comparison of measured and calculated values of pressure drop from Equation (10).

Table 2. Parameters of approximating Equations (13), (14), (16) and (18).

$i =$	RMSR 25-3			RMSR 40-3			RMSR 50-4		
	1	2	3	1	2	3	1	2	3
a_i	0.00784	1.165	0.254	0.009427	0.853	0.145	0.008945	0.542	0.0319
b_i	72.92	0.418	0.0787	65.21	0.4181	0.0952	51.28	0.3839	0.0780
d_i	0.001929	0.719	—	0.001113	0.788	—	0.001041	0.794	—
e_{i1}	0.057451	0.2678	-0.0197	-0.2289	0.6643	-0.1393	-0.2443	0.4261	-0.0878
e_{i2}	0.4975	-0.0442	0.04031	0.4504	0.04774	0.0125	0.4257	0.2889	-0.0452
e_{i3}	-0.1674	0.14838	-0.0619	-0.0793	-0.019	-0.013	-0.1023	-0.0997	0.00938

HYDRAULIC AND MASS TRANSFER CHARACTERISTICS OF RMSR PACKING

Pressure Drop

The pressure drop of RMSR as a function of gas and liquid flow rates is described well by a correlation presented by Robbins⁸:

$$\frac{dP}{H} = 1.972 Q + 6.061 \cdot 10^{-9} Q^4 S^{0.1} \quad (11)$$

where

$$Q = F^2 F_{pd} \cdot 10^{0.001236 \cdot S}$$

$$S = B F_{pd}^{0.5} \mu_L^{0.1} \quad (12)$$

The dry-bed packing factors F_{pd} given by Robbins for Intalox packings differ slightly from those obtained by fitting of our pressure drop data, see Table 1. Measured and calculated values of pressure drop from the correlation are compared in Figure 1. The mean value of the relative difference of both values is 20%. Using the original values of the dry-bed packing factor F_{pd} given by Robbins for Intalox packing the relative difference is 50%.

Liquid Hold-Up

The liquid hold-up dependencies on gas and liquid flow rates for RMSR packings are shown in Figure 2. The

dependencies for gas flow velocity 2.3 and 2.89 m/s include two or three points only for each packing size due to flooding. The data are correlated by the following equation

$$\varepsilon_L = a_1 B^{a_2 - a_3 \log B} \quad (13)$$

with standard deviations 7.3%, 7.6% and 6.9% for RMSR 25-3, 40-3 and 50-4, respectively. The parameters a_i for the packings are given in Table 2. The ε_L values predicted by Billet's model¹³ are also given in the Figure 2. Fairly good agreement (differences up to 25%) was found for RMSR 50-4 but in the case of RMSR 25-3 the differences between Billet's prediction and the experimental data reach 50%.

Interfacial Area

Figure 3 shows the a/a_i values of the RMSR packings measured at various gas and liquid velocities. The effective area is independent of gas velocity over the range of measurements. The following equation fits the data well with standard deviations of 16%, 8.1% and 10%, for RMSR 25-3, 40-3 and 50-4, respectively:

$$a = b_1 B^{b_2 - b_3 \log B} \quad (14)$$

The parameters b_i are given in Table 2. The a/a_i values predicted by Billet's model¹³ are also presented in Figure 3. They are significantly lower than the present experimental

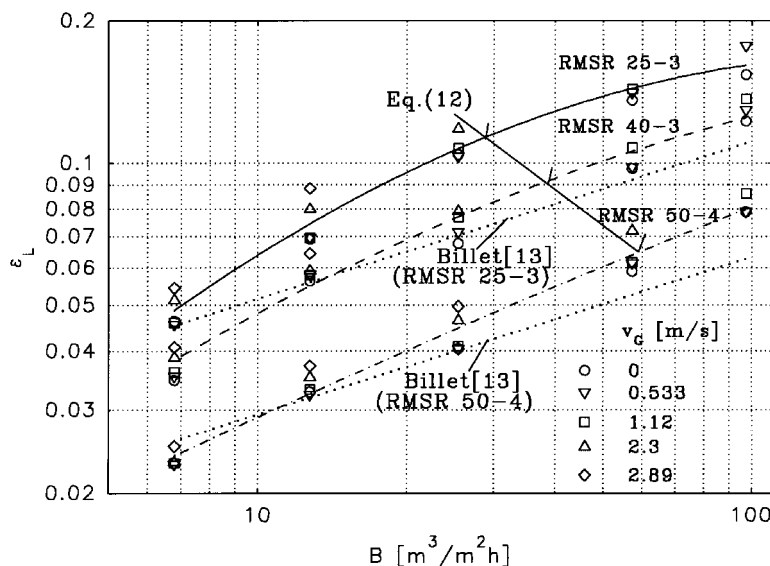


Figure 2. Liquid holdup ε_L as a function of gas and liquid flow rates and the comparison with the prediction of Billet's model¹³.

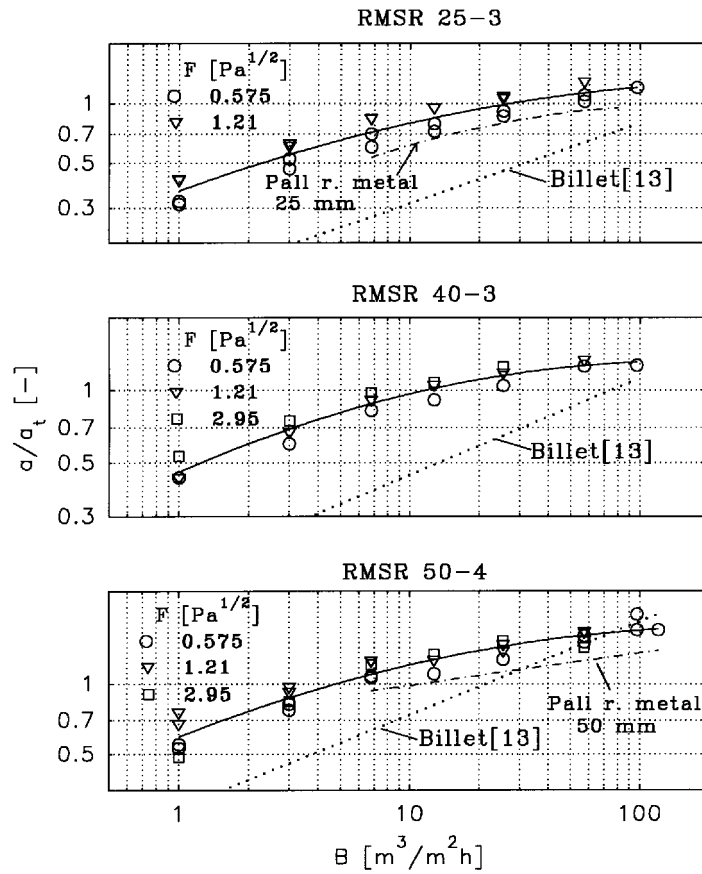


Figure 3. Effective to total surface area ratio a/a_t , as a function of gas and liquid flow rates. Comparison with data for 25 and 50 mm metal Pall rings and comparison with Billet's model³.

values, especially at lower liquid loads. In Figure 3 the comparison is also shown of the a/a_t values with those measured previously⁶ for 25 and 50 mm metal Pall rings. The values a/a_t are practically the same for both the packings of the same nominal size.

In Figure 4 our data are compared with data from Norton⁹ given in the form of $K_G a$ for 1% CO_2 absorption into 4% NaOH (= 1 M) solution at 24°C, 25% conversion to carbonate and gas flow rate $1.22 kg m^{-2} s^{-1}$. Norton's $K_G a$ data were recalculated for a temperature of 20°C using literature

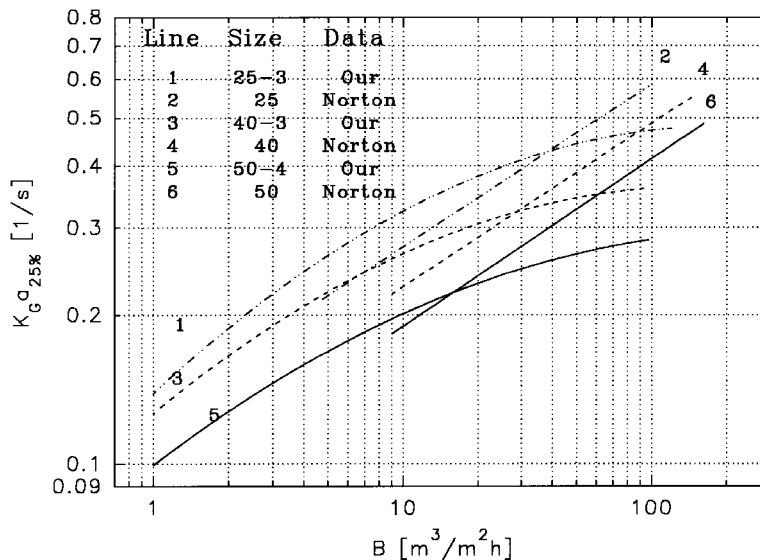


Figure 4. Comparison of our $k_G a$ data with data by Norton⁹ which were recalculated for 20°C and 25% conversion to carbonate using Equation (15).

data¹⁰ on the kinetics, diffusivity and solubility of CO₂ in the solution from following relation:

$$(K_G a)_{20} = (K_G a)_{24} \frac{(H_{\text{CO}_2} \sqrt{D_{\text{CO}_2} k_2})_{20}}{(H_{\text{CO}_2} \sqrt{D_{\text{CO}_2} k_2})_{24}}$$

$$= (K_G a)_{24} \frac{2.24 \cdot 10^{-3}}{2.51 \cdot 10^{-3}} \quad (15)$$

At higher liquid flow rates the data of Norton are higher than our data. At $B = 100 \text{ m}^{-3} \text{ m}^{-2} \text{ h}^{-1}$ the overestimation reaches 50% for packings of nominal sizes 40 and 50 mm.

Liquid-Film Mass Transfer Coefficient $k_L a$

The $k_L a$ data for all packing sizes measured at low gas velocity $F = 0.023 \text{ Pa}^{1/2}$ are given in Figure 5. They are well fitted by the following expression:

$$k_L a = d_1 B^{d_2} \quad (16)$$

with standard deviations of 5.5%, 6.6% and 3.6% for RMSR 25-3, 40-3 and 50-4, respectively. The parameters d_i for the packings are given in Table 2. To compare the experimental data with literature we fitted Billet's model¹³ to our $k_L a$ data and obtained the characteristic constants C_L , which are not available for RMSR or Intalox metal packing. C_L values of 1.362, 1.075 and 1.158 with standard deviations of 5.9%, 12.5% and 10.2% were obtained for RMSR 25-3, 40-3 and 50-4, respectively. In Figure 5 a comparison is also shown of the $k_L a$ values with those measured previously⁶ for 25 and 50 mm metal Pall rings. The values are practically the same for the packings of the nominal size 50 mm. For the smaller packings (25 mm) the data for RMSR are higher by up to 50% at low liquid rates.

For liquid-side mass transfer coefficient k_L of oxygen to water at 20°C it follows from Equations (14) and (16):

$$k_L = \frac{d_1}{b_1} B^{d_2 - b_2 + b_3 \log B} \quad (17)$$

The parameters d_i and b_i are given in Table 2. The values of k_L ranged from $2.7 \cdot 10^{-5}$ to $2.8 \cdot 10^{-4} \text{ m s}^{-1}$ for B in the

range from 3 to $100 \text{ m}^3 \text{ m}^{-2} \text{ h}^{-1}$. The values of k_L are needed when absorption with chemical reaction take place and a chemical enhancement factor has to be calculated.

Gas-Film Mass Transfer Coefficient $k_G a$

The experimental $k_L a$ data for RMSR packing are given in Figure 6. They are well fitted by the following expressions

$$k_G a = 10^{e_1} B^{e_2 + e_3 \log B} \quad (18)$$

$$e_j = e_{1j} + e_{2j} F + e_{3j} F^2 \quad \text{for } j = 1, 2, 3$$

The parameters e_{ij} for the packings are given in Table 2. Lines in the figure represent Equation (18) and the standard deviations are also given there for individual packing sizes.

A comparison with Billet's mode¹³ has been made again with characteristic constants C_V obtained by fitting the model to our experimental data. Comparison of the data calculated using these constants in Billet's model with the experimental data is given in Figure 7. In contrast to the $k_L a$ data Billet's model shows higher deviations, and especially in the region of lower liquid loads the differences reach more than 50%.

A comparison of the $k_G a$ values for RMSR 25-3 with those measured previously⁶ for metal Pall rings 25 is shown in Figure 8. The differences between the characteristics of both packing types are not higher than 25%. Pall rings gave higher $k_G a$ in the middle part of the gas velocity range while the RMSR gave rather higher $k_G a$'s at the lowest and highest gas velocities.

HETP

The measured values of HETP are compared with those calculated from absorption mass transfer data in Figure 9 for the different sizes of RMSR packing and distillation systems. The calculated values of HETP differ by less than $\pm 15\%$ from the experimental values for the distillation systems studied. An exception are the data obtained at extremely low gas flow rates ($F < 0.3 \text{ Pa}^{1/2}$) in the system ethanol-methanol for which the respective difference reached 46%.

CONCLUSIONS

Hydraulic and mass transfer characteristics are given for Rauschert-Metall-Sattel-Rings 25, 40 and 50 in the form of the relations which describe the influence of gas and liquid flow rates.

The data are compared with literature models and deviations can reach more than 50% even if the characteristic constants specific for the packing type and size are obtained by fitting to the same set of experimental data ($k_G a$ data). In the case of general models without characteristic constants specific for each packing the predicted values can differ from the experimental data by multiples (effective surface area). In the range of gas and liquid velocities used in transport characteristics determination it is worth using empirical correlations in column design. The RMSR characteristics are compared with data for metal Pall rings and Intalox packing which are of the same size as RMSR. The absorption mass transfer data are used for calculation of HETP for atmospheric distillation of methanol-ethanol, ethanol-water and

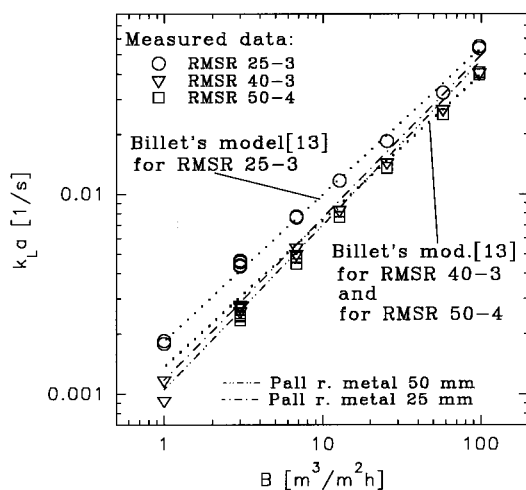


Figure 5. Liquid-side volumetric mass transfer coefficient $k_L a$ as a function of liquid flow rate. Comparison with data for 25 and 50 mm metal Pall rings and comparison with Billet's model fitted to our data.

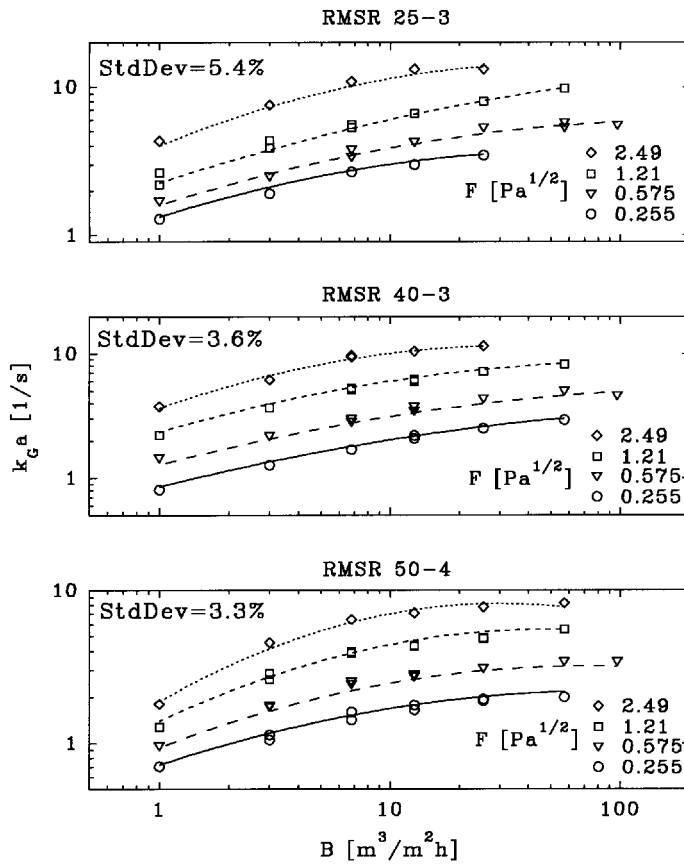


Figure 6. Gas-side volumetric mass transfer coefficient k_Ga as a function of gas and liquid flow rates. Lines: Equation (18).

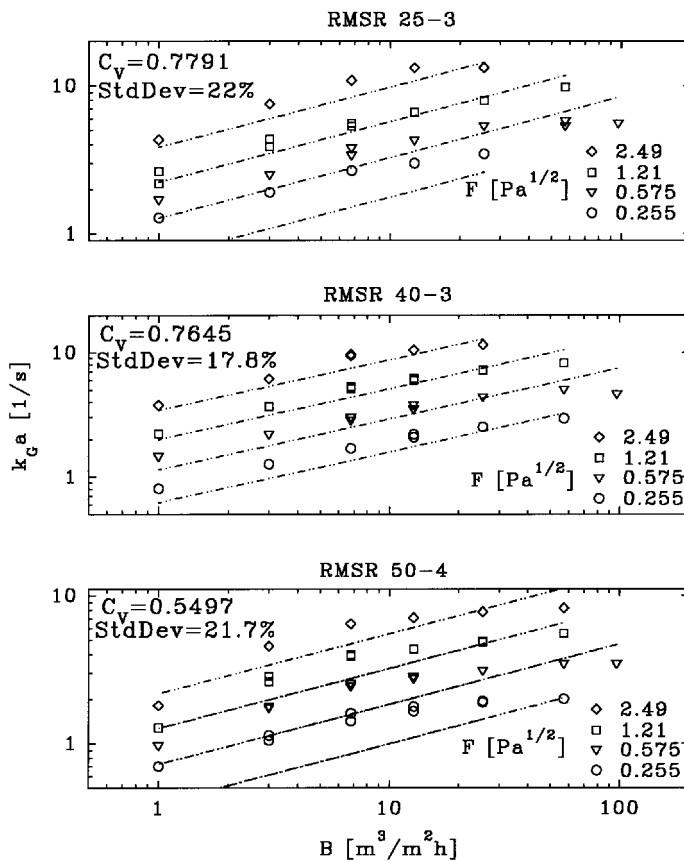


Figure 7. Gas-side volumetric mass transfer coefficient k_Ga : comparison of our experimental data with Billet's model fitted to them.

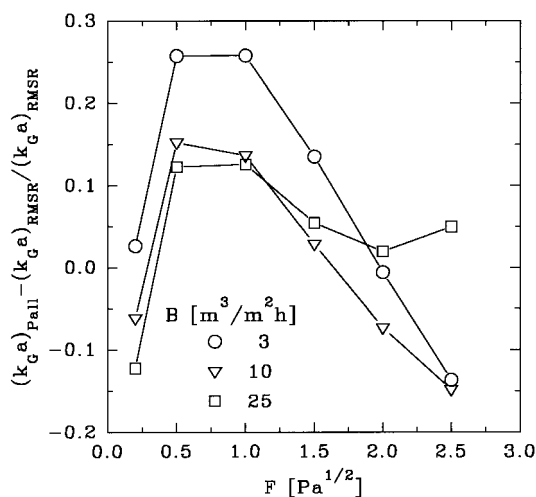


Figure 8. Comparison of the $k_G a$ values for RMSR 25-3 with those for metal Pall rings 25.

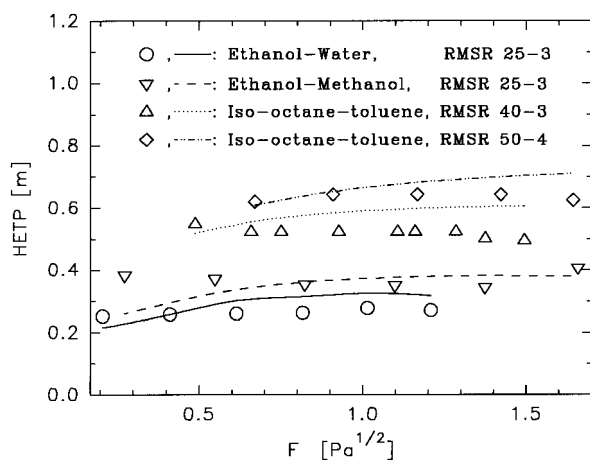


Figure 9. Comparison of measured values of HETP with those calculated from absorption mass transfer data using Equation (7).

isooctane-toluene systems. The calculated values differ from the experimental values of HETP by less than 15% in most cases.

NOMENCLATURE

a	effective interfacial area per unit packed volume, m^{-1}
a_t	geometric surface of packing per unit packed volume, m^{-1}
B	liquid load, $m^3/m^2 h$
D	molecular diffusivity, $m^2 s^{-1}$
dP/H	pressure drop, $Pa m^{-1}$
F	$= v_G \rho_G^{1/2}$, gas flow rate, $Pa^{1/2}$

F_{pd}	dry-bed packing factor
H	height of packed bed, m
H_{CO_2}	distribution coefficient for CO_2
K_i	overall mass transfer coefficient, $m s^{-1}$
k_i	mass transfer coefficient, $m s^{-1}$
M_i	molecular weight of phase i , $kmol kg^{-1}$
m	local slope of equilibrium curve
n	number of pieces of packing per unit volume, m^{-3}
r	oxygen probe signal, Pa
$s(t)$	time dependent conductivity probe signal
t	time, s
x_G	signal of gas analyzer, ppm
x_i	liquid phase molar fraction of component i in liquid-vapour equilibrium
y_i	vapour phase molar fraction of component i in liquid-vapour equilibrium

Greek symbols

ε	holdup
μ	viscosity, cP
v_i	flow rate of phase i , $m s^{-1}$
ρ	density $kg m^{-3}$
τ	residence time, s

Indexes

A	absorption column
D	distillation column
G	gas phase
L	liquid phase

REFERENCES

1. Fair, J.R., 1988, *Trans IChemE, Part A, Chem Eng Res Des*, 66: 363.
2. Linek, V., Sinkule, J. and Hovorka, F., 1994, *Chem Prüm*, 44/69: 130.
3. Linek, V., Sinkule, J. and Hovorka, F., 1995, *Chem Prüm*, 45/70: 3.
4. Linek, V. and Sinkule, J., 1997, *Chem Listy*, 91: 54.
5. Linek, V., Petříček, P., Beneš, P. and Brun, R., 1984, *Trans IChemE, Part A, Chem Eng Res Des*, 62: 13.
6. Linek, V., Sinkule, J. and Brekke, K., 1995, *Trans IChemE, Chem Eng Res Des*, 73, Part A: 398.
7. Gmehling, J. and Onken, N., 1981, *Collection Dachema-Chemistry Data Series*.
8. Robbins, L.A., 1991, *Chem Eng Progress*, May: 87.
9. Norton, *Intalox Metal Tower Packing*, Bulletin IM-82.
10. Pohorecki, R. and Moniuk, W., 1988, *Chem Eng Sci*, 43: 1677.
11. Onda, K., Sada, E. and Takeuchi, A., 1968, *J Chem Eng Japan*, 1: 612.
12. Onda, K., Takeuchi, A. and Okumoto, Y., 1968, *J Chem Eng Japan*, 1: 56.
13. Billet, R. and Schultes, M., 1993, *Chem Eng Technol*, 16: 1.
14. Perry, R.H. and Green, D., 1992, *Chemical Engineers Handbook, 6th edition* (McGraw-Hill Inc., New York).
15. Strigle, R.F. and Rukovena, F., 1979, *Chem Eng Progress*, March: 86.

ACKNOWLEDGEMENT

This work was supported by the Grant Agency of Czech Republic through the project No. 104/00/0574 and by the Czech Ministry of Education through the scientific project No. 07/409050702.

ADDRESS

Dr. T. Moucha, Department of Chemical Engineering, Prague Institute of Chemical Technology, Technika 3, 166 28 Praha 6, Czech Republic. E-mail: mouchat@vscht.cz

This manuscript was received 13 April 2000 and accepted for publication after revision 23 January 2001.

Absorption Mass-Transfer Characteristics of Mellapak Packings Series

L. Valenz, F. J. Rejl, J. Šíma, and V. Linek*

Department of Chemical Engineering, Prague Institute of Chemical Technology, CZ-166 28 Prague 6, Czech Republic

ABSTRACT: Mass-transfer characteristics were measured for the Mellapak structured packing series 250Y, 350Y, 452Y, and 500Y. $k_L a$ was measured by oxygen desorption from water and the effective mass-transfer area a by absorption of CO_2 into NaOH solution and also by oxygen absorption into a sulfite solution. Using Bodenstein numbers determined by means of the “cold” air–water dynamic experiments, effects of gas- and liquid-phase axial mixing on the characteristics were evaluated for Mellapak 250Y. Strikingly large differences found between the mass-transfer parameters and their flow dependencies measured in this work and those predicted by models especially designed for the prediction of the parameters in corrugated sheet structured packings (Billet, R.; Schultes, M. *Chem. Eng. Res. Des.* **1999**, *77*, 498; Rocha, J. A.; Bravo, J. L.; Fair, J. R. *Ind. Eng. Chem. Res.* **1996**, *35*, 1660; Olujić, Ž.; Kamerbeek, A. B.; Graauw, J. *Chem. Eng. Process.* **1999**, *38*, 683) demonstrate the bad physical relevance of the parameters predicted.

1. INTRODUCTION

Sulzer Mellapak corrugated-metal-sheet structured packings, apart from the Montz B1, Koch-Glitsch Flexipac, and Raschig Superpak packing series, are those most frequently used for the intensification of the interfacial mass transfer between gas/vapor and liquid in absorption and distillation columns. The most fundamental parameters describing the transfer in the packings are the contact (interfacial) area between gas and liquid (a) and the volumetric gas- and liquid-side mass-transfer coefficients (k_{GA} and $k_L a$). These parameters are used in the rational design of the columns, to enable the comparisons between the performance of the various commercial packings, and for vendors they facilitate the negotiations with the customer.

Test absorption systems are used for measuring the gas- and liquid-side mass-transfer coefficients, in which the mass-transfer resistance is concentrated either in the gas (k_{GA}) or the liquid phase ($k_L a$). The effective mass-transfer area is measured by chemisorption systems whereby the rate of absorption depends solely on the reaction rate constant of the reaction that accompanies the absorption, solubility, and diffusivity of the gas absorbed, i.e., on the quantities already well-established by independent experiments.

The wide differences between the transport parameters measured by various authors using the same packing and the same absorption test system have highlighted the need for the standardization of the methods for their measurement. This is demonstrated in Figure 1, where the contact area are shown as they were measured using the CO_2 /air–NaOH test system by four research teams (de Brito et al.,¹ Tsai et al.,² Murieta et al.,³ Linek and Sinkule⁴) in Mellapak 250Y and in the very similar Flexipac 2 packing.

Hoffmann et al.⁵ and Rejl et al.,⁶ who dealt with the standardization of the measuring methods of mass-transfer characteristics in absorption columns, have recommended the absorption/desorption of O_2 in/from water for the measurement of $k_L a$. CO_2 absorption is unsuitable due to its greater solubility and the possibility of a dissociation or precipitation reaction with components that are usually present in drinking water, which adhere to the packing surface, affecting its wettability. For the

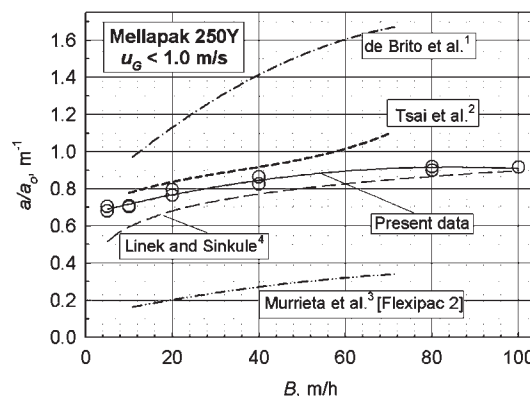


Figure 1. Gas–liquid contact area measured on Mellapak 250Y and Flexipac 2 packings by different research teams using the CO_2 /air–NaOH test system.

measurement of the gas–liquid contact area they recommended the chemisorption of a CO_2 /air mixture in a NaOH solution. For the evaluation of these experiments, both the physical properties, such as solubility H and diffusivity D_{CO_2} , and the reaction kinetic constant k_{OH} , originating from one research team should be utilized.² This recommendation stems from the fact that most of the kinetic constants published in the literature have been determined from absorption data, and therefore, the diffusion coefficient and solubility values used need to be identical to those used by the author team of the corresponding kinetic constant.

In this study, the recommended testing methods are used for the $k_L a$ and a measurement of the Mellapak packing series aimed at a thorough evaluation of the three well-established correlations for their prediction on conventional corrugated sheet structured packings, namely, the correlations of Billet and Schultes,⁸ Rocha

Received: March 22, 2011

Accepted: September 21, 2011

Revised: August 10, 2011

Published: September 21, 2011

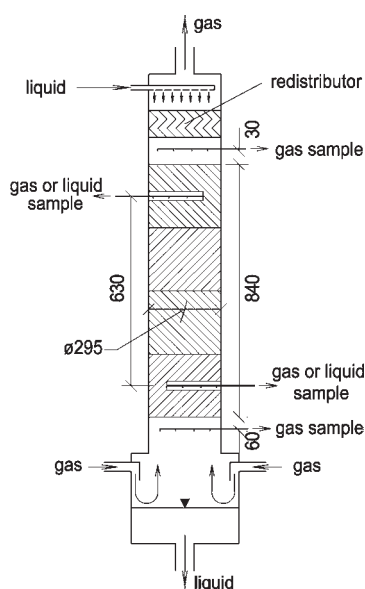


Figure 2. Configuration of the absorption column.

et al.,⁹ and Olujić et al.¹⁰ The gas-phase axial mixing effect on the measured values of the effective interfacial area is also tested.

2. EXPERIMENTAL SECTION

2.1. Configuration of the Absorption Test Column. The column, with a 0.29 m inner diameter, containing four elements of packing with a total bed height of 0.84 m, was equipped with four openings in which sampling devices for the withdrawal of liquid and gas samples could be placed at various cross-sections along the column (see Figure 2). The packings used were Mellapak 250Y, 350Y, 452Y, and 500Y. Uniform liquid distribution over the cross-section of the column was carried out by the pipe liquid distributor with drip-point density of 630 drip points/m². Since such distributors deliver inferior quality of initial liquid distribution, the Raschig liquid redistributor was situated beneath it. Used as the absorption liquids was distilled water ($k_L a$ measurements) and solutions of 1 kmol of NaOH/m³ or 0.8 kmol of Na₂SO₃ solutions (measurements of a). These solutions were recirculated. The experiments were performed with the temperature of the gas and liquid entering the column maintained at 20 °C; the gas was saturated with water vapor. The liquid velocities of 2.5, 5, (8), 10, (13), 20, 40, 60, 80, and 100 m³/(m² h) (or only to loading point) and gas velocities of 0.5, 1.0, 1.5, 2.0, and 2.5 m/s were utilized. The velocity of the nitrogen in the column during the measuring of $k_L a$ was approximately 0.03 m/s, ensuring that the oxygen concentration in the effluent gas was lower than 0.15 vol %. The temperature was maintained at a constant 20 °C during all the experiments.

The gas and liquid can be sampled at two different levels, two being located in the packed bed and one just above (0.03 m) and one just below (0.06 m) the packing. The openings for the sampling devices, shown in Figure 2, were drilled through the structured packing using an electrical-discharge technique. The height of a measuring section of the packing H , i.e., the height of packing between the sampling points, was 0.63 m for sampling in the bed and 0.84 m for sampling outside the bed. Great attention was paid to obtain the liquid and the gas samples uniformly from

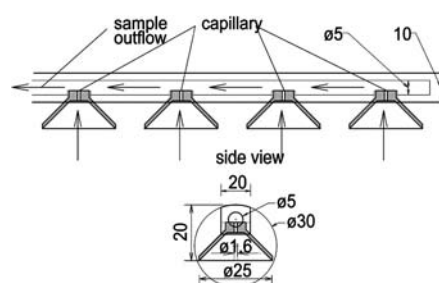


Figure 3. Detail of the sampling device.

the entire cross-section of the column. The sampling device (see Figure 3) was of a special design; the samplers enabled sampling from four regularly spaced points along a radial cross-section of the column. The main pressure drop in the individual sampling lines was concentrated in the capillaries placed in each of the lines. The capillaries are of the same size, ensuring thus the same sample flow rate in all the lines. The sampling device was turned downward for gas sampling and upward for liquid sampling.

Two optical oxygen probes Fibox 3 (PreSens) were used to measure the oxygen concentration in liquid samples withdrawn from the column continuously. Flow rates of the samples were very small because the optical probe does not consume oxygen, and thus, the steady-state probe signal is not affected by the liquid flow rate before the probe membrane. Similarly, the CO₂ concentration was measured in the gas samples withdrawn from the column continuously using IR analyzer S710 (Maihak). The sulfite concentration was determined using the classic back-iodometric titration.

2.2. Experimental and Evaluation Procedures. **2.2.1. $k_L a$ Measuring Procedure.** The volumetric liquid-side mass-transfer coefficient was measured using oxygen desorption from air-saturated water into a stream of nitrogen. Details of the method are given elsewhere by Linek et al.¹¹ The desorption experiment is simpler to carry out, and thus we prefer it to the absorption version. Nitrogen gas flow rate through a column is used low ($u_G \geq 0.03$ m/s), but it is sufficient to keep the oxygen concentration in the effluent gas lower than 0.2 vol %. This ensures negligible back-pressure of oxygen and negligible influence of axial dispersion in the gas phase. The $k_L a$ value was calculated from the readings of oxygen probes in liquid samples taken from the upper ($c_{O_2}^u$) and the lower ($c_{O_2}^l$) sampling points of the measuring section from

$$k_L a = \frac{u_L}{H} \ln \left(\frac{c_{O_2}^l}{c_{O_2}^u} \right) \quad (1)$$

where H is the height of the packed bed between two sampling points and u_L is the superficial liquid velocity. The effect of liquid-phase axial mixing on the $k_L a$ values is analyzed in the Appendix. There is shown that the axial mixing increases $k_L a$ values in comparison with the plug flow model. Their difference decreases with increasing liquid flow rate, is lower than 10% for the rates higher than 15 m/h, and reaches up to 43% at the lowest rate of 2.5 m/h.

2.2.2. Interfacial Area Measuring Procedures. The interfacial area of the packing was measured by using two different chemisorption systems: CO₂/air–NaOH and O₂–Na₂SO₃.

2.2.2.1. Chemisorption of Diluted CO₂ (1 vol % in Air) into Aqueous NaOH Solution of Initial Concentration of 1 kmol/m³. Details of this method have been presented by Linek et al.¹¹

The lye solution was replenished when the concentration of OH^- dropped below 0.4 kmol/m^3 . Assuming the plug flow and the negligible gas-phase mass-transfer resistance, the following relation is derived for the evaluation of the specific mass-transfer area (a) from CO_2 concentrations measured at the lower ($c_{\text{CO}_2}^l$) and upper ($c_{\text{CO}_2}^u$) sampling points in the column

$$a = \frac{u_G}{HK\sqrt{c_{\text{OH},\text{av}}}} \ln\left(\frac{c_{\text{CO}_2}^l}{c_{\text{CO}_2}^u}\right) \quad (2)$$

with

$$K = \text{He}\sqrt{D_{\text{CO}_2}k_{\text{OH}}} \quad (3)$$

He and D_{CO_2} are the distribution coefficient and diffusion coefficient of carbon dioxide, $c_{\text{OH},\text{av}}$ is an average OH-ion concentration in lye solution in the column, k_{OH} is the second-order kinetic constant of the reaction between carbon dioxide and OH-ions, and u_G is the superficial gas velocity. Validity of the assumptions used was carefully analyzed: Rejl et al.¹¹ evaluated gas-phase relative mass-transfer resistance occurring in the effective mass-transfer area measurements of various authors. They have shown that when the gas velocity is higher than 0.5 m/s , the errors in a are lower than 6%. The effect of gas-phase axial mixing on a values is evaluated in the Appendix, and it is shown there that the effect is negligible in our experiments.

The experimental value of $K = (2.24 \pm 0.08) \cdot 10^{-3} \text{ m/s}$ related to $c_{\text{OH}} = 1 \text{ kmol/m}^3$ measured by Linek et al.¹¹ was utilized. This value is in full agreement with that calculated from eq 3 using the recommended data of Pohorecki and Moniuk.⁷

2.2.2.2. Chemisorption of Oxygen into Aqueous Na_2SO_3 . Details of this method have been given by Linek et al.¹² The concentration of SO_3^{2-} ions did not drop below 0.4 kmol/m^3 during the experiments. The following relation was derived by Linek et al.¹³ for the oxygen absorption rate into the 0.8 kmol/m^3 sulfite solution from our own and all of the other available literature regarding kinetic data concerning the reaction between oxygen and sulfite in the presence of a cobalt catalyst

$$N/(\text{kmol}/(\text{m}^2 \text{ s})) = 4.469 \cdot 10^{-5} c_{\text{CoSO}_4}^{0.496} (\text{pH} - 6.459) \exp\left\{-\frac{E}{R}\left(\frac{1}{T} - \frac{1}{303.15}\right)\right\} \left(\frac{p_{\text{O}_2}}{9.5058 \cdot 10^4}\right)^{3/2} \quad (4)$$

N is oxygen flux at partial pressure of oxygen p_{O_2} (Pa) into 0.8 kmol/m^3 sulfite solution in the presence of cobalt catalyst concentration c_{CoSO_4} (kmol/m^3) at temperature T (K) and pH. The activation energy $E = 19000 \text{ kJ/kmol}$ is independent of pH and comprises the activation energy for the solubility and the molecular diffusivity of oxygen and for the second-order rate constant. The relation may be used for the interpretation of the oxygen absorption rate into a sodium sulfite solution provided that the following three conditions, discussed in detail by Linek and Vacek,¹⁴ are fulfilled:

(i) The concentration of sulfite should not drop below 0.45 kmol/m^3 in order to maintain a zero order of the reaction with respect to sulfite.

(ii) The oxygen concentration at the interface $c_{\text{O}_2}^*$ must be lower than $6 \cdot 10^{-4} \text{ kmol/m}^3$ in order to reach second order of the reaction with respect to oxygen. For air and oxygen absorption into 0.8 M sulfite this condition is fulfilled at a temperature of $20 \text{ }^\circ\text{C}$ and higher.

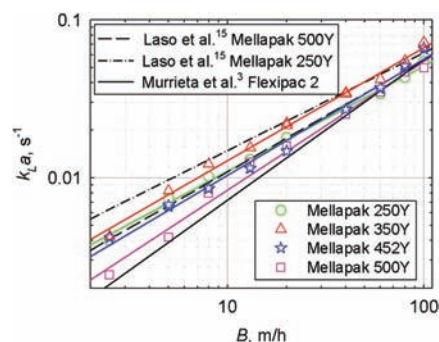


Figure 4. Volumetric mass-transfer coefficients for the Mellapak packings series.

(iii) Cobalt catalyst concentration, c_{CoSO_4} , must be greater than $3 \cdot 10^{-5} \text{ kmol/m}^3$. Then the oxygen absorption rate does not depend on the agitation intensity of the liquid phase.

The following relation can be derived for the evaluation of the specific mass-transfer area from sulfite concentrations measured at the upper ($c_{\text{Na}_2\text{SO}_3}^u$) and lower ($c_{\text{Na}_2\text{SO}_3}^l$) sampling points in the column taking into account axial dispersion in the liquid phase

$$a = \frac{(c_{\text{Na}_2\text{SO}_3}^u - c_{\text{Na}_2\text{SO}_3}^l)u_L}{2NH} + \frac{u_L}{2NB_{\text{OL}}}\left[\left(\frac{dc_{\text{Na}_2\text{SO}_3}}{dz}\right)_{z=l} - \left(\frac{dc_{\text{Na}_2\text{SO}_3}}{dz}\right)_{z=u}\right] \quad (5)$$

N in the equation is constant along the column and is calculated from eq 4 for the catalyst concentration, the partial pressure of oxygen in the gas phase, the mean temperature values, and the pH that persisted in the absorption column during the measuring of the area. The second term on the right side of the equation, representing the effect of liquid-phase axial mixing on sulfite balance, was not taken into account as it is negligible. It is demonstrated on the data of Mellapak 250Y in Appendix. The term's equal to $0.31 - 0.033 \text{ m}^{-1}$, while the first terms of the equation are higher than 150 m^{-1} for liquid flow rates from 40 to 100 m/h , i.e., when pure oxygen absorption was used.

The results measured using the sulfite method were not affected by the axial mixing either of the liquid phase (because absorption rate N does not change along the column) nor of the gas phase due to the small change in the oxygen concentration along the column. The air velocity in the column was 1 m/s , which ensures negligible oxygen concentration change along the column, or pure oxygen at a flow rate of 0.1 m/s was used. In our experiments, 0.8 kmol/m^3 sulfite solution with $5 \cdot 10^{-4} \text{ kmol/m}^3$ of CoSO_4 , initial pH 8.65 and temperature $20 \text{ }^\circ\text{C}$, was used. Absorption of air was used in the experiment performed at a liquid flow rate of 10 m/h and pure oxygen absorption in the experiments performed at liquid flow rates of 40, 80, and 100 m/h .

3. RESULTS AND DISCUSSION

3.1. Volumetric Liquid-Side Mass-Transfer Coefficient $k_L a$.

The experimental results presented in Figure 4 are well-correlated by the following relation

$$k_L a = a_1 B^{a_2} \quad (6)$$

The correlation is based on the experimental data in the range of liquid flow rate from 2.5 through 100 m/h . The constants a_1 and

Table 1. Constants and Ranges of Validity of the Correlations 6 and 7

Mellapak	a_1	$10^3, s^{-1}$	α	range of B , m/h	b_1	β	range of B , m/h	γ
250Y	2.37		0.668	(2.5; 100)	0.573	0.104	(5; 100)	0.565
350Y	2.48		0.717	(2.5; 100)	0.521	0.0962	(5; 50)	0.618
452Y	1.92		0.735	(2.5; 100)	0.536	0.0911	(5; 90)	0.643
500Y	1.28		0.816	(2.5; 100)	0.417	0.116	(5; 100)	0.698

α are given in Table 1 for all of the packings tested. The k_1a values differ from one another only slightly, and only Mellapak 500Y shows up to 2-fold lower values at liquid flow rates lower than 10 m/h. These results confirm the findings of Laso et al.¹⁵ that an additional increase in the geometric area of the packing above $350 m^{-1}$ is not reflected in a corresponding enhancement in the k_1a value. The practical conclusion is that the application of Mellapak 500Y does not intensify physical mass-transfer processes (e.g., beer or beverage carbonation) in comparison with the application of Mellapak 250Y. The data measured by Murrieta et al.³ on Flexipac 2 (Koch-Glitch) are up to 2-fold lower than the data on the geometrically almost identical Mellapak 250Y packing. Similarly to us, all mentioned authors have used the plug flow model in evaluating their results.

3.2. Effective Mass-Transfer Area a . Experimental results measured using the CO_2 /air–NaOH system are presented in Figure 5a,b as a function of the gas and liquid flow rates. The lines presented in the figure end at the liquid velocities that correspond to the loading points. The results can be summarized as follows:

(a) The effective mass-transfer area measured using sampling points inside ($H = 0.63$ m) and outside the bed ($H = 0.84$ m) did not differ as demonstrated by the results presented in Table 2. This finding indicates that the end effects on the upper and lower sides of the packing are negligible.

(b) The effect of gas velocity on the wetted area on the high-performance Mellapak 452Y differs considerably from the effect observed on the other classic Mellapak packings. For the high-performance packing, the area is not practically affected by the gas velocity up to the loading point while, for all the other packings, the area increases with gas velocity and increases sharply just before the loading point. The phenomena conform to the flow pattern deduced from the pressure drop measurements on the Mellapak packing series. The main difference between high performance packings such as Mellapak 452Y and the other classic Mellapak packings used in this work lies in the gas–liquid interaction just at the transitions between the packing elements (entrance effects). At both ends of the high-performance packing pieces, the corrugation smoothly changes its orientation from 45° to the vertical, eliminating so the right angle change of gas flow occurring at the interfaces in the classic Mellapak packings. The intensive gas–liquid interaction gives rise to gas–liquid dispersion and to the formation of foam bubbles, resulting in backflow of gas and finally starts flooding of packing.

(c) The ratio of the wetted to the geometric area a/a_0 on most Mellapak packings achieved a value of a maximum of 0.8. The ratio of unity, i.e., a completely wetted geometric surface of the packing, was achieved only on Mellapak 250Y. A ratio slightly above unity was observed recently on this type of packing by Tsai et al.,² though their data measured on Mellapak 500Y are much lower than ours, achieving a maximum of 0.55 (see Figure 5a). The ratios greater than unity, measured by de Brito et al.,¹ and usually observed on dumped packings, were not observed at all.

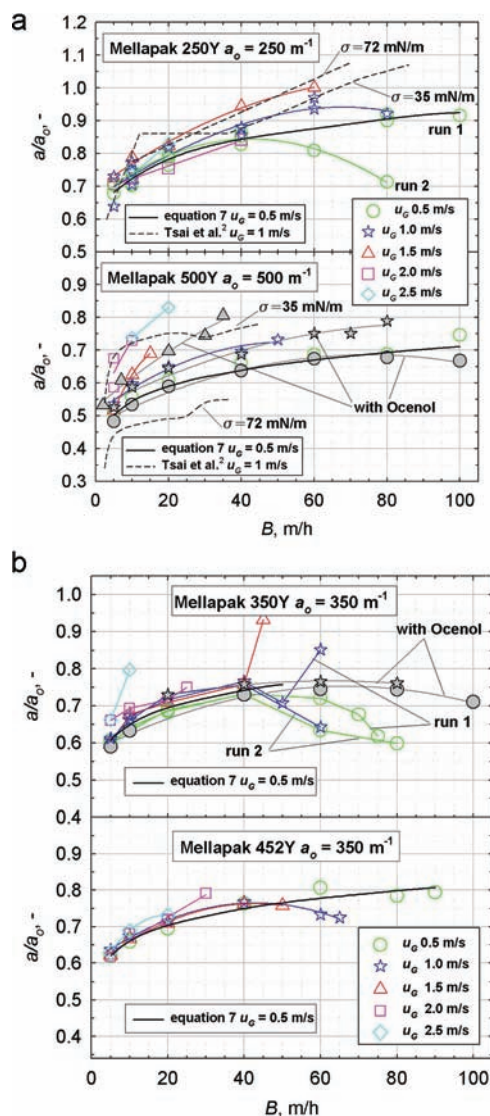


Figure 5. Relative wetted area of (a) Mellapak 250Y and 500Y and (b) Mellapak 350Y and 452Y packings measured using the CO_2 /air–NaOH system.

(d) On Mellapak 350Y, and to a lesser extent on Mellapak 250Y, a significant decrease of the wetted area was observed at low gas velocities (<1.0 m/s) with high liquid velocities exceeding 40 m/h. We attribute this phenomenon to the increased hydrodynamic interaction between gas and liquid at the transitions between packing elements as described above. It occurs at liquid velocities higher than the critical values, which induces a backflow of gas. Results of the CO_2 –lye method are critically dependent on the validity of the plug flow concept of the gaseous phase in the column. The plug flow model ceases to be valid at

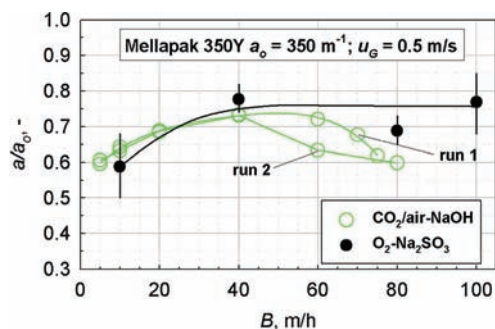
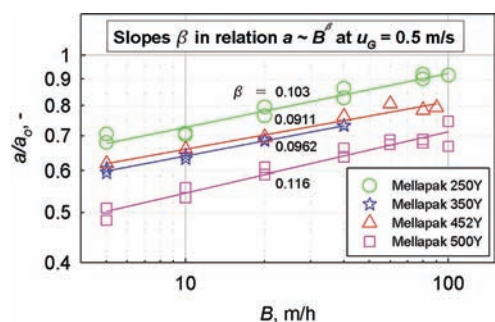
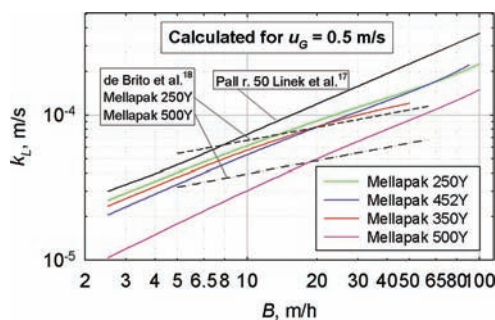
Table 2. Comparison of Data with Sampling Inside (0.63 m) and Outside (0.84 m) the Bed of Mellapak 250Y

B , m/h	u_G , m/s	a , m ⁻¹		u_G , m/s	a , m ⁻¹	
		0.63 m	0.84 m		0.63 m	0.84 m
5	0.5	177	176	1.0	160	182
10		177	187		187	193
20		191	196		209	205
40		216	213		220	220
60		208	202		243	234

these “supercritical” liquid flow rates. As a consequence, the driving force of absorption deduced from the plug flow model is overestimated and the evaluated area is then underestimated. It was also observed that this phenomenon is enhanced by the carbonization of the solution, which increases the foaming tendency of the lye. This is demonstrated in the experiments performed with fresh and somewhat carbonated solution labeled as “run 1” and “run 2” in Figure 5a,b.

(e) Addition of antifoamer Ocenol (1 ppm by volume) eliminated the decrease of the wetted area measured for Mellapak 350Y at the higher liquid rates of $B > 40$ m/h, while the area measured at lower liquid rates was not affected. Ocenol lowered the surface tension of the solution from 77 to 45 mN/m as we found using the ring method for measuring the surface tension. It was observed visually that the addition of Ocenol essentially lowered the number of bubbles in the liquid emanating from the packing and eliminated the creation of liquid films between the liquid streams. These findings confirm that a decrease in the area is a phenomenon caused by the backflow of the gas phase, induced by the liquid flow. Recently, Tsai et al.² studied the effect of the surface tension. For Mellapak 250Y, this effect was not significant. Similarly in our experiments with Mellapak 250Y, Ocenol did not affect the wetted area at low liquid flow rates ($B < 40$ m/h). For Mellapak 500Y, its decrease from 72 to 35 mN/m even raised the area by 50%, while in our work no significant effect was observed.

The crucial role of gas-phase axial mixing in the decrease of the wetted area observed at low gas and high liquid velocities was also confirmed by experiments performed using the sulfite system. The application of pure oxygen for absorption or air absorption (with the small change in the oxygen concentration along the column due to low solubility of oxygen) prevents possible effect of the gas-phase axial mixing. The results measured on Mellapak 350Y are compared with those measured using the CO₂ system in Figure 6. The sulfite system data are quite scattered, though they show no decrease in the wetted area of the packing at high liquid velocities as appears in the data using the CO₂ system. The large scatter of the data measured using the sulfite system is partially the result of the lack of experience of the working team with the methodology of this new measuring system. The crucial problem of this method is the accurate determination of the small sulfite concentration differences between the samples withdrawn from the upper and lower sampling points in the column. The vertical lines in Figure 6 represent differences caused by scatter in the two repeated titrations of the sulfite samples. In subsequent experimentation, more convenient and accurate in-line monitoring of the sulfite concentration by UV absorption at the wavelength of 255 nm will be used instead of the iodometric back-titration. The UV method was improved recently by Kordač et al.¹⁶

**Figure 6.** Comparison of the relative wetted area of packing measured using the CO₂/air–NaOH and O₂–Na₂SO₃ systems.**Figure 7.** Relative wetted area measured at $u_G = 0.5$ m/s vs liquid flow rate plotted in log scale.**Figure 8.** Liquid-side mass-transfer coefficients as a function of the liquid flow rate.

The relative wetted to geometric area measured at a gas velocity of 0.5 m/s is well-correlated by the following relation

$$\frac{a}{a_0} = b_1 B_L^\beta \quad \text{for } u_G = 0.5 \text{ m/s} \quad (7)$$

The b_1 and β constants are given in Table 1 for all packings tested, together with the ranges of their validity in the liquid flow rate B . For the purposes of illustration, the data measured at $u_G = 0.5$ m/s are plotted in Figure 7 in a logarithmic scale that apparently shows to what extent this relation matches the experimental data. The revealed values of the exponent are around $\beta_{av} = 0.1$ and correspond well with that predicted by the Olujić et al.¹⁰ model ($\beta = 0.12$) but are much lower than those predicted by the Billet and Schultes⁸ and Rocha et al.⁹ models ($\beta = 0.4$).

3.3. Liquid-Side Mass-Transfer Coefficient k_L . Coefficients k_L calculated as the ratio of $k_{L,a}$ (calculated from correlation 6) and a (calculated from eq 7) are plotted in Figure 8 as a function of the

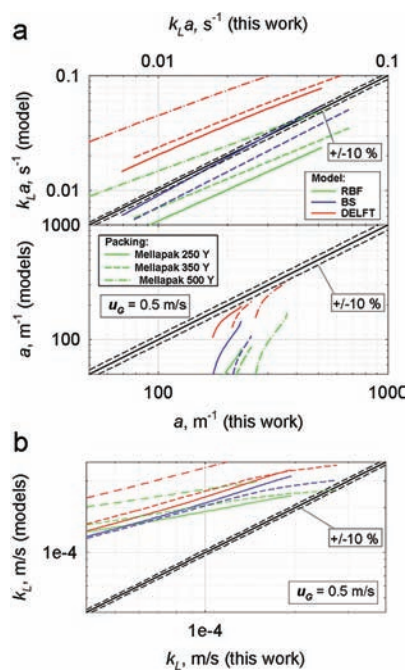


Figure 9. (a) Comparison of the volumetric liquid-side mass-transfer coefficients and the effective mass-transfer areas measured in this work with those calculated from RBF, BS, and DELFT models. (b) Comparison of the liquid-side mass-transfer coefficients measured in this work with those calculated from RBF, BS, and DELFT models.

liquid flow rate. k_L values for all of the packings differ from each other only slightly, and only Mellapak 500Y shows 2-fold lower k_L values. De Brito et al.¹⁷ found a similarly lower k_L value on 500Y in comparison with 250Y. This is due to the fact that the liquid film spread on the packing of a larger surface is thinner than that on the packing of a smaller surface, and therefore the liquid film flows at a lower velocity on the larger packing surface and has lower k_L coefficients compared to those on a smaller packing surface.

Higher mass-transfer coefficients are usually measured on dumped packings, particularly on packings of a larger size. This is due to the intensive mixing of the liquid phase by bouncing droplets and by the mixing of the liquid film upon contact with the packing body. This is illustrated in Figure 8, in which k_L data measured on metal Pall rings 50 are shown and they are up to twice as high as compared to Mellapak 250Y and three times as high, compared to Mellapak 500Y.

The γ exponents in the relation $k_L \propto u_L^\gamma$ can be calculated as a difference of the exponents, $\alpha - \beta = \gamma$, and in Table 1 are defined for all the packings tested. On average, they equal 0.631 and therefore this value is much higher than the value of 0.302 measured by de Brito et al.¹⁷ on Mellapak 250Y and 500Y. They substantiated the lower value of the exponent using a theoretical value deduced from a mass-transfer model of laminar liquid film flowing on the packing surface. It seems that the laminar flow model is not a good approximation for the description of absorption rate to the liquid film flowing over the surface of these packings.

4. EVALUATION OF THE MASS-TRANSFER MODEL FOR CORRUGATED SHEET STRUCTURED PACKINGS

The parameters measured in this work were compared with those calculated from the BS (Billet and Schultes⁸), RBF (Rocha et al.⁹), and DELFT (Olujic et al.¹⁰) models. These results are plotted in Figure 9a,b in a logarithmic scale which enables one to

Table 3. Exponents α , β , γ , and δ in Power Dependences $k_L a \propto u_L^\alpha$; $a \propto u_L^\beta$; $k_L \propto u_L^\gamma$; and $k_G a \propto u_L^\delta$

model	α	β	γ	δ
BS	0.733	0.4	0.333	1.16
RBF	0.597	0.4	0.197	1.20
DELFT	0.445	0.125	0.32	0.845
this work	0.734	0.1	0.631	
"Profile Method" M–E, E–P, and M–P Distillation Systems				
piston flow ²⁰	1.18			0.771
axial dispersion ²¹	1.00			0.512

estimate directly the relative differences between the calculated and the experimental data. Except for a small discrepancy ($\pm 10\%$) of the $k_L a$ values on Mellapak 250Y for the BS model, all of these models underestimate the effective mass-transfer area, even multifold (e.g., RBF three times), and overestimate the liquid-side mass-transfer coefficient to a similar extent (e.g., RBF 2-fold, DELFT up to four times). The volumetric mass-transfer coefficient is either largely overestimated (DELFT) or largely underestimated (BS and RBF).

Similar discrepancies also exist between the predicted and the measured dependencies of these parameters on the phase flow rate. The exponents α , β , γ , and δ in the relations $k_L a \propto u_L^\alpha$, $a \propto u_L^\beta$, $k_L \propto u_L^\gamma$, or $k_G a \propto u_L^\delta$ measured on Mellapak 250Y in this work and those predicted by the models are compared in Table 3. These differ, especially the exponent β that is four times higher than the predicted value and the exponent γ that is approximately half of the predicted value.

Recently, the "profile method" for the measurement of vapor- and liquid-side volumetric mass-transfer coefficients directly in distillation columns was developed. This method, described in detail by Rejl et al.,¹⁸ evaluates the coefficients by comparing the vapor and liquid concentration profiles with those calculated from a rate-based distillation model. This makes it possible to validate the models more conclusively than by means of comparing the experimental and the calculated HETP values. The exponents α and δ of the $k_L a$ and $k_G a$ flow dependencies measured by the profile method by the distillation of the three different mixtures of alcohols (methanol–ethanol, ethanol–propanol, and methanol–propanol) on Mellapak 250Y are presented in Table 3. A striking finding is that the BS and RBF models predict the exponents α and δ as 0.7 and 1.2, respectively, while the profile method provides approximately the same values of the exponents but in the opposite sequence, i.e., 1.2 and 0.7, respectively.

The significant differences between the absolute values of the parameters and their flow dependencies indicate an insufficient relevance of the model parameters. The predictive accuracy of the existing models can be improved empirically on the basis of experiments performed on different packing sizes, using different testing systems and under different operating conditions for the measuring and evaluating procedures that produce mass-transfer parameters of clear physical meaning which is not affected by any artifacts such as axial mixing of the phases or the end effects in apparatus. In this situation, comparison of the absorption coefficients with those measured in distillation columns using the profile method might have an instructive significance. The distillation coefficients are usually measured at higher temperatures in liquids with a lower surface tension. These wet the packing surface more thoroughly than do aqueous absorption

solutions; therefore, the size of the installed surface that is effectively used as the interface for the mass transfer in absorption and distillation may differ significantly and should be identified first.

5. CONCLUSIONS

Similar $k_L a$ values were obtained for all of the packings studied (Mellapak structured packing series 250Y, 350Y, 452Y, and 500Y) except for Mellapak 500Y showing two-time lower values at low liquid flow rates (<10 m/h).

The slight increase of the mass-transfer area with liquid flow rate was well-described by the relation $a \propto u_L^{0.1}$ for all of the packings. The gas velocity did not affect the a values for high-performance Mellapak 452Y and increases them slightly for all other packings. The ratio of wetted to geometric area (a/a_o) reached a maximum of 0.8 for all the packings except for Mellapak 250Y for which a completely wetted geometric surface of the packing was achieved.

A marked effect of gas-phase axial mixing was observed on the data measured by the CO₂/air–NaOH system at low gas and high liquid velocities for all packings except of Mellapak 452Y in which the interaction between the gas and liquid at the interfaces between individual packing elements is suppressed substantially. The marked effect of the axial dispersion on other packings was eliminated by the addition of antifoamer Ocenol to a lye solution and was not observed in the sulfite system which does not have a tendency to foam.

k_L values of all the packings studied differ only a little from each other; only Mellapak 500Y shows two-time lower values.

Large differences were revealed between the mass-transfer parameters measured in this work and those predicted by models especially designed for the prediction of the parameters in corrugated sheet structured packings (Billet and Schultes,⁸ Rocha et al.,⁹ and Olujic et al.¹⁰). Except for a small discrepancy ($\pm 10\%$) of the $k_L a$ values on Mellapak 250Y for the BS model, all of these models underestimate the effective mass-transfer area (e.g., RBF three times) and overestimate the liquid-side mass-transfer coefficient k_L to a similar extent (e.g., RBF 2-fold, DELFT up to four times). The volumetric mass-transfer coefficient $k_L a$ is either largely overestimated (DELFT) or largely underestimated (BS and RBF). Similar discrepancies also exist between the predicted and the measured dependencies of these parameters on the phase flow rate.

APPENDIX

Effect of gas and liquid axial mixing on the mass-transfer parameters measured in this work under conditions when foaming of absorbing solution does not occur.

A1. Oxygen Desorption from Water, Carbon Dioxide Absorption in Lye Solution. Axial mixing of phases lowers the driving force of the interfacial mass transfer in the absorption columns compared with the force calculated from plug flow model used in the evaluating of $k_L a$ and a parameters. As a result, the apparent plug flow parameters, $k_L a_{\text{plug}}$ and a_{plug} , are overestimated compared with the true parameters, $k_L a_{\text{true}}$ and a_{true} . In the absorption systems used for their measuring, the axial mixing is decisive only in one of the phases; the liquid phase for $k_L a$ measuring and the gas phase for measurement of a . For the case of significant axial dispersion of just one phase, Miyachi and Vermeulen²¹ derived following relation between numbers of the

Table 4. Relative Increases R_a of a Values Due to Gas- and Liquid-Phase Axial Mixing

B , m/h	u_G , m/s	a_{plug} , m ⁻¹	Bo_G	N_{plug}	N_{true}	R_a , %	a_{true} , m ⁻¹
5	0.5	170	264	0.4233	0.4239	0.14	170
100		229	264	0.5395	0.5405	0.19	229
5	1.5	181	261	0.1376	0.13765	0.07	181
60		250	269	0.1881	0.1882	0.07	250

true (N_{true}) and the plug flow (N_{plug}) transfer units

$$\exp(-N_{\text{plug}}) = \frac{4b \exp(Bo/2)}{(1+b)^2 \exp(bBo/2) - (1-b)^2 \exp(-bBo/2)}$$

$$N_{\text{plug}} = \ln\left(\frac{c^d}{c^u}\right); \quad b = \sqrt{1 + 4N_{\text{true}}/Bo}$$
(A1)

Axial dispersion in the respective phase is expressed by means of the Bodenstein number Bo . The numbers were calculated from the following correlations deduced²² by means of the ‘cold’ air-water dynamic experiments performed under similar hydraulic conditions as the measurement of mass-transfer parameters were measured for Mellapak 250Y in this work (Bo numbers are related to the packing height of 1 m)

$$Bo_L = 1.022 Fr^{0.478} \left(\frac{3}{\sin^2 \alpha}\right)^{1.159} (da_o)^{6.337}$$
(A2)

$$Bo_G = 2.807 \quad 10^6 Re_G^{-0.00895} (10^{-0.00394 Re_L})(da_o)^{-7.792}$$
(A3)

Validity ranges of phase flow rates: $0 < B < 40 \text{ m}^2/(\text{m}^3 \text{ h})$; $0 < u_G < 2 \text{ m/s}$. The characteristic dimension d of Mellapak 250Y, $d = 0.01277 \text{ m}$.

Relative increase of the true values of the mass transfer parameters, p_{true} , related to the plug flow value p_{plug} is given by following relation

$$R_p/\% = \frac{p_{\text{true}} - p_{\text{plug}}}{p_{\text{plug}}} \quad 100 = \frac{N_{\text{true}} - N_{\text{plug}}}{N_{\text{plug}}} \quad 100$$

$$p = k_L a \text{ or } a$$
(A4)

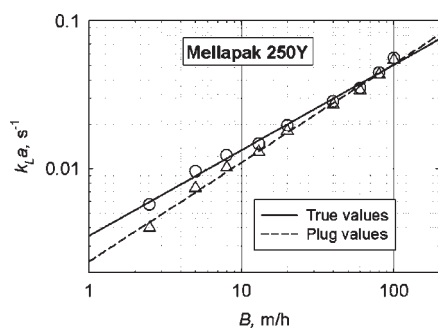
The R_a values (Table 4) calculated for limiting gas and liquid flow rates used in the measurement of interfacial area show that the a values are not affected by gas phase axial mixing. On the other hand, the $R_{k_L a}$ values (Table 5) show that the $k_L a_{\text{true}}$ values are higher (by up to 43% at the lowest liquid load of $2.5 \text{ m}^2/(\text{m}^3 \text{ h})$) than the $k_L a_{\text{plug}}$ values, and differ in their dependence on the liquid flow rate (see Figure 10) as follows

$$\begin{aligned} k_L a_{\text{true}} &= 3.50 \quad 10^{-3} B^{0.581} \\ k_L a_{\text{plug}} &= 2.37 \quad 10^{-3} B^{0.668} \end{aligned}$$
(A5)

We are investigating the effect of axial mixing of both phases on mass transfer coefficients in absorption and distillation columns in more detail now. Absorption columns operate usually at liquid flow rates higher than 20 m/h; i.e., the correlation based on the plug flow model are acceptably accurate for their design. On other side, liquid flow rates in distillation columns are usually low,

Table 5. Relative Increases $R_{k_L a}$ of $k_L a$ Values Due to Liquid-Phase Axial Mixing

B m/h	$k_L a_{\text{plug}}$ 10^{-2} s^{-1}	Bo_L	N_{plug}	N_{true}	$R_{k_L a}$ %	$k_L a_{\text{true}}$ 10^{-2} s^{-1}
2.5	0.40	7.32	3.628	5.207	43	0.57
5	0.74	10.1	3.356	4.359	29	0.96
8	1.02	12.7	2.892	3.500	21	1.23
13	1.30	16.1	2.268	2.569	13	1.47
20	1.79	19.7	2.030	2.227	9.7	1.96
40	2.70	27.5	1.531	1.613	5.3	2.84
60	3.39	33.4	1.281	1.329	3.7	3.52
80	4.33	38.3	1.228	1.267	3.1	4.47
100	5.45	42.6	1.236	1.271	2.8	5.60

**Figure 10.** Effect of liquid-phase axial mixing on $k_L a$ values measured for Mellapak 250Y.

often lower than 20 m/h and the effect of liquid phase axial mixing should be taken into account. Some first results concerning this effect on mass transfer coefficient in distillation column we published elsewhere.²⁰

A2. Oxygen Absorption in Sulfite Solution. The local slope of sulfite concentration profile in the column occurring in the second term on the right side of eq 5 were calculated from sulfite concentration profile deduced from following differential mass balance of sulfite

$$N_t + X - \frac{1}{Bo_L} \frac{dX}{dZ} = 0 \quad (\text{A6})$$

where

$$Z = \frac{z}{0.84}, \quad N_t = \frac{2NaH}{u_L}, \quad X = \frac{dc_{\text{Na}_2\text{SO}_3}}{dZ} \quad (\text{A7})$$

Solution with boundary condition $X(1) = 0$ gives

$$X(Z) = \frac{dc_{\text{Na}_2\text{SO}_3}}{dZ} = -N_t [1 - \exp\{-Bo_L(1-Z)\}] \quad (\text{A8})$$

Samples of sulfite solution were withdrawn from the packing at $Z^0 = 0.105/0.84 = 0.125$ and $Z^1 = 0.735/0.84 = 0.875$ where 0.84 m is the total height of four packing pieces installed in the column. Values of the second term corresponding to the limiting liquid flow rates 40 and 100 m/h used in the work for pure oxygen absorption are as follows. Corresponding Bo_L and N

values were taken from Table 2A and calculated from eq 4, respectively.

$$\begin{aligned} & \frac{u_L}{(2)(0.84)NB_{oL}} (X(0.875) - X(0.125)) \\ &= \frac{40 \div 100}{(2)(0.84)(1.7 \cdot 10^{-5})(3600)(27.5 \div 42)} \\ & \quad (2.17 \cdot 10^{-3} \div 1.42 \cdot 10^{-4}) \\ & \frac{u_L}{2N Bo_L} \left[\left(\frac{dc_{\text{Na}_2\text{SO}_3}}{dz} \right)_{z=0.735} - \left(\frac{dc_{\text{Na}_2\text{SO}_3}}{dz} \right)_{z=0.105} \right] \\ &= 0.31 \div 0.033 \text{m}^{-1} \quad (\text{A9}) \end{aligned}$$

AUTHOR INFORMATION

Corresponding Author

*E-mail: linekv@vscht.cz.

ACKNOWLEDGMENT

Financial support from the Ministry of Education (Grant MSM 6046137306) is gratefully acknowledged. Sulzer Ltd. is acknowledged for providing the packing free of charge.

Nomenclature

- a = effective specific mass-transfer area, 1/m
- a_o = specific geometrical area of the packing, 1/m
- B = superficial liquid velocity, $\text{m}^3/(\text{m}^2 \text{ h})$
- $Bo = uH/D_e$, Bodenstein number
- b = defined by eq A1
- c = molar concentration, kmol/m^3
- d = packing characteristic dimension, m
- D = diffusion coefficient, m^2/s
- D_e = axial dispersion coefficient, m^2/s
- E = activation energy, kJ/kmol
- $Fi = \eta_L u_L / d^2 \rho_L g$
- g = gravity acceleration, m/s^2
- H = packing height between two sampling points, m
- He = distribution coefficient
- K = mass-transfer coefficient defined by eq 3, $\text{m}^{5/2}/(\text{kmol}^{1/2} \text{ s})$
- $k_{L,G}$ = liquid-/gas-side mass-transfer coefficient, m/s
- k_{OH} = second-order kinetic constant, $\text{m}^3/(\text{kmol s})$
- N = oxygen flux into sulfite solution given by eq 4, $\text{kmol}/(\text{m}^2 \text{ s})$
- N_p = number of transfer units given by eq A1 (p = plug or thru)
- N_t = number of transfer units defined by eq A7, kmol/m^3
- p = pressure, Pa
- R = gas constant, $\text{kJ}/(\text{kmol K})$
- R_p = relative increase of the true to the plug flow parameters $p = k_L a$ or a given by eq A4
- $Re_G = u_G d \rho_G / \eta_G$
- T = temperature, K
- u_j = superficial velocity ($j = L, G$), m/s
- X = slope of concentration profile in column defined by eq A7, kmol/m^3
- z = packing height coordinate taken from top of the packing ($z = 0$), m
- $Z = z/0.84$ dimensionless packing height coordinate

Subscripts

- G = gas phase
- L = liquid phase

plug = based on plug flow model
true = based on axial dispersion model

Superscripts

α = exponent in relation to $k_L a \propto u_L^\alpha$

β = exponent in relation to $a \propto u_L^\beta$

γ = exponent in relation to $k_L \propto u_L^\gamma$

δ = exponent in relation to $k_G a \propto u_L^\delta$

σ = surface tension, mN/m

l = lower sampling points of the measuring section

u = upper sampling points of the measuring section

REFERENCES

- (1) de Brito, H. M.; Stockar, U.; Bangerter, A. M.; Bomio, P.; Laso, M. Effective mass transfer area in a pilot plant column equipped with structured packings and with ceramic rings. *Ind. Eng. Chem. Res.* **1994**, *33*, 647.
- (2) Tsai, R. E.; Schultheiss, P.; Kettner, A.; Lewis, J. C.; Seibert, A. F.; Eldridge, R. B.; Rochelle, G. T. Influence of surface tension on effective packing area. *Ind. Eng. Chem. Res.* **2008**, *47*, 1253.
- (3) Murrieta, C. R.; Seibert, A. F.; Fair, J. R.; Rocha, J. A. Liquid-side mass-transfer resistance of structured packings. *Ind. Eng. Chem. Res.* **2004**, *43*, 7113.
- (4) Linek, V.; Sinkule, J. Hydraulic and transport characteristic of new type packing for absorption and distillation columns (in Czech). *Chem. Listy* **1997**, *91*, 54.
- (5) Hoffmann, A.; Mackowiak, J. F.; Gorak, A.; Haase, M.; Loning, J. M.; Runiowski, T.; Hallenberger, K. Standardization of mass transfer measurements. Basis for the description of absorption processes. *Chem. Eng. Res. Des.* **2007**, *85*, 40.
- (6) Rejl, J. F.; Linek, V.; Moucha, T.; Valenz, L. Methods standardization in the measurement of mass transfer characteristics in packed absorption/distillation columns. *Chem. Eng. Res. Des.* **2009**, *87*, 695.
- (7) Pohorecki, R.; Moniuk, W. Kinetics of reaction between carbon dioxide and hydroxyl ions in aqueous electrolyte solutions. *Chem. Eng. Sci.* **1988**, *43*, 1677.
- (8) Billet, R.; Schultes, M. Prediction of mass transfer columns with dumped and arranged packings. *Chem. Eng. Res. Des.* **1999**, *77*, 498.
- (9) Rocha, J. A.; Bravo, J. L.; Fair, J. R. Distillation columns containing structured packings: A comprehensive model for their performance. 2. Mass-transfer model. *Ind. Eng. Chem. Res.* **1996**, *35*, 1660.
- (10) Olujić, Ž.; Kamerbeek, A. B.; Graauw, J. Corrugation geometry based model for efficiency of structured distillation packings. *Chem. Eng. Process.* **1999**, *38*, 683.
- (11) Linek, V.; Petříček, P.; Beneš, P.; Braun, R. Effective interfacial area and liquid side mass transfer coefficients in absorption columns packed with hydrophilised and untreated plastic packing. *Chem. Eng. Res. Des.* **1984**, *62*, 13.
- (12) Linek, V.; Stoy, V.; Machoň, V.; Krivský, Z. Increasing the effective interfacial area in plastic packed absorption columns. *Chem. Eng. Sci.* **1974**, *29*, 1955.
- (13) Linek, V.; Kordač, M.; Moucha, T. Mechanism of mass transfer from bubbles in dispersions: Part I. Danckwerts' plot method with sulfite solutions at the presence of viscosity and surface tension changing agents. *Chem. Eng. Process.* **2005**, *44*, 353.
- (14) Linek, V.; Vacek, V. Chemical engineering use of catalyzed sulfite oxidation kinetics for the determination of mass transfer characteristics of gas–liquid contactors. *Chem. Eng. Sci.* **1981**, *36*, 1747.
- (15) Laso, M.; Brito, M.; Bomio, H.; Stockar, P. U. Liquid-side mass transfer characteristics of a structured packing. *Chem. Eng. J.* **1995**, *58*, 251.
- (16) Kordač, M.; Opletal, M.; Linek, V. Measurement of mass transfer characteristics of gas–liquid reactors by sulfite system using on-line monitoring UV absorption. *Chem. Eng. J.* **2011**, *167*, 314.
- (17) de Brito, H. M.; Stockar, U.; Bangerter, A. M.; Bomio, P.; Laso, M. Predicting the liquid-phase mass transfer coefficients $k_L a$ for the Sulzer structured packing Mellapak, distillation and absorption. *Inst. Chem. Eng. Symp. Ser.* **1992**, *128*, 137.
- (18) Rejl, F. J.; Valenz, L.; Linek, V. "Profile method" for the measurement of $k_L a$ and k_{va} in distillation column. Validation of rate-based distillation models using concentration profiles measured along the column. *Ind. Eng. Chem. Res.* **2010**, *49*, 4383.
- (19) Rejl, F.; Linek, V.; Moucha, T.; Prokopová, E.; Valenz, L.; Hovorka, F. Vapour- and liquid-side volumetric mass transfer coefficients measured in distillation column. Comparison with data calculated from absorption correlations. *Chem. Eng. Sci.* **2006**, *61*, 6096.
- (20) Valenz, L.; Rejl, F. J.; Linek, V. Effect of gas and liquid phase axial mixing on the rate of mass transfer in a distillation column packed with Mellapak 250Y. *Ind. Eng. Chem. Res.* **2011**, *50*, 2262.
- (21) Miyachi, T.; Vermeulen, T. Longitudinal dispersion in two-phase continuous-flow operations. *Ind. Eng. Chem. Fundam.* **1963**, *2*, 113.
- (22) Valenz, L.; Rejl, F. J.; Linek, V. Gas and liquid axial mixing in the column packed with Mellapak 250Y, Intalox saddles and Pall rings 25 under flow conditions prevailing in distillation columns. *Ind. Eng. Chem. Res.* **2011**, *50*, 2262.

Gas and Liquid Axial Mixing in the Column Packed with Mellapak 250Y, Pall Rings 25, and Intalox Saddles 25 under Flow Conditions Prevailing in Distillation Columns

L. Valenz,* F. J. Rejl, and V. Linek*

Prague Institute of Chemical Technology, Department of Chemical Engineering, CZ-166 28 Prague 6, Czech Republic

The axial dispersions of gas and liquid phase in a column of inner diameter 0.297 m packed with random packing of metal Pall rings 25 and Intalox saddles 25 and structured packing of Mellapak 250Y were measured using a dynamic method under hydraulic conditions common in distillation columns, i.e., liquid flow rate from 6.94×10^{-4} to 0.0111 m/s and gas flow rate from 0.25 to 2 m/s. The two-response method with a diffusion-type model was used to reproduce the experimental response curves. Axial mixing in the gas increases with gas and liquid rates for both random and structured packings, but the dependence on the gas rate is very weak for the structured packing. The largest gas mixing was found for the Pall rings at the highest gas rate; the least was found for the structured packing at the lowest gas and liquid rates. Liquid-phase axial mixing increases with decreasing liquid flow rate and is independent of gas flow rate for both random and structured packings. The largest liquid mixing was found for the Intalox saddles at the lowest liquid rate; the least was found for the structured packing. The correlations of Bo_L and Bo_G numbers deduced for all types of packings used reproduced the experimental data within $\pm 22\%$.

1. Introduction

In our recent paper¹ we presented the “profile method”, which evaluates the vapor- and liquid-side volumetric mass transfer coefficients k_{va} and k_{la} by comparing the concentration profiles measured along the distillation column with the simulated profiles. The method was applied in a distillation column packed with random packing of Intalox saddles 25 or structured packing of Mellapak 250Y. It was revealed that experimental liquid and vapor concentration profiles along the column under total reflux do not superimpose (Figure 1). However, the plug flow model that was used in the simulation¹ predicts their agreement. The difference between the phases' concentrations is apparently a consequence of the longitudinal mixing in the packed bed. The differences observed for the structured packing are lower in comparison to those for the random packing. Therefore, the volumetric mass transfer coefficients evaluated from each one-phase concentration profile were nearly the same¹ for the structured packing whereas they differ for the random packing. A clear physical meaning of the mass transfer coefficients underlies their applicability/transferability to other conditions than those in which they were measured. The aim of our further investigation is to include the effect of the longitudinal mixing into the evaluation procedure of the distillation volumetric mass transfer coefficients by the profile method. The mass transfer coefficients are used as the process parameters in rate-based models for the distillation column's design from the first principles, and neglecting its effect may substantially reduce the reliability of the column's design.

Longitudinal mixing has been studied thoroughly in first-generation random packings (Raschig rings, Berl saddles). For example, studied were the effects of (i) mutual phase interaction,^{2–6} (ii) response evaluation method,⁷ (iii) end effects,⁸ (iv) packing length and its diameter,^{4,5,9,10} (v) wall flow,¹⁰ (vi) static and dynamic holdups,^{11,12,15} (vii) viscosity and surface tension,¹³ (viii) a complete dynamic approach to characterize gas–liquid

columns (axial dispersions, mass transfer coefficient, holdups) by using transient techniques with transferable tracer,^{14,26} and (ix) elevated pressure.¹⁶ On the other hand, the data of the longitudinal mixing for modern random (Intalox saddles) and structured (Mellapak) packings are rather limited,^{17–21} and the data available do not cover gas and liquid flow rates used in a distillation column where gas- and liquid-side volumetric mass transfer coefficients were evaluated by the profile method.^{1,22,23}

This work aims at providing these data by means of the “cold” air–water dynamic experiments performed under hydraulic conditions, by which the concentration profiles were measured²² in the distillation column.

2. Experimental Section

The axial dispersion of gas and liquid phases in packed columns was measured using a dynamic method based on injecting the step concentration impulse of a tracer into the inlet stream and subsequent monitoring of the response patterns at

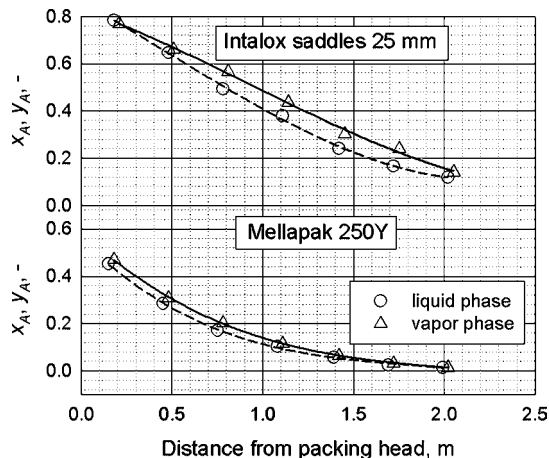


Figure 1. Vapor and liquid concentration profiles measured in column packed with random (Intalox saddles) and structured (Mellapak 250Y) packing for ethanol–propanol distillation system.

* Corresponding author. E-mail: linekv@vscht.cz (V. Linek); valenzl@vscht.cz (L. Valenz).

two different points downstream from the injection point. Gas-phase dispersion was evaluated from two responses monitored in gas samples withdrawn from the packing at two sampling points in the column packing. In the liquid phase, the two responses were obtained by monitoring the tracer concentration in the outlet liquid from the column with different packing heights. The concentration step change was carried out by momentarily stopping the tracer injection into the input-phase flow after achieving a steady-state tracer concentration in the column. Helium gas and an aqueous solution of NaCl were used as the inert tracers in the gas and the liquid phase, respectively.

2.1. Column. The column body was formed by a varying number of flange Perspex tubes of inner diameter 0.297 m filled with packing. Using a different number of the tubes enabled measurement at different packing heights, keeping the distance between the liquid distributor and the packing the same. The extent of axial mixing greatly depends on the uniformity of the phase distribution in the bed. This is why great attention was paid to the uniformity of gas and liquid distribution onto the bed. The distributors were of special design, enabling us to introduce the step concentration change of the tracer uniformly across the column cross section into the inlet streams of gas and liquid and, in the case of the gas distributor, to allow monitoring of the response in the liquid leaving the column. Their construction minimized the tracer holdups between the injection point and the packing and therefore minimized the end effects.

2.1.1. Bottom of the Column. Gas entered the bottom of the column through 16 cups regularly spaced over the column base cross section. Helium tracer was injected into the gas entering the column packing through a three-way solenoid valve and a small retention cylindrical vessel (volume 300 cm³). The vessel was used to distribute helium through 16 flexible tubes of the same length (30 cm) and diameter (6 mm) into each of the 16 cups in the gas distributor. At the end of the tubes were 10 cm long Perspex tubes drilled with four 1.5 mm orifices that controlled the main pressure drop of the whole dosing system and thereby ensured the same helium inflow to each of the cups. The solenoid valve was also connected to a diaphragm vacuum pump to remove the helium from the dosing pipes at the same moment as the implementation of the step concentration change in the input gas flow was performed. This prevents the slow helium flushing from the supply sleeves after interruption of its feeding. Liquid leaves the column bottom through four symmetrically distributed channels of diameter 30 mm, each equipped with conductance probes. The same liquid level was maintained by overflow in all four channels under the various flow rates used. Details of the distributor, helium dosing system, and liquid outflow channels equipped with conductance sensors are given in Figure 2.

2.1.2. Head of the Column. Uniform liquid distribution onto the bed was realized via 16 regularly spaced exchangeable nozzles of different diameters (2, 3, 5, and 7 mm), providing 242 pour points per m². The different nozzle diameters were used to keep the liquid discharge velocity lower than 2 m/s at various liquid flow rates and, at the same time, to keep the pressure drop on the nozzle higher than 2 cm of H₂O. The pressure drop ensured the same discharge velocity in the nozzles. NaCl solution was injected into each of the nozzles by syringe needles with a diameter of 0.5 mm and length of 8 cm, which came through the column head. The needles ended 2 mm below the edge of the nozzles. The salt solution was fed into the individual needles by flexible tubes with a diameter of 6 mm. A strictly uniform tracer flow rate was assured by an overflow

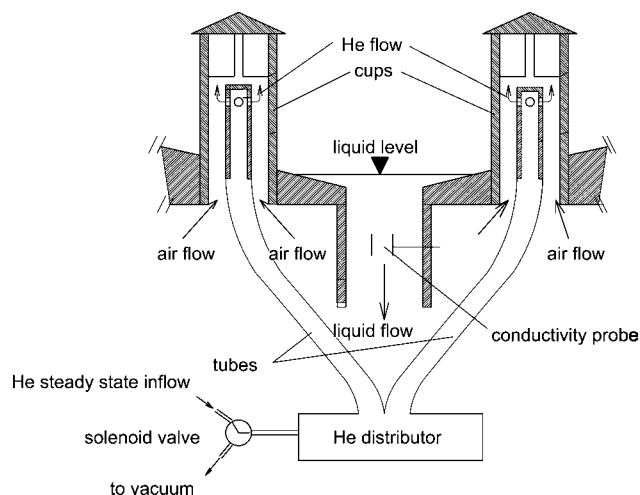


Figure 2. Details of the gas inlet tubes, gas-phase tracer (helium) injection system, liquid outflow tube, and location of the conductivity probe.

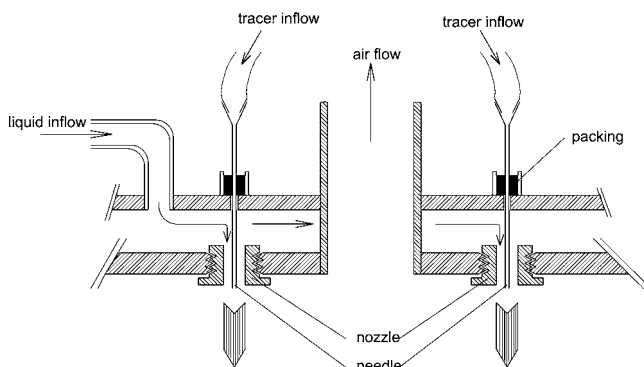


Figure 3. Details of the liquid distributor and liquid-phase tracer injection system.

Table 1. Combinations of the Gas and Liquid Flow Rates Used in This Work

		liquid-phase axial dispersion					
u_L	mm/s	6.86	14.4	23.9	33.9	55.6	111
u_G	m/s	0		1		2	
		gas-phase axial dispersion					
u_L	mm/s	0	13.9	27.8	55.6	111	
u_G	m/s	0.25	0.50	1.0	1.5	2.0	

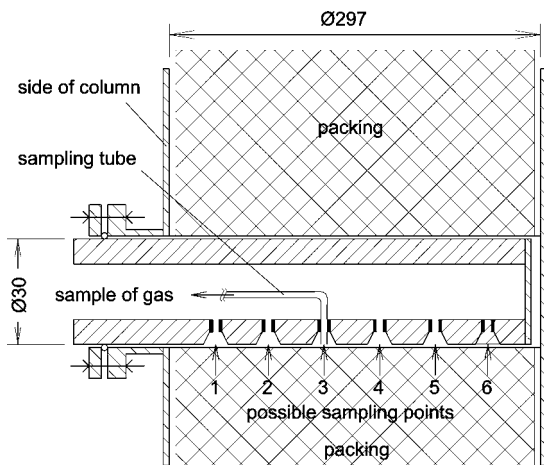
placed 2 m above the column head. The main pressure drop of the whole NaCl tracer dosing system was concentrated in the capillaries, thus ensuring the same tracer flow rate in each nozzle. Gas was drawn from the column by 9 openings with diameters of 30 mm passing through the distributor. Injection of the solution directly into the liquid entering the distributor led to large scatter in the data. Details of the distributor, NaCl tracer dosing system, and air exhaust tube are given in Figure 3.

2.2. Experimental Conditions, Types of Packings, and Experiment Procedure. Experiments were performed in a column at ambient temperature (~ 22 °C) and pressure. In these experiments, two types of packing (metal Intalox saddles 25 mm and Mellapak 250Y) were investigated with water flow rates up to 40 m/h and air flow rates up to 2 m/s. These flow ranges are valid for measuring the gas and liquid mass transfer coefficients in a distillation column.^{22,23} Gas-to-liquid flow rate combinations used in this work are given in Table 1. A packing of metal Pall rings 25 was also investigated because, for this packing, it is possible to find some literature data^{15,17,18} for

Table 2. Characteristics of the Packings and Lengths of the Test Sections Used in This Work

		Intalox saddles	Pall ring	Mellapak 250Y ^c
d_{eq}	mm	25.4	25.4	12.77 ^a
a_p	m ⁻¹	205	205	250
L	m	0.89/0.92 ^b	1.46/1.47 ^b	0.84/0.84 ^b

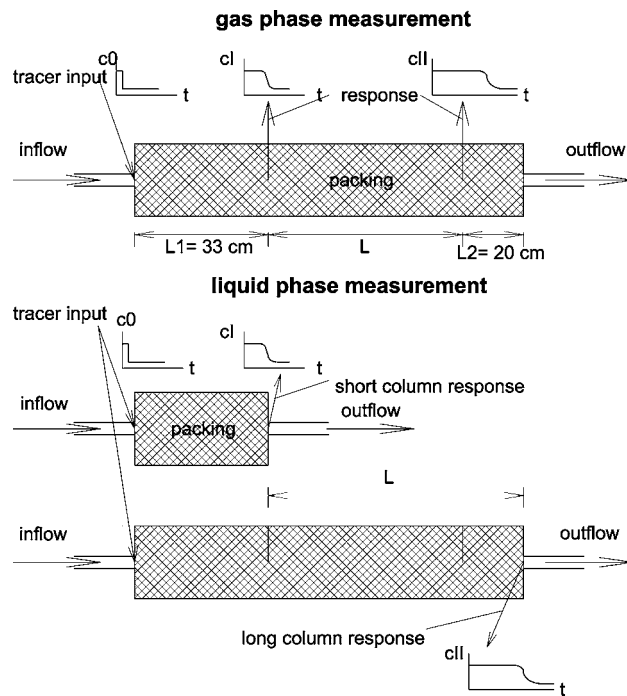
^a Calculated from eq 18 in ref 17. ^b Length of the test section used in measuring Bo_G/Bo_L . ^c $\alpha = 45^\circ$.

**Figure 4.** Gas sampling device.

comparison. The results measured on structured packing Mellapak 250Y and on similar structured packing Flexipac 2 are rather scarce.^{18,20}

Concentration of the liquid tracer was monitored by flow conductance cells installed in each of the four liquid outlet tubes of the column. The NaCl concentration during the liquid experiments was kept to a value of 1.2 g/L. Under this condition, it was experimentally observed that conductivity cell signal is linearly proportional to the NaCl concentration. The size of the cells was modified, to give the same signal in solutions of the same salt concentration. Thus, the contributions of the single cells to the overall signal after their mutual electric interconnection were the same. Differences of the packing heights of the short and long columns, L , used for measuring the axial dispersion in the liquid phase, are given in Table 2, together with the characteristics of the packings used. In these measurements, the spacings between the liquid distributor and the top of the packed bed were the same in the short and long columns.

The gas tracer concentration was monitored in sample gas withdrawn continuously from the column by two gas samplers. The samplers were placed in the bed so that the spacing between gas distributor and the first gas sampling point was filled with Pall rings 25 to the height of 33 cm. Holes for the sampling devices, depicted in Figure 4, were drilled through the structured packing by an electric discharge technique. The distances of the sampling points L used in this work are given in Table 2. The samplers enable sampling of gas from six points regularly spaced along the radial cross section of the column. In all experiments, gas was sampled from the center of the cross section, i.e., from position 3 (see Figure 4), except the situation when the effect of the radial concentration profile of the tracer was studied (section 4.1). Steady flow of the gas samples sucked into the thermal conductivity detector through a 35 cm long tube of 1 mm diameter was held to 150 mL/min by a mass flow controller (the residence time of gas in the tube was 0.12 s). The experiments were performed with the He concentration up to 5% vol. In this concentration range, the signal of the thermal

**Figure 5.** Experimental scheme for dynamic response studies in both phases.

conductivity detector is linearly dependent on the He concentration, which was experimentally verified.

3. Data Evaluation Method

Axial dispersion of a tracer that flows along column mass transfer exchangers has been described in this work, similarly as it is in the works of other authors, by Fick's diffusion model. In this model, the molecular diffusion coefficient is replaced by an effective dispersion coefficient D_e . Then the tracer movement in the column is described through the material balance of the tracer over a differential element dz of the packing bed:

$$\frac{\partial c}{\partial t} = D_e \frac{\partial^2 c}{\partial z^2} - u_i \frac{\partial c}{\partial z} \quad (1)$$

The solution of this equation, with the initial and boundary conditions corresponding to experimental conditions and the tracer concentration pulse at the input to the packing test section, provides a model tracer concentration response for a place where the second response is measured. Matching the model response onto the experimental one, the best-fit values of the model parameters, effective dispersion coefficient, and mean residence time are then obtained by an optimization procedure. This two-response method cancels the effects of the probe dynamics, the imperfection of the tracer concentration step change, and the ends of the column.

As the dispersion model (eq 1) is linear, the convolution integral can be used to calculate the normalized profile of the tracer concentration $c_{II}(t)$ at a distance L downstream in the column (see Figure 5) from the experimentally determined profile $c_I(t)$ at an arbitrary place z in the column by using the pulse, $E(t)$, or transient, $F(t)$, characteristic of the section L of the packing:

$$c_{II}(t) = \int_0^t c_I(\tau) \cdot E(t - \tau) d\tau = \int_0^t c_I(\tau) \cdot \frac{\partial F(t - \tau)}{\partial t} d\tau \quad (2)$$

The pulse characteristic $E_o(t)$ of the part L of the packing is obtained by solving eq 1 with the following initial and boundary conditions corresponding to an open system:

$$\begin{aligned} c(z, 0) &= \delta(z) \\ c(z = \pm\infty, t) &= 0 \end{aligned} \quad (3)$$

An analytical solution was presented by Levenspiel and Smith²⁴ in the form

$$\begin{aligned} E_o(t; t_m, Bo) &= \left(\frac{Bo}{4\pi\theta}\right)^{1/2} \exp\left\{-Bo\frac{(1-\theta)^2}{4\theta}\right\} \\ Bo &= \frac{u_i L}{D_e}; \theta = \frac{u_i t}{L} = \frac{t}{t_m} \end{aligned} \quad (4)$$

The pulse characteristic $E_c(t; L)$ deduced from an analytical solution of eq 1 with the following initial and boundary conditions corresponding to a closed system

$$\begin{aligned} c(z, 0) &= 0 \\ -\frac{1}{Bo} \frac{\partial c(0^+, t)}{\partial z} + c(0^+, t) &= c(0^-, t) = 1 \\ \frac{\partial c(0^+, t)}{\partial z} - Bo[c(0^+, t) - 1] &= 0 \\ \frac{\partial c(L, t)}{\partial z} &= 0 \end{aligned} \quad (5)$$

is deduced in ref 23 in the form

$$E_c(t; t_m, Bo) = -\frac{8}{t_m} \exp\left\{\frac{Bo}{2}\right\} \sum_{j=1}^{\infty} k \frac{B_j^2}{4B_j^2 + Bo^2 + 4Bo} \times \exp\left\{-\frac{4B_j^2 + Bo^2}{4Bo \cdot t_m} t\right\} \quad (6)$$

where B_j are roots of equations

$$\begin{aligned} 2B_j \cot g(B_j/2) + Bo &= 0 & \text{for } k = 1 \\ 2B_j \tan g(B_j/2) - Bo &= 0 & \text{for } k = -1 \end{aligned} \quad (6a)$$

One thousand members in the series (eq 6) were used when the response E_c was calculated. The same responses were obtained using 500 members.

The parameters characterizing the axial dispersion flow, mean residence time t_m , and effective mixing coefficient D_e were determined from both gas- and liquid-side dynamic response data using the two-point detection technique as is described below. The detector signals measured on the short, $s_I(t)$, and the long, $s_{II}(t)$, column packing were transformed to a normalized profile of the tracer concentration $c_{I,exp}$ and $c_{II,exp}$,

$$c_{I,exp}(t) = \frac{s_I(t) - s_{I,0}}{s_{I,\infty} - s_{I,0}}; \quad c_{II,exp}(t) = \frac{s_{II}(t) - s_{II,0}}{s_{II,\infty} - s_{II,0}} \quad (7)$$

where s_0 and s_∞ are initial and final steady-state probe signals, respectively. The experimental responses $c_{II,exp}$, measured at the end of the test section (gas-phase measurement) or at the outlet of the long column (liquid-phase measurement), were compared to those, $c_{II,cal}$, predicted by the theoretical transformation of the experimental concentration profiles $c_{I,exp}$, measured at the inlet into the test section (gas-phase measurement) or at the outlet of the short column. The transformation was made via

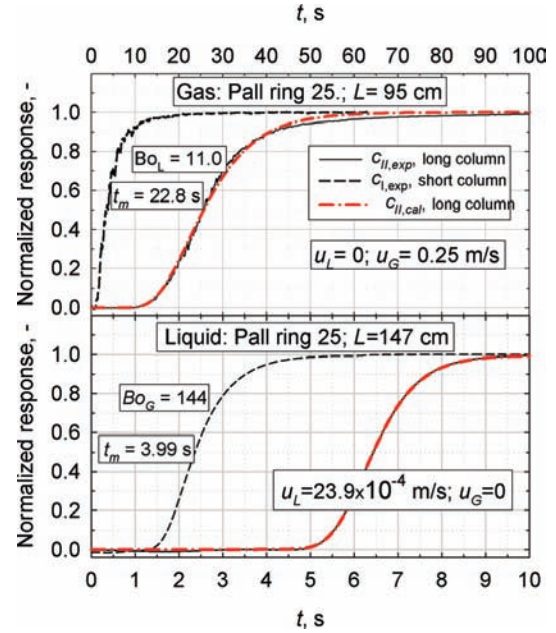


Figure 6. Liquid and gas experimental responses and the responses fitted.

Table 3. Parameter Bo_L Evaluated Using Open or Closed System Pulse Characteristic, E_o or E_c , Respectively

u_G , m/s	0				1			
u_L , mm/s	14.4	33.9	14.4	33.9	14.4	33.9	14.4	33.9
characteristics	E_c	E_o	E_c	E_o	E_c	E_o	E_c	E_o
Bo_L	14.0	15.0	21.2	22.1	12.4	13.5	20.2	21.2

the convolution integral (eq 2) using the pulse characteristic (eq 4 or 6) in evaluating gas or liquid responses, respectively

$$c_{II,cal}(t; t_m, Bo) = \int_0^t c_{I,exp}(t - \tau) E_i(\tau; t_m, Bo) d\tau; \quad i = o, c \text{ for gas and liquid, respectively} \quad (8)$$

Equation 8 was solved using numerical integration with integration steps of 0.05 and 0.005 s when the liquid and the gas responses were evaluated, respectively. The same results were achieved using twice higher integration steps, i.e., 0.1 and 0.01 s, respectively.

The best-fit values of the model parameters t_m and Bo were obtained by minimizing the objective function

$$R(t_m, Bo) = \sum_{j=1}^n (c_{II,exp,j} - c_{II,cal,j})^2 \quad (9)$$

The simplex method has been used to search for the optimal pair of parameters $[t_m, Bo]$. Minimization has been performed until the differences in the values of the parameters in the two following steps were lower than 10^{-5} .

An example of gas and liquid experimental and calculated responses is shown in Figure 6. The axial dispersion model fits the experimental responses accurately. The standard deviations of the experimental and the calculated responses in liquid phase were <0.015 and in gas phase were <0.004 .

There were some doubts concerning an application of the closed system pulse characteristic E_c . Thus, we have also used the open system pulse characteristic E_o in evaluating the liquid-phase responses. The results in Table 3 show insignificant (compared with their parameter sensitivity on experimental errors) differences between Bo_L numbers evaluated using either E_o or E_c .

Table 4. Radial Distribution of Tracer Concentration and Its Effect on the Parameters t_m and Bo

position	1	2	3	4	5	6
tracer concentration differences from the mean value, %						
section I	4.48	-9.43	-9.37	-1.25	7.71	7.86
section II	0.72	0.75	-0.76	-0.98	-0.17	0.43
effect of radial distribution on evaluated parameters t_m and Bo						
repetition	1	2	1	2	1	2
t_m^a , s	0.89	0.90	0.92	0.91	0.91	0.91
avg t_m^a , s	0.908 ± 0.024					
Bo_G^a	129	135	129	127	114	113
avg Bo_G^a	117 ± 10.0					

^a The parameters recalculated for $L = 1$ m.

Table 5. Deviations between the Parameters Evaluated from Individual Experiments and Their Mean Value, Which Have Been Used in Figures

	Pall rings		Intalox saddles		Mellapak	
	t_m	Bo	t_m	Bo	t_m	Bo
mean deviation measured in gas phase, %						
0.06	6.12	1.01	16.1	0.74	23.4	
mean deviation measured in liquid phase, %						
1.19	4.95	1.24	6.95	0.93	5.88	

The parameters t_m and Bo_L evaluated on various packing heights L_{exp} were recalculated on the height of 1 m to be mutually comparable. So, all the data presented below were recalculated using the ratio $1/L_{exp}$.

4. Results

4.1. Radial Scatter of the Gas-Phase Tracer Concentration. The model of the tracer axial dispersion assumes that no concentration gradient exists in the radial direction. The radial scatter of helium tracer concentration was measured in the column packed with Pall rings 25. The height of the first part of the packing was $L_1 = 0.33$ m, of the test section was $L = 0.95$ m, and of the packing height above the test section was $L_2 = 0.20$ m. The helium concentration differences relative to the mean of the values taken at six regularly distributed points over the column cross section are given in Table 4. At the entrance into the test section ($L_1 = 0.33$ m), the relative differences reach 9.47% at maximum, whereas at the outlet of this section ($L_1 + L = 1.28$ m), the differences are all <1%. This confirms the assumption of the model on the uniform radial tracer concentration. The parameters t_m and Bo evaluated from the responses sampled at the individual radial positions show similarly small differences. Thus, we believe that our results measured in the center of column (position 3) represent well the nonideal flow conditions in the whole column cross section.

4.2. Sensitivity of the Parameters on Experimental Errors and Their Scatter. Experiments were repeated 4 times for each gas-to-liquid flow rate combination. To reduce the scatter of the experimental points, the mean values of the parameters t_m and Bo have been used in further calculations. Mean deviation of the parameters of the repeated experiments from their mean value are given in Table 5. Bo parameters have larger scatter than t_m ($\pm 1\%$). The largest observed scatter ($\pm 24\%$) was in the Bo_G numbers of Mellapak 250Y.

The parameters t_m and Bo were studied for their sensitivity to the probe signal $s_{II,0}$ (used in normalizing the second response, c_{II}) and to the time shift t_0 of the response c_{II} measured with the long column. The following expressions represent the ratio of relative errors of the parameter p , t_m , or Bo , and of experimentally measured values $s_{II,0}$ and t_0 . These ratios were

evaluated by numerical derivation for some experiments exhibiting the highest scatter, i.e., measurement of Bo_G numbers of Mellapak 250Y.

$$\frac{\Delta_{rel} p}{\Delta_{rel} s_{II,0}} = \left(\frac{\partial p}{\partial s_{II,0}} \right) \frac{s_{II,0}}{p}; \quad \frac{\Delta_{rel} p}{\Delta_{rel} t_0} = \left(\frac{\partial p}{\partial t_0} \right) \frac{t_0}{p}; \quad p = t_m \text{ or } Bo \quad (10)$$

The highest values of the ratios, indicating the highest effect of experimental errors on the measured parameters, were found for the experiments for Mellapak 250Y. In Table 6, the ratios calculated for some experiments are given together with the relative errors of Bo induced by following probable experimental errors of t_0 and $s_{II,0}$: the probable error of t_0 is 0.04 s for gas and 0.4 s for liquid responses, and the relative errors of normalized response $\Delta_{rel} s_{II,0}$ are 0.3 and 3% for gas and liquid responses, respectively. The results show that the parameter sensitivity, both of t_m and Bo , increases with decreasing residence time in the tested section of the bed. The parameters measured for liquid phase exhibit lower error/scatter than those measured for gas phase, which can reach up to 50% at the shortest residence time, i.e., at gas flow rate $u_G = 2$ m/s. This has fully confirmed our following experimental results, e.g., see the highest scatter of Bo_G numbers measured at this gas flow rate for Mellapak packing in Figure 12. The analysis of the errors presented here can be used for calculation of the height L of test section needed to keep up the accuracy of the parameters on controlled level.

4.3. Holdup. Total liquid holdup $H_t (= u_L t_m / L)$ for random packings Pall rings and Intalox saddles and for structured packing Mellapak are compared with available literature^{15,17,20} data in Figure 7. The holdups for Pall and Mellapak packings for nonzero gas flow rate are only slightly higher (at maximum 20%) compared with zero gas flow rate. This confirms findings by others that liquid holdup is not significantly affected by gas rate but only by liquid loading and packing geometry. Holdup was correlated by using the following correlation, which was deduced²⁵ from dimensionless analysis of quantities affecting decisively the holdup, i.e., liquid flow character, gravitational force, and packing geometry. For the random packing

$$H_t = a_1 Re_L^{a_2} Ga^{-1/3} (d_{eq} a_p)^{4.945} \quad (11)$$

and for structured packing

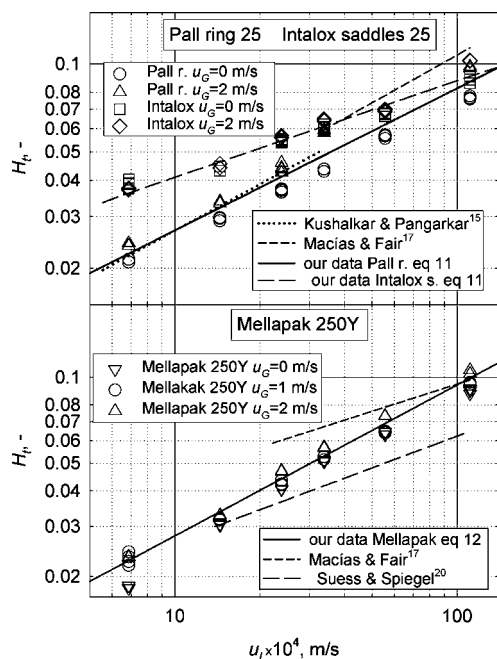
$$H_t = a_1 Ft^{a_2} \left(\frac{3}{\sin^2 \alpha} \right)^{0.877} (d_{eq} a_p)^{2.405} \quad (12)$$

The exponents of the packing geometry characteristics were taken to be the same as those found by Macías and Fair,¹⁷ and the constants a_1 and a_2 were obtained by multiple nonlinear regression analysis of experimental data. These constants and

Table 6. Effect of Experimental Errors of $t_0 = 0.04$ s for Gas and of $t_0 = 0.4$ s for Liquid and of $\Delta_{rel}S_{II,0} = 0.003$ for Gas and $\Delta_{rel}S_{II,0} = 0.03$ for Liquid Responses on the Parameters t_m and Bo Evaluated on Mellapak 250Y Evaluated from Eq 10

no.	conditions						$(\Delta_{rel}Bo)/(\Delta_{rel}S_{II,0})$	$(\Delta_{rel}t_m)/(\Delta_{rel}S_{II,0})$	$(\Delta_{rel}Bo)/(\Delta_{rel}t_0)$	$(\Delta_{rel}t_m)/(\Delta_{rel}t_0)$	$\pm Bo, \%$
	$u_G, \text{ m/s}$	$B, \text{ m/h}$	L	$t_m, \mu\text{s}$	Bo_i	i					
1	0.25	10	0.84	3.33	139	G	10.9	0.52	2.00	1.01	5.7
2	0.5	10	0.84	1.66	171	G	22.7	0.78	2.00	1.01	12
3	2	20	0.84	0.411	105	G	94.7	3.36	2.01	1.02	48
4	1.5	5	0.84	0.556	296	G	151	2.24	2.06	1.01	60
5	1.5	10	0.84	0.540	211	G	123	2.40	2.01	1.01	52
6	1.5	20	0.84	0.535	88	G	55.5	2.48	1.97	1.02	31
7	0.5	0	0.84	1.81	258	G	29.7	0.72	2.35	1.01	14
8*	0.25	0	0.95	3.99	145	G	9.15	0.46	2.01	1.01	4.8
9	0	2.74	0.84	22.8	9.25	L	5.7	0.68	2.59	0.97	10
10	0	8.60	0.84	14.3	23.0	L	5.1	0.48	2.24	0.98	11
11	0	20.0	0.84	9.53	20.4	L	4.9	0.45	2.17	0.98	14
12	2	8.60	0.84	16.5	17.9	L	5.3	0.51	2.24	0.98	11

* Data for Pall rings 25.

**Figure 7.** Effect of liquid flow rate on the total holdup of the liquid. Comparison with literature data.

standard deviations of the correlations are given in Table 7. The data for Pall rings coincide with data by Kushalkar and Pangarkar¹⁵ and are only 20% lower than Macías-Salinas and Fair¹⁷ data. Holdup of Intalox saddles is up to two times higher at low liquid rates ($u_L < 27.8 \times 10^{-4}$ m/s) compared to Pall rings. Our data for structured packing Mellapak 250Y lie between the Suez and Spiegel²⁰ data measured on Mellapak 250Y, Mellapak 250X, and Mellapak 500Y packings and the Macías-Salinas and Fair¹⁷ correlation deduced from data measured on Flexipak 2 and Sulzer BX.

4.4. Liquid-Phase Axial Dispersion. Bodenstein numbers Bo_L of the random packing Pall rings 25 and Intalox saddles 25 and the structured packing Mellapak 250Y (related to packing height $L = 1$ m) are plotted in Figure 8. For all the packings, the axial mixing in the liquid decreases with increasing liquid rate and is unaffected by the gas rate in the range investigated. It is evidenced by Figure 9 in which Bo_L are plotted as a function of gas flow rate. Bo_L numbers measured at 0 and 2 m/s gas flow rates do not differ, compared with the data scatter. Mellapak produced the lowest and Intalox packing the highest axial mixing results. The mixing on Pall rings lies between them and lies also between literature data by Kushalkar and Pangarkar,¹⁵ which are up to two times lower, and Macías-Salinas

and Fair,¹⁸ which are two times higher than our data (Figure 8). Axial dispersion of Mellapak presented by Zhang et al.²¹ is higher, i.e., Bo_L numbers are lower by multiples compared with our data. The multiple lower values of Bo_L ascertained in refs 15 and 21 are probably due to the experimental technique used by the authors. Their experiments were performed on one packing height, the responses were sampled in the outlet flow of the column, and the end effects were ignored in the evaluating procedure. The evaluation without considering the end effects leads to lower value of Bodenstein number.

Correlation of Bo_L numbers of structured packings Flexipak 2 and Sulzer BX by Macías-Salinas and Fair¹⁷ gives ~ 2 times lower values compared with our experimental data. Nevertheless, the experimental data of Sulzer BX packing overtaken from Figure 14 of their work¹⁸ coincide practically with our data, as shown in Figure 8.

Our experimental mixing results were correlated using the form given by Macías-Salinas and Fair.¹⁸ For random packings

$$Bo_L = b_1 Re_L^{b_2} Ga^{-1/3} (d_{eq} a_p)^{2.11} \quad (13)$$

and for structured packing

$$Bo_L = b_1 Fi^{b_2} \left(\frac{3}{\sin^2 \alpha} \right)^{1.159} (d_{eq} a_p)^{6.337} \quad (14)$$

The values of the correlating constants b_1 and b_2 were obtained by multiple nonlinear regression analysis of the data, whereas the exponents of the packing geometry characteristics were retained the same as in the original correlations. The constants are given in Table 7 together with the standard deviations of the experimental data from the correlations.

4.5. Gas-Phase Axial Dispersion. The studies on the gas-phase axial mixing through metal Pall rings 25 are relatively available. Our results obtained for this packing were compared to those correlated by previous investigators. For this purpose, we have used the correlation deduced by Macías-Salinas and Fair¹⁸ for random packings

$$Bo_G = c_1 Re_G^{c_2} 10^{c_3 Re_L} (d_{eq} a_p)^{c_4} \quad (15)$$

The values of the correlating constants c_1 – c_4 obtained by the authors¹⁸ using multiple nonlinear regression analysis of the data measured for Raschig and Pall rings 25 are given in Table 8 together with the standard deviation of the experimental data from the correlation. Our results for Pall rings measured within the operating ranges of Macías-Salinas and Fair¹⁸ ($u_L < 9.44$ mm/s; $0.86 < u_G < 3.5$ m/s) agree well with theirs, as illustrated

Table 7. Constants of the Regression Eqs 11–14

a_1	a_2	$\sigma \times 10^3$	eq	b_1	b_2	σ	eq	source
Pall ring 25								
8.17e-4	0.5442		11	26.75 ^a	0.5544		13	refs 17 and 18
8.65e-4	0.4863	4.97	11	13.45	0.5557	1.25	13	our data ^b
Intalox saddle 25								
2.17e-3	0.3309	3.54	11	0.5642	1.0575	0.88	13	our data ^b
Mellapak 250Y								
0.0557	0.3165		12	8.917 ^a	0.7082		14	refs 17 and 18
0.6844	0.5296	3.12	12	1.022	0.4784	3.76	14	our data [#]

^a Recalculated from $L = 0.914$ m, used in ref 17, onto $L = 1$ m, used in this work. ^b Operating ranges: $22 < Re_L < 281$; $0 < Re_G < 3240$; $Ga = 1.60 \times 10^8$; $d_{eq}a_p = 5.21$. [#] Operating ranges: $8 < Re_L < 141$; $0 < Re_G < 3240$; $4.3 \times 10^{-7} < Fi < 6.96 \times 10^{-6}$; $d_{eq}a_p = 3.19$; $\alpha = 45^\circ$.

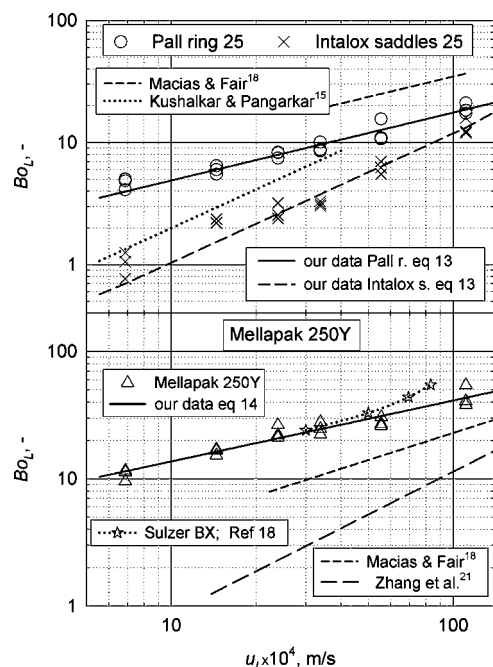


Figure 8. Experimental Bo_L numbers on random and structured packings ($L = 1$ m) as a function of liquid flow rate. Comparison with literature data.

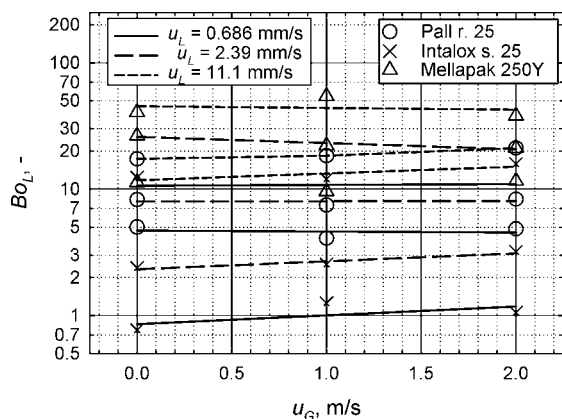


Figure 9. Experimental Bo_L numbers as a function of gas flow rate.

in Figure 10. The coincidence of our data with the literature correlation for the relatively well studied packing of Pall rings supports/confirms the correctness of the measuring technique. The filled points in the figure, which differ from the correlation significantly, were measured outside the operating ranges of the correlation ($u_G < 1$ m/s; $u_L > 83.3 \times 10^{-4}$ m/s).

The correlating form of eq 15 was used to regress our Bo_G data measured for Pall rings 25 (except the data for the highest

liquid load 111×10^{-4} m/s) and all data measured for Intalox saddles 25. The magnitude of the axial dispersion for Intalox saddles was lower than for Pall rings. The resulting constants c_1 – c_3 (the exponent c_4 of the packing geometry characteristics was retained the same as in the original correlation¹⁸) were obtained by multiple nonlinear regression analysis of our data and are given in Table 8 for both packings. The correlations acceptably reproduce the experimental data within $\pm 13\%$ and $\pm 22\%$ for the Pall and Intalox packing, respectively, as is shown in Figure 11. Axial mixing in the gas increases with both gas and liquid rates for both random packings, but the extent of the dependence on gas flow rate is much weaker compared with the Macías-Salinas and Fair¹⁸ correlation. This is illustrated in Figures 13 and 14 in which the Bo_G numbers are plotted for all three packings as a function of liquid and gas flow rate, respectively. Note also the lower value of the exponent c_2 in the correlations of our data compared with the one in the original correlation,¹⁸ as is given in Table 8.

Similar comparisons, which were done for the random packings, were done also for the structured packing, Mellapak 250Y. The comparison with the Macías-Salinas and Fair¹⁸ correlation (deduced from Bo_G data for Flexipak 2 and Sulzer BX) is presented in Figure 10. Bo_G numbers, which we measured for Mellapak within the operating range of the Macías-Salinas and Fair¹⁸ correlation ($33 \times 10^{-4} < u_L < 85 \times 10^{-4}$ m/s; $1 < u_G < 3.5$ m/s; see Figure 6 of their work), are up to four times higher compared with those calculated from their¹⁸ original correlation. Using the form of eq 15 to regress our all Bo_G data measured for Mellapak packing resulted in the constants c_1 – c_3 , which are given in Table 8. The correlation acceptably reproduces the experimental data within $\pm 20\%$ difference between measured and predicted values; see Figure 12.

Our Bo_G numbers for Mellapak 250Y exhibit a substantially lower level of axial mixing (up to three times, see Figure 10) and much weaker dependence of the axial mixing on gas flow rate (see exponents c_2 in Table 8) than the Macías-Salinas and Fair data¹⁸ for similar Flexipak 2 packing. They¹⁸ found approximately the same Bo_G numbers for Pall rings and Flexipak 2 (see Figure 7 of their work), whereas we obtained the numbers for Mellapak up to six times higher than those for Pall rings, as is shown in Figure 13. We believe that our data describe the physical reality more accurately for the following reasons. The axial mixing is caused by the instable gas flow, which results in the formation of eddies in the flow channels available for gas flow in the bed. In packings within random structure, the random variation of the channel geometry may produce higher turbulence intensity than gas flow through a structured packing, which has regular pores. This could provide an explanation for the increased amount of dispersion in the gas phase for the random packings in comparison with the structured packing. This explains also the weaker dependence of the axial mixing

Table 8. Constants of the Regression Equation 15

c_1	$-c_2 \times 10^2$	$-c_3 \times 10^3$	c_4	Re_G	Re_L	σ	source
0.09602 ^a	89.15	0.75	Pall ring 25	340/4066	90/237	8.5	ref 18
0.00169	37.33	1.164	8.231	405/3241	0/141	10.8	our data
0.00200	30.16	1.136	8.231	405/3241	0/282	33.6	ref 18
4.644 × 10 ⁸ ^a	89.6	2.08	Mellapak 250Y	381/3516	25/122	4.37	ref 18
2.807 × 10 ⁶	0.895	3.94	-7.792	204/1630	0/142	41.8	our data

^a Recalculated from $L = 0.914$ m, used in ref 17, onto $L = 1$ m, used in this work.

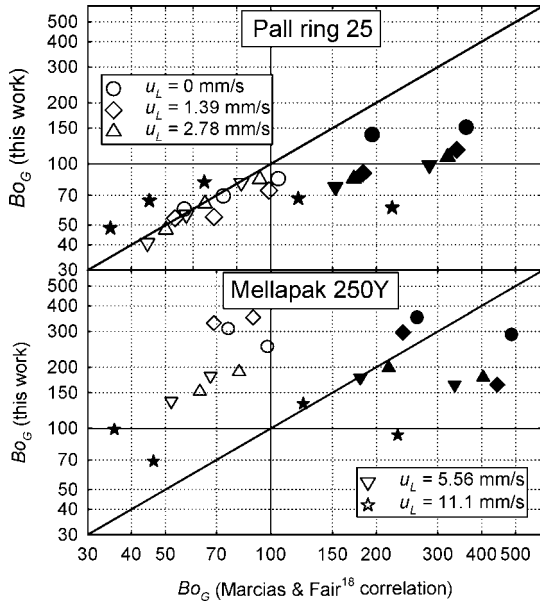


Figure 10. Comparison of experimental Bo_G numbers with Macías-Salinas and Fair correlation. The filled points were measured outside the operating ranges of the correlation (Pall ring: $u_L < 9.44$ mm/s; $0.86 < u_G < 3.5$ m/s. Mellapak 250Y: $3.3 < u_L < 8.5$ mm/s; $1 < u_G < 3.5$ m/s).

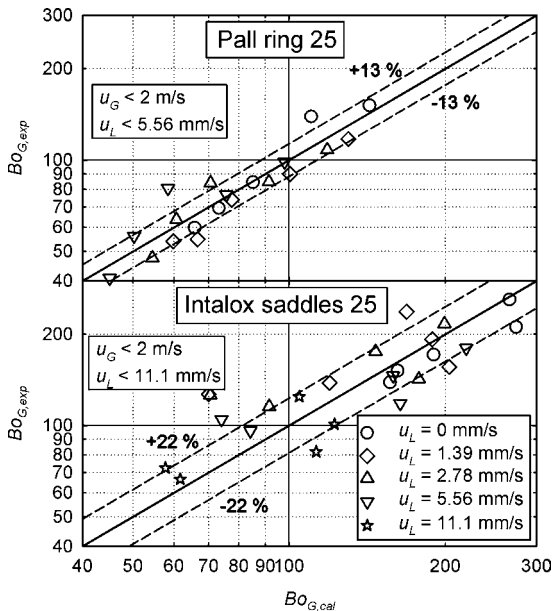


Figure 11. Comparison of our experimental Bo_G numbers for Pall rings and Intalox saddles with values calculated by eq 15.

on gas flow rate occurring for structured packing. This type of packing exhibits less increase of pressure drop with increasing gas flow rate, i.e., less energy dissipation due to turbulence, and thus less increase of the axial mixing.

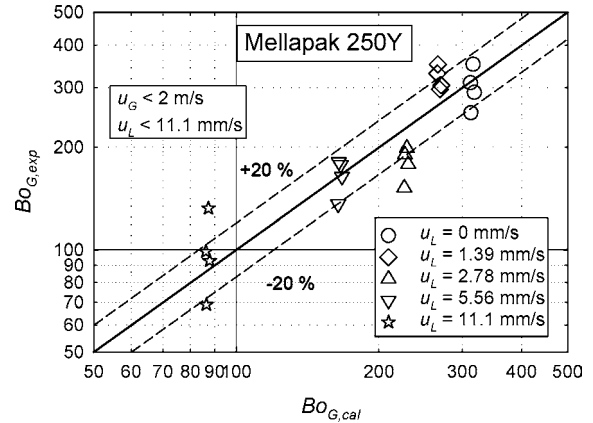


Figure 12. Comparison of experimental Bo_G numbers for Mellapak 250Y with the values calculated by eq 15.

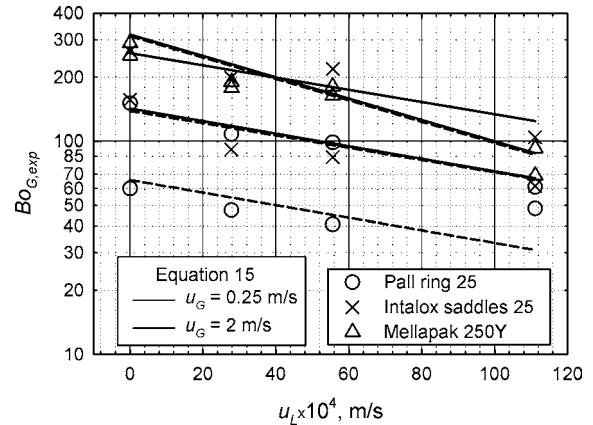


Figure 13. Gas-phase mixing numbers Bo_G vs liquid flow rate measured for two different gas flow rates.

5. Conclusions

The axial dispersion of gas and liquid phases in columns packed with metal Pall rings 25, Intalox saddles 25, and Mellapak 250Y were measured using a dynamic method under hydraulic conditions common in distillation columns. Flow rates used in the experiments were within the ranges $0 < u_L < 111 \times 10^{-4}$ m/s and $0 < u_G < 2$ m/s.

Gas and liquid distributors of a special design were used for introduction of a step concentration change of tracer uniformly across the column cross section into the inlet streams of gas and liquid. The radial scatter of the helium tracer concentration was measured, and it was found that our results measured in the center of the column using the bottom packing height of 33 cm of Pall rings represent well the nonideal flow conditions in the whole column cross section.

Bo_L and Bo_G numbers for Pall rings were found to be close to the ones calculated by the Macías-Salinas and Fair¹⁸

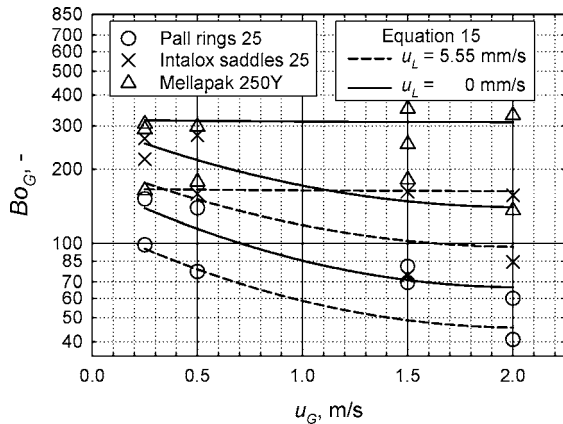


Figure 14. Gas-phase mixing numbers Bo_G as a function of gas flow rate.

correlation. This agreement validates our measuring technique, especially that used in the liquid phase. It is based on the reproduction of the experimental response curves measured at the outlet of the long column by the response predicted by the theoretical transformation of the experimental concentration profiles measured at the outlet of the short column using a diffusion-type model. The technique circumvents the effect of the probe dynamic, the imperfection of the tracer concentration step change, and the end effects on the evaluated parameters. Pulse characteristics of the open and closed systems used for the response evaluation gave practically the same results.

The results confirmed the dependence trends of gas and liquid longitudinal mixing on the rates of phases revealed by the Macías-Salinas and Fair's data¹⁸ for random and structured packings, but our Bo_G numbers for structured packing of Mellapak 250Y show up to three times lower level of axial mixing and much weaker dependence on gas flow rate than their data for similar Flexipak 2 packing.

The following correlations were developed for the prediction of axial mixing in both phases under countercurrent, two-phase flow conditions.

For random packing of metal Pall rings 25,

$$Bo_L = 13.45 Re_L^{0.556} Ga^{-1/3} (d_{eq} a_p)^{2.11} \quad (16)$$

with a valid operating range of $22 < Re_L < 281$; $0 < Re_G < 3240$; $Ga = 1.60 \times 10^8$; and $d_{eq} a_p = 5.21$, and

$$Bo_G = 0.00169 Re_G^{-0.3733} 10^{-0.001164 Re_L} (d_{eq} a_p)^{8.231} \quad (17)$$

with a valid operating range of $0 < Re_L < 141$; $405 < Re_G < 3240$; and $d_{eq} a_p = 5.21$.

For random packing of metal Intalox saddles 25,

$$Bo_L = 0.564 Re_L^{1.058} Ga^{-1/3} (d_{eq} a_p)^{2.11} \quad (18)$$

with a valid operating range of $22 < Re_L < 281$; $0 < Re_G < 3240$; $Ga = 1.60 \times 10^8$; and $d_{eq} a_p = 5.21$, and

$$Bo_G = 0.002 Re_G^{-0.3016} 10^{-0.001136 Re_L} (d_{eq} a_p)^{8.231} \quad (19)$$

with a valid operating range of $0 < Re_L < 281$; $405 < Re_G < 3240$; $d_{eq} a_p = 5.21$.

For structured packing of Mellapak 250Y,

$$Bo_L = 1.022 Fi^{0.4784} \left(\frac{3}{\sin^2 \alpha} \right)^{1.159} (d_{eq} a_p)^{6.337} \quad (20)$$

with a valid operating range of $8 < Re_L < 141$; $0 < Re_G < 3240$; $4.3 \times 10^{-7} < Fi < 6.96 \times 10^{-6}$; $d_{eq} a_p = 3.19$; and $\alpha = 45^\circ$, and

$$Bo_G = 2.807 \times 10^6 Re_G^{-0.00895} 10^{-0.00394 Re_L} (d_{eq} a_p)^{-7.792} \quad (21)$$

with a valid operating range of $0 < Re_L < 141$; $204 < Re_G < 1630$; and $d_{eq} a_p = 3.19$. The correlations reproduce the experimental data within $\pm 22\%$ of the measured values.

Acknowledgment

Financial support from the Ministry of Education (MSM 6046137306) is gratefully acknowledged.

Nomenclature

- a_p = packing geometrical area, 1/m
- Bo_i = $Lu_{i,j}/D_{e,i}$, Bodenstein number
- c = normalized concentration response
- d_{eq} = nominal diameter (random packing), equivalent diameter (structured packing), m
- D_e = effective dispersion coefficient, m^2/s
- E = pulse characteristic
- F = transient characteristic
- Fi = $\eta_L u_i / d_{eq}^2 \rho_L g$, film number
- g = gravity acceleration, m/s^2
- Ga = $d_{eq}^3 \rho_L^2 g / \eta_L^2$, Galileo number
- H_t = $u_L t_m / L$, total liquid holdup, m^3/m^3
- L = height of test section of packing, m
- $L_{1,2}$ = packing heights before and behind the test section, m
- R = objective function eq 9
- Re_i = $u_i d_{eq} \rho_i / \eta_i$, Reynolds number
- s = probe signal, V
- t = time, s
- t_m = mean residence time, s
- t_0 = time shift of the responses on short and long column, s
- u_i = superficial gas/liquid velocity, m/s
- u_j = interstitial velocity (velocity in actual flow cross section), m/s
- z = packing height coordinate, m

Greek symbols

- α = corrugation inclination angle
- δ = Dirac function
- η = viscosity, Pa s
- ρ = density, kg/m^3
- σ = standard deviation
- $\theta = t/t_m$, dimensionless time

Subscripts

- axial = axial dispersion considered
- c = closed system
- cal = predicted value
- exp = measured value
- i = G or L, gas or liquid phase
- o = open system
- plug = plug flow considered
- I = first measuring point, short column
- II = second measuring point, long column
- 0 = initial steady-state probe signal
- ∞ = final steady-state probe signal

Literature Cited

- (1) Rejl, F. J.; Valenz, L.; Linek, V. "Profile method" for the measurement of k_a and $k_v a$ in distillation columns. Validation of rate-based distillation models using concentration profiles measured along the column. *Ind. Eng. Chem. Res.* **2010**, *49*, 4383.
- (2) Kramers, H.; Alberta, G. Frequency response analysis of continuous flow systems. *Chem. Eng. Sci.* **1958**, *2*, 173.

- (3) DeMaria, F.; White, R. R. Transient response study of gas flowing through irrigated packing. *AIChE J.* **1960**, *6*, 473.
- (4) Otake, T.; Kunugita, E. Mixing characteristics of irrigated packed towers. *Chem. Eng. Jpn.* **1958**, *22*, 144.
- (5) Hoogendoorn, C. J.; Lips, J. Axial mixing of liquid in gas-liquid flow through packed columns. *Can. J. Chem. Eng.* **1965**, *43*, 125.
- (6) Dunn, W. E.; Vermeulen, T.; Wilke, Ch. R.; Word, T. T. Longitudinal dispersion in packed gas absorption columns. *Ind. Eng. Chem. Fundam.* **1977**, *16*, 116.
- (7) Polk, E. M.; Clements, W. C. *Liquid phase dynamics of a packed absorption column using pulse testing methods*; Vanderbilt Univ. Tech. Rep. No. 10; Vanderbilt University: Nashville, TN, 1966.
- (8) Sater, V. E.; Levenspiel, O. Two-phase flow in packed beds evaluation of axial dispersion and holdup by moment analysis. *Ind. Eng. Chem. Fundam.* **1966**, *5*, 86.
- (9) Carleton, A. J.; Flain, R. J.; Rennie, J.; Valentin, F. H. H. Some properties of a packed bubble column. *Chem. Eng. Sci.* **1977**, *22*, 1839.
- (10) Farid, M. M.; Guán, D. J. Dispersion in trickle and two-phase flow in packed columns. *Chem. Eng. Sci.* **1979**, *34*, 579.
- (11) Bennett, A.; Goodridge, F. Hydrodynamic and mass transfer studies in packed absorption columns. Part I: Axial dispersion. *Trans. Inst. Chem. Eng.* **1970**, *48*, T232.
- (12) Van Swaaij, W. P. M.; Charpentier, J. C.; Villiermaux, J. Residence time distribution in the liquid phase of trickle flow in packed columns. *Chem. Eng. Sci.* **1969**, *24*, 1083.
- (13) Stovkã, U.; Cevey, P. F. Influence of the physical properties of the liquid on axial dispersion in packed columns. *Ind. Eng. Chem. Process Des. Dev.* **1984**, *23*, 717.
- (14) Perrin, S.; Chaudourne, S.; Jallut, C.; Lieto, J. Transient state techniques for mass transfer characterization of a gas-liquid packed column. *Chem. Eng. Sci.* **2002**, *57*, 3335.
- (15) Kushalkar, K. B.; Pangarkar, V. G. Liquid holdup and dispersion in packed columns. *Chem. Eng. Sci.* **1990**, *45*, 759.
- (16) Benadda, B.; Kafou, K.; Monkam, P.; Otterbein, M. Hydrodynamics and mass transfer phenomena in counter-current packed column at elevated pressures. *Chem. Eng. Sci.* **2000**, *55*, 6251.
- (17) Macías-Salinas, R.; Fair, J. R. Axial mixing in modern packings, gas and liquid phases: I. Single-phase flow. *AIChE J.* **1999**, *45*, 222.
- (18) Macías-Salinas, R.; Fair, J. R. Axial mixing in modern packings, gas and liquid phases: II. Two-phase flow. *AIChE J.* **2000**, *46*, 79.
- (19) Noeres, C.; Hoffmann, A.; Górak, A. Reactive distillation: Non-ideal flow behavior of the liquid phase in structured catalytic packings. *Chem. Eng. Sci.* **2002**, *57*, 1545.
- (20) Suez, P.; Spiegel, L. Hold-up of Mellapak structured packings. *Chem. Eng. Process.* **1992**, *31*, 119.
- (21) Zhang, P.; Liu, Ch.; Tang, Z.; Juan, X.; Yu, G. Gas-liquid two-phase axial backmixing through structured packing at elevated pressure. *Chin. J. Chem. Eng.* **2003**, *11*, 504.
- (22) Linek, V.; Moucha, T.; Prokopová, E.; Rejl, J. F. Simultaneous determination of vapor- and liquid-side volumetric mass transfer coefficients in distillation column. *Trans. Inst. Chem. Eng., Chem. Eng. Res. Des.* **2005**, *83* (A8), 979.
- (23) Valenz, L. Study of interfacial heat and mass transfer in packed distillation and absorption columns. An effect of axial dispersion in both phases. Ph.D. Dissertation, Prague Institute of Chemical Technology, Prague, Czech Republic, 2009.
- (24) Levenspiel, O.; Smith, W. K. Notes on the diffusion-type model for the longitudinal mixing of fluids in flow. *Chem. Eng. Sci.* **1957**, *6*, 227.
- (25) Otake, T.; Okada, K. Liquid holdup in packed towers. *Chem. Eng. Jpn.* **1953**, *17*, 176.
- (26) Linek, V.; Beneš, P.; Sinkule, J.; Kivský, Z. Simultaneous determination of mass transfer coefficient and of gas and liquid axial dispersions and hold-ups in a packed absorption column by dynamic response method. *Ind. Eng. Chem. Fundam.* **1978**, *17*, 298.

Received for review May 14, 2010

Revised manuscript received August 20, 2010

Accepted August 31, 2010

IE101092E

Contents lists available at [ScienceDirect](http://www.sciencedirect.com)

Chemical Engineering Research and Design

journal homepage: www.elsevier.com/locate/cherd

IChemE

On the modeling of gas-phase mass-transfer in metal sheet structured packings



F.J. Rejl*, L. Valenz, J. Haidl, M. Kordač, T. Moucha

Institute of Chemical Technology Prague, Technická 5, 166 28 Praha 6, Czech Republic

ABSTRACT

This paper refers on gas mass-transfer characteristics of several metal sheet Mellapak structured packings (M250Y, M350Y, M452Y, M500Y) under absorption conditions. These characteristics have been measured using standard absorption systems of SO₂ chemisorption into the NaOH aqueous solution ($k_G a$) and CO₂ chemisorption into the NaOH aqueous solution (effective area a). Measurements were performed with four elements of the packing with diameter of 0.29 m and total height of 0.84 m. Gas-phase mass-transfer coefficients for all studied packings have been correlated by the dimensionless equation $Sh_G = 0.409 \cdot Re_G^{0.622} \cdot Re_L^{0.0592}$. The experimental values of k_G are in the most cases significantly under-predicted by fundamental mass-transfer models, wetted-wall column correlations and by the model packages developed for structured packing. The exponent 0.622 of gas Reynolds criteria is lower than expected by the models starting from the imagination of the flow through the channel and corresponding experiments with wetted-wall columns. The revealed value of the exponent agrees better with those found for flow around submerged objects like spheres or through the bed consisting of random packing, suggesting that the wetted wall column is not a suitable experimental simplification for the study of structured packings.

© 2014 The Institution of Chemical Engineers. Published by Elsevier B.V. All rights reserved.

Keywords: Absorption; Mass-transfer; Structured packing; Mellapak

1. Introduction

Structured packings are now widely utilized due to their low pressure drop per unit of separation efficiency. Since their introduction number of models predicting their mass-transfer performance has been published. Comprehensive review of mass-transfer models for packed columns has been provided by Wang et al. (2005). While new and new models are created (some of them are incorporated into the simulation programs) their reliability is still not broadly acknowledged (Crause and Nieuwoudt, 1999).

Principally, all gas-phase mass transfer correlations developed for structured packings are based on the following fundamental models of mass transfer of gas component from interface to the bulk phase: (i) wetted wall mass transfer model, (ii) boundary layer model and (iii) turbulent flow models utilizing “Chilton–Colburn analogy” (Chilton and Colburn, 1934).

(i) Wetted wall mass transfer models utilize the relation

$$Sh = C Re^m Sc^n \quad (1)$$

with the parameters C , m and n optimized on the basis of experiments in the wetted wall column performed with various absorption and/or distillation systems.

(ii) *Boundary layer models* assume development of boundary layer along the surface. Below the critical Reynolds number this layer remains laminar. For laminar boundary layer developing along the flat plate, while bulk remains turbulent, following formula has been derived

$$Sh = C Re^{1/2} Sc^{1/3} \quad Re < 5 \times 10^5 \quad (2)$$

(iii) *Turbulent flow models* assume dominant form of transport from the interface by turbulent eddies and analogy between momentum, heat and mass transfer. The

* Corresponding author. Tel.: +420 220 44 3299.

E-mail address: frantisek.rejl@vscht.cz (F.J. Rejl).

Available online 10 June 2014

<http://dx.doi.org/10.1016/j.cherd.2014.06.004>

0263-8762/© 2014 The Institution of Chemical Engineers. Published by Elsevier B.V. All rights reserved.

Nomenclature

a	effective interfacial area (m^2/m^3)
a_g	geometrical area of the packing (m^2/m^3)
B	liquid superficial velocity (m/h)
C_p	isobaric heat capacity ($\text{J}/\text{kg}/\text{K}$)
C_V	packing characteristic constant in Eqs. (9) and (10)
c_A	concentration of solute A (mol/m^3)
D	diffusion coefficient (m^2/s)
d_{eq}	packing equivalent diameter in Eq. (32); $d_{\text{eq}} = 0.01277 \text{ m}$
d_p	packing characteristic diameter (m); $d_p = 4\varepsilon/a_g$ (m)
f	friction factor
Fi_L	liquid film number; $Fi_L = \mu_L u_L / d_{\text{eq}}^2 \rho_L g$
H	packing height (m)
He	liquid–gas equilibrium constant, $He = c_L/c_G$
h	heat transfer coefficient ($\text{J}/\text{m}^2/\text{K}$)
h_L	liquid hold-up (m^3/m^3)
j_H	Chilton–Colburn’s heat transfer j -factor
j_M	Chilton–Colburn’s mass transfer j -factor
K_{OG}	overall gas mass transfer coefficient (m/s)
K_{OGa}	overall gas volumetric mass transfer coefficient (s^{-1})
k_G	gas mass-transfer coefficient (m/s)
k_{Ga}	volumetric gas mass transfer coefficient (s^{-1})
k_{OH}	kinetic constant of the second order between CO_2 and OH^- ($\text{m}^3/\text{s}/\text{mol}$)
l	length (m)
Pr	Prandtl number; $Pr = c_p \mu_L / h$
Re	Reynolds number; $Re = d_p u \rho / \mu$
R_G	gas-phase relative resistance
Sc	Schmidt number; $Sc = \mu / D \rho$
Sh	Sherwood number; $Sh = (k \cdot d_p) / D$
u	phase velocity (m/s)

Greek letters

ε	packing void fraction (m^3/m^3)
θ	inclination of the channels from horizontal plane ($^\circ$)
μ	dynamic viscosity (Pa s)
ξ_{GL}	gas–liquid friction factor
ρ	density (kg/m^3)
σ_{rel}	relative standard deviation, RSD
φ	fraction of the channel occupied by liquid

Indexes

E	effective
G	gas-phase
i	interstitial
IN	at the inlet
L	liquid-phase
lam	laminar
OUT	at the outlet
turb	turbulent

Chilton–Colburn analogy postulates equality of j -factors

$$j_M \equiv \frac{f}{2} = j_H \equiv \frac{h}{C_p \rho u} Pr^{2/3} = j_M \equiv \frac{k_G}{u} Sc^{2/3} \quad (3)$$

These factors are functions of Reynolds number and the dependence must be determined experimentally. This dependence is rather weak for flow in tubes

$$j_i = 0.023 Re^{-0.2} \quad Re > 10^4 \quad (4)$$

resulting in

$$Sh = 0.023 Re^{0.8} Sc^{1/3} \quad (5)$$

and more pronounced for the flow around submerged object such as single sphere

$$j_i = 0.37 Re^{-0.4}; \quad 20 < Re < 10^4; \quad Sh = 0.37 Re^{0.6} Sc^{1/3} \quad (6)$$

or around submerged objects, where abrupt changes in gas flow direction and its velocity occurs like in the flow through the packed bed for which was found

$$j_i = 1.17 Re^{-0.415}; \quad 10 < Re < 2500; \quad Sh = 0.37 Re^{0.585} Sc^{1/3} \quad (7)$$

Eqs. (4)–(7) have been taken from Henley et al. (2011).

There is usually assumed, that the gas flows upwards through the system of mutually perpendicular 45° (Y-type) inclined, triangular channels with one side open and the gas does not change its direction until reaching edge of the element or the wall of the column. Due to the inclination of the channels, true gas velocity through the channel is higher than the superficial velocity by factor $\sqrt{2}$ (for Y-type). No slip condition is assumed for the gas at the interface. The determinative for hydrodynamic and mass-transfer calculations of counter-current absorption and distillation columns is therefore the sum of interstitial liquid and superficial gas velocities, “effective velocity” – u_E . Determination of the interstitial liquid velocity out of superficial velocity might be tricky and desires at least knowledge of liquid hold-up.

There is necessary to determine the characteristic dimension of the packing, d_p , for calculation of the Reynolds number. It is usually identified with the hydraulic diameter of the packing, $4\varepsilon/a_g$, or the length of the channel. Turbulent flow is usually tacitly assumed for the gas-phase hydrodynamics, although the Re_G calculated with the hydraulic diameter of the packing taken as the characteristic dimension is relatively low. For example the gas-phase Reynolds number equals only $Re_G = 1455$ for superficial velocity of 1 m/s, air at ambient conditions and M250Y. However, as the power law slope on the pressure drop curve versus gas rate is very close to 2 even for the smallest gas rates, the character of the flow is probably really close to the fully developed turbulent one. The intricate geometry of the channels and the roughness of tube walls induce turbulent flow in the channels or the gas flow path is more complicated than simple channel flow. The value of the critical Re -number for the transition to the turbulent flow decreases from 2100 down to the value, which is probably in the order of few hundreds.

It should be noted, that recommended correlations binds together velocity and characteristic dimension dependence of k_G e.g., $k_G \propto u_G^m d_p^{m-1}$ for most frequently used type of correlation (Eq. (1)).

2. Survey of correlations of gas-phase mass-transfer in structured packings

Models of gas-phase mass-transfer for the structured packing are often based on the experiments in the wetted-wall column, e.g. on the study of [Johnstone and Pigford \(1942\)](#). They optimized the parameters m and C in Eq. (1) on the basis of experiments performed with four distillation and two absorption systems. They found the values $m=0.77$ and $C=0.0328$. The exponent $n=0.33$ was taken over from [Chilton and Colburn \(1934\)](#) because their experiments covered only a narrow range of Sc values and it was not possible to determine the effect of this criteria.

[Rocha et al. \(1996\)](#) modeled mass-transfer in the gas-phase in the dimensionless form (Eq. (1)) where characteristic dimension is calculated from geometry of corrugation (further referred to as (RBF)). They correlated the HETP data of Sulzer BX packing measured on four distillation systems under various pressures with assumptions of fully wetted area of the packing and the mass transfer resistance limited to the gas-phase and found the relation

$$Sh_G = 0.054 Re_G^{0.8} Sc_G^{0.33} \quad (8)$$

[Billet and Schultes \(1999\)](#) (further referred to as (BS)) proposed gas-phase mass-transfer model

$$k_G = C_V \left[\frac{a_g}{d_p(\varepsilon - h_L)} \right]^{1/2} D_G \left(\frac{u_G \rho_G}{a_g \mu_G} \right)^{3/4} Sc_G^{1/3} \quad (9)$$

which can be redrawn as

$$Sh_G = C_V \left(\frac{4\varepsilon}{\varepsilon - h_L} \right)^{0.5} Re_G^{0.75} Sc_G^{1/3} \quad (10)$$

where C_V is the packing specific constants and the hydraulic dimension of the packing d_p

$$d_p = \frac{4\varepsilon}{a_g} \quad (11)$$

[Olujic et al. \(1999, 2004\)](#) assume that for gas velocities prevailing in distillation columns hydrodynamic conditions correspond rather to transient than turbulent behavior (their model is further referred to as (DELFT)). In order to cover the whole range of operating conditions encountered in typical total reflux distillation tests, the authors takes vapor side mass transfer coefficient comprises both a laminar and a turbulent part and is described as

$$Sh_G = \sqrt{Sh_{G,lam}^2 + Sh_{G,turb}^2} \quad (12)$$

Expressions for Sherwood numbers have been deduced from analogy with the heat transfer and the source relations are chosen that for short tubes with pronounced entrance effects for which the flow is not stabilized.

$$Sh_{G,lam} = 0.664 Re_G^{1/2} Sc_G^{1/3} \left(\frac{d_p}{l_G} \right)^{1/2} \quad (13)$$

$$Sh_{G,turb} = \frac{\left(\frac{Re_G Sc_G \varepsilon_{GL} \psi}{8} \right) \left(\frac{d_p}{l_G} \right)^{1/2}}{1 + 12.7 \sqrt{\frac{\varepsilon_{GL} \psi}{8}} (Sc_G^{2/3} - 1)} \quad (14)$$

[Crause and Nieuwoudt \(1999\)](#) and [Nieuwoudt and Crause \(1999\)](#) considered earlier performed tests on wetted wall columns as inappropriate to be a basis for structured packings due to the length to diameter ratio far greater than that occurring in structured packings. They performed experiments on the wetted-wall column with a length of four diameters using pure liquids. For low viscosity liquids they found

$$Sh_G = 0.054 Re_G Sc_G^{0.33} Re_L^{0.08} \quad (15)$$

Model of [Hanley and Chen \(2012\)](#) is based on the dimension analysis of the quantities describing gas-phase mass-transfer, which results in dimensionless Eq. (1) (further referred to as (Hanley)). Values of exponent m and n are specified using Chilton–Colburn analogy in the form

$$j_M = \frac{Sh_G}{Re_G Sc_G^{1/3}} = \frac{f(Re_G)}{2} \quad (16)$$

For larger channels of metal sheet packings the Reynolds number dependence of the friction factor is assumed negligible and therefore

$$Sh_G = C Re_G Sc_G^{1/3} \quad (17)$$

For smaller channels assumed for gauze packings the Reynolds number dependence of the friction factor is assumed non-negligible and the resulting relation takes form of

$$Sh_G = C Re_G^{1/2} Sc_G^{1/3} \quad (18)$$

Constant C has been validated through the fit to distillation data only, absorption experiments served for fit of liquid side mass-transfer coefficient solely.

The model should not be applied below minimum liquid rate expected for good performance of the packing – typically about 30–40% of the flood.

Only limited absorption gas-phase mass-transfer data are published for size series of the structured packings. Aim of this work is therefore focused on measurement of volumetric mass-transfer coefficients in the gas-phase, $k_G a$, for the three metal structured Sulzer Mellapak packings differing in nominal geometric area – Mellapak 250Y (M250Y), Mellapak 350Y (M350Y), Mellapak 500Y (M500Y) and one high-capacity packing of the same vendor Mellapak M452Y (M452Y). Mass-transfer coefficients in the gas-phase, k_G , are determined using the data of independently measured effective interfacial area published recently in [Valenz et al. \(2011a,b\)](#).

These data shall serve as a base for correlation of the mass-transfer coefficients with the gas velocity and packing characteristic dimension. The data and the revealed dependences will be compared with the predictions of the models developed or used in the connection with the investigation of the structured packings.

3. Experimental

The experiments have been carried out in the column with a 0.29 m inner diameter. The packed bed consisted of four elements of the packing rotated mutually by 90° with a total bed height of 0.84 m. The packings used were M250Y, M350Y, M452Y, and M500Y. Each element of the packing was horizontally drilled by electrical discharge machinery to enable

installation of a sampling device for the withdrawal of the gas samples. This sampling device is a virtually tube of a diameter of 30 mm with four downward conical openings collecting solely the gas and performing so uniformly along the packing diameter. The effect of the sampling device installation on the measured data has been published together with detailed drawing of the absorption column and sampling device in Valenz et al. (2011a,b). The authors concluded on the basis of the effective mass-transfer area measurement using sampling points inside and outside the bed of the packing are negligible. Liquid distribution over the cross-section of the column was carried out by the pipe liquid distributor with drip-point density of 630 dp/m². Gas entered the column through a large drum where the flow was calmed and proceeded into the column through the grid which secured its uniform distribution. Absorption liquid was the aqueous solution of NaOH with concentration of 1 kmol/m³. The solution was recirculated. The batch was superseded when the concentration of OH⁻ dropped under certain limit; 0.5 kmol/m³ – in the case of interfacial area measurement; 0.1 kmol/m³ – in the case of $k_G a$ measurement. The gas circuit was open. The experiments were performed at atmospheric pressure with the temperature of the gas and liquid entering the column maintained at 20 °C. The gas was saturated with water vapor. The experiments were carried out up to flooding conditions with liquid velocities of 5, 10, 20, 40, 60, 80, 100 m³/(m² h) and gas superficial velocities of 0.5, 1.0, 1.5, 2.0, 2.5, 3.0 m/s.

The tracer gas was introduced into the gas-phase long before it entered the column and was therefore well mixed. Tracer gas flow was set to maintain its concentration at the lowest sampling point at least 1000 ppm. The gas was sampled from each element at four different levels of the packed bed. The height of the packing between the sampling points corresponded to the height of the element and was 0.21 m. Mass-transfer characteristics were evaluated from concentrations measured in only two sampling points, however. Their choice has been done on the basis of an effort to cover as long packed bed as possible, but the top concentration must not drop below about 20 ppm. Below this limit the error in concentration determination would be unbearable. For measurement of the interfacial area this politics meant most often utilization of 0.63 m of the bed, while for $k_G a$ determination 0.21 m or 0.42 m of the bed was utilized.

The CO₂ and SO₂ concentration in the gaseous samples were measured continuously using IR analyzer S710 (Sick). Before entering the analyzer the gas was dried by a passage through the cartridge filled by crushed CaCl₂ (CO₂ analysis) or Mg(ClO₄)₂ (SO₂ analysis).

3.1. $k_G a$ determination

Measurement of the volumetric mass-transfer coefficients, $k_G a$, is performed through experiments with systems, for which the mass-transfer resistance is limited to the gas-phase. Evaporation or absorption accompanied by the instantaneous reaction of the transferring gaseous solute at the interface is commonly utilized (Danckwerts, 1970; Rejl et al., 2009). In this work, absorption of SO₂ into the lye has been used. Under the assumptions of the plug flow of the gas-phase, instantaneous reaction between SO₂ and OH⁻ ions resulting in zero concentration of SO₂ at the interface and the low concentration of the

absorbed component, the $k_G a$ value can be calculated from the following relation:

$$k_G a = \frac{u_G}{H} \cdot \ln \frac{c_{\text{SO}_2}^{\text{IN}}}{c_{\text{SO}_2}^{\text{OUT}}} \quad (19)$$

which also predicts arrangement of the experiment and necessary quantities to be measured. The assumptions of the instantaneous reaction at the interface and negligible mass transfer resistance in the liquid phase were verified by measuring the dependence of $k_G a$ value on the NaOH concentration in Linek et al. (1995). The authors have shown an independence of $k_G a$ on OH⁻ concentration in the range of NaOH concentration from 0.1 M to 1.0 M.

3.2. Effective area determination

Experimental set-up for the effective interfacial area measurement consists in the absorption of the diluted CO₂ from the air into the aqueous NaOH solution, which is the system, where the gas-phase relative mass-transfer resistance is low and the rapid reaction of CO₂ with OH⁻ consumes quantitatively CO₂ within the liquid film. In such case, the mass-transfer rate is determined by the reaction-transport phenomena in the liquid film and is determined solely by the physical quantities of the system. Effective interfacial area can be calculated by combination of the relation for the CO₂ local mass-transfer rate and its balance along the height of the packing (Linek et al., 1984)

$$\begin{aligned} a_{R_G=0} &= \frac{(K_{OG} a)_{\text{CO}_2}}{He \sqrt{D_{L,\text{CO}_2} k_{\text{OH}^-\text{COH,ave}}}} \\ &= \frac{1}{He \sqrt{D_{L,\text{CO}_2} k_{\text{OH}^-\text{COH,ave}}}} \cdot \frac{u_G}{H} \cdot \ln \frac{c_{\text{CO}_2}^{\text{IN}}}{c_{\text{CO}_2}^{\text{OUT}}} \end{aligned} \quad (20)$$

Value of the reaction term $He \sqrt{D_{L,\text{CO}_2} k_{\text{OH}^-\text{COH,ave}}} = 2.24 \times 10^{-3}$ m/s (20 °C and 1 M NaOH solution) was determined by still level experiments (Linek et al., 1995) as this procedure circumvents the errors induced by application of different physical data of solubility and diffusivity by the authors. The data of the effective interfacial area for all Mellapak packing types were originally published by Valenz et al. (2011a,b). In this work effective area data were corrected to the gas-phase mass transfer resistance using relation

$$a = \frac{a_{R_G=0}}{1 - R_G} \quad (21)$$

taken from Hoffmann et al. (2007) where R_G stands for the relative mass transfer resistance. For systems used in this work is R_G defined as

$$R_G = \frac{(K_{OG} a)_{\text{CO}_2}}{(K_{OG} a)_{\text{SO}_2}} \cdot \left(\frac{D_{G,\text{SO}_2}}{D_{G,\text{CO}_2}} \right)^{2/3} \quad (22)$$

The R_G reaches 11% at the lowest gas velocity used 0.5 m/s and decreases with increasing the liquid and gas velocities to 3% evaluated for gas superficial velocity of 2.5 m/s.

3.3. k_G determination

The absorption experiments related with $k_G a$ as well as a determination have been performed using lye as a liquid

Table 1 – Constants of correlations (24), (25) and (26).

	C_1	α	β	$\sigma_{rel}(k_G a)$	C_2	γ	δ	$\sigma_{rel}(a)$	C_3	ζ	η	$\sigma_{rel}(k_G)$
M250Y	4.37	0.651	0.137	2.3%	156	0.010	0.106	4.8%	0.028	0.642	0.031	5.3%
M350Y	5.64	0.643	0.164	4.9%	214	0.016	0.066	5.0%	0.026	0.626	0.098	7.0%
M452Y	5.92	0.624	0.146	3.6%	202	-0.009	0.085	1.5%	0.029	0.632	0.061	3.9%
M500Y	6.08	0.746	0.278	6.7%	243	0.136	0.112	3.7%	0.025	0.610	0.166	7.7%

phase and air as the gas-phase. Under the same liquid and gas flow rate, effective interfacial area for both experiments can be therefore considered equal, as usage of CO₂ or SO₂ cannot effectively change hydrodynamic conditions. Mass transfer coefficient was therefore determined as

$$k_G = \frac{k_G a}{a} \quad (23)$$

4. Results

4.1. Correlation of the experimental data

Values of volumetric mass-transfer coefficient ($k_G a$) and effective interfacial area (a) resulting from the experiments have been correlated in the power law form (Eqs. (24) and (25)).

$$k_G a = C_1 \cdot u_G^\alpha \cdot B^\beta \quad (24)$$

$$a = C_2 \cdot u_G^\gamma \cdot B^\delta \quad (25)$$

The correlations have been constructed for each of the packing individually in order to provide correlations most closely fitting experimental data. The sum of squares of differences between measured and calculated quantity have been used as the objective function; points contributing to the value of the objective function represented more than five times the value of the average contribution were excluded from the set of correlated data as outlying ones and the correlation procedure was repeated. Altogether 12 experimental values have been excluded from the overall number of 98 $k_G a$ experiments performed. The constants of Eqs. (24) and (25) for individual packings are given in Table 1.

Range of flows, for which the correlations are valid, corresponds with the range of the experimental data plotted in the Fig. 1a–d.

As can be seen from these figures, for given load, M250Y packing provides the lowest $k_G a$ values, while M500Y packing achieves the highest absolute values of $k_G a$. M350Y and M452Y packings provide similar mass-transfer behavior in the preloading region with intermediate values of $k_G a$. Highest capacity has been achieved with M452Y packing.

Values of the mass transfer coefficients (k_G) for each packing are presented in the power law form

$$k_G = C_3 \cdot u_G^\zeta \cdot B^\eta \quad (26)$$

where constants for this correlation have been obtained by division of Eq. (24) by Eq. (25). Values of the constants C_3 , ζ , η can be found in Table 1. These correlations fit experimental data well for phase velocities up to about 2/3 of those at flooding as is demonstrated in the parity graphs (Figs. 2 and 3) and in Fig. 1a–d presenting $k_G a$ values for all studied packings.

As the recalculation of the $k_G a$ data to conditions of other systems is challenging, the data have been compared to those obtained for Mellapak 250Y and SO₂–air–lye system by

Klement (2002) with good results (see Fig. 1a). The correlation of the effective area of M250Y is in good agreement with the correlation published by Tsai et al. (2009).

Constants of Eq. (26) for the mass-transfer coefficient k_G (C_3 , ζ , η) reveal, that dependence of k_G on the superficial gas-phase velocity is for all packings close to $k_G \propto u_G^{0.63}$, while dependence of k_G on the liquid flow rate is rather weak $k_G \propto B^{0.166}$.

As the geometry of the studied packing series is similar, it there should be possible to correlate resulting values of the mass-transfer coefficient k_G for all the packing types with a single dimensionless equation. When hydraulic diameter of the channel has been utilized as a characteristic dimension of the packing correlation of experimental data for all packing types is found to be

$$Sh_G = 0.409 \cdot Re_G^{0.622} \cdot Re_L^{0.0592} \quad \text{st. dev.} = 6\% \quad (27)$$

for the range of $Re_G = 240$ – 2500 and $Re_L = 10$ – 300 .

Correlation (27) fits well with experimental data of all packing types used as demonstrates the parity graph in Fig. 4. Schmidt number has been omitted from the correlation as the physical properties of the gas-phase were not changed throughout the experiments and its influence on the Sherwood number could not be determined. Experimentally, mass-transfer coefficients k_G were studied independently as a functions of the phase flows and of the packing dimension. However, Eq. (27) postulates single dependence of Sh_G on Re_L and Re_G , which makes the $k_G = k_G(d_p)$ relation dependent.

$$k_G \propto d_p^{(m+n-1)} = d_p^{-0.319} \quad (28)$$

Low dispersion of the correlation (27) validates also the analogy between the mass-transfer phenomena on the various Mellapak packing types and usefulness of the choice of the channel hydraulic diameter as a packing characteristic dimension (Tables 2 and 3.).

4.2. Use of the effective mutual phase velocity

Gas-phase mass-transfer coefficient is often suggested (as in DELFT, RBF model) as a function of the single mutual

Table 2 – Geometrical properties of the packings.

	a_G (m ⁻¹)	d_p (m)	ε	Θ
M250Y	250	0.0155	0.97	45
M350Y	350	0.0106	0.93	45
M452Y	350	0.0106	0.93	45
M500Y	500	0.00728	0.91	45

Table 3 – Gas-phase properties of the system air–SO₂.

D_{SO_2} (m ² /s)	ρ_G (kg m ⁻³)	μ_G (Pa s)
1.22×10^{-5}	1.21	$18.2 \cdot 10^{-6}$

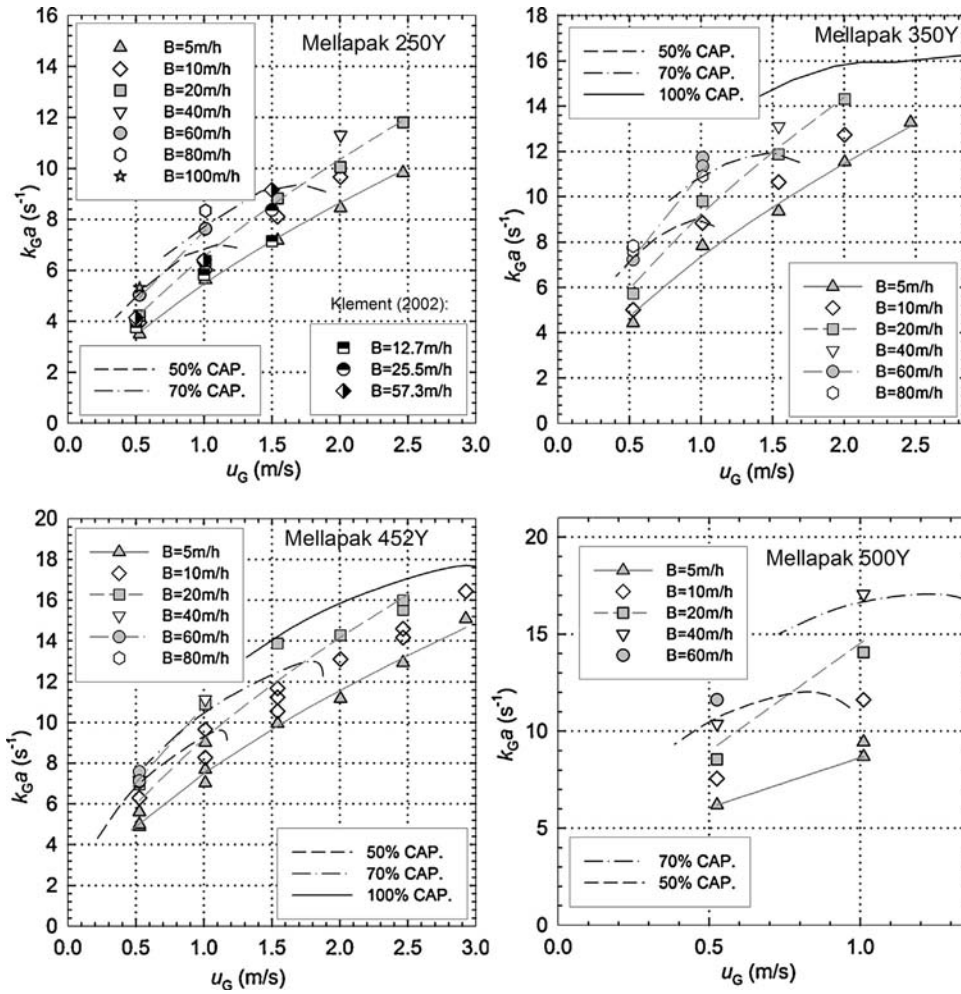


Fig. 1 – (a) M 250Y: volumetric mass-transfer coefficients $k_{G,a}$ data used for construction of the correlation Eq. (24). The lines represent the correlation. Comparison with the data of Klement (2002). (b) M350Y: volumetric mass-transfer coefficients $k_{G,a}$ data used for construction of the correlation Eq. (24). The lines represent the correlation. (c) M452Y: volumetric mass-transfer coefficients $k_{G,a}$ data used for construction of the correlation Eq. (24). The lines represent the correlation. (d) M500Y: volumetric mass-transfer coefficients $k_{G,a}$ data used for construction of the correlation Eq. (24). The lines represent the correlation.

“effective” phase velocity, u_E , rather than as the function of the gas and the liquid superficial velocity.

$$u_E = u_{L,i} + u_{G,i} \tag{29}$$

Interstitial gas velocity differs from superficial velocity due to the inclination of channels (and corresponding prolonging of the flow path through the element) and due to liquid hold-up restricting available channel

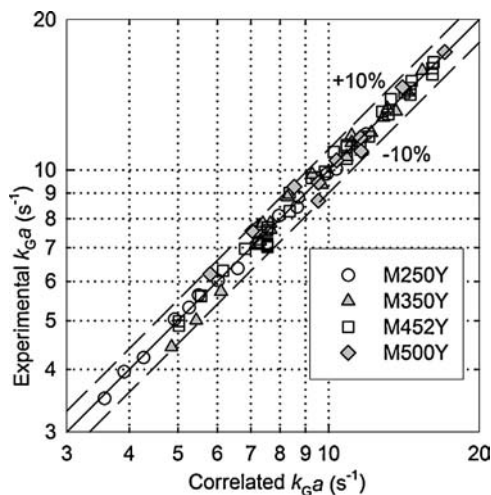


Fig. 2 – Comparison of experimental and from correlation (24) calculated $k_{G,a}$.

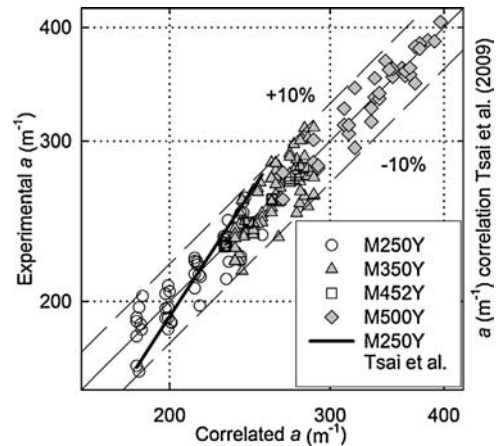


Fig. 3 – Comparison of experimental and from correlation (25) calculated interfacial area. Comparison with the correlation by Tsai et al. (2009) for aqueous system and M250Y packing.

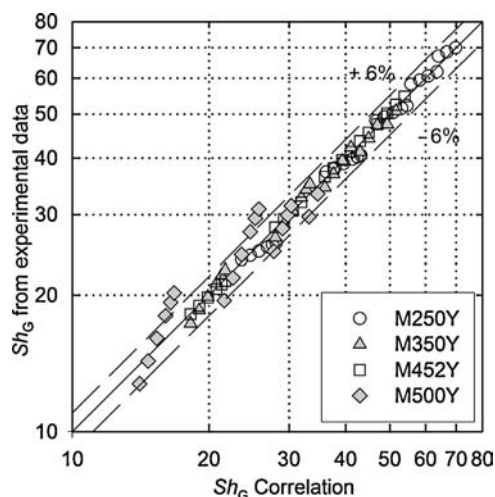


Fig. 4 – Comparison of experimental and from the correlation (27) calculated Sh_G .

cross-section.

$$u_{G,i} = \frac{u_G}{\sin\theta \cdot (\varepsilon - h_L)} \quad (30)$$

Interstitial liquid velocity is assumed to be such that enables the volumetric flow of the liquid through the column to be achieved through the cross-section provided by the liquid hold-up.

$$u_{L,i} = \frac{u_L}{\sin\theta \cdot \varepsilon \cdot h_L} \quad (31)$$

The effect of using the effective phase velocity instead of the superficial one for correlation of the gas-phase mass-transfer data has been tested for M250Y. Required liquid hold-up has been measured with M250Y earlier (Valenz et al., 2011a,b) using the same apparatus with water–air system providing regression

$$h_L = 0.571 \cdot Fi^{0.519} \cdot \left(\frac{3}{\sin^2\theta}\right)^{0.877} \cdot (d_{eq} a_g)^{2.405} \quad (32)$$

Shape of the correlation as well as the dependence on the packing geometry was adopted from Macías-Salinas and Fair (1999).

Mass-transfer coefficients, k_G , evaluated from Eq. (26) for M250Y and for all experimental conditions have been correlated in two different ways – utilizing either effective phase velocity, u_E , or superficial velocity of the gas, u_G .

$$k_G = 0.0308 \cdot u_G^{0.628} \quad \text{rel. st. dev} = 3.16\% \quad (33a)$$

$$k_G = 0.0209 \cdot u_E^{0.703} \quad \text{rel. st. dev} = 2.85\% \quad (33b)$$

Utilization of the effective velocity improves fit of the k_G data as can be deduced from the value of the relative standard deviation (RSD) of the correlation by Eq. (33) provided in Table 1. Optimized value of the exponent at the velocity, ϕ , changes substantially from 0.628 to 0.703 when the effective phase velocity is used instead of the superficial one.

5. Discussion of the results

Ability of the relations/models presented in the literature to describe gas-phase mass-transfer in the structured packings

Table 4 – Comparison of k_G calculated from the model packages for standard conditions.

Author	Dependences	k_G , nominal (m/s)
Johnstone and Pigford (1942)	$k_G \propto u_G^{0.77} d_p^{-0.23}$	7.5×10^{-3}
Hanley and Chen (2012)	$k_G \propto u_G^1 d_p^0$	7.3×10^{-3}
Rocha et al. (1996) (RBF)	$k_G \propto u_G^{0.8} d_p^{-0.2}$	16×10^{-3}
Olujic et al. (2004) (DELFT)	No explicit relation	9.6×10^{-3}
Billet and Schultes (1999) (BS)	$k_G \propto u_G^{3/4} d_p^{-5/4}$	45×10^{-3}
Nieuwoudt and Crause (1999)	$k_G \propto u_G^1 d_p^0$	4.7×10^{-3}
Onda et al. (1968)	$k_G \propto u_G^{0.7} d_p^{-2}$	48×10^{-3}
This work	$k_G \propto u_G^{0.622} d_p^{-0.319}$	30×10^{-3}

can be studied through comparison of predicted absolute k_G values, dependences of k_G on gas velocity or characteristic dimension they predict.

5.1. Values of k_G predicted by gas-phase mass-transfer models

For simplicity, following “standard” conditions corresponding with actual experimental system has been chosen for calculation of the “nominal” k_G value: $u_G = 1$ m/s, $d_p = 0.0155$ m (M250Y), $\rho_G = 1.21$ kg/m³, $\mu_G = 18.2 \times 10^{-6}$ Pa s, $D_G = 1.22 \times 10^{-5}$ m²/s ($Re_G = 1455$, $Sc_G = 1.23$); physical data correspond to dilute SO₂ in the air at 20 °C and atmospheric pressure.

Experiments reveal values of k_G of about 0.030 m/s for the standard conditions. These values are largely under-predicted by model packages from Table 4, in some cases almost by an order of magnitude. Only exception is that of BS model, which adjusts the results to the experimental values through usage of packing specific constants. For comparison, the results of the Onda’s model (Onda et al., 1968) developed for random packing are also enlisted.

As can be seen from Fig. 5a–c, under the same phase velocities, the value of the mass-transfer coefficient k_G increases with geometrical area of the packing, these differences are more pronounced for high liquid velocities.

5.2. Dependence of k_G on phase velocities

The exponent on the gas velocity in the dependences of k_G predicted by correlations of wetted-wall column experiments $k_G \propto u_G^{0.8-1}$ is too high in comparison with the one found here for structured packings. Experiments performed here provide quite convincingly dependence $k_G \propto u_G^{0.62}$. When more elaborate approach utilizing mutual effective phase velocity has been applied, dependence $k_G \propto u_G^{0.7}$ was found for M250Y. Similar performance $k_G \propto u_G^{0.6-0.7}$ has been found earlier for random packings e.g. by Onda et al. (1968). On the other hand, exponent of the dependence $k_G \propto u_G^{0.5}$ predicted by the penetration theory and by the laminar boundary layer model is bit too low.

It leads us to the belief, that modeling of the gas-phase mass-transfer in the structured packings on the basis of the flow through the straight channel and on wetted-wall experiments is not (at least not universally) appropriate. The value of the exponent in the velocity dependence of k_G dropping to 0.62 is characteristic for flow around submerged objects, where abrupt change in gas flow direction and its velocity occurs. CFD simulations (Saleh et al., 2011) indicate, that the gas is actually proceeding vertically through the packing in all

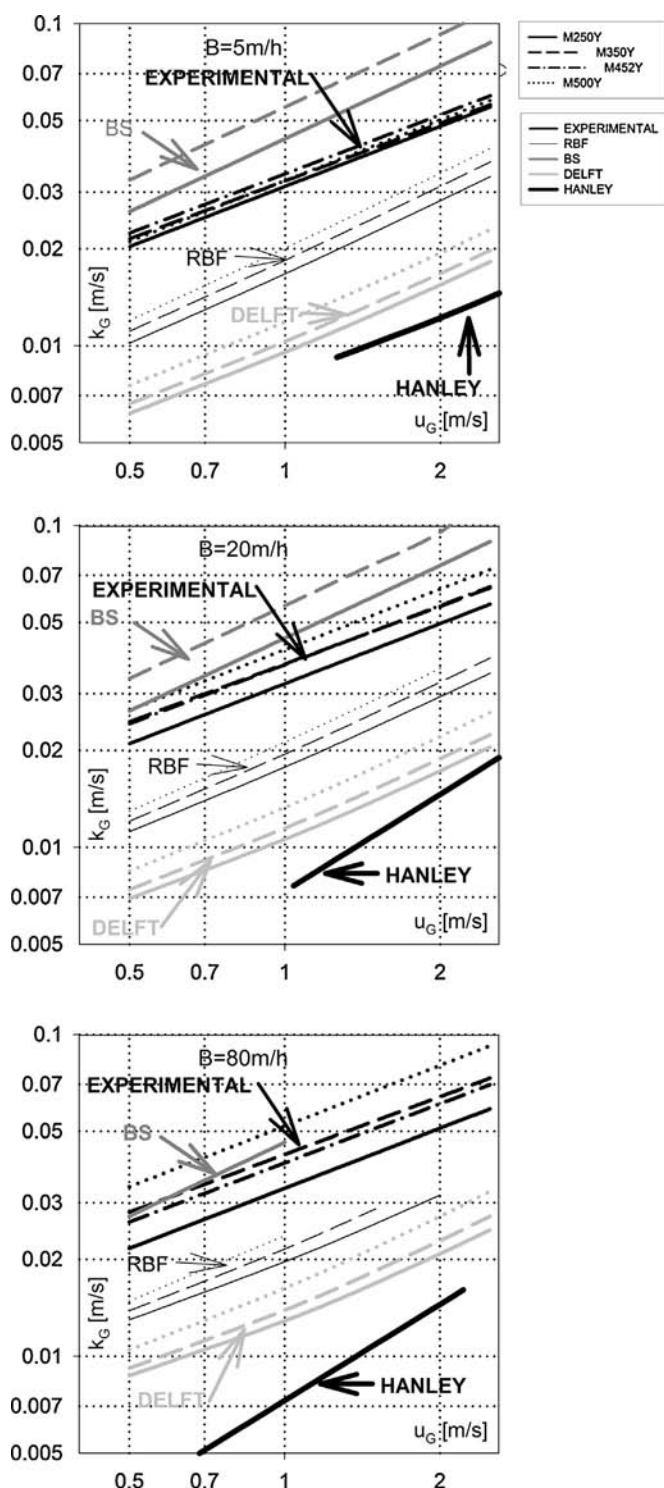


Fig. 5 – (a) Comparison of the experimental and from model package predicted dependence of k_G on the gas velocity for liquid load $B = 5 \text{ m/h}$. (b) Comparison of the experimental and from model package predicted dependence of k_G on the gas velocity for liquid load $B = 20 \text{ m/h}$. (c) Comparison of the experimental and from model package predicted dependence of k_G on the gas velocity for liquid load $B = 80 \text{ m/h}$.

directions from -45° to $+45^\circ$ with respect to the vertical, what suggests, that fair amount of the gas moves around the crimps instead of flowing straightly along the corrugation of the packings. Perpendicular and skewed arrangement of the channels also implies inevitable formation of rotational component of the velocity vector. There is also interesting, that absolute

k_G values and its dependence on the gas velocity are quite well described by venerable model Onda characterizing first generation packings. These packings (Raschig rings, spheres, saddles) certainly do not form straight channels, rather lead to the imagination of flow around an object.

5.3. Dependence of k_G on packing characteristic dimension

Mass-transfer coefficient k_G can be successfully correlated by the dimensionless correlation (27) which proved to fit well experimental data measured for all the packing types with relative standard deviation of 6% and with the hydraulic diameter of the channel taken as the packing characteristic dimension. The dependence of the mass-transfer coefficient on the packing characteristic dimension is according to the correlation $k_G \propto d_p^{-0.32}$. Close fit indicates that the gas-phase mass-transfer phenomena for various dimensions of Mellapak packing are indeed analogical and that the packing characteristic dimension has been chosen properly.

6. Conclusions

Mass-transfer characteristics of metal sheet structured Mellapak-Y packings have been measured using standard methods and the values of the gas-phase mass-transfer coefficient have been evaluated in the dependence on phase flows for each packing. The data has been correlated by Eqs. (24)–(26) with the relative standard deviation lower than 8%.

Gas flow through the structured packing is usually modeled on the basis of turbulent flow through the channel of the triangular cross-section. Long or short wetted-wall column is taken as a corresponding experimental set-up. Alternatively results of heat-transfer in the straight tube are utilized using analogy between heat and mass-transfer. Values of k_G acquired from this geometrical arrangement are substantially lower than those found experimentally in this work, i.e. k_G of about 0.030 m/s for here defined standard condition. The dependence of k_G on gas velocity is found also different, $k_G \propto u_G^{0.62}$.

It suggests that modeling of the gas-phase mass-transfer in the structured packings on the basis of the flow through the straight channel and on wetted-wall experiments is not appropriate. Conversely, the value of exponent in velocity dependence of k_G dropping to 0.62 is characteristic for flow around objects, suggesting that fair amount of the gas moves around the crimps instead of flowing straightly along the corrugation of the packings.

Mass-transfer data measured for all studied types of Mellapak packing has been successfully correlated by the dimensionless correlation (27), which interrelates the effect of the packing geometry and the phase velocities on the mass-transfer. Close fit with relative standard deviation of 6% indicates that the gas-phase mass-transfer phenomena for various dimensions of Mellapak packing are indeed analogical and that the packing characteristic dimension defined by Eq. (11) has been chosen properly.

Acknowledgements

Authors are grateful to Sulzer Co. for providing of the packings and to the Czech Science Foundation for supporting the project through Grant 13-01251S.

References

- Billet, R., Schultes, M., 1999. Prediction of mass transfer columns with dumped and arranged packings. Updates summary of the calculation method of Billet and Schultes. *Trans IChemE* 77 (Part A), 498–504.
- Chilton, T.H., Colburn, A.P., 1934. Mass transfer (absorption) coefficients. Prediction from data on heat transfer and fluid friction. *Ind. Eng. Chem* 26, 1183–1187.
- Crause, J.C., Nieuwoudt, I., 1999. Mass transfer in a short wetted-wall column. 1. Pure components. *Ind. Eng. Chem. Res.* 38, 4928–4932.
- Danckwerts, P.V., 1970. *Gas-Liquid Reactions*. McGraw-Hill Book Company, New York.
- Hanley, B., Chen, Ch., 2012. New mass-transfer correlations for packed towers. *AIChE J.* 58 (1), 132–152.
- Henley, E.J., Seader, J.D., Roper, D.K., 2011. *Separation Process Principles*, third ed. John Wiley & Sons, Asia.
- Hoffmann, A., Mackowiak, J.F., Gorak, A., Haase, M., Loning, J.-M., Runiowski, T., Hallenberger, K., 2007. Standardization of mass transfer measurements. Basis for the description of absorption processes. *Chem. Eng. Res. Des.* 85 (A1), 40–49.
- Johnstone, H.F., Pigford, R.L., 1942. Distillation in a wetted wall column. *Trans. AIChE* 38, 25–51.
- Klement, M., (Diploma thesis) 2002. *Studium transportních charakteristik výplní Mellapak (Study of the transport characteristics of the Mellapak packings)*. ICT, Prague.
- Linek, V., Petříček, P., Beneš, P., Braun, R., 1984. Effective interfacial area and liquid side mass transfer coefficients in absorption columns packed with hydrophilised and untreated plastic packing. *Chem. Eng. Res.Des.* 62, 13–21.
- Linek, V., Sinkule, J., Brekke, K., 1995. A critical evaluation of the use of absorption mass transfer data for the design of packed distillation columns. *Chem. Eng. Res. Des.* 73 (Part A), 398–405.
- Macías-Salinas, R., Fair, J.R., 1999. Axial mixing in modern packings, gas and liquid phases. I. Single-phase flow. *AIChE J.* 45 (2), 222–239.
- Nieuwoudt, I., Crause, J.C., 1999. Mass transfer in a short wetted-wall column. 2. Binary systems. *Ind. Eng. Chem. Res.* 38, 4933–4937.
- Olujic', Ž., Behrens, M., Colli, L., Paglianti, A., 2004. Predicting the efficiency of corrugated sheet structured packings with large specific surface area. *Chem. Biochem. Eng. Q* 18 (2), 89–96.
- Olujic', Ž., Kamerbeek, A.B., de Graauw, J., 1999. A corrugation geometry based model for efficiency of structured distillation packing. *Chem. Eng. Proc.* 38, 683–695.
- Onda, K., Takeuchi, H., Okumoto, Y., 1968. Mass transfer coefficients between gas and liquid phases in packed columns. *J. Chem. Eng. Jpn.* 1 (1), 56–62.
- Rejl, F.J., Linek, V., Moucha, T., Valenz, L., 2009. Methods standardization in the measurement of mass-transfer characteristics in packed absorption columns. *Chem. Eng. Res. Des.* 87, 695–704.
- Rocha, J.A., Bravo, J.L., Fair, J.R., 1996. Distillation columns containing structured packings: a comprehensive model for their performance. 2. Mass transfer model. *Ind. Eng. Chem. Res.* 35, 1660–1667.
- Saleh, A.R., Hosseini, S.H., Shojaee, S., Ahmadi, G., 2011. CFD studies of pressure drop and increasing capacity in MellapakPlus 752.Y structured packing. *Chem. Eng. Technol.* 34 (9), 1402–1412.
- Tsai, R.E., Seibert, A.F., Eldridge, E.B., Rochelle, G.T., 2009. Influence of viscosity and surface tension on the effective mass transfer area of structured packing. *Energy Procedia* 1, 1197–1204.
- Valenz, L., Rejl, F.J., Linek, V., 2011a. Effect of gas- and liquid-phase axial mixing on the rate of mass transfer in a pilot-scale distillation column packed with Mellapak 250Y. *Ind. Eng. Chem. Res.* 50 (4), 2262–2271.
- Valenz, L., Rejl, F.J., Šíma, J., Linek, V., 2011b. Absorption mass-transfer characteristics of mellapak packing series. *Ind. Eng. Chem. Res.* 50, 12134–12142.
- Wang, G.Q., Yuan, X.G., Yu, K.T., 2005. Review of mass-transfer correlations for packed columns. *Ind. Eng. Chem. Res.* 44, 8715–8729.



Contents lists available at ScienceDirect

Chemical Engineering Research and Design

IChemE

journal homepage: www.elsevier.com/locate/cherd

Methods standardization in the measurement of mass-transfer characteristics in packed absorption columns

J.F. Rejl, V. Linek*, T. Moucha, L. Valenz

Institute of Chemical Technology Prague, Department of Chemical Engineering, Technická 5, 166 28 Prague 6, Czech Republic

ABSTRACT

This paper supports the drive to standardize methods used in the measurement of mass-transfer characteristics ($k_L a$, $k_G a$, a) in packed absorption columns. Using 25 mm Pall rings as packing, Hoffmann et al. [Hoffmann, A., Mackowiak, J.F., Gorak, A., Haase, M., Loning, J.-M., Runiowski, T. and Hallenberger, K., 2007, Standardization of mass transfer measurements. Basis for the description of absorption processes, TranslChemE, Part A, Chem Eng Res Des 85(A1): 40–49] recently proposed various such methods. Their recommendations are assessed in the light of the results reported by other researchers using the same type of packing of different sizes (25 and 50 mm) in different absorption systems. Data differences between these authors are analyzed, and the reasons for them explained. On this basis, absorption systems and measurement procedures are proposed capable of providing consistent data for primary quantities ($k_G a$, $k_L a$, a). We recommend to use only such absorption systems and under such conditions, in which interfacial mass-transfer resistance is fully concentrated in single, addressed phase. Thus, for the measurement of $k_L a$, we recommend the absorption/desorption of sparingly soluble gases, such as oxygen or carbon dioxide in/from water, i.e. systems in which mass-transfer resistance is fully concentrated in the liquid phase. The absorption of NH_3 in water is not recommended as approx. 50% mass-transfer resistance is concentrated in gas phase and has to be measured and subtracted by independent experiment. Suitable system for the measurement of $k_G a$ is the absorption of SO_2 in NaOH solution. For the measurement of the effective interfacial area, we recommend the absorption of CO_2 in aqueous NaOH solution under conditions in which the gas-phase mass-transfer resistance is negligible (i.e. $u_G \geq 0.5$ m/s, $c_{\text{OH}} \leq 1$ M). It is emphasized that the values of the physical properties (diffusivity, solubility) used in the evaluation of the area must be the same as those used in the evaluation of the kinetic constant (of the reaction of CO_2 and the OH^- ions). To eliminate end-effects, the gas and liquid phases should be sampled directly from the packing rather than from the inlet and outlet pipes.

© 2008 The Institution of Chemical Engineers. Published by Elsevier B.V. All rights reserved.

Keywords: Absorption; Interfacial area; Mass-transfer coefficient; Standardization

1. Introduction

It is currently difficult to predict mass-transfer absorption characteristics with any degree of certainty. While a lot of data exists, much of it has been measured using various different, and often erroneous, methods. This has resulted in the publication of vastly conflicting data, which force plant engineers to greatly overestimate column parameters in their designs. Recently, Hoffmann et al. (2007) proposed the development

of a set of standardized procedures for the measurement of mass-transfer absorption characteristics. Having previously highlighted the need for such standardization and attempted to galvanize action towards it (Linek and Moucha, 2000), we, in particular, support such efforts.

Models of the processes that take place in absorption columns have become more sophisticated in recent years. However, as such models only produce useful results when the parameters on which they are based have been determined

* Corresponding author.

E-mail address: linekv@vscht.cz (V. Linek).

Received 12 May 2008; Received in revised form 21 August 2008; Accepted 29 September 2008

Nomenclature

a	effective gas/liquid interfacial area per volume (m^{-1})
a_t	geometric surface of packing per volume (m^{-1})
B	liquid load (m^3/h)
Bo	Bodenstein number ($=uH/E$)
c	concentration (kmol/m^3)
c^*	equilibrium concentration (kmol/m^3)
d	characteristic dimension of packing (m)
D	diffusion coefficient (m^2/s)
E	dispersion coefficient (m^2/s)
F	gas capacity factor ($=u_G(\rho_G)^{1/2}$) ($\text{Pa}^{1/2}$)
H	packing height (m)
He	distribution coefficient of carbon dioxide
I	ionic strength (kmol/m^3)
k	mass-transfer coefficient (m/s)
$k_G a$	gas-phase volumetric mass-transfer coefficient (piston flow) (s^{-1})
$k_L a$	liquid-phase volumetric mass-transfer coefficient (piston flow) (s^{-1})
k_{OH}	second-order kinetic constant ($\text{m}^3/(\text{kmol}\cdot\text{s})$)
K_G	$= He \sqrt{D_{CO_2,L} k_{OH}}$ ($\text{m}^{5/2}/(\text{kmol}^{1/2}\cdot\text{s})$)
K_{OG}	overall gas-phase mass-transfer coefficient (m/s)
NTU	number of transfer units
p	mass-transfer parameters ($k_L a$, $k_G a$ or a)
r	relative mass-transfer resistance
Re	Reynolds number ($=u\rho d/\mu$)
u	superficial velocity in the column (m/s)

Greek symbols

μ	viscosity ($\text{Pa}\cdot\text{s}$)
ρ	density (kg/m^3)

Sub- and superscripts

CO_2	carbon dioxide
G	gas phase
i	G or L
in	input value
L	liquid phase
NH_3	ammonia
out	output value
O_2	oxygen
p	plug flow
SO_2	sulphur dioxide
true	plug flow with superimposed axial dispersion
*	at equilibrium

with sufficient accuracy, it is surprising that far more attention has been paid to enhancing the models than to identifying the values of the parameters underlying them. Therefore, in this paper we focus on the development of an absorption measurement database which contains quantities with clear physical meanings that condition their transferability to absorption/distillation systems in general. Such quantities should neither be influenced by the effects of phenomena not included in the $k_G a$, $k_L a$, a evaluation models (e.g. differences in wetted area, axial dispersion in combined experiments) nor by artefacts caused by the usage of incorrect equilibrium or kinetic data for the evaluation of experimental data.

Recently, Hoffmann et al. (2007) recommended the following: the absorption of SO_2 in an aqueous NaOH solution for the determination of the volumetric mass-transfer coefficient in the gas phase; the absorption of CO_2 in an aqueous NaOH solution for the measurement of the effective interfacial area; and physical absorption systems (i.e. the absorption of NH_3 in water or the stripping of CO_2 from water) for the determination of the volumetric mass-transfer coefficient in the liquid phase.

In this paper we evaluate the methods proposed by Hoffmann et al. (2007) to determine whether or not their data is consistent with the literature data. There is analyzed, whether physical-chemistry data used for mass-transfer experiments evaluation are consistent and whether other phenomena usually not taken in account (like axial dispersion) affect the results. The results of this analysis should be taken into account before recommendation of these methods as the standard ones.

2. Analysis of measurement methods

2.1. Methods for the measurement of $k_L a$

Although the absorption/desorption of sparingly soluble gases, typically oxygen or carbon dioxide in/from water, is generally used to measure $k_L a$, Hoffmann et al. (2007) recently recommended using the absorption of NH_3 in water. Various researchers, including Hoffmann et al. (2007) have measured $k_L a$ values for 25 mm and/or 50 mm metal Pall rings in different absorption systems operating under conditions below the loading point (see Table 1). Physical-chemical properties at 20°C and packing data used in calculations in this paper are given in Table 2. Fig. 1, which compares the results of these authors, shows that the data are in good agreement, except in the case of Hoffmann et al. (2007), whose data deviates from the others by up to almost 100%. In addition, as is well known, $k_L a$ is proportional to the liquid flow rate (B) to some power. Almost all authors report this power to be around 0.8 at all gas velocities, while, in stark contrast, Hoffmann et al. (2007) reported power of 0.358, 0.479 and 0.7 at $u_G = 0.9$, 1.8 and 2.3 m/s, respectively. Further, only their data show marked dependence on gas flow rate below the loading point.

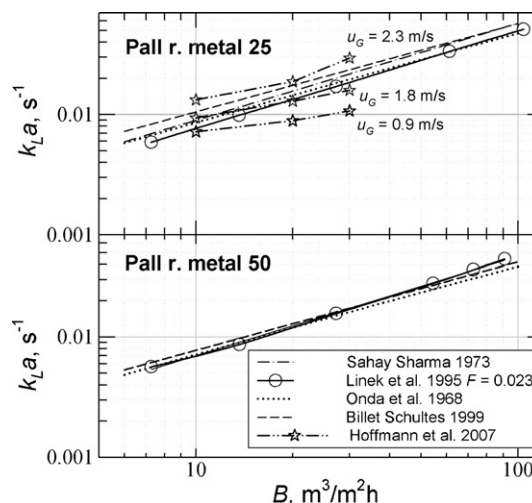


Fig. 1 – Comparison of $k_L a$ values measured by various authors for metal Pall rings in different absorption systems below the loading point (see Table 1).

Table 1 – Methods used by various authors to measure $k_L a$, $k_G a$ and a .

Author	System $k_L a$	System a	System $k_G a$
Sahay and Sharma (1973)	CO ₂ -H ₂ O	CO ₂ -1 M NaOH Air-dithionite	Cl ₂ -1 M NaOH
Onda et al. (1968)	CO ₂ -H ₂ O	CO ₂ -1 M NaOH	Evaporation NH ₃ -H ₂ O
Billet and Schulte (1999)	CO ₂ -H ₂ O	CO ₂ -1 M NaOH	SO ₂ -1 M NaOH NH ₃ -1 M H ₂ SO ₄
Hoffmann et al. (2007)	NH ₃ -H ₂ O	CO ₂ -1 M NaOH	SO ₂ -1 M NaOH
Linek et al. (1984, 1995, 2001)	O ₂ -H ₂ O	CO ₂ -1 M NaOH	SO ₂ -1 M NaOH

Table 2 – Physical-chemical properties at 20 °C and packing data used in calculations.

$D_{SO_2, Air}$	1.22E-5 m ² /s	$D_{O_2, water}$	2.12E-9 m ² /s
$D_{CO_2, Air}$	1.54E-5 m ² /s	$D_{CO_2, water}$	1.80E-9 m ² /s
$D_{NH_3, Air}$	2.37E-5 m ² /s	$D_{NH_3, water}$	1.98E-9 m ² /s
$D_{Cl_2, Air}$	1.26E-5 m ² /s	$D_{Cl_2, water}$	2.12E-9 m ² /s
ρ_{Air}	1.205 kg/m ³	μ_{Air}	1.82E-6 Pa s
$He_{O_2, water}$	0.0334	$He_{NH_3, water}$	1854
$He_{CO_2, water}$	0.950	a_t (Pall 25)	200 m ⁻¹
a_t (Pall 50)	99 m ⁻¹		

Using Eq. (1), we evaluated the liquid-phase relative mass-transfer resistance, r_L , from $k_L a$ and $k_G a$ values calculated from the HTU values published by Hoffmann et al. (2007):

$$r_L = \left(1 + \frac{k_L \cdot He}{k_G}\right)^{-1} \cong \left(1 + \frac{k_L a \cdot He}{k_G a}\right)^{-1} \quad (1)$$

As about 50% of mass-transfer resistance is concentrated in the gas phase in the absorption system used by Hoffmann et al. (2007) (see Table 3), the authors have evaluated $k_L a$ by subtracting the gas-phase resistance measured by the absorption of SO₂ in lye from the total mass-transfer resistance measured by the absorption of NH₃ in water. This calculation procedure assumes that the effective mass-transfer areas in both absorption systems, namely NH₃-water and SO₂-lye, are the same. However, the effective area for a physical absorption experiment is lower than that for evaporation or chemisorption experiments, this being true over a wide range of gas flow rates unless the surface is completely wetted (Yoshida and Koyanagi, 1962; Danckwerts, 1970). We suppose this is the main reason why their $k_L a$ data differs from those of other authors. These facts lead us to suggest not to use the absorption of NH₃ in water for the measurement of $k_L a$, even if the gas-phase resistance measured by SO₂ absorption in NaOH solution is taken into account. We prefer system of oxygen desorption from air-saturated water into gaseous nitrogen. In our introducing work (Linek et al., 1984), we proved experimentally that the values of $k_L a$ derived from oxygen absorption and desorption are identical and that the transport coefficients are gas flow independent. All the $k_L a$ values measured since (Linek et al., 1995, 2001; Linek and Sinkule, 1997) were obtained by desorption experiments which

were the simple of the two to carry out. Nitrogen gas flow rate through a column is low ($u_G \approx 0.03$ m/s) but sufficient to keep the oxygen concentration in the effluent gas lower than 0.2 vol%. This ensures negligible back pressure of oxygen and negligible influence of axial dispersion in the gas phase.

2.2. Methods for the measurement of effective interfacial area

The effective interfacial area, a , is usually measured using the absorption of carbon dioxide-enriched air in 1 M NaOH solution, although Sahay and Sharma (1973) additionally used an air-dithionite system (see Table 1). Fig. 2 compares the effective areas measured by various authors using different absorption systems with the same packing of Pall rings. The

Table 3 – Relative resistance (r_L , %) of NH₃ absorption in water in the liquid phase.

u_G (m/s)	B (m/h)		
	10	20	30
0.9	44	45	42
1.9	51	48	48
2.3	47	45	37

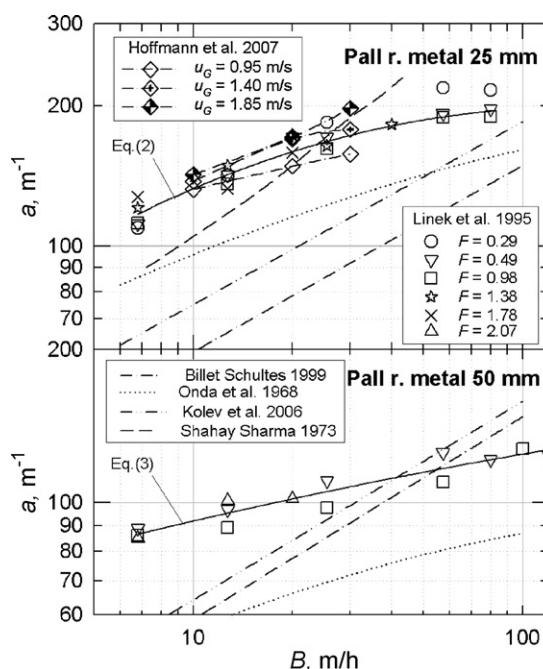


Fig. 2 – Comparison of effective areas measured by various authors for the same type of packing in different absorption systems (see Table 1).

data plotted for Hoffmann et al. (2007) are those corrected for the effect of gas-phase resistance. Our data (Linek et al., 1995) measured at various gas flow rates illustrate well negligible effect of gas velocity on the effective interfacial area. The data for $u_G \geq 0.5$ m/s were correlated using the following relations:

$$a = 48.9B^{(0.567-0.132 \log B)} \quad (\text{S.D.} = 3.4\%) \quad \text{for Pall 25 mm} \quad (2)$$

$$a = 62.3B^{(0.187-0.0184 \log B)} \quad (\text{S.D.} = 3.5\%) \quad \text{for Pall 50 mm} \quad (3)$$

We did not find good agreement between these results, with differences as high as 200% being observed in some cases. Similar disagreement was found among the values reported for the reaction kinetic constant and other physical properties used by the individual authors to evaluate their experimental data.

To precisely define the physical quantities discussed below, it is first necessary to present the relations used to evaluate the effective area. Assuming plug flow and negligible gas-phase mass-transfer resistance, this relation is obtained by integrating the equation for carbon dioxide balance in a differential section of a column, dH , as follows:

$$-u_G dc_{\text{CO}_2,G} = c_{\text{CO}_2,L}^* \sqrt{D_{\text{CO}_2,L} c_{\text{OH}} k_{\text{OH}}} a dH = c_{\text{CO}_2,G} K_G \sqrt{c_{\text{OH}}} a dH \quad (4)$$

where

$$K_G = He \sqrt{D_{\text{CO}_2,L} k_{\text{OH}}}, \quad He = \frac{c_{\text{CO}_2,L}^*}{c_{\text{CO}_2,G}} \quad (5)$$

Subsequently, the integration of (4) with the limits $0 \rightarrow H$ and $c_{\text{CO}_2,G}^{\text{in}} \rightarrow c_{\text{CO}_2,G}^{\text{out}}$ results in the following relation:

$$a = \frac{(K_{OG}a)_{\text{CO}_2}}{K_G \sqrt{c_{\text{OH},\text{ave}}}} \quad (6)$$

where overall gas-phase volumetric mass-transfer coefficient of carbon dioxide into NaOH solution is calculated as

$$(K_{OG}a)_{\text{CO}_2} = \frac{u_G}{H} \ln \frac{c_{\text{CO}_2,G}^{\text{in}}}{c_{\text{CO}_2,G}^{\text{out}}} \quad (7)$$

Hoffmann et al. (2007) recommended taking into account the gas-phase mass-transfer resistance using volumetric mass-transfer coefficient determined from SO_2 absorption in NaOH solution recalculated on the influence of the gas-phase diffusion coefficient. Eq. (6) can be then rewritten as

$$a = \left[\frac{1}{(K_{OG}a)_{\text{CO}_2}} - \frac{1}{(k_G a)_{\text{SO}_2}} \left(\frac{D_{G,\text{SO}_2}}{D_{G,\text{CO}_2}} \right)^{2/3} \right]^{-1} \frac{1}{K_G \sqrt{c_{\text{OH},\text{ave}}}} \quad (8)$$

The difference between the simple relation (6), used, for example, by Linek et al. (1984, 1995, 2001), Linek and Sinkule (1997), Billet and Schulte (1999) and Kolev et al. (2006), and the calculation procedure (8) recommended by Hoffmann et al. (2007) is illustrated in Fig. 3. In the figure, the gas-phase relative mass-transfer resistance, r_G , are presented which occurred in the effective mass-transfer area measurements of various authors. The r_G values were calculated from the relation:

$$r_G = \frac{(K_{OG}a)_{\text{CO}_2}}{(k_G a)_{\text{SO}_2}} \left(\frac{D_{G,\text{SO}_2}}{D_{G,\text{CO}_2}} \right)^{2/3} \quad (9)$$

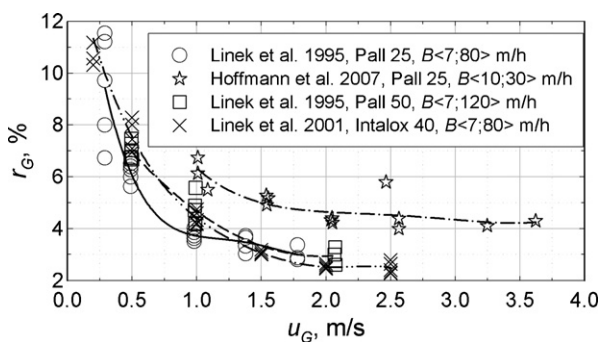


Fig. 3 – Gas-phase relative mass-transfer resistance, r_G , occurring in the effective mass-transfer area measurements of various authors.

The results in this figure show that when the gas velocity is higher than 0.5 m/s, the errors in a are lower than 6%. Therefore, when the gas velocity ≥ 0.5 m/s, the omission of gas-phase resistance is an acceptable method for the measurement of the effective area by the absorption of carbon dioxide-enriched air in lye.

The dependence of the carbon dioxide absorption rate on the square root of the concentration of hydroxyl ions included in Eqs. (6) and (8) was verified experimentally by Linek et al. (1984) for the concentration range 0.1–1 M. Because this dependence results from the first-order reaction occurring between carbon dioxide and hydroxyl ions in liquid film no mistake or approximation is factored into the evaluation. Even after multiple passages the concentration of hydroxyl ions changes only insignificantly as the liquid phase passes through the column. Therefore, an average OH^- concentration can be used in the column, $c_{\text{OH},\text{ave}}$, and can be considered to be equal to that in the inlet stream. This holds while the concentration of carbon dioxide in the gas phase is low (usually 1 vol%).

The accumulation of carbonate in the circulating NaOH absorption solution increases its ionic strength, I , which, because the reaction kinetics depends on it, must be taken into account. The effect of the kinetic constant and physical properties (solubility and diffusivity of carbon dioxide) on the calculation of the effective area is expressed by K_G in Eqs. (6) and (8). In accordance with the theory of absorption in fast chemical reactions, K_G can be determined experimentally under conditions where the rate of carbon dioxide absorption in an NaOH solution is not dependent on the physical mass-transfer coefficient k_L or, in other words, on the hydrodynamic conditions prevailing at the liquid interface. As most of the kinetic constants published in the literature have been determined from absorption data (e.g. Pohorecki and Moniuk, 1988), when using a published kinetic constant to calculate the effective area from the absorption rate, the diffusion coefficient and solubility values used must be the same as those used by the author of the corresponding kinetic constant. Hence, the way proposed by Hoffmann et al. (2007) on improvement the accuracy of physical properties for the system by using kinetic constant by Pohorecki and Moniuk (1988) and values of others needed physical quantities (solubility and diffusivity) from more accurate but different sources from those used by Pohorecki to evaluation of the kinetic constant is wrong.

Table 4 shows K_G values calculated from the physico-chemical data published by some authors for 1M NaOH at a temperature of 20 °C, together with K_G values used by other authors to calculate the effective area. While the value employed by Linek et al. (1984, 1995, 2001) and Linek and

Table 4 – K_G values calculated from consistent data (kinetic constant, diffusivity and solubility of CO_2) published by various authors for 1 M NaOH at a temperature of 20 °C and $(K_G)_{\text{used}}$ values used for calculation of α shown where available.

Authors	$D_{\text{CO}_2, \text{L}}$ ($\times 10^{-9} \text{ m}^2/\text{s}$)	k_{OH} ($\text{m}^3 \text{ mol}^{-1} \text{ s}^{-1}$)	He_{CO_2}	K_G ($\times 10^3 \text{ m}^2.5 \text{ kmol}^{-1/2} \text{ s}^{-1}$)	$(K_G)_{\text{used}}$ ($\times 10^3 \text{ m}^2.5 \text{ kmol}^{-1/2} \text{ s}^{-1}$)
Kolev et al. (2006)		6.47		2.38	
Kucka et al. (2002)	1.45	6.54	0.684	2.11	
Pohorecki and Moniuk, 1988	1.41	9.43	0.684	2.49	
Linek et al. (1984)					2.24 ^a
Hoffmann et al. (2007)	1.65 ^b	10.6 ^b	1.00 ^b		4.17 ^b
Weimer and Schaber, 1996					2.80 ^c
Tsai et al. (2008)					2.74 ^d
de Brito et al. (1994)					1.25 ^d

^a Experimental value.

^b Author's information.

^c 1 M KOH.

^d Recalculated for 1 M NaOH.

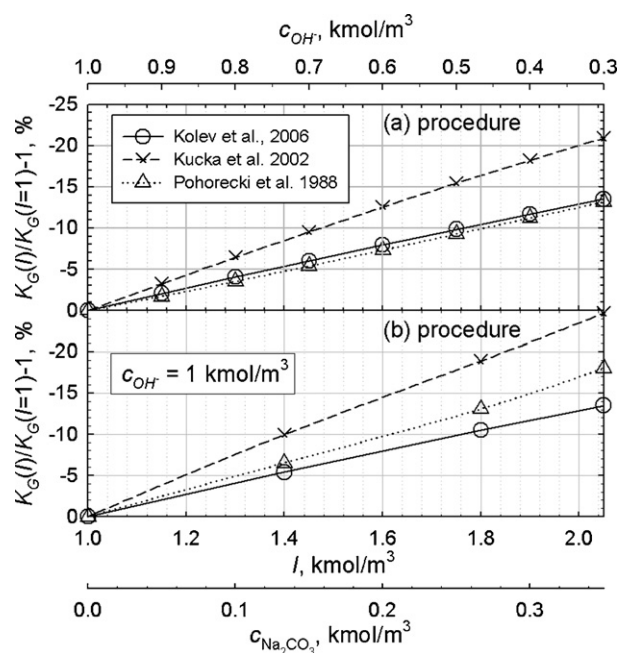


Fig. 4 – Effect on K_G of changes in the ionic strength of NaOH solution during procedures (a) and (b).

Sinkule (1997) differed only slightly (about 5%) from those recommended in the literature (Pohorecki and Moniuk, 1988; Kucka et al., 2002; Kolev et al., 2006), de Brito et al. (1994) used approximately half the K_G value used by Linek and Sinkule (1997) and Tsai et al. (2008) to evaluate the effective wetted area of Mellapak 250.Y packing. Consequently, de Brito reported a suspiciously high-wetted area (375 m^{-1}) compared with other authors using the same packing, who reported values only slightly higher than the geometric area of the packing (250 m^{-1}). Hoffmann et al. (2007) recently used a value of $4.17 \times 10^{-3} \text{ m/s}$, which, calculated from physical-chemical data (obtained, on enquiry, from the author), was 86% higher than the literature and our data.¹ Nevertheless, the resulting values of effective interfacial area are similar! It is due to the fact that the experimental values of overall gas-phase volumetric mass-transfer coefficient of carbon dioxide inter NaOH solution, measured by Hoffmann and by Linek for the same hydrodynamic conditions differ in similar scope (83% higher, see Table 5) as the K_G values used by the authors.

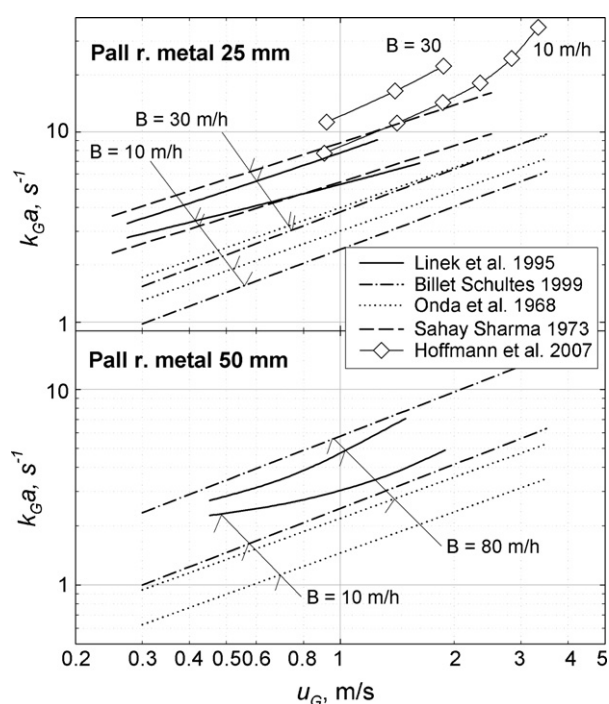
Fig. 4 plots the effect on K_G of relative changes in the ionic strength, I , of the circulating NaOH solution. Results are shown for carbon dioxide absorption without the addition of NaOH concentrate (Fig. 4(a)), and with NaOH concentrate added to maintain a constant concentration of 1 M NaOH (Fig. 4(b)). As the effect of these changes is significant, they should be taken into account in the calculation of the effective area. Procedure (a) comes out better from this comparison because, as $I = 2.5 - 1.5c_{\text{OH}}$, it does not require the concentrations of both Na_2CO_3 and NaOH to be simultaneously monitored. Additionally, changes in the ionic strength occurring during procedure (a) have slightly less effect on K_G than those taking place during procedure (b).

Following our analysis, we recommend usage of the physical property values and reaction kinetic constants published

¹ Also, surprisingly distribution coefficient used by Hoffmann was high ($\text{He} = 1.00$), which is close to the solubility of carbon dioxide in pure water ($\text{He} = 0.95$).

Table 5 – Comparison of overall gas-phase volumetric mass-transfer coefficient of carbon dioxide into NaOH solution, $(K_{OG}a)_{CO_2}$, measured for metal Pall ring 25 mm.

u_G (m/s)	B (m/h)	Hoffmann ^a $(K_{OG}a)_{CO_2}$ (s^{-1})	Linek ^b $(K_{OG}a)_{CO_2}$ (s^{-1})	Relative increase Hoff/Lin (%)
~0.9	10	0.510	0.287	78
	20	0.576	0.361	59
	30	0.572	0.401	43
~1.4	10	0.550	0.295	86
	20	0.672	0.353	90
	30	0.712	0.382	87
~1.85	10	0.570	0.303	88
	20	0.687	0.346	99
	30	0.794	0.364	118
Mean relative increase				83

^a Hoffmann et al. (2007).^b Linek et al. (1995).**Fig. 5 – Comparison of $k_G a$ values measured by various authors for metal Pall rings in different absorption systems below the loading point (see Table 1).**

either by Pohorecki and Moniuk (1988) or Kolev et al. (2006) in the evaluation of the resulting experimental data.

2.3. Methods for the measurement of $k_G a$

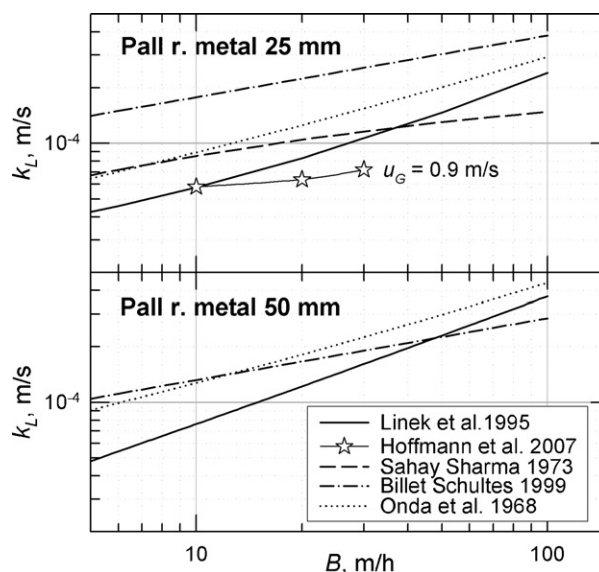
The gas-phase volumetric mass-transfer coefficient, $k_G a$, is typically measured using systems whose mass-transfer resistance is limited to the gas phase. Data from evaporation experiments can be utilized for such measurements, as well as data from absorption experiments in which an instantaneous reaction occurred in the liquid phase. Sahay and Sharma used the absorption of chlorine in lye. Both Linek et al. (1984, 1995, 2001), Linek and Sinkule (1997) and Hoffmann et al. (2007) used SO_2 absorption in lye, while Billet (1995) and Billet and Schulte (1999) used SO_2 absorption in lye as well as NH_3 absorption in sulphuric acid solution. Onda et al. (1968) used evaporation experiments in an air-water system and experiments involving the absorption of NH_3 in water, the latter involving the subtraction of liquid-phase mass-transfer

resistance. The instantaneous course of the reaction of SO_2 with OH^- ions at the interface was experimentally proven by Linek et al. (1995), who, across a range of concentrations down to almost zero ($c_{OH} \approx 0.01$ M), demonstrated the independence of the absorption rate from the concentration of OH^- ions.

Fig. 5 presents the $k_G a$ values calculated from correlations published by various authors and Hoffmann's experimental data. The data reported by Hoffmann et al. (2007), Linek et al. (1995) and Sahay and Sharma (1973) for 25 mm Pall rings are in relatively good agreement (differences less than 50%). However, the data calculated from correlations published by Onda et al. (1968) and Billet and Schulte (1999) underestimate $k_G a$ values by 100–200%. Only the values predicted by Billet and Schulte (1999) correlation for data measured for 50 mm Pall rings is in good agreement with our data.

2.4. Mass-transfer coefficient k_L in the liquid phase

Fig. 6 shows k_L values calculated using various literature correlations for $k_L a$ and a , and shows large differences of up to 200%. As there is generally good agreement among the published $k_L a$ data (Fig. 1), these differences are due to the lack of agreement

**Fig. 6 – Comparison of liquid-phase mass-transfer coefficients k_L calculated either from experimental data or using various literature correlations of $k_L a$ and a .**

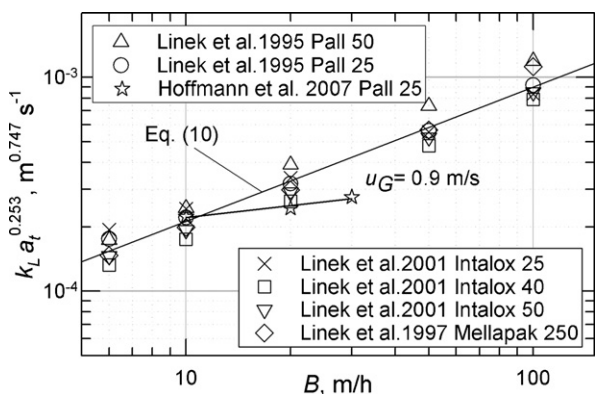


Fig. 7 – Correlation of k_L data measured over several years in a single laboratory for various packing types and sizes (Linek et al., 1995, 2001; Linek and Sinkule, 1997).

among literature effective area values (Fig. 2). However, dispersion among the k_L data decreases significantly when only data measured in a single laboratory for various packing types and sizes (Linek et al., 1995, 2001; Linek and Sinkule, 1997) are used in the calculation. When only these data were fitted (Fig. 7) using the regression relation:

$$k_L = 5 \times 10^{-5} B^{0.628} (a_t)^{-0.253} \quad (\text{S.D.} = 12\%) \quad (10)$$

A low mean deviation of 12% was obtained between the experimental data and the values calculated using Eq. (10). In close agreement with the correlations published by Billet and Schulte (1999) and Onda et al. (1968), who stated that $k_L \sim B^{2/3}$, the k_L coefficient is proportional to the liquid velocity to the power of 0.628. Conversely, the data measured by Hoffmann et al. (2007) was less proportional to the liquid load ($k_L \sim B^{0.18}$). The negative value of the power in Eq. (10) applied to the geometric area of the packing, a_t , corresponds to the fact that the thickness of the liquid film on the packing, and, thus, k_L increases with the wetting rate, u_L/a_t . The value of the power in our relation approximates to those used by Billet and Schulte (1999) and Onda et al. (1968); namely, -0.333 and -0.267 , respectively.

2.5. Mass-transfer coefficient k_G in the gas phase

For one type of packing (25 mm metal Pall rings), Fig. 8 shows the k_G calculated from either experimental data or calculated using various literature correlations. Although not as pro-

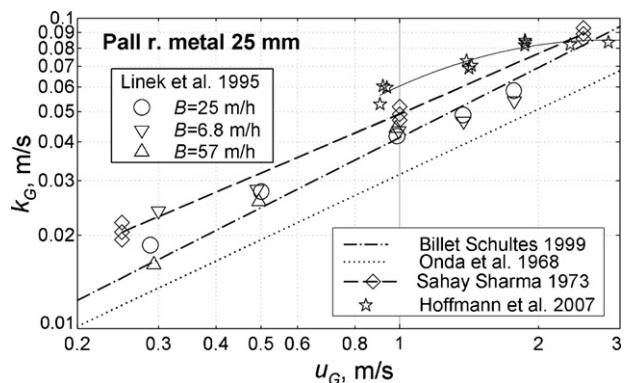


Fig. 8 – Comparison of gas-phase mass-transfer coefficients k_G calculated for 25 mm metal Pall rings either from experimental data or using various literature correlations for $k_G a$ and a .

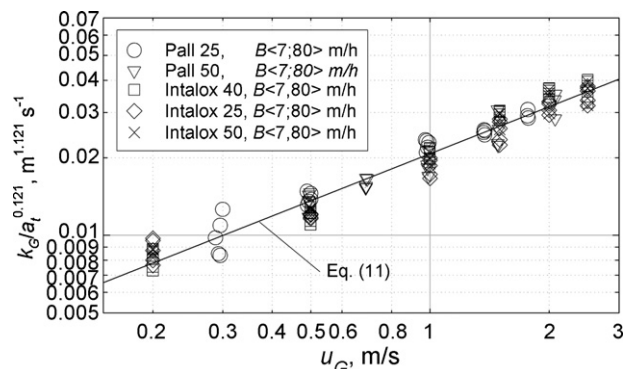


Fig. 9 – Correlation of k_G data measured over several years in a single laboratory for various packing types and sizes (Linek et al., 1995, 2001; Linek and Sinkule, 1997).

nounced as in the case of k_L , the differences still reach 100%, possibly as a result of errors in the determination of $k_G a$ and/or the interfacial area. However, again differences among the k_G data decrease significantly when only data measured in a single laboratory for various packing types and sizes (Linek et al., 1995, 2001; Linek and Sinkule, 1997) are used in the calculation. When only these data were correlated (Fig. 9) using the relation:

$$k_G = 2.06 \times 10^{-2} u_G^{0.608} (a_t)^{0.121} \quad (\text{S.D.} = 8.2\%) \quad (11)$$

A mean deviation of just 8% resulted, with the k_G coefficient being proportional to the gas velocity to the power of 0.608. The correlations published by Billet and Schulte (1999) and Onda et al. (1968) predict $k_G \sim u_G^{3/4}$ and $k_G \sim u_G^{0.7}$, respectively. The positive value of the power of a_t corresponds to the fact that, at a fixed superficial gas velocity, turbulence in the gas phase (and thus gas-phase mass-transfer coefficient) is higher when passing through finer ribbing of packing with a higher geometric area, a higher pressure drop and higher energy dissipation. The value of the power in our relation approximates to those used by Billet and Schulte (1999) and Onda et al. (1968); namely, 0.25 and 0.3, respectively.

Successful calculation of the fundamental transport coefficients k_L and k_G requires the utilization of flexible, empirical, multi-parameter correlations able to interpolate and smooth experimental data with sufficient accuracy. For example, Linek et al. (2001) used the following formula to correlate $k_G a$ data:

$$k_G a = 10^{e_1} B^{e_2 + e_3 \log B}, \quad e_j = e_{1j} + e_{2j} u_G + e_{3j} u_G^2 \quad \text{for } j = 1, 2, 3 \quad (12)$$

This formula has been shown to fit experimental data with a mean deviation of just 6% when the gas velocity range is 0.2–2.5 m/s and the liquid load range is 1–100 m/h. The calculation of mass-transfer coefficients using this complex, physically unfounded, but close-fitting relation can significantly reduce the dispersion of k_L and k_G as correlated with physico-chemical properties and flow rates.

Using correct methods for the determination of $k_L a$, $k_G a$ and a , good agreement and a low degree of dispersion was found in both k_L and k_G data calculated from primary data ($k_L a$, $k_G a$, a) measured on different types of random and structured packing. This suggests that the establishment a set of recognised methods for the measurement of mass-transfer characteristics in absorption columns would prove to be of considerable benefit.

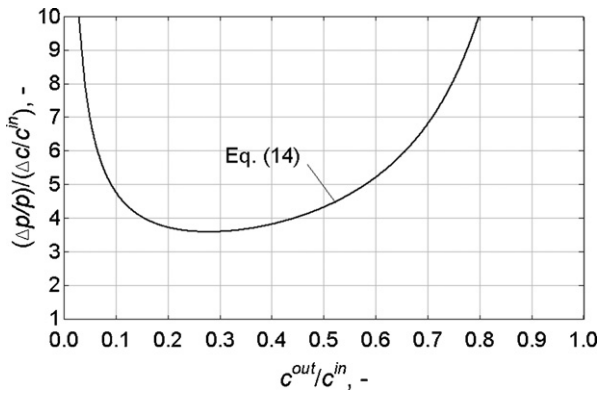


Fig. 10 – Relation between the relative error of the parameter p , $\Delta p/p$, and that of the concentrations, $\Delta c/c^{in}$, as a function of the ratio of outlet to inlet concentration.

3. Experimental setup

We echo the experimental setup recommendations expressed by Hoffmann et al. (2007). Attention should also be paid to sampling. In particular, to avoid end effects, we recommend that sampling should be performed directly from the packing, not from the streams going in and out the column as Hoffmann et al. do. In our forgoing works (Linek et al., 1984, 1995, 2001; Linek and Sinkule, 1997), samples of gas were withdrawn from the packing through three funnels distributed regularly over the column cross-section while those of liquid were taken from a free-flow channel placed across the column diameter. Now, we use another system: six small funnels drilled into Perspex rod of diameter 30 mm and length equal to column diameter of 300 mm. For the sampling of liquid or gas, the funnels/rod are directed up or down, respectively. The funnel stems are equipped with adjustable resistive elements, which enable to adjust the same sampling rate of fluid through the individual funnels. Installation of the sampling rods into the column with random packing brings no problem. With the structured packing, the rods are inserted into the holes (of diameter 34 mm) cut out by water jet cutter horizontally to the packing elements at required positions.

Transport parameters p ($k_L a$, $k_G a$ and a) are calculated from the concentrations measured in continuously sampled fluid at the input, c^{in} , and output, c^{out} , of measuring section of the packing from following relation:

$$p = \frac{u_i}{zH} \ln \frac{c_i^{in}}{c_i^{out}} \quad p = k_G a, a; \quad i = G \quad (13)$$

$$p = k_L a; \quad i = L$$

where $z=1$ for $k_L a$ and $k_G a$ evaluation and $z = K_G \sqrt{C_{OH,ave}}$ for evaluation of a . The height of the measuring section H should be chosen with respect to accuracy of the concentrations measuring methods. Following relationship, between relative error of the parameter p , $\Delta p/p$, and relative error of the concentrations relative to the concentration at the input of measuring section, $\Delta c/c^{in}$, follows from Eq. (13):

$$\frac{\Delta p/p}{\Delta c/c^{in}} = \frac{(1 + (c^{in}/c^{out}))}{\ln(c^{in}/c^{out})} \quad (14)$$

Fig. 10 shows that the height limitation is based on the ratio of outlet to inlet concentration: the height of measuring section must not lead to output concentration below 5% of the input because it produces an unacceptable error in the measured parameter. For this reason, the height of the measuring

section was 1 m in measuring $k_L a$ and a using oxygen–water and CO_2 –1 M NaOH systems, respectively and only 0.5 m in measuring $k_G a$ using SO_2 –1 M NaOH system (Linek et al., 1995, 2001; Linek and Sinkule, 1997).

4. Assessment of the influence of axial dispersion on the measurement of mass-transfer parameters

The true values of the mass-transfer parameters, p_{true} , with axial dispersion in the respective phase expressed by means of the Bodenstein number (Bo), was calculated using the equation described by Miyauchi and Vermeulen (1963):

$$p_{i,true} = p_i \frac{NTU_{i,true}}{NTU_{i,p}} \quad i = G, L; \quad p = k_L a, k_G a \quad (15)$$

where $NTU_{i,p}$ and $NTU_{i,true}$ is the number of transfer units assuming plug flow and assuming plug flow with superimposed axial dispersion, respectively. $NTU_{i,p}$ is given by the relation:

$$NTU_{i,p} = \frac{uL}{H} \ln \frac{c_i^{in}}{c_i^{out}} \quad i = G, L \quad (16)$$

and $NTU_{i,true}$ is obtained by solving the following implicit relation between $NTU_{i,true}$, $NTU_{i,p}$ and Bo_i

$$\exp(-NTU_{i,p}) = \frac{4b \exp(Bo_i/2)}{(1+b)^2 \exp(bBo_i/2) - (1-b)^2 \exp(-bBo_i/2)} \quad i = G, L \quad (17)$$

where

$$b = \sqrt{1 + \frac{4NTU_{i,true}}{Bo_i}} \quad (18)$$

Axial mixing of the phases in terms of Bodenstein numbers, Bo_i ($i=G$ or L), has been measured in an absorption column of inner diameter 0.29 m with air–water system packed with 25 mm metal Pall rings using dynamic measuring methods. The experiments consisted in monitoring of the exit response on the sudden change of the concentration of the tracer in the inlet stream. The tracer was helium for the gas phase (concentration determined through thermal conductivity measurement) and aqueous solution of NaCl for the liquid phase (conductivity measurement). To eliminate end effects, Bodenstein numbers have been evaluated via analysis of response obtained by deconvolution of responses measured for the two heights of the packing. The difference height of the packing and the characteristic dimension for Bo_i numbers was 1.47 m. The following regression relations were derived from our hitherto unpublished measurements for gas phase

$$Bo_G = 3.94 \times 10^4 Re_G^{-0.894} \quad (19)$$

and for liquid phase

$$Bo_L = 6.11 + 0.525 \cdot B - 10^{-3} B^2 \quad (20)$$

The effect of phase axial dispersion on $k_G a$ and $k_L a$, by comparing the values obtained when axial dispersion is taken into account, $p_{i,true}$, with those obtained when it is not, p_i , illustrate

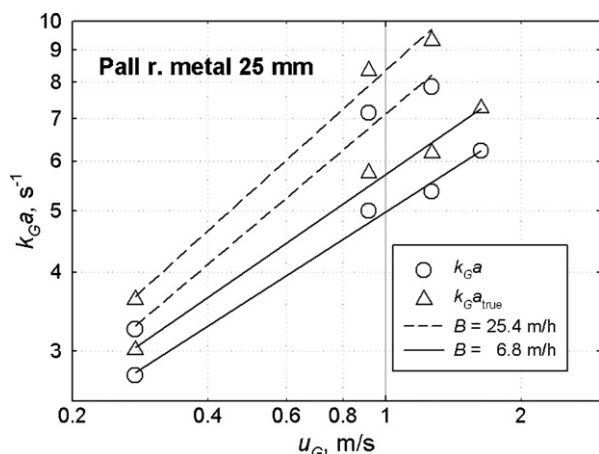


Fig. 11 – Effect of gas-phase axial mixing on $k_G a$ values measured by Linek et al. (1995) for 25 mm metal Pall rings.

Figs. 11 and 12, respectively using absorption data by Linek et al. (1995) measured in a column of inner diameter 0.29 m packed with 1.04 m of 25 mm metal Pall rings. For the measurement of $k_L a$, oxygen was desorbed from water to nitrogen. As the increase in the oxygen concentration in the column was negligible during the gas phase (due mainly to the low solubility of oxygen and sufficiently large flow of nitrogen), the effect of gas-phase axial dispersion was insignificant in these $k_L a$ measurements. Similarly, using absorption of SO_2 in NaOH solution, the effect of liquid-phase axial dispersion was insignificant in $k_G a$ measurements.

Fig. 11 shows the dependencies of $k_G a_{\text{true}}$ and $k_G a$ on the superficial gas velocity for two values of the liquid load, B . The $k_G a_{\text{true}}$ values, calculated with axial dispersion taken into account, are 10–15% higher than those calculated with plug flow assumed. Therefore, axial dispersion cannot be used to explain differences in the literature data of up to 200%. We suggest that the cause of these discrepancies is most likely to be found in experimental technique; namely, in sampling procedures (non-elimination of end effects) and in initial non-uniform distribution of the gas and liquid phases.

Fig. 12 plots the dependence of $k_L a_{\text{true}}$ and $k_L a$ on the liquid load B . The $k_L a_{\text{true}}$ values are higher (by up to almost 30% at low loads) than the $k_L a$ values, and differ in their dependence on the liquid load ($k_L a_{\text{true}} \sim B^{0.71}$; $k_L a \sim B^{0.81}$). We are investigating the effect of liquid-phase axial dispersion in more detail now because the effect is comparable with the differences in the literature data and might negatively influence correlation of the

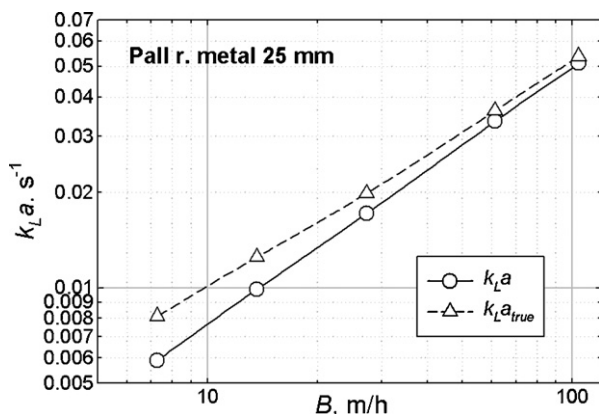


Fig. 12 – Effect of liquid-phase axial mixing on $k_L a$ values measured by Linek et al. (1995) for 25 mm metal Pall rings.

mass-transfer coefficient with properties of the system and their application/transfer onto other absorption/distillation systems.

5. Conclusions

In this paper we have assessed various procedures for the measurement of the effective interfacial area a and the volumetric mass-transfer coefficients, $k_G a$, and $k_L a$. On this basis, we herein propose the procedures that we believe should become the standard methods of the future.

We tested these methods for 25 and 50 mm metal Pall rings, and compared our results with the experimental data reported by Hoffmann et al. (2007) and Sahay and Sharma (1973), as well as with data resulting from use of the correlations published by Billet and Schulte (1999) and Onda et al. (1968); all data obtained below the loading point.

The $k_L a$ data measured using different absorption systems with mass-transfer resistance limited to the liquid phase (absorption/desorption of oxygen/carbon dioxide in water) are in good agreement. We, therefore, recommend the use of these systems as standard methods in the determination of $k_L a$. However, the absorption of NH_3 in water, as recommended by Hoffmann et al. (2007), is not an appropriate method because of the inaccuracy introduced by combining the results of two separate experiments measured in different phases. This conclusion is supported by the fact that the data measured by Hoffmann et al. (2007) was less proportional to the liquid load ($k_L \sim B^{0.18}$) compared with other data ($k_L \sim B^{2/3}$).

For the measurement of $k_G a$, we recommend the absorption of SO_2 in NaOH solution. For the determination of the effective interfacial area, a , we recommend the chemisorption of CO_2 in NaOH solution. Large differences exist between the effective area values published by various authors; differences that are due to inconsistencies in the kinetic, solubility and diffusivity data used in their evaluation. It is therefore necessary to unify the physical property and kinetic constant values used in the evaluation of a from absorption data. For this purpose we recommend the data presented by Pohorecki and Moniuk (1988) or Kolev et al. (2006) because they are complete and because the K_G values calculated from them are similar to those measured experimentally by many other authors.

To eliminate end effects we emphasise the need to sample the gas and liquid directly from the packing instead of from the top and bottom of the column.

For the calculation of the mass-transfer coefficients k_L and k_G we advise the use of flexible, empirical, multi-parameter interpolation formulas capable of smoothing the experimental data with sufficient accuracy. The use of such formulas can significantly reduce the dispersion of k_L and k_G as correlated with the physical-chemical properties and flow rates in the column.

Acknowledgments

Support from the Ministry of Education (MSM 6046137306) and from the Grant Agency of Czech Republic through the project no. 104/06/0736 are gratefully acknowledged.

References

- Billet, R., 1995, A, Packed Towers in Processing and Environmental Technology (VCH Verlagsgesellschaft mbH, D-69451 Weinheim, BRD) (English translation).

- Billet, R. and Schulte, M., 1999, Prediction of mass transfer columns with dumped and arranged packings. *Trans IChemE*, 77: 498–504.
- Danckwerts, P.V., (1970). *Gas-Liquid Reactions*. (McGraw-Hill, New York, USA).
- Henriques de Brito, M., von Stockar, U., Bangerter, A.M., Bomio, P. and Laso, M., 1994, Effective mass transfer area in a pilot plant column equipped with structured packings and with ceramic rings. *Ind Eng Chem Res*, 33: 647–656.
- Hoffmann, A., Mackowiak, J.F., Gorak, A., Haase, M., Loning, J.-M., Runiowski, T. and Hallenberger, K., 2007, Standardization of mass transfer measurements. Basis for the description of absorption processes. *Trans IChemE, Part A, Chem Eng Res Des*, 85(A1): 40–49.
- Kolev, N., Nakov, S., Ljutzkanov, L. and Kolev, D., 2006, Effective area of a highly efficient random packing. *Chem Eng Proc*, 45: 429–436.
- Kucka, L., Kenig, E.Y. and Gorak, A., 2002, Kinetics of the gas-liquid reaction between carbon dioxide and hydroxide ions. *Ind Eng Chem Res*, 41: 5952–5957.
- Linek, V. and Moucha, T., 2000, Mass transfer characteristics of packings for absorption and distillation columns, In *Lecture Held on Working Party of the Group Absorption and Distillation*. (The European Federation of Chemical Engineers, Winthertur, Switzerland)
- Linek, V., Petříček, P., Beneš, P. and Braun, R., 1984, Effective interfacial area and liquid side mass transfer coefficients in absorption columns packed with hydrophilised and untreated plastic packings. *Chem Eng Res Des*, 62: 13–21.
- Linek, V. and Sinkule, J., 1997, Hydraulické a transportní charakteristiky nových typů výplní absorpčních a rektifikačních kolon. Nerezová fóliová orientovaná výplň NFOV 350. *Chem Listy*, 91: 54–58.
- Linek, V., Sinkule, J. and Brekke, K., 1995, A critical evaluation of the use of absorption mass transfer data for the design of packed distillation columns. *Trans IChemE, Part A, Chem Eng Res Des*, 73: 398–405.
- Linek, V., Moucha, T. and Rejl, F.J., 2001, Hydraulic and mass transfer characteristics of packings for absorption and distillation columns, Rauschert-Metall-Sattel-Rings. *Trans IChemE, Part A, Chem Eng Res Des*, 79: 725–732.
- Miyauchi, T. and Vermeulen, T., 1963, Longitudinal dispersion in two-phase continuous-flow operations. *Ind Eng Chem Fundam*, 2: 113–126.
- Onda, K., Takeuchi, H. and Okumoto, Y., 1968, Mass transfer coefficients between gas and liquid phases in packed columns. *J Chem Eng Jpn*, 1: 56–62.
- Pohorecki, R. and Moniuk, W., 1988, Kinetics of reaction between carbon dioxide and hydroxyl ions in aqueous electrolyte solutions. *Chem Eng Sci*, 43: 1677–1684.
- Sahay, B.N. and Sharma, M.M., 1973, Effective interfacial area and liquid and gas side mass transfer coefficients in a packed column. *Chem Eng Sci*, 28: 41–47.
- Tsai, R.E., Schultheiss, P., Kettner, A., Lewis, J.C., Seifert, A.F., Eldridge, R.B. and Rochelle, G.T., 2008, Influence of surface tension on effective packing area. *Ind Eng Chem Res*, 47: 1253–1260.
- Weimer, T. and Schaber, K., 1996, Ermittlung effektiver Phasengrenzflächen durch Kohlendioxidabsorption aus Luft. *Chem Tech*, 48: 237–249.
- Yoshida, F. and Koyanagi, T., 1962, Mass transfer and effective interfacial areas in packed columns. *AIChE J*, 8: 309–316.

“Profile Method” for the Measurement of $k_L a$ and $k_V a$ in Distillation Columns. Validation of Rate-Based Distillation Models Using Concentration Profiles Measured along the Column

F. J. Rejl, L. Valenz, and V. Linek*

Department of Chemical Engineering, Prague Institute of Chemical Technology, CZ-166 28 Prague 6, Czech Republic

The “profile method” enables the determination of vapor- and liquid-side volumetric mass-transfer coefficients $k_V a$ and $k_L a$ by comparing the concentration profiles measured in both phases in a distillation column with the simulated profiles. The method is based on the fact that the shape of the concentration profiles along the column depend significantly on the distribution of the mass-transfer resistance between the liquid and vapor phases. This makes it possible to measure $k_L a$ and $k_V a$ directly in the distillation columns, in the same manner that is possible in absorption columns, and therefore to validate the distillation models more conclusively than by means of comparing the experimental and calculated height equivalent to a theoretical plate values. The coefficients were measured on structured packing Mellapak250Y. A small axial mixing of phases on this type of packing enables the use of a plug-flow model for both phases. Three distillation systems, methanol–ethanol, ethanol–propanol, and methanol–propanol, were used under total reflux and atmospheric pressure. Samples of the phases were withdrawn directly from the column packing by means of special sampling devices. The dependence of the individual transport coefficients on the phase flow rate was obtained by changing the reboiler duty. The dependencies were compared with those predicted by the following three mass-transfer correlations developed for packed columns: RBF (Rocha et al. *Ind. Eng. Chem. Res.* **1996**, *35*, 1660), BS (Billet, R.; Schultes, M. *Trans. Inst. Chem. Eng.* **1999**, *77*, 498), and DELFT (Olujic et al. *Chem. Eng. Proc.* **1999**, *38*, 683). The coefficients obtained by the profile method differ substantially from those calculated from the original models. Specifically, all of the original models considerably overvalue the $k_L a$ coefficients (RBF by up to 2 times, BS by up to 1.5 times, and DELFT by up to 6.3 times) and undervalue the $k_V a$ coefficients (all by up to 2 times). The dependence of the mass-transfer coefficients on the rate of the phases predicted by any of the original models is not consistent with that of the profile method. It has also been shown that the experimental concentration profiles strongly differ from the profiles calculated from the Aspen Plus simulation program. The correlations of the $k_L a$ and $k_V a$ coefficients with improved flow dependencies according to the profile method are presented. The concentration profiles calculated from the improved correlations fit the profiles accurately.

1. Introduction

1.1. Transport Parameters in Rate-Based Models of a Packed Distillation Column. Many correlations have been published for the calculation of the partial transport coefficients k_L and k_V and the effective mass-transfer area a on random and structured packing. Wang et al.¹ reviewed the correlations developed during the last decades, from among which we employ in this work the models presented by Rocha et al.^{2,3} (RBF), Billet and Schultes⁴ (BS), and Olujic et al.⁵ (DELFT). The forms of the correlations are derived from simple hydrodynamic and transfer models, which are then designed or rectified, according to the results of the absorption experiments, which enable the measurement of these transport coefficients separately. Validation of these relations has hitherto been carried out by comparing the predicted height equivalent to a theoretical plate (HETP) values with the experimental values established by the product concentrations.

Taylor⁶ gave a telling assessment of the present state-of-the-art in distillation model validation with the following conclusion: “To properly validate *any* column model (be it EQ with efficiencies, NEQ, or CFD), it is necessary to measure composition profiles along the flow path(s)—not at all an easy task (especially for packed columns). Such data are, however,

essential. Product concentrations are useless for evaluating column models, as almost any model, sometimes even relatively simple black boxes, can be validated with such data. Measured composition profiles, especially in reactive and three-phase distillation processes, would be especially welcome, much more so than more profiles computed from increasingly sophisticated models.”

Validation of the models by means of the product concentrations has led to situations in which the resulting HETP values, predicted by various models, agree well with the experimental data, despite the fact that the values of the transport parameters differ by multiples. An example is shown in Table 1: The models predict an almost identical value of HETP = 0.31 m for atmospheric rectification of the methanol–propanol (M–P) mixture. Nevertheless, the DELFT model presumes a $k_L a$ value of double and a $k_V a$ value of half in comparison with the RBF model, and the BS model presumes an a value of half in comparison with the RBF and DELFT models. This indicates an unsatisfactory relevance of the parameters used in the simulation models of the processes occurring in distillation

Table 1. Transport Data of M–P ($x_A = 0.0782$; $P = 40$ kW)

model	$k_L a$, s ⁻¹	$k_V a$, s ⁻¹	a , m ⁻¹	HETP, m
RBF	0.0322	7.91	208	0.313
BS	0.0303	9.55	106	0.304
DELFT	0.0755	4.34	235	0.311

* To whom correspondence should be addressed. E-mail: linekv@vscht.cz.

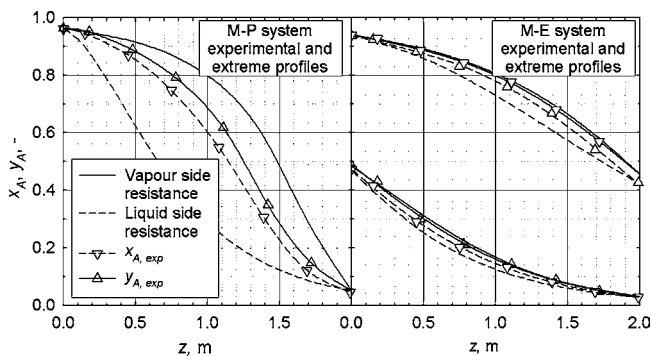


Figure 1. Comparison of concentration profiles calculated, provided the mass-transfer resistance is concentrated in the liquid or vapor phase, with the experimental profiles measured at identical product concentrations.

columns and their degradation into purely matching parameters with no clear physical meaning. However, the clear physical meaning of these parameters underlies their applicability for other distillation systems and the loadings of the column and condition their transferability to similar processes like absorption.

The aim of this work is to determine the $k_{L,a}$ and $k_{V,a}$ in the distillation column by the profile method^{7,8} applied to experimental data measured on the structured packing Mellapak250Y. A small axial mixing of phases on this often used packing makes it attractive for the profile method because the results are less biased by the hydrodynamic plug-flow model utilized. The values of $k_{L,a}$ and $k_{V,a}$ and their dependence on the rate of phases are then utilized for qualitatively higher validation of the models presently in use for the calculation of these parameters in the rate-based models of distillation.

1.2. "Profile Method" Measurement of Volumetric Vapor and Liquid Mass-Transfer Coefficients in a Distillation Column. The effect of the resistance in individual phases on the local mass-transfer intensity changes significantly along the distillation column depending on the local slope of the equilibrium curve, as results from eq 1 for the overall mass-transfer coefficient

$$\frac{1}{K_{L,a}} = \frac{1}{m_A k_{V,a}} + \frac{1}{k_{L,a}} \quad \text{or} \quad R_{\text{total}} = R_{\text{vapor}} + R_{\text{liquid}} \quad (1)$$

where m_A is the local slope of the equilibrium curve. As a result, the hypothetical concentration profiles in the column differ considerably, when calculated as providing the resistance against the interfacial mass transfer, which is concentrated in the vapor or liquid phase. This is demonstrated in Figure 1, where the hypothetical profiles are compared with the experimental data measured at identical product concentrations. The experimental profile lies between the hypothetical extremes.

The profile method applies the fact that the relative resistance of the individual phases varies along the column, according to eq 1, for the separate determination of the volumetric mass-transfer coefficients in the vapor and liquid phases. Simulated concentration profiles are calculated by integration of the rate-based model, with $k_{L,a}$ and $k_{V,a}$ as the matching parameters. The profile method modifies the values of $k_{L,a}$ and $k_{V,a}$, calculated from the original model RBF, BS, or DELFT, by multiplication with the correction factors b_L and b_V to fit the experimental profiles. The best fit with the experimental profiles is obtained with the optimal values of the pair (b_L, b_V) , which is unambiguous. The data obtained from these three different models by the profile method provide similar values of the volumetric mass-transfer coefficient. This supports the premise that the $k_{L,a}$ and $k_{V,a}$ data obtained by the profile method are unique.

2. Mass-Transfer Parameter (k_L , k_V , and a) Correlations Used in This Work

2.1. RBF Model. The Rocha et al.^{2,3} relation for the liquid-side mass-transfer coefficient is based on the penetration theory, with the contact time expressed in terms of the average liquid velocity u_{LE} in an actual liquid-phase-flow cross section and a characteristic length, which is identified with the corrugation length d_s of the packing. The resulting value is reduced by a factor of 0.9

$$k_L = 2\sqrt{\frac{0.9D_L u_{LE}}{\pi d_s}} \quad (2)$$

The liquid velocity is given by

$$u_{LE} = \frac{u_L}{\varepsilon h_{LR} \sin \alpha} \quad (3)$$

and h_{LR} is the total liquid holdup given by eq 19 in ref 3.

The relation for the vapor-side mass-transfer coefficient is based on earlier investigations on absorption in a wetted-wall column

$$k_V = 0.054 \frac{D_V}{d_s} \left[\frac{(u_{VE} + u_{LE}) \rho_V d_s}{\mu_V} \right]^{0.8} Sc_V^{0.33} \quad (4)$$

u_{VE} denotes the average gas velocity in an actual gas-phase-flow cross section

$$u_{VE} = \frac{u_V}{\varepsilon(1 - h_{LR}) \sin \alpha} \quad (5)$$

For calculation of the effective mass-transfer area below the loading point, the authors start from the Shi and Mersmann⁹ correlation and suggest the following relation:

$$a = a_p F_{SE} \frac{29.12 \left(\frac{u_L^2 \rho_L d_s}{\sigma} \frac{u_L^2}{d_s g} \right)^{0.15} d_s^{0.359}}{\left(\frac{u_L \rho_L d_s}{\mu_L} \right)^{0.2} \varepsilon^{0.6} (1 - 0.93 \cos \gamma) (\sin \alpha)^{0.3}} \quad (6)$$

For sheet-metal packing, they give $\cos \gamma = 0.9$ for $\sigma < 0.055 \text{ N m}^{-1}$. This is the case for the alcohol systems used in this work.

2.2. BS Model. The Billet and Schultes⁴ relation for the liquid-side mass-transfer coefficient is also based on the penetration theory, but the contact time is expressed in terms of the superficial liquid velocity u_L and the mixing length is defined as the equivalent hydraulic diameter d_h of a channel in the packing fully filled with liquid. The resulting value is multiplied by a constant C_L , specific for each type of packing

$$k_L = C_L 12^{1/6} \sqrt{\frac{u_L D_L}{h_{LB} d_h}} \quad (7)$$

$$d_h = \frac{4\varepsilon}{a_p} \quad (8)$$

h_{LB} is the total holdup given by eqs 11 and 12 in ref 4.

For calculation of the vapor-side mass-transfer coefficient, the dependence on diffusivity, based on a penetration model in a laminar film from the hindered side, is used and the dependence on the vapor flow rate is deduced from experimental

data. The resulting value is multiplied by a constant C_V , specific for each type of packing.

$$k_V = C_V \frac{a_p^{1/2} D_V}{\sqrt{d_h} (\epsilon - h_{LB})} \left(\frac{u_V \rho_V}{a_p \mu_V} \right)^{3/4} Sc_V^{1/3} \quad (9)$$

The effective mass-transfer area below the loading point is calculated from the following relation:

$$a = \frac{1.5 a_p}{\sqrt{d_h} a_p} \left(\frac{u_L d_h \rho_L}{\mu_L} \right)^{0.2} \left(\frac{u_L^2 \rho_L d_h}{\sigma} \right)^{0.75} \left(\frac{u_L^2}{d_h g} \right)^{-0.45} \quad (10)$$

It was shown that, below a lower limit for the surface tension of 30 mN m⁻¹, the surface of metals, plastics, or ceramic is completely wetted. If a real liquid has a surface tension below this value (as it is in our case; see Table 3), the calculations have to be performed with the limiting value of 30 mN m⁻¹.

2.3. DELFT Model. The Olujic et al.⁵ relation for the liquid-side mass-transfer coefficient is also based on the penetration theory, with the contact time expressed in terms of the effective liquid velocity and the mixing length

$$k_L = 2 \sqrt{\frac{D_L u_{LE}}{0.9 \pi d_{hV}}} \quad (11)$$

The liquid-phase interfacial velocity u_{LE} is defined by eq 3 in which the total liquid holdup h_{LR} is calculated from eq 11 in ref 5 and the hydraulic diameter d_{hV} of the triangular channel is given as

$$d_{hV} = \frac{\frac{(bh - 2\delta d_s)^2}{bh}}{\left[\left(\frac{bh - 2\delta d_s}{2h} \right)^2 + \left(\frac{bh - 2\delta d_s}{b} \right)^2 \right]^{0.5} + \frac{bh - 2\delta d_s}{2h}} \quad (12)$$

The thickness of the liquid film δ is calculated from following relation:

$$\delta = \left(\frac{3\mu_L u_L}{\rho_L g a_p \sin \alpha} \right)^{1/3} \quad (13)$$

It is assumed in this model that the liquid-side mass-transfer coefficient k_L does not depend on the vapor-phase velocity up to the loading point.

The vapor-side mass-transfer coefficients were calculated assuming that the transitional phase flow and, by analogy with heat transfer the overall coefficient, was a geometric mean of the coefficients calculated in the laminar and turbulent regimes, respectively.

$$k_V = \sqrt{k_{V,\text{lam}}^2 + k_{V,\text{turb}}^2} \quad (14)$$

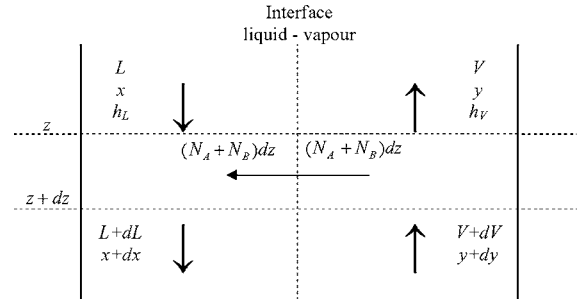


Figure 2. Differential control volume of a distillation column.

where

$$k_{V,i} = \frac{Sh_{V,i} D_V}{d_{hV}} \quad i = \text{lam or turb} \quad (15)$$

$$Sh_{V,\text{lam}} = 0.664 Sc_V^{1/3} \sqrt{Re_{Vrv} \frac{d_{hV}}{l_{V,pe}}} \quad (16)$$

$$Sh_{V,\text{turb}} = \frac{(Re_{Vrv} Sc_V \xi_{VL} \phi / 8) [1 + (d_{hV} / l_{V,pe})^{2/3}]}{1 + 12.7 \sqrt{\xi_{VL} \phi / 8} (Sc_V^{2/3} - 1)} \quad (17)$$

$$l_{V,pe} = \frac{h_{pe}}{\sin \alpha}; \quad Re_{Vrv} = \frac{\rho_V (u_{VE} + u_{LE}) d_{hV}}{\mu_V} \quad (18)$$

$$\xi_{VL} = \left\{ -2 \log \left[\frac{\delta}{d_{hV}} - \frac{5.02}{Re_{Vrv}} \log \left(\frac{\delta}{3.7} + \frac{14.5}{Re_{Vrv}} \right) \right] \right\}^{-2} \phi = \frac{2d_s}{b + 2d_s} \quad (19)$$

The vapor-phase interfacial velocity u_{VE} is defined by eq 5.

Calculation of the effective mass-transfer area started from the Onda et al.¹⁰ correlation, which is multiplied by the expression $1 - \Omega$, taking into account the perforation of the structured packing

$$a = a_p (1 - \Omega) \left\{ 1 - \exp \left[-1.45 \left(\frac{0.075}{\sigma} \right)^{0.75} \left(\frac{\rho_L u_L}{a_p \mu_L} \right)^{0.1} \left(\frac{u_L^2 a_p}{g} \right)^{-0.05} \left(\frac{\rho_L u_L^2}{a_p \sigma} \right)^{0.27} \right] \right\} \quad (20)$$

where Ω means the portion of the packing surface occupied by holes. In this work, the decrease of the effective mass-transfer area due to the perforation was not considered, $\Omega = 0$.

3. Theoretical Section

3.1. Distillation-Column Model. The distillation process has been modeled as continuous and one-dimensional. The model has been based on mass and energy balances and the mass-transfer relation to a differential control volume $S dz$ of the column (see Figure 2) developed on the basis of the following assumptions: (i) the process is the distillation of a binary mixture under total reflux, i.e., $L = V$ and $x = y$ at one/the same cross section of the column; (ii) the process is adiabatic and steady state; (iii) the overall pressure is constant throughout the column; (iv) there is plug flow in both phases; (v) interfacial mass transport is described using a film model in which the convective flow is taken into account; (vi) the rate of heat transfer is such as to keep the vapor and liquid phases just at their dew point and boiling point, respectively; (vii) there is

thermodynamic equilibrium at the interface. A complete set of corresponding model equations can be found in work by Rejl et al.,⁸ the algorithm for their solution can be found in work by Linek et al.⁷

3.2. Method of Concentration Profile Calculation. The concentration profile of the liquid phase $x_A(z)$ along the column has been obtained by means of the simultaneous integration of the differential equations

$$\begin{aligned} \frac{dL}{dz} &= f\left(\frac{dx_A}{dz}, \frac{dh_V}{dz}, \frac{dh_L}{dz}, N_A, N_B, x_A, L, h_V, h_L, k_L a, k_V a\right) \\ \frac{dx_A}{dz} &= f\left(\frac{dL}{dz}, \frac{dh_V}{dz}, \frac{dh_L}{dz}, N_A, N_B, x_A, L, h_V, h_L, k_L a, k_V a\right) \end{aligned} \quad (21)$$

with the initial conditions

$$\begin{aligned} x_A(z=0) &= x_{A0} \\ L(z=0) &= L_0 \end{aligned} \quad (22)$$

The molar flow of the liquid phase at the inlet of the column, L_0 , is determined experimentally from the volumetric flow F , concentration $x_{A0,exp}$, and temperature of the reflux. The molar fraction of the more volatile component, x_{A0} , in the liquid-phase inlet of the column either is determined experimentally or is subject to optimization (see further). The molar fluxes transferred per unit height of packing N_A and N_B were calculated either with convective flow taken into account from the equation

$$\begin{aligned} N_A &= k_V a c_V r \ln\left[\frac{y_{Aw} - r}{x_A - r}\right] S = k_L a c_L r \ln\left[\frac{x_A - r}{x_{Aw} - r}\right] S \\ r &= \frac{N_A}{N_A + N_B} \end{aligned} \quad (23)$$

or by assuming equimolar counterdiffusion (i.e., the convective flow is not taken into account) from the equation

$$N_A = k_L a c_L (x_{Aw} - x_A) S = k_V a c_V (x_A - y_{Aw}) S \quad (24)$$

The volumetric mass-transfer coefficients $k_L a$ and $k_V a$ are not considered constant along the column. Their dependence on phase flows and physicochemical properties has therefore been left in the form assumed by the RBF, BS, or DELFT model, and their variability, required for the purpose of optimization, has been retained by application of the multiplication parameters b_L and b_V

$$\begin{aligned} k_L a &= b_L (k_L^{model} a^{model}) \\ k_V a &= b_V (k_V^{model} a^{model}) \end{aligned} \quad \text{model is RBF, BS or DELFT} \quad (25)$$

Enthalpies were calculated from equations

$$\begin{aligned} h_L(x_A, t_L) &= [c_{pLA} x_A + c_{pLB} (1 - x_A)] t_L + \\ &\Delta h_{mix} h_V(x_A, t_V) = [c_{pLA} t_{bpA} + \Delta h_{vapA}] x_A + \\ &[c_{pLB} t_{bpB} + \Delta h_{vapB}] (1 - x_A) + c_{pVA} x_A (t_V - t_{bpA}) + \\ &c_{pVB} (1 - x_A) (t_V - t_{bpB}) \end{aligned} \quad (26)$$

and their derivatives

$$\begin{aligned} \frac{dh_L}{dz} &= \left[\left(\frac{\partial h_L}{\partial x_A} \right)_{t_L} + \left(\frac{\partial h_L}{\partial t_L} \right)_{x_A} \frac{dt_L}{dx_A} \right] \frac{dx_A}{dz} \\ \frac{dh_V}{dz} &= \left[\left(\frac{\partial h_V}{\partial x_A} \right)_{t_V} + \left(\frac{\partial h_V}{\partial t_V} \right)_{x_A} \frac{dt_V}{dx_A} \right] \frac{dx_A}{dz} \end{aligned} \quad (27)$$

were obtained numerically using dt_L/dx_A and dt_V/dx_A from the dependence of the boiling and dew points on the concentration of the mixture, respectively.

In the calculation, the thermodynamic properties ρ_L , ρ_V , c_{pL} , c_{pV} , Δh_{mix} , Δh_{vap} , σ , μ_L , μ_V , D_L , and D_V were considered as functions of the concentration and temperature, and hence they vary along the column. The corresponding functions were taken from the literature: the molar densities of the liquid mixtures according to Barner-Quinlan's rule, using data from Vargaftik;¹¹ the vapor phase was considered as ideal, molar heats according to Zábanský et al.;¹² heats of mixing were not considered because the enthalpy change of the liquid phases along the column is 400 times greater than the enthalpy change due to the heat of mixing; the molar heat of vaporization according to Majer and Svoboda,¹³ the surface tensions according to Yaws,¹⁴ viscosities according to Reid et al.¹⁵ with the exception of propanol vapor viscosity according to Chung et al.;¹⁶ the vapor-liquid equilibria have been taken from Gmehling et al.¹⁷ and the diffusion coefficients from Zarzycki and Chacuk¹⁸ and those in the liquid using a thermodynamic correcting factor in accordance with Krishna and Wesselingh.¹⁹

Using the auxiliary relations (23)–(27), the differential equations 21 can be transformed to

$$\begin{aligned} \frac{dL}{dz} &= f(x_A, L; b_L, b_V) \\ \frac{dx_A}{dz} &= f(x_A, L; b_L, b_V) \end{aligned} \quad (21a)$$

The equations, after their replacement with the set of difference equations, have been solved by the Gauss method with b_L and b_V as the sought parameters.

3.3. b_L and b_V Optimization Procedure. Four concentration profiles were calculated according to the procedure described in section 3.2 with estimated values $[b_{L0}, b_{V0}]$ identical for all of these profiles and with the initial conditions \bar{L}_0 and \bar{x}_{A0} corresponding with four experimental series, measured at the same reboiler duty. Their mutual consistency was quantified using the objective function

$$s = \sqrt{\left[\sum_{i=1}^n (x_{A,i,cal} - x_{A,i,exp})^2 + \sum_{i=1}^n (y_{A,i,cal} - y_{A,i,exp})^2 \right] / 2n} \quad (28)$$

$$x_{A,i,cal} = y_{A,i,cal}$$

where s represents the standard deviation of the experimental and calculated molar fractions. The simplex method has been used to search for the optimal pair of parameters $[b_L, b_V]$. Minimization has been performed until the difference in the values of the objective function s in the two following steps was lower than $10^{-7}\%$ of its value and the differences in the parameter values were lower than $10^{-4}\%$ of their values.

In this manner, the profile method provides a set of correction parameters b_L and b_V , which modify values $k_L^{model} a^{model}$ and $k_V^{model} a^{model}$ for the real values in the column according to eq 25, for each of the RBF, BS, and DELFT models and for one reboiler duty. The pairs of parameters b_L and b_V , obtained by minimizing the objective function eq 28, represent the global minimum. This confirmed therefore that the parameters for the different initial estimates $[b_{L0}, b_{V0}]$ do not differ significantly.

4. Experimental Section

4.1. Distillation Column. The experiments were performed in a stainless steel atmospheric distillation column (see Figure 3) with an interior diameter of 0.15 m, packed with 10 pcs of Mellapak250Y, to a height of 2.1 m. Each of the packing pieces was equipped with two wall wipers that redirect the wall flow

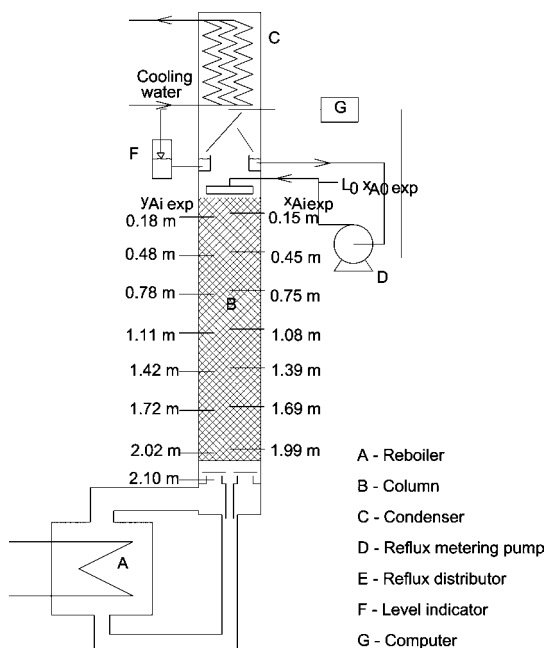


Figure 3. Schematic drawing of the packed distillation column operating under total reflux.

Table 2. Characteristics of Mellapak250Y

a_p (m^{-1})	ε	h (m)	B (m^{-1})	d_s (m)	α (deg)	FSE	Ω	σ_c (N/m)	h_{pe} (m)	
250	0.97	0.0117	0.22	0.016	06	45	0.35	0	0.071	0.21

back into the packing. The small diameter of the column and the high number of the wipers justify our assumption that even a small maldistribution of the liquid (higher liquid flow near the column wall) is suppressed substantially in our column. The characteristics of the packing are described in Table 2. An electrically heated reboiler, equipped with an electric power regulator (up to 60 kW), was used to maintain a constant rate of boiling. The power was measured with a three-phase wattmeter (Orbit Merret 405, accuracy 240 W). The complete spiral condenser with a height of 1 m was mounted at the top of the column. The column and reboiler were covered with Orsil insulation. The heat loss, measured by independent experiments, was less than 3% of the reboiler duty.

The column was operated under total reflux, which was maintained by PI regulation of the liquid level in the reflux head. The reflux flow was measured with a radial turbine flowmeter (Omega FTB9510, with an accuracy of 0.001 L min^{-1}). Reflux flow was distributed on the packing using a shower distributor with 25 openings (see Figure 4; $1472 \text{ holes m}^{-2}$). Vapor from the reboiler was introduced into the column by a distributor with four openings regularly spaced over the column base cross section.

The column was equipped with seven openings for the placement of thermistors and sampling devices for the withdrawal of liquid and vapor samples along the column (see Figure 3). A platinum thermometer (Pt 100, accuracy $0.05 \text{ }^\circ\text{C}$) was installed in the collecting channel of the sampling device (Figure 5). Note that the sampling tubes were equipped with an overlap, preventing a mixture of the wall-flow liquid with the liquid sampled from the packing. Holes for the sampling devices were drilled through the structured packing with a water jet. We believe the sample points do not affect the phase flow in the packing, notably because the volume of the holes occupies 3.3% of the packing volume only. The column also enables the

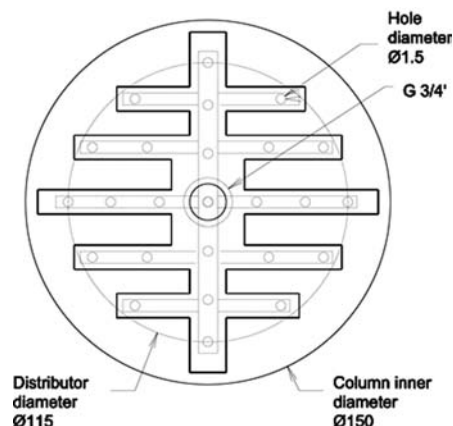


Figure 4. Schematic drawing of the liquid distributor.

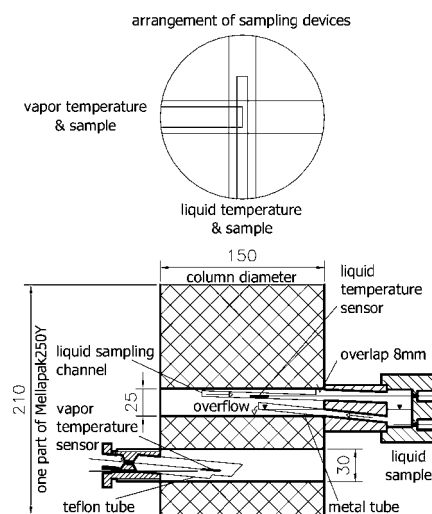


Figure 5. Sampling and measuring device assembly.

withdrawal of samples of the liquid reflux and of the vapor entering the bottom of the column from the reboiler.

4.2. Experimental Procedures, Conditions, and Analytical Methods. Three distillation systems were used: methanol–ethanol (M–E), ethanol–propanol (E–P), and methanol–propanol (M–P). About 45 L of the distillation mixture was poured into the reboiler, and the electric power input to the reboiler was adjusted to the desired level. Four of the power input levels were employed, namely, $P = 10, 20, 30,$ and 40 kW . The column was operated for a sufficient length of time to achieve a steady state, which usually took 1 h. Liquid and vapor samples (2.5 mL) were withdrawn by means of glass syringes from all of the sampling devices simultaneously over a period of approximately 6 min. The vapor phase was withdrawn into a syringe by self-suction due to the self-condensation of vapor inside the syringe, which was cooled by acetone evaporation from the cotton-wool wrapping of the syringe. Analysis of the samples was carried out using a tempered digital refractometer, the Atago RX5000, at $20 \text{ }^\circ\text{C}$. The refractometer measures the refractive index with an accuracy of 10^{-5} . The indexes n_D of the pure components of the mixtures differ significantly (n_D : for methanol, 1.32854; ethanol, 1.36123; propanol, 1.38516); the dependence of the mixture indexes on their concentrations does not manifest any extremes, and the accuracy of the molar fraction determination is better than 0.001.

These experiments were repeated four times for every power input with four different concentrations of the mixture in the

Table 3. Vapor and Liquid Flow Rates in the Distillation Column at Limiting Reboiler Duties and Physical Properties of the Distillation Systems Used ($p = 101.3$ kPa)

x_A	$P = 10$ kW		$P = 40$ kW		$t_{bp},$ °C	$\Delta h_{vap},$ kJ mol ⁻¹	$c_L \times 10^{-4},$ mol m ⁻³	$c_V,$ mol m ⁻³	$D_{AB,L} \times 10^9,$ m ² s ⁻¹	$D_{AB,V} \times 10^5,$ m ² s ⁻¹	$\mu_L \times 10^4,$ Pa s	$\mu_V \times 10^4,$ Pa s	$s \times 10^3,$ N m ⁻¹
	$B, \text{m h}^{-1}$	$u_V, \text{m s}^{-1}$	$B, \text{m h}^{-1}$	$u_V, \text{m s}^{-1}$									
Methanol–Ethanol													
0	3.30	0.42	13.2	1.69	78.3	38.6	1.60	34.7	5.28	1.34	4.30	10.4	17.5
0.2	3.14	0.43	12.5	1.70	75.2	38.0	1.71	35.0	5.16	1.35	4.14	10.3	17.8
0.4	2.97	0.43	11.9	1.71	72.2	37.4	1.83	35.3	5.06	1.33	3.96	10.3	18.1
0.6	2.80	0.43	11.2	1.73	69.4	36.8	1.98	35.6	4.97	1.31	3.79	10.2	18.3
0.8	2.63	0.44	10.5	1.74	66.9	36.2	2.14	35.8	4.92	1.27	3.61	10.1	18.6
1	2.45	0.44	9.80	1.76	64.6	35.6	2.34	36.1	4.93	1.25	3.44	10.1	18.8
Ethanol–Propanol													
0	3.97	0.41	15.9	1.64	97.0	41.9	1.23	32.9	4.13	0.95	4.94	9.59	17.6
0.2	3.81	0.41	15.3	1.64	91.7	41.4	1.29	33.4	3.84	0.93	4.88	9.45	17.7
0.4	3.67	0.41	14.7	1.64	87.4	40.9	1.36	33.8	3.67	0.91	4.76	9.34	17.8
0.6	3.54	0.41	14.2	1.65	83.9	40.2	1.43	34.1	3.61	0.89	4.61	9.24	17.8
0.8	3.42	0.42	13.7	1.67	80.9	39.4	1.51	34.4	3.64	0.88	4.46	9.16	17.7
1	3.30	0.42	13.2	1.69	78.3	38.6	1.60	34.7	3.76	0.87	4.30	9.09	17.5
Methanol–Propanol													
0	3.97	0.41	15.9	1.64	97.0	41.9	1.23	32.9	4.99	1.24	4.94	9.59	17.6
0.2	3.64	0.41	14.5	1.63	87.6	41.1	1.36	33.8	4.61	1.18	4.74	9.34	18.2
0.4	3.33	0.41	13.3	1.64	79.6	40.0	1.53	34.6	4.39	1.14	4.45	9.13	18.6
0.6	3.03	0.42	12.1	1.66	73.1	38.7	1.74	35.2	4.18	1.10	4.11	8.95	18.9
0.8	2.74	0.43	11.0	1.70	68.0	37.2	1.99	35.7	3.73	1.07	3.77	8.82	19.0
1	2.45	0.44	9.80	1.76	64.6	35.6	2.34	36.1	4.24	1.05	3.44	8.73	18.8

Table 4. b_L and b_V Parameters Calculated with Fixed and Optimized Initial Conditions: System M–P, Model RBF

P, kW	fixed initial conditions			optimized initial conditions			
	b_L	b_V	s	b_L	b_V	s	shift x_A^*
10	0.342	3.01	0.0367	0.441	2.11	0.0335	0.0121
20	0.453	1.85	0.0349	0.620	1.32	0.0303	0.0159
30	0.598	1.45	0.0341	0.853	1.08	0.0300	0.0142
40	0.734	1.27	0.0345	1.09	0.993	0.0266	0.0100

* Absolute value of the difference of optimized $x_A(z=0)$ and fixed (measured) $x_{A0,exp}$. Mean values of four series.

reboiler. The concentrations were chosen in order to encompass the entire concentration range of the measured concentration profiles in the column. The result of these experiments is 16 sets of data, each of which includes a set of seven liquid, x_{Ai} , and vapor concentrations, y_{Ai} , along the packing, the liquid concentration in the reflux tube $x_{A0,exp}$, the vapor concentration entering at the base of the column from the reboiler (in the shell of the plate) y_{A8} ; the volumetric flow rate of the liquid reflux F , the barometric pressure p , and the average temperature of each phase at the time of withdrawal t_{Li} and t_{Vi} . A complete list of the source data is given in the Appendix. Illustrative vapor and liquid flow rates in the column calculated from the reboiler duties and some physical properties of the distillation systems used are defined in Table 3.

4.3. Data Evaluation Method. Before the final evaluation of all of the experiments, the effect of the three following conditions of the model and their integration with the best-fit parameters b_L and b_V was tested on a narrow set of data: (i) fixed versus optimized initial conditions; (ii) transverse convective flow; (iii) optimization toward the profiles in separate liquid and vapor phases.

(i) Effect of the Fixed or Optimized Initial Conditions in the Search for Parameters b_L and b_V . Within the scope of this test, the parameters b_L and b_V evaluated with the fixed initial conditions $x_A(z=0) = y_A(z=0) = x_{A0,exp}$ were compared with the values evaluated with the initial conditions $x_A(z=0) = y_A(z=0)$ optimized simultaneously in accordance with the parameters b_L and b_V for every set of data measured at the same reboiler duty. The same value of L_0 was used for both initial conditions.

From the results summarized in Table 4, it is apparent that

the parameters b_L and b_V evaluated with the fixed and optimized initial conditions differ about 22–49%, but the optimized $x_A(z=0)$ values differ from the measured values $x_{A0,exp}$ just about less than 0.015(!) on average. It is thus evident that the sensitivity of the parameters on the initial conditions is high. Because the optimized values $x_A(z=0)$ did not take any unrealistic values, we have presumed that the optimization of the initial conditions together with the parameters b_L and b_V is a correct method and, hence, this method has been used further.

(ii) Effect of Convective Flow. Convective flow of methanol (A component) $x_A(N_A + N_B)$ induced by the total flow of the mixture through an interface ($N_A + N_B$) relative to the flow N_A is presented for M–P and M–E distillation systems as a function of the concentration of methanol in Figure 6. The convective flow reaches up to 25% and 12% of the flow of methanol at the top of the column in M–P and M–E systems, respectively, and flows from the liquid into the vapor along the whole column. No reversal of the direction of the convective

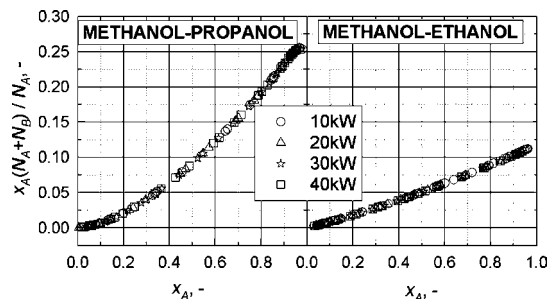
**Figure 6.** Convective flow of methanol (A component), $x_A(N_A + N_B)$, relative to the flow N_A as a function of the concentration of component A.

Table 5. b_L and b_V Parameters Calculated with (Eq 23) or without (Eq 24) Equimolar Counterdiffusion Considering Convective Flow: System M–P, Model RBF

P , kW	With convective flow			equimolar counterdiffusion		
	b_L	b_V	s	b_L	b_V	s
10	0.449	2.05	0.0335	0.475	2.02	0.0336
20	0.628	1.29	0.0303	0.658	1.28	0.0304
30	0.862	1.06	0.0300	0.907	1.06	0.0301
40	1.098	0.971	0.0266	1.181	0.965	0.0266

flow was observed, in contrast to the system ethanol–water presented in ref 8. An effect of the convective flow on parameters b_L and b_V is, however, minimal. The results presented in Table 5 show that differences of the parameters b_L and b_V evaluated assuming equimolar counterdiffusion, i.e., using eq 24 in the rate-based model of the column, or taking the convective flow into account, i.e., using eq 23, reach 6% at most. Because the calculation with eq 23 does not bring any other problems, except for an increase in the computation time, and is physically more consistent, this model has been used further.

(iii) Effect of Optimization toward the Profiles in the Liquid and Vapor Phases Separately. Experimental liquid and vapor profiles do not coincide with each other (see Figure 7). This is apparently a consequence of the longitudinal mixing of the phases. The plug-flow model was used in both phases of this work in spite of the fact that the model assumes the coincidence of both profiles. The reasons for its application follow. Our hitherto unpublished data²⁰ concerning the axial dispersion in the absorption tower packed with random (Intalox25) or structured packing (Mellapak250Y) revealed multiple lower longitudinal mixing of the structured packing. Also, the distillation profiles for Mellapak250Y indicate a lesser mutual spacing of vapor and liquid profiles in comparison with the spacing on the random packing (see ref 20). The parameters b_L and b_V , obtained by the adjustment of the liquid concentration profiles and of the vapor profiles, differ only about 10% on average, and the parameters obtained by the adjustment of both of the profiles together constitute roughly their average, as is demonstrated in Table 6. Another reason is that this model has also been used by the authors of mass-transfer correlations, which are compared with the data measured by the profile method in this work.

5. Results

5.1. Temperature of Phases. The liquid phase was found to be overheated at whichever location in the packing for all three distillation systems. This overheating was highest for the M–P system, reaching 3 °C. Vapor was found to be roughly saturated, with the highest deviation from saturation discovered for the M–P system, namely, subcooling by 1 °C. Further

analysis of the experimental data achieves these findings: (i) there is no clear relationship between the overheating/subcooling of the phases and the reboiler duty; (ii) the scatter of the overheating/subcooling data is less when it is plotted as a function of the concentration phase than when it is plotted as a function of its position in the column; (iii) subcooling of the vapor phase and overheating of the liquid phase have their maxima at around the equimolar concentration of the mixture, at which the temperature difference of the phases and mass-transfer intensity achieve their maximum values (see the experimental data in Tables A1–A3 in the Appendix).

5.2. Parameters b_L and b_V and Concentration Profiles Evaluated by the Profile Method. The pairs of the best-fit parameters [b_L , b_V], obtained by minimizing the objective function eq 13, are shown in Table 7, together with the standard deviations s of the experimental and calculated concentrations. The s values show that all of the models with the best-fit parameters obtained by the profile method fit the concentration profiles with practically the same precision. The most precise are the fitted data of the M–E system ($s < 0.018$), and the worst are those of the M–P system ($s < 0.034$). That is why the data for the M–P system are used to illustrate the data behavior obtained by the profile method in the calculations of this work because the deviations for this system are the largest and therefore our conclusions are on the safe side. This is demonstrated clearly in Figure 8, in which the experimental concentration profiles $x_{A,\text{exp}}$ and $y_{A,\text{exp}}$ are compared with those calculated from the RBF model with the best-fit parameters b_L and b_V for the M–P and E–P distillation systems.

The parameters b_L and b_V depend on the reboiler duty P or, in other words, on the phase flow rates (Table 7). The b_L values increase and the b_V values decrease with P as much as 2-fold in the range of the reboiler duties utilized. This indicates that the individual models do not fit the dependence of the volumetric mass-transfer coefficients on the phase velocities well. This is discussed in section 5.4.

5.3. $k_L a$ and $k_V a$ Evaluated according to the Profile Method. The dependence of the volumetric mass-transfer coefficients calculated from the models RBF, BS, and DELFT using the best-fit parameters b_L and b_V on the superficial vapor and liquid phase velocities is shown in Figure 9, together with the coefficients calculated from the original models presented in the literature. The $k_V a$ dependence on the vapor flow rate shows a wide dispersion due to the $k_V a$ dependence on the physical properties of the distillation mixtures, which, not having been eliminated, infiltrates these plots. The differences between the coefficients determined by the profile method and those calculated from the original models can be estimated from the ratio of the corresponding model parameters b . The parameters $b_{L,\text{orig}}$ and $b_{V,\text{orig}}$ of the original correlations are also give in Table 7. For example, the ratios $b_{L,\text{orig}}/b_{L,\text{RBF}} = 1/0.474 = 2.11$ and $b_{V,\text{orig}}/b_{V,\text{RBF}} = 1/2.00 = 0.5$ indicate that the RBF model gives 111% higher $k_L a$ and 50% lower $k_V a$ data on average, compared with the profile method in the M–E system at a reboiler duty of 10 kW. From these ratios, it follows that the

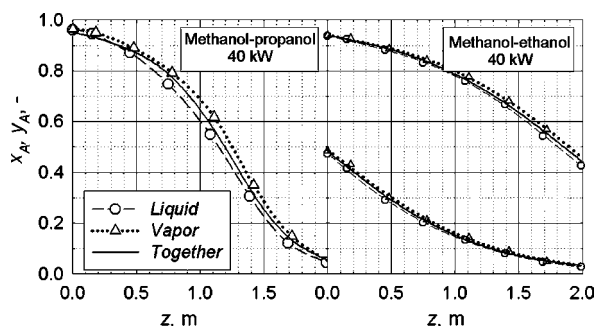


Figure 7. Vapor and liquid concentration profiles adjusted together and separately by the profile method using the RBF model.

Table 6. b_L and b_V Parameters Calculated from Liquid or Vapor and/or Both Concentration Profiles: System M–P, Model RBF

P , kW	liquid profile		vapor profile		both profiles	
	b_L	b_V	b_L	b_V	b_L	b_V
10	0.413	2.27	0.498	1.94	0.449	2.05
20	0.636	1.25	0.595	1.41	0.628	1.29
30	0.825	1.04	0.851	1.13	0.862	1.06
40	1.020	0.990	1.193	0.969	1.098	0.971

Table 7. Best-Fit Parameters b_L and b_V Obtained by the Profile Method

	$b_{L,orig}^a$	$b_{V,orig}^a$	P , kW	methanol–ethanol			ethanol–propanol			methanol–propanol		
				b_L	b_V	s	b_L	b_V	s	b_L	b_V	s
RBF	1	1	10	0.474	2.00	0.018	0.418	2.14	0.025	0.449	2.05	0.034
			20	0.564	1.50	0.014	0.580	1.38	0.022	0.628	1.29	0.030
			30	0.763	1.27	0.014	0.794	1.18	0.020	0.861	1.06	0.030
			40	0.971	1.16	0.012	1.025	1.09	0.015	1.098	0.97	0.027
BS ^b	1.334	0.385	10	0.917	0.580	0.018	0.755	0.650	0.025	0.858	0.592	0.034
			20	0.971	0.444	0.014	0.937	0.428	0.022	1.060	0.378	0.030
			30	1.242	0.382	0.014	1.192	0.375	0.020	1.353	0.320	0.030
			40	1.494	0.356	0.012	1.442	0.350	0.015	1.621	0.298	0.027
DELFT	1	1	10	0.196	1.56	0.018	0.158	1.96	0.025	0.178	1.68	0.033
			20	0.259	1.59	0.014	0.249	1.71	0.022	0.289	1.45	0.030
			30	0.392	1.59	0.014	0.369	1.72	0.020	0.447	1.40	0.030
			40	0.534	1.63	0.012	0.493	1.76	0.015	0.596	1.43	0.026

^a Values of the multiplication parameters used in the original models. ^b Billet and Schultes⁴ did not present the constant for Mellapak250Y. For comparison, the constants are presented for similar packing Ralu-Pak.

coefficients predicted by the original RBF model most closely match the coefficients obtained by the profile method at the highest reboiler duty of 40 kW, i.e., at flow rates near the loading point: the differences between k_{VA} coefficients do not exceed 10% and 16% for k_{LA} coefficients in all of the distillation systems employed. At this reboiler duty, a similar congruence exists between the coefficients calculated from the BS model (the differences do not exceed 22%). In all remaining situations (reboiler duties and distillation systems), all of the original models considerably overvalue the k_{LA} coefficients (by up to 6.3 times; DELFT model) and undervalue the k_{VA} coefficients (by up to 2 times).

The conclusion is that none of the literature correlations (RBF, BS, or DELFT) describes the distillation mass-transfer coefficients along the column sufficiently accurately for all of the distillation systems used in this work. An encouraging fact is that the volumetric mass-transfer coefficients evaluated from these three different models (RBF, BS, and DELFT), after correction by the profile method, demonstrate mutual compatibility.

5.4. Dependence of k_{LA} and k_{VA} on Phase Flow Rates. The dependence of the mass-transfer coefficients and interfacial area on the physicochemical properties and on the flow rate of phases allows, to a certain extent, validation of the models for k_{LA} and

k_{VA} evaluation. The physicochemical properties of the alcoholic systems utilized in this work do not vary much. The greatest differences exist between the M–E and E–P systems (see Table 5). The differences in the surface tension and vapor viscosity do not exceed 3% and 10%, respectively, but more noticeable differences occur in the viscosity of the liquid phase (by an average 21%) and in the diffusivity, namely, 34% and 45% on average for the liquid and vapor phases, respectively. The b_L values (see Table 7) evaluated by the profile method in the M–E and E–P systems, utilizing the RBF, BS, and DELFT models, differ on average by about 6%, 7%, and 11%, respectively, for the same reboiler duties, i.e., at the same rate of phases, and similarly the b_V values differ on average by about 7%, 8%, and 12%, respectively. This is why, in this work, the dependence

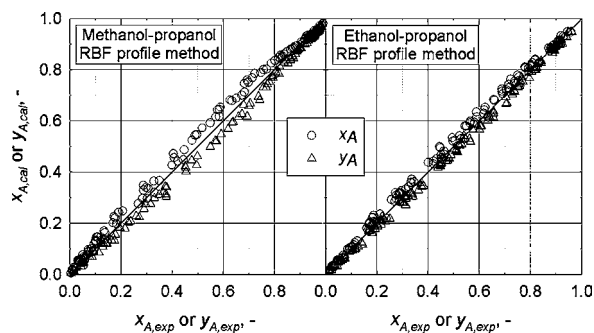


Figure 8. Experimental concentration profiles compared with those calculated from the RBF model with the best-fit parameters b_L and b_V evaluated by the profile method for the M–P and E–P distillation systems.

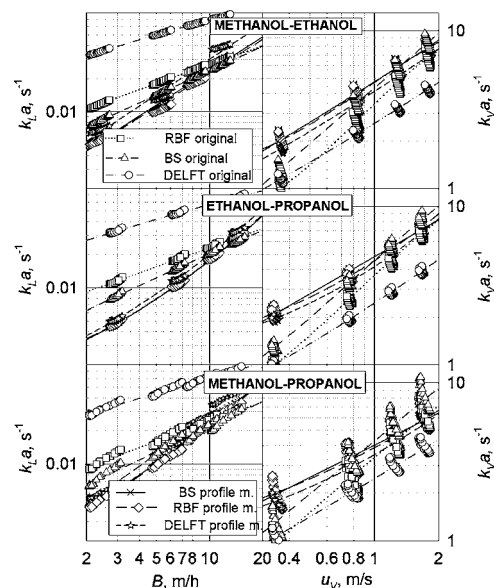


Figure 9. Volumetric mass-transfer coefficients calculated from the models RBF, BS, and DELFT using the best-fit parameters b_L and b_V as a function of the superficial vapor and liquid phase velocities and from the original model correlations.

Table 8. Values of the Exponents in Relations (29) and (33)

	methanol–ethanol			ethanol–propanol			methanol–propanol		
	RBF	BS	DELFT	RBF	BS	DELFT	RBF	BS	DELFT
$\alpha + \varepsilon$	0.597	0.733	0.445	0.596	0.733	0.445	0.597	0.733	0.450
β	-0.015	0	0	-0.020	0	0	-0.017	0	0
ε	0.4	0.4	0.125	0.4	0.4	0.125	0.4	0.4	0.125
$\alpha + \beta + \varepsilon$	0.582	0.733	0.445	0.576	0.733	0.445	0.580	0.733	0.450
λ	0.506	0.339	0.735	0.610	0.432	0.776	0.622	0.437	0.851
$\alpha + \beta + \varepsilon + \lambda$	1.09	1.07	1.19	1.19	1.17	1.22	1.20	1.17	1.30
$\delta + \varepsilon$	0.435	0.408	0.192	0.436	0.408	0.202	0.436	0.408	0.200
γ	0.759	0.750	0.631	0.764	0.750	0.670	0.761	0.750	0.644
$\gamma + \delta + \varepsilon$	1.19	1.16	0.823	1.20	1.16	0.872	1.20	1.16	0.844
ν	-0.350	-0.317	0.025	-0.454	-0.420	-0.078	-0.502	-0.466	-0.111
$\gamma + \delta + \varepsilon + \nu$	0.844	0.843	0.848	0.747	0.740	0.794	0.695	0.693	0.733

of the volumetric mass-transfer coefficients on the rate of the phases predicted by the models was tested because it was only possible to change the rates in a wide range, approximately four times, by changing the input into the reboiler.

5.4.1. $k_L a$ and $k_V a$ Dependence on the Rates of Phases Predicted by the RBF, BS, and DELFT Models. It follows from the forms of the correlation that the dependence of the transport characteristics on the rate of the phases can be represented by the following power dependence:

$$k_L \propto u_L^\alpha; k_L \propto u_V^\beta; k_V \propto u_L^\delta; k_V \propto u_V^\varepsilon; a \propto u_L^\varepsilon \quad (29)$$

We assume that the vapor velocity does not affect the mass-transfer area up to the loading point ($a \propto u_V^0$). Then the dependence of the volumetric coefficients will have the following form:

$$\begin{aligned} k_L a &\propto u_L^\alpha u_V^\beta u_L^\varepsilon \\ k_V a &\propto u_L^\delta u_V^\varepsilon u_L^\varepsilon \end{aligned} \quad (30)$$

At total reflux, it holds the following mass balance:

$$u_L S \rho_L = u_V S \rho_V \quad (31)$$

Relations (30) may therefore be rewritten for the column working under total reflux as follows:

$$\begin{aligned} k_L a &= b_{L,\text{orig}} A_L(\text{phys properties}) u_L^{\alpha+\beta+\varepsilon} \\ k_V a &= b_{V,\text{orig}} A_V(\text{phys properties}) u_V^{\gamma+\delta+\varepsilon} \end{aligned} \quad (32)$$

$A_{L,V}$ are functions of the physicochemical properties of the system itself that are given by the original models RBF, BS, or DELFT, and $b_{L,V,\text{orig}}$ are multiplication parameters used in the models that are given in Table 7. The exponents of the power dependence in eq 29, predicted by the RBF, BS, and DELFT models, were obtained by smoothing the data calculated from the respective model within the range of experimental rates (see Table 5) under the following conditions:

$$\begin{aligned} k &\propto u_L^\chi|_{u_V=\text{const.}}; k \propto u_V^\chi|_{u_L=\text{const.}}; u_{L,\text{const.}} = \\ &0.118 \text{ m s}^{-1}; u_{V,\text{const.}} = 1 \text{ m s}^{-1}; x_{A,\text{const.}} = 0.5; t = t_{\text{boiling}} \end{aligned}$$

where k stands for the transport characteristics (k_L , k_V , and a) and χ for the exponents (α , β , γ , δ , and ε). The exponents evaluated are presented in Table 8 for all of the distillation systems.

The overall exponents, $\alpha + \beta + \varepsilon$ and $\gamma + \delta + \varepsilon$, evaluated from the individual models do not depend in practical terms on the rate, concentration, and distillation system within the

range of conditions of our experiments. For example, the exponents calculated from the RBF model for the rates $u_L = 0.236 \text{ m s}^{-1}$ and $u_V = 1.8 \text{ m s}^{-1}$ and the system M–P, $\alpha + \beta + \varepsilon = 0.580$ and $\gamma + \delta + \varepsilon = 1.19$, hardly differ from the exponents presented in Table 8 for the half rates, namely, 0.580 and 1.20, respectively.

5.4.2. $k_L a$ and $k_V a$ Dependence on the Rate of Phases Predicted by the Profile Method. When the power input into the reboiler is altered, only the rate of the phases changes significantly in relation to eq 32 (see Table 5). The rate of liquid and vapor in the column rises proportionately to the power. If the $k_L a$ and $k_V a$ dependence on the rate of the phases of the RBF, BS, and DELFT models is described well, the parameters b_L and b_V , obtained by optimization, should not be dependent on the power input to the reboiler. However, the value of the parameter b_L increases with the power for all of the models, and the value of the parameter b_V decreases for the RBF and BS models. This indicates inaccurate $k_L a$ and $k_V a$ dependence on the rate of the phases included in the original RBF, BS, and DELFT models.

The dependence of the experimentally determined parameters b_L and b_V on the power P , i.e., on the mean velocity of the phases in the column, was adjusted in regard to the power relation, in analogy to relations according to eq 29 for the transport coefficients

$$\begin{aligned} b_L &\propto P^\lambda \\ b_V &\propto P^\nu \end{aligned} \quad (33)$$

The λ and ν exponents found are shown in Table 8. Relations (32) rewritten so as to include the effect of the rate of the phases on the b_L and b_V parameters revealed by the profile method are the following:

$$\begin{aligned} k_L a &= b_{L,\text{profile}} A_L(\text{phys properties}) u_L^{\alpha+\beta+\varepsilon+\lambda} \\ k_V a &= b_{V,\text{profile}} A_V(\text{phys properties}) u_V^{\gamma+\delta+\varepsilon+\nu} \end{aligned} \quad (34)$$

Corrected values of the overall exponents $\alpha + \beta + \varepsilon + \lambda$ and $\gamma + \delta + \varepsilon + \nu$, presented in Table 8, show that the RBF, BS, and DELFT models considerably undervalue the $k_L a$ dependence on the rate (the exponents in the original models range from 0.445 to 0.733, while the profile method yields values in the range from 1.06 to 1.37) and considerably overestimate the $k_V a$ dependence (the exponents in the original models range from 1.16 to 1.20, and those in the profile method range from 0.682 to 0.846).

The best-fit parameters $b_{L,\text{profile}}$ and $b_{V,\text{profile}}$ were obtained by the profile method with the corrected dependence of

Table 9. Best-Fit Parameters $b_{L,profile}$ and $b_{V,profile}$ Obtained by the Profile Method

	P , kW	methanol–ethanol			ethanol–propanol			methanol–propanol		
		$b_{L,profile}$	$b_{V,profile}$	s	$b_{L,profile}$	$b_{V,profile}$	s	$b_{L,profile}$	$b_{V,profile}$	s
RBF	10	17.2	1.35	0.018	30.1	1.42	0.025	36.0	1.35	0.033
	20	13.5	1.24	0.014	25.2	1.31	0.022	30.1	1.24	0.030
	30	14.5	1.27	0.014	26.1	1.36	0.020	30.7	1.27	0.030
	40	15.7	1.35	0.012	27.6	1.45	0.015	32.0	1.35	0.027
BS	10	10.07	0.445	0.018	15.50	0.440	0.025	17.63	0.408	0.033
	20	8.104	0.444	0.014	13.40	0.404	0.022	15.53	0.368	0.030
	30	8.837	0.437	0.014	14.02	0.424	0.020	16.37	0.374	0.030
	40	9.504	0.449	0.012	14.76	0.451	0.015	16.04	0.419	0.026
DELFT	10	36.6	1.72	0.018	36.6	1.94	0.025	72.9	1.65	0.033
	20	26.8	1.72	0.014	30.2	1.79	0.022	59.2	1.51	0.030
	30	29.1	1.67	0.014	31.3	1.84	0.020	61.1	1.51	0.030
	40	31.1	1.69	0.012	32.6	1.92	0.015	62.3	1.59	0.026

Table 10. Mean Values of the Corrected Overall Exponents and the Best-Fit Parameters

	all systems			
	RBF	BS	DELFT	all models
$\alpha + \beta + \varepsilon + \lambda$	1.16 ± 0.050	1.14 ± 0.06	1.24 ± 0.05	1.18 ± 0.066
$\gamma + \delta + \varepsilon + \nu$	0.762 ± 0.062	0.759 ± 0.066	0.792 ± 0.047	0.771 ± 0.061
$b_{L,profile}$	24.9 ± 7.4	13.3 ± 3.2	42.5 ± 15	
$b_{V,profile}$	1.33 ± 0.064	0.422 ± 0.027	1.71 ± 0.136	
λ	0.579	0.403	0.787	
ν	-0.435	-0.401	-0.055	

volumetric mass-transfer coefficients on the velocity of the phases using the following relations:

$$k_L a = b_{L,profile} u_L^\lambda (k_L^{model} a^{model})$$

$$k_V a = b_{V,profile} u_V^\nu (k_V^{model} a^{model}) \quad \text{model is RBF, BS or DELFT} \quad (35)$$

for calculation of the coefficients in optimizing the procedure instead of the relation (25). $b_{L,profile}$ and $b_{V,profile}$ are given in Table 9. The s values, practically the same as those in Table 7, demonstrate that the concentration profiles are fitted with the same accuracy as previously, but the $b_{L,profile}$ and $b_{V,profile}$ values are now practically independent of the phase flow rates and therefore the dependence of the coefficients on the rate is substantively better described.

5.5. $k_L a$ and $k_V a$ Evaluated by the Profile Method with Correction of the Dependence on the Flow Rates of the Phases. The corrected values of the overall exponents $\alpha + \beta + \varepsilon + \lambda$ and $\gamma + \delta + \varepsilon + \nu$ presented in Table 8 for different models and distillation systems differ very little from each other. The same holds true for the best-fit parameters $b_{L,profile}$ and $b_{V,profile}$ obtained in different distillation systems. Their mean values are listed in Table 10, together with their standard deviations. Making use of these mean values of the parameters and exponents, the final forms of the mass-transfer correlations referred to in the literature, adjusted according to the profile method, are as follows:

Corrected RBF^{2,3} model.

$$(k_L a)_{PM,RBF} = 24.9 u_L^{0.579} (k_L a)_{RBF,orig}$$

$$(k_V a)_{PM,RBF} = 1.33 u_V^{-0.435} (k_V a)_{RBF,orig} \quad (36)$$

fits the experimental concentration profiles of all distillation systems used with the standard deviation $s_{PM,RBF} = 0.0373$, while the original RBF correlation with $s_{RBF,orig} = 0.121$.

Corrected BS⁴ model.

$$(k_L a)_{PM,BS} = 13.3 u_L^{0.403} (k_L a)_{BS,orig}$$

$$(k_V a)_{PM,BS} = 0.422 u_V^{-0.401} (k_V a)_{BS,orig} \quad (37)$$

fits the profiles with $s_{PM,BS} = 0.0383$, while the original BS correlation with $s_{BS,orig} = 0.0765$.

Corrected DELFT⁵ model.

$$(k_L a)_{PM,DELFT} = 42.5 u_L^{0.787} (k_L a)_{DELFT,orig}$$

$$(k_V a)_{PM,DELFT} = 1.71 u_V^{-0.055} (k_V a)_{DELFT,orig} \quad (38)$$

fits the profiles with $s_{PM,DELFT} = 0.0393$, while the original DELFT correlation with $s_{DELFT,orig} = 0.145$.

Other forms of the correlations may be discussed; e.g., the Reynolds number may be used in place of the velocity. However, such a discussion would perhaps be premature at this time because it is based on a very narrow database of only three distillation systems, with little variance in the physicochemical properties. In this situation, it is difficult to distinguish the exponent values λ and ν , revealed by the profile method, between the exponents of the Reynolds, Weber, and Froude criteria, which include velocity in the original RBF, BS, or DELFT models.

These experimental concentration profiles are compared with those calculated from the corrected RBF model (36) for the M–P and E–P distillation systems in Figure 10. The most accurate are the data of the E–P system and the least accurate those of the M–P system. The standard deviations of the experimental concentrations and those concentrations calculated from eq 36 for the M–E, E–P, and M–P systems are $s = 0.035$, 0.028, and 0.042, respectively. In any case, the correlation (36) is much more precise than the original RBF model with the standard deviations $s = 0.069$, 0.078, and 0.164 for these same systems. Improved accuracy can also be demonstrated for the BS and DELFT models.

The experimental concentration profiles are also compared with those calculated from the *Aspen Plus* simulation program for the M–P and M–E distillation systems in Figure 11 on the log–log scale, which enables detection of the relative differences of the data. In the simulation program, the rate-based model of the distillation columns utilizes either RBF mass-transfer coefficients published by Bravo et al.²² or BS mass-transfer coefficients published by Billet and Schultes.²³ The profiles

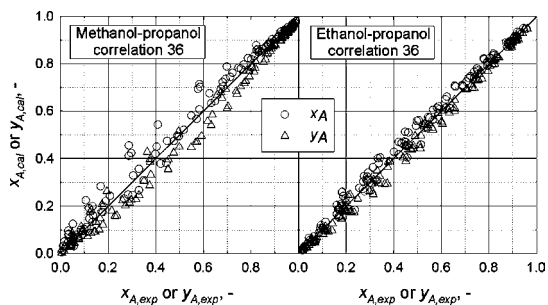


Figure 10. Comparison of the experimental concentrations with those calculated from the corrected RBF model, i.e., from eq 36.

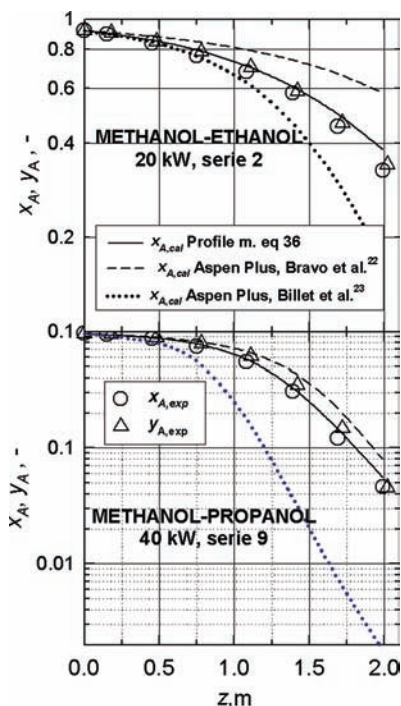


Figure 11. Experimental concentration profiles and profiles calculated from the *Aspen Plus* simulation model and from the profile method correlation (36).

calculated from the profile method correlations (36) and (37) are also plotted in the figure. The product concentrations measured on our distillation column having 5.5 theoretical plates differ considerably from those calculated by the *Aspen Plus* program. The RBF model gives 30% and 70% higher and the BS model (Dr. Schultes informed us that ASPEN has made noticeable mistakes incorporating the BS model into the program simulation and that ASPEN has been informed about these mistakes; unfortunately, it will take some time before corrections will be made) 250 and 1800% lower product concentrations in comparison with the experimental values. The profile method correlations (36) and (37) fit the profiles accurately.

5.6. HETP Values and Relative Liquid-Side Mass-Transfer Resistance. The experimental HETP values were calculated from a number of theoretical plates, as part of the packing, delineated by the liquid concentrations measured at the top and base of the packing part and by the actual height of this part. These are compared with the HETP values evaluated from the concentration profiles calculated by integration of the rate-based model (21), using k_{LA} and k_{VA} values, calculated from the original RBF, BS, and DELFT models or from their corrected versions, i.e., from eqs 36–38, respectively. The resultant values are plotted in Figure 12 for the M–P and M–E

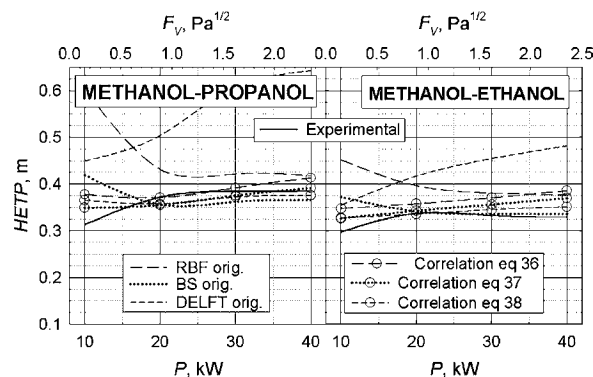


Figure 12. HETP evaluated from the original models RBF, BS, and DELFT or their corrected versions by the profile method, i.e., from eqs 36–38 respectively.

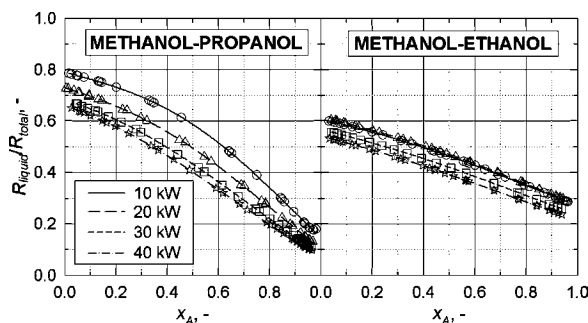


Figure 13. Relative liquid-side mass-transfer resistances calculated from eq 1 using k_{LA} and k_{VA} obtained by the profile method, using the RBF model with corrected dependence on the velocity of the phases, i.e., with $b_{L,profile}$ and $b_{V,profile}$.

distillation systems. The following conclusions result from the data presented in the figure: (i) HETP values predicted by the original RBF and DELFT models differ considerably from the experimental results; the differences amount to as much as 100%; the original BS model fits the experimental HETP values the best; the maximum difference makes 20% only. (ii) the experimental HETP values are consistent with the values calculated from the three corrected models, RBF, BS, and DELFT, i.e., from the correlations (36), (37), and (38), respectively. (iii) HETP values calculated from these three correlations practically coincide; the differences between them amount to 8% at most.

Variations of the relative liquid-side mass-transfer resistance along the column underlie the applicability of the profile method for the separate evaluation of k_{LA} and k_{VA} from the concentration profile in the distillation column. The resistance calculated from eq 1 using the mass-transfer coefficients obtained by the profile method, using the RBF model with corrected dependence on the velocity of the phases, is shown in Figure 13. The resistance decreases from the base to the top of the column in all of the distillation systems used and does not manifest any extreme such as, e.g., the ethanol–water system.⁸ The greatest change in the resistance occurs in the M–P system at the lowest reboiler duty of 10 kW (from 80% to 20%), and the least change occurs in the M–E system at the highest reboiler duty of 40 kW (from 50% to 10%). In any case, the variation is sufficient for the successful application of the profile method in these distillation systems.

6. Conclusions

The profile method for the simultaneous determination of vapor- and liquid-side volumetric mass-transfer coefficients in

a distillation column was successfully applied on structured packing Mellapak250Y for the atmospheric distillation of three alcoholic systems: M–E, E–P, and M–P. This method calculates the transport coefficients by comparing the concentration profiles measured in both phases with the simulated profiles. The dependence of the coefficients $k_L a$ and $k_V a$ on the phase flows and physicochemical properties has been considered in the form assumed in the RBF, BS, or DELFT models, and their variances, which are necessary for the purpose of optimization, have been retained by application of the multiplication parameters b_L and b_V . The choice of the structured packing with minor axial mixing of the phases was driven by the intention to apply a simple plug-flow model for both phases.

It was discovered that the relative liquid-side mass-transfer resistance decreases from the base to the top of the column in all of the distillation systems used and does not manifest any extreme. Variations in the resistance along the column range between 80% and 10% for the M–P system and between 50% and 20% for the M–E system.

The liquid phase along the entire column is overheated for all of the three distillation systems. The highest overheating was registered for the M–P system, reaching 3 °C around the equimolar concentration of the mixture, in which the temperature difference of the phases and mass-transfer intensity achieve maximum values. The vapor phase was more or less saturated.

The convective flow of a more volatile ingredient, methanol, induced by the total flow of the mixture through an interface, reaches up to 25% and 12% of the flow of methanol in the M–P and M–E systems, respectively, but its influence on the parameters b_L and b_V in comparison with their evaluated values, assuming equimolar counterdiffusion, reaches 6% at the most.

The volumetric mass-transfer coefficients obtained by the profile method differ considerably from those calculated from the original RBF, BS, and DELFT models. The original models overvalue the $k_L a$ coefficients (by up to 6.3 times; DELFT model) and undervalue the $k_V a$ coefficients (by up to 2 times). The coefficients evaluated by the profile method with these three different RBF, BS, and DELFT models, using the best-fit parameters b_L and b_V , demonstrate mutual compatibility.

The best-fit b_L and b_V parameters depend on the reboiler duty, i.e., on phase flow rates. This indicates that none of the models fits precisely with the dependence of the volumetric mass-transfer coefficients on the phase velocities. According to the profile method, $k_L a$ depends on the phase flow in accordance with the relation $k_L a \propto u_L^{1.18}$, which is considerably greater than what the original models predict (approximately $k_L a \propto u_L^{0.7}$), and $k_V a$ is in accordance with the relation $k_V a \propto u_V^{0.775}$, which is considerably less than what the models predict (approximately $k_V a \propto u_V^{1.2}$). The best-fit parameters $b_{L,profile}$ and $b_{V,profile}$ evaluated by the profile method using this corrected dependence of the coefficients on the velocity of phases depend neither on the reboiler duty nor on the distillation system and are specific only for the model (RBF, BS, or DELFT). Correlations of $k_L a$ and $k_V a$ coefficients with the improved flow dependence according to the profile method are presented in the form of eqs 36, 37 and 38. HETP values calculated according to the three suggested correlations practically coincide, with the differences between them reaching 8% at most.

The experimental concentration profiles differ from the profiles calculated from the *Aspen Plus* simulation program. The differences reach up to 70% for the RBF model and 1800% for the BS model. The profile method correlation (36) fits the profiles accurately.

The profile method allows evaluation of the volumetric mass-transfer coefficients in the individual phases in distillation columns, in a manner similar to that also possible in absorption columns, and thereby substantial improvement to the mass-transfer models of distillation and to their validation.

Appendix

A full list of the source data is given in Tables A1–A3 for the distillation systems M–E, E–P, and M–P, respectively.

Nomenclature

- a = effective mass-transfer area, m^{-1}
 a_p = packing geometrical area, m^{-1}
 B = superficial liquid velocity, $m\ h^{-1}$
 b = triangular channel base dimension, m^{-1}
 $b_{L,V}$ = empirical correction factors obtained by using eq 25 in the profile method
 $b_{L,V,profile}$ = empirical correction factors obtained by using eq 35 in the profile method
 $b_{L,V,orig}$ = multiplication parameters used in the original models RBF, BS, and DELFT
 C_V, C_L = packing-specific constant for the BS model
 c = molar concentration, $mol\ m^{-3}$
 c_p = molar heat, $kJ\ kmol^{-1}\ K^{-1}$
 D = diffusion coefficient, $m^2\ s^{-1}$
 d_h = equivalent hydraulic diameter defined in eq 8, m
 d_{hV} = packing characteristic dimension, eq 12, m
 d_s = side dimension of packing corrugation, m
HETP = height equivalent to a theoretical plate, m
 F = volumetric flow rate of reflux, $L\ min^{-1}$
 $F_V = u_V \sqrt{\rho_V} =$ gas capacity factor, $Pa^{1/2}$
 F_{SE} = surface enhancement factor
 g = gravity acceleration, $m\ s^{-2}$
 h = triangular channel height, m
 h_{pe} = height of the packing element, m
 h = molar enthalpy, $kJ\ kmol^{-1}$
 h_{LB} = liquid holdup given by eqs 11 and 12 in ref 4
 h_{LR} = liquid holdup given by eq 19 in ref 3
 Δh_{mix} = heat of mixing, $kJ\ kmol^{-1}$
 Δh_{vap} = molar heat of vaporization, $kJ\ kmol^{-1}$
 K_V = overall mass-transfer coefficient, $m\ s^{-1}$
 K_A = equilibrium coefficient in the equation $y_A = K_A x_A$
 k_L = liquid-side mass-transfer coefficient on a more volatile component concentration, $m\ s^{-1}$
 k_V = vapor-side mass-transfer coefficient on a more volatile component concentration, $m\ s^{-1}$
 $k_L a$ = liquid-side volumetric mass-transfer coefficient, s^{-1}
 $k_V a$ = vapor-side volumetric mass-transfer coefficient, s^{-1}
 $l_{V,pe}$ = length of the gas flow channel in a packing element, m
 L = liquid-phase molar flow, $kmol\ s^{-1}$
 $m_A = dc_{AV}^*/dc_{AL}^* =$ local slope of equilibrium curve
 n_D = refractive index
 N = molar flux transferred per unit height of packing, $kmol\ m^{-1}\ s^{-1}$
 p = atmospheric pressure, Torr
 P = reboiler duty, kW
 r = quantity defined by eq 23
 R_{liquid} = relative liquid-phase mass-transfer resistance defined by eq 1
 Re_{vrv} = Reynolds number defined by eq 18
 s = objective function defined by eq 28
 S = column cross section, m^2
 $Sc_i = \mu_i / \rho_i D_i =$ Schmidt number ($i = V, L$)

Table A2. Source Experimental Data System E-P

z, m	series 1			series 2			series 3			series 4			series 5			series 6			series 7			series 8					
	t_{sat} , °C	x_A , yA	t_{exp} , °C	t_{sat} , °C	x_A , yA	t_{exp} , °C	t_{sat} , °C	x_A , yA	t_{exp} , °C	t_{sat} , °C	x_A , yA	t_{exp} , °C	t_{sat} , °C	x_A , yA	t_{exp} , °C	t_{sat} , °C	x_A , yA	t_{exp} , °C	t_{sat} , °C	x_A , yA	t_{exp} , °C	t_{sat} , °C	x_A , yA	t_{exp} , °C	t_{sat} , °C	x_A , yA	
	P = 40 kW, F = 3.955 L min ⁻¹ , p = 749 Torr			P = 30 kW, F = 2.86 L min ⁻¹ , p = 749 Torr			P = 20 kW, F = 1.82 L min ⁻¹ , p = 749 Torr			P = 10 kW, F = 0.81 L min ⁻¹ , p = 749 Torr			P = 40 kW, F = 3.98 L min ⁻¹ , p = 749 Torr			P = 30 kW, F = 2.87 L min ⁻¹ , p = 749 Torr			P = 20 kW, F = 1.8 L min ⁻¹ , p = 745 Torr			P = 10 kW, F = 0.795 L min ⁻¹ , p = 745 Torr					
0.00	79.05	0.9113	79.09	0.9085	79.33	0.9199	78.44	0.9592	81.19	0.7542	81.21	0.7527	80.48	0.7947	80.48	0.7947	80.48	0.7527	81.21	0.7527	80.48	0.7947	80.48	0.7947	80.48	0.7947	80.48
0.15	79.38	0.8862	79.64	0.8767	79.71	0.8901	78.82	0.9292	81.89	0.7064	82.09	0.6929	81.28	0.7388	81.28	0.7388	81.28	0.6929	82.09	0.6929	81.28	0.7388	81.28	0.7388	81.28	0.7388	81.28
0.45	80.50	0.8035	80.94	0.7921	81.17	0.7995	79.46	0.8806	79.68	0.5652	84.87	0.5454	83.57	0.5890	83.57	0.5890	83.57	0.5454	84.87	0.5454	83.57	0.5890	83.57	0.5890	83.57	0.5890	83.57
0.75	81.77	0.7141	82.53	0.6891	83.09	0.6894	80.83	0.7799	81.42	0.4330	87.65	0.4012	86.03	0.4457	86.03	0.4457	86.03	0.4012	87.65	0.4012	86.03	0.4457	86.03	0.4457	86.03	0.4457	86.03
1.08	83.81	0.5824	85.15	0.5495	85.65	0.5495	82.59	0.6598	83.90	0.2870	90.86	0.2705	89.38	0.3251	89.38	0.3251	89.38	0.2705	90.86	0.2705	89.38	0.3251	89.38	0.3251	89.38	0.3251	89.38
1.39	86.63	0.4207	88.05	0.4211	88.05	0.4574	85.24	0.4974	87.02	0.1652	93.26	0.1721	91.95	0.2372	91.95	0.2372	91.95	0.1721	93.26	0.1721	91.95	0.2372	91.95	0.2372	91.95	0.2372	91.95
1.69	89.55	0.2762	90.98	0.2563	91.41	0.2781	88.34	0.3338	89.88	0.0919	94.92	0.0919	94.92	0.1223	94.92	0.1223	94.92	0.0919	94.92	0.0919	94.92	0.1223	94.92	0.1223	94.92	0.1223	94.92
1.99	92.21	0.1612	93.40	0.1607	93.50	0.1682	91.71	0.1819	93.17	0.0492	95.93	0.0492	95.93	0.0492	95.93	0.0492	95.93	0.0492	95.93	0.0492	95.93	0.0492	95.93	0.0492	95.93	0.0492	95.93
2.10																											
	Liquid			Liquid			Liquid			Liquid			Liquid			Liquid			Liquid			Liquid			Liquid		
0.00	80.44	0.8943	80.82	0.8862	80.99	0.8960	79.33	0.9415	79.49	0.7252	84.34	0.7045	84.61	0.7569	83.37	0.7569	83.37	0.7045	84.61	0.7045	83.37	0.7569	83.37	0.7569	83.37	0.7569	83.37
0.18	82.13	0.8202	82.68	0.8144	82.77	0.8253	80.54	0.8901	80.83	0.5853	87.42	0.5743	87.61	0.6305	86.33	0.6305	86.33	0.5743	87.61	0.5743	86.33	0.6305	86.33	0.6305	86.33	0.6305	86.33
0.48	83.94	0.7365	84.53	0.7297	84.61	0.7384	82.10	0.8213	82.48	0.4522	89.94	0.4479	89.94	0.5080	88.71	0.5080	88.71	0.4479	89.94	0.4479	88.71	0.5080	88.71	0.5080	88.71	0.5080	88.71
1.11	86.57	0.6076	87.31	0.6011	87.36	0.6048	84.61	0.7049	84.96	0.3052	92.61	0.3122	92.48	0.3621	91.39	0.3621	91.39	0.3122	92.48	0.3122	91.39	0.3621	91.39	0.3621	91.39	0.3621	91.39
1.42	89.56	0.4470	90.34	0.4387	90.45	0.4501	88.18	0.5232	88.81	0.1829	94.61	0.1814	94.58	0.2339	93.65	0.2339	93.65	0.1814	94.58	0.1814	93.65	0.2339	93.65	0.2339	93.65	0.2339	93.65
1.72	92.26	0.2884	92.91	0.2987	92.71	0.3140	90.81	0.3752	91.34	0.0919	95.82	0.1041	95.61	0.1398	94.92	0.1398	94.92	0.1041	95.61	0.1041	94.92	0.1398	94.92	0.1398	94.92	0.1398	94.92
2.02	94.14	0.1691	94.81	0.1711	94.69	0.1790	93.53	0.2088	94.04	0.0492	96.56	0.0518	96.43	0.0699	96.03	0.0699	96.03	0.0518	96.43	0.0518	96.03	0.0699	96.03	0.0699	96.03	0.0699	96.03
2.10																											
	Vapor			Vapor			Vapor			Vapor			Vapor			Vapor			Vapor			Vapor			Vapor		
0.00	84.67	0.5224	84.35	0.5416	84.35	0.5416	82.80	0.6373	79.22	0.9168	79.18	0.9196	79.31	0.9099	79.31	0.9099	79.31	0.9168	79.22	0.9168	79.31	0.9099	79.31	0.9099	79.31	0.9099	79.31
0.15	85.92	0.4518	87.06	0.4518	87.04	0.4540	85.15	0.4948	86.82	0.8925	79.67	0.8925	79.67	0.8925	79.67	0.8925	79.67	0.8925	79.67	0.8925	79.67	0.8925	79.67	0.8925	79.67	0.8925	79.67
0.45	89.13	0.2893	90.43	0.2856	90.47	0.2724	88.13	0.3371	89.30	0.8195	80.80	0.8195	80.80	0.8195	80.80	0.8195	80.80	0.8195	80.80	0.8195	80.80	0.8195	80.80	0.8195	80.80	0.8195	80.80
0.75	91.50	0.1849	92.83	0.1716	93.02	0.1721	91.44	0.1873	92.68	0.7236	82.53	0.7236	82.53	0.7236	82.53	0.7236	82.53	0.7236	82.53	0.7236	82.53	0.7236	82.53	0.7236	82.53	0.7236	82.53
1.08	93.59	0.1021	94.86	0.1026	94.76	0.1092	93.28	0.1137	94.66	0.6201	84.58	0.6201	84.58	0.6201	84.58	0.6201	84.58	0.6201	84.58	0.6201	84.58	0.6201	84.58	0.6201	84.58	0.6201	84.58
1.39	94.98	0.0513	95.75	0.0570	95.61	0.0735	93.46	0.0663	95.46	0.5156	86.40	0.5156	86.40	0.5156	86.40	0.5156	86.40	0.5156	86.40	0.5156	86.40	0.5156	86.40	0.5156	86.40	0.5156	86.40
1.69	95.71	0.0258	96.38	0.0253	96.34	0.0310	95.45	0.0347	96.13	0.3325	90.18	0.3325	90.18	0.3325	90.18	0.3325	90.18	0.3325	90.18	0.3325	90.18	0.3325	90.18	0.3325	90.18	0.3325	90.18
1.99	96.10	0.0127	96.67	0.0143	96.59	0.0169	95.94	0.0179	96.48	0.2122	92.72	0.2122	92.72	0.2122	92.72	0.2122	92.72	0.2122	92.72	0.2122	92.72	0.2122	92.72	0.2122	92.72	0.2122	92.72
2.10																											
	Liquid			Liquid			Liquid			Liquid			Liquid			Liquid			Liquid			Liquid			Liquid		
0.00	88.79	0.4825	89.39	0.4708	89.59	0.4756	87.26	0.5648	87.81	0.8998	80.61	0.8998	80.61	0.8998	80.61	0.8998	80.61	0.8998	80.61	0.8998	80.61	0.8998	80.61	0.8998	80.61	0.8998	80.61
0.18	91.69	0.3149	92.49	0.3080	92.43	0.3209	90.68	0.3748	91.35	0.8408	82.14	0.8408	82.14	0.8408	82.14	0.8408	82.14	0.8408	82.14	0.8408	82.14	0.8408	82.14	0.8408	82.14	0.8408	82.14
0.48	93.63	0.1932	94.23	0.2025	94.03	0.2155	92.74	0.2496	93.34	0.7699	83.83	0.7699	83.83	0.7699	83.83	0.7699	83.83	0.7699	83.83	0.7699	83.83	0.7699	83.83	0.7699	83.83	0.7699	83.83
1.11	94.94	0.1066	95.56	0.1163	95.38	0.1258	94.40	0.1428	94.96	0.6551	86.39	0.6551	86.39	0.6551	86.39	0.6551	86.39	0.6551	86.39	0.6551	86.39	0.6551	86.39	0.6551	86.39	0.6551	86.39
1.42	95.66	0.0575	96.39	0.0642	96.27	0.0689	95.39	0.0761	96.09	0.5110	89.70	0.5110	89.70	0.5110	89.70	0.5110	89.70	0.5110	89.70	0.5110	89.70	0.5110	89.70	0.5110	89.70	0.5110	89.70
1.72	96.13	0.0242	96.73	0.0316	96.58	0.0363	95.84	0.0446	96.38	0.3721	91.30	0.3721	91.30	0.3721	91.30	0.3721	91.30	0.3721	91.30	0.3721	91.30	0.3721	91.30	0.3721	91.30	0.3721	91.30
2.02	96.32	0.0111	96.99	0.0143	96.90	0.0164	96.15	0.0232	96.75	0.2204	94.25	0.2204	94.25	0.2204	94.25	0.2204	94.25	0.2204	94.25	0.2204	94.25	0.2204	94.25	0.2204	94.25	0.2204	94.25
2.10																											
	Vapor			Vapor			Vapor			Vapor			Vapor			Vapor			Vapor			Vapor			Vapor		
0.00	84.67	0.5224	84.35	0.5416	84.35	0.5416	82.80	0.6373	79.22	0.9168	79.18	0.9196	79.31	0.9099	79.31	0.9099	79.31	0.9168	79.22	0.9168	79.31	0.9099	79.31	0.9099	79.31	0.9099	79.31
0.15	85.92	0.4518	87.06	0.4518	87.04	0.4540	85.15	0.4948	86.82	0.8925	79.67	0.8925	79.67	0.8925	79.67	0.8925</											

Table A3. Source Experimental Data System M-P

z, m	series 1			series 3			series 8			series 9			series 12			series 13			series 14			series 15		
	t_{sat} , °C	x_A , yA	t_{exp} , °C	t_{sat} , °C	x_A , yA	t_{exp} , °C	t_{sat} , °C	x_A , yA	t_{exp} , °C	t_{sat} , °C	x_A , yA	t_{exp} , °C	t_{sat} , °C	x_A , yA	t_{exp} , °C	t_{sat} , °C	x_A , yA	t_{exp} , °C	t_{sat} , °C	x_A , yA	t_{exp} , °C	t_{sat} , °C	x_A , yA	
0.00	67.44	0.8028		65.12	0.9320		64.66	0.9615		64.36	0.9814		64.75	0.9557		64.60	0.9657		64.45	0.9757		64.45	0.9757	
0.15	70.54	0.6728	72.43	65.49	0.9081	66.18	64.91	0.9453	65.44	64.60	0.9656	65.17	65.09	0.9337	64.97	0.9417	65.86	64.62	64.62	0.9644	65.86	64.62	0.9644	64.88
0.45	78.94	0.4045	80.19	67.79	0.7880	69.06	66.15	0.8706	67.26	65.32	0.9193	65.98	66.77	0.8374	66.27	0.8639	67.34	65.35	65.35	0.9176	67.34	65.35	0.9176	65.97
0.75	87.45	0.1903	88.48	71.86	0.6258	74.16	68.71	0.7475	70.67	67.21	0.8156	68.91	70.32	0.6824	69.54	0.7130	71.81	66.89	66.89	0.8317	71.81	66.89	0.8317	68.19
1.08	91.84	0.0938	93.05	79.19	0.3987	81.26	74.14	0.5491	76.54	71.19	0.6500	74.33	76.47	0.4768	78.71	0.4968	84.59	78.62	70.31	0.6830	84.59	78.62	0.6830	72.45
1.39	93.75	0.0542	94.50	87.84	0.1822	89.13	78.37	0.4215	80.60	77.58	0.4442	80.57	84.26	0.2667	85.80	0.3027	84.59	82.82	82.82	0.4473	84.59	82.82	0.4473	79.76
1.69	95.95	0.0101	96.45	93.14	0.0673	93.84	88.04	0.1776	89.53	88.26	0.1726	89.67	91.86	0.0940	91.54	0.1009	92.37	86.78	86.78	0.2065	92.37	86.78	0.2065	88.13
1.99	96.22	0.0050	96.67	95.32	0.0234	95.87	94.19	0.0460	95.00	92.93	0.0717	93.98	94.63	0.0371	94.54	0.0389	95.17	92.30	92.30	0.0849	95.17	92.30	0.0849	93.24
2.10																								
	Liquid																							
0.00																								
0.18	77.86	0.7416	77.24	68.89	0.9205	69.02	67.05	0.9507	67.27	65.53	0.9733	65.90	67.69	0.9410	67.72	66.76	0.9549	66.92	65.85	0.9684	66.92	65.85	0.9684	66.05
0.48	86.38	0.4758	85.60	73.93	0.8175	74.62	68.69	0.8893	70.57	68.26	0.9324	68.29	71.98	0.8699	71.47	71.12	0.8855	70.65	68.46	0.9292	70.65	68.46	0.9292	68.32
0.78	91.25	0.2711	90.93	79.50	0.6787	80.24	75.80	0.7915	75.43	72.40	0.8620	72.07	77.32	0.7557	76.66	76.35	0.7789	75.58	72.33	0.8633	75.58	72.33	0.8633	72.06
1.11	94.44	0.1124	94.54	86.39	0.4533	87.00	82.29	0.6178	81.66	79.32	0.7043	78.58	84.39	0.5487	83.41	83.85	0.5671	82.75	78.06	0.7372	82.75	78.06	0.7372	77.44
1.42	95.74	0.0416	96.20	92.21	0.2151	92.46	89.54	0.3492	89.17	87.07	0.4506	86.54	90.90	0.2888	90.42	90.73	0.2965	90.11	85.81	0.4984	90.11	85.81	0.4984	85.20
1.72	96.22	0.0147	96.65	95.59	0.0766	95.14	93.80	0.1478	93.84	92.02	0.2365	91.84	94.18	0.1280	94.17	93.94	0.1404	93.74	91.53	0.2595	93.74	91.53	0.2595	91.36
2.02	96.39	0.0047	96.93	97.00	0.0231	96.11	95.71	0.0454	96.18	95.18	0.0743	95.47	95.80	0.0401	96.15	95.77	0.0422	96.10	94.88	0.0906	96.10	94.88	0.0906	95.07
2.10				0.0068		0.0386	0.0195		0.0368			0.0368		0.0192			0.0216							0.0469
	Vapor																							
0.00																								
0.18																								
0.48																								
0.78																								
1.11																								
1.42																								
1.72																								
2.02																								
2.10																								
	Liquid																							
0.00																								
0.15	64.56	0.9684		64.62	0.9645		64.61	0.9698		64.31	0.9893		64.58	0.9667		64.56	0.9685		64.39	0.9797		64.39	0.9797	
0.45	65.92	0.8835	66.84	64.85	0.9491	65.22	64.99	0.9446	65.83	64.50	0.9765	64.96	65.24	0.9241	66.39	65.16	0.9292	66.26	64.76	0.9555	66.26	64.76	0.9555	65.50
0.75	68.49	0.7570	70.28	68.20	0.7694	69.98	66.62	0.8487	67.20	65.02	0.9425	65.55	67.04	0.8238	68.61	66.94	0.8291	68.54	65.82	0.8892	68.54	65.82	0.8892	66.98
1.08	73.46	0.5710	75.73	73.07	0.5842	75.53	69.38	0.7222	71.57	67.14	0.8227	68.49	73.27	0.5775	75.66	72.98	0.5871	75.51	69.92	0.6982	75.51	69.92	0.6982	72.51
1.39	80.99	0.3499	82.99	81.80	0.3288	83.51	81.82	0.3299	83.31	83.51	0.2871	85.29	90.65	0.1199	91.85	89.94	0.1352	91.43	88.45	0.1683	91.43	88.45	0.1683	89.58
1.69	90.01	0.1338	91.12	89.89	0.1363	90.78	91.66	0.0997	92.49	91.40	0.1054	91.71	94.84	0.0330	95.22	94.79	0.0338	95.13	93.93	0.0513	95.13	93.93	0.0513	94.17
1.99	93.81	0.0536	94.51	93.84	0.0530	94.53	94.43	0.0424	95.11	94.95	0.0321	95.38	95.91	0.0117	96.36	95.97	0.0105	96.37	95.68	0.0162	96.37	95.68	0.0162	96.06
2.10																								
	Vapor																							
0.00																								
0.18	66.57	0.9578	66.72	66.75	0.9551	66.90	66.68	0.9571	66.87	64.97	0.9835	65.26	67.25	0.9477	67.52	66.99	0.9516	67.36	65.85	0.9685	67.36	65.85	0.9685	66.24
0.48	70.07	0.9035	69.71	70.44	0.8972	70.05	70.72	0.8935	70.37	67.34	0.9473	67.46	73.72	0.8362	72.86	73.36	0.8435	72.60	70.45	0.8971	72.60	70.45	0.8971	70.09
0.78	74.79	0.8139	74.26	75.21	0.8047	74.71	75.81	0.7928	75.16	71.83	0.8738	71.68	80.95	0.6583	79.65	80.45	0.6727	79.22	76.84	0.7674	79.22	76.84	0.7674	76.06
1.11	81.79	0.6330	80.80	81.64	0.6377	80.83	83.19	0.5911	82.23	79.80	0.6929	78.75	88.93	0.3755	87.66	88.94	0.3750	87.50	85.90	0.4951	87.50	85.90	0.4951	84.21
1.42	88.98	0.3733	88.36	88.86	0.3784	88.21	90.07	0.3293	89.50	89.28	0.3632	88.43	94.27	0.1233	94.03	94.17	0.1285	93.87	92.88	0.1943	93.87	92.88	0.1943	92.36
1.72	93.23	0.1768	93.06	93.44	0.1659	93.26	93.60	0.1616	93.44	93.36	0.1736	92.99	95.64	0.0489	95.75	95.61	0.0510	95.71	94.97	0.0858	95.71	94.97	0.0858	94.87
2.02	95.50	0.0569	95.72	95.56	0.0536	95.83	95.79	0.0445	96.09	95.74	0.0478	95.96	96.24	0.0153	96.70	96.27	0.0138	96.70	96.11	0.0231	96.70	96.11	0.0231	96.48
2.10																								

Series 2, 4-7, 10, 11, and 16 were not utilized for evaluation because molar fractions of one of components reached values higher than 0.99 at the top or bottom of the column.

$Sh_{V,i}$ = Sherwood number (i = turd, lam) defined by eq 16 or 17
 t = temperature, °C

u = superficial velocity, m s^{-1}

u_{LE} = average liquid velocity in an actual liquid-flow cross section defined by eq 3, m s^{-1}

u_{VE} = average liquid velocity in an actual liquid-flow cross section defined by eq 5, m s^{-1}

x_A = mole fraction of a more volatile component in the liquid phase

y_A = mole fraction of a more volatile component in the vapor phase

z = packing height coordinate taken from the top ($z = 0$), m

Subscripts

L = liquid phase

V = vapor/gas phase

PM = profile method

profile = profile method

orig = original RBF, BS, or DELFT model

w = vapor–liquid interface

Superscripts

$\alpha, \beta, \gamma, \delta, \varepsilon$ = exponents in relation (29)

λ, ν = exponents in relation (33)

* = equilibrium value

Greek Symbols

α = corrugation angle, deg

δ = liquid film thickness defined by eq 13 or 29, m

ε = packing porosity

φ = fraction of the channel occupied by the liquid defined by eq 19

γ = contact angle, deg

μ = viscosity, Pa s

ρ = density, kg m^{-3}

σ = surface tension, N m^{-1}

ξ_{VL} = friction factor defined by eq 19

Ω = packing surface void fraction

Acknowledgment

Financial support from the Ministry of Education (Grant MSM 6046137306) is gratefully acknowledged.

Literature Cited

(1) Wang, G. Q.; Yuan, X. G.; Yu, K. T. Review of mass-transfer correlations for packed columns. *Ind. Eng. Chem. Res.* **2005**, *44*, 8715.

(2) Rocha, J. A.; Bravo, J. L.; Fair, J. R. Distillation columns containing structured packings: A comprehensive model for their performance. 2. Mass-transfer model. *Ind. Eng. Chem. Res.* **1996**, *35*, 1660.

(3) Rocha, J. A.; Bravo, J. L.; Fair, J. R. Distillation columns containing structured packings: A comprehensive model for their performance. 1. Hydraulic models. *Ind. Eng. Chem. Res.* **1993**, *32*, 641.

(4) Billet, R.; Schultes, M. Prediction of mass transfer columns with dumped and arranged packings. Updated summary of the calculation method of Billet and Schultes. *Trans. Inst. Chem. Eng.* **1999**, *77*, 498.

(5) Olujić, Ž.; Kamerbeek, A. B.; de Graauw, J. A. Corrugation geometry based model for efficiency of structured distillation packing. *Chem. Eng. Proc.* **1999**, *38*, 683.

(6) Taylor, R. (Di)Still modeling after all these years: A view of the state of the art. *Ind. Eng. Chem. Res.* **2007**, *46*, 4349.

(7) Linek, V.; Moucha, T.; Prokopová, E.; Rejl, J. F. Simultaneous determination of vapour- and liquid-side volumetric mass transfer coefficients in distillation column. *Trans. Inst. Chem. Eng., Chem. Eng. Res. Des.* **2005**, *83* (A8), 979.

(8) Rejl, F.; Linek, V.; Moucha, T.; Prokopová, E.; Valenz, L.; Hovorka, F. Vapour- and liquid-side volumetric mass transfer coefficients measured in distillation column. Comparison with data calculated from absorption correlations. *Chem. Eng. Sci.* **2006**, *61*, 6096.

(9) Shi, M. G.; Mersmann, A. Effective interfacial area in packed columns. *Ger. Chem. Eng.* **1985**, *8*, 87.

(10) Onda, K.; Takeuchi, H.; Okumoto, Y. Mass transfer coefficients between gas and liquid phases in packed columns. *J. Chem. Eng. Jpn.* **1968**, *1*, 56.

(11) Vargaftik, N. B. *Tables on the Thermophysical Properties of Liquids and Gases*, 2nd ed.; Wiley: New York, 1975.

(12) Zábanský, M.; Růžička, V.; Majer, V.; Domalski, E. S. Heat Capacities of Liquids, Critical Review and Recommended Values. *Journal of Physical and Chemical Reference Data, Monograph*; American Chemical Society: Washington, DC, 1996; No. 6.

(13) Majer, V.; Svoboda, V. Enthalpies of Vaporization of Organic Compounds. *IUPAC Chemical Data Series No. 32*; Blackwell: Oxford, U.K., 1985.

(14) Yaws, C. L. *Chem. Eng.* **1976**, Oct 25.

(15) Ried, R. C.; Prausnitz, J. M.; Poling, B. E. *The Properties of Gases and Liquids*, 4th ed.; McGraw-Hill Book Company: Singapore, 1988.

(16) Chung, T. H.; Lee, L. L.; Starling, K. E. Applications of Kinetic Gas Theories and Multiparameter Correlation for Prediction of Dilute Gas Viscosity and Thermal Conductivity. *Ind. Eng. Chem. Fundam.* **1984**, *23*, 8.

(17) Gmehling, J.; Onken, N. Vapor–Liquid Equilibrium Data Collection, Alcohols—Supplement 3, Chemistry Data Series. *Dechema, Frankfurt am Main* **1991**, *1*, Part 2e.

(18) Zarzycki, R.; Chacuk, A. *Absorption Fundamentals & Applications*; Pergamon Press: London, 1993; p 42.

(19) Krishna, R.; Wesselingh, J. A. The Maxwell–Stefan approach to mass transfer. *Chem. Eng. Sci.* **1997**, *52*, 861.

(20) Valenz, L. Study of interfacial heat and mass transfer in packed distillation and absorption columns. An effect of axial dispersion in both phases. Dissertation, Prague Institute of Chemical Technology, Prague, Czech Republic, 2009.

(21) Rejl, J. F.; Linek, V.; Moucha, T.; Valenz, L. Methods standardization in the measurement of mass transfer characteristics in packed absorption columns. *Chem. Eng. Res. Des.* **2009**, *87*, 695.

(22) Bravo, J. L.; Rocha, J. A.; Fair, J. R. A comprehensive model for the performance of columns containing structured packings. *Inst. Chem. Eng. Symp. Ser.* **1992**, *128*, A489 Distillation and Absorption '92, Vol. 1.

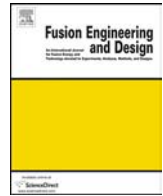
(23) Billet, R.; Schultes, M. Predicting mass transfer in packed columns. *Chem. Eng. Technol.* **1993**, *16* (1), 1.

Received for review October 28, 2009

Revised manuscript received February 11, 2010

Accepted March 4, 2010

IE901690M



The engineering sizing of the packed desorption column of hydrogen isotopes from Pb–17Li eutectic alloy. A rate based model using experimental mass transfer coefficients from a Melodie loop

V. Linek^{a,*}, L. Košek^b, T. Moucha^a, F.J. Rejl^a, M. Kordač^a, L. Valenz^a, M. Opletal^a

^a Prague Institute of Chemical Technology, Department of Chemical Engineering, CZ-166 28 Prague 6, Czech Republic

^b Research Centre Řež, CZ-250 68 Husinec-Řež, Czech Republic

HIGHLIGHTS

- The model of hydrogen isotopes desorption from lead lithium alloy in packed column is presented.
- Mass transfer coefficient $k_L a$ are evaluated from Alpy's Melodie loop experiments.
- Packing height and efficiency of packed columns in DEMO plant for DCLL and HCLL are evaluated.
- Effects of liquid phase axial dispersion, surface tension and wettability of packing are evaluated.
- Effect of flow rate of the purge gas on packing height and desorption efficiency is evaluated.

ARTICLE INFO

Article history:

Received 27 February 2014

Received in revised form 24 May 2014

Accepted 28 May 2014

Available online 26 June 2014

Keywords:

Fusion

Tritium desorption from Pb–Li

Tritium extraction

Blanket concepts DCLL and HCLL

ABSTRACT

The model of the desorption of hydrogen isotopes from lead lithium alloy in a packed column is derived from the first principles using the plug flow in the liquid phase either the plug flow or ideal mixing in the gas phases. Sievert's law of non-linear equilibrium is followed. The volumetric mass transfer coefficient $k_L a$ and its dependence on the liquid metal flow rate are evaluated on the basis of the Melodie loop experiments.

The presented model is used for evaluation of the minimum flow rate of the purge gas for which the concentration of the isotope in the gas leaving the column is at its highest, while the driving force of the interfacial transport of the isotope is still not reduced and the tritium desorption efficiency is therefore retained. The potential effect of the axial dispersion in the gas and liquid phase is evaluated. Highlighted are the issues of the optimum packing geometric surface area, above which the efficiency starts to decrease, and of the role of the surface tension and the contact angle with regard to the wettability of the packing. On the basis of the findings related to these factors, the Mellapak 500 Y and Mellapak packings with flat surfaces are recommended for the tests aiming to intensify the tritium desorption efficiency in the packed columns. The models were used for the engineering sizing of the packed columns in two breeding blanket concepts for the DEMO plant – utilizing DCLL (dual coolant lead lithium) and HCLL (helium cooled lithium lead).

© 2014 Elsevier B.V. All rights reserved.

1. Introduction

Desorption from the liquid lead lithium eutectic alloy into an inert gas (He, H₂) in the column packed with structured packing was selected [1] as a favorable candidate for the process of tritium extraction. Using this system, the mass transfer resistance is concentrated in the liquid phase and there is no boundary layer at the

interface as there is with the metal membranes. The eddies ensuing from the bulk of the liquid bring a melt with a higher content of tritium to the interface, which is a faster process in comparison with diffusion through a boundary layer on a solid membrane surface.

Mohan et al. [2] presented a model of packed columns design for tritium desorption based on the HTU concept. Plug flow is applied and mass transfer resistances are considered in both phases. The mass transfer coefficients are evaluated using the correlations by Rocha et al. [3,4]. The stripping factor utilized for evaluating the overall mass transfer coefficient was calculated as the average slope of the equilibrium curve. The evaluation of the gas phase flow rate

* Corresponding author. Tel.: +420 220 443 298.
E-mail address: linekv@vscht.cz (V. Linek).

Nomenclature

A	$=\pi d^2/4$, cross section of column, m^2
A_c	parameters defined in Eq. (7), mol/m^3
A_p	parameters defined in Eq. (8), $Pa^{1/2}$
a	specific effective interfacial area, m^{-1}
a_t	specific geometric area of packing, m^{-1}
B	liquid load, m/h
$Bo_{G,L}$	$=u_{G,L}Z/E_{G,L}$ gas/liquid Bodenstein number
b	channel base of packing corrugation, m
$c_{G,L}$	bulk gas/liquid isotope concentration, mol/m^3
$c_{G1,L1}$	gas/liquid isotope concentration at inlet of the column, mol/m^3
$c_{G2,L2}$	gas/liquid isotope concentration at outlet of the column, mol/m^3
c_L^*	equilibrium isotope concentration at interface, mol/m^3
D_L	diffusion coefficient, m^2/s
d	diameter of column, m
d_h	hydraulic diameter $= 4\varepsilon/a_t$, m
d_s	characteristic length of packing (Mellapak 250Y = 16.1 mm), m
E	axial dispersion coefficient, m^2/s
Fi	film number $= \mu_L u_L / (d_s^2 \rho_L g)$
h	packing channel dimension – crimp height, m
K_S	Sievert constant, $mol/m^3 Pa^{1/2}$
k_L	mass transfer coefficient, m/s
$k_L a$	volumetric mass transfer coefficient, $1/s$
N, N_t	number of the plug flow and the true transfer units, respectively
p_G	partial pressure, Pa
p_L	equilibrium partial pressure, Pa
p_t	total pressure, Pa
$Q_{G,L}$	volumetric gas/liquid flow rate, Nm^3/h
R	gas constant $= 8.31 Pa m^3/mol, K$
Re_i	Reynolds number $= u_i d_s \rho_i / \eta_i$, ($i=L$ or G)
R_G	$= Q_G / Q_L = u_{GN} / u_L$ relative gas to liquid flow rate
R_T	relative tritium production rate per volume of liquid metal $= T_o / Q_L$, mol/m^3
r	roughness factor
s	packing channel side, m
t, T	temperature $^{\circ}C, K$
T_o	tritium production rate, mol/s
U_α	quantity defined in Eq. (14)
$u_{G,L}$	superficial gas/liquid velocity, m/s
$u_{GE,LE}$	interstitial/true gas/liquid velocity of the liquid film, m/s
u_{GN}	superficial gas velocity at normal conditions, m/s
V	quantity defined in Eq. (17)
z	longitudinal coordinate taken from the top of column, m
Z	height of packing, m
Z_t	true height of packing, m
Greek symbols	
α	relative increase of packing height $= Z/Z_{min}$
β	relative liquid metal flow rate led into packed column $= Q_L / Q_{LR}$
Γ	volumetric flow rate of the fluid per wetted perimeter in cross-sectional slice of the packing, $m^3/m s$
δ	corrugation angle, $^{\circ}$
ε	void fraction of packing

μ	viscosity, $Pa s$
η	$= (c_{L1} - c_{L2}) / c_{L1}$ desorption efficiency of the column
ρ	density, kg/m^3
σ	surface tension, N/m
θ	intrinsic contact angle, deg
Φ	apparent contact angle, deg

was based on the non-flooding criterion. This form of the column design for the desorption from liquid metal suffers from inaccuracies due to the prediction of the transport characteristics by using correlations based on the data obtained with aqueous systems. Aqueous systems have significantly different transport properties (in terms of their density, viscosity, surface tension) from those found in liquid metals.

The aim of this paper is to present the mass transfer model of the hydrogen isotopes desorption derived from first principles. The interfacial mass transfer of an isotope is described in terms of the liquid side volumetric mass transfer coefficient of hydrogen evaluated from the desorption experiments carried out by Alpy et al. [5,6] Mass transfer resistance in the gas-phase is neglected and the non-linear Sievert's law is used. This model is used for the sizing of the columns in two facilities, absorption/desorption circulation experimental loop and the columns at the DEMO plant for both the HCLL and the DCLL breeding blanket systems.

2. Model of the desorption of hydrogen isotopes from the Pb–17Li eutectic alloy

2.1. The plug flow model of phases

Assuming negligible gas side mass transfer resistance, the isotope mass balances can be recorded in a differential section dz of the column for both phases drawn schematically in Fig. 1 as follows:

$$u_L dc_L = -k_L a (c_L - c_L^*) dz \quad (1)$$

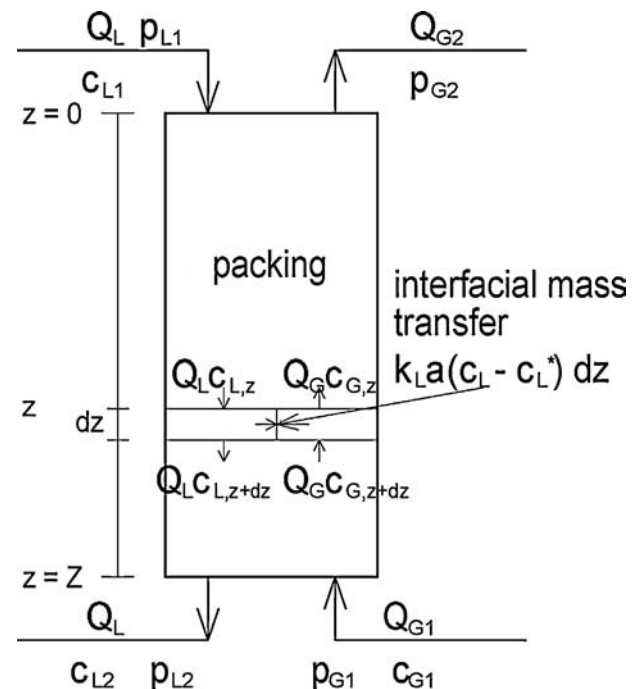


Fig. 1. Schema of the column.

$$u_G dc_G = -u_L dc_L = k_L a (c_L - c_L^*) dz \quad (2)$$

where u_G and u_L are superficial gas and liquid velocities in column, c_G and c_L are local bulk gas and liquid isotope concentrations, c_L^* is equilibrium isotope concentration at the interface and $k_L a$ is a volumetric mass transfer coefficient. Low solubility and diffusivity of the isotopes in the liquid alloy compared with that in the gas phase confirms the validity of the negligible gas side mass transfer resistance. The isotope concentration at the interface c_L^* is in equilibrium with the local gas phase concentration and is given by Sievert's law

$$\left[\frac{c_L^*}{K_S} \right]^2 = p_G = c_G RT \quad (3)$$

The local gas phase concentration is given by the overall mass balance

$$c_G = -\frac{u_L}{u_G} (c_{L1} - c_L) + c_{G2} = -\frac{u_L}{u_G} (c_{L2} - c_L) + c_{G1} \quad (4)$$

Explanation of the used symbols gives Fig. 1. Combination of relations (1) through (4) and integration of the resulting differential equation provides the following relation:

$$Z = \frac{u_L}{k_L a} \int_{c_{L2}}^{c_{L1}} \frac{dc_L}{c_L - K_S (u_L RT / u_G)^{1/2} (c_L - c_{L2} + c_{G1} u_G / u_L)^{1/2}} \quad (5)$$

among the height of packing Z , an isotope concentration in the outlet liquid metal c_{L2} , a flow rate of purge gas u_G and of lead lithium alloy u_L , an isotope concentration in the melt c_{L1} and in the purge gas c_{G1} entering the desorption column.

If the concentrations in the liquid phase are expressed in terms of the equilibrium partial pressures of the isotope, the relation (5) reduces to

$$Z = \frac{u_L}{k_L a} \int_{p_{L2}^{1/2}}^{p_{L1}^{1/2}} \frac{d(p_L^{1/2})}{p_L^{1/2} - (K_S p_t \cdot 0.0224 / R_G)^{1/2} (p_L^{1/2} - p_{L2}^{1/2} + R_G p_{G1} / K_S p_t \cdot 0.0224)^{1/2}} \quad (6)$$

$$c_{Li} = K_S p_{Li}^{1/2}; \quad R_G = \frac{u_G p_t T_0}{u_L p_0 T} = \frac{u_G p_t \cdot 0.0224}{u_L RT} = \frac{u_{GN}}{u_L}$$

2.2. A plug flow model of the liquid, a perfect mixing model of the gas

At very low gas velocity through the packing, the gas can be considered ideally mixed (see Section 3.2.1). In this case, the partial pressure of the isotope in the gas is constant along the column and is equal to its concentration in the gas leaving the column c_{G2} and Eq. (5) reduces to the following explicit relation for the packing height

$$Z = \frac{u_L}{k_L a} \ln \frac{c_{L1} - A_c}{c_{L2} - A_c}; \quad A_c = K_S \left(\frac{u_L RT}{u_G} \right)^{1/2} (c_{L1} - c_{L2} + c_{G1} \cdot u_G / u_L)^{1/2} \quad (7)$$

Using the equilibrium partial pressures of the isotopes instead of their molar concentrations in the liquid phase leads to the relations

$$Z = \frac{u_L}{k_L a} \ln \frac{p_{L1}^{1/2} - A_p}{p_{L2}^{1/2} - A_p}; \quad A_p = \left(\frac{K_S p_t \cdot 0.0224}{R_G} \right)^{1/2} \times (p_{L1}^{1/2} - p_{L2}^{1/2} + p_{G1} \cdot R_G / (K_S p_t \cdot 0.0224))^{1/2} \quad (8)$$

At a sufficiently low concentration of isotopes in gas, the parameter A_p is negligible with respect to the pressure $p_{L2}^{1/2}$ i.e., $p_{L2}^{1/2} \gg A_p$ and the relation (8) reduces to

$$Z = \frac{u_L}{k_L a} \ln \frac{p_{L1}^{1/2}}{p_{L2}^{1/2}}; \quad (9)$$

2.3. The effect of the axial mixing of the phases

The axial mixing of the phases in columns is an undesirable phenomenon since it lowers the driving force of the interfacial mass transfer. As a result a higher packing height of Z_t is necessary to obtain the same output concentration of the transferred species in both phases, compared with that of Z for the plug flow. In situations in which the axial mixing and mass transfer resistance are significant in one phase only, the effect of axial mixing is described by the following relation adapted from Ref. [7].

$$\exp(-N) = \frac{4b \exp(Bo/2)}{(1+b)^2 \exp(bBo/2) - (1-b)^2 \exp(-bBo/2)} \quad (10)$$

$$b = \sqrt{1 + 4 \frac{N_t}{Bo}}; \quad Bo = \frac{uZ}{E}; \quad N = \ln \frac{c_1}{c_2}; \quad \frac{N}{N_t} = \frac{Z}{Z_t};$$

where the Bodenstein number Bo characterizes the effect of axial mixing through the axial dispersion coefficient E of the phase and c_1 and c_2 are concentrations in the inlet and the outlet of the phase from the column. The relative increase of the packing height, Z_t/Z , compensating the effect of axial mixing is obtained by solving the implicit relation (10) where N and N_t are numbers of the transfer units for the plug flow and for the true flow, respectively. The relation (10) is plotted in Fig. 2.

The Bo -number correlations deduced [8] from the 'cold' air-water dynamic experiments performed in the column packed with

Mellapak 250Y structured packing (the Bo number is related to the packing height of 1 m).

$$Bo_L = 1.022 \quad Fi^{0.478} \left(\frac{3}{\sin^2 \delta} \right)^{1.159} (d_s a_t)^{6.337} \quad (11)$$

$$Bo_G = 2.807 \cdot 10^6 \quad Re_G^{-0.00896} 10^{-0.00394 Re_L} (d_s a_t)^{-7.792}$$

The correlations were deduced from experiments made in the following ranges of phase flow rates: $0 < B < 40$ m/h; $0 < u_G < 2$ m/s.

3. The physical data and the mass transfer characteristic $k_L a$ for the design of columns packed with structured packings

There exist three models that are most frequently used for the design of packed columns filled with structured packings: the model presented by Rocha et al. [3,4] (further denoted as RBF), by Billet and Schultes [9] (further denoted as BS) and by Olujic et al. [10] (further denoted as Delft). These models were based on the data measured using aqueous solutions and organic solvents but their application to a quite different physical system such as liquid metal can lead to considerable errors (see Fig. 3).

3.1. Physical properties of lead lithium alloy used in this paper

Lead lithium eutectic alloy (17 at% = 15.7 wt% of Li): [11]

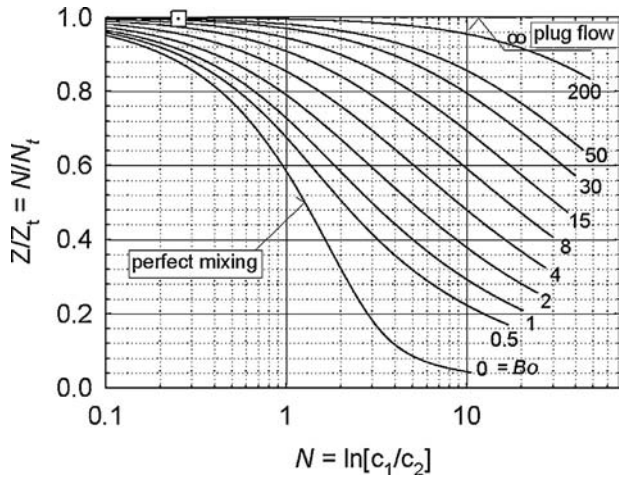


Fig. 2. Relative increase of the column packing height, Z_t/Z , eliminating an effect of the axial dispersion in the liquid phase characterized by the Bo_L number. Points represent Alpy's experiment presented in the first row of Table 1.

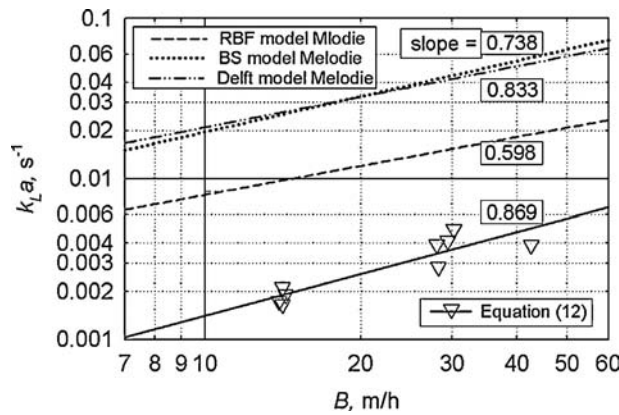


Fig. 3. Mass transfer coefficients of hydrogen $k_L a$ into lead lithium alloy at 673 K evaluated from the experiments of Alpy et al. [5,6] using Eq. (9) and from the RBF [3,4], the BS [9] and the Delft [10] models.

Melting point: $T = 508 \text{ K}$;
 Density: $\rho_L = 10.52 (1 - 1.13 \cdot 10^{-4} T) \text{ kg/m}^3$; $\rho_L(673 \text{ K}) = 9720 \text{ kg/m}^3$
 Viscosity: $\mu_L = 1.87 \cdot 10^{-4} \exp[1400/T] \text{ Pa s}$; $\mu_L(673 \text{ K}) = 0.0015 \text{ Pa s}$
 Surface tension: $\sigma = 0.52 - 1.1 \cdot 10^{-4} \cdot T \text{ N/m}$; $\sigma(673 \text{ K}) = 0.446 \text{ N/m}$
 Molecular weight: $Mw = 0.176 \text{ kg/mol}$;

Table 1
 Mass transfer coefficients calculated from Alpy et al. [5,6] data.

T (K)	Q_L (L/h)	B (m/h)	$Q_G \cdot 10^3$ (Nm ³ /h)	A_p (Pa)	p_{L1H}^* (Pa)	p_{L2H}^* (Pa)	$k_L a \cdot 10^3 \text{ s}^{-1}$ Eq. (8)	$k_L a \cdot 10^3 \text{ s}^{-1}$ Eq. (9)	$k_L a \cdot 10^2 \text{ s}^{-1}$ BS	$k_L a \cdot 10^2 \text{ s}^{-1}$ RBF
Ref. [5]; $Z = 0.6 \text{ m}$; $d = 0.06 \text{ m}$										
673	71	30.2	3	7.83	1085	653	4.87	3.55	4.42	1.54
673	66	28.0	6	5.17	1003	613	3.92	3.19	4.18	1.47
673	69	29.4	9	4.29	927	557	4.13	3.47	4.32	1.51
673	100	42.6	6	5.50	1188	858	3.88	3.21	5.69	1.89
713	61	26.0	3	8.23	1258	682	5.06	3.68	3.95	1.56
713	68	28.9	6	5.70	1152	670	4.50	3.63	4.70	1.66
713	68	28.9	9	5.00	1158	612	5.16	4.27	4.70	1.66
713	100	42.6	6	7.04	1228	712	6.99	5.37	6.27	2.10
713	70	29.8	6	7.91	2490	1215	6.12	4.95	4.72	1.69
Ref. [6]; $Z = 0.8 \text{ m}$; $d = 0.06 \text{ m}$										
673	80	28.2	6	5.92	1275	796	2.84	2.31	4.20	1.48
673	40	14.1	6	4.77	1050	515	2.12	1.75	2.52	0.97
673	40	14.1	30	2.10	988	484	1.90	1.75	2.52	0.97
673	40	14.1	6	3.48	463	267	1.66	1.35	2.52	0.97
673	40	14.1	6	2.90	225	130	1.73	1.34	2.52	0.97

Tritium:

[12]: $D_{L,T} = 2.50 \cdot 10^{-7} \exp\left\{-\frac{27000}{RT}\right\} \text{ m}^2/\text{s}$;
 $D_{L,T}(673 \text{ K}) = 2.00 \cdot 10^{-9} \text{ m}^2/\text{s}$

[13]: $K_{S,T} = 1.24 \cdot 10^{-3} \exp\left\{-\frac{1350}{RT}\right\} \text{ mol/m}^3 \text{ Pa}^{1/2}$;
 $K_{S,T}(673 \text{ K}) = 9.74 \cdot 10^{-4} \text{ mol/m}^3 \text{ Pa}^{1/2}$

Hydrogen:

[14]: $D_{L,H} = 8.18 \cdot 10^{-8} \exp\left\{-\frac{15800}{RT}\right\} \text{ m}^2/\text{s}$;
 $D_{L,H}(673 \text{ K}) = 4.85 \cdot 10^{-9} \text{ m}^2/\text{s}$

[15]: $K_{S,H} = 1.33 \cdot 10^{-4} \exp\left\{-\frac{1350}{RT}\right\} \text{ mol/m}^3 \text{ Pa}^{1/2}$;
 $K_{S,H}(673 \text{ K}) = 1.04 \cdot 10^{-4} \text{ mol/m}^3 \text{ Pa}^{1/2}$

3.2. Analysis of the mass transfer data from a Melodie loop

Alpy et al. [5,6] presented hydrogen desorption rates for liquid lead lithium eutectic alloy measured in the Melodie loop using a column with a 6 cm diameter packed with Mellapak 750Y to the heights of 0.6 and 0.8 m and at various gas and alloy flow rates. Alpy's data are reproduced in Table 1. The estimation of the gas and liquid phase axial mixing in the column has enabled to find the proper relation for evaluation of the volumetric mass transfer coefficients from their [5,6] experiments.

3.2.1. Effect of gas and liquid phase axial mixing

When gas velocity through the packing is very low gas maldistribution may occur. In this case pressure drop of the packing is too low to offer the proper resistance to the gas flow, allowing the spread of the gas in radial directions: maldistribution leads to channeling phenomena resulting in high axial dispersion, with a drastic reduction of the mass transfer efficiency. The longitudinal mixing of the gas flowing through the column at extremely low rates may be enhanced by a counter currently flowing liquid. In most situations, for example in the Melodie loop, the actual gas flow rate was as low as 1 mm/s ($u_{GE} = u_G/\varepsilon = 1/0.93 = 1.1 \text{ mm/s}$) (see Table 1). A film of liquid metal flows counter-currently at a much higher interstitial velocity such as 169 mm/s ($u_{LE} = u_L/(1 - \varepsilon) = 11.8/(1 - 0.3) = 169 \text{ mm/s}$) promoting the longitudinal mixing of the gas phase in the column.

The significance of the longitudinal mixing utilized in these experiments can be also judged from the diagram in Fig. 2. The relative increase in the packing height, Z_t/Z , eliminating the effect of the longitudinal dispersion in the gas and liquid phase, is characterized by the Bo_G or Bo_L number which can be estimated using Eq. (11) for similar packing, i.e. Mellapak 250Y: $d_s = 0.01606 \text{ m}$; $\delta = 45^\circ$;

$u_G = (0.73–7.3)$ mm/s; $u_L = (3.92–11.8)$ mm/s. Even the correlation (11) was deduced from the ‘cold’ air–water dynamic experiments, its applicability to describe axial dispersion might not be lost. The axial dispersion, unlike the molecular diffusion, is connected with macroscopic hydrodynamic behavior, and it can be assumed that the measure of non-ideality in liquid flow will be similar in the case of hot gas or liquid metal.

The physical data of Pb–Li/He system were taken from Section 3.1 at temperature of 673 K and the resulting Bo numbers lie in the following intervals: $Bo_G (1.69–1.73) \cdot 10^{-2}$ $Bo_L (38.2; 64.6)$. The Bo_L number of Mellapak 750Y would still be higher than that for 250Y. The low values of Bo_G number and the high number of Bo_L in Alpy’s experiments indicate perfect mixing of the gas phase in the column and plug flow of the liquid metal which underlies negligible effect of the axial dispersion on the mass transfer in the column. For illustration, the values corresponding to the liquid phase of the experiment presented in the first row of Table 1 ($N_L = 0.5 \cdot \ln[p_{L1}/p_{L2}] = 0.254$; $Bo_L = 54.9$) are plotted in Fig. 2.

3.2.2. Evaluation of the $k_L a$ -correlation of hydrogen and tritium from Alpy’s data

The A_p -values calculated from Eq. (8) and presented in Table 1 do not unambiguously confirm the validity of the $A_p \ll p_{L2}^{1/2}$ relation for all of Alpy’s experiments. Therefore the non-simplified relation (8) was used for the evaluation of the volumetric mass transfer coefficients of hydrogen $k_L a_H$ based on Alpy’s experimental data. The resulting $k_L a_H$ -values are given in Table 1 and are plotted as a function of liquid load B in Fig. 3. There is consistency between the experimental value of the exponent in the dependence of $k_L a$ on the flow rate of the alloy and that predicted by the RBF [3,4], the BS [9] and the Delft [10] models, however the coefficients calculated from the model are three-fold (RBF) and ten-fold (BS, Delft) higher (see Fig. 3). The regression of the experimental data from the Melodie loop identifies the following relation for the volumetric mass transfer coefficient of hydrogen on Mellapak 750Y at 673 K

$$k_L a_H = 1.90 \cdot 10^{-4} \cdot B^{0.869} \quad (12)$$

This correlation for hydrogen can be recalculated for tritium using following relation between mass transfer coefficient and diffusivity resulting from the penetration model of unhindered liquid flow along the interface $k_L \propto D^{0.5}$. The diffusivity of tritium was taken from Section 3.1. The final correlation for tritium is

$$k_L a_T = k_L a_H \left(\frac{D_T}{D_H} \right)^{0.5} = 1.90 \cdot 10^{-4} \cdot B^{0.869} \left(\frac{2.00 \cdot 10^{-9}}{4.85 \cdot 10^{-9}} \right)^{0.5} \quad (13)$$

$$k_L a_T = 1.22 \cdot 10^{-4} \cdot B^{0.869}$$

The correlations (12) and (13) are derived from the data for the system Pb–17Li at 673 K, the packing Mellapak 750Y, a liquid flow rates from 10 to 50 m/h and a gas flow rates from 0.3 to 3.0 Nm³/m²s.

It should be emphasized that the values of $k_L a_H$ measured in this manner do not depend on the solubility and the diffusivity of hydrogen and thus, the correlation (12) does not suffer from their experimental errors. The reliability of the $k_L a_T$ correlation derived in this manner depends only on the reliability/accuracy of the hydrogen to tritium diffusivity ratio.

4. A sensitivity analysis of the desorption efficiency of the column

The sensitivity analysis presented below is performed in regard to hydrogen transfer i.e. Eq. (12) is used to calculate $k_L a_H$ and the $K_{S,H}$ solubility is used. The same behavior of the model would also be obtained using these quantities for tritium.

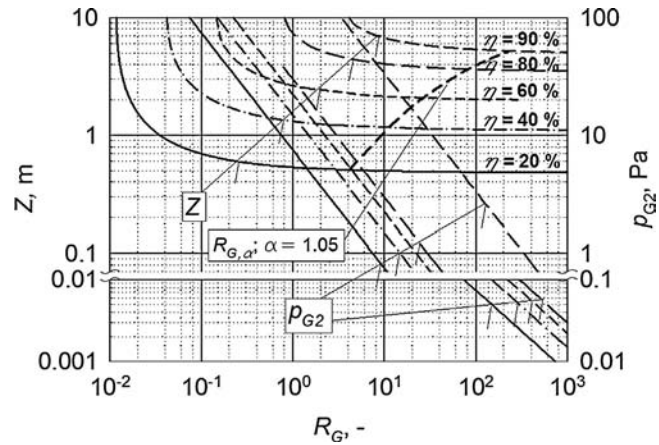


Fig. 4. The dependence of the packing height Z and of the concentration of hydrogen p_{G2} the gas leaving the column on the relative gas flow rate R_G for its requisite desorption efficiencies η calculated from Eq. (14). ($p_{L1} = 1000$ Pa; $B = 20$ m/ho).

4.1. The effect of the gas flow rate on the performance of a packed column

The usual practice in the design of absorption columns is to choose a column working point close to the loading point, and to evaluate the diameter of the column out of the gas flow rate at which the flooding condition occurs. A choice of this kind is not suitable for tritium desorption as there is endeavor to obtain high concentration of tritium in the exiting gas. In such a situation, the gas flow rate should be deduced from the minimum gas flow rate for which the concentration of the isotope in the leaving gas is the highest but the driving force of desorption is still not reduced and the column height does not have to be seriously increased.

Model of the perfect mixing of the gas and the piston flow of liquid metal is used to evaluate the effect of the throughput of the inert gas on the performance of the column. The relationship between the packing height Z , absorption efficiency η , the relative flow rate of the purge gas R_G and the isotope concentration in the gas leaving the column p_{G2} provides relation (8) which is simplified if pure tritium not containing purging gas is used $c_{G1} = 0$

$$\begin{aligned} Z &= \frac{u_L}{k_L a} \ln \frac{p_{L1}^{1/2} - A_p}{p_{L1}^{1/2}(1 - \eta) - A_p}; \\ A_p &= \left(\frac{K_S p_t \cdot 0.0224}{R_G} \right)^{1/2} (p_{L1}^{1/2} - p_{L2}^{1/2})^{1/2}; \\ p_{G2} &= 0.0224 \frac{p_{L1}^{1/2} p_t K_S \eta}{R_G}; \\ R_{G,\alpha} &= 0.0224 \frac{K_S p_t \eta}{U_\alpha^2 p_{L1}^{1/2}}; \quad U_\alpha = \frac{(1 - \eta)^{1-\alpha} - 1}{(1 - \eta)^{-1} - 1}; \\ \alpha &= \frac{Z}{Z_{min}} \end{aligned} \quad (14)$$

A calculation was performed with regard to the conditions under which the measurement on the Melodie loop was effected: $p_{L1} = 1000$ Pa; $p_{L2} = (100; 900)$ Pa; $B = 20$ m/h; $K_{S,H}$ from Section 3.1 and $k_L a_H$ from Eq. (12) at a temperature of 673 K were utilized. These results are plotted in Fig. 4. When the gas flow rate decreases below a certain minimum gas flow rate R_{Gmin} , the concentration of the isotope in the gas in the column increases so that the driving force of the mass transfer of the isotope starts to reduce and the packing height has to be increased to maintain its required efficiency. In the figure, the line of thick, short dashes corresponds to

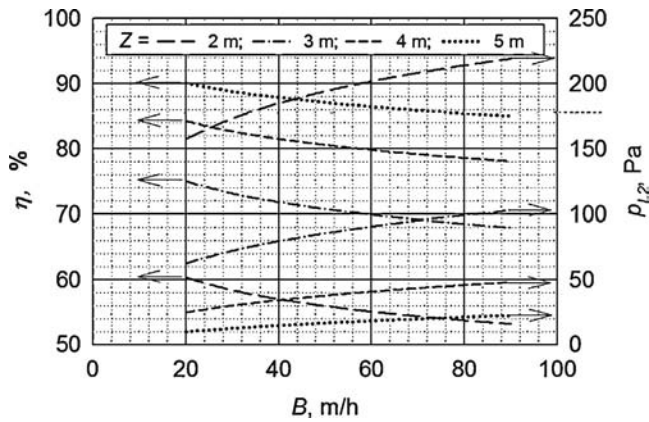


Fig. 5. Effect of the lead–lithium liquid eutectic flow rate B on desorption efficiency η and hydrogen concentration p_{L2} in the eutectic leaving the column of different packing heights Z calculated from Eq. (15) for $p_{L1} = 1000$ Pa.

the relative gas flow rate at which the relative increase $\alpha = Z/Z_{min}$ of the packing height needed to maintain the efficiency constant is 5%. Gas flow rates higher than R_{Gmin} do not increase the desorption efficiency and only diminish the isotope concentration in the gas leaving the column. This is illustrated in Fig. 4. For example: if the hydrogen concentration in the lead lithium liquid eutectic is $p_{L1} = 1000$ Pa and the specific liquid metal flow rate $B = 20$ m/h, 60% of the hydrogen should be removed and the minimum relative gas flow rate $R_G = 24$ was used, the sufficient minimum packing height is 2 m and the hydrogen concentration in the outlet gas is 0.8 Pa. If in this situation a 100 times lower gas flow rate $R_G = 0.24$ was used the requisite packing height would increase to 6 m while the same amount of hydrogen would be removed and its outlet concentration would increase 100-fold to $p_{G2} = 80$ Pa. Similarly, if in this situation a gas flow 10 times higher than the minimum rate $R_G = 240$ is used the sufficient packing height (2 m) would not change, the same quantity of hydrogen would be removed, but its concentration in the gas leaving the column will decrease 10-fold to $p_{G2} = 0.07$ Pa.

Using this procedure it is possible to calculate the packing height Z and the gas flow rate R_G needed to achieve the required efficiency of the column η and the isotope concentration in the outlet gas p_{G2} for the given flow rate of lead lithium alloy u_L and the isotope concentration p_{L1} .

4.2. The effect of the liquid flow rate on packed column performance

As was explained above, the model of the piston flow of liquid metal is used for evaluating the effect of the liquid flow rate on the performance of the column. The gas flow rate is used higher than the minimum gas flow rate R_{Gmin} whereby the effect of the gas phase on the column desorption efficiency is negligible. This situation describes the relation (9) which is used to the following sensitivity analysis of the effect of liquid flow on the column desorption efficiency η . The relation can be redrawn as follows:

$$\eta = 1 - \exp \left\{ -\frac{Zk_L a}{u_L} \right\}; \quad p_{L2} = p_{L1} \exp \left\{ -2\frac{Zk_L a}{u_L} \right\} \quad (15)$$

Calculations are carried out for the hydrogen content in the metal $p_{L1} = 1000$ Pa. The liquid flow rate effect on desorption efficiency η and hydrogen concentration p_{L2} in the lead–lithium liquid eutectic is illustrated in Fig. 5 as their dependences on the liquid load B for different packing heights Z . As follows from Eq. (15), the flow dependence is moderate because it is diminished by the flow dependence of $k_L a$ on u_L ($\sim u_L/k_L a \sim B^{1-0.869} \sim B^{0.31}$).

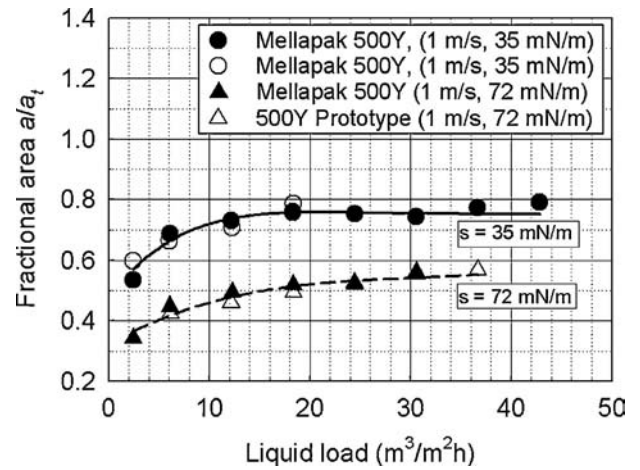


Fig. 6. Relative wetted area of Mellapak 500Y, a/a_t , as a function of the liquid flow rate. Slightly modified version of figure from Ref. [17].

4.3. Effect of the geometric surface area of the packing

It is a usual practice to increase the mass transfer efficiency of packed column by using packing with a higher geometric area (a_t). This is successful only to the certain value of the geometrical area of the packing. The effective interfacial area (a) responsible for the desorption efficiency of the column, represents only the part of the geometric surface area of the packing which is actually wetted by the liquid metal. This is why the current correlations for the effective area are based on the study the falling liquid film spreading on the packing surface [16].

Decisive parameters affecting the spreading process are density, viscosity, surface tension and contact angle of the liquid on the packing material and the volumetric flow rate of the fluid per wetted perimeter in cross-sectional slice of the packing Γ ($m^3/m s$) = u_L/L where wetted perimeter $L = (4s)/(bh)$. The dimensions of packing channels b (channel base) h (crimp height) and s (channel side) are presented for various sizes of Mellapak in Ref. [16]. The film thickness and its tendency to spread over the packing surface increase with increasing Γ . For physical systems which do not wet the packing completely (like water or Pb–Li) in the columns packed with the same type of the packing (Mellapak) of different geometric area, the wetted perimeter L increases with increasing geometric packing area ($a_t = 250 m^{-1}$, $L = 0.237 m^{-1}$; $a_t = 500 m^{-1}$, $L = 0.531 m^{-1}$) and the flow rate Γ decreases producing thinner liquid film with lower tendency to spread over the packing surface. As a result, further increase of geometric area of the packing above a certain limiting value need not lead to the further increase in the mass transfer efficiency. The efficiency may even decrease if other phenomena e.g. the decrease of mass transfer coefficient from the attenuated liquid film, also takes place.

This explains the significantly lower utilization of the geometric area of Mellapak 500Y [17] by higher surface tension liquid (water $\sigma = 72$ mN/m, only 55% at liquid load 30 m/h; see Fig. 6) in comparison with the practically complete wetting of Mellapak 250Y [17] (water $\sigma = 72$ mN/m, 95% at liquid load 30 m/h; see Fig. 7). The two times higher liquid flow rate per packing perimeter on Mellapak 250Y also leads to the thicker liquid film with higher mass transfer coefficients k_L . As a result, the coefficients $k_L a$ of Mellapak 250 and 350 with a lower geometric area are even 30% higher than the coefficients of the Mellapak 500Y with a liquid load of 30 m/h [18]; see the data in Fig. 8. Note that this phenomenon did not occur on the packing perfectly wetted by the low surface tension liquid.

These experimental results and theoretically non-predicted limiting value of the geometric area of packing lead us to recommend

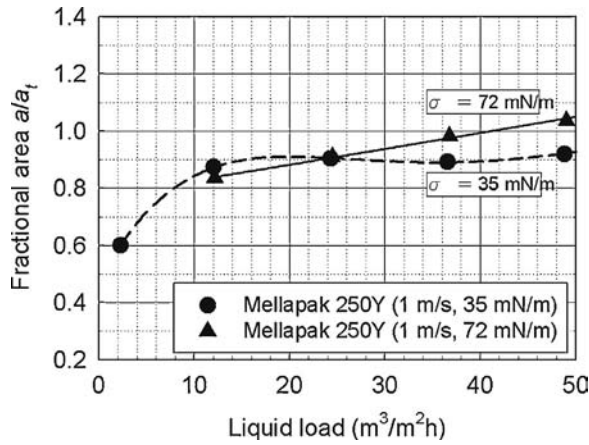


Fig. 7. Relative wetted area of Mellapak 250Y, a/a_t , as a function of the liquid flow rate. Slightly modified version of figure from Ref. [17].

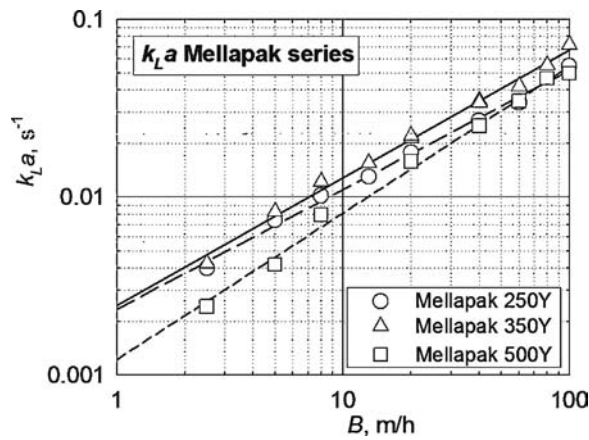


Fig. 8. The dependence of the mass transfer coefficients $k_L a$ on liquid loading B of the Mellapak series. Taken from Ref. [18]. The air–water system.

Mellapak 500Y as an alternative packing to the proposed Mellapak Plus 752Y in the experiments for determination of the mass transfer data for the sizing of tritium extraction units.

5. Engineering sizing of the desorption columns

5.1. The absorber/desorber circulating system for experimental study

The flow-sheet shown in Fig. 9 simulates an experimental loop that is usually utilized for the kinetic study of the hydrogen isotopes desorption in packed columns. Specifically it comprises of an absorber and a stripper. The liquid metal tank and the pumps and blowers are omitted as they are not relevant components for describing the mass transfer rates and the concentration distribution in the system. The circulating system with the packed absorption column is more suitable than the bubble column utilized in the Melodie loop. It may provide absorption and desorption kinetic mass transfer data measured simultaneously under the same operating conditions. Their comparison/reversibility would contribute to the solution of the still unanswered question whether the interfacial mass transfer process is controlled by the diffusion of gas atoms through the boundary layer or whether the recombination/dissociation reactions of tritium atoms and molecules at the liquid–gas interface also affect the rate of the transfer process significantly [19–21].

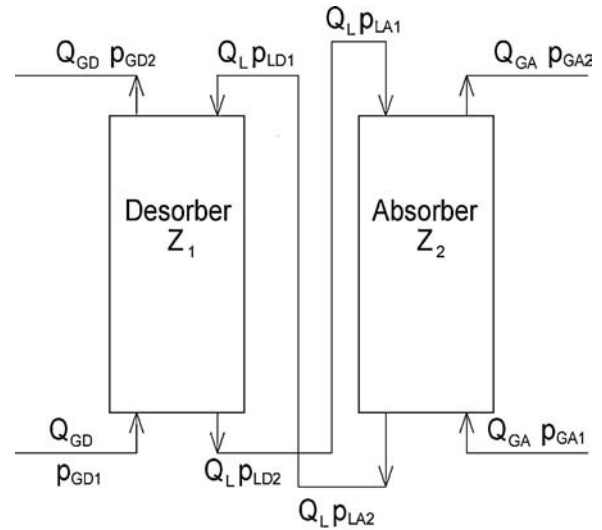


Fig. 9. Flow-sheet of the experimental setup normally utilized for the kinetic study of tritium desorption in a packed column.

The calculations have been carried out using the same process parameters in accordance with those at which the experiments for the Melodie loop were performed. The authors [5] used a high gas flow rate and therefore $p_{GD} = 0$. Using a similarly high gas flow rate in the absorption column it then holds $p_{GA1} = p_{GA2} = p_{GA}$ and the mass transfer in both the desorber and the absorber is well described by the Eq. (9). The steady-state distribution of the hydrogen isotope concentration in the system is described by the following equations of the mass transfer rates in the columns. (The symbols utilized are described in Fig. 9 in the flow-sheet.)

Desorber

$$Z_1 = \frac{u_L}{k_L a} \ln \frac{p_{LD1}^{1/2}}{p_{LD2}^{1/2}}$$

Absorber, assuming $p_{LA1} = p_{LD2}$ and $p_{LA2} = p_{LD1}$

$$Z_2 = \frac{u_L}{k_L a} \ln \frac{p_{GA}^{1/2} - p_{LA1}^{1/2}}{p_{GA}^{1/2} - p_{LA2}^{1/2}} = \frac{u_L}{k_L a} \ln \frac{p_{GA}^{1/2} - p_{LD2}^{1/2}}{p_{GA}^{1/2} - p_{LD1}^{1/2}}$$

By combining the relations the steady state concentrations of the isotope in all the streams of the circulation system are obtained

$$p_{LD2}^{1/2} = p_{LA1}^{1/2} = p_{GA}^{1/2} \frac{1 - K_2}{1 - K_1 K_2}; \quad p_{LD1}^{1/2} = p_{LA2}^{1/2} = K_1 p_{GA}^{1/2} \frac{1 - K_2}{1 - K_1 K_2};$$

$$K_i = \exp \left\{ \frac{Z_i k_L a}{u_L} \right\} \quad (16)$$

This illustrative calculation is created by using the process variable for the desorber of Alpy et al. [5]. Desorber: $Z_1 = 0.6$ m; $B = 30.2$ m/h; $p_{GD} = 0$; $T = 673$ K; $k_L a = 3.46 \cdot 10^{-3} \text{ s}^{-1}$. Absorber: $Z_2 = 0.8$ m; $B = 30.2$ m/h; $p_{GA} = 2500$ Pa ($x_{GA} = 0.02$; $p = 125$ kPa); 673 K; $k_L a = 3.46 \cdot 10^{-3} \text{ s}^{-1}$.

The results calculated from Eq. (16) are following: hydrogen concentration in the liquid leaving the absorption column and then entering the desorption column is $p_{LD1} = p_{LA2} = 1026$ Pa and in the liquid leaving desorption and then entering the absorption column is $p_{LD2} = p_{LA1} = 623$ Pa. The efficiencies of both columns are the same and equal to $\eta = 22\%$. Its efficiency is consistent with that obtained by Alpy et al. [5,6]; compare these results with the data provided in the first line of Table 1.

This model, based on realistic modeling and experimental data originating from Alpy [5,6], can be utilized to predict the

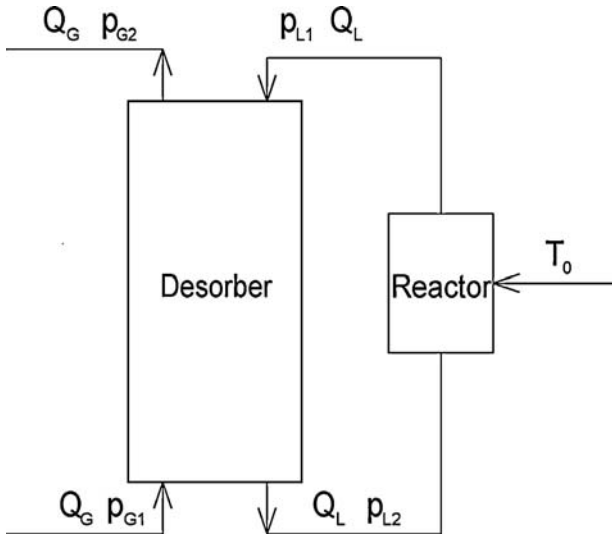


Fig. 10. Flow-sheet of simplified tritium extraction process in packed column of HCLL system and symbols used. Losses of tritium in piping and blanket are neglected.

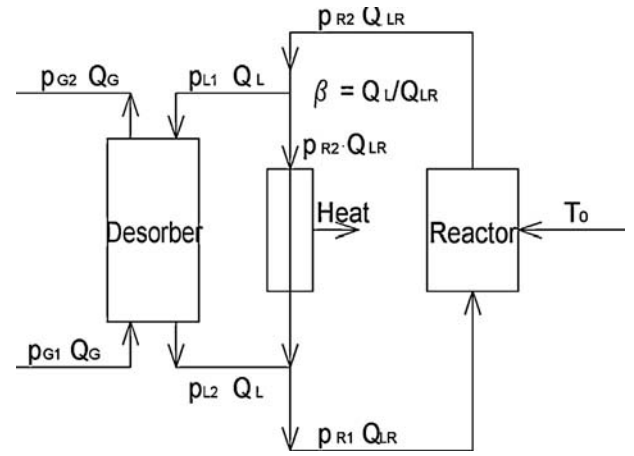


Fig. 11. Flow-sheet of simplified tritium extraction process in packed column of DCLL system and symbols used. Losses of tritium in piping and blanket are neglected.

performance of the experimental apparatus for investigating the mass transfer of hydrogen isotopes in packed columns and for estimating the anticipated concentrations as a function of the flow rate of the eutectic and of the concentration of the isotope in absorbed gas.

5.2. Sizing of the column for the DEMO plant for HCLL and DCLL breeding blankets

The 2300 MW reactor was selected for the purpose of column sizing. This reactor produces 385 g of tritium daily. The Pb–Li flow rate through the HCLL blanket is 810 kg/s [22]. A comparable example of the use of DCLL is a blanket for the Chinese FDS-II reactor with 2500 MW of power producing 405 g of tritium per day and a PbLi mass flow of 55,000 kg/s [23].

The objective of the column sizing described in this paper is to provide dimensions for the tritium desorption column for both the blanket concepts. The sizing is based on realistic modeling and experimental data from Alpy et al. [5,6]. The flow-sheet of the facility and the symbols utilized are defined in Fig. 10 of the HCLL system and in Fig. 11 of the DCLL system. In order not to underestimate the heights of packing in the columns, the gas is considered ideally mixed in further calculation as predicts the lowest driving force of absorption and thus leads to the highest packing height in the column. The model (8) of the perfect mixing of the gas and the piston flow of liquid metal was used for the calculation. When this model is applied to the blankets it leads to the following relations in regard to the evaluation of the main parameters of the device which are on the safe side of the estimation.

$$Z[R_G, R_T, \eta, B] = \frac{B}{3600 \cdot k_L a} \ln \frac{1 - V}{(1 - \eta) - V}; V = \left(0.0224 \frac{p_t K_{S,T}^2 \eta^2}{R_G R_T} \right)^{1/2}; p_{G2} = 0.0224 \frac{p_t R_T}{R_G} \tag{17}$$

$$R_{G,\alpha} = 0.0224 \frac{p_t K_{S,T}^2 \eta^2}{U_\alpha^2 R_T}; U_\alpha = \frac{(1 - \eta)^{1-\alpha} - 1}{(1 - \eta)^{-1} - 1}; p_{L2} = \left[\frac{(1 - \eta) R_T}{K_{S,T} \eta} \right]^2; p_{L1} = \left[\frac{R_T}{K_{S,T} \eta} \right]^2$$

Input parameters for evaluation of the packing heights Z in HCLL and DCLL systems are the relative purge gas flow rate R_G, the relative tritium production rate per volume of liquid metal R_T, efficiency of desorption column η and liquid metal load B of the column.

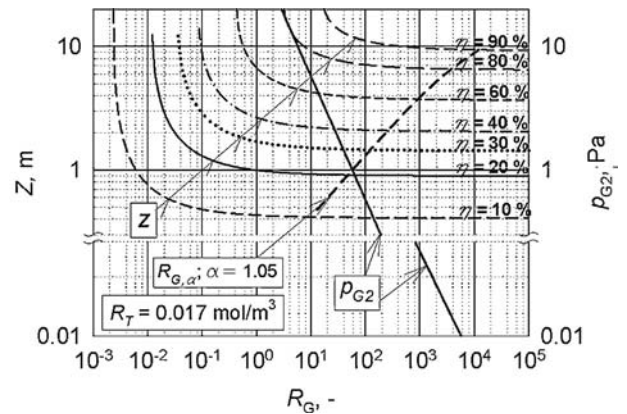


Fig. 12. Packing height Z and tritium concentration p_G2 in the gas leaving desorption column and the efficiency of the columns of the HCLL blanket. Tritium production rate T_0 = 385 g/day; flow rate of Pb–Li = 0.81 t/h; B = 60 m/h; d = 2.58 m.

5.2.1. The HCLL breeding blanket

The relative production rate of tritium using the HCLL system amounts to $R_T = (T_0/Q_L) = (385/3 \cdot 24 \cdot 3600)/(9273/810) = 1.017 \text{ mol/m}^3$. The pressure in the column was considered as being 1.5 kPa and the tritium losses were ignored for column sizing. The results calculated for this R_T value are presented in Fig. 12 in terms of the dependence of the packing height Z and of the concentration of tritium in the gas leaving the column p_G2 at the relative gas flow rate R_G and the efficiency of desorption column η. The tritium concentration c_L2 in the lead lithium alloy exiting from the desorption column and the superficial gas velocity in the column of the blanket are presented in Fig. 13. As can be seen below, the graphs enable the rapid estimation of the impact of the various process parameters on the tritium desorption column design based on the more

realistic mass transfer data deduced from the actual data regarding the hydrogen desorption from the Pb–17Li melt.

In the DEMO global balance study [22] an efficiency of the Tritium Extraction System of between 70–90% was assumed,

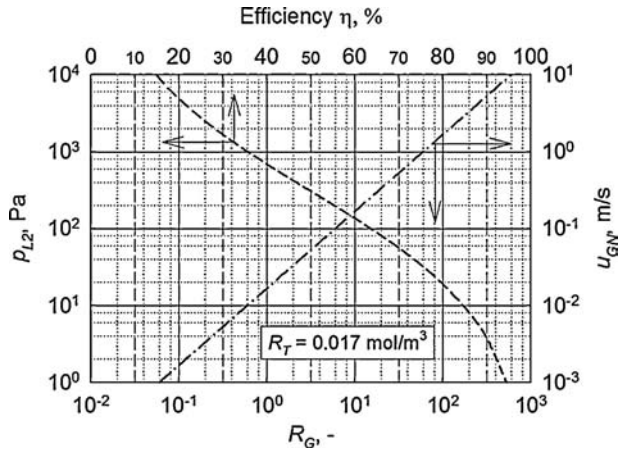


Fig. 13. Tritium concentration p_{L2} in the lead lithium alloy exiting the desorption column and the superficial gas velocity in the columns of the HCLL blanket. Tritium production rate $T_o = 385$ g/day; flow rate of Pb–Li = 0.81 t/h; $B = 60$ m/h; $d = 2.58$ m.

i.e. values significantly higher than the up-to-date experimental results obtained (30%). Packing height Z may be read from Fig. 12. For greater efficiency 90%, the tritium column is rather high (10 m). The lower 60% requirement leads to a more realistic packing height estimation of 3.8 m. The column diameter depends on the lead lithium alloy flow rate maintaining a reasonable liquid load B higher than 50 m/h. The column diameter requisite for the HCLL blanket to maintain $B = 60$ m/h is 2.6 m.

The lines corresponding to the gas flow rate below which the packing height should be increased to maintain constant desorption efficiency are also illustrated in Fig. 12 for the relative increase of the packing height $\alpha = 1.05$. For example, if the minimum gas flow rate $R_{G,1.05} = 10^3$ is utilized and the desorption efficiency needed is 60%, the requisite packing height is 3.8 m (see Fig. 12), the tritium partial pressure in the gas leaving the column is 0.02 Pa, the corresponding superficial gas velocity in the column is an unrealistically high 20 m/s and the tritium concentration in the eutectic leaving the desorption column c_{L2} and flowing into the main area of the DEMO facility is 135 Pa (see Fig. 13). If the thousand times lower gas flow rate $R_G = 1$ is utilized, the requisite height of the column increases to 6.5 m, but the tritium partial pressure in the gas leaving the column increases to 58 Pa, while the corresponding superficial gas velocity in the column decreases to 0.02 m/s (which promotes the creation of a perfect mixing gas phase in the column) and the tritium concentration in the eutectic leaving the desorption column remains unchanged and is equal to 135 Pa.

It should be noted that only the tritium concentration in the gas leaving the desorption column p_{G2} and the packing height Z are dependent on the tritium solubility $K_{S,T}$ and only at significantly low flow rates of purge gas whereby the mass transfer driving force starts to decrease as is explained in Section 4.2. In this situation, the value of parameter V is not negligible in comparison with the value of $(1 - \eta)$ (see Eq. (17)) and the relation $(1 - \eta) \gg V$ is no more valid.

5.2.2. DCLL breeding blanket

The main difference between the HCLL and the DCLL blankets in regard to the operation of the desorption column is that in the DCLL blanket, only part $\beta = Q_L/Q_{LR}$ of the circulating eutectic is led into the desorption column. The blankets are compared with regard to the situation in which the same desorption columns are used in both the systems. This is achieved by using the same parameter values for determining the size of the columns. In the illustrative calculations presented below, the same values for the parameters are used as were used for the HCLL breeding blanket: $R_G = 1$; $R_T = 0.017$ mol/m³; $\eta = 60\%$; $B = 60$ m/h. This solution is reached if

the following gas and liquid flow rates and column diameter are utilized.

$$R_T = \frac{T_o}{Q_L} = \frac{T_o}{\beta Q_{LR}} = 0.017 = \frac{405 \cdot 9273}{3 \cdot 24 \cdot 3600 \cdot Q_L}; \quad Q_L = 852 \text{ kg/s};$$

$$R_G = 1 = Q_G \frac{9273}{852 \cdot 3600}; \quad \Rightarrow \quad Q_G = 331 \text{ Nm}^3/\text{h};$$

$$B = 60 \text{ m/h} = \frac{852 \cdot 3600 \cdot 4}{9257 \cdot \pi d^2}; \quad \Rightarrow \quad d = 2.65 \text{ m}$$

In this situation only 1.55% of the circulating eutectic is led into the desorption column ($\beta = 852/55,000 = 0.0155$). The values of the parameters calculated based on Eq. (17) describing the operation of desorption column in the DCLL breeding blanket are also the same as in the HCLL blanket i.e., the necessary height of the column $Z = 6.5$ m, the tritium partial pressure in the gas that leaves the column $p_{G2} = 58$ Pa and the tritium concentrations in the eutectic alloy flowing into and leaving the desorption column $p_{L1} = 991$ Pa and $p_{L2} = 135$ Pa.

The concentration of tritium in the eutectic leaving the reactor p_{R2} and flowing into the desorption column p_{L1} equal to $p_{R2} = p_{L1} = 991$ Pa and the concentration in the eutectic entering the reactor p_{R1} and circulating in the main part of the DCLL breeding blanket of the DEMO facility equals to $p_{R1} = (1 - \beta) p_{L1} + \beta p_{L2} = (1 - 0.0155) \cdot 991 + 0.0155 \cdot 135 = 978$ Pa. This concentration is substantially higher as compared to the tritium concentration in the eutectic alloy circulating in the HCLL breeding blanket. This may increase the loss of tritium in the piping of the blanket.

6. Analysis of the effect of the wettability of the packing

The surface tension and the contact angle are decisive quantities for determining the spreading of a liquid film on the packing surface and thereby making the effective surface area available for a mass transfer.

6.1. The effect of surface tension

Low surface tension liquids ($\sigma < 30$ mN/m) such as alcohols or hydrocarbons, spread very easily on metallic or plastic surfaces whereas water and most of aqueous systems of higher surface tension (approx. 72 mN/m) wet these surfaces substantially less. This is illustrated in Fig. 6, taken from Tsai et al. [17] The decrease in the surface tension of the water from 72 to 35 mN/m (induced by the addition of a surfactant) increased the wetted area of the Mellapak 500Y two-fold. The high value of the surface tension of the liquid metal Pb–Li ($\sigma = 446$ mN/m) indicates ineffective wetting of the packing. The wetted area of packing, a , relative to the geometric area, a_t , can be estimated from the relation (18) of Onda et al. [24] For Mellapak 750Y and the Pb–17Li melt at a flow rate of 30 m/h and 673 K it gives (physical data taken from Section 3.1, hydraulic diameter of the packing $d_h = 4\varepsilon/a_t = 4 \cdot 0.95/750 = 0.00507$ m)

$$\frac{a}{a_t} = \frac{1.5}{\sqrt{d_h a_t}} \left(\frac{u_L d_h \rho_L}{\mu_L} \right)^{-0.2} \left(\frac{u_L^2 \rho_L d_h}{\sigma} \right)^{0.75} \left(\frac{u_L^2}{d_h g} \right)^{-0.45} = 0.12 \quad (18)$$

Similarly, a low value of the wetted area of the packing is predicted by the RBF model [3,4] (12%), and a somewhat higher value is predicted by models BS [9] and Delft [10] (35%), see Fig. 14. The extremely low wetted area of the packing is caused by the extremely high surface tension of the Pb–17Li melt, however these data may be unreliable, because the relations were derived for liquid systems with a substantially lower surface tension < 80 mN/m.

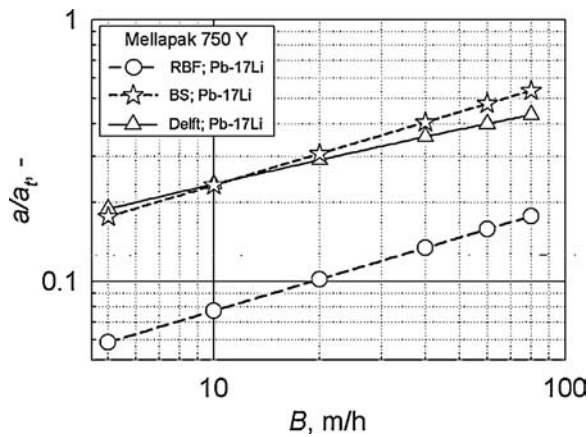


Fig. 14. Relative wetted area of the packing calculated for the Pb–17Li system from the RBF [3,4], BS [9] and Delft [10] models.

Nevertheless, serious wetting of the packing cannot be expected in regard to liquid with such a high surface tension and its lowering by the application of some additives to the eutectic alloy is hardly feasible. In the case of liquids badly spreading over the surface of packing is also very important its good initial distribution over the column cross-section. This is why the liquid distributors with sufficiently high number of drip points per unit area should be used. A minimum of the drip points/m² depends also on the ability of the packing to spread the liquid phase over the packing cross-section. This depends on the geometry of the packing and can hardly be predicted for the liquid metal from present correlations based on the data measured using aqueous solutions and organic solvents.

6.2. The effect of the contact angle

The capability or the tendency of liquid film to spread over a packing surface depends, apart from the surface tension, on the contact angle. A limiting value of the contact angle determining the transition from no spreading to spreading film is 90°. A marked decrease of the contact angle to below this value leads to a similar increase in the wetting of the packing and thereby also of mass transfer efficiency of the column. This effect was already being utilized in the industry [25] (Raschig GmbH, Ludwigshafen) to improve the wettability of plastic packings (PP: $\theta = 102^\circ$; PE: $\theta = 96^\circ$) by means of aqueous media. The decrease of the contact angle of the plastic packing by aqueous media ($\theta < 5^\circ$) using chemical hydrophilization of their surface enhances their wetting two-fold as compared to the untreated ones, as shown by the data measured on PP Mellapak 250Y (Fig. 15) or to the random packings shown in [26]. The data have also shown decisive role of contact angle in comparison with the effect of surface tension. The increase in wetted area is achieved in liquid (1 M NaOH solution) of rather high surface tension (72 mN/m) in the group of liquids, for which the models of RBF [3,4], BS [9] and Delft [10] have been derived.

In contrast to the surface tension, the contact angle of the liquid metal on a metal surface can be essentially affected by any roughness or impurities, particularly oxygen which forms a layer of oxides at the interface. Wettability of the rough surfaces is described by Wenzel's relation between intrinsic (θ) and apparent (Φ) contact angles

$$\cos \Phi = r \cos \theta \quad (19)$$

r represents the roughness factor defined as the ratio of the real area of the solid body to the apparent area of a plane with the same macroscopic dimensions. One fundamental observation is that roughening the surface improves wetting if $\theta < 90^\circ$, whereas, it

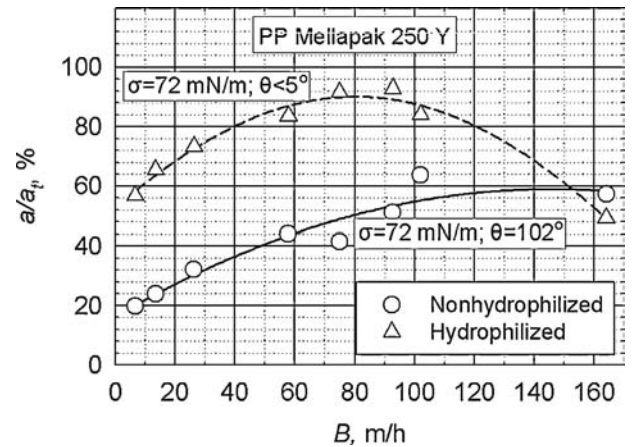


Fig. 15. Relative wetted area of polypropylene Mellapak 250Y of a hydrophilized ($\theta < 5^\circ$) and untreated ($\theta = 102^\circ$) surface.

decreases the wetting if $\theta > 90^\circ$. Steel surfaces, if they are not specially treated become covered by an oxide layer that manifests poor wettability, the contact angle typically being greater than 120° . Thereby the roughness of metal surfaces may not improve their wettability as it is applicable safely for water and other liquids with surface tension below 90° . The wettability of Fe–Cr steel by lead and Pb–Li alloys was studied by Protsenko et al. [27] and Gubzhokov et al. [28]. Their main results are shown in Figs. 16 and 17.

The results of Protsenko et al. [27] have shown, see Fig. 16, that in a high vacuum, pure lead does not wet ($\theta = 150^\circ$) oxidized steel at temperatures lower than 600°C . At higher temperatures (600 – 800°C), the contact angle is lower, but it remains very close to the non-wetting/wetting transition value of 90° . The addition of Li to Pb decreases the contact angle of Pb on oxidized steel by more than 20° and thereby improves the wetting of the steel ($\theta \sim 60^\circ$).

The most recent results of Gubzhokov et al. [28], reproduced in Fig. 17 and also measured on the oxidized steel surface, are quite different. They show a decrease of the contact angle with the addition of Li to Pb, but the values of θ (110 – 135°) are higher as compared with those published by Protsenko et al. [27] indicating the non-wetting of the steel.

These ambiguous results concerning the effect of the roughness of the packing surface on its wettability by Pb–Li alloys have also led us to recommend the use of the Mellapak packings with flat surfaces for experiments testing the efficiency of hydrogen isotopes desorption in packed columns. The fundamental science behind wetting

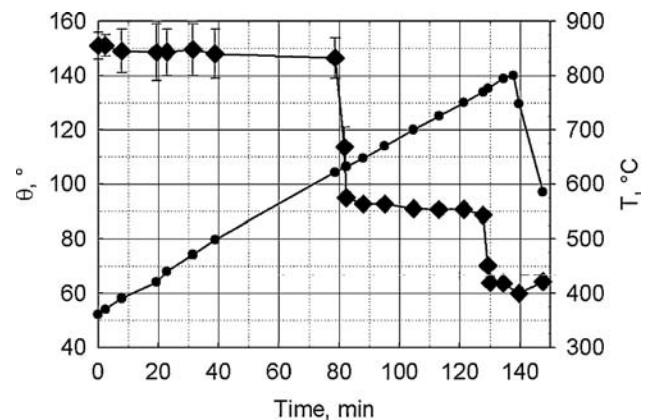


Fig. 16. Contact angle of Pb on untreated i.e. partially oxidized stainless steel as a function of time in the course of a temperature cycle in high vacuum, studied using the sessile drop method.

Source: Adapted from Ref. [27].

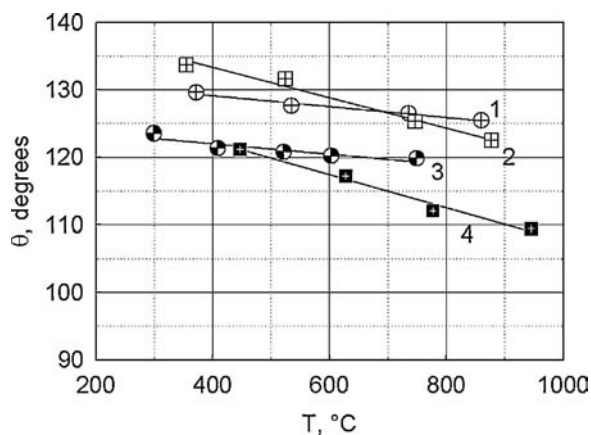


Fig. 17. Temperature dependence of the contact angle for the following Pb–Li melt on the 12Cr18Ni9Ti steel: 1 – 0.03 at.% Li; 2 – 0.1 at.% Li; 3 – 0.3 at.% Li; 4 – 0.5 at.% Li. Source: Adapted from Ref. [28].

and the contact angle phenomena for this system might bring similar practical benefits in this instance, as it has already brought about the improved wetting of plastic packings.

7. Conclusions

The correlations (12) and (13) for $k_L a$ of hydrogen and tritium on Mellapak 752Y at 673 K are deduced from the data measured by Alpy et al. [5,6] on the Melodie loop. The $k_L a$ values are three times lower than that predicted by the RBF [3,4] model.

The coefficients are used in the model of the hydrogen isotope desorption efficiency of the packed column. Introduction of the experimental Bodenstein number into the model of axial mixing effect on the efficiency of desorption shows, that the axial mixing of the liquid phase is negligible. The relation for the calculation of the minimal gas flow rate is presented; application of the minimal gas flow rate leads to the highest concentration of the isotope in the gas leaving the column, while the mass-transfer driving force is still not reduced and the height of the column does not need to be lengthened for keeping the efficiency.

The model developed was applied to describe a steady-state mass transfer in a closed loop for the absorption/stripping of the hydrogen isotopes experiments and also to the DEMO sized reactor. Essential input data for the design of desorption column were the breeder mass flow, the tritium concentration in the breeder at the column inlet and some requirements for the desorption process. While the desorption efficiency has been used for the determination of the column packing height in this paper, other design specifications can also be utilized, such as the tritium concentration in the breeder at the column outlet or the outlet isotope concentration in the stripping gas. Optimal choice of the specifications is not yet well documented in the open literature.

The results of the simulation showed that a packed column can be used for both types of blanket, however the application on the DCLL blanket leads to a higher tritium concentration in the circulating eutectic alloy as compared to the HCLL breeding blanket. To improve this comparison the real geometry of the system must be taken into account to include the actual tritium losses in the analysis. Geometry inputs indicate rough blanket geometry (wetted surface and wall thickness), pipe dimensions (length and thickness), breeder temperatures and construction material.

Larger wetted area and mass transfer coefficient on Mellapak 250Y than on Mellapak 500Y with twofold larger geometric area are foreseen due to the higher liquid flow rate per perimeter of the M 250Y packing. This is why we also recommend the testing

of the desorption efficiency of the Mellapak 500Y, apart from the Mellapak 750Y.

The roughness of the packing surface may increase its wettability if the contact angle is lower than 90° . It has been shown that the literature data on the contact angle of lead lithium alloys to the oxidized steel surface are ambiguous. This is why parallel tests of the desorption efficiency of the packings with smooth and with rough surfaces are recommended.

Acknowledgments

The supports from The Czech Science Foundation through the project no. 13-01251S and The Ministry of Education, Youth and Sports through program EUPRO II no. LE11012 are gratefully acknowledged.

References

- [1] A. Aiello, A. Ciampichetti, M. Utili, G. Benamati, TRIEX facility: an experimental loop to test tritium extraction systems from lead lithium, *Fusion Eng. Des.* 82 (2007) 2294–2302.
- [2] S. Mohan, K. Bhanja, K.C. Sandeep, Experimental design of tritium extraction loop from lead lithium eutectic, *Fusion Eng. Des.* 85 (2010) 803–808.
- [3] J.A. Rocha, J.L. Bravo, J.R. Fair, Distillation columns containing structured packings: a comprehensive model for their performance. 2. Mass transfer model, *Ind. Eng. Chem. Res.* 35 (1996) 1660–1669.
- [4] J.A. Rocha, J.L. Bravo, J.R. Fair, Distillation columns containing structured packings: a comprehensive model for their performance. 1. Hydraulic models, *Ind. Eng. Chem. Res.* 32 (1993) 641–648.
- [5] N. Alpy, T. Dufrenoy, A. Terlain, Hydrogen extraction from Pb–17Li: tests with a packed column, *Fusion Eng. Des.* 39–40 (1998) 787–792.
- [6] N. Alpy, A. Terlain, V. Lorenz, Hydrogen extraction from Pb–17Li: results with 800 mm high packed column, *Fusion Eng. Des.* 49–50 (2000) 775–780.
- [7] T. Miyauchi, T. Vermeulen, Longitudinal dispersion in two-phase continuous-flow operations, *Ind. Eng. Chem. Fundam.* 2 (1963) 113–116.
- [8] L. Valenz, F.J. Rejl, V. Linek, Gas and liquid axial mixing in the column packed with Mellapak 250Y, Pall rings and Intalox saddles 25 under flow conditions prevailing in distillation columns, *Ind. Eng. Chem. Res.* 49 (2010) 10016–10025.
- [9] R. Billet, M. Schultes, Prediction of mass transfer columns with dumped and arranged packings. Updated summary of the calculation method of Billet and Schultes, *Trans. Inst. Chem. Eng.* 77 (1999) 498–504.
- [10] Z. Olujic, A.B. Kamerbeek, J.A. de Graauw, Corrugation geometry based model for efficiency of structured distillation packing, *Chem. Eng. Proc.* 38 (1999) 683–697.
- [11] E. Mas de les Valls, L.A. Sedano, L. Batet, I. Ricapito, A. Aiello, O. Gastaldi, F. Gabriel, Lead–lithium eutectic material database for nuclear fusion technology, *J. Nucl. Mater.* 376 (2008) 353–357.
- [12] T. Terai, S. Nagai, T. Yoneoka, Y. Takahashi, Diffusion coefficient of tritium in molten lithium–lead alloy (Li 17 Pb 83) under neutron irradiation at elevated temperatures, *J. Nucl. Mater.* 187 (1992) 247–253.
- [13] F. Reiter, Solubility and diffusivity of hydrogen isotopes in liquid Pb–17Li, *Fusion Eng. Des.* 14 (1991) 207–211.
- [14] Y. Edao, H. Noguchi, S. Fukada, Experiments of hydrogen isotope permeation, diffusion and dissolution in Li–Pb, *J. Nucl. Mater.* 417 (2011) 723–726.
- [15] A. Aiello, A. Ciampichetti, G. Benamati, Determination of hydrogen solubility in lead lithium using sole device, *Fusion Eng. Des.* 81 (2006) 639–644.
- [16] R.E. Tsai, A.F. Seibert, R.B. Eldridge, G.T. Rochelle, A dimensionless model for predicting the mass-transfer area of structured packing, *AIChE J.* 57 (2011) 1173–1184.
- [17] R.E. Tsai, P. Schultheiss, A. Kettner, J.C. Lewis, A.F. Seibert, R.B. Eldridge, G.T. Rochelle, Influence of surface tension on effective packing area, *Ind. Eng. Chem. Res.* 47 (2008) 1253–1259.
- [18] L. Valenz, F.J. Rejl, V. Linek, Absorption mass-transfer characteristics of Mellapak packings series, *Ind. Eng. Chem. Res.* 50 (2011) 12134–12142.
- [19] (a) V. Viola, G. Perini, G. Lolligeroni, Kinetics of deuterium desorption from Pb–Li eutectic, *Fusion Eng. Des.* 14 (3–4) (1991) 249–260; (b) C. Malara, G. Casini, V. Viola, Analysis of tritium behavior and recovery from water-cooled Pb17Li blanket, *Fusion Eng. Des.* 28 (1995) 299–312.
- [20] T. Terai, S. Nagai, T. Yoneoka, Y. Takahashi, Mass transfer coefficient of tritium from molten lithium–lead alloy (Li₁₇Pb₈₃) to environmental gas under neutron irradiation, *Fusion Eng. Des.* 17 (1991) 237–241.
- [21] H. Feuerstein, F. Grabner, S. Horn, J. Oschinski, Transport of deuterium and rare gases by flowing molten Pb–17Li, *J. Nucl. Mater.* 179–181 (1991) 882–885.
- [22] O. Gastaldi, N. Ghirelli, F. Gabrieli, L. Giancarli, J.F. Salavy, Tritium transfers and main operating parameters impact for demo lithium lead breeding blanket (HCLL), *Fusion Eng. Des.* 83 (2008) 1340–1347.
- [23] Y. Song, Q. Huang, Y. Wang, M. Ni, Analysis on tritium controlling of the dual-cooled lithium lead blanket for fusion power reactor FDS-II, *Fusion Eng. Des.* 84 (2009) 1779–1783.

- [24] K. Onda, H. Takeuchi, Y. Okumoto, Mass transfer coefficients between gas and liquid phases in packed columns, *J. Chem. Eng. Jpn.* 1 (1968) 56–62.
- [25] Z. Křivský, M. Strnad, V. Linek, P. Beneš, J. Šulc, A. Stoy, Fillers with hydrophilic surfaces for installations for interphase mass and/or heat exchange. Application: DE 80-3035483 Patent No. 19800919.
- [26] V. Linek, P. Petříček, P. Beneš, R. Braun, Effective interfacial area and liquid side mass transfer coefficients in absorption columns packed with hydrophilized and untreated plastic packings, *Chem. Eng. Res. Des.* 62 (1984) 13–21.
- [27] P. Protsenko, A. Terlain, M. Jeymond, N. Eustathopoulos, Wetting of Fe–7.5%Cr steel by molten Pb and Pb–17Li, *J. Nucl. Mater.* 307 (2002) 1396–1399.
- [28] M.M. Gubzhokov, M.K. Ponegev, A.B. Sozaeva, V.A. Sozaev, Temperature dependences of wetting angles of steel 12Cr18Ni9Ti and ceramics by the melts with least additions of alkali metals, *J. Phys.: Conf. Ser.* 98 (2008) 062028.



Laboratory differential simulation design method of pressure absorbers for carbonization of phenolate solution by carbon dioxide in coal-tar processing

V. Linek*, J. Sinkule, T. Moucha, J.F. Rejl

Institute of Chemical Technology Prague, Department of Chemical Engineering, Technická 5, 16628 Prague 6, Czech Republic

ARTICLE INFO

Article history:

Received 14 May 2008

Received in revised form 4 September 2008

Accepted 22 September 2008

Available online 27 September 2008

Keywords:

Absorption column design

Coal-tar processing

Phenolate carbonization

Carbon dioxide absorption

ABSTRACT

A laboratory differential simulation method is used for the design of carbonization columns at coal-tar processing in which phenols are regenerated from phenolate solution by carbon dioxide absorption. The design method is based on integration of local absorption rates of carbon dioxide along the column. The local absorption rates into industrial phenolate mixture are measured in a laboratory model contactor for various compositions of the gas and liquid phases under the conditions that ensure the absorption rates in the laboratory absorber simulate the local rates in the industrial column. This condition is the same value of physical liquid-side mass transfer coefficients in the laboratory model contactor and in the absorption column. As the model contactor a stirred cell is used in which the interfacial area is well defined. By using an auxiliary surface stirrer the values of the physical mass transfer coefficient are extended up to the values encountered in packed absorbers. In experiments, carbon dioxide was absorbed into industrial phenolate mixture containing Na-phenolate of the phenol-mixture of the following approximate composition: phenol 44%, *o*-cresol 9%, *p*-cresol 10%, *m*-cresol 15%, 2,4-xyleneol 2%, 2,5-xyleneol 1%, 2,6-xyleneol 0.5%, 2,3-xyleneol 0.5%, 3,4-xyleneol 1%, 3,5-xyleneol 2%, *o*-ethyl-phenol 0.5%, *m*-ethyl-phenol 2%, *p*-ethyl-phenol 1.5%, others 11%. The experiments were performed in the following ranges of temperature 50–90 °C and pressure 100–700 kPa. An explicit formula correlating the absorption rates with carbonization of phenolate solution, partial pressure of carbon dioxide and temperature was derived which facilitated an assessment of various technological variants.

On the bases of the calculations, two-step carbonization columns were designed for 30 000 t/year of the phenolate solution treatment by carbon dioxide. The absorption proceeds at higher pressure of 500 kPa and temperatures from 50 to 65 °C, pure carbon dioxide is used and toluene is added. These conditions have the following favourable effects: (i) significant size reduction of the columns, (ii) it is possible to process more concentrated solutions without danger of silting the columns by crystallization of NaHCO₃ on the packing, (iii) small amount of inert gas is released; from environmental standpoint, this process arrangement represents an encapsulated technology without harmful influence on environment, (iv) lower alkalinity and better separability of the organic phase (phenols with toluene) from water phase (soda or bicarbonate solution) in separators.

© 2008 Elsevier B.V. All rights reserved.

1. Introduction

A fundamental quantity for the design of packing height in an absorption column is absorption rate of the gas into the absorption solution used. The industrial absorption solutions are often a mixture of substances for which all required physical and kinetic data necessary for the design from first principles are not known. An empirical simulation method is then practically the only feasible approach for the calculation of the column packing height.

In this method, the absorption rate is measured directly in the given absorption system in a laboratory apparatus under the same conditions as are in the industrial column.

The laboratory differential simulation method was proposed by Danckwerts and Gillham [1] and developed by other authors [2–4]. The reliability of the method was tested by the simulated design of an existing industrial packed column for CO₂ scrubbing at a high pressure (28 kPa) with a mixed solution of 30% triethanolamine and 3% diethanolamine. They found an excellent agreement between the calculated (23.1 m) and the actual (24.5 m) height of packing. To allow more flexible design and optimization with respect to changes in process conditions (activator concentration, temperature, and gas and liquid flow rate), Linek et al. [5] have presented

* Corresponding author.

E-mail address: linekv@vscht.cz (V. Linek).

a new version of the method allowing also a simple way of the inclusion of an axial mixing of gas phase into the design.

The laboratory differential simulation method, using a stirred cell in a batch arrangement as a model contactor, is employed in this work to design high-pressure CO₂ absorber for carbonization of 30 000 t/year of phenolate solution in the treatment of a coal-tar. The aim is also to find suitable temperature and pressure for absorption and to evaluate a possible effect of addition of toluene into the absorption process.

2. Scheme of industrial carbonization unit

Phenols are usually separated from coal-tars by extraction into lye solution in the form of phenolates. From the solution of the industrial phenolate mixture (IPM), the phenols are regenerated by absorption of carbon dioxide performed in carbonization unit. During the absorption, soda produced by neutralization of Na-phenolate stays in aqueous phase while released phenols pass into newly formed organic phase of phenols. The carbonization unit should ensure: (i) minimum content of Na⁺-ions in organic phase of phenols, (ii) minimum quantity of gaseous outlets, which contain carcinogenic vapour of phenols, (iii) minimum content of phenolates in the outgoing soda solution, (iv) minimum content of bicarbonate in outgoing soda solution. Increasing carbonization affects contradictory the requirements: favourably affects the requirements (i) and (iii) and unfavourably (ii) and (iv). Accordingly, it was suggested to carry out the carbonization of the IPM in two counter current pressure absorbers using pure carbon dioxide in the following way.

In the first absorber, the IPM is saturated by carbon dioxide to the extent that its alkalinity will be converted into Na₂CO₃. Bicarbonate solution flowing out of the second column is fed to lower section of the first column to be converted back onto soda before leaving the bottom of the first column. Addition of toluene to the solution outgoing from first column may markedly lower water content and residual alkalinity of not-fully saturated carbolic acid (NSCA) which forms in separator after first column. Toluene also facilitates phase segregation in the funnel by increasing density difference of the separated phases.

In the second absorber, the NSCA with addition of a little water is fully saturate by carbon dioxide, i.e. Na⁺ in aqueous phase convert to NaHCO₃. In this situation, alkalinity of organic phase of saturated carbolic acid (SCA) which is formed in separator after second column, achieves its minimum attainable under given operational conditions (temperature and pressure). An application of pure carbon dioxide for absorption minimize amount of the gaseous outlets from the first absorber.

Technological scheme with notation of streams and equipments is shown in Fig. 1. The industrial phenolate mixture 1 is pumped to the head of the first absorber **D** from compensatory reservoir **A** by pump **C**. Part of IPM is recycled back to the reservoir **A** through the small packed column **B**. In this column, the remnants of CO₂ are entrapped from waste gases 17 drained from whole this carbonization unit to incineration plant. Carbon dioxide in the stream 9 from the top of the first column **D** and in the stream 16, generated by the pressure release of the saturated carbolic acid in the expander **J**, is returned into the process and its losses are so minimized. These streams, led above water level in the storage tank **A**, contain except of CO₂ remnants also vapours of phenols, water, and toluene and inert from the feed of pressurized carbon dioxide 7. Into the lower part of the first absorber there are led carbon dioxide 8 from the bottom of the second column **H**, bicarbonate solution 5 and toluene 10. Liquid mixture 11 is from the bottom of the first absorber led to the separator **E**, from which stream 3 of the NSCA and the final

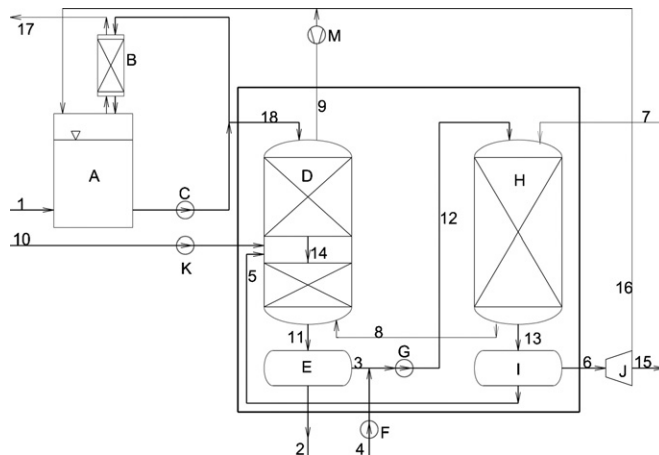


Fig. 1. Scheme of the carbonization technology.

soda solution 2 issue. Water, stream 4, is added into the stream 3 by means of dosing pump **F**. The liquids after mixture in the pump **G** are led at the top of the second absorber **H**. Liquid mixture 13 is from the second absorber led into the separator **I** from which is bicarbonate solution 5 returned back to the first column and stream 6 of SCA is led into the expander **J**. Gases 16, released from the SCA (practically pure CO₂ + vapour of toluene), are led into the storage tank **A** where all CO₂ is absorbed into the fresh solution of IPM in the column **B**. Practically pure CO₂ is feed to the top the second column as stream 7.

Pressurized part of the equipment is delimited by bold line on the scheme. Absorption of pure carbon dioxide under pressure has a number of advantages compared to the absorption at normal pressure: (i) the equipments are of smaller sizes, (ii) in the small equipment, the recirculation of the solution for achieving a minimum wetting rate for prevention crystallization of NaHCO₃ on the packing is not necessary, (iii) minimize escape of gas waste to the surroundings (encapsulated technology on the side of gaseous CO₂).

3. Laboratory differential simulation method of the carbonization packed column absorber

The laboratory differential simulation method is based on experimentally measured absorption rates of carbon dioxide, N_A , into the industrial phenolate mixture in a laboratory model absorber under the conditions prevailing in the industrial column. The total interfacial area in the column, A_w , needed for the required carbonization of the phenolate mixture is found by numerical integration of the local absorption rates along the column

$$A_w = \dot{V}_L \int_{c_{A2}}^{c_{A1}} \frac{dc_A}{N_A} \quad (1)$$

c_{A1} and c_{A2} are carbonizations of the input and the output liquid stream, respectively. This area is subsequently converted to column diameter d and packing height H for packing type chosen. To allow more flexible design and optimization with respect to possible changes in concentration, temperature, and gas and liquid flow rate, the absorption rates, N_A , must be measured at different levels of temperature t , carbon dioxide partial pressure p_A and carbonization c_A to the extent assumed in the industrial absorber. This approach, using a stirred cell in a batch arrangement as a model contactor, is employed in this work to simulate the high-pressure CO₂ absorber.

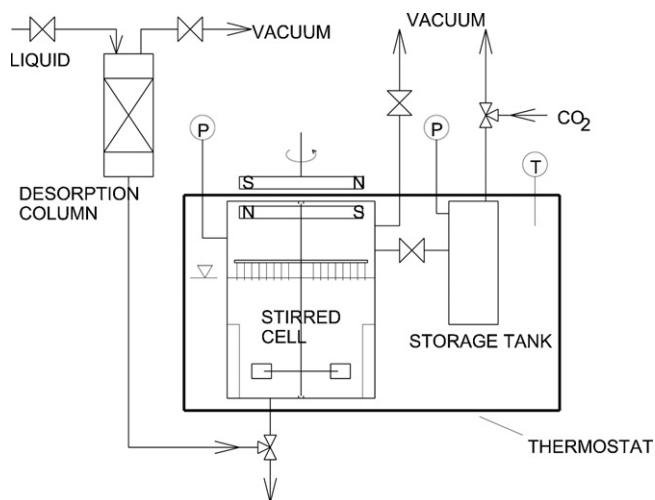


Fig. 2. Laboratory model contactor.

The conditions ensuring the same absorption rates in laboratory absorber as the local rates in the industrial column follow from the theory of absorption accompanied by chemical reaction. For absorption with rapid chemical reaction taking part in the liquid film (e.g. neutralization reaction), the conditions were defined by Laurent and Charpentier [3]: if the laboratory experiment is performed with the same absorption solution, temperature and compositions of both phases as the absorption proceeds at a given section of the industrial absorber, then the agreement of physical mass transfer coefficients k_G and k_L in both equipments ensures the usability of the laboratory results for the design. If the resistance against mass transfer in the gas phase is negligible, e.g. when pure gas is absorbed, the coefficient k_G is irrelevant. The agreement of k_L values guarantees the same hydrodynamic conditions at the interface in both apparatuses.

4. Experimental

4.1. Laboratory model contactor

Apparatus, schematically drawn in Fig. 2 and described in detail elsewhere [4], is made of stainless steel and is immersed into the bath, which maintains temperature with accuracy of $\pm 0.02^\circ\text{C}$. It consists of a desorption column, the stirred cell, a gas storage tank ($V_{GS} = 599.3\text{ cm}^3$) and two accurate pressure transducers in the cell and the tank. The apparatus enables to measure an equilibrium vapour pressure of the absorbing solutions, to dose an accurate amount of CO_2 above the solution level and to follow an absorption rate of gas in the solution as a function of pressure and carbonization of the absorbing solution.

The stirred cell is a cylindrical vessel with a diameter of 0.08 m, a liquid volume of 212.6 cm^3 , and a total volume of 915.3 cm^3 , equipped with a magnetically driven six-blade turbine stirrer in the bulk liquid and an auxiliary liquid surface stirrer on a common shaft. The surface stirrer allows one to attain high k_L values commonly encountered in packed columns. The stirrer is a PTFE disk bearing an array of 64 needles (1 mm in diameter). The tips of the needles reach 2 mm beneath the liquid surface.

4.2. Experimental condition

Experiments were performed with the industrial phenolate mixture. The mixture contains Na-phenolate of the phenol-mixture of the following approximate composition: phenol 44%, *o*-cresol

9%, *p*-cresol 10%, *m*-cresol 15%, 2,4-xyleneol 2%, 2,5-xyleneol 1%, 2,6-xyleneol 0.5%, 2,3-xyleneol 0.5%, 3,4-xyleneol 1%, 3,5-xyleneol 2%, *o*-ethyl-phenol 0.5%, *m*-ethyl-phenol 2%, *p*-ethyl-phenol 1.5%, others 11%. Alkalinity of streams expressed in kg NaOH/m^3 was measured by titration with 0.1 N HCl using methyl orange as indicator. The alkalinity of the industrial phenolate mixture was equal to 124 kg NaOH/m^3 .

Experiments were performed in the stirred cell at agitator frequency of 230 min^{-1} , when the value of k_L equals to $2 \times 10^{-4}\text{ m/s}$. This value well represents mass transfer coefficients in packed columns (e.g. for Pall rings 50 mm within the liquid loading interval from 40 through $100\text{ m}^3/\text{m}^2\text{ h}$ $k_L = 1.7$ through $2.8 \times 10^{-4}\text{ m/s}$, Linek et al. [6]). Absorption rate at chemisorption depends on k_L only a little; even the absorption accompanied by pseudo-first order reaction (e.g. absorption of diluted CO_2 into NaOH solution) does not depend [6] on k_L at all.

An aim of the experiments was to obtain absorption rates of carbon dioxide N_A at nodal points of the absorbers designed by integration Eq. (1). Measurements were performed with the industrial phenolate mixture (IPM) and the mixture of not-fully saturated carbolic acid (NSCA) with toluene and water mixed in the proportion of 1:0.23 with resulting constitution 47.4% toluene, 7.7% water and 44.9% phenols. Such conditions of the experiments were selected to cover the possible conditions in the industrial absorption columns, i.e. temperatures 50, 70 and 90°C , partial pressures of CO_2 from equilibrium pressure through 700 kPa, carbonization of solution from 0 till $1.5\text{ kmol CO}_2/\text{m}^3$ for IPM and 0 till $0.25\text{ kmol CO}_2/\text{m}^3$ for NSCA.

4.3. Measurement and evaluation methods

The methods employed were similar to those used in our previous work [5]. The absorption rate of carbon dioxide into the IPM and the mixture of NSCA, water and toluene were measured as follows. The evacuated cell was filled with degassed absorption liquid and after the desired temperature had been established the equilibrium pressure of water, phenols and toluene vapours above the solution, p_{vapor}^0 , was recorded. Then the solution was exposed to pure CO_2 and the time course of pressure in the cell was recorded. When equilibrium was attained (i.e., the pressure in the cell reached a steady-state) the equilibrium pressure of CO_2 , p_A , was recorded. Afterwards a further amount of pure CO_2 was added into the cell and the procedure was repeated with the same initial pressure. The initial pressure ranged from 100 to 750 kPa. The time courses of the pressure in the cell in each experiment, $p(t)$, were fitted by the multinomial of the shape

$$p(t) = b_0 + b_1 t + b_2 t^2 + b_3 t^3 + b_4 t^4 \quad (2)$$

Correlation coefficients of the equation were higher than 0.9999 in all the experiments. The instantaneous absorption rates of carbon dioxide were calculated from the relation

$$N_A = -\frac{V_G}{A_{\text{cell}} RT} \frac{dp_A}{dt} = -\frac{V_G}{A_{\text{cell}} RT} (b_1 + 2b_2 t + 3b_3 t^2 + 4b_4 t^3) \quad (3)$$

because the partial pressure of carbon dioxide is given by the relation

$$p_A = p - p_{\text{vapor}}^0 \quad (4)$$

and tension of vapours above the solution p_{vapor}^0 is constant during the experiment. Instantaneous carbonization of solution, c_A , expressed as number of CO_2 -kmoles absorbed in 1 m^3 of absorbing solution, was evaluated from the difference of the amount of CO_2 introduced to the cell from the storage tank, n_{A0} , and the amount of CO_2 , which remained in gaseous phase in the cell at the given

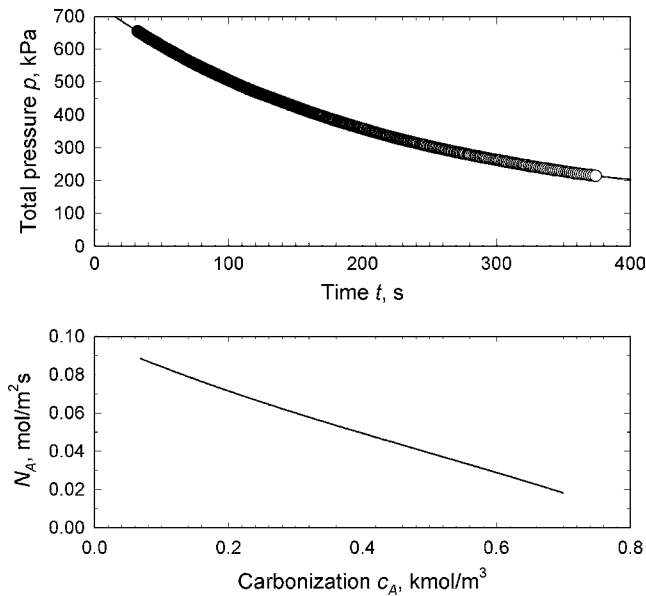


Fig. 3. Course of experiment performed with IPM at 50 °C.

moment, n_{AG} ,

$$c_A = \frac{n_{A0} - n_{AG}}{V_L} = \frac{V_{SG} \Delta p_{SG} - V_G (b_0 + b_1 t + b_2 t^2 + b_3 t^3 + b_4 t^4)}{V_L RT} \quad (5)$$

For illustration, results of one experiment performed with industrial mixture phenolate (IPM) at 50 °C are plotted in Fig. 3. The time profile of pressure in the cell, fitted by the relation (2), is given as well as the dependence of carbon dioxide absorption rate on the solution carbonization.

Solubility of CO₂ in the saturated carbonic acid with toluene was determined as follows. Known amount of the liquid was fed to the cell and was saturated by carbon dioxide at about 500 kPa. In this way, all alkalinity was removed from the sample, which could bind CO₂ chemically. Then, all physically dissolved CO₂ together with other gases were removed from the sample by vacuum, vapour pressure was determined and subsequently, a known amount of carbon dioxide was introduced to the cell from the gas storage. The solubility was calculated from the liquid sample volume, the amount of carbon dioxide added and final equilibrium pressure in the cell.

5. Results and discussion

5.1. Equilibrium data

An average equilibrium partial pressures of water and phenols vapours above the IPM, p_{vapor}^o , measured at the beginning of the experiments performed at 50, 70 and 90 °C were 9.18, 21.05 and 55.72 kPa, respectively and are well correlated by the relation of Antoine type

$$\ln p_{\text{vapor}}^o = -11.5876 - \frac{4703.7}{t - 391.45} \quad (6)$$

Average equilibrium partial pressures of water, phenols and toluene vapours above the mixture of NSCA with toluene measured at the beginning of the experiments performed at 50 °C equals to 26.01 kPa.

The equilibrium partial pressure of carbon dioxide, p_A^+ , above the saturated carbonic acid with toluene as a function of physically

Table 1
Empirical parameters of Eq. (9).

T (°C)	50	70	90
a_1			
a_{01}	-0.5547	-0.5440	-0.5595
a_{11}	2.936e-5	5.343e-5	9.890e-5
a_2			
a_{02}	-1.400e-3	-1.657e-2	-1.838e-2
a_{12}	-1.163e-4	-1.783e-4	-3.260e-4
a_3			
a_{03}	2.952	1.582	1.174
a_{13}	-2.100e-3	-3.448e-4	3.339e-4
a_4	0.5580	0.5428	0.5545

dissolved carbon dioxide, c_A^+ , in the solution at 50 °C was fitted well as

$$p_A^+ = 1758c_A^+ \quad (7)$$

5.2. Absorption rate of carbon dioxide into IPM and NSCA with toluene

The experimental absorption rates, N_A , into the IPM were measured at three temperatures (50, 70, and 90 °C) and into the NSCA mixture with toluene at 50 °C only. Their dependences on partial pressure of carbon dioxide p_A and carbonization of the solutions c_A were correlated at individual temperatures t_i by the formula

$$N_A(c_A, p_A; t_j) = a_1 [1 - a_2(2 - c_A)^{a_3}]^{1/a_3} + a_4 \quad \text{for IPM} \quad (8)$$

where a_i are linear function of p_A

$$a_i = a_{0i} + a_{1i}p_A \quad i = 1, 2, 3 \quad (9)$$

and

$$N_A(c_A, p_A; t_j) = b_1 + b_2(c_A)^{b_3} \quad \text{for NSCA with toluene} \quad (10)$$

where b_i are linear function of p_A

$$b_i = b_{0i} + b_{1i}p_A \quad i = 1, 2 \quad (11)$$

The parameters a_i and b_i were established by minimizing the sum of squares of relative errors. The results are given in Tables 1 and 2 together with the relative mean deviations between experimental and from the relations (8) and (10) calculated values. The experimental absorption rates into IPM and NSCA determined at 50 °C are plotted in Figs. 4 and 5, respectively. It is apparent from Fig. 6, in which the absorption rates for all temperatures and the mean relative deviations are given, that a good agreement was achieved between the experimental and from the relations (8) and (10) calculated values.

Table 2
Empirical parameters of Eq. (11).

t (°C)	50
b_1	
b_{01}	8.934e-4
b_{11}	1.233e-4
b_2	
b_{02}	-1.498
b_{12}	1.809e-3
b_3	
b_{03}	3.646
b_{13}	-2.437e-3

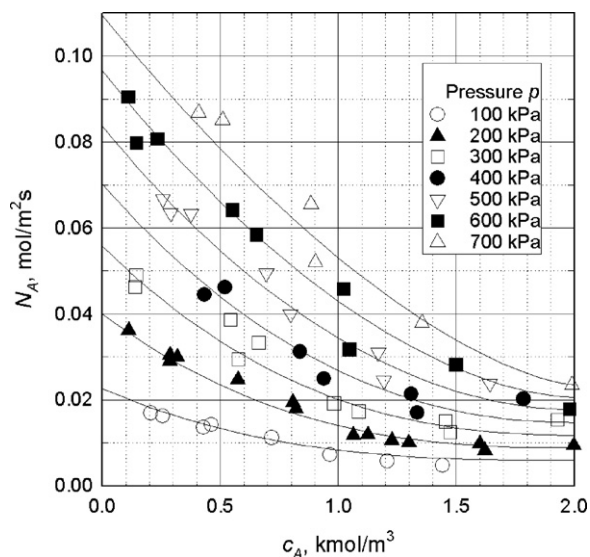


Fig. 4. Carbon dioxide absorption rate in IPM at 50 °C. Lines calculated from Eq. (8).

5.3. Mass balances of the industrial carbonization unit working at various pressures

Input data of the mass balances of the carbonization unit presented in Fig. 1 are given in Table 3. Assuming the same composition of the streams 1 and 18 (see Table 3), we obtain dimensions of the columns D and H on the safe side of the design compared to the situation when carbon dioxide in the streams 9 and 16 is absorbed into the IPM in the column B. Balance-sheet for total pressures of 250 and 500 kPa are given in Table 4. The results show advantages of the higher-pressure technology: (i) amount of degassed stream 9, released from the first column, is lower about 14%. (ii) Total con-

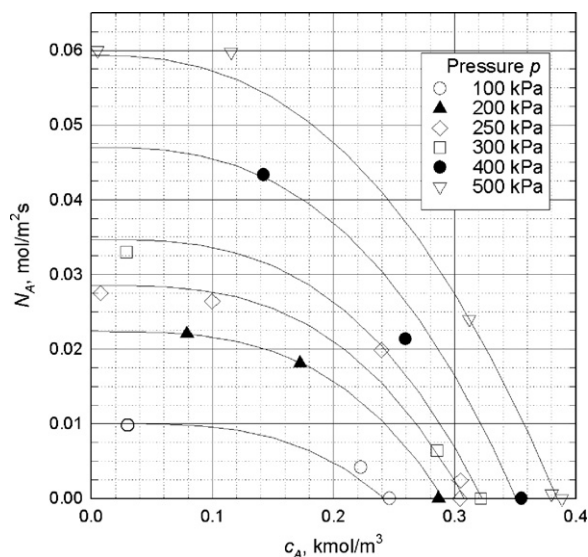


Fig. 5. Carbon dioxide absorption rate in NSCA at 50 °C. Lines calculated from Eq. (10).

sumption of carbon dioxide is lower. If CO₂ released in the stream 16 is reused for carbonization of IPM in the column B, the total consumption reduces about 11%. (iii) Amount of CO₂ released in expander J from SCA is 2.6 times higher.

5.4. Calculation of the packing height of the industrial absorption column

Interfacial areas, $A_{w,i}$, needed to meet the required carbonizations for the individual technological variants were calculated from relation (1) by integration of local absorption rates along the column.

Table 3

Input data of the mass balances of the carbonization unit given in Fig. 1.

Stream	Flow (t/h)	Composition	ρ (kg/m ³)
1, 18	3.75	10.8% NaOH	1150
2	–	% NaHCO ₃ / % Na ₂ CO ₃ = 0.38	
3	–	47.4% toluene; 7.7% H ₂ O; 44.9% phenols; 13.4 g NaOH/1 kg	
4	–	$M_4/m_3 = 0.23$	
6	–	5% H ₂ O; 0.03% NaOH	
7	–	99 vol. CO ₂ ; 1% vol. inerts	
10	0.9264	Toluene	

Table 4

Mass balances of the carbonization unit at the total pressures of 250/500 kPa.

Stream	Flow (t/h)	Alkalinity (kmol Na ⁺ /t)	Carbonization (kmol CO ₂ /t)	Flow (kmol/h)	CO ₂ (% vol.)	t (°C)
1, 18	3.75	2.70	0		0	50
2	3.23	3.14	1.82			50
3	1.95	0.335	0.168			50
4	0.450	0	0			50
5	0.505	1.27	1.27			50
6	1.90	0.0075	0.160			50
7				6.32/6.01 ^a	99	50
8				6.36/5.44 ^a	88.7	50
9				0.152/0.131 ^a	50	50
10	0.926					50
11	5.18	2.08	1.198			60.8
12	2.40	0.272	0.136			50
13	2.40	0.272	0.136			50
14	3.75	2.71	1.48			63.3
15	1.90	0.0075	0.052/0.0477 ^a			50
16				0.276/0.716 ^a	74.1	50

^a The data for the total pressures of 250/500 kPa.

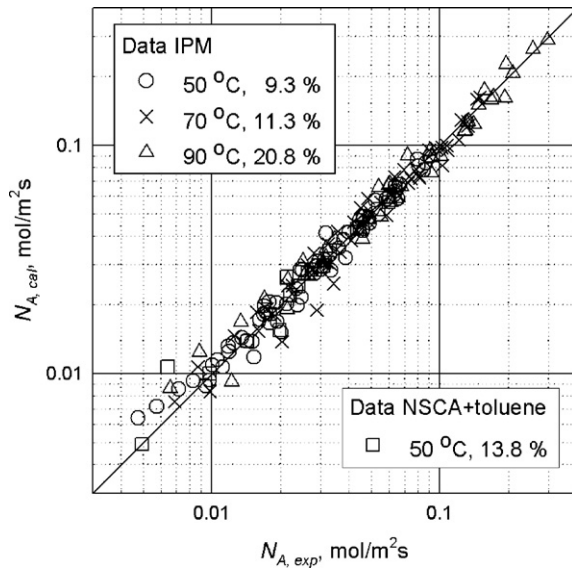


Fig. 6. Comparison of experimental and from regressions (8) and (10) calculated absorption rates and mean relative differences between them.

The local absorption rates, N_A , were calculated from relations (8) for solution IPM at temperatures of 50, 70, 90 °C and from relation (10) for NSCA at 50 °C. For other than mentioned temperatures, the rates were calculated from Arrhenius interpolation formula

$$N_A(c_A, p_A, t) = \alpha \exp \left\{ \frac{\beta}{t + 273.15} \right\} \quad (12)$$

α and β were determined from the rates at the nearest temperatures t_i and t_j

$$\beta = \left(\frac{1}{t_i + 273.15} - \frac{1}{t_j + 273.15} \right)^{-1} \ln \frac{N_A(c_A, p_A, t_i)}{N_A(c_A, p_A, t_j)} \quad (13)$$

$$\alpha = N_A(c_A, p_A, t_i) \exp \left\{ -\frac{\beta}{t_i + 273.15} \right\}$$

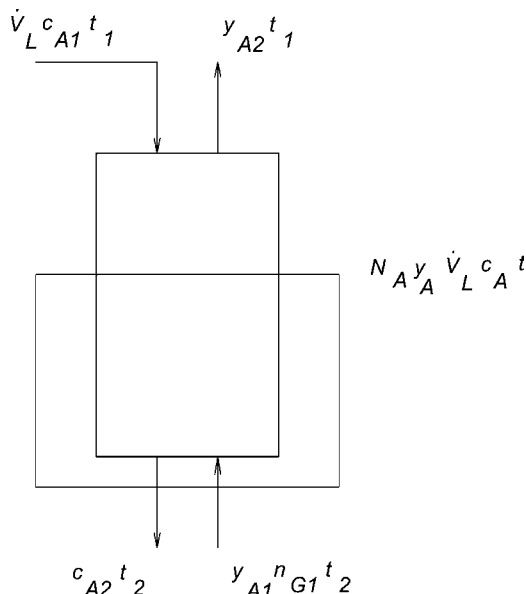


Fig. 7. Schema of the slice balance of column.

Table 5

Packing heights in the second carbonization column H for temperature 50 °C at pressures of 250 and 500 kPa.

p (kPa)	250			500		
A_w (m ²)	15.4			10.9		
B (m/h)	35	40	50	35	40	50
d (m)	0.303	0.28	0.27	0.303	0.28	0.27
H (m)	1.48	1.69	1.90	1.05	1.19	1.34

Input data for the integration of Eq. (1) were as follows (see Fig. 7): (i) volumetric liquid flow rate, \dot{V}_L , (ii) carbonization of input solution, c_{A1} , and required carbonization of output solution, c_{A2} , (iii) volumetric fraction of carbon dioxide in entering, y_{A1} , and exiting gas, y_{A2} .

The relations $p_A(c_A)$ and $t(c_A)$ follow from the slice mass and enthalpy balances of absorber. Following assumptions were used: (i) plug flow of phases, (ii) inert present in carbon dioxide does not dissolve in liquid, (iii) the heat capacity of gas is negligible compared to the liquid one, (iv) gas phase in absorber is saturated with water, phenols and toluene, (v) adiabatic absorption and the liquid temperature increase is proportional to the amount of carbon dioxide absorbed. These assumptions – except of (i) – underestimate mass transfer driving force of absorption and thus, lead to the design on the safe side. Then the relations have the following forms:

$$p_A(c_A) = y_{A2} p = [p - p_{\text{vapor}}^o(t) - p_T^o(t)] \frac{n_{G1} y_{A1} - \dot{V}_L (c_A - c_{A2})}{n_{G1} - \dot{V}_L (c_A - c_{A2})} \quad (14)$$

$$t(c_A) = t_1 - (c_A - c_{A1}) \Delta t \quad (15)$$

Gas flow rate at the inlet to the absorber n_{G1} is calculated from following overall CO₂ mass balance

$$n_{G1} = \dot{V}_L (c_{A1} - c_{A2}) \frac{1 - y_1^o - y_{A2}}{y_{A1} (1 - y_1^o) - y_{A2}} \quad (16)$$

where $y_1^o = [p_{\text{vapor}}^o(t) + p_T^o(t)]/p$ and toluene vapour pressure is

$$\log p_T^o(t) = 6.07954 - \frac{1344.8}{t + 219.482} \quad (17)$$

Measured value of the adiabatic temperature rise of liquid due to CO₂ absorption in IPM was $\Delta t = 9 \text{ K m}^3 \text{ IPM/kmol CO}_2$. This value was used also for calculations in NSCA.

Eq. (1) was integrated numerically by using the net of 200 nodal points. In calculations, zero carbonization of IPM entering the first column was considered, although can be expected that the entering IPM will already be partially carbonized at finish-cleaning column B (see schema Fig. 1). The calculations were done for two pressure levels (250 and 500 kPa) and three liquid loads B (35, 40 and 50 m³/m² h) preventing crystallization of bicarbonate on the packing. The areas A_w were then converted to packing height H and column diameter d for the selected liquid loads and packing type of Ralu flow ring no. 1 of geometric specific area $a_w = 144 \text{ m}^2/\text{m}^3$. The packing heights of the first carbonization column are given in Fig. 8 for various liquid temperatures at the inlet of the column t_1 and those in the second column are in Table 5 for temperature 50 °C. The high packing heights at high temperatures are due to high vapour tensions of the solution and toluene which lower driving force of absorption.

6. Final production industrial columns

On the basis of the performed calculations, two carbonization columns working at pressure of 500 kPa and temperature in interval 50–60 °C with pure carbon dioxide of the purity better than 99% have been used for carbonization of 30 000 t/year of phenolate

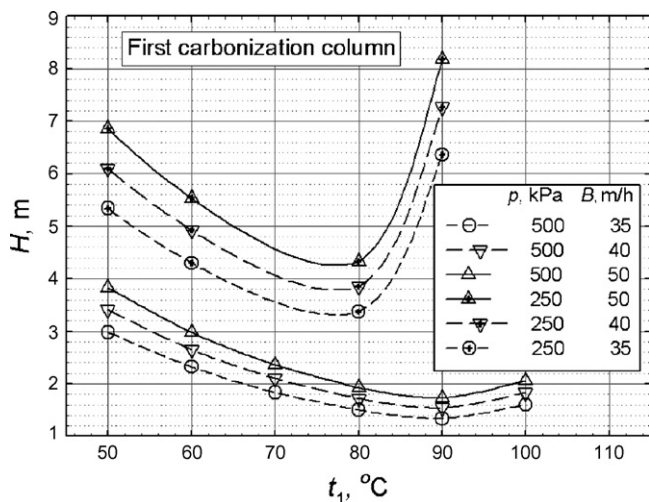


Fig. 8. Packing height H in the first carbonization column packed with Ralu flow ring no. 1 as a function of inflowing liquid temperature t_1 at three liquid loadings B and two pressures.

solution in coal-tar processing at DEZA a.s., Valašské Meziříčci, Czech Republic. Alkalinity of the final organic phase of the saturated carbonic acid in the output stream of the second carbonization column did not exceed $0.009 \text{ kmol Na}^+/\text{t}$.

6.1. Construction of the first carbonization column

Inner diameter of the column is 0.35 m, packing height 3.2 m of metal Ralu ring 25 mm. The packing is divided into three sections namely 0.5, 2.2 and 0.5 m separated by redistributors of liquid with separated flow of phases. In the upper section, inert components presented in the “pure” carbon dioxide accumulate. The redistributor reduces their transport into lower parts of the column by axial dispersion. On the lower redistributor (situated 0.5 m above the column bottom), toluene and recycled stream of bicarbonate from the second column are fed. In the low section, the liquid phases are well mixed and the bicarbonate is converted back onto carbonate. Carbon dioxide is fed into the bottom and, at the same time, above the low redistributor to prevent flooding in the column owing to possible foaming of the solution in lower parts of the column.

6.2. Construction of the second carbonization column

Inner diameter of the column 0.3 m, packing height 1.5 m of metal Ralu ring 25 mm. Carbon dioxide is fed to the head of the column. Co-current configuration has been used to prevent from flooding the column.

7. Conclusions

The empirical simulation method, developed by Danckwerts and Gillham [1] and Laurent and Charpentier [2] for calculation of the packing height of industrial packing absorption column for complicated absorption systems, was successfully used in the design of pressurized carbonization columns for regeneration of phenols from phenolate solution by carbon dioxide absorption. Stirred cell was used as a model contactor. Correlations for the

rate of carbon dioxide absorption by phenolate solution valid in a wide range of temperatures (50–90 °C) and partial pressures of carbon dioxide (0–700 kPa), enabling this design, are presented as Eqs. (8)–(13).

Acknowledgments

Support from the Ministry of Education (MSM 6046137306) is gratefully acknowledged.

Appendix A. Nomenclature

a_w	specific geometrical area of packing (1/m)
A_{cell}	gas–liquid interfacial area in stirred cell (m^2)
A_w	gas–liquid interfacial area in packed column (m^2)
B	liquid load (m/h)
c_A	concentration of carbon dioxide (mol/m^3)
d	column diameter (m)
H	height of packing (m)
k_G	mass transfer coefficient in gas (m/s)
k_L	mass transfer coefficient in liquid (m/s)
N_A	absorption rate of carbon dioxide ($\text{mol}/\text{m}^2\text{s}$)
n_{A0}	amount of CO_2 introduced to the cell from the storage tank (mol)
n_{AG}	carbon dioxide in gas phase in the cell (mol)
n_{G1}	gas flow rate at inlet to absorption column (mol/s)
p	total pressure (Pa)
p_A	partial pressure of carbon dioxide (Pa)
p_{vapor}^o	partial pressures of water and phenols vapours above the IPM (Pa)
p_T^o	vapour pressure of toluene (Pa)
Δp_{SG}	pressure drop in the storage tank (Pa)
R	gas constant ($\text{Pa m}^3/\text{mol K}$)
t	time/temperature ($\text{s}/^\circ\text{C}$)
T	temperature (K)
V_L	liquid volume in stirred cell (m^3)
V_G	gas volume in stirred cell (m^3)
V_{SG}	volume of dosing CO_2 -reservoir into stirred cell (m^3)
\dot{V}_L	liquid volume flow rate in to column (m^3/s)
y	molar fraction
y_1^o	$= [p_{vapor}^o + p_T^o]/p$

References

- [1] P.V. Danckwerts, A.J. Gillham, The design of gas absorbers. I—methods for predicting rates of absorption with chemical reaction in packed columns, and tests with 1 1/2 in. Raschig rings, *Trans. IChemE* 42 (1966) 42–54.
- [2] P.V. Danckwerts, E. Alper, Design of gas absorbers. III—laboratory point model of a packed column absorber, *Trans. IChemE* 53 (1975) 34–40.
- [3] A. Laurent, J.C. Charpentier, The use of experimental laboratory-scale models in predicting the performance of gas–liquid reactors, *Inst. Chem. Eng.* 23 (1983) 265–275.
- [4] V. Linek, J. Sinkule, M. Richter, J. Pospilil, Verification of the design methods for industrial carbon dioxide-triethanolamine absorbers: laboratory differential simulation and computational methods, *Ind. Eng. Chem. Res.* 29 (1990) 1676–1681.
- [5] V. Linek, J. Sinkule, P. Havelka, Empirical design method of industrial carbon dioxide-mixed solvent absorbers with axial dispersion in gas, *Ind. Eng. Chem. Res.* 33 (1994) 2731–2737.
- [6] V. Linek, P. Petříček, P. Beneš, R. Braun, Effective interfacial area and liquid side mass transfer coefficients in absorption columns packed with hydrophilised and unaterated plastic packings, *Chem. Eng. Res. Des.* 62 (1984) 13–21.

Liquid-phase mass-transfer coefficients of Mellapak structured packings under desorption of oxygen from primary alcohols

F.J. Rejl^{1,a}, J. Haidl^a, L. Valenz^a, A. Marchi^b, T. Moucha^a, R. Petříček^a, E. Brunazzi^b

a) University of Chemistry and Technology Prague,

Technická 5, 166 28 Praha 6, Czech Republic

Tel.: +420 220 44 3299

e-mail: frantisek.rejl@vscht.cz

b) Università di Pisa

Keywords: absorption, mass transfer, mass-transfer coefficient, structured packing

Abstract

Volumetric mass-transfer coefficient in the liquid phase, $k_L a$, for Mellapak 250.Y, 350.Y and 500.Y structured packings has been measured by standard method of desorption of oxygen into nitrogen from pure methanol, ethanol and n-propanol in the column of i.d. of 150 mm. Although utilization of organic solvents for absorption experiments provides valuable behavior interlink between properties of aqueous absorption systems and ordinary (organic) systems under distillation conditions, studies of such kind are not published in the open literature.

The behavior of the $k_L a$ data on alcohol systems do not differ significantly from that found for aqueous system, the $k_L a$ values rise with the liquid superficial powered to $\sim 0.5 - 0.78$. For one solvent the $k_L a$ are almost identical for all three packings under the same superficial velocity. According to the expectations the $k_L a$ values under the same superficial liquid flow rate are highest for the solvent with the lowest viscosity and the highest diffusivity of oxygen, methanol, and decrease in the order ethanol, n-propanol and water.

¹ corresponding author

The k_L data for all three packings, alcohols and also for water has been successfully correlated by dimensionless correlation $Sh = 0.207 \cdot Re^{0.798} Fr^{-0.563} We^{0.511} Sc^{0.528}$ with mean relative deviation of 12 %.

1 Introduction

As an important step for more reliable design of packed absorption and distillation columns we see adoption of the rate-based approach for their modeling. Utilization of the rate-based modeling demands reliable and accurate knowledge of its parameters, volumetric mass-transfer coefficients. These coefficients can be predicted from various models which also describe their dependence on the process conditions. To make sure that these predictions are reliable and the models are generally true, they should be based or verified against experimental data obtained by standard procedures under as broad as possible conditions, namely also under distillation ones.

Evaluation of the volumetric mass-transfer coefficients, $k_L a$, $k_G a$, under distillation conditions by the novel “profile method” [1], [2], [3] provided very reasonable results in terms of gas-phase ones, but results in dependence of $k_L a$ values on liquid flow rate of $k_L a \sim u_L^1$, which is steeper than that found during absorption experiments, where $k_L a \sim u_L^{0.62-0.9}$. The significant difference in the properties of the distillation mixtures and mostly aqueous systems used for the absorption experiments was suspected as a possible cause of the difference.

This paper refers on $k_L a$ data obtained for Mellapak 250.Y, 350.Y and 500.Y structured packings by desorption of oxygen into nitrogen from oxygen saturated methanol, ethanol and n-propanol at 20°C. The alcohols have been chosen as the constituents of the distillation mixtures used for the profile method experiments. They also differ significantly in viscosity and oxygen diffusivity and therefore cover broad spectra of the physical properties. Although only Mellapak 250.Y has been used for the mirrored distillation experiments, usage of the other packings broadens the experimental portfolio by geometrically similar packings of different size.

2 Literature review

Volumetric mass-transfer coefficient in the liquid phase, $k_L a$, on structured packings has been measured under absorption / desorption conditions with water as a liquid phase by stripping of low soluble gases [4], [5], [6], [7] or toluene [8] into the inert gas. The results are shown in the Fig. 1.

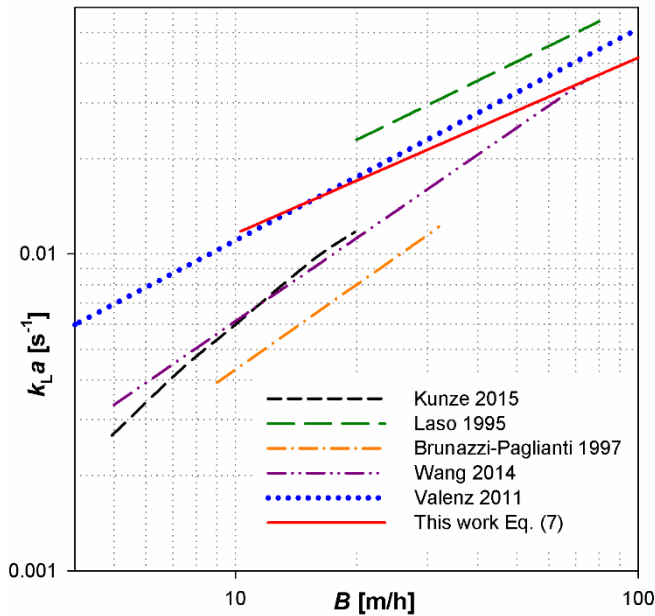


Fig. 1 – Liquid phase volumetric mass-transfer coefficient, $k_L a$. Experimental data for Mellapak 250.Y. Measured with, or recalculated to the $O_2 - H_2O$ system.

For the mutual recalculation of the results obtained with different absorbed / desorbed solutes i, j equation based on the penetration theory (1) was used

$$\frac{k_L a(i)}{k_L a(j)} \propto \sqrt{\frac{D_i}{D_j}} \quad (1)$$

The $k_L a$ values reported by the investigators are given either only in the graphical form [6] or correlated [4], [5] as a dependence of $k_L a$ on the liquid velocity u_L in the power law form (2) with α in the range of 0.62 - 0.9 (see

Table 1).

$$k_L a \propto u_L^{C_0} \quad (2)$$

Table 1: $k_L a$ values and their trend with liquid velocity for metal Mellapak 250.Y and oxygen stripping from water

		C_0 in the equation (2)	$k_L a$ [1/s] for $B = 20$ m/h
Laso (1995)	oxygen stripping	0.62	0.0229
Brunazzi (1997)	CO ₂ stripping	0.90	0.0080 (bed height = 0.84m)
Valenz (2011)	oxygen stripping	0.668	0.0175
Wang (2014)	toluene stripping	0.875	0.0114*

* - recalculated to O₂-H₂O system according to Eq. (1)

Some authors performed $k_L a$ measurements using aqueous systems with modified physical properties [9] or with packings of different geometry [8] what enabled more elaborated dimensional or dimensionless correlation of the data. While dependence of $k_L a$ on the gas velocity up to the loading point was found negligible [7], significant dependence of the $k_L a$ on the total packed bed height has been reported for random [10] as well as structured [7] packings. Large difference in experimentally obtained $k_L a$ values can be observed and the recent urge for the measurement and evaluation method standardization [11], [12], [13] is therefore comprehensible.

Many mass-transfer models for packed columns have been developed on the basis of the experimental data and theoretical considerations; summary of the models developed until 2005 can be found in [14] and recent actualization on the limited topic of the liquid side mass-transfer coefficient models on

structured packings in [15]. The $k_L a$ data calculated out of several models [16], [7], [17], [18], [19], [8] for several conditions treated in this work are depicted in the Figs 2-2a,b,c.

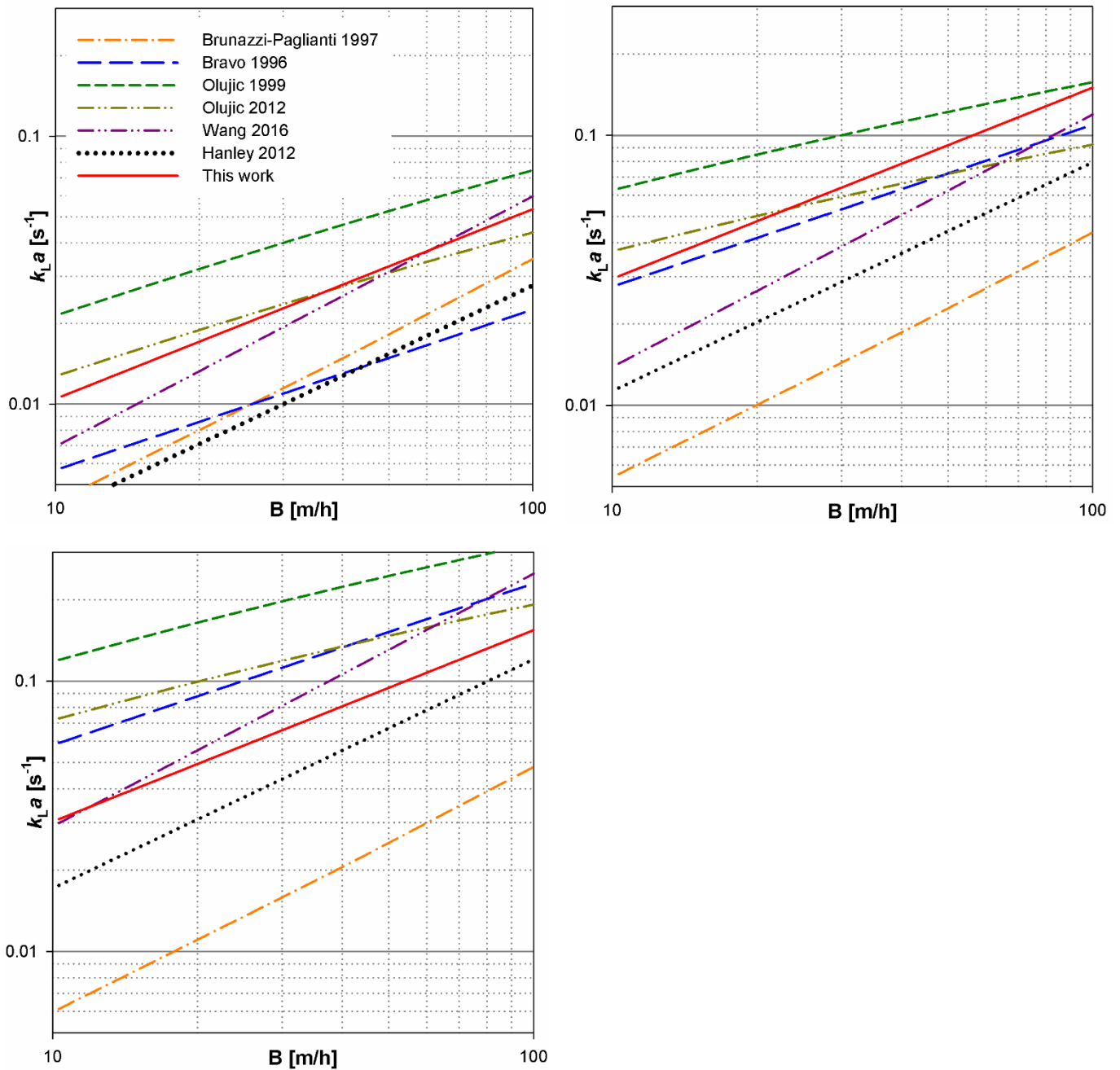


Fig. 2 – Liquid phase volumetric mass-transfer coefficient, $k_L a$. Prediction of the literature models. (a) Mellapak 250.Y (H_2O-O_2). (b) Mellapak 250.Y ($MeOH-O_2$). (c) Mellapak 500.Y ($MeOH-O_2$)

The $k_L a$ data predicted by the models for water (Fig. 2a) exhibit similar scatter as the experimental data (Fig. 1). The scatter increases when non-aqueous system (Fig. 2b) and different packing (Fig. 2c) is

introduced, demonstrating unsatisfactory knowledge of the k_L dependence on the physical properties of the liquid and size of the packing.

The data obtained with the water-inert gas system serve often as an experimental base for development of mass-transfer models which are usually assumed to be valid also for distillation conditions. However, water is a substance with high surface tension, far from the properties of the organic systems treated by distillation. There can be anticipated that the organic liquid phase in distillation experiments behaves significantly differently in terms of the liquid phase mass-transfer than aqueous systems under the desorption conditions.

Only few papers report on absorption/desorption from/into organic liquids in any packed device [20], [21]. Desorption experiments with organic liquid phase have been performed recently at our workplace using the wetted-wall column [22], however, although the device was often taken as a basis for development of mass-transfer correlations for structured packings, the effect of the liquid side hydrodynamics on the liquid-side mass-transfer coefficient is completely different.

There is currently no study dealing with absorption/desorption from/into organic liquids for structured packings published in the open literature. This article aims to fill this gap.

3 Theoretical background

The data for absorption of different gases into the liquid on the packing has been many times successfully correlated using penetration theory based on the imagination of unsteady diffusion of the solute into the liquid behaving like a semi-infinite slab for the period of exposure time τ after which the liquid is well mixed. The corresponding mass-transfer coefficient, k_L , is obtained through time averaging of the molar flux as

$$k_L = \sqrt{\frac{4D}{\pi\tau}} \quad (3)$$

As can be seen, the penetration theory doesn't directly describe either the influence of the liquid flow rate or the physical properties of the liquid on the mass-transfer rate. Their possible effect can be anticipated to be hidden in the value of the exposure time which can be assumed to be dependent on the liquid film hydrodynamics. The lack of prediction tools for determination of the exposure time on the basis of viscosity and surface tension can be attributed to relatively low number of experiments performed with different solvents.

Forces acting on the liquid film flowing down the column on the packing and forming its velocity profile and thickness are the inertial, gravitational, viscous and surface ones. The hydrodynamics of the film is therefore described by the values of *Reynolds*, *Froude* and *Weber* numbers, *Re*, *Fr*, *We*. The relation of the hydrodynamics to the mass-transfer is usually expressed by introduction of the *Sherwood* and *Schmidt* numbers, *Sh*, *Sc*. The final correlation can take dimensionless form

$$Sh = C_1 Re^{C_2} Fr^{C_3} We^{C_4} Sc^{C_5} \quad (4)$$

4 Experimental

Experimental set-up

Experiments have been carried out in the PVC-U column with of an i.d. of 150 mm (see Fig. 3). The packing was stainless steel Mellapak 250.Y, 350.Y and 500.Y with height of the element equal 0.21 m provided by Sulzer in the year 2000 and equipped with plain sheet extra wall-wipers designed at the workplace (see Fig. 4)². The liquid phase flowing in the closed circuit has been pumped from the main tank into the column by centrifugal pump P1 through the set of turbine flowmeters F1, F2 and

² The extra wall-wipers were made from the 0.1 mm thick stainless steel band with the total height of 40 mm. The lower half was cut to form downward pointing triangles. The tips of the triangles were manually bended into the packing element. The extra wall-wipers were placed just under the lower original ones.

distributed over the packing by pipe-type distributor with 25 openings (1415 openings/m²). The liquid flowing from the packing has been collected in the liquid collector / chimney gas-distributor and flew back to the main tank by means of gravity. The nitrogen from the cylinder has been fed under the gas-distributor. Its flow was controlled by control valves.

When tap water was the liquid phase, the batch of 300-400 l was maintained at constant temperature of 20 °C and saturated with oxygen in the agitated 500 l stainless steel tank H1.

In the case of alcohols the main storage tank was a 30 l PVC-U vessel H2 submerged in the H1 tank filled with water. The water served as a supportive heat transfer medium and also as a safety measure for the case of a major leak from the vessel. The alcohols used were of p.a. grade. The vessel was also connected to the saturation loop made of i.d. 25mm glass tube with a total length of about 3 m in which the liquid was cooled down and saturated with oxygen. The flow of the liquid was driven by centrifugal pump P2 and cooled by means of the plate heat exchanger. The oxygen with a flow of approximately 10 nl/min was introduced into the pipeline by i.d. 4 mm blunt ended steel capillary.

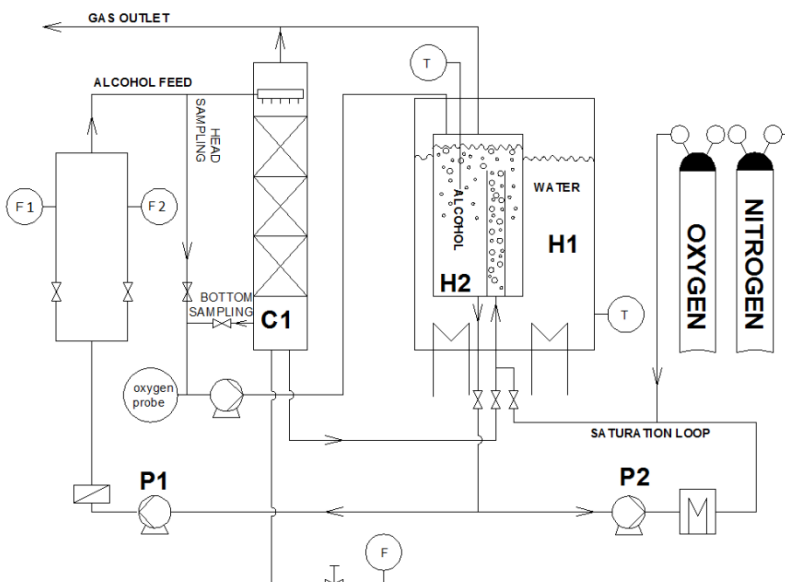


Fig. 3 – Sketch of the experimental apparatus.

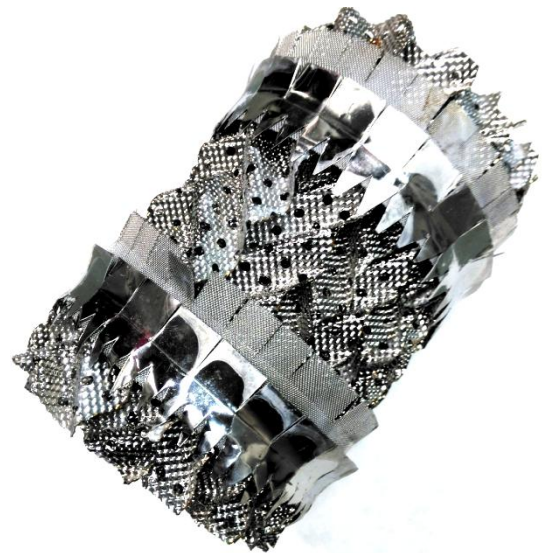


Fig. 4 – Packing with the extra wall-wipers.

Sampling and analytics

The sample of the liquid from the head had been taken from the pipe-line feeding the liquid distributor. The sample from the bottom had been taken from five points of the liquid collector. Sampling lines were switched by the three-way valve to the oxygen probe overflown by the sample. Sampling rate from each line was 6 g/s.

Optical oxygen probe (PSt3, PreSens) was calibrated using its response in the environment of the measured liquid saturated with nitrogen, air and oxygen at 20 °C. The probe is manufactured for measurement of the oxygen fugacity in the gas or aqueous media in the fugacity range of 0 – 21 kPa, but it proved to be stable in the alcohol environment with the daily drift of 1.5 % on average. In the environment of alcohols the probe did not provide linear response with the oxygen fugacity in the entire 0 – 100 kPa range and the second order polynomial calibration curve was therefore constructed during the calibration process and further utilized for evaluation of the results. The accuracy of the probes is assumed to be around 1.5 % for the 100 kPa oxygen fugacity and around 10 % for the 0.5 kPa oxygen fugacity.

Table 2: Physical properties of the systems

	ρ [kgm ⁻³]	η [mPas]	σ [mNm ⁻¹]	D_{O_2} [m ² /s]	H [Pa]
<i>MeOH</i>	794	0.579	22.5	5.34×10^{-9}	2.46×10^8
<i>EtOH</i>	790	1.207	21.6	3.61×10^{-9}	1.70×10^8
<i>PrOH</i>	804	2.215	23.7	2.35×10^{-9}	1.47×10^8
<i>WATER</i>	998	1.002	72.8	1.90×10^{-9}	4.05×10^9

The physical properties of the systems used for the calculations are summarized in the Table 2. The densities have been calculated according to the Yaws et. al. [23], viscosities according to the Reid et. al. [24], surface tension according to the Yaws [23], the diffusivities have been calculated according to the Tyn and Calus method [25] and the solubility data were taken from APV86 HENRY database of Aspen SW.

Volumetric mass-transfer coefficient, $k_L a$, evaluation

As the samples were not taken out of the packing there was necessary to subtract end-effects formed by 1) mass-transfer in the space between the packing and the liquid distributor as well as between the packing and the liquid collector and in the liquid collector itself; 2) different gas-liquid behavior of the packing close to its upper and bottom edge and the middle section of the packed bed. The subtraction was performed by measurements with 'short' and 'long' bed under the same liquid flow rate, as discussed e.g. by Billet [26]. The distance of the liquid distributor and liquid collector from the edge of the packed bed was kept constant for both cases. The $k_L a$ for given liquid flow rate with the end-effects subtracted has been evaluated using

$$k_L a = \frac{u_L}{H^{long} - H^{short}} \ln \left(\frac{f_h^{long} f_b^{short}}{f_b^{long} f_h^{short}} \right) \quad (5)$$

For measurements performed with water the 'short' bed consisted of two packing elements while the 'long' bed consisted of four, six or eight elements. For the measurements with methanol and ethanol the maximum number of elements forming the 'long' bed were three, otherwise the bottom fugacity of oxygen in the liquid was below that the probe was able to determine with reasonable accuracy. For measurements with all three alcohols the 'short bed' therefore consisted of only a single element ($H = 0.21$ m) in order to keep possibility to check agreement of the results obtained with at least two heights of the 'long' bed (two elements: $H = 0.42$ m, three elements: $H = 0.63$ m) and to keep procedure for all alcohols constant. The $k_L a$ data evaluated from the measurements with the 'long' bed consisting of two elements (together with the data measured with single element 'short' bed) are further denoted as "2-1" while the data evaluated from the measurements with three elements 'long' bed (together with the data measured with single element 'short' bed) are denoted "3-1". Intense mass-transfer in the liquid collector and mass transfer in subtracted part of the packing was also found sufficient for saturation of the nitrogen with alcohol vapors.

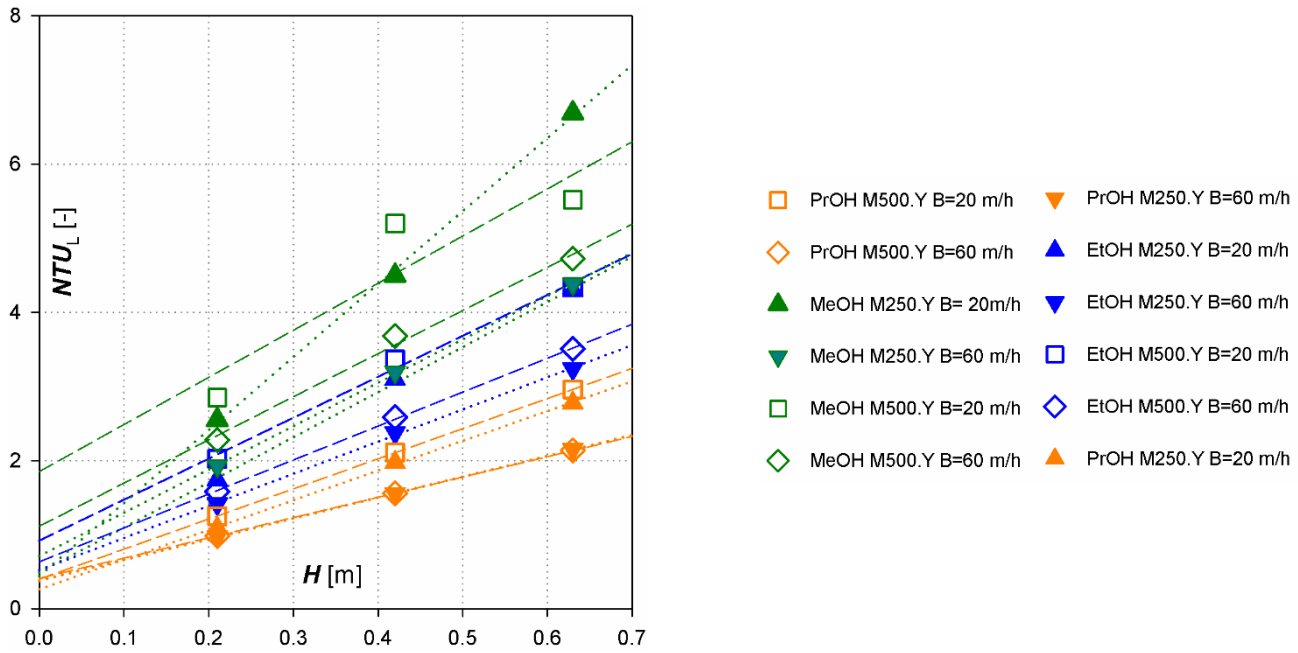


Fig. 5 – End-effect evaluation. NTU_L dependence on the height of the packed-bed, H .

Legend for Fig. 5

Following treatment by Billet [26], the raw number of transfer units in the liquid, NTU_L , was evaluated out of the head and bottom fugacity of the oxygen for all three heights of the packed bed and $NTU_L(H)$ dependence was fitted with a straight line. For several conditions it is depicted in the Fig. 5.

$$NTU_L = \ln \frac{f_h}{f_b} \quad \text{Eq. (6)}$$

With exception of the outlying data for Mellapak 500.Y and B=60 m/h one can observe that 1) the dependences $NTU_L(H)$ is linear; 2) these dependences intercept the vertical axis in the limited range (around value of $NTU_L = 1$).

This suggests that 1) all the external and internal end-effects affecting the measurements with ‘long’ bed configuration are completely developed already for the ‘short’ bed, and can be therefore subtracted according to (5); 2) the end-effects are of similar magnitude for all conditions.

5 Results

The PVC-U i.d. 150 mm column was a new experimental set-up and therefore the measurement method has been first thoroughly verified by the experiments with water on Mellapak 250.Y packing. A significant dependence of the obtained $k_L a$ on the packed bed height as well as noticeable wall flow have been observed. Both phenomena have been suppressed by installation of additional plain sheet wall wiper on each packing element – after its installation the dependence of $k_L a$ on the height of the packed bed almost vanished and $k_L a$ values nearly matched those found for the i.d. 300 mm column (Fig. 6a).

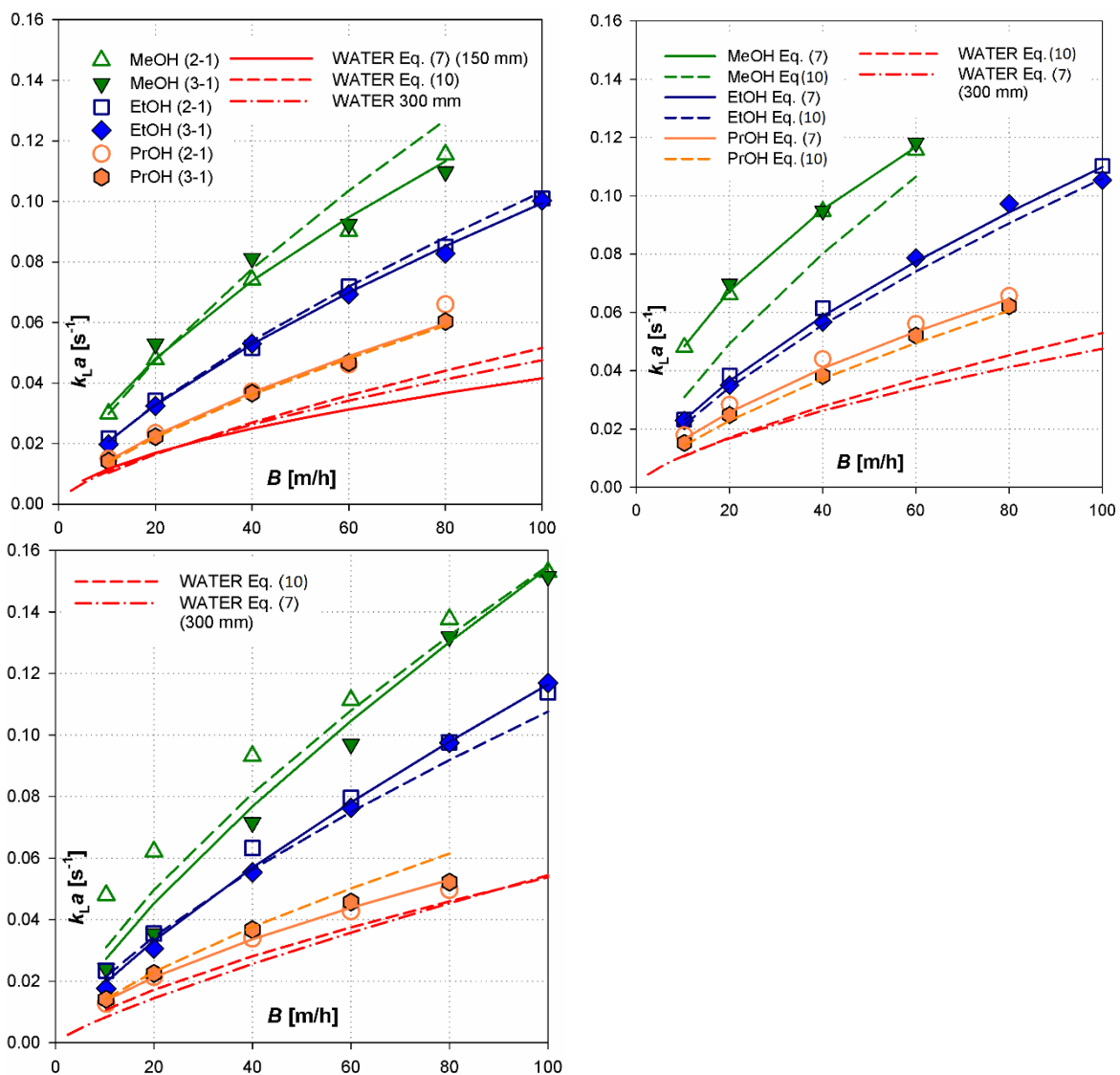


Fig. 6 – Experimental data and their correlation (Eqs. 7, 10). (a) Mellapak 250.Y. (b) Mellapak 350.Y. (c) Mellapak 500.Y.

Measurement of the $k_L a$ with methanol proved difficult due to its high degree of desaturation and corresponding low values of the bottom oxygen fugacity, which determined the lowest achievable liquid flows. High oxygen solubility in alcohols necessitated introduction of the maximum achievable stable flow of the nitrogen and it became a limiting factor for the achievement of the valid data for high liquid superficial flow.

Conversely, liquid collector / gas distributor hydraulic behavior was a limiting factor for achievement of high liquid superficial flows with n-propanol.

The measured $k_L a$ data for all three packings and all three alcohols in the dependence on liquid superficial velocity are depicted in the Fig. 6a,b,c. The numbers in the brackets depict number of elements for 'long' and 'short' bed. Out of the 97 obtained experimental $k_L a$ values 5 were discarded as outlying. The data have been correlated with average *R.S.D.* of 8% by the equation

$$k_L a = C_1 B^{C_2} \tag{7}$$

with optimized constants provided in the Table 3.

Table 3: Constants of the Eq. (7)

	Mellapak 250.Y		Mellapak 350.Y		Mellapak 500.Y	
	C ₁	C ₂	C ₁	C ₂	C ₁	C ₂
MeOH	0.00754	0.618	0.00151	0.499	0.00463	0.761
EtOH	0.00416	0.689	0.00472	0.684	0.00319	0.781
PrOH	0.00286	0.693	0.00355	0.662	0.00298	0.656
WATER	0.00320	0.557	0.00243	0.720	0.00124	0.821

The $k_L a$ values measured for "2-1" and "3-1" configurations are almost identical for the most experimental conditions, proving successful subtraction of the end-effects. The behavior also suggest sufficient stripping gas saturation with alcohol vapors before entering the measurement section and

maintenance of the sufficiently low oxygen concentration in the stripping gas in the frame of the bed. Only exception are the data for the methanol and Mellapak 500.Y packing (Fig. 6c).

The $k_L a$ values for the same liquid superficial velocity and the same alcohol do not increase systematically with packing geometrical area. Such behavior has been observed for water [5] as well. Assuming increasing effective interfacial area with the geometrical one this finding implies decreasing values of the mass-transfer coefficient, k_L . This in turn can be explained by decreasing liquid interstitial velocity on the individual packing sheet as the same liquid flow needs to be distributed on the higher number of sheets for the packing with higher geometrical area.

Mass-transfer coefficient, k_L , evaluation

The data processing consisted of extraction of the mass-transfer coefficient k_L from $k_L a$ data

$$k_L = \frac{k_L a}{a_{CH}} \quad (8)$$

The effective area for the conditions of $k_L a$ measurement (physical absorption) is not known and its closest experimentally achievable approximation was assumed to be the effective area, a_{CH} , obtained for the same packing types by the chemisorption of CO_2 into aqueous solution of sodium hydroxide [5]. The values were calculated according to (9) with constants from the Table 2, the data are graphically presented in the Fig. 7.

$$a_{CH} = C_3 B^{C_4} \quad (9)$$

Table 4: Constants of the Eq. (9)

PACKING	C_3	C_4
Mellapak 250.Y	135	0.110
Mellapak 350.Y	206	0.0626
Mellapak 500.Y	186	0.112

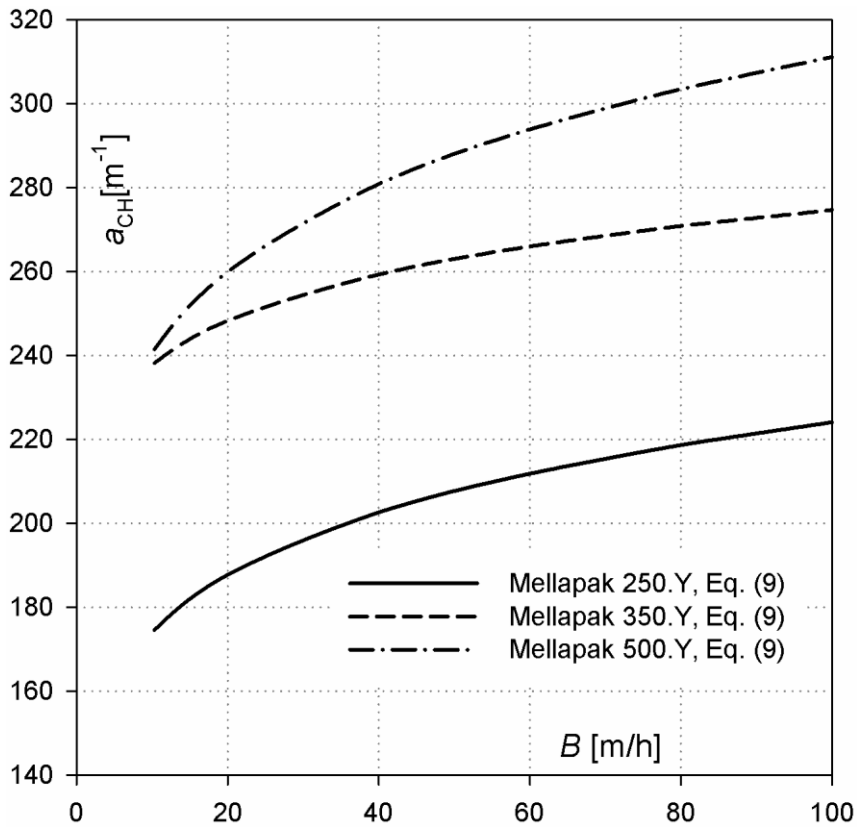


Fig. 7 – Effective interfacial area, a_{CH} , from chemisorption experiments.

Usage of chemisorption area, a_{CH} , for extraction of the k_L from $k_L a$ data mostly proved to provide better match of developed correlations to the experimental data than usage of geometrical area, a_G .

Mass-transfer coefficient, k_L , dimensionless correlation

The k_L data for all alcohols, water and for all packings have been correlated in the dimensionless form

$$Sh_L = 0.207 \cdot Re^{0.798} Fr^{-0.563} We^{0.511} Sc^{0.528} \quad (10)$$

with *R.S.D.* of 12.1%, its success in data fit is shown in the Fig. 8. The similar absolute value of the powers at Froude and Weber numbers suggests that the effect of the inertia forces connected with these numbers cancels and the numbers can be combined into the Eötvös (Bond) number. After the optimization the correlation results in

$$Sh_L = 0.586 \cdot Re^{0.695} Eo^{0.505} Sc^{0.468} \quad (11)$$

with only minor increase in *R.S.D.* to the value of 12.6%.

The dependence of k_L on individual physical quantities as predicted by the Eq. (10) in the form of simple power-law dependence

$$k_L \propto \text{quantity}^{\text{power}} \quad (12)$$

is shown in the Table 5.

Table 5: Dependence of k_L on physical quantities according to the Eq. (10).

Quantity	u_L	ρ	a	η	g	σ	D
Power	0.694	0.781	-0.872	-0.27	0.563	-0.511	0.472

The correlation Eq. (10) predicts dependence of the mass-transfer coefficient on the diffusivity with power of 0.472 and 0.538, respectively, close to the prediction of the penetration theory (which predicts 0.5). The correlation predicts the same magnitude but opposite effect of the gravity acceleration and the surface tension and relatively small effect of the viscosity. An increase in the packing area has significant negative effect on the value of the mass-transfer coefficient. This corresponds with the fact that the $k_L a$ values for the packings of different sizes (i.e. of geometrical areas) do not change significantly. The 0.7 dependence of the k_L on the liquid superficial velocity is in approximate agreement with prediction of the models but is too low for explanation of the data evaluated from the distillation experiments. In the same time it is higher than predicted by penetration theory. Significant dependence on density suggests, that out of various extensive quantities it is in fact mass-flow what directly affects mass-transfer on the packing.

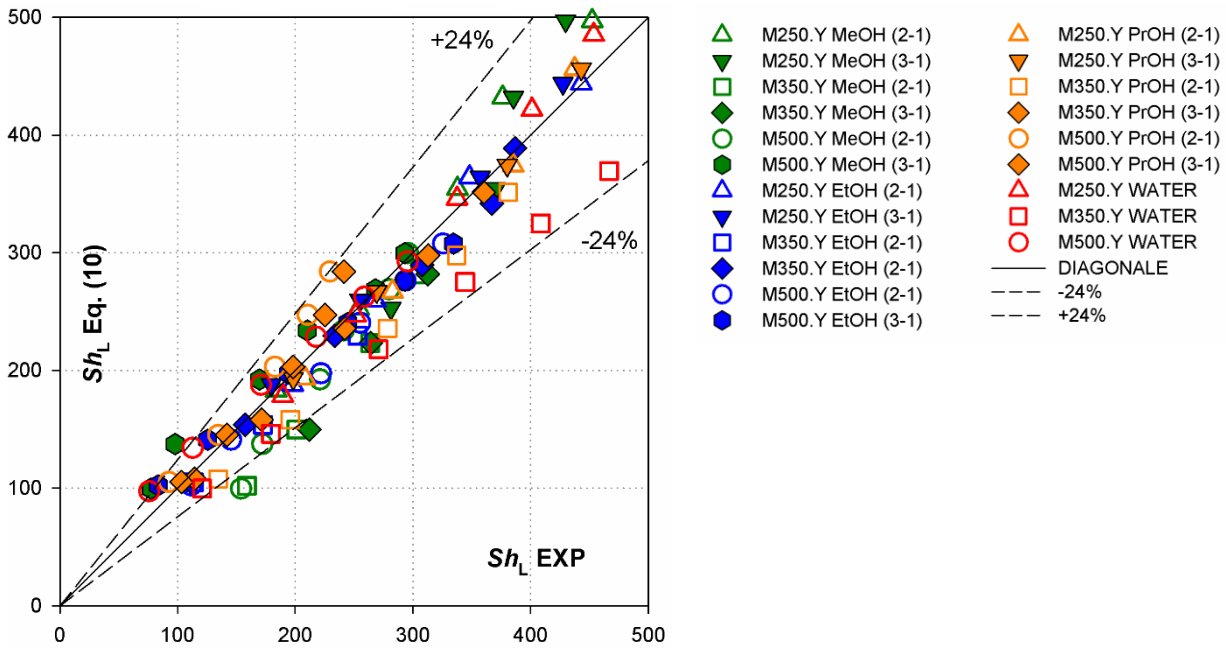


Fig. 8 - Sh_L parity graph. Experimental data and those calculated from Eq. (10).

Legend for Fig. 8

6 Conclusions

Volumetric mass-transfer coefficient, $k_L a$, were measured on three sizes of metal Mellapak structured packing (M250.Y, M350.Y, M500.Y) by desorption of oxygen from water and also from methanol, ethanol and n-propanol. When the packing was equipped with plain sheet extra wall-wipers suppressing significantly wall-flow of the liquid, the $k_L a$ values were found constant for different heights of the packed bed and for different diameter of the column.

Under otherwise similar conditions the $k_L a$ values are similar for all packing sizes as the higher interfacial area is compensated by lower mass-transfer coefficient with possible slight optimum found for M350.Y.

The mass-transfer coefficient has been successfully correlated for all packings, alcohols and water with R.S.D. of 12 % by dimensionless equations (10) and (11) based on the analysis of the forces acting on the liquid film flowing down the packing. The diffusivity power of just a little under 0.5 supports the penetration theory model for mass-transfer description. The inertial and gravitational forces were found supportive for the mass transfer while the viscous and surface forces were found to be suppressive for the process. On the basis of the correlations the k_L values rise approximately with 0.7 power of the

liquid load. The 0.7 power dependence of the k_L on the liquid superficial velocity is close to the prediction of many mass-transfer models but doesn't bring any new clue for explanation for the $k_L a$ behavior evaluated from the distillation experiments.

7 Acknowledgement:

Authors are grateful to the Czech Science Foundation for supporting the project through Grant 13-01251S and to the financial support from specific university research (MSMT No 20/2016).

Workplace is grateful to Sulzer Ltd. for providing of packing samples.

8 List of symbols

a	interfacial area of the packing, (m^2/m^3)
a_G	geometrical area of the packing, (m^2/m^3)
a_{CH}	effective area measured by chemisorption experiments, (m^2/m^3)
B	liquid superficial velocity, (m/h)
C_i	multiplication constant or power of a quantity
c	molar concentration of a solute in the liquid, (mol/m^3)
D	Diffusivity, (m^2/s)
f	fugacity of the oxygen in the liquid, (Pa)
g	gravity acceleration, $g = 9.81 \text{ m/s}^2$
H	height of the packed bed, (m)
H	Henry constant, (Pa)
k_L	liquid phase mass-transfer coefficient, (m/s)
$k_G a$	volumetric gas phase mass-transfer coefficient, (1/s)
NTU_L	number of transfer units in liquid, $NTU_L = \ln \frac{f_h}{f_b}$
$k_L a$	volumetric liquid phase mass-transfer coefficient, (1/s)

u_L liquid superficial velocity, (m/s)

Greek symbols

α power of a quantity

ν kinematic viscosity, (m²/s)

η dynamic viscosity, (Pa·s)

ρ density, (kg/m³)

σ surface tension, (N/m)

τ exposure time, (s)

Subscripts

b bottom

h head

s superficial

i interstitial

i,j individual solutes

Superscripts

long long bed

short short bed

Dimensionless numbers

$EO = \frac{\rho g}{a_{CH}^2 \sigma}$ liquid phase Eötvös (Bond) number

$Fr = \frac{u_L^2 a_{CH}}{g}$	liquid phase Froude number
$Re = \frac{u_L \rho}{\eta a_{CH}}$	liquid phase Reynolds number
$Sc = \frac{\nu}{D}$	liquid phase Schmidt number
$Sh = \frac{k_L}{D a_{CH}}$	liquid phase Sherwood number
$We = \frac{\rho u_L^2}{a_{CH} \sigma}$	liquid phase Weber number

Abbreviations

i.d.	inner diameter
M250.Y	Mellapak 250.Y
M350.Y	Mellapak 350.Y
M500.Y	Mellapak 500.Y
EtOH	ethanol
MeOH	methanol
PrOH	<i>n</i> -propanol
R.S.D	relative standard deviation

9 Literature cited

- [1] V. Linek, T. Moucha, E. Prokopová, J.F. Rejl, Simultaneous Determination of Vapour- and Liquid-Side Volumetric Mass Transfer Coefficients in Distillation Column, Chem. Eng. Res. Des. 83 (2005) 979–986. doi:10.1205/cherd.03311.
- [2] J.F. Rejl, V. Linek, T. Moucha, E. Prokopová, L. Valenz, F. Hovorka, Vapour- and liquid-side volumetric mass transfer coefficients measured in distillation column. Comparison with data calculated from absorption correlations, Chem. Eng. Sci. 61 (2006) 6096–6108. doi:10.1016/j.ces.2006.06.003.
- [3] F.J. Rejl, L. Valenz, V. Linek, “Profile Method” for the Measurement of $k_L a$ and $k_V a$ in Distillation Columns. Validation of Rate-Based Distillation Models Using Concentration Profiles Measured along the Column, Ind. Eng. Chem. Res. 49 (2010) 4383–4398. doi:10.1021/ie901690m.
- [4] M. Laso, M.H. Debrito, P. Bomio, U. Vonstockar, Liquid-Side Mass-Transfer Characteristics of a

- Structured Packing, Chem. Eng. J. Biochem. Eng. J. 58 (1995) 251–258.
- [5] L. Valenz, F.J. Rejl, J. Šíma, V. Linek, Absorption mass-transfer characteristics of mellapak packings series, Ind. Eng. Chem. Res. 50 (2011) 12134–12142. doi:10.1021/ie200577k.
- [6] A.-K. Kunze, P. Lutze, M. Kopatschek, J.F. Maćkowiak, J. Maćkowiak, M. Grünewald, A. Górak, Mass transfer measurements in absorption and desorption: Determination of mass transfer parameters, Chem. Eng. Res. Des. 1 (2015) 440–452. doi:10.1016/j.cherd.2015.08.025.
- [7] E. Brunazzi, A. Paglianti, Liquid-Film Mass-Transfer Coefficient in a Column Equipped with Structured Packings, Ind. Eng. Chem. Res. 36 (1997) 3792–3799. doi:10.1021/ie970045h.
- [8] C. Wang, M. Perry, F. Seibert, G. Rochelle, Packing characterization for post combustion CO₂ capture: Mass transfer model development, Energy Procedia. 63 (2014) 1727–1744. doi:10.1016/j.egypro.2014.11.180.
- [9] R.J. Mangers, A.B. Ponter, Effect of Viscosity on Liquid Film Resistance to Mass Transfer in a Packed Column, Ind. Eng. Chem. Process Des. Dev. 19 (1980) 530–537.
- [10] R.J. Mangers, A.B. Ponter, Liquid-Phase Resistance to Mass Transfer in a Laboratory Absorption Column Packed with Glass and Polytetrafluoroethylene Rings Part I . The Effects of Flowrate Sequence , Repacking , Packing Depth and Initial Liquid Distribution The experimental apparatus, 19 (1980) 139–146.
- [11] A. Hoffmann, J.F. Maćkowiak, A. Górak, M. Haas, J.-M. Löning, T. Runowski, K. Hallenberger, Standardization of Mass Transfer Measurements, Chem. Eng. Res. Des. 85 (2007) 40–49. doi:10.1205/cherd06134.
- [12] J.F. Rejl, V. Linek, T. Moucha, L. Valenz, Methods standardization in the measurement of mass-transfer characteristics in packed absorption columns, Chem. Eng. Res. Des. 87 (2009) 695–704. doi:10.1016/j.cherd.2008.09.009.
- [13] A.K. Kunze, P. Lutze, H. Schoenmakers, S. Müller, M. Kopatschek, J. Maćkowiak, J. Maćkowiak, A. Górak, M. Grünewald, Die notwendigkeit einer standardisierung von stofftransportmessungen in der Ab- und desorption, Chemie-Ingenieur-Technik. 84 (2012) 1931–1938. doi:10.1002/cite.201200045.
- [14] G.Q. Wang, X.G. Yuan, K.T. Tu, Review of mass-transfer correlation for packed columns, Ind. Eng. Chem. Res. 44 (2005) 8715–8729.
- [15] Ž. Olujić, a. F. Seibert, Predicting the Liquid Phase Mass Transfer Resistance of Structured Packings, Chem. Biochem. Eng. Q. 28 (2014) 409–424. doi:10.15255/CABEQ.2014.1934.
- [16] J.A. Rocha, J.L. Bravo, J.R. Fair, Distillation-Columns Containing Structured Packings - a Comprehensive Model for Their Performance. 2. Mass-Transfer ModelModels, Ind. Eng. Chem. Res. 35 (1996) 1660–1667.
- [17] Ž. Olujić, M. Behrens, L. Colli, A. Paglianti, Predicting the Efficiency of Corrugated Sheet Structured Packings with Large Specific Surface Area, Chem. Biochem. Eng. Q. 18 (2004) 89–96. doi:10.15255/CABEQ.2014.19344.
- [18] Ž. Olujić, T. Rietfort, H. Jansen, B. Kaibel, E. Zich, G. Frey, G. Ruffert, T. Zielke, Experimental Characterization and Modeling of High Performance Structured Packings †, (2012).
- [19] B. Hanley, C.-C. Chen, New Mass-Transfer Correlations for Packed Towers, AIChE J. 58 (2012) 132–152.
- [20] K. ONDA, H. TAKEUCHI, Y. OKUMOTO, Mass Transfer Coefficients Between Gas and Liquid Phases in Packed Columns, J. Chem. Eng. Japan. 1 (1968) 56–62. doi:10.1252/jcej.1.56.
- [21] F. Yoshida, T. Koyanagi, Liquid phase mass transfer rates and effective interfacial area in packed absorption columns, Ind. Eng. Chem. 50 (1958) 365–374. <http://pubs.acs.org/doi/abs/10.1021/ie50579a038>.
- [22] J. Haidl, F.J. Rejl, L. Valenz, M. Kordač, T. Moucha, L. Labík, M. Schultes, Absorption in wetted-wall column with phase properties close to distillation conditions, Chem. Eng. Sci. 144 (2016) 126–134.

doi:10.1016/j.ces.2015.12.027.

- [23] C.L. Yaws, Chem. Eng. (1976).
- [24] R.C. Reid, J.M. Prausnitz, B.E. Poling, The Properties of Gases and Liquids, 4th ed., MacGraw Hill, New York, 1987.
- [25] M.T. Tyn, W.F. Calus, Diffusion coefficients in dilute binary liquid mixtures, J. Chem. Eng. Data. 20 (1975) 106–109. doi:10.1021/je60064a006.
- [26] R. Billet, Packed Towers in Processing and Environmental Technology, VCH Verlagsgesellschaft mbH, Weinheim, VCH Publishers, Inc., Weinheim, New York, 1995.



Contents lists available at ScienceDirect

Chemical Engineering Research and Design

journal homepage: www.elsevier.com/locate/cherdiChemE
ADVANCING
CHEMICAL
ENGINEERING
WORLDWIDE

General mass-transfer model for gas phase in structured packings

J. Haidl*, F.J. Rejl, L. Valenz, T. Moucha, R. Petříček

University of Chemistry and Technology Prague, Technická 5, 166 28 Praha 6, Czech Republic

ARTICLE INFO

Article history:

Received 14 February 2017
Received in revised form 11 June 2017
Accepted 31 July 2017
Available online 7 August 2017

Keywords:

Absorption
Distillation
Mass transfer
Structured packing

ABSTRACT

Volumetric mass-transfer coefficient in the gas phase, $k_G a$, for Mellapak 250.X and 250.Y structured packings has been measured by standard method of absorption of SO₂ from carrier gas to aqueous solution of NaOH in the i.d. 150.6 mm absorption column. Three carrier gases – He, N₂ and SF₆ – have been utilized providing wide range of Sc_G from 0.49 to 2.32. The gas-phase mass-transfer coefficient, k_G , has been calculated from the experimental $k_G a$ data as the ratio of $k_G a$ and of the effective interfacial area, a , measured utilizing CO₂/NaOH system. The experimental and literature k_G data for Mellapak 250.X, 250.Y, 350.Y and 500.Y have been correlated by dimensionless correlation $Sh_G = 2.7 + 0.038 \cdot Re_{LG}^{0.88} \cdot Sc_G^\beta$ with $\beta = 0.33 + 0.9 \cdot \exp(-0.6 \cdot Sc_G)$. The correlation fits the data in the wide range of Re_{LG} and Sc_G covering the process conditions of common absorption and distillation columns.

© 2017 Institution of Chemical Engineers. Published by Elsevier B.V. All rights reserved.

1. Introduction

Counter-current gas–liquid contactors – absorption and distillation columns – are the most widely used separation devices in the chemical industry. Humphrey (1995) estimated that only in US there are more than 40 000 of distillation towers which handle almost 90% of all separation processes. The columns are equipped either with trays or with random or structured packings. The latter are widely used in these contactors because of the low ratio of pressure drop to separation efficiency. Their mass-transfer efficiency is usually described by means of HETP or, in the case of the rate-based modeling, by the mass-transfer coefficients in the liquid and gas/vapor phase – k_L and k_G – and the effective interfacial area a .

Numerous models of the mass transfer in structured packings can be found in literature; their comprehensive overview and comments are given in Wang et al. (2005). Some of them are already incorporated into Aspen Plus or CHEMCAD engineering packages and they are routinely used in a column design. In our previous papers (Rejl et al., 2015; Valenz et al., 2011) we discussed the reliability of k_G and $k_G a$ values predicted by these models for absorption and distillation conditions and Mellapak 250.Y structured packing. Significant differences in predicted k_G and $k_G a$ values have been revealed; the predictions differ not only in the values of these parameters but also in their dependencies on gas/vapor flow rate. The power-law dependence of $k_G \propto u_{G,s}^\alpha$ with α

ranging from 0.6 to 1 is predicted according to these models. Almost all models (except of the correlation of Wang et al. (2016)) involve the dependence of $k_G \propto D_{12,G}^{2/3}$ taken from the Chilton–Colburn analogy (Chilton and Colburn, 1934). The differences found in existing models led us to re-opening of the question about modeling of the gas-phase mass transfer in structured packings.

For the purpose of the gas-phase mass-transfer modeling the structured packing is usually described as a bundle of inclined channels of hydraulic diameter d_h . The modeling of the mass transfer in the packing channel is then based on the correlations for k_G in a wetted wall column.

The turbulent character of the gas flow in the packing channel is tacitly assumed due to frequent direction changes in the gas flow.

The gas-phase mass-transfer characteristics of the wetted wall column are usually published in a dimensionless form as a dependence of gas phase Sherwood number, Sh_G , on system properties characterized by Schmidt number, Sc_G , and the hydrodynamic conditions characterized by Reynolds number, Re_G .¹

The simplest and often utilized relation for Sh_G is a simple power-law form

$$Sh_G = A \cdot Re_{LG}^\alpha Sc_G^\beta \quad (1)$$

* Corresponding author.

E-mail address: jan.haidl@vscht.cz (J. Haidl).
<http://dx.doi.org/10.1016/j.cherd.2017.07.034>

0263-8762/© 2017 Institution of Chemical Engineers. Published by Elsevier B.V. All rights reserved.

¹ Similarly the heat-transfer characteristics are correlated as a dependence of Nusselt number on Prandtl and Reynolds numbers.

Nomenclature

List of symbols

A (–)	Correlation parameter independent on Sc and Re
A_{Sc} (–)	Correlation parameter dependent on Sc_G
a (m^2/m^3)	Effective interfacial area of the packing
a_g (m^2/m^3)	Geometrical area of the packing
B (m/h)	Liquid superficial velocity
b (m)	Length of the channel base
c (mol/m^3)	Molar concentration
D_{12} (m^2/s)	Binary diffusion coefficient
d_{eq} (m)	Equivalent diameter of the packing
d_h (m)	Hydraulic diameter of the packing channel
g (m/s^2)	Gravitational acceleration, $g=9.81\text{ m/s}^2$
h (m)	Height of the packing channel
h_L (m^3/m^3)	Liquid hold-up
k_G (m/s)	Mass-transfer coefficient in the gas phase
$k_G a$ (s^{-1})	Volumetric mass-transfer coefficient in the gas phase
l_h (m)	Characteristics length of the packing channel
o (m)	Channel perimeter
p (Pa)	Pressure
S (m^2)	Channel cross-section
s (m)	Length of the channel side
u (m/s)	Velocity
x, y, z (m)	Spatial coordinates in Eq. (15)
y_i (–)	Molar fraction of component i

Greek symbols

α (–)	Correlation parameter, power at Re
β (–)	Correlation parameter, power at Sc (Pr)
ε (m^3/m^3)	Packing void fraction
θ	Channel inclination angle
ϑ	Liquid effective angle of channel
ξ	Gas–liquid interaction parameter (DELFT model)
μ (Pa s)	Dynamic viscosity
ρ (kg/m^3)	Density

Dimensionless numbers

Mi	Mixing number
Nu	Nusselt number
Pr	Prandtl number
Re	Reynolds number
Sc	Schmidt number
Sh	Sherwood number

Subscripts, superscripts

E	Effective (velocity)
G	Gas phase
h	Hydraulic
L	Liquid phase
LG	Gas phase related to liquid phase (Reynolds number)
lam	Laminar
$turb$	Turbulent

with parameters A , α and β evaluated on the basis of experimental data or taken from the heat-transfer correlations utilizing the analogy of heat and mass transfer. This form of the Sh_G correlation with the parameters $A=0.023$, $\alpha=0.83$ and $\beta=0.44$ was published by Gilliland and Sherwood (1934) who evaporated several liquids into the turbulent

air stream in the wetted wall column. Their data had been taken by Chilton and Colburn (1934) for simultaneous correlation of heat and mass-transfer coefficients resulting in famous analogy of momentum, heat and mass-transfer with values of $A=0.029$, $\alpha=0.78$ and $\beta=1/3$. The value of exponent $\beta=1/3$ was later confirmed by Linton and Sherwood (1950) who measured the mass-transfer characteristics of turbulent liquids with high values of Sc . Johnstone and Pigford (1942) performed a series of distillation experiments in the wetted wall column and reported good agreement of evaluated distillation Sh_G values with those calculated according to correlations of Gilliland and Sherwood and Chilton and Colburn. Years later Crause and Nieuwoudt (1999) performed a series of evaporation experiments in a short wetted wall column representing the channel of a structured packing and published the values of $\alpha=1$ and $\beta=0.5–0.55$. Recently, we have performed absorption experiments in a wetted wall column with three carrier gases having significantly different values of Sc_G (the same ones were used in this work) and found values of $\alpha=0.9$ and $\beta=0.6$ (Haidl et al., 2016). The usability of our correlation was confirmed also for distillation conditions proving the concept of absorption and distillation process analogy (Rejl et al., 2016).

In our previous work (Rejl et al., 2015) we performed series of absorption experiments on Mellapak 250.Y, 350.Y, 452.Y and 500.Y utilizing air/ SO_2 /NaOH_(aq.) system for $k_G a$ measurement and air/ CO_2 /NaOH_(aq.) for a measurement. The $k_G = k_G a/a$ values for all packings were correlated in a dimensionless form

$$\left(\frac{k_G d_{eq}}{D_{12,G}}\right) = 0.409 \left(\frac{d_{eq} u_{G,s} \rho_G}{\mu_G}\right)^{0.622} \left(\frac{d_{eq} u_{L,s} \rho_L}{\mu_L}\right)^{0.0592} \quad (2)$$

with $d_{eq}=4\varepsilon/a_g$. The results indicate the value of $\alpha=0.622$ which is in agreement with findings of Wang et al. (2016) made for various structured packings using the same absorption systems. It is, however, significantly lower than the values used in the wetted wall column correlations and in other models (from 0.75 according to Billet and Schultes (1999) to 1 used in the correlation of Hanley and Chen (2012)).

This paper is focused on the experimental study of k_G dependence on physical properties of gas, i.e. Sc_G , in the range of common absorption and distillation systems. For this purpose, the absorption of SO_2 from three different carrier gases – He, N_2 and SF_6 – into aqueous solution of NaOH has been utilized for the $k_G a$ measurements providing the range of Sc_G from 0.49 to 2.32. The k_G data measured in this work together with the literature data are correlated resulting in one dimensionless correlation.

2. Experimental

The $k_G a$ measurements have been performed with a proven method of absorption of diluted SO_2 from carrier gas (N_2 , He, SF_6) into the aqueous solution of NaOH (Rejl et al., 2009). In this system, the mass-transfer resistance is concentrated only in the gas phase due to the instantaneous reaction of SO_2 with sodium hydroxide at the gas–liquid interface. Assuming plug flow of the gas phase, $k_G a$ can be calculated from the molar fraction of SO_2 in the gas sampled at the bottom and at the top of the packed bed according to Eq. (3).

$$k_G a = \frac{u_{Gs}}{h_{bed}} \ln \frac{y_{SO_2, bottom}}{y_{SO_2, top}} \quad (3)$$

The experiments have been carried out in a 150.6 mm i.d. absorption column made of transparent PVC-U packed with Mellapak 250.X (M250X) or Mellapak 250.Y (M250Y) packing. The packed bed consisted of six elements of packing for measurements using N_2 and He as a carries gas (total bed height of 1.26 m with M250Y or 1.32 m with M250X) and of two packing elements for measurement using SF_6 (total bed height of 0.42 m with M250Y). The individual packing elements were rotated around vertical axes by 90° with respect to each other.

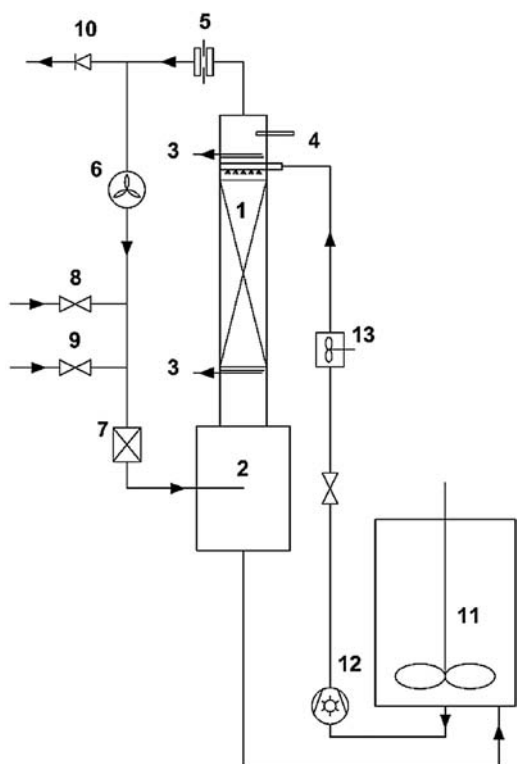


Fig. 1 – Experimental setup. 1-PVC-U column; 2-gas mixing drum; 3-sampling devices; 4-oxygen probe; 5-calibrated orifice; 6-fan; 7-static mixer; 8-make-up gas; 9-tracer gas; 10-outgas; 11-absorption liquid storage vessel; 12-pump; 13-turbine flow meter.

The packed bed was installed 0.4 m above the mixing drum providing the calming section for the gas entering the packing — see Fig. 1.

The absorption liquid — aqueous solution of NaOH of initial concentration of 0.5 kmol/m^3 — was fed to the column by means of pressurized pipe-type liquid distributor with 25 drip points. In order to minimize the liquid entrainment from the top of the packing the liquid distributor was placed right on the packing. Two liquid flow rates corresponding to liquid superficial velocities of 20 and $40 \text{ m}^3/\text{m}^2/\text{h}$ were utilized; the liquid flow rate was measured with the turbine flow meter.

The carrier gas was recirculated in a closed loop by means of high speed fan; its flow rate was controlled via the fan revolutions and measured via the pressure drop across a calibrated orifice.² For each carrier gas the lowest gas flow rate was limited by the detection limit of the analyzer at the top of the packed bed; the highest flow rate was limited by the fan capacity and column hydraulics. The pressure in the loop was maintained approx. 200 Pa higher than the atmospheric pressure to prevent ambient air from being sucked in. Moreover, the content of the closed loop was continuously purged with small amount of pure carrier gas from pressure cylinder to ensure high purity of the gas inside the loop. Assuming air to be the only gas penetrating into the loop, its concentration inside the loop was monitored as an oxygen level by means of the oxygen optical probe; the concentration of air was main-

² The calibration of the orifice for each individual carrier gas was checked as a steady increase of CO_2 concentration in the gas stream in front of the column after mixing the gas leaving the column (lean on CO_2 due to its reaction with NaOH) with known amount of pure CO_2 .

tained lower than 3 %. The density of the carrier gas used for the evaluation of the measured data has been corrected for the presence of air and water vapor in the carrier gas.

The tracer gas — SO_2 — was fed into the carrier gas in front of the static mixer; its flow rate was controlled by means of Bronkhorst® flow meter. The gas samples were withdrawn from the column by means of two sampling devices located immediately below the packed bed and above the liquid distributor. The construction of the sampling devices ensures that the gas sample is taken across the whole diameter of the column and prevents the liquid phase to influence the samples. The gas samples taken below the bed (and also above in the measurements with SF_6) have been analyzed with Sick S710 IR spectrometer calibrated for the range 50–3000 ppm of SO_2 , the samples taken above the bed have been analyzed with Horiba APSA-370 SO_2 analyzer calibrated for a range of 20–800 ppb SO_2 .³ The experimental setup is drawn in Fig. 1.

3. Results and discussion

3.1. Evaluation of k_G , comparison with literature

The k_G values have been calculated as a ratio of the $k_G a$ measured in this work and the effective interfacial area, a , measured independently by absorption of CO_2 into the NaOH solution.⁴

$$k_G = \frac{k_G a}{a} \quad (4)$$

The values of a used in this paper and the geometrical characteristics of individual packings — see Fig. 3 — are listed in Table 1.

The experimental k_G and $k_G a$ data measured on Mellapak 250.Y at $B=20 \text{ m/h}$ are compared with the values predicted by the most used mass-transfer models in Fig. 2a–c.⁵ It can be concluded that no single model is capable to predict both, the k_G and $k_G a$ values of those three absorption systems accurately.

The experimental k_G data have been correlated in a power-law form

$$k_G = A \cdot u_{G,s}^\alpha \quad (5)$$

with parameters A and α evaluated for each packing and each carrier gas separately. The parameters of the correlation and its relative standard deviation (RSD) are listed in Table 2.

³ It was not possible to use the Horiba analyzer for experiments carried with SF_6 due to the interference of the carrier gas with the analyzer, therefore these experiments have been carried with a lower bed (2 elements only) using Sick analyzer for the samples taken above and below the packing.

⁴ Detailed description of a measurement with $\text{CO}_2/\text{air}/\text{NaOH}$ system, $k_G a$ measurement with SO_2/air and results of those measurements for Mellapak 250.X, 250.Y, 350.Y and 500.Y are given in our previous papers (Rejl et al., 2015; Valenz et al., 2011).

⁵ The brief description of the models is given in Appendix A. A special attention is paid to the dependence of Sh_G on Re_G and Sc_G .

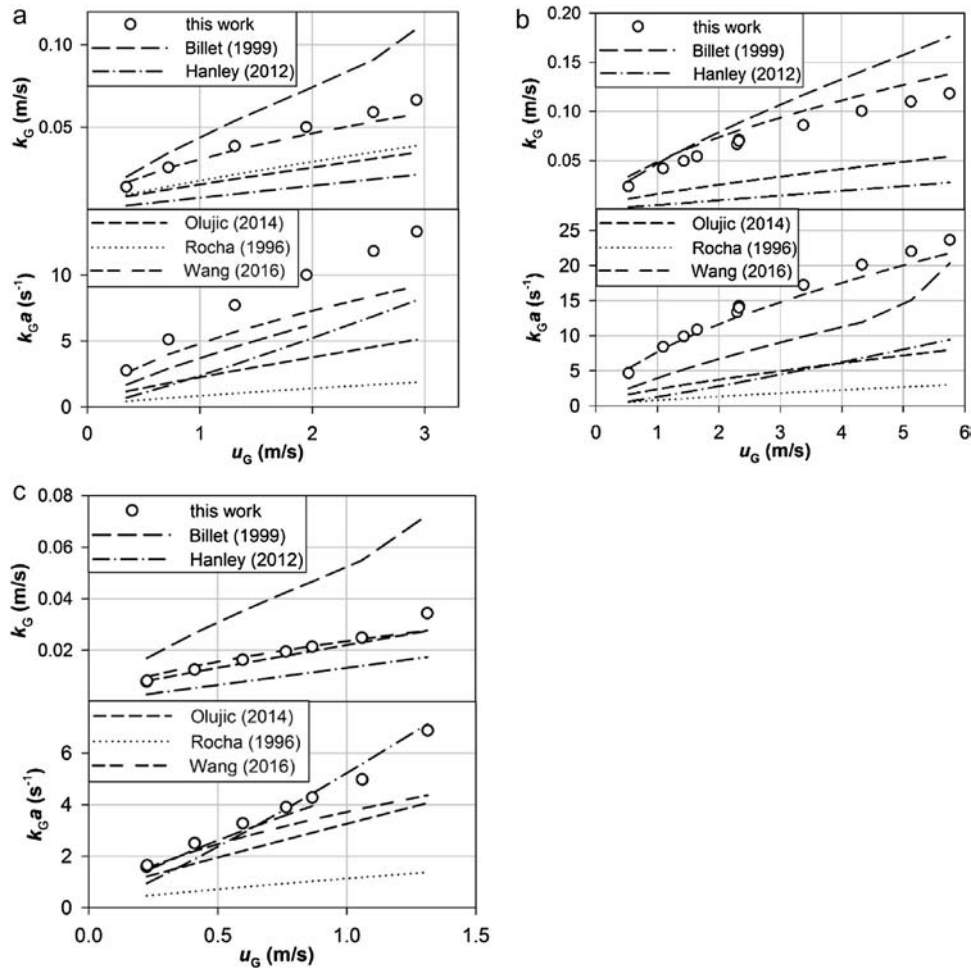


Fig. 2 – Comparison of experimental and predicted k_G and $k_G a$ data for M250Y packing and (a) SO_2/N_2 ; (b) SO_2/He ; (c) SO_2/SF_6 system. $B = 20$ m/h.

Table 1 – Packing parameters and effective interfacial area used in this paper.

	b (m)	h (m)	s (m)	a_g (m^2/m^3)	ε (m^3/m^3)	θ ($^\circ$)	a (m^2/m^3)	
							$B = 20$ m/h	$B = 40$ m/h
M250X	0.022	0.012	0.016	250	0.987	60	205	220
M250Y	0.022	0.012	0.016	250	0.987	45	200	218
M350Y	0.016	0.0084	0.012	350	0.982	45	243	260
M500Y	0.010	0.0063	0.0080	500	0.975	45	335	360

Table 2 – Parameters of correlation of k_G in power-law form (Eq. (5)).

Packing	System	u_{GS} (m/s)	\overline{Re}_{LG}	A	α	RSD
M250Y	SO_2/N_2	0.7–2.5	1500	0.0312	0.71 ± 0.01	0.03
	SO_2/He	1.1–5.1	400	0.0397	0.64 ± 0.01	0.02
	SO_2/SF_6	0.2–1.1	4050	0.0261	0.75 ± 0.04	0.09
M250X	SO_2/N_2	0.2–2.6	1100	0.0254	0.66 ± 0.01	0.03
	SO_2/He	0.7–5.3	250	0.0331	0.53 ± 0.01	0.02

Experimental velocity ranges for higher density gases were lower than for low density gases due to lower hydraulic capacity of the column.

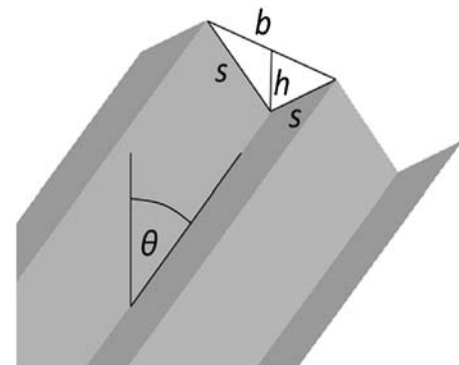


Fig. 3 – Geometrical characteristics of structured packings.

3.2. Dimensionless correlation of k_G data

It is usual to correlate k_G in the form of Sh_G

$$Sh_G = \frac{k_G \cdot d_h}{D_{12,G}} \quad (6)$$

as a function of physical properties characterized by Schmidt number

$$Sc_G = \frac{\mu_G}{D_{12,G} \cdot \rho_G} \quad (7)$$

and hydrodynamic conditions characterized by Reynolds number

$$Re_{LG} = \frac{(u_{G,e} + u_{L,e}) \cdot \rho_G \cdot d_h}{\mu_G} \quad (8)$$

In this paper we follow the approach of Rocha et al. (1993) and Olujić et al. (2004) to model the packing as a bundle of inclined triangular channels of base b , height h and sides s . The geometry of the packing is defined by its geometrical area a_g , void fraction ε , inclination angle ϑ and channel dimensions b , h and s (see Fig. 3). The hydraulic diameter of the channel is defined as

$$d_h = \frac{4S}{o} = (1 - h_L) \frac{2bh}{b + 2s} \quad (9)$$

The relation for the liquid hold-up, h_L , was taken from (Olujić et al., 2004).

$$h_L = a_g \left(\frac{3\mu_L u_{L,s}}{\rho_L g a_g \sin \vartheta} \right)^{1/3} \quad (10)$$

with a_g being the geometrical area of the packing and ϑ the effective liquid flow angle defined as

$$\vartheta = \arctan \left[\frac{\cos \left(\frac{\pi}{2} - \theta \right)}{\sin \left(\frac{\pi}{2} - \theta \right) \cos \left[\arctan \left(\frac{b}{2h} \right) \right]} \right] \quad (11)$$

Gas flows through the packing channel with the effective velocity

$$u_{G,e} = \frac{u_{G,s}}{(\varepsilon - h_L) \sin \vartheta} \quad (12)$$

whilst liquid flows down the packing in thin films with the effective velocity

$$u_{L,e} = \frac{u_{L,s}}{\varepsilon h_L \sin \vartheta} \quad (13)$$

A simple power-law correlation in the form of Eq. (1) is often used for the description of Sh_G dependence on Re_G and Sc_G . However, the results listed in Table 2 show that the value of α ($k_G \propto u_{G,s}^\alpha$; $Sh_G \propto Re_{LG}^\alpha$) varies from 0.53 to 0.75; α convincingly increases with increasing value of \overline{Re}_{LG} . The variance in the value of α precludes correlating the data in the simple power-law form.

Moreover, the shape of Eq. (1) implies that at low values of Re_{LG} the value of Sh_G will limit to zero which conflicts with the meaning of Sherwood number as a ratio of total mass flux across the gas-liquid interface and of the mass flux induced solely by diffusion in a stagnant gas. This disadvantage can be avoided by specifying the lowest Reynolds number, $Re_{LG,trans}$, the correlation is valid to with another correlation to be used for values of $Re_{LG} < Re_{LG,trans}$. The value of $Re_{LG,trans}$ is usually identified as a transition from laminar to turbulent flow regime. In our Sh_G data measured in the wetted wall column (Haidl et al., 2016) the transition from laminar to turbulent flow regime was observed as a steep change in the dependence of Sh_G on Re_{LG} . As it can be seen in Fig. 2a–c, the experimental data measured in this work do not exhibit such phenomenon so the identification of the transition from the laminar to the

Table 3 – Range of simulation conditions used as input for solution of Eq. (15).

d_h/L (-)	D_{12} (10^{-6} m ² /s)	μ (10^{-6} Pa s)	u_s (m/s)	Re	Sc
0.017–1.05	1–20	5–20	0.003–1.34	2.8–1300	0.5–10

turbulent flow regime cannot be performed. As the value of Sh_G must have some positive limit a correlation in the form of

$$Sh_G = Sh_{G,0} + A_{Sc} \cdot Re_{LG}^\alpha \quad (14)$$

has been proposed instead of Eq. (1). A_{Sc} in Eq. (14) represents an unknown function of Sc_G ; its value for each physical system is assumed to be constant. The shape of this function is discussed later.

The quantity of $Sh_{G,0}$ represents the limit of Sh_G for low Re_{LG} and/or Sc_G values thus it should be dependent on the packing geometry only. Its value for corrugated-sheet packing was obtained through numerical solution of the set of partial differential equations describing the momentum- and mass transfer within the fluid flowing through the V-channel under laminar flow conditions:

$$\begin{aligned} -\frac{dp}{dz} &= \mu \left(\frac{\partial^2 u}{\partial x^2} + \frac{\partial^2 u}{\partial y^2} \right) \\ u(x, y) \cdot \frac{\partial c}{\partial z} &= D_{12} \left(\frac{\partial^2 c}{\partial x^2} + \frac{\partial^2 c}{\partial y^2} \right) \end{aligned} \quad (15)$$

with the boundary conditions

$$\begin{aligned} x = 0 : \quad u &= 0, \quad c = 0 \\ y = 0 : \quad u &= 0, \quad c = 0 \\ y = x : \quad u &= 0, \quad \frac{\partial c}{\partial x} = \frac{\partial c}{\partial y} = 0 \end{aligned} \quad (15a-d)$$

which describe the conditions (velocity and concentration) on the channel perimeter. The solution has been obtained for numerous d_h/L , dp/dz , D_{12} and μ combinations — see Table 3. From all the numerical solutions, the limit

$$Sh_{G,0} = \lim_{Re \rightarrow 0} Sh_G = \lim_{Sc \rightarrow 0} Sh_G \approx 2.70 \pm 0.05 \quad (16)$$

has been evaluated. With $Sh_{G,0} = 2.7$ the experimental data can be individually correlated using Eq. (14) with value of α in the range of 0.82–0.90 with value of α seemingly independent on Re_{LG} . The scatter of α can be probably accounted to the uncertainties in concentration and gas flow rate measurements.

In order to extend the experimental Sh_G database we supplemented the data measured in this work also with the data for air/SO₂/NaOH_(aq) system on Mellapak 250.X, 250.Y, 350.Y and 500.Y for superficial liquid velocities from 5 to 40 m/h measured in our previous work (Rejl et al., 2015) and also with the data of Kunze et al. (2015) measured on Mellapak 250Y using air/NH₃/H₂SO_{4(aq)} system. All the data have been correlated simultaneously with Eq. (14) resulting in the value of $\alpha = 0.88$ and values A_{Sc} listed in Table 5. The value of the relative standard deviation (RSD) has been used as the objective function in the correlation. The data whose relative deviation from the correlation exceeded twice the RSD value of the correlation have been excluded from the dataset and the values of A_{Sc} and α have been re-evaluated resulting on lower value of RSD. This procedure has been repeated until relative deviations of

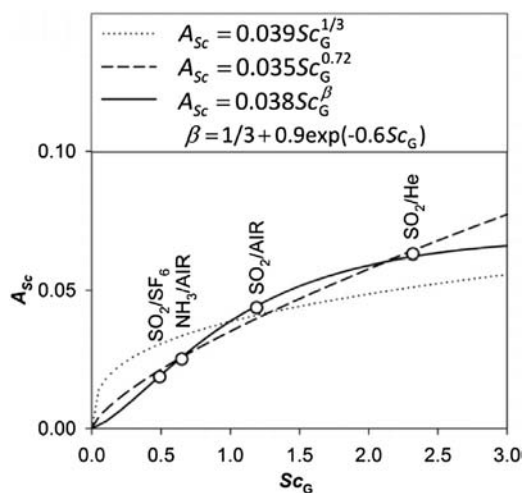
Table 4 – Physical properties of absorption systems.

	ρ_G (kg/m ³)	μ_G (Pa s)	$D_{12,G}$ (m ² /s)	Sc_G	Re_{LG}
SO ₂ /He	0.187 ^a	2.00×10^{-5}	4.63×10^{-5}	2.32	85–740
SO ₂ /N ₂	1.14	1.75×10^{-5}	1.28×10^{-5}	1.20	320–2700
SO ₂ /air	1.17	1.80×10^{-5}	1.30×10^{-5}	1.18	250–2300
SO ₂ /SF ₆	5.78 ^a	1.55×10^{-5}	5.48×10^{-6}	0.49	2000–5900
NH ₃ /air	1.17	1.80×10^{-5}	2.36×10^{-5}	0.65	1300–2500

^a Density of the pure carrier gas corrected to the low content of air.

Table 5 – Optimized values of A_{Sc} for each physical system, $\alpha = 0.88$.

System	Sc_G	A_{Sc}
Air, N ₂ /SO ₂ /NaOH(aq.)	1.19	0.0437
He/SO ₂ /NaOH(aq.)	2.32	0.0629
SF ₆ /SO ₂ /NaOH(aq.)	0.49	0.0186
Air/NH ₃ /H ₂ SO ₄ (aq.)	0.65	0.0251

**Fig. 4 – The optimized values of A_{Sc} . Comparison with simple power-law correlations.**

all the remaining data were lower than double of RSD. The physical properties of individual absorption systems are listed in Table 4.

The shape of Eq. (1) implies A_{Sc} being a power-law function of Sc_G . The optimized values of A_{Sc} listed in Table 5 have been therefore fitted in this form resulting in correlation

$$A_{Sc} = 0.035 \cdot Sc_G^{0.72} \quad (17)$$

with the RSD of 11%.

The value of $\beta = 0.72$ implies the dependence of $k_G \propto D_{G,12}^{0.28}$. In Fig. 4 are shown the values of A_{Sc} evaluated from the experimental data using Eq. (14) with $\alpha = 0.88$ in the dependence on Sc_G and their comparison with the widely accepted dependence of $Sh_G \propto Sc_G^{1/3}$ and the optimized dependence of $Sh_G \propto Sc_G^{0.72}$. It can be concluded, that the power of 1/3 which is suitable for the mass- and heat-transfer data measured on the wetted-wall column in the wide range of Sc and Pr numbers, respectively, doesn't fit the data measured in this work.

The relatively high value of RSD of Eq. (17) together with the surprisingly high value of β led us to the deeper investiga-

Table 6 – The values of β evaluated according to Eq. (18).

Pair	SO ₂ /SF ₆ – NH ₃ /air	NH ₃ /air – SO ₂ /air	SO ₂ /air – SO ₂ /He
β	1.05	0.92	0.50

tion of function A_{Sc} . The power-law form of A_{Sc} can be easily rewritten in the form of

$$\frac{A_{Sc,1}}{A_{Sc,2}} = \left(\frac{Sc_{G,1}}{Sc_{G,2}} \right)^\beta \quad (18)$$

which can be used, for example, for recalculation of the known value of $A_{Sc,1}$ from system characterized by $Sc_{G,1}$ to the system characterized by $Sc_{G,2}$. If this form was used for evaluation of β from the following pairs of Sc_G the values of β listed in Table 6 were obtained.

Apparently the value of β decreases with increasing Sc_G . This observation corresponds with the findings made for heat and mass transfer in turbulent pipe flow which can be found in the literature: the correlations describing the heat transfer in liquid metals ($Pr \approx 0.1$) (Mikityuk, 2009) involve the value of $\beta = 0.5–0.9$; the correlations of Gilliland and Sherwood (1934) and Crause and Nieuwoudt (1999) for Sh_G measured by evaporation of various liquids into the air stream ($Sc_G = 0.6–2.2$) involve $\beta = 0.44–0.55$; our own measurements (Haidl et al., 2016) in the wetted wall column with the same physical systems as used in this paper give $\beta = 0.61$; and finally the heat-transfer (Dittus and Boelter, 1930; Gnielinski, 1976) and mass-transfer (Linton and Sherwood, 1950) correlations for wide range of Pr and Sc , respectively, involve the value of $\beta = 0.3–0.4$. These findings have been deeply examined by Notter and Sleicher (1972). They solved a PDE describing the heat (or mass) transfer in a turbulent pipe flow (Graetz problem) for wide range of Pr (Sc) and Re using a concept of turbulent quantities (viscosity, diffusivity, temperature conductivity) and published their results in the form of a dimensionless correlation for the range of $Re = 10^4 – 10^6$ and $Pr = 0.1–10^4$:

$$Nu = 5 + 0.016 Re^\alpha Pr^\beta$$

$$\alpha = 0.88 - \frac{0.24}{4 + Pr} \quad (19)$$

$$\beta = 0.33 + 0.5 \cdot \exp(-0.6 \cdot Pr)$$

In this paper, we adopted the shape of relation for calculation of β in order to describe the dependence of A_{Sc} on Sc_G resulting in the final correlation

$$Sh_G = 2.7 + 0.038 \cdot Re_{LG}^{0.88} \cdot Sc_G^\beta$$

$$\beta = 0.33 + 0.9 \cdot \exp(-0.6 \cdot Sc_G) \quad (20)$$

which fits the experimental Sh_G data with RSD of 5%.⁶ The agreement of the experimental data with the correlation is shown in the parity chart (Fig. 5) and illustrated on the experimental Sh_G data of Mellapak 250.Y in Fig. 6. The correlation

⁶ The RSD of 5% is calculated on the basis of the dataset which remains after outliers have been excluded (14 of 110 data points). The original dataset which corresponds with the results listed in Table 2 provides RSD of 7%. It should, however, be noted, that the data measured on M250X packing using helium as the carrier gas exhibit the highest deviation from the correlation with RSD of 13%.

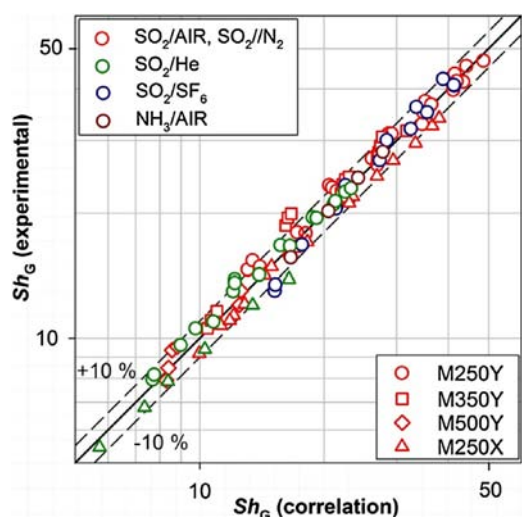


Fig. 5 – Parity chart. Comparison of experimental data and correlation in Eq. (20).

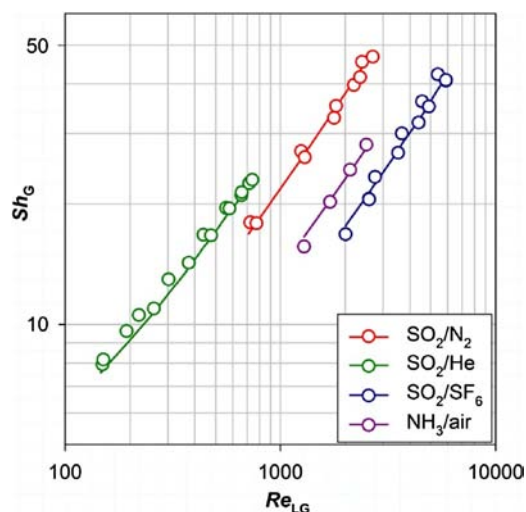


Fig. 6 – Mellapak 250.Y. Comparison of experimental Sh_G with data calculated according to Eq. (20).

is valid for M250X, M250Y, M350Y and M500Y structured packings in pre-loading region and the range of $Re_{LG} = 85\text{--}5900$ and $Sc_G = 0.49\text{--}2.32$.

The correlation in the form of Eq. (20) implies the following:

- at low values of Re_{LG} and/or Sc_G the value of Sh_G limits to the value of $Sh_{G,0} = 2.7$;
- at high values of Re_{LG} (usually the distillation conditions) the dependence of Sh_G on Re_{LG} will take a form $Sh_G \propto Re_{LG}^{0.9}$ which agrees with most of the distillation mass-transfer models;
- at very low value of Sc_G the second term of Eq. (20) vanishes resulting in the dependence of $k_G \propto D_{G,12}^1$ which corresponds to the “film theory” proposed by Lewis and Whitman (1924);
- at high value of Sc_G the dependence of Sh_G on Sc_G takes a form of $Sh_G \propto Sc_G^{1/3}$ which is in an agreement with the Chilton–Colburn analogy or with the laminar boundary layer theory.

The range of the conditions, Eq. (20) has been built on, covers the range of process conditions prevailing in common absorption and distillation columns — see Table 7. It can be,

Table 7 – Estimation of industrial columns operating conditions at 50% of their capacity provided by Aspen Plus for column packed with Mellapak 250.Y.

	System	p (bar)	Re_{LG}	Sc_G
Distillation	<i>p</i> -Xylene/ <i>m</i> -xylene	0.133	2500	0.70
Distillation	Methanol/ethanol	1	2400	0.81
Distillation	Cyclohexane/ <i>n</i> -heptane	1.013	5300	0.70
Absorption	CO ₂ /H ₂	20	1500	1.04
Absorption	H ₂ S/H ₂	20	1200	1.91

therefore, assumed that the correlation is valid not only for absorption conditions, but it can be also used for predictions of Sh_G in distillation columns. This assumption is supported by our previous work on the wetted wall column for which the Sh_G correlation built on the absorption data measured by the same systems as in this work was later successfully used for the prediction of the separation efficiency under distillation conditions (Rejl et al., 2016). However, the validation of the correlation transferability to the distillation conditions has to be performed in a future work.

4. Conclusions

In this work the gas phase mass-transfer coefficients, k_G , of Mellapak 250.X and 250.Y structured packings have been measured using absorption of SO₂ from carrier gas to the aqueous solution of NaOH. Three carrier gases – N₂, He and SF₆ – have been used in these measurements providing wide range of gas transport properties characterized by Sc_G from 0.49 to 2.32. It was found that the Sh_G data is possible to correlate in a simple power-law dependence on Re_{LG} if the limiting value of $Sh_{G,0} = 2.7$ is subtracted from the experimental data; the dependence of $(Sh_G - Sh_{G,0}) \propto Re_{LG}^{0.88}$ has been evaluated on the basis of the experimental data.

The data measured in this work have been supplemented with the literature data for Mellapak 250.X, 250.Y, 350.Y and 500.Y measured with air/SO₂/NaOH_(aq.) system and the data for Mellapak 250.Y measured with air/NH₃/H₂SO_{4(aq.)} system. All the data have been correlated in the dimensionless form with Eq. (20). The correlation was built on the data measured in wide range of Re_{LG} and Sc_G which covers the range of operation conditions of many industrial columns. In our previous work the possibility of recalculation of the absorption Sh_G to distillation conditions was successfully proved therefore it can be expected the correlation Eq. (20) will be valid for both absorption and distillation conditions.

Acknowledgments

Authors are grateful to the Czech Science Foundation for supporting the project through Grant 13-01251S and to the financial support from specific university research (MSMT No 20/2016). Workplace is grateful to Sulzer Ltd. for providing of packing samples.

Appendix A. Review of gas-phase mass-transfer models

(A1) Billet and Schultes

Model of Billet and Schultes (1999) is a comprehensive model initially built for design of the absorption and distillation columns packed with random packings. Later the model has

been broadened to enable its use also for the structured packings. The model consists from the relations for the prediction of the hydraulic (liquid hold-up, effective interfacial area and pressure drop) and mass-transfer (gas- and liquid-phase mass-transfer coefficients) characteristics of the packing. The packing in this model is characterized by its geometry (geometrical area, void fraction) and by six packing characteristic constants; their values have been optimized on the basis of results of numerous experimental data. The relation for k_G involved in this model is based on the penetration theory and adjusted to fit the wide database of absorption and distillation data resulting in Eq. (A1).

$$\frac{k_G \cdot a_g}{D_{12,G}} = C_G \frac{a_g^2}{2\varepsilon^{1/2}(\varepsilon - h_L)^{1/2}} \left(\frac{u_G \cdot \rho_G}{a_g \cdot \mu} \right)^{3/4} Sc_G^{1/3} \quad (A1)$$

Due to this adjustment, the dependence of $Sh_G \propto Re_G^{1/2} \cdot Sc_G^{1/2}$ originally assumed according to the penetration theory was changed to the dependence of $Sh_G \propto Re_G^{3/4} \cdot Sc_G^{1/3}$.

(A2) Rocha, Bravo and Fair

This comprehensive model has been built for prediction of the mass-transfer performance of the packed distillation columns. The model consists of two parts — hydraulic (Rocha et al., 1993) and mass-transfer (Rocha et al., 1996). The packing is characterized by its geometry (geometrical area, inclination angle, channel dimensions, void fraction) and by the surface parameter (surface enhancement factor). The liquid phase mass-transfer coefficient, k_L , is calculated according to the penetration theory. For the calculation of k_G the packing is modeled as a bundle of inclined triangular pipes and the correlation of Johnstone and Pigford (1942) for Sh_G in the wetted wall column is utilized in the form

$$Sh_G = A \cdot Re_{LG}^{0.8} Sc_G^{1/3}. \quad (A2)$$

The front factor $A = 0.054$ has been adjusted to fit the HETP data measured on numerous packings and distillation systems.

(A3a) DELFT model

The model (Olujić et al., 2012, 2004) has been designed for prediction of structured packings efficiency under distillation conditions. In this model the packing is characterized by the packing geometry only. Similarly, as in the Rocha, Bravo and Fair model only negligible mass-transfer resistance is assumed in distillation processes; the liquid-side mass transfer coefficient is calculated according to the penetration theory and for the gas-phase mass transfer the packing is modeled as a bundle of inclined triangular pipes. The analogy of the heat and mass transfer in packed columns is assumed; the relations for prediction of Sh_G are based on the relations for prediction of Nusselt number for laminar and turbulent flow in pipes

$$Sh_{G,lam} = 0.644 \cdot Sc_G^{1/3} \cdot \sqrt{Re_{LG} \frac{d_{hG}}{l_{hG}}} \quad (A3a)$$

$$Sh_{G,turb} = \frac{Re_{LG} Sc_G^{\frac{\xi}{8}} + 1.27 \sqrt{\frac{\xi}{8}} (Sc_G^{2/3} - 1)}{1 + \left(\frac{d_{hG}}{l_{hG}} \right)^{2/3}} \quad (A3b)$$

with $\xi(d_{hG}, Re_{LG})$ being gas–liquid interaction factor. The relation for ξ estimation is based on the fit of experimental HETP and pressure drop data. A transitional character of the flow is assumed in the packing; the transitional Sh_G is calculated by addition of laminar and turbulent contributions.

$$Sh_G = \sqrt{Sh_{G,lam}^2 + Sh_{G,turb}^2} \quad (A4)$$

Unlike the other correlations, the DELFT model does not implies a simple power law dependence of Sh_G on Re_{LG} and Sc_G . At the low values of $Re_{LG} \approx 500$ the dependence of $Sh_G \propto Re_{LG}^{-0.6} Sc_G^{0.15}$ can be observed on the basis of predicted data while at the high values of $Re_{LG} \approx 10\,000$ the dependence takes a form $Sh_G \propto Re_{LG}^{0.9} Sc_G^{0.3}$.

(A5) Hanley and Chen

The model of Hanley and Chen (2012) is a mass-transfer model designed for prediction of k_G , k_L and a of random and structured packings under absorption and distillation conditions. The power-law dependencies of a/a_g , Sh_L and Sh_G on the other dimensionless quantities are assumed in the model; namely for Sh_G the dependence of $Sh_G \propto Re_G Sc_G^{1/3}$ taken from the Chilton–Colburn analogy is assumed. The front factors of the power-law relations have been fitted to the database of HETP data and to the temperature profiles along the amine absorption columns resulting in the following relation for Sh_G in metal sheet structured packings:

$$Sh_G = 0.0084 \cdot Re_G Sc_G^{1/3} \cdot \left(\frac{\cos(\theta)}{\cos(\pi/4)} \right)^{-3.072} \quad (A5)$$

According to the authors the model predicts reliable values of the mass-transfer parameters of the packing at the operating condition of the column, on the other hand wrong values can be predicted by this model for very low or very high loads.

7. Wang et al.

This model (Wang et al., 2016) brings a novel approach to the modeling of the mass transfer in structured packings. The packing in this model is characterized by the geometrical area and the inclination angle only. According to the model the inclination angle specifies the Mixing number (Mi) of the packing which represents the dimensionless form of mixing point density.⁷ The parameters of the model were adjusted to fit absorption k_L , k_G and a data measured on numerous packings using aqueous systems. Similarly, as in this work, k_G has been measured using absorption of SO_2 into the diluted solution of NaOH and the results have been correlated in a dimensionless form

$$\frac{k_G}{a_g D_{12,G}} = 14 \left(\frac{\rho \cdot u_{GS}}{a_g \mu_G} \right)^{0.59} Sc_G^{1/2} \cdot Mi^{1.1} \quad (A6)$$

This correlation predicts the dependence of $Sh_G \propto Re_G^{0.59}$ which is in a close agreement with the dependence of $Sh_G \propto Re_G^{0.62}$ published in our previous paper (Rejl et al., 2013) for Mellapak Y packing series and SO_2 /air system $Sh_G \propto Re_G^{0.59}$. The

⁷ “Mixing points are the contact points of metal sheets in structured packings and are believed to enhance mass transfer.” (Wang et al., 2016).

power of $\frac{1}{2}$ at Sc_G was taken from Mehta and Sharma (1966). The applicability of this model for other than the experimental conditions has been never verified nor commented by the authors.

References

- Billet, R., Schultes, M., 1999. Prediction of mass transfer columns with dumped and arranged packings updated summary of the calculation method of Billet and Schultes. *Chem. Eng. Res. Des.* 77, 498–504, <http://dx.doi.org/10.1205/026387699526520>.
- Chilton, T.H., Colburn, A.P., 1934. Mass transfer (absorption) coefficients prediction from data on heat transfer and fluid friction. *Ind. Eng. Chem.* 26, 1183–1187, <http://dx.doi.org/10.1021/ie50299a012>.
- Crause, J.C., Nieuwoudt, I., 1999. Mass transfer in a short wetted-wall column. 1. Pure components. *Ind. Eng. Chem. Res.* 38, 4928–4932, <http://dx.doi.org/10.1021/ie990029f>.
- Dittus, F.W., Boelter, L.M.K., 1930. *Heat Transfer in Automobile Radiator of the Tubular Type*, 2nd ed. University of California at Berkley Publ., Eng, Berkley.
- Gilliland, E.R., Sherwood, T.K., 1934. Diffusion of vapors into air streams. *Ind. Eng. Chem.* 26, 516–523, <http://dx.doi.org/10.1021/ie50293a010>.
- Gnielinski, V., 1976. New equation for heat and mass transfer in turbulent pipe and channel flow. *Int. Chem. Eng.* 16, 359–368.
- Haidl, J., Rejl, F.J., Valenz, L., Kordač, M., Moucha, T., Labík, L., Schultes, M., 2016. Absorption in wetted-wall column with phase properties close to distillation conditions. *Chem. Eng. Sci.* 144, 126–134, <http://dx.doi.org/10.1016/j.ces.2015.12.027>.
- Hanley, B., Chen, C.C., 2012. New mass-transfer correlations for packed towers. *AIChE J.* 58, 132–152, <http://dx.doi.org/10.1002/aic.12574>.
- Humphrey, J.L., 1995. Separation processes: playing a critical role. *Chem. Eng. Prog.* 91, 31–41.
- Johnstone, H.F., Pigford, R.L., 1942. Distillation in a wetted wall column. *Trans. Am. Inst. Chem. Eng.* 38, 25.
- Kunze, A.-K., Lutze, P., Kopatschek, M., Maćkowiak, J.F., Maćkowiak, J., Grünwald, M., Górak, A., 2015. Mass transfer measurements in absorption and desorption: determination of mass transfer parameters. *Chem. Eng. Res. Des.* 104, 440–452, <http://dx.doi.org/10.1016/j.cherd.2015.08.025>.
- Lewis, W.K., Whitman, W.G., 1924. Principles of gas absorption. *Ind. Eng. Chem.* 16, 1215–1220.
- Linton, W.H., Sherwood, T.K., 1950. Mass transfer from solid shapes to water in stream-line and turbulent flow. *Chem. Eng. Prog.* 46, 258–264.
- Mehta, V.D., Sharma, M.M., 1966. Effect of diffusivity on gas-side mass transfer coefficient. *Chem. Eng. Sci.* 21, 361.
- Mikityuk, K., 2009. Heat transfer to liquid metal: review of data and correlations for tube bundles. *Nucl. Eng. Des.* 239, 680–687, <http://dx.doi.org/10.1016/j.nucengdes.2008.12.014>.
- Notter, R.H., Sleicher, C.A., 1972. A solution to the turbulent Graetz problem-III Fully developed and entry region heat transfer rates. *Chem. Eng. Sci.* 27, 2073–2093, [http://dx.doi.org/10.1016/0009-2509\(72\)87065-9](http://dx.doi.org/10.1016/0009-2509(72)87065-9).
- Olujić, Ž., Behrens, M., Colli, L., Paglianti, A., 2004. Predicting the efficiency of corrugated sheet structured packings with large specific surface area. *Chem. Biochem. Eng. Q.* 18, 89–96, <http://dx.doi.org/10.15255/CABEQ.2014.19344>.
- Olujić, Ž., Rietfort, T., Jansen, H., Kaibel, B., Zich, E., Frey, G., Ruffert, G., Zielke, T., 2012. Experimental characterization and modeling of high performance structured packings. *Ind. Eng. Chem. Res.* 51, 4414–4423.
- Rejl, F.J., Haidl, J., Valenz, L., Moucha, T., Schultes, M., 2016. Analogy of absorption and distillation processes. Wetted-wall column study. *Chem. Eng. Sci.* 153, 146–154, <http://dx.doi.org/10.1016/j.ces.2016.07.021>.
- Rejl, F.J., Valenz, L., Haidl, J., Kordač, M., Moucha, T., 2015. On the modeling of gas-phase mass-transfer in metal sheet structured packings. *Chem. Eng. Res. Des.* 93, 194–202, <http://dx.doi.org/10.1016/j.cherd.2014.06.004>.
- Rejl, J.F., Linek, V., Moucha, T., Valenz, L., 2009. Methods standardization in the measurement of mass-transfer characteristics in packed absorption columns. *Chem. Eng. Res. Des.* 87, 695–704, <http://dx.doi.org/10.1016/j.cherd.2008.09.009>.
- Rocha, J.A., Bravo, J.L., Fair, J.R., 1996. Distillation columns containing structured packings: a comprehensive model for their performance. 2. Mass-transfer model. *Ind. Eng. Chem. Res.* 35, 1660–1667, <http://dx.doi.org/10.1021/ie9910773>.
- Rocha, J.A., Bravo, J.L., Fair, J.R., 1993. Distillation-columns containing structured packings—a comprehensive model for their performance. 1. Hydraulic models. *Ind. Eng. Chem. Res.* 32, 641–651, <http://dx.doi.org/10.1021/ie9910773>.
- Valenz, L., Rejl, F.J., Šíma, J., Linek, V., 2011. Absorption mass-transfer characteristics of Mellapak packings series. *Ind. Eng. Chem. Res.* 50, 12134–12142, <http://dx.doi.org/10.1021/ie200577k>.
- Wang, C., Song, D., Seibert, F.A., Rochelle, G.T., 2016. Dimensionless models for predicting the effective area, liquid-film, and gas-film mass-transfer coefficients of packing. *Ind. Eng. Chem. Res.* 55, 5373–5384, <http://dx.doi.org/10.1021/acs.iecr.5b04635>.
- Wang, G.Q., Yuan, X.G., Yu, K.T., 2005. Review of mass-transfer correlations for packed columns. *Ind. Eng. Chem. Res.* 44, 8715–8729, <http://dx.doi.org/10.1021/ie050017w>.